INSTITUTE OF PHYSICS PUBLISHING REPORTS ON PROGRESS IN PHYSICS

Rep. Prog. Phys. **68** (2005) 1997–2265 doi:10.1088/0034-4885/68/9/R01

Spin-polarized charged particle beams in high-energy accelerators

S R Mane[1,4], **Yu M Shatunov**[2] **and K Yokoya**[3]

[1] Convergent Computing Inc., PO Box 561, Shoreham, NY 11786, USA
[2] Budker Institute of Nuclear Physics, Novosibirsk 630090, Russia
[3] National Laboratory for High-Energy Physics (KEK), 1-1 Oho, Tsukuba, Ibaraki 305-0801, Japan

E-mail: srmane@optonline.net and kaoru.yokoya@kek.jp

Received 5 April 2005, in final form 15 June 2005
Published 16 August 2005
Online at stacks.iop.org/RoPP/68/1997

Abstract

We present a comprehensive survey of the dynamics of spin-polarized beams in high-energy particle accelerators. A major theme of this review is to clarify the distinction between the properties of an *individual* particle—a *spin*—and that of a *beam*—the *polarization*. We include work from a number of institutions, including high- and medium-energy facilities, synchrotron light sources and muon storage rings (including a proposal to measure the muon electric dipole moment) and, briefly, linear accelerators and recirculating linacs. High-precision tests of the Standard Model using spin-polarized beams are reviewed; also innovative studies using spin dynamics as a tool for accelerator physics *per se*. We include important historical works as well as modern developments in the field. The fundamental theory is derived in detail, starting from the basic principles of quantum mechanics, electrodynamics and statistical mechanics, as well as 'accelerator physics'. The principal theoretical formulae in the field (Froissart–Stora, Sokolov–Ternov and Derbenev–Kondratenko) are presented, with in-depth attention to the quantum-statistical mechanics, as opposed to purely 'accelerator physics'.

(Some figures in this article are in colour only in the electronic version)

SRM dedicates this paper to the memory of Robert Glasser: physicist, mentor and friend.

[4] Author to whom any correspondence should be addressed.

0034-4885/05/091997+269$90.00

Contents

1. Introduction

All of the particle species commonly accelerated in modern particle accelerators have spin. This immediately suggests the possibility of utilizing the particle spins as an additional experimental tool. High-energy and nuclear physics using accelerators has reached a point where a very large fraction of the experiments require polarized beams. Essentially all research electron accelerators use polarized beams—Jefferson Lab exclusively, for a number of years now (since 1999). At ELSA (the Electron Stretcher Accelerator facility), it is stated that polarized electron beams will play a major role in their future research programme. Most proton (or hadron) machines desire polarized beams—e.g. RHIC, the Relativistic Heavy Ion Collider at BNL (Brookhaven National Laboratory). The recent successes at BNL to accelerate, store and collide counter-rotating polarized proton beams at high energy, by using so-called 'Siberian Snakes', 'spin rotators' and 'partial Snakes' mark the successful culmination of three decades of both theoretical ideas and experimental work in the field. (*Note:* As of the date of writing this paper, RHIC has accelerated polarized proton beams to 100 GeV. All the material on RHIC in this paper will discuss only 100 GeV beams. However, the top design energy of RHIC is 250 GeV, and RHIC will undoubtedly accelerate polarized proton beams to a higher energy in the future.) Anyone looking at the underlying physics will appreciate that this reality (the need for polarized relativistic particle beams) is likely to remain the case for a long time, and thus, that new generations of physicists—both accelerator builders and research users—will need to understand these phenomena. Presently, there is no one place for a student/researcher to obtain pertinent information. One wonders how much time and effort is lost by people seeking such information (in many sub-fields), when in reality, the field is mature enough for a comprehensive review. Several years ago, Courant (1990) and Shatunov (1990) wrote a pair of back-to-back reviews on spin dynamics in high-energy accelerators, but there have been many advances since then, e.g. the Siberian Snakes, spin rotators and partial Snakes mentioned above. This is therefore, a propitious time to write a broad, but also detailed, survey of the dynamics of spin-polarized beams in high-energy particle accelerators.

This paper is one of two that jointly aim to provide a comprehensive and in-depth review of the field of polarized beams in high-energy accelerators, including important historical works, as well as modern experiments and, also, the supporting theory and open questions in the field. The companion paper (Mane *et al* 2005) will be denoted MSY1 below, the current paper being MSY2. MSY1 reviewed the important subject of 'Siberian Snakes' and spin rotators. Siberian Snakes are essential devices to enable the acceleration of spin-polarized beams to high energies without crossing so-called depolarizing spin resonances. However, they are also useful at lower energy facilities, and have been employed with success at the electron storage rings AmPS and SHR, where the beam energy is less than 1 GeV. MSY1 reviewed not only the theory of Snakes and spin rotators, but also several practical designs, e.g. solenoids and 'full-twist helical magnetic fields' and 'Steffen Snakes'. MSY1 also reviewed the practical accelerator physics experience with such devices, including the so-called 'Snake resonances', which are depolarizing resonances in rings equipped with Siberian Snakes. MSY1 did *not*, however, treat the important subject of 'partial Snakes'. This is one of the topics we shall address below.

The present paper (MSY2) is a longer paper, and will cover a broader range of topics. It will review the fundamental theory of spin dynamics in accelerators, including the principal formulae for both radiative and nonradiative polarization, e.g. the Froissart–Stora, Sokolov–Ternov and Derbenev–Kondratenko formulae. Experimental work at a number of facilities will be reviewed, including 'case studies' at various laboratories, to illustrate the practical issues one encounters when working with polarized beams in actual accelerators. Important

achievements using spin-polarized beams, including precision tests of the Standard Model, will be treated. Particular attention will be paid to the fundamental physical principles of statistical mechanics, (semiclassical) electrodynamics, dynamical systems theory as well as so-called 'accelerator physics'. We emphasize the distinction between a *spin*—a property of an individual particle—and the *polarization*—a property of the entire beam.

While the aim of both MSY1 and MSY2 is to provide a broad yet comprehensive survey of spin dynamics in accelerators, this paper is not a compilation of every paper published in the field. In general, we try to cite significant works, and to stress positive achievements. In some cases, we have not cited certain papers which seem to be inadequate. As stated above, we review experimental work at several accelerator laboratories to illustrate a number of fundamental points of spin physics. However, we are well aware that many of those points could be made using work done at other accelerators, or by citing experiments other than those we mention below. The Nuclotron at Dubna, for example, delivers the highest-energy polarized deuteron beams in the world, but we do not discuss the work at the Nuclotron in this paper. Another facility we do not discuss in detail is COSY, the COoler SYnchrotron at Jülich. COSY accelerates beams of polarized and unpolarized protons and deuterons in the momentum range between 300 MeV c^{-1} and 3650 MeV c^{-1} (Lorentz *et al* 2004). Vertically polarized proton beams with over 80% polarization have been delivered to internal targets and external experiments. Since 2003, polarized deuterons have also been delivered to users. We also do not discuss the important subject of spin-polarized beams of radioactive nuclei, e.g. ^{7}Be or ^{8}Li, as at CERN's ISOLDE facility, or at ISAC at TRIUMF, etc.

Note also, that although we shall touch on various topics of particle physics throughout this paper, our focus is on accelerator physics, not particle physics. An excellent modern text titled 'Spin in Particle Physics' is by Leader (2001), which, as the title states, describes many of the important roles that spin-polarized beams have played, and continue to play, in high-energy physics.

We shall mainly treat only spin $\frac{1}{2}$ particles. Almost all the particle species we shall discuss, e.g. electrons, positrons, muons and protons, have spin $\frac{1}{2}$. However, there is increasing interest at modern accelerator facilities in the availability of polarized deuteron beams. Deuterons have spin 1, so we shall discuss the polarization of spin 1 particles, but only briefly. We shall *not* discuss neutrons: as the title states, we discuss only *charged* particles. Although we shall mainly treat circular accelerators (synchrotrons and storage rings), we do include two sections at the end, on linear accelerators (at SLAC) and recirculating linacs (CEBAF). While on the subject of linear accelerators, we mention here a significant achievement, namely, the first measurement of the proton's 'weak magnetism' obtained by the SAMPLE experiment (Hasty *et al* 2000), using a longitudinally polarized electron beam from the linac at the MIT-Bates Linear Accelerator Laboratory. This is the weak-interaction analogue of the magnetic dipole moment. Its existence was predicted theoretically in the 1950s. A longitudinally polarized electron beam (i.e. electrons in helicity eigenstates) was essential to perform this measurement.

We include not only the highest energy rings such as RHIC and LEP, but also lower energy facilities such as ELSA, IUCF, JLAB/CEBAF, KEK-PS, VEPP-2M and VEPP-4, etc. A list of the names (acronyms) of the various machines mentioned in the text, and the institutions where they are located, is given in table 1. Some machines, like SPEAR, DORIS or TRISTAN, have acronyms, for historical reasons, that do not fit their actual operation; we have placed the acronym in parentheses. (SPEAR was retrofitted to mean Stanford Positron Electron Accelerating Ring.) For BESSY the acronym was too long and we could not find the meaning of SATURNE. Note also that several of the machines have been decommissioned; accelerators do not operate forever.

Table 1. Names and locations of accelerators referenced in the text, listed alphabetically by institution.

Institution	Location	Machine	Acronym
ANL	Argonne, IL, USA	ZGS	Zero Gradient Synchrotron
Berlin	Berlin, Germany	BESSY-I, II	—
BINP	Novosibirsk, Russia	VEPP-(2, 2M, 3, 4)	Colliding Electron–Positron Beams
BNL	Upton, NY, USA	AGS	Alternating Gradient Synchrotron
		RHIC	Relativistic Heavy–Ion Collider
CERN	Geneva, Switzerland	LEP	Large Electron–Positron Project
Cornell	Ithaca, NY, USA	CESR	Cornell Electron Storage Ring
DESY	Hamburg, Germany	DORIS	(Doppel Ring Speicher)
		HERA	Hadron–Elektron Ring Anlage
		PETRA	Positron–Electron Tandem Ring Accelerator
ELSA	Bonn, Germany	ELSA	Electron Stretcher Accelerator
IUCF	Bloomington, IN, USA	IUCF Cooler	Indiana University Cyclotron Facility Cooler
KEK	Tsukuba, Japan	KEK-B	KEK B-Factory
		KEK-PS	KEK Proton Synchrotron
		TRISTAN	(Tri-Ring Intersecting Storage Accelerators at Nippon)
LBNL	Berkeley, CA, USA	ALS	Advanced Light Source
MIT-Bates	Middleton, MA, USA	SHR	South Hall Ring
NIKHEF	Amsterdam, Netherlands	AmPS	Amsterdam Pulse Stretcher
Orsay	Gif-sur-Yvette, France	ACO	Anneau de Collisions d'Orsay
PSI	Villigen, Switzerland	SLS	Swiss Light Source
Saclay	Gif-sur-Yvette, France	SATURNE	—
SLAC	Palo Alto, CA, USA	PEP-2	PEP B-Factory
		SLC	Stanford Linear Collider
		SPEAR	(Stanford Positron Electron Asymmetric Rings)
TJLab	Newport News, VA, USA	CEBAF	Continuous Electron Beam Accelerator Facility

Perhaps the greatest triumph of modern times, a success for both theory and experiment, is the recent successful installation and commissioning of 'Siberian Snakes' and spin rotators at RHIC, the Relativistic Heavy-Ion Collider at BNL. RHIC is the world's first (and to date, only) polarized proton collider. As of the time of writing this paper, RHIC has stored and collided 100 GeV polarized proton beams (Roser *et al* 2003). A schematic view of the BNL complex showing RHIC and its injector chain is shown in figure 1. The structure of the complex is a cascaded chain of accelerators, fairly typical for modern laboratories, and will serve as a useful example to explain some important concepts. A polarized proton source produces a spin-polarized beam which is injected into a linear accelerator (linac), from which the beam is then transferred to a Booster synchrotron. The particles are then transferred to a second synchrotron, the AGS (Alternating Gradient Synchrotron), and then to RHIC. The beam energy increases in each machine in the chain. The AGS, which today serves as the final injector leading to RHIC, is a venerable synchrotron in its own right. Work on polarized proton beams at the AGS has pioneered many techniques for spin dynamics in accelerators. The AGS work on polarized proton beams will be reviewed below. The above example of the BNL complex demonstrates several important lessons:

- A source of polarized particles (in this case, protons) is required. The majority of charged particle sources produce *un*polarized beams. It is much more difficult to create a beam of polarized charged particles than an unpolarized beam; the beam intensity may be lower by a factor of 1000 or more. The available intensity of polarized beams is itself a problem, but one which we shall not address.

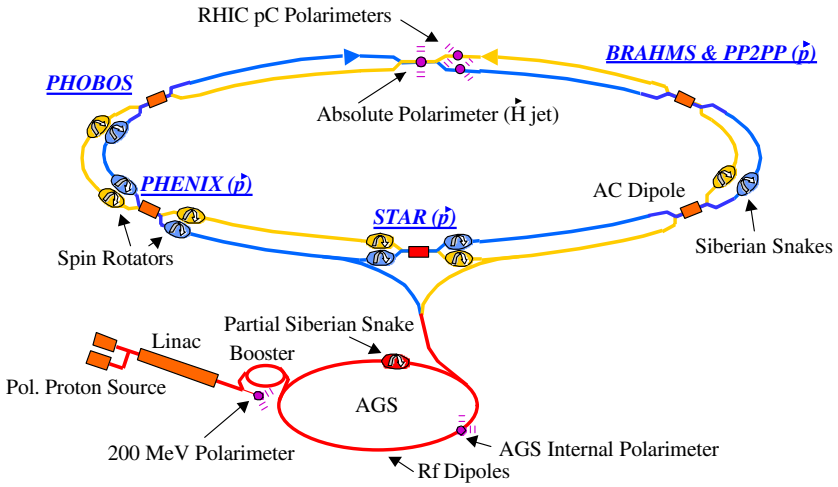

Figure 1. Schematic layout of BNL complex for polarized proton operations. Courtesy of MacKay (private communication) and BNL Collider Accelerator Department.

- The beam must be accelerated and transferred from one machine to another. There are any number of mechanisms which can depolarize the beam along the way; much of the text will be devoted to explaining the various sources of depolarization and the techniques to avoid or overcome them.
- The polarization must be measured: polarimeters are required. The design and operation of polarimeters, especially for hadrons, is also a nontrivial task. Although polarimetry is not really within the scope of this paper, we do include a section on polarimetry because the subject is important and cannot be ignored completely.
- Consulting figure 1, the Siberian Snakes and spin rotators are indicated in RHIC, also an 'ac dipole'. A 'partial Snake' is indicated at the AGS. We shall explain all of these devices below.
- Lastly, it must always be remembered that if the beam is lost, for whatever reason, then there is no polarization—there is no beam! The spin dynamics always sits on top of the orbital dynamics. The various machines must be adjusted to preserve (or optimize) the beam intensity (in the case of colliders, the appropriate term is 'luminosity'). In some cases, such requirements on the machine can conflict with those to optimize the polarization.

The above ideas give a conceptual view of the issues involved in dealing with hadron beams. The situation is somewhat different for ultrarelativistic electron and positron beams. Such beams emit synchrotron radiation. At the simplest level, synchrotron radiation is a classical phenomenon, and was so discussed in the classic paper by Schwinger (1949). However, synchrotron radiation does, after all, consist of photons, and at the higher orders of QED perturbation theory, it was shown that photon emission couples to the electron (or positron) spin. The emission of a photon can flip the particle spins, and because this flip takes place in a background guiding magnetic field, the spins actually polarize spontaneously. This phenomenon is called *radiative polarization*, also called the Sokolov–Ternov effect. Sokolov and Ternov (1964) solved the electron motion in a homogeneous magnetic field, and showed that the polarization builds up exponentially (starting from zero), according to

$$P(t) = P_{\mathrm{ST}}(1 - \mathrm{e}^{-t/\tau_{\mathrm{pol}}}), \tag{1.1}$$

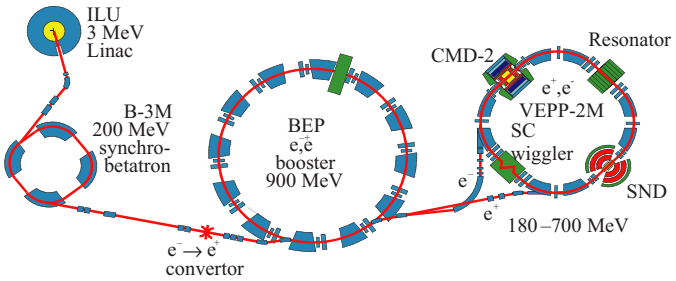

Figure 2. Schematic layout of VEPP-2M complex.

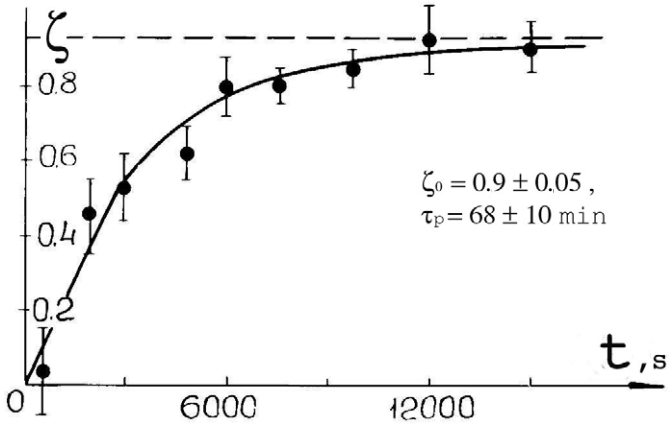

Figure 3. An early observation of radiative polarization buildup in an e^+e^- storage ring (VEPP-2M). The degree of polarization is denoted by ζ. From Serednyakov *et al* (1976). Copyright (1976) by the American Institute of Physics.

to an asymptotic value of

$$P_{\rm ST} = \frac{8}{5\sqrt{3}} \simeq 92.376\%, \tag{1.2}$$

with a time constant $\tau_{\rm pol}$ which we shall discuss shortly, below. The direction of the asymptotic polarization is antiparallel to the guiding magnetic field for electrons, and parallel for positrons. Hence, for ultrarelativistic e^+e^- beams, it is not always necessary to employ a polarized particle source, etc: the beams can be polarized *in situ*. An early observation of radiative polarization was at the VEPP-2M e^+e^- storage ring (Serednyakov *et al* 1976). A schematic layout of the VEPP-2M complex is shown in figure 2. Note that the figure is a modern version of the ring; not all of the hardware was in existence in the 1970s.

The exponential buildup of the polarization buildup at VEPP-2M is shown in figure 3. The asymptotic polarization equals the theoretical maximum ($P = 0.9 \pm 0.05$ in figure 3). The time constant τ is indicated as (68 ± 10) min. Radiative polarization buildup is not necessarily a fast process. Figure 4 shows the polarization buildup at VEPP-4. The asymptotic polarization is 65%. Note that the beam was deliberately depolarized at the end of the graph and we shall (later) discuss why one would wish to do this. Figure 5 is a graph of the record radiative polarization level of 57% attained at LEP. We shall soon discuss why $P < P_{\rm ST}$ at most storage rings.

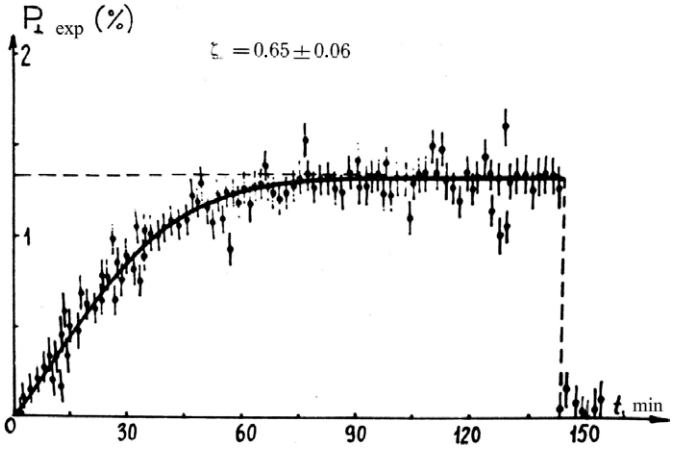

Figure 4. Measurement of the radiative beam polarization at the VEPP-4 storage ring. The vertical axis denotes the polarimeter asymmetry.

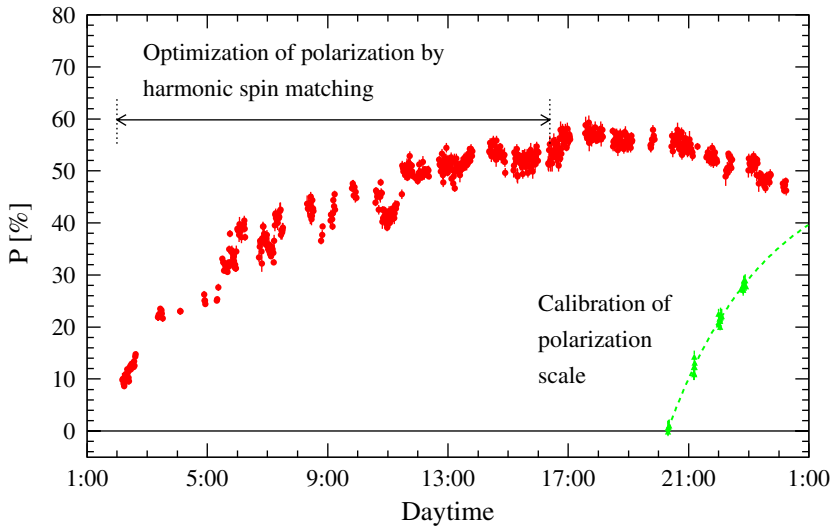

Figure 5. Record polarization of 57% attained at LEP. Courtesy of J Wenninger (private communication) and CERN.

Radiative polarization is a slow process in most machines. The time constant for the polarization buildup is strongly energy dependent: for a beam of energy E circulating in a uniform magnetic field B, it is given by

$$\tau_{\text{pol}} \propto \frac{1}{B^3 E^2}. \tag{1.3}$$

Hence, in low-energy electron storage rings such as AmPS at NIKHEF or SHR at MIT-Bates, for example, where the beam energy is less than 1 GeV, the radiative polarization buildup time is hundreds of hours or more. A polarized electron source is required at such rings.

One of the most beautiful graphs of the measurement of the polarization in a storage ring, is the SPEAR polarization data (Johnson *et al* 1983). The measurements are shown

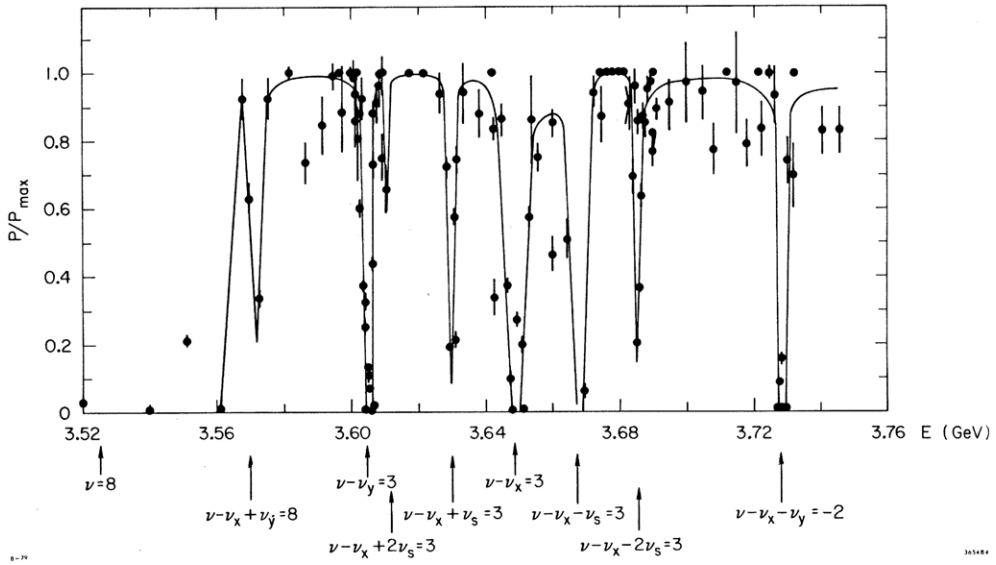

Figure 6. Measurement of the positron beam polarization in the SPEAR storage ring. The value of the parameter $P_{\max}$ is 92.4%. The orbital tunes (to be defined later in the text) are denoted by $\nu_{x,y,s}$, and the spin tune (also to be defined later) is denoted by ν. Reprinted from Johnson *et al* (1983). Copyright (1983) with permission from Elsevier.

in figure 6. The positron beam polarization was measured parasitically over several shifts during accelerator studies in single-beam (non-colliding) mode. The curve through the data is a guide to the eye, not a theoretical calculation. The most striking feature of the SPEAR polarization data is the appearance of several depolarizing spin resonances, labelled in figure 6. We shall explain the notation $\nu_{x,y,s}$, etc, later. The essential point here is that, there is more to the polarization than just a simple exponential buildup to some asymptotic value. There can be numerous depolarizing effects in a storage ring.

The SPEAR polarization data were fitted by four sets of authors, all using different theoretical formalisms. We shall review the theoretical explanation of the SPEAR polarization data in section 29. One fit to the data was by Mane (1988a) and is shown in figure 7. Evidently there is a rich spectroscopy of spin resonances in storage rings.

Equally beautiful observations of spin resonances have been obtained at proton storage rings. An example of synchrotron sideband resonances in proton storage rings is shown in figure 8, displaying polarized beam data taken by the Alan Krisch group at the IUCF Cooler Ring (see van Guilder (1993), Lee and Berglund (1996), Chu *et al* (1998)). Both the vertical and radial polarization are shown; the IUCF polarimeter could measure both the vertical and radial asymmetries. The figure shows a parent resonance and synchrotron sidebands. Note that P_0 is just an arbitrary normalization constant, hence the fact that $P_v/P_0 > 1$ at some points in figure 8 is not an error. A polarized particle source is required at proton rings; proton beams emit no significant synchrotron radiation, and therefore do not polarize spontaneously.

Obviously then, spin-polarized beams in all types of accelerators are subject to depolarizing resonances. A major theoretical problem of spin dynamics in accelerators is to calculate the strengths of these depolarizing resonances, and to devise ways to avoid, overcome or eliminate them, or, alternatively, to *use* them—more accurately, to use the spectroscopy provided by the resonances for useful physics.

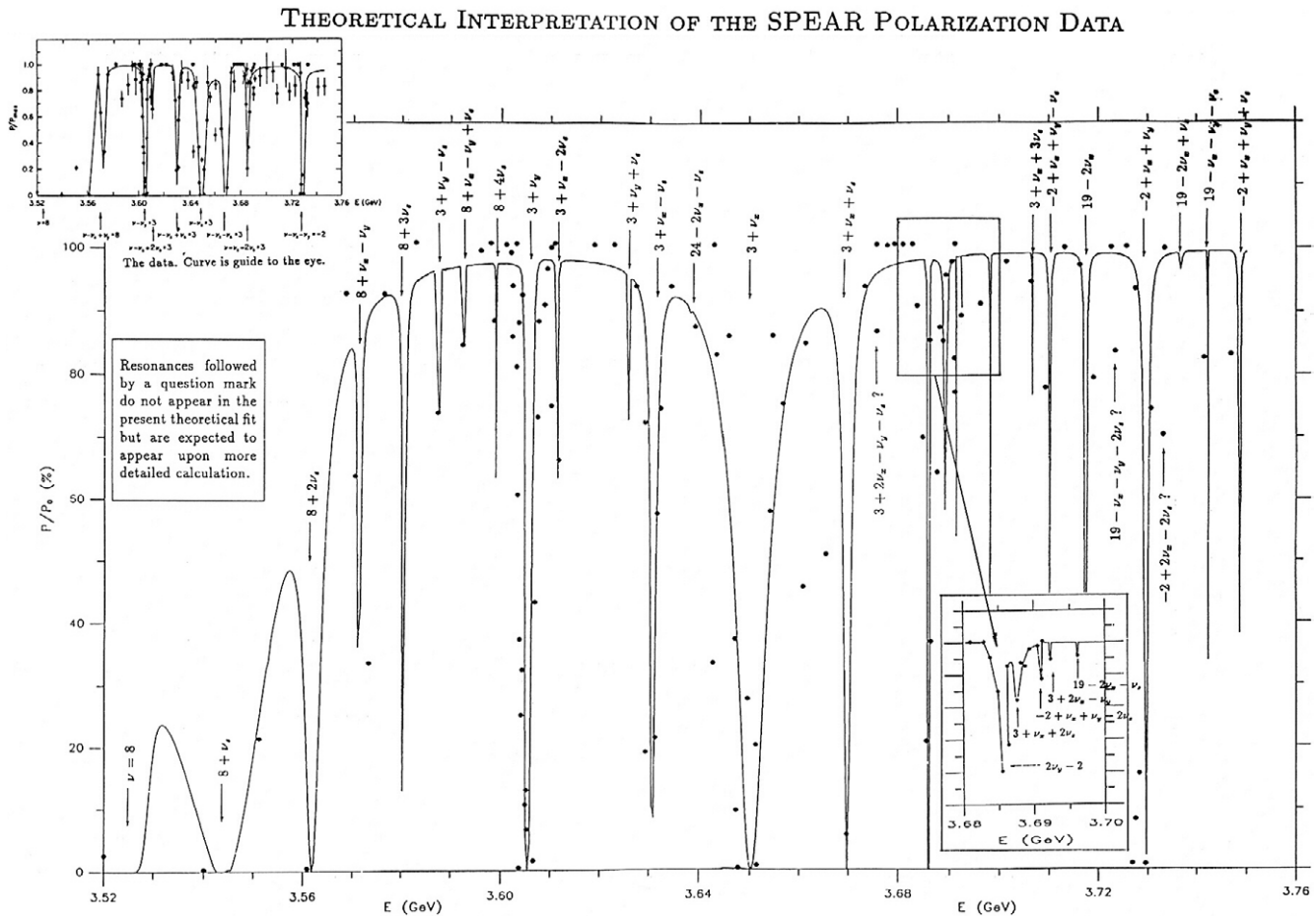

Figure 7. Theoretical fit of the SPEAR polarization data using SMILE. From Mane (1988a).

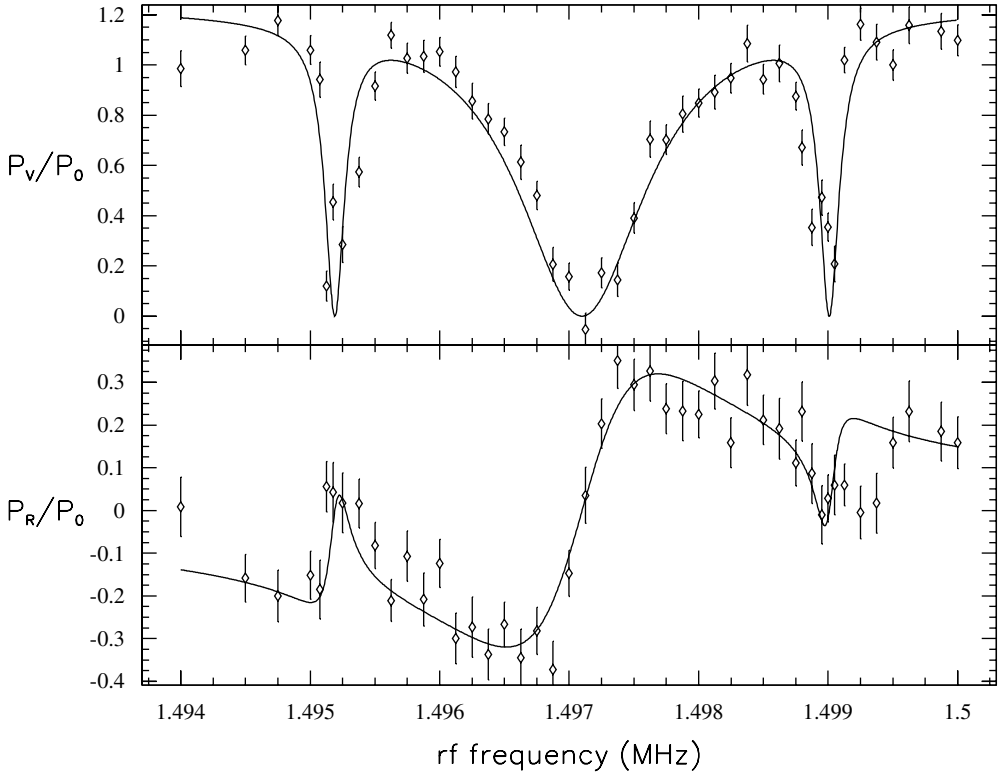

Figure 8. Parent and synchrotron sideband resonances at the IUCF Cooler. Both the vertical and radial polarization are shown. The curve is a theoretical fit. Reprinted with permission from Lee and Berglund (1996). Copyright (1996) by the American Physical Society.

We classify the types of rings we shall review in the text:

- Nonradiatively polarized beams in storage rings, e.g. RHIC, IUCF Cooler, AmPS and SHR. The above rings are, in fact, the only storage rings to be equipped with Siberian Snakes to date. We mean here, full-strength Snakes, to avoid murky historical priority claims. RHIC and the Cooler store(d) polarized protons and AmPS and SHR store(d) polarized electrons. Schematic layouts of the IUCF Cooler, AmPS and SHR are shown in figures 9, 10 and 11, respectively.
- Synchrotrons, e.g. the AGS and KEK-PS for polarized protons, and ELSA for polarized electrons, and others to be mentioned later. The KEK-PS was historically the first cascaded accelerator chain where polarized protons were transferred from one synchrotron (Booster) to another (Main Ring). The acceleration of nonradiatively polarized beams will be reviewed in section 25. Schematic layouts of the KEK-PS and ELSA facilities are shown in figures 12 and 13, respectively. A graph of the polarization level attained at ELSA as a function of the extracted beam energy is shown in figure 14, indicating the progress from about 1997. The various major depolarizing resonances encountered during the acceleration of the beam are marked in the figure. Recall from figure 6, that the locations of the spin resonances depend on the beam energy. For nonradiatively polarized beams, several depolarizing spin resonances are encountered during acceleration to the top energy.

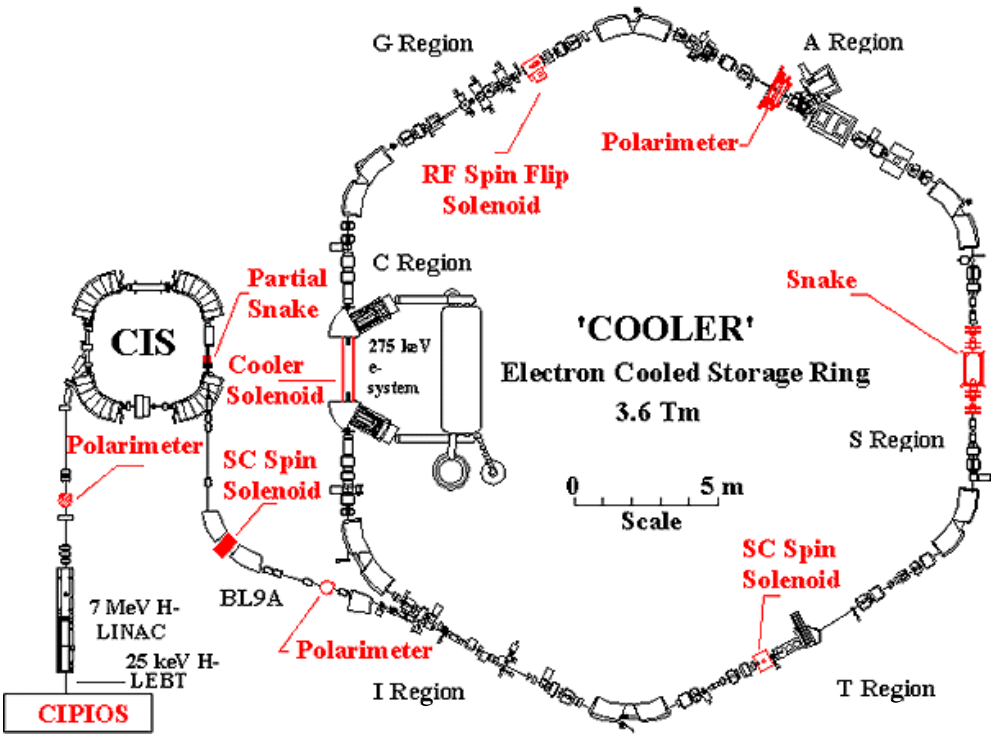

Figure 9. Schematic of the IUCF CIS/Cooler layout. Courtesy of Friesel (private communication) and IUCF.

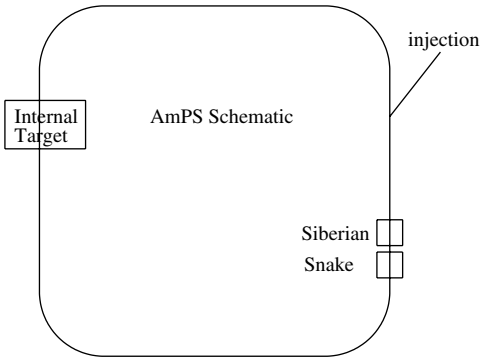

Figure 10. Schematic layout of AmPS.

- Electron (and e^+e^-) rings with radiatively polarized beams. This includes the proton–lepton ($p/e^{\pm}$) collider HERA. VEPP-2M is the lowest energy e^+e^- storage ring we shall treat below. At the other extreme is LEP (at CERN), the largest accelerator ever built (27 km circumference), and also the highest energy e^+e^- collider. A schematic of LEP is shown in figure 15. Section 31 is entirely devoted to LEP.
- A somewhat fringe topic is the work with radiatively polarized beams at *synchrotron light sources*. A principal goal in such rings is to maintain a very stable beam energy; for this, an accurate relative calibration of the beam energy is required. The work at synchrotron

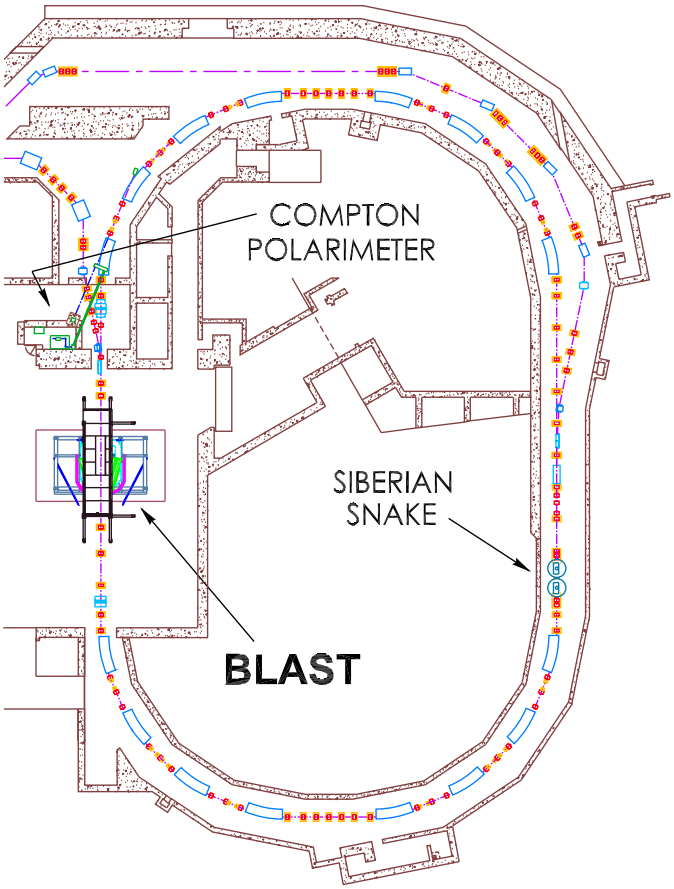

Figure 11. Schematic layout of the SHR at MIT-Bates. Courtesy of MIT-Bates Linear Accelerator Center.

light sources is reviewed in section 30. Schematic layouts of two light sources, namely, the ALS and the SLS, are shown in figures 16 and 17, respectively.

- Muon storage rings: these are also lepton rings, but do not emit any appreciable synchrotron radiation. Muons however, are polarized at birth via the parity-violating decay of the pion. A schematic layout of a 50×50 GeV muon collider is shown in figure 18. This is a proposed machine, a collider of the future. We shall also review the recently completed E821 experiment at BNL to measure the anomalous magnetic moment of the muon, and a new proposal to measure the *electric dipole moment* of the muon. *Spin* does not always mean the *magnetic* dipole moment.
- We also include brief sections on linear machines, namely, the SLC (linear collider), and CEBAF (recirculating linacs). A schematic view of the 'polarized SLC' is shown in figure 19. A schematic layout of CEBAF is shown in figure 20.

Historically, research using nonradiatively polarized beams typically involved accelerating polarized beams in synchrotrons for delivery to external fixed-target experiments, whereas research using radiatively polarized beams employed storage rings (colliders and/or internal targets). However, the situation is now quite different. RHIC is a polarized *proton* collider. In fact, of the four storage rings which have been equipped with Siberian Snakes,

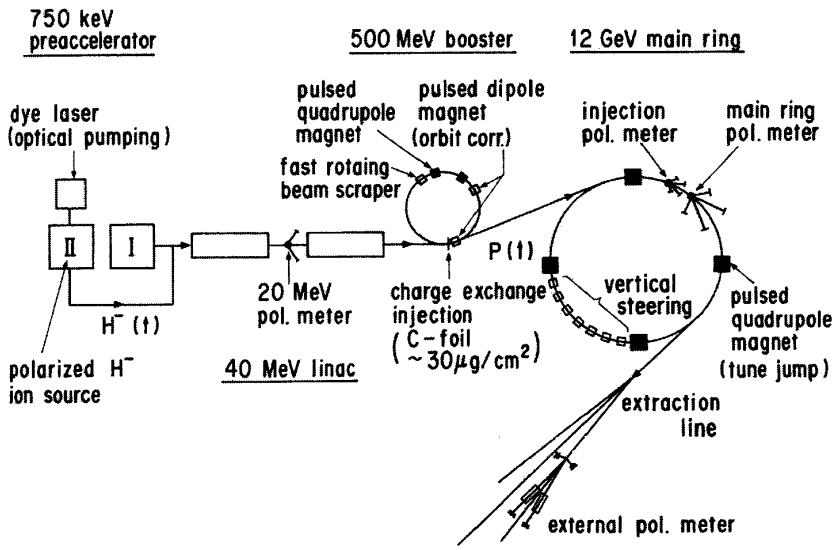

Figure 12. Schematic layout of the KEK-PS injector and Main Ring complex. Courtesy of Sato (private communication) and KEK.

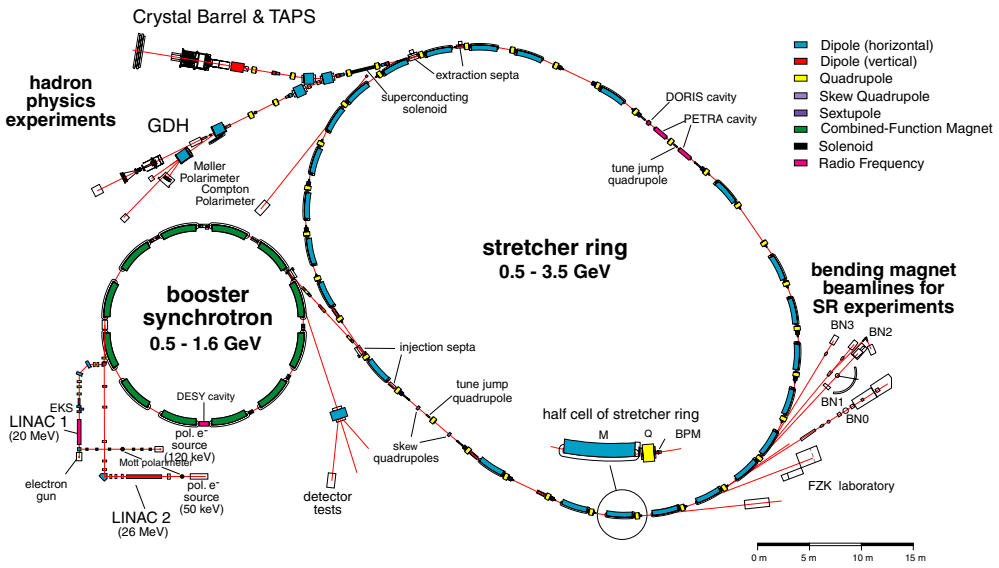

Figure 13. Schematic layout of the ELSA facility. Courtesy of Frommberger (private communication) and ELSA.

to date, two of them (AmPS and SHR) stored *electron* beams (which were nonradiatively polarized). Hence, we made the decision to treat, as far as possible, the basic concepts of spin dynamics in accelerators on a unified footing, *without* regard as to whether the results apply to radiative or nonradiative systems. We recognize that our decision did make the paper harder to write, and the structure of this paper is somewhat complicated. Nevertheless, we feel it is a worthy goal to present a unified treatment of the basic concepts in the field.

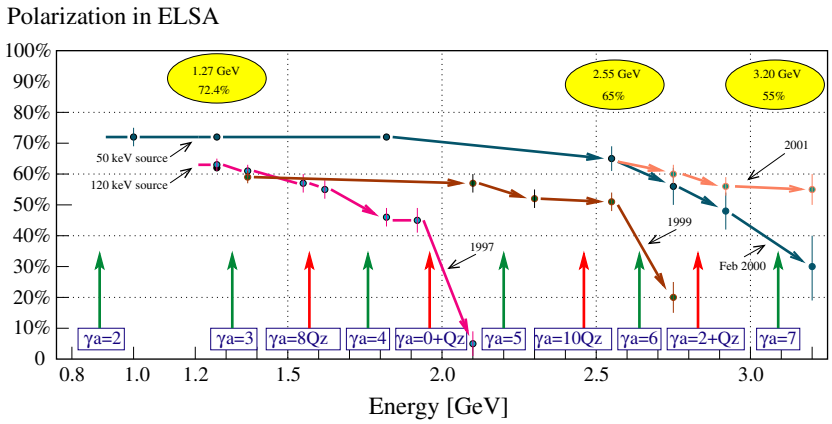

Figure 14. Polarization at ELSA as a function of extracted beam energy. From Hoffmann (2001).

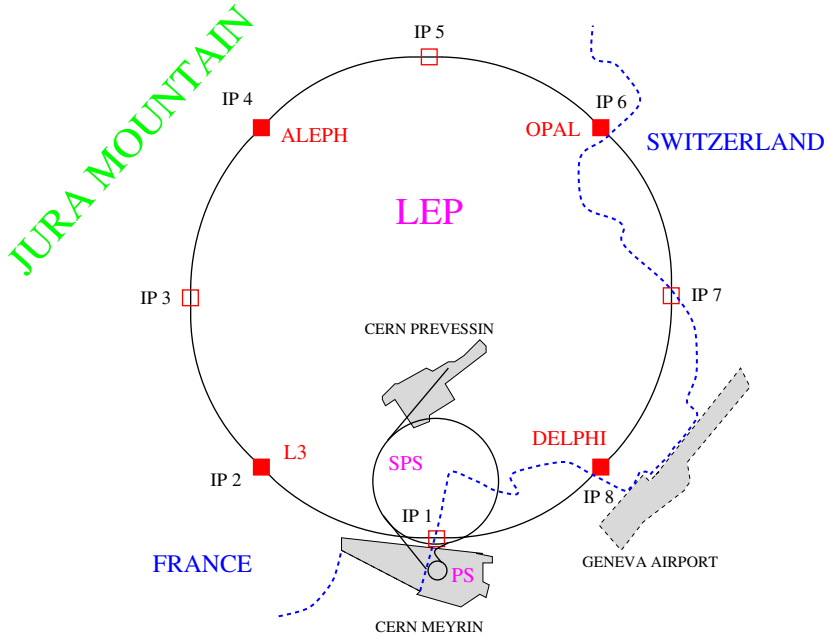

Figure 15. Schematic layout of LEP. Courtesy of Wenninger (private communication) and CERN.

The overall structure of the text is as follows. In the next section we review the Sokolov–Ternov formula, which gives the degree of the radiative polarization in a high-energy e^+e^- storage ring. We follow with 'chapter zero', which is explicitly intended to be a (relatively) nontechnical summary of the principal 'tacit assumptions' and 'unstated approximations', etc that the experts do not bother to mention. We attempt to clarify the foundations of the subject by a greater level of detail than seen in any other review, or textbook in the field. We follow chapter zero with a discussion of the Hamiltonian and the classical spin model. We present next, another major formula, namely, the Froissart–Stora formula, in

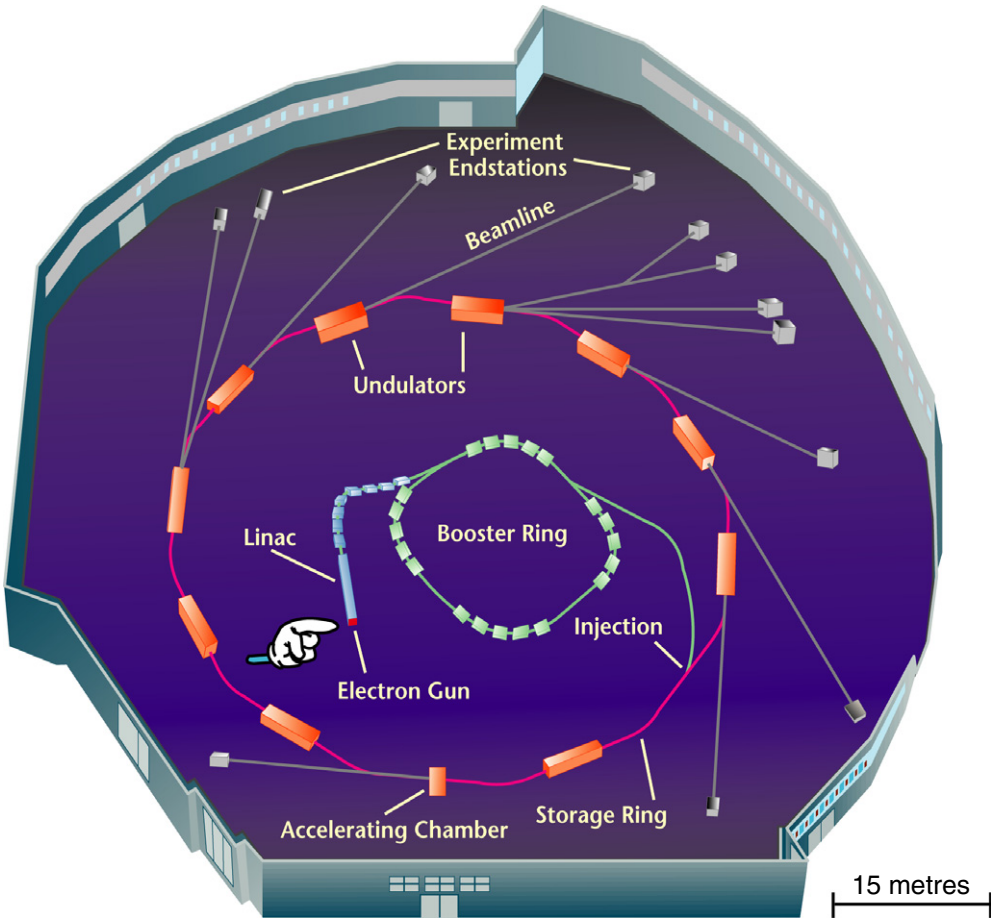

Figure 16. Schematic layout of the ALS. Courtesy of Byrd (private communication) and ALS.

section 6. Sections 7–10 develop foundational material, e.g. the basic notation, equations of motion and coordinate systems, also the orbital dynamics. The next section is on muon storage rings. Section 12 on polarimetry was originally intended to be a very brief summary of the subject, but grew to include some very important ideas and also experiments. Sections 14–23 return to formalism and develop the theory of the fundamental notion of the quantization axis of the spin eigenstates ('diagonalization of the Hamiltonian'). A great deal of formalism will be developed in these sections, including both perturbation theory and nonperturbative formalisms, to calculate the spin motion for off-axis trajectories. Once again, experiments will be mixed with theory. Sections 24 and 25 describe the acceleration of nonradiatively polarized beams to high energies in synchrotrons. Section 26 is devoted to the BNL polarized proton complex; this is where much of the theory, some of it proposed thirty years ago, has been vindicated with spectacular success. Sections 27–31 discuss radiative polarization, including several high-precision measurements made using polarized beams. Some of the best experimental work with polarized beams is contained in these sections. Sections 32 and 33 describe linear accelerators (SLAC) and recirculating linacs (CEBAF). The appendix contains the formal canonical transformation theory to diagonalize the spin–orbit Hamiltonian.

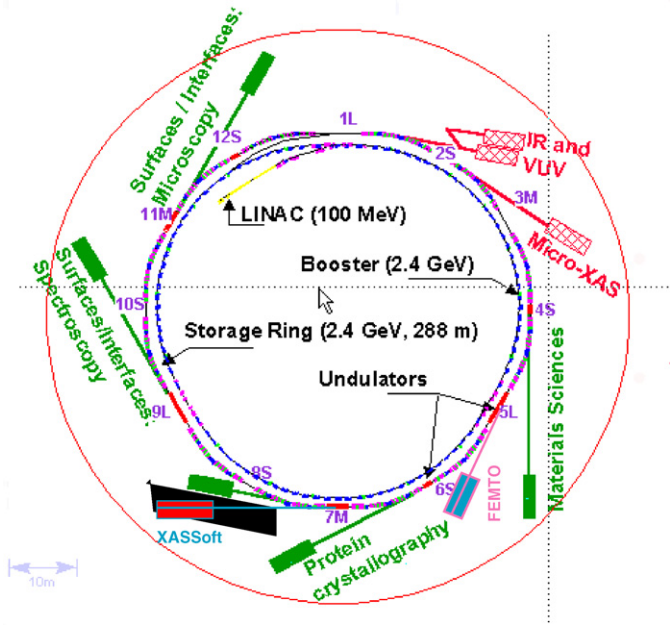

Figure 17. Schematic layout of the SLS complex. Courtesy of Leemann (private communication) and SLS.

We employ cgs units, the same as in the classic textbook by Jackson (1998). Hence the Lorentz force is written as $\boldsymbol{E} + \boldsymbol{\beta} \times \boldsymbol{B}$, and not $\boldsymbol{E} + \boldsymbol{v} \times \boldsymbol{B}$, where $\boldsymbol{\beta} = \boldsymbol{v}/c$. (See (5.66) below, and also (5.64) for the magnetic dipole interaction.) Here $\boldsymbol{v}$ is the particle velocity and c the speed of light, and $\boldsymbol{E}$ and $\boldsymbol{B}$ are the electric and magnetic fields which have the same dimensions. We do *not* set $\hbar$ and c to unity.

2. Sokolov–Ternov effect

2.1. Background

In this section, we review one of the outstanding theoretical ideas in the field, namely, the Sokolov–Ternov effect (Sokolov and Ternov 1964). It is the spontaneous buildup of radiative polarization in high-energy e^+e^- storage rings, via the emission of spin-flip synchrotron radiation. It is the basis for a great deal of excellent experimental work, including many high-precision tests of the Standard Model. We present this work at such an early stage deliberately, to demonstrate that it is possible to convey fundamental ideas without heavy formalism.

Radiative electron polarization is one among those phenomena that were predicted theoretically before being observed experimentally. The basic notion, that the photon emission couples to the particle spin operator at the higher orders of QED perturbation theory, was first noted by Ternov *et al* (1962). A quantitative solution for motion in a homogeneous field, based on calculation using the Dirac equation, was given by Sokolov and Ternov (1964). Authors coming after Sokolov and Ternov used semiclassical QED instead of solving the Dirac equation. However, see also a calculation by Schwinger and Tsai (1974) using a 'modified electron propagator' technique. An excellent review of the electrodynamics of spin-flip synchrotron radiation has been given by Jackson (1976).

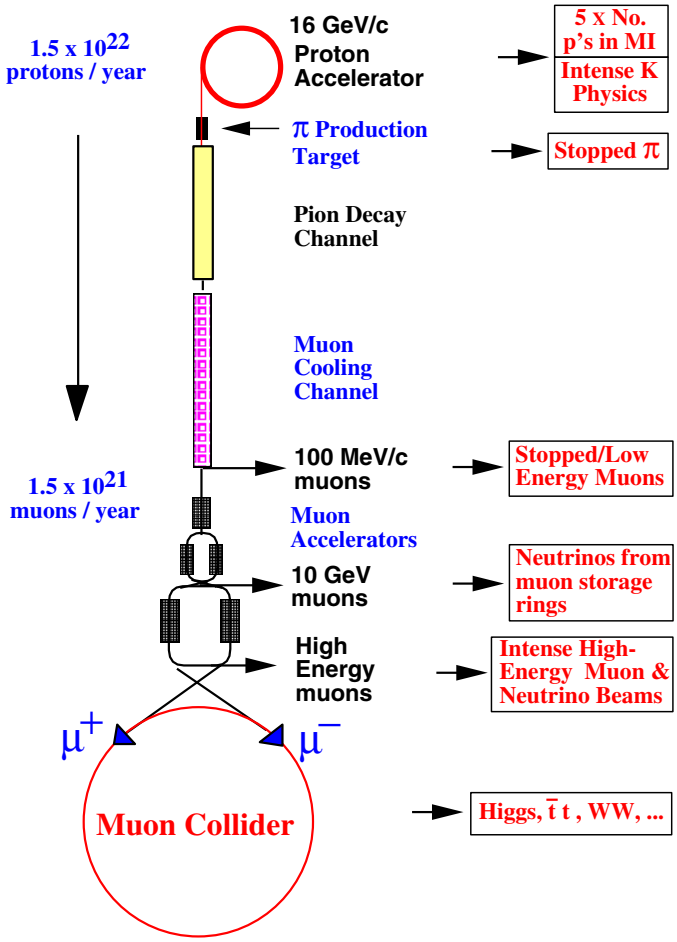

Figure 18. Schematic layout of a proposed muon collider. Reprinted with permission from Alsharo'a *et al* (2003). Copyright (2003) by the American Physical Society. Courtesy of Raja (private communication) and the Muon Collider Collaboration.

2.2. Early measurements of radiative polarization

The first experimental observation of Sokolov–Ternov radiative polarization was at ACO (Orsay Storage Ring Group 1971) and VEPP-2 (Baier 1972). Later, a higher degree of polarization was obtained at ACO (Le Duff *et al* 1973) and at VEPP-2M (Serednyakov *et al* 1976). A large value for the polarization of the electron and positron beams ($P \simeq 85\%$) was measured in the e^+e^- collider SPEAR1 (Camerini *et al* 1975), and shortly thereafter ($P \simeq 76\%$), in the upgraded machine SPEAR2 (Learned *et al* 1975). The measurements in the first three cases above, employed the Touschek effect (the intrabeam scattering of electrons, i.e. Møller scattering). The later measurements in VEPP-2M and SPEAR1 employed the azimuthal dependence of the $e^+e^- \to \mu^+\mu^-$ annihilation cross-section. The polarization measurements at SPEAR2 employed the above reaction, and in addition, measurements of the elastic scattering reaction $e^+e^- \to e^+e^-$ (Bhabha scattering). For electron and positron beams with polarizations P_1 and P_2 (transverse to the beam direction),

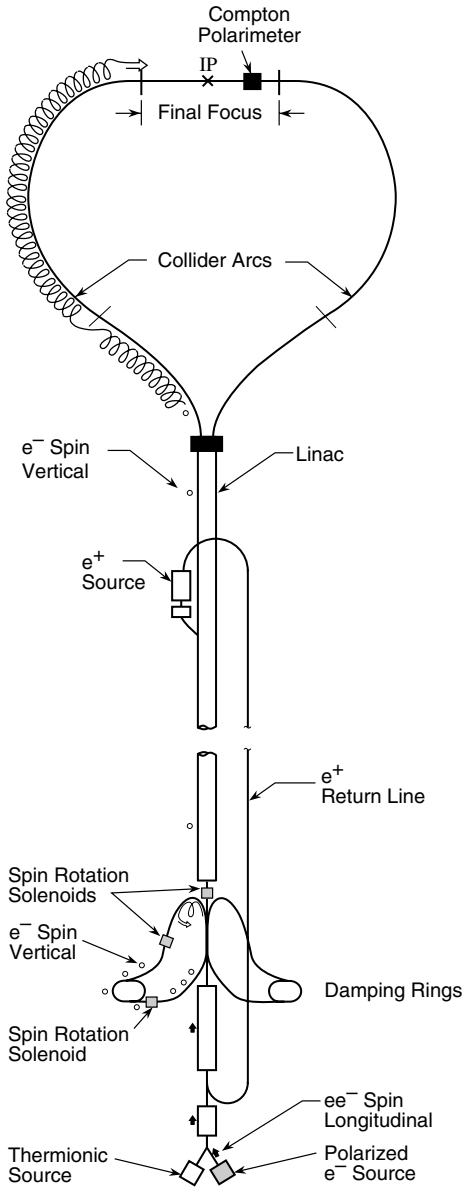

Figure 19. 'The polarized SLC' schematic layout. Courtesy of Woods (private communication) and SLAC.

the differential cross-sections in the centre-of-mass frame are (Baier 1969)

$$\frac{\mathrm{d}\sigma}{\mathrm{d}\Omega}(\mathrm{e}^+\mathrm{e}^- \to \mu^+\mu^-) = \frac{r_0^2}{16\gamma^2}\,\beta_\mu\,\{2 - \beta_\mu^2\,\sin^2\theta[1 - |P_1||P_2|\cos(2\phi)]\},$$
$$\frac{\mathrm{d}\sigma}{\mathrm{d}\Omega}(\mathrm{e}^+\mathrm{e}^- \to \mathrm{e}^+\mathrm{e}^-) = \frac{r_0^2}{16\gamma^2}\left(\frac{3+\cos^2\theta}{1-\cos\theta}\right)^2\left\{1 + \frac{|P_1||P_2|\sin^4\theta}{(3+\cos^2\theta)^2}\,\cos(2\phi)\right\}, \tag{2.1}$$
$$\frac{\mathrm{d}\sigma}{\mathrm{d}\Omega}(\mathrm{e}^+\mathrm{e}^- \to \gamma\gamma) = \frac{r_0^2}{4\gamma^2(1-\beta_\mathrm{e}^2\cos^2\theta)}\,\{1 + \cos^2\theta + |P_1||P_2|\sin^2\theta\,\cos(2\phi)\},$$

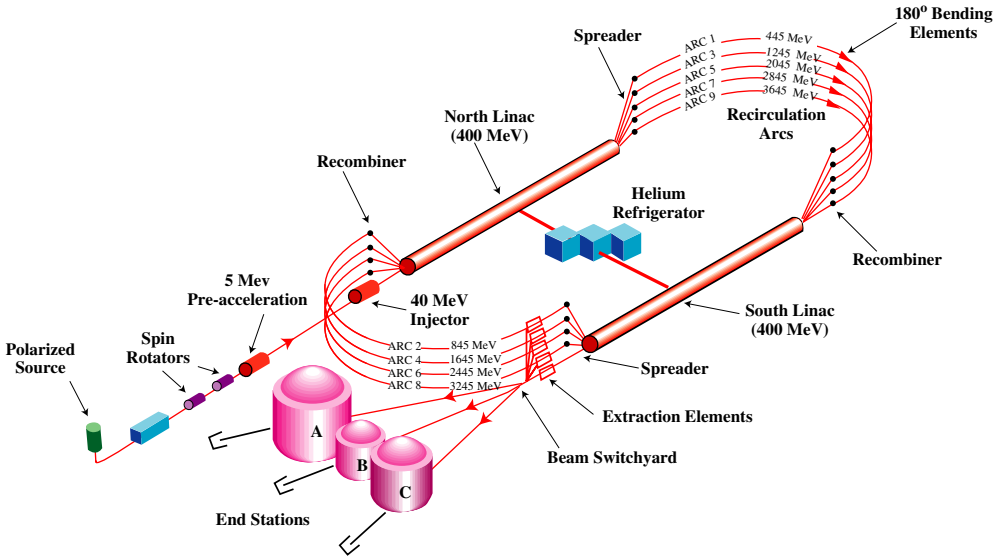

Figure 20. Schematic layout of CEBAF. Courtesy of Grames (private communication) and CEBAF/JLab.

where r_0 is the classical electron radius, θ is the scattering angle, ϕ is the azimuthal angle around the beam axis, with $\phi = 0$ being parallel to the direction of the polarization, i.e. vertical, and β_e and β_μ are the dimensionless velocities of the electrons and muons, respectively. (We typically expect $P_1 = -P_2$.) We also displayed the cross-section for $e^+e^- \to \gamma\gamma$. See also calculations by Ford *et al* (1972) for the Touschek effect and HEP interactions in e^+e^- storage rings. The above measurements served to confirm the validity of the basic Sokolov–Ternov theory and employed standard equipment such as beam loss monitors, or else the high-energy particle detectors themselves, as polarimeters. The more usual Compton backscattering polarimeters were later installed in many e^+e^- colliders (first at SPEAR by Gustavson *et al* (1979)).

2.3. Basic formulae

We denote the particle charge and mass by e and m, respectively. Readers should be able to apply the formulae to electrons or positrons, as appropriate. The particle velocity, momentum and energy are denoted by $\boldsymbol{v}$, $\boldsymbol{p}$ and E, respectively. The dimensionless particle velocity is $\boldsymbol{\beta} = \boldsymbol{v}/c$, and the Lorentz factor is $\gamma = (1-\beta^2)^{-1/2}$ and $E = \gamma mc^2$ and $\boldsymbol{p} = \beta\gamma mc$. Sokolov and Ternov (1964) treated a model of circular motion in a homogeneous magnetic field. The formulae for the polarization buildup and the asymptotic polarization were given in (1.1) and (1.2), but we repeat them here for self-containedness. For initially unpolarized particles, the polarization builds up in the vertical direction according to

$$P(t) = P_{\rm ST}\,(1 - {\rm e}^{-t/\tau_{\rm pol}}), \tag{2.2}$$

where $P_{\rm ST}$ is the asymptotic (equilibrium) degree of the polarization, and $\tau_{\rm pol}$ is the polarization buildup time. Sokolov and Ternov (1964) obtained an equilibrium degree of polarization of

$$P_{\rm ST} = \frac{8}{5\sqrt{3}} \simeq 92.376\%. \tag{2.3}$$

This is frequently called the 'Sokolov–Ternov polarization'. As can be seen from the experimental results mentioned above, the beam polarization can, and does, approach the

theoretical limit. For the polarization buildup time they obtained

$$\tau_{\rm ST}^{-1} = \frac{5\sqrt{3}}{8}\frac{e^2\hbar\gamma^5}{m^2c^2\rho^3} = \frac{5\sqrt{3}}{8}c\lambda_{\rm e}r_{\rm e}\frac{\gamma^5}{\rho^3}, \tag{2.4}$$

where ρ is the radius of the orbit, $\lambda_{\rm e} = \hbar/(mc)$ is the electron Compton wavelength and $r_{\rm e} = e^2/(mc^2)$ is the classical electron radius. If the bending radius ρ is not a constant, e.g. if the ring consists of a set of circular arcs joined by straight lines, then one must replace ρ^3 by

$$\frac{1}{\rho^3} \to \oint \frac{1}{|\rho(\theta)|^3}\frac{{\rm d}\theta}{2\pi} = \frac{1}{2\pi R}\oint \frac{1}{|\rho(s)|^3}\,{\rm d}s, \tag{2.5}$$

where θ is the machine azimuth, and R is the average ring radius. Here s is the arc-length around the circumference, not to be confused with the spin $\boldsymbol{s}$. The prescription works even if ρ is locally negative, hence the absolute value signs on $|\rho(\theta)|^3$. For the common case of 'isomagnetic' fields, where $\rho(\theta)$ has the same value in all the dipole bending magnets, the above expression simplifies to $\rho^{-3} \to (\rho^2 R)^{-1}$. A simple practical guide for most machines is then

$$\tau_{\rm pol}({\rm s}) \simeq 3654\frac{(R/\rho)}{[B({\rm T})]^3[E({\rm GeV})]^2}. \tag{2.6}$$

To a good accuracy, 3654 s is 1 h, so we can, instead, measure $\tau_{\rm pol}$ in hours and drop the factor of 3654 above. We have seen that the radiative polarization buildup time can range from several minutes to several hours in modern storage rings. Note in passing, that the equilibrium polarization level is now

$$P_{\rm eq} = \frac{8}{5\sqrt{3}}\frac{\oint({\rm d}s/|\rho(s)|^3)\,\boldsymbol{b}\cdot\boldsymbol{e}_3}{\oint({\rm d}s/|\rho(s)|^3)}, \tag{2.7}$$

where $\boldsymbol{b}$ is a unit vector in the direction of the local magnetic field and $\boldsymbol{e}_3$ is a vertical unit vector. If there are reverse bends, i.e. $\boldsymbol{b}\cdot\boldsymbol{e}_3 = -1$, the equilibrium polarization will be less than 92.4%. If all the bends have the same sign, then $P_{\rm eq} = P_{\rm ST}$.

In fact, one must go to $\mathrm{O}(\hbar^2)$ in the radiated power spectrum, and not merely $\mathrm{O}(\hbar)$, to obtain a spin-flip asymmetry. Following Sokolov and Ternov (1964), we write the classical radiation intensity as (assuming a constant radius of curvature ρ)

$$W^{\rm cl} = \frac{2}{3}\frac{{\rm e}^2 c\gamma^2}{\rho^2}. \tag{2.8}$$

We set $v = c$ whenever possible in the radiated intensities. The classical radiated power per unit frequency has a broad peak at the critical frequency $\omega_{\rm crit} = \frac{3}{2}(c\gamma^3/\rho)$ (Schwinger 1949). Dividing the critical photon energy $\hbar\omega_{\rm crit}$, by the particle energy γmc^2, yields the dimensionless parameter

$$\xi = \frac{3}{2}\frac{\hbar\gamma^2}{mc\rho}. \tag{2.9}$$

In present-day storage rings ξ is a small number, of $\mathrm{O}(10^{-6})$ or less. Then, up to terms in ξ^2, Sokolov and Ternov obtained

$$\begin{aligned}
W_\sigma^{\uparrow\uparrow} &= W^{\rm cl}\left\{\frac{7}{8} - \xi\left(\frac{25\sqrt{3}}{12} - \zeta\right) + \xi^2\left(\frac{335}{18} + \frac{245\sqrt{3}}{48}\,\zeta\right) + \cdots\right\},\\
W_\sigma^{\uparrow\downarrow} &= W^{\rm cl}\frac{\xi^2}{18},\\
W_\pi^{\uparrow\uparrow} &= W^{\rm cl}\left\{\frac{1}{8} - \xi\frac{5\sqrt{3}}{24} + \xi^2\frac{25}{18} + \cdots\right\},\\
W_\pi^{\uparrow\downarrow} &= W^{\rm cl}\,\xi^2\frac{23}{18}\left\{1 + \zeta\frac{105\sqrt{3}}{184}\right\}.
\end{aligned} \tag{2.10}$$

The arrows show the relative direction of the spin in the initial and final spin states. The initial spin state is specified by $\zeta = \pm 1$, if the initial spin is directed along/against the field. The ratio of the spin-flip radiated power, to classical synchrotron radiation is

$$\frac{\mathcal{P}_{\text{spin-flip}}}{\mathcal{P}_{\text{cl}}} = \frac{W_\sigma^{\uparrow\downarrow} + W_\pi^{\uparrow\downarrow}}{W^{\text{cl}}} = \frac{4}{3}\xi^2\Big(1 \pm \frac{35\sqrt{3}}{64}\Big). \tag{2.11}$$

Substituting numbers for a machine with the approximate dimensions of HERA, say $\rho = 1000\,\text{m}$ and $E = 30\,\text{GeV}$, yields $\xi \simeq 9 \times 10^{-7}$, and so the ratio of spin-flip to classical radiated power is roughly 5×10^{-12}. This exemplifies the claim that spin-flip photon emissions are rare, compared with the emission of ordinary synchrotron radiation.

Note also, that for the non-flip terms $W_\sigma^{\uparrow\uparrow} \gg W_\pi^{\uparrow\uparrow}$, i.e. the radiation is emitted mainly in the horizontal plane. It is well-known that classical synchrotron radiation is strongly linearly polarized in the plane of the particle orbit. For the spin-flip terms, the opposite is true: $W_\sigma^{\uparrow\downarrow} \ll W_\pi^{\uparrow\downarrow}$. The spin-flip radiation is not only weaker, but also strongly polarized along the normal to the orbit. Note also, that $W_\sigma^{\uparrow\uparrow}$ and $W_\pi^{\uparrow\uparrow}$ depend on ζ, at order ξ, but this does not contribute to the polarization. This is discussed in the next paragraph.

We can express the radiation intensities in terms of the spectral power density $\mathscr{P}(\omega)$. Specifically, for the spin-flip terms, we can write, summing over the σ and π modes,

$$W^{\uparrow\downarrow}(\zeta) = \int_0^\infty \mathscr{P}^{\uparrow\downarrow}(\zeta, \omega)\,\mathrm{d}\omega. \tag{2.12}$$

Expressions for $\mathscr{P}^{\uparrow\downarrow}(\zeta, \omega)$ are given by Jackson (1976). The number of spin-flip photons emitted per unit frequency interval per unit time is

$$\mathscr{N}^{\uparrow\downarrow}(\zeta, \omega) = \frac{\mathscr{P}^{\uparrow\downarrow}(\zeta, \omega)}{\hbar\omega}. \tag{2.13}$$

The spin-flip transition probabilities per unit time, from up to down and vice-versa, are given by

$$p_\pm = \int_0^\infty \mathscr{N}^{\uparrow\downarrow}(\zeta = \mp 1, \omega)\,\mathrm{d}\omega. \tag{2.14}$$

Let us also denote the 'up' and 'down' spin populations by N_+ and N_-. In equilibrium, one must have $N_+ p_- = N_- p_+$. The equilibrium degree of polarization is

$$P_{\text{eq}} = \frac{N_+ - N_-}{N_+ + N_-} = \frac{p_+ - p_-}{p_+ + p_-}. \tag{2.15}$$

Hence, only the spin-flip amplitudes determine the equilibrium polarization level. This explains why the nonflip radiation, given by $W_\sigma^{\uparrow\uparrow}$ and $W_\pi^{\uparrow\uparrow}$ in (2.10), does not contribute to the equilibrium degree of polarization. Hence, it is irrelevant that $W_\sigma^{\uparrow\uparrow}$ and $W_\pi^{\uparrow\uparrow}$ depend on ζ in (2.10). We shall see later, that the situation is more subtle than this. The so-called nonflip radiation *does* matter, in two distinct ways. One mechanism is obvious: the nonflip radiation mixes up the 'up' and 'down' spin populations among themselves, i.e. it equilibrates the orbital phase–space distribution. The other mechanism requires a much deeper analysis of the physics. We shall not get to it until section 27.

2.4. Spin light: observation of spin-dependent synchrotron radiation

Although the spin-dependent component of the synchrotron radiation intensity is small, it has been observed. This phenomenon is called 'spin light'. Experiments at the VEPP-4

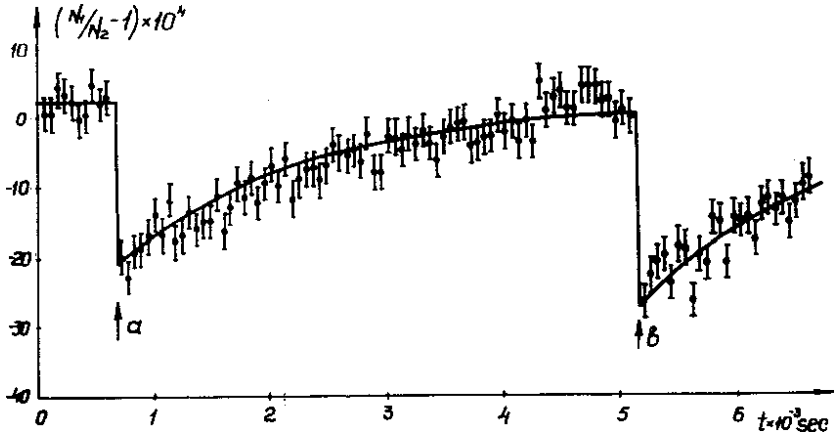

Figure 21. Measurement of the synchrotron radiation intensity as a function of the degree of the polarization of the beam. At the points '*a*' and '*b*', one of the bunches was quickly depolarized. Reprinted from Belomesthnykh *et al* (1984). Copyright (1984) with permission from Elsevier.

storage ring recorded the variation in the synchrotron radiation intensity with the polarization level (Belomesthnykh *et al* 1984). The basic theory (and also a proposed measurement technique) was described by Bondar and Saldin (1982). A more recent theoretical paper is by Bordovitsyn *et al* (1995), where it is pointed out that the radiation from a relativistic neutron would be pure spin light.

The spin-dependent term in the radiated intensity is of $O(\xi)$, multiplied by the polarization level. Note that the polarization buildup itself is proportional to the $O(\xi^2)$ terms, but the asymmetry in the radiated power can be observed in the $O(\xi)$ term. The information below is taken from Belomesthnykh *et al* (1984). Since $\xi \ll 1$, a direct observation of the spin-dependent radiated power is difficult. In the VEPP-4 experiment, two bunches of electrons (or two positron bunches), of equal beam current, were circulated in the ring. The bunches were injected and the beam currents equalized to one part in 10^3 by scraping the bunch with a higher current. The bunches were then allowed to polarize. One bunch was selectively depolarized and the difference in the radiated power output recorded. To increase the spin-flip power output, a three-pole asymmetric wiggler was inserted in the ring. The wiggler had a strong central field (short bend radius). By the $1/\rho^3$ dependence of the spin-flip component of the synchrotron radiation, the spin-flip radiation from the wiggler dominated that of the rest of the machine. The photon counts from passage through the wiggler were recorded in the detectors. The measured quantity was $(1 - \dot{N}_1/\dot{N}_2)$ where $\dot{N}_1$ and $\dot{N}_2$ were the counting rates of the detector coinciding with the passage of the first (second) bunch through the wiggler central field. After the beams had been polarized to close to the asymptotic level, one of them was fully depolarized using a TEM wave created by a pair of vertically separated conducting plates connected to an rf generator. The value of $(1 - \dot{N}_1/\dot{N}_2)$ dropped in a jump-like manner when the depolarizer was activated. After the depolarizer was switched off, the value of $(1 - \dot{N}_1/\dot{N}_2)$ increased exponentially as the depolarized beam regained its polarization. The result is shown in figure 21. The measurement time at each point was 60 s. The Sokolov–Ternov polarization time was 1740 ± 20 s. The asymptotic polarization level was 0.726. Additional details, and descriptions of other measurements, are given by Belomesthnykh *et al* (1984). For example, the depolarizer was kept on for 1000 s, before allowing the bunch to repolarize. The direction of the wiggler field was also reversed, and it was verified that the sign of the asymmetry reversed, in concert with the direction of the wiggler central field.

3. Chapter zero

3.1. General remarks

Often, the most important part of a scientific paper is the material *not* stated. 'Page zero' of the paper contains the fundamental mindset of the author; the unstated assumptions and approximations, etc which determine the whole outlook of the paper. For example, what does the author consider to be a 'high' energy, or a 'short' timescale? Unless one understands these hidden assumptions, it is often difficult to understand properly the contents of the paper. Hence this section is titled chapter zero. Here, we shall explicitly discuss basic material (possibly *very* basic), to elucidate the foundations on which the subject of spin dynamics and polarization in accelerators rests. There are indeed many unstated assumptions in the literature, and their origins (or justifications) are frequently forgotten, because they have become ingrained by now.

First, a typical particle energy for us will be roughly hundreds of MeV or 1 GeV up to tens or hundreds of GeV. For electrons, this is ultrarelativistic, while for protons, it spans the moderately relativistic (1 GeV) to ultrarelativistic (few hundred GeV) range. A typical accelerator has a circumference of tens to thousands of metres. The timescale for storage of a particle beam will be seconds to several hours. There are many other length-scales and time-scales, e.g. the timescale of the emission of a photon of synchrotron radiation, or the height and width of a particle beam. We shall work through the various scales below.

3.2. Basic model of orbital motion

Modern beam transport systems, i.e. accelerators, are designed to channel a set of particles—a 'bunch' or a beam—along some reference trajectory, or *design orbit*. In a circular accelerator, i.e. a synchrotron or a storage ring, the design orbit closes on itself: it is a loop. The design orbit usually lies in a plane which we shall call the 'horizontal' plane. (In LEP the normal to the plane of the machine was tilted by 0.8° to the vertical.) Dipole bending magnets (vertical magnetic fields) are used to bend the particles in the circular portions of the reference orbit. In a real accelerator, due to unavoidable tolerances of manufacture and alignment, etc, the actual *closed orbit* is still a loop but perturbed slightly from the design orbit. The individual particles do not all follow the closed orbit, of course. There is necessarily a spread of the particle coordinates and momenta around the reference value. The transverse oscillations of the particles around the closed orbit are called 'betatron oscillations'. There are both horizontal and vertical betatron oscillations. The betatron oscillations are focused using quadrupole magnets. A symbolic sketch of the design orbit, imperfect closed orbit and a horizontal betatron oscillation is shown in figure 22.

In addition to the transverse oscillations, the particles in a beam also execute *longitudinal* oscillations. Such oscillations are called 'synchrotron oscillations'. Two particles of different energy will circulate around the circumference at different frequencies, and therefore, will separate longitudinally. Hence, the synchrotron oscillations are $(\Delta t, \Delta E)$ or (time-of-arrival, energy offset) oscillations, where the Δ signifies an offset relative to the reference particle. Longitudinal electric fields in so-called rf (radio-frequency) cavities—essentially waveguides operating in a TM mode—are used to supply a differential push to the particles based on their time of arrival at the cavities. The rf cavities are also used to replenish the energy loss due to synchrotron radiation (for e^+e^- rings), and also, to ramp the beam energy from injection to the top energy.

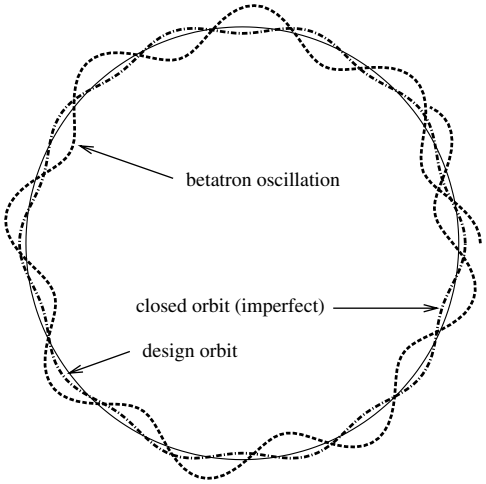

Figure 22. Sketch of the design orbit, imperfect closed orbit and a horizontal betatron oscillation in a synchrotron. The amplitudes of the imperfections and oscillations are highly exaggerated.

3.3. Stern–Gerlach force

The first tacit assumption to be explicitly pointed out is that, the particle spins play *no role* in the design of the orbital oscillation guiding and focusing system. Many years of experience with subatomic beams in particle accelerators, electron microscopes, etc, demonstrate that the optical transport and focusing of charged particle beams is wholly determined by the Lorentz force. The force due to the spin, via the Stern–Gerlach effect (Gerlach and Stern 1922) is negligible. Beams in accelerators do not separate into spin 'up' and 'down' beamlets. For charged particles, the Stern–Gerlach force is dominated by the Lorentz force, even for nonrelativistic systems. See, e.g., the text by Kessler (1985) for a discussion of this point. For relativistic systems, the magnitude of the Stern–Gerlach force drops off very rapidly with increasing Lorentz factor γ, and the Lorentz force dominates it completely, for all practical purposes in modern accelerators. We can, therefore, validly speak of the 'orbital motion' without reference to the spin, as anyone who has worked with charged particle optical systems knows. We shall neglect the Stern–Gerlach force in this paper, unless specifically noted otherwise.

3.4. Spin precessions

Although the orbital motion does not depend on the spin, the spin motion depends crucially on the orbital motion. For example, if two particles enter the same quadrupole magnet but with different orbital coordinates, they will encounter different magnetic fields as they traverse the magnet. Hence, their spins will precess around different axes, and rotate through different angles. What this means is that, the description of the spin dynamics sits on top of a description of the orbital motion. There is also another very important consequence. Most reviews of the orbital motion treat the reference trajectory as a given quantity, usually denoted by '$z = 0$' or some such. It is simply a 'fixed point' of map methods. The interesting physics lies in the analysis of the off-axis trajectories, e.g. the focusing of the orbits and the correction of the aberrations, etc. However, in the case of the spin, there is considerable interesting physics to be had just by examining the spin precessions on the reference orbital trajectory itself. Hence, a good deal of this paper will treat just the spin precessions on the reference orbit.

3.5. Statistical mechanical facts

We begin with some simple, but fundamental, consequences of statistical mechanics. To illustrate the concepts, we perform some *gedanken* experiments. As our candidate accelerator, we select Enrico Fermi's hypothetical accelerator which circumnavigates the equator of the Earth.

The simplest typical model of a storage ring is a uniform vertical magnetic field. The particles circulate in horizontal circles, and the particle spins precess around the vertical axis, i.e. the direction of the magnetic field. The spin states are quantized along/against the direction of the local magnetic field. If the particles emit synchrotron radiation and polarize spontaneously, the equilibrium polarization points vertically, of course. Let us examine the matter step by step, and challenge the 'of course'.

Let us suppose our gedanken accelerator to have a uniform vertical magnetic field all around the circumference, *plus* a small solenoid localized at one point in the ring. The magnetic field integral $\int \boldsymbol{B}_{\rm sol} \cdot \mathrm{d}\boldsymbol{\ell}$ of the solenoid is just sufficient to rotate a particle spin by 180° around the longitudinal (solenoidal) axis. The solenoid has no effect on the orbital motion because $\boldsymbol{v} \times \boldsymbol{B}_{\rm sol} = 0$, to the leading approximation, anyway. The vertical magnetic field is (by hypothesis), not strong enough to induce significant synchrotron radiation. Suppose that a particle (say a proton) with spin vertically up, is injected into the ring. Because of the solenoid, the spin direction will reverse on every pass around the ring. The direction of the long-term equilibrium polarization in this ring is therefore *not* vertical.

Note that it does *not* matter how big the ring is—the one little solenoid affects the polarization vector around the *entire* circumference. This gedanken experiment is sufficient to dispel the notion that the direction of the polarization (or of the spin eigenstates) is determined by the direction of the local magnetic field. The direction of the polarization is determined by the structure of the *entire* accelerator. (Actually, it is more subtle than this. See below.) If the polarization is vertical in the arcs of a storage ring, it is so *by design*.

Now, suppose that the accelerator magnetic field *is* strong enough to induce significant synchrotron radiation, and the particle spins polarize spontaneously. We may as well say the particles are electrons or positrons. Two important questions must be dealt with:

- how does one calculate the synchrotron radiation emitted in one magnet?
- how does one calculate the equilibrium polarization, and also the equilibrium beam emittances?

It is crucial to realize these are two different issues, and the answers are *not* the same. To calculate the synchrotron radiation emitted in a magnet, i.e. the photon emission matrix elements, it is sufficient to know that an electron moves locally in a circular arc in a locally uniform magnetic field. All that matters is the electron motion in the one magnet. Actually, we need to take a convolution of the photon spectrum from one electron with the equilibrium distribution of electrons in the beam, to get the overall photon angular distribution, etc. This leads to the second question—what is the equilibrium electron distribution? *That* question *cannot* be answered by examining the electron motion in only one magnet (a locally circular arc, etc). We need to do the following:

- we express the electron motion around the reference trajectory as a sum of betatron and synchrotron oscillations;
- we then say that the recoils from the emission of distinct photons induce 'jumps' in the orbital oscillations;
- we average over the effects of the recoils, etc, to arrive at the equilibrium electron beam distribution.

Now the structure of the orbital oscillations (and also the spin trajectories) can only be determined by knowing the *full* structure of the accelerator. A 'bump' in one part of the ring will affect the motion (and the spin precession—recall the solenoid) *everywhere* around the ring.

In other words, to determine a photon emission matrix element, it is sufficient to know an electron's motion only in the magnet where the photon is emitted, but to know the effect of that recoil on the motion of the electron, we need to know the structure of the whole accelerator. In terms of our gedanken accelerator, the synchrotron radiation spectrum is affected not a whit by the presence of the solenoid, but the effect of that radiation on the equilibrium polarization depends critically on the little solenoid. Indeed, the equilibrium polarization will be zero because of the reversal of the spin directions by the solenoid.

Once again, this sounds obvious enough, but, really, why is it so? Suppose that a mechanism could be found such that an electron beam could achieve equilibrium in just a *single pass* through a magnet. In such a situation, the equilibrium beam distribution *could* be calculated by only examining the motion of the electrons locally in that magnet. The rest of the accelerator would not matter. The spin eigenstates *would* be quantized along and against the direction of the local magnetic field. Our little solenoid in our gedanken accelerator would not then matter.

This finally gets to the heart of the matter—the *timescales* of the processes involved. A single photon emission takes place very rapidly—the standard approximation is to treat the process as a 'point' photon emission. Only the local electron motion matters. The time to equilibrate the electron beam (say $\tau_{\rm orbit}$ and $\tau_{\rm pol}$ for the orbit and spins, respectively) is much longer than a pass through one magnet. In fact, it is much longer than the revolution time around the circumference of the ring (say $\tau_{\rm rev}$). It is for this reason that we need to know the structure of the entire accelerator, in order to determine the betatron oscillations and spin trajectories, etc. This is also the reason why the magnitude of the polarization is uniform around the ring.

It is, of course, true that one can construct combinations of magnets to rotate the direction of the polarization locally, say, at the interaction point, from the vertical to the longitudinal and back again. Such devices are called spin rotators, and have been successfully operated in various machines, e.g. RHIC. However, one cannot construct (a combination of) magnets to locally enhance the magnitude of the polarization.

At the root of all this, we must realize that we are dealing not merely with single-particle dynamics, but with *statistical mechanics* as well. This fact cannot be overemphasized. *The statistical mechanics determines how we formulate the single-particle dynamics*. As noted above, if we could introduce some new type of interaction which could equilibrate the orbital and spin motion in a single pass through a magnet, the characterization of the Hamiltonian and the eigenstates would change radically.

Another simple but profound fact is that the equilibration time of the orbital motion (the so-called beam emittance) is much smaller than the equilibration time of the spins (the polarization): $\tau_{\rm orbit} \ll \tau_{\rm pol}$. Hence, the orbital coordinates and momenta can be assumed to be already in equilibrium when calculating the polarization. An electron (or positron) traverses the orbital phase-space many times between successive spin-flip photon emissions. Hence the polarization is uniform across the orbital phase-space. One does not have higher polarization in the core of the beam and less in the tails. Note, however, that this may not be true for nonradiatively polarized beams. For nonradiative systems such as proton beams, the orbital motion is *not* ergodic. The spins at the core of the beam do not mix with those in the tails. For muon beams, the muon polarization *is* correlated with the particle momentum. A 'luminosity weighted' polarization was also required to analyse the polarized electron beam at the SLC.

3.6. Point photon emission

We treat only *incoherent* synchrotron radiation in this paper. The emission of distinct photons is assumed to be uncorrelated, and the motion of the individual particles (electrons or positrons) is independent. Synchrotron radiation is highly peaked in the forward direction. A photon is emitted within an angle of order $1/\gamma$, relative to the particle velocity (or momentum) vector. It is (almost) universal, when calculating the effects of photon emissions on the particle orbits, to assume 'point' photon emission. Point photon emission implies two things:

- we consider the photon emission to be instantaneous;
- the photon direction is parallel to the particle momentum vector at the instant of emission.

The above assumptions have significant consequences. The orbital coordinates are thus *continuous* at the instant of emission. Next, point photon emission implies the electron recoil is parallel to its momentum. Hence the particle momentum is not continuous (because of the energy lost to the photon), but, denoting the horizontal, vertical and longitudinal components of the momentum vector by (p_x, p_y, p_z), the *ratios* p_x/p_z and p_y/p_z remain unchanged across the emission process. Denoting the horizontal and vertical slopes of the trajectory by x' and y', respectively, we model a photon emission (for ultrarelativistic motion) by keeping the values of x' and y' fixed and decrementing $p_z \to p_z(1-\hbar\omega/E)$, where the photon energy is $\hbar\omega$, and the particle energy is E. This is a very good approximation in practice.

We do not treat any other stochastic interaction in detail in this paper, e.g. beam–gas scattering (collisions with residual molecules or ions in the beam vacuum chamber), although such effects are potentially important in some machines. We do not treat collective effects on the beam motion (collective instabilities, etc), even though such effects are important in high-intensity beams.

3.7. An individual (un)polarized particle

It is possible for an individual particle to be unpolarized. The fact that a particle has a definite value of its total spin, does not mean it has a polarization of 100%. The spin state could vary randomly as a result of stochastic interactions, hence the polarization might be zero. In the case of an individual particle, the polarization is defined as a time average over many observations of its spin.

3.8. Classical versus quantum spin

Most calculations in the accelerator physics literature on polarized beams treat the spin using a classical model of a three-component unit vector. We have already done so above. Let us examine the matter. First, note that the particle coordinates and momenta are always treated classically, without comment, using the Lorentz force to determine the particle motion in the prescribed accelerator electric and magnetic fields. But we do need to comment, because we treat the spin, and the value of $\hbar$ is therefore significant. At the energies of typical modern-day accelerators, the de Broglie wavelength of the particles is much smaller than the dimensions of the magnet apertures. It is an excellent approximation to treat the orbital motion classically. This is analogous to the case of geometric optics, where the wavelength should be much less than the dimensions of the apertures. Furthermore, the de Broglie wavelength of the particles is much smaller than the root mean square (rms) beam size. More accurately, the phase-space area occupied by an individual particle is much smaller than the beam emittance. Under this circumstance, there is negligible overlap between the particle wavefunctions, and so one can treat the particles as distinct. There is no need for Fermi–Dirac statistics (or Bose–Einstein, for

deuterons). The beam is 'dilute' as opposed to 'degenerate'. Note also, that the interaction of a particle with the accelerator electric and magnetic fields, even in the highest-energy present-day accelerators, does not result in pair production. There is no need for the Dirac equation. This is so even for photon emission at present-day accelerator energies, because the emitted photon energy is much less than the particle energy.

The above statements are not true if an individual interaction changes the orbital motion drastically. For example, the orbital motion cannot be treated classically to analyse e^+e^- annihilation. Hence, one employs both a classical and a quantum description of the particle motion in different parts of an accelerator, depending on circumstances.

Consider a simple model of a uniform vertical magnetic field and solve the Schrödinger equation (or the Dirac equation for relativistic particles). The orbital eigenstates are known as Landau levels. The nth level has a radius $r_n \propto \sqrt{n}$, with the ground state having a typical radius of $r_1 = \mathrm{O}(1)$ Å. For a highly excited state with $n \simeq 10^{20}$, the orbit will have a radius of approximately 1 m. In this circumstance, the orbital states form a continuum to a very good approximation. One can construct localized wavepackets, which can be treated as classical 'point' particles. They have a well-defined energy and angular momentum to a sufficiently good approximation, without violating the Heisenberg Uncertainty Principle. Experience shows that the use of the semiclassical approximation to treat the orbital motion is excellent.

For the spin, there is no semiclassical limit when the orbital quantum number is large. Even at the highest energies, an electron, or a proton, etc, remains a spin $\frac{1}{2}$ particle. There is no continuum of spin states. The justification for the classical spin model therefore takes a different route and will be discussed in detail in section 5. We begin with protons, or other particles for which synchrotron radiation is negligible. The only significant interaction the spins encounter is that with the prescribed accelerator electric or magnetic fields. The evolution of a quantum spin state is a precession, which is *continuous* in time. Under these circumstances, a classical model of the spin will suffice.

However, if the spin state changes *discontinuously* from an 'up' to a 'down' state, as it can when emitting a photon, then quantum mechanics must necessarily be employed. Once again, we are led to distinguish between the local interaction of a spin with a photon in a single magnet, and the influence of that interaction on the motion of that spin in the rest of the accelerator. For ultrarelativistic electrons and positrons, a classical spin model is adequate to describe the spin motion for almost everything except the photon emissions. Spin-flip photon emissions are rare, but when they do occur, cause the spin orientation to abruptly change from 'up' to 'down'. The spin then continues along the new semiclassical orbit.

Another situation is when the particles collide with some target/obstacle in the accelerator, e.g. molecules of residual gas in the vacuum chamber, or an internal gas jet target, etc. This also includes intrabeam scattering, i.e. collisions of the particles in a beam with each other. A quantum treatment of the spin is also required in any polarimetry measurement.

Nevertheless, the quantum nature of the spin does constrain the usage of the classical spin model. For spin $\frac{1}{2}$ particles, we *cannot* use the classical spin model to calculate anything other than a vector polarization. Suppose we have a set of classical spins all aligned vertically, with 75% up and 25% down. Now consider 'another' distribution of classical spin vectors, distributed uniformly around an upright cone with an opening angle of 60°. Quantum mechanically, the polarization vector is vertical and the degree of the polarization is 50% in both cases:

$$P_a = \frac{0.75 - 0.25}{0.75 + 0.25} = 0.5, \qquad P_b = \cos 60^\circ = 0.5. \tag{3.1}$$

There is *no* additional information about the polarization, for spin $\frac{1}{2}$ particles. From a classical spin perspective, therefore, we must treat the above two systems as equivalent.

Having agreed upon the use of a classical spin model, note that many authors do *not* use a three-component classical unit vector $\boldsymbol{s}$ to describe the spin, but instead, prefer to use a spinor Ψ. The relation between $\boldsymbol{s}$ and Ψ is $\boldsymbol{s} = \Psi^\dagger \boldsymbol{\sigma} \Psi$, also written in bracket notation as $\boldsymbol{s} = \langle \Psi | \boldsymbol{\sigma} | \Psi \rangle$. Certainly, Ψ exhibits all the 'double-valuedness', etc, of a quantum spinor, and we shall see below, that the equation of motion for Ψ bears a great formal resemblance to the Schrödinger equation. However, Ψ is a classical variable, defined within the framework of the classical spin model.

3.9. Spin-flip

We use the term 'spin-flip' above to denote the abrupt (discontinuous) change in the spin state which can occur when a particle emits a photon. There is no deterministic time evolution linking the spin states before and after a spin-flip photon emission. If one runs time backwards, the spin does not return from the 'down' to the 'up' state.

There is, however, another widely employed usage for the term 'spin-flip'. This alternative usage is generally employed when discussing nonradiative polarization. It simply means a reversal of the spin direction, i.e. a 180° spin rotation, but not a discontinuous change of the spin state. In this case, there *is* a deterministic time evolution linking the final spin state to the initial spin state, although it may be complicated to calculate. If one runs time backwards, the spin *does* return to its original state. Indeed, the classical spin model is used to describe the spin motion throughout such a spin-flip process. We shall see the usage of the term 'spin-flip' when we discuss the Froissart–Stora formula (Froissart and Stora 1960) in section 6.

In fact, there are devices called 'spin-flippers' which have been successfully operated in storage rings. They consist of radio-frequency magnetic fields, which rotate the spins through 180°. Note, therefore, that the spins are *not* rotated through 180° in a single pass, but a little at a time, over many passes around the accelerator circumference, although the overall rotation is still fairly rapid. Note also that *all* of the spins in the beam are rotated. (This is in contrast to radiative spin-flip, where only one spin in the beam changes its state, and the spin-flips of different particles are incoherent.) It is more accurate to say that the *polarization* rotates through 180°, which is, in fact, what happens. Spin flippers are used to rapidly reverse the polarization of a beam of, say, polarized proton beams *in situ* in an accelerator. This is an important technique to reduce any systematic errors arising from the accelerator itself, in experiments with polarized beams.

3.10. Spin eigenstates

We have seen that, to calculate the direction of the polarization, one needs to know the structure of the accelerator around the entire circumference. Merely knowing the orbital and spin motion in one magnet is not enough. Related to the above, we also noted an important fact which we shall encounter repeatedly throughout this paper: *the spin precession depends on the particular orbital trajectory of the particle*. The significance for spin physics is profound: it means that the (direction of the) spin eigenstates *depends on the location of the particle in the orbital phase-space*.

In other words, 'the' direction of the spin eigenstates is actually a *vector field* of spin quantization axes, that is conventionally denoted by $\boldsymbol{n}$. It is one of the central ideas for the consideration of polarized particle motion in a circular machine. The idea of a vector field of spin quantization axes was formulated in 1972–3 by Derbenev, Kondratenko and Skrinsky. The definitive publication is by Derbenev and Kondratenko (1973). The vector field $\boldsymbol{n}$ is a function of the orbital coordinates and momenta, and the azimuth around the

ring circumference. To determine the direction of the polarization vector requires a phase-space average over a cone of unit vectors. This does not contradict the earlier statement, that there is only one polarization vector for the entire beam, e.g. in the case of radiative electron polarization. There is, indeed, only one polarization vector, but many spin quantization axes.

This indicates, incidentally, that the direction of the equilibrium polarization vector is not necessarily the direction of the individual spin eigenstates. One must always bear in mind the distinction between the polarization (a property of the beam), and the spin (a property of an individual particle). Since the polarization vector (or density matrix) belongs collectively to the whole beam, it is *not* attached to any one particle, nor to any one point in the orbital phase-space. The direction of the (equilibrium) polarization cannot, in general, coincide with the spin quantization axis of every individual particle.

3.11. A fallacious argument

The interested reader may wish to try their hand at discerning the weak spot in the following fallacious argument. The answer is given in the succeeding paragraph. Consider a ring containing only magnetic fields and no electric fields. The magnetic fields are arbitrary, subject to the proviso that they are transverse to the design orbit and symmetric about the median plane of the accelerator. More precisely, using (x, y) transverse coordinates, the vertical component of the magnetic field has the property $B_y(x, y) = B_y(x, -y)$. To satisfy Maxwell's equations, we then also need $B_x(x, y) = -B_x(x, -y)$, which means that $B_x = 0$ when $y = 0$. The above restrictions on B_x and B_y are quite mild. It allows all standard dipole, quadrupole, sextupole, etc, magnets. Solenoids, however, are excluded. Such an accelerator is said to have 'midplane symmetry' or 'median plane symmetry'. Most modern accelerators do, in fact, possess midplane symmetry, at least in the ideal design on paper. Here is the fallacious claim: 'by parity invariance under a spatial reflection in the horizontal (median) plane, the direction of the (equilibrium) polarization is vertical, hence the spins should be quantized vertically'.

What is the weak point here? Actually, the above argument does correctly point out that the direction of the equilibrium polarization is vertical. The mistake is to then further conclude that this fact implies that the spins should *all* be quantized vertically. The correct statement is that, the above argument proves that the set of spin quantization axes is *symmetrically distributed* about the vertical axis.

As a matter of fact, the above argument also proves that the orbit of the reference particle (the design orbit) must lie in the horizontal (median) plane. Does anyone therefore conclude that all of the particle orbits therefore lie in the horizontal plane? The correct answer is that the set of vertical betatron oscillations is symmetrically distributed about the median plane. For every betatron trajectory $(y_\beta, p_{y\beta})$, there is an 'image' orbit $(-y_\beta, -p_{y\beta})$, which also satisfies the equations of motion.

3.12. a or G?

Everyone agrees on the notation μ for the magnetic moment (with subscripts $\mu_{\rm p}$, $\mu_{\rm e}$, etc, for the particle species), and on the use of g for the g-factor, and $(g-2)/2$ for its anomalous part (which is also known as the magnetic moment anomaly). This harmonious state of affairs ends there. In the electron (lepton) literature, the standard notation is $a \equiv \frac{1}{2}(g-2)$. One further writes $a_{\rm e}$, a_μ for electrons and muons, etc, respectively. In the proton (hadron) literature, the notation is $G \equiv \frac{1}{2}(g-2)$. When discussing work on leptons, we use a, and when discussing hadrons we use G. We employ the notation a for $(g-2)/2$ in general for formulae that are common to both particle species.

3.13. Orbital tunes

At the simplest level, the transverse and longitudinal oscillations (betatron and synchrotron oscillations) are modelled as simple harmonic oscillations. The Hamiltonian is expanded up to quadratic terms in the dynamical variables (canonical coordinates and momenta). This approximation is known as linear orbital dynamics because the equations of motion are linear differential equations. The main point here is that the frequencies of the betatron oscillations are conventionally expressed as 'tunes'. The (horizontal or vertical) betatron tune is the betatron oscillation frequency divided by the orbital revolution frequency of the reference particle. There is, correspondingly, a synchrotron tune, which is the frequency of a synchrotron oscillation, divided by the orbital revolution frequency of the reference particle. We shall denote the orbital tunes by Q_x, Q_y and Q_s (for 'synchrotron').

There is, correspondingly, a spin tune, usually denoted by ν or ν_{spin}. We shall discuss it later, after we have written down precise equations of motion, etc. The alert reader may note, that since there is a vector field of spin quantization axes, the spin tune might also be a field, a scalar field in this case. This is correct.

3.14. Spin resonance formula

Resonances in the orbital motion occur when the tunes are not incommensurate, i.e. when an integer linear combination of the tunes adds up to an integer

$$m_0 + \boldsymbol{m} \cdot \boldsymbol{Q} = 0. \tag{3.2}$$

Here, the m_j are integers, including zero. Similarly, a spin resonance occurs whenever the spin tune equals an integer plus an integer combination of the orbital tunes, i.e.

$$\nu_{\text{spin}} = m_0 + \boldsymbol{m} \cdot \boldsymbol{Q}. \tag{3.3}$$

Basically, the spin precession resonates with a linear combination of orbital oscillations. Strictly speaking, as we shall show in the formal theory below, in the above formula, ν_{spin} should be the off-axis spin tune on a given orbital trajectory, and the orbital tunes should also include the dependence on the particle orbit. The coefficient of the spin tune in the resonance formula is always unity, although the orbital tunes can appear with multiple harmonics. This is because the Hamiltonian for the spin–orbit motion is linear in the spin $\boldsymbol{s}$. The orbital terms can, however, appear in the Hamiltonian with multiple powers, e.g. x^2, y^3 or xy, etc.

In practice, a simpler and more successful usage of (3.3), is to take ν_{spin} as just $\nu_{\text{c.o.}}$, the spin tune on the design orbit. However, there *is* experimental evidence of orbital tune spread in some spin resonances, due to a distribution of the orbital amplitudes. The orbital tune spread increases the widths of some experimentally observed spin resonances.

3.15. Coordinate systems and conventions

Unfortunately, there is a wide variety of coordinate bases and notations in the literature. There is no standard notation in the field. Some authors use (x, y, z) or (x, y, s), where x is radial, y is vertical and z or s is longitudinal, and increases clockwise around the circumference. Other authors use the basis (x, s, z), so that 'z' refers to the vertical (here 's' increases in the counterclockwise sense). We chose the notation $(\boldsymbol{e}_1, \boldsymbol{e}_2, \boldsymbol{e}_3)$, where $\boldsymbol{e}_1$ points radially outwards, $\boldsymbol{e}_2$ points longitudinally (counterclockwise) and $\boldsymbol{e}_3$ points vertically up. A sketch of the coordinate basis is shown in figure 23. We use this coordinate basis partly to avoid choosing between the above notations, and also, because we want the positive sense of rotation to be counterclockwise. However, because of the wide scope of our review, we include formulae

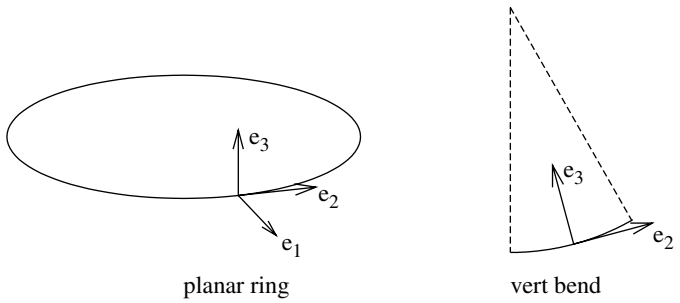

Figure 23. Sketch of the coordinate basis for a planar ring and a vertical bend.

by many authors, and it is too difficult (and prone to errors), to transcribe every formula to an $(\boldsymbol{e}_1, \boldsymbol{e}_2, \boldsymbol{e}_3)$ basis. Furthermore, to do so would break contact with the original literature. When reproducing formulae from the literature, e.g. the 'Chao–Yokoya spin integrals' (see (28.25)), we explain the basis used (which is (x, y, z) in the case of (28.25)). The reader is *strongly* advised to *always* consult the original literature to obtain the definitive formulae, and to verify the notations and coordinate conventions used. In general, we use the notation 'x' for the radial motion, 'y' for the vertical motion and either 'z' or 's' for the longitudinal motion.

Note that we denoted the tunes by $Q_{x,y,s}$. Many authors denote the orbital tunes by the notation $\nu_{x,y,z}$ or $\nu_{x,z,s}$ (see figure 6) or $Q_{x,y,z}$, etc. All authors, fortunately, denote the spin tune simply by ν, without a subscript, although we shall sometimes write ν_{spin} to avoid ambiguity.

In addition to the orbital rotations, it is even more important for this review that the positive sense of a *spin* rotation be counterclockwise. The Pauli matrix $\mathrm{e}^{-\mathrm{i}\psi\boldsymbol{\sigma}\cdot\boldsymbol{e}/2}$ denotes a right-handed (counterclockwise) rotation through an angle ψ around the unit vector (spin rotation axis) $\boldsymbol{e}$. Successive rotations are carried out by multiplying from the left:

$$|\Psi'\rangle = \cdots \mathrm{e}^{-\mathrm{i}\psi''\boldsymbol{\sigma}\cdot\boldsymbol{e}''/2}\mathrm{e}^{-\mathrm{i}\psi'\boldsymbol{\sigma}\cdot\boldsymbol{e}'/2}\mathrm{e}^{-\mathrm{i}\psi\boldsymbol{\sigma}\cdot\boldsymbol{e}/2}|\Psi\rangle. \tag{3.4}$$

To take a concrete example, let the spinor $|\Psi\rangle$ be defined such that

$$\langle\Psi|\boldsymbol{\sigma}|\Psi\rangle = \boldsymbol{e}_1, \tag{3.5}$$

then the spinor

$$|\Phi\rangle = \mathrm{e}^{-\mathrm{i}\psi\sigma_3/2}|\Psi\rangle \tag{3.6}$$

(we have chosen $\boldsymbol{e} = \boldsymbol{e}_3$) yields the vector

$$\langle\Phi|\boldsymbol{\sigma}|\Phi\rangle = \boldsymbol{e}_1 \cos\psi + \boldsymbol{e}_2 \sin\psi. \tag{3.7}$$

We shall make heavy use of Pauli matrix algebra in this paper.

3.16. Electrons and protons: E versus p

As is evident by now, much of the dichotomy in the spin physics literature is between 'electron' polarization and 'proton' polarization, but it is really more accurate to say that the distinction lies between ultrarelativistic, radiative polarization and nonradiative polarization. There are machines, such as the muon storage ring at BNL, to measure the anomalous magnetic moment of the muon, which are leptonic but nonradiative systems.

However, in this section we shall consider another distinction, namely, ultrarelativistic versus non-ultrarelativistic systems. We pointed out above that the longitudinal orbital oscillations are energy oscillations. It is more usual to employ the relative energy offset $\Delta E/E_0$,

where E_0 is the energy of the reference particle, than to use the energy offset ΔE itself. However, in proton (or hadron) accelerators, it is more common to use the longitudinal momentum offset $\Delta p/p_0$, where p_0 is the longitudinal momentum of the reference particle. The relation between the two variables is

$$\frac{\Delta E}{E_0} = \beta^2 \frac{\Delta p}{p_0}, \tag{3.8}$$

where $\beta = v/c$ is the dimensionless longitudinal speed of the particle. For ultrarelativistic particles, $\beta \simeq 1$, and the distinction is not important. However, in many proton accelerators, the value of β is significantly less than unity, and the distinction *does* matter.

The distincton between $\Delta E/E_0$ and $\Delta p/p_0$ is important because of concepts such as the chromaticity. It is conventional in the literature on hadron accelerators, to define the chromaticities via

$$Q_x = Q_{x0} + \xi_x \frac{\Delta p}{p_0}, \qquad Q_y = Q_{y0} + \xi_y \frac{\Delta p}{p_0}. \tag{3.9}$$

The corresponding formulae for electrons usually employ $\Delta E/E_0$, which is the limiting case for $\beta \to 1$. We shall employ the definition (3.9) in this paper. Note that there is also another definition of chromaticity in the literature, which is basically, ξ_j/Q_j $(j = x, y)$. We shall not employ this alternative definition.

3.17. Emittances

Up to now the discussion of the orbital motion has been for individual orbits. We now briefly discuss the statistical distribution of the particles. For simplicity, consider linear orbital dynamics. The particles in the beam have a statistical distribution of oscillation amplitudes and phases. The average value of the phase-space area occupied by the beam is (π times) the horizontal or vertical beam 'emittance'. We generally assume a uniform distribution over the orbital phases. The above emittances pertain to the transverse oscillations. There is also a longitudinal emittance.

For an ultrarelativistic electron or positron beam, radiating significant synchrotron radiation, the orbital oscillations mix up ergodically in the orbital phase-space and the beam settles down, in equilibrium, to a self-consistent statistical distribution of values for the orbital amplitudes. For less relativistic electron/positron beams, or for proton beams, the statistical distribution depends on the beam profile at injection. When a beam is first injected into an accelerator, it may not be exactly matched to the design orbit of the machine, and there may be transient motions of the beam centroid, i.e. coherent betatron oscillations. Our interest in this paper is principally after such transients have died out, i.e. the steady-state or long-term values of the beam emittances.

We remark in passing, that it is tacitly assumed that the emittance, after multiplying by mc to fix the dimensions, is very much greater than $\hbar$. It is also assumed that the uncertainty in the phase-space location of an individual particle is much greater than $\hbar$. This is necessary to justify a classical treatment of the orbital motion.

4. Hamiltonian

4.1. QED and accelerator Hamiltonians

It is usual to simply write down an 'accelerator Hamiltonian', but we wish to examine in more detail the approximations involved in deriving it. We saw above, that it is adequate to treat the orbital and spin motions classically, except for spin-flip photon emissions. Hence, it is

necessary to treat the spin as a quantum operator $\boldsymbol{s}_{\rm op}$, if radiative photon emission is being considered.

We treat only spin $\frac{1}{2}$ particles below. Hence, the Hamiltonian is linear in the spin operator: any product of spin $\frac{1}{2}$ operators is a linear combination of the unit operator and spin $\frac{1}{2}$ operators. We can, therefore, write the Hamiltonian in the form

$$H = \mathscr{A}(\boldsymbol{q}, \boldsymbol{p}, \hbar) + \mathscr{B}(\boldsymbol{q}, \boldsymbol{p}, \hbar) \cdot \boldsymbol{s}_{\rm op}. \tag{4.1}$$

Here $\boldsymbol{q}$ and $\boldsymbol{p}$ are the canonical coordinates and momenta, respectively. The independent variable is time. The functions $\mathscr{A}$ and $\mathscr{B}$ contain arbitrary powers of $\hbar$. We now treat $\hbar$ as an infinitesimal quantity, and retain terms only up to the first order in $\hbar$. Then, $\mathscr{A}$ and $\mathscr{B}$ are independent of $\hbar$. This leads to the usual semiclassical electrodynamic expression for the Hamiltonian

$$H = \left[\left(\boldsymbol{p} - \frac{e}{c}\boldsymbol{A}\right)^2 c^2 + m^2 c^4\right]^{1/2} + eV + \boldsymbol{\Omega} \cdot \boldsymbol{s}_{\rm op}. \tag{4.2}$$

The notation is fairly standard, e.g. $\boldsymbol{A}$ and V are the electromagnetic vector and scalar potentials, respectively, etc. To treat radiative photon emission, we separate $\boldsymbol{A}$, etc, into external (accelerator) and radiation (photon) fields,

$$\boldsymbol{A} = \boldsymbol{A}_{\rm ext} + \boldsymbol{A}_{\rm rad}, \qquad V = V_{\rm ext} + V_{\rm rad}, \qquad \boldsymbol{\Omega} = \boldsymbol{\Omega}_{\rm ext} + \boldsymbol{\Omega}_{\rm rad}. \tag{4.3}$$

Treating the radiation fields as a perturbation, which is standard, we can write

$$H = \left[\left(\boldsymbol{p} - \frac{e}{c}\boldsymbol{A}_{\rm ext}\right)^2 c^2 + m^2 c^4\right]^{1/2} + eV_{\rm ext} + \boldsymbol{\Omega}_{\rm ext} \cdot \boldsymbol{s} + e\left(V_{\rm rad} - \frac{\boldsymbol{v}}{c} \cdot \boldsymbol{A}_{\rm rad}\right) + \boldsymbol{\Omega}_{\rm rad} \cdot \boldsymbol{s}. \tag{4.4}$$

This Hamiltonian can be used to derive spin-flip photon emission matrix elements, etc. The recoils due to photon emissions can then be used to calculate changes to the synchrotron and betatron oscillations and spin trajectories, etc.

To calculate the structure of those synchrotron and betatron trajectories, we solve for the motion in the prescribed accelerator magnetic and electric fields. It is conventional to employ the arc-length as the independent variable for this purpose. The new Hamiltonian is the negative of the longitudinal momentum: $H' = -p_{\rm long}$, where

$$p_{\rm long} = \frac{e}{c} A_{\rm long} + \left[\frac{1}{c^2}\left(\mathrm{H} - eV - \boldsymbol{\Omega} \cdot \boldsymbol{s}_{\rm op}\right)^2 - m^2 c^2 - \left(\boldsymbol{p}_\perp - \frac{e}{c}\boldsymbol{A}_\perp\right)^2\right]^{1/2}. \tag{4.5}$$

We again appeal to the properties of spin $\frac{1}{2}$ operators and write this as a linear expression in $\boldsymbol{s}_{\rm op}$. We also switch the independent variable from the arc-length to the azimuth θ (which just implies scaling H' by the average machine radius R, i.e. $\mathscr{H} = RH'$),

$$\mathscr{H} = \mathscr{A}'(\boldsymbol{q}, \boldsymbol{p}, \hbar) + \mathscr{B}'(\boldsymbol{q}, \boldsymbol{p}, \hbar) \cdot \boldsymbol{s}. \tag{4.6}$$

To avoid too many symbols, we still denote the conjugate coordinates and momenta by $\boldsymbol{q}$ and $\boldsymbol{p}$, but they are different from the variables in (4.1). We again retain terms only to first order in $\hbar$. Then $\mathscr{A}'$ and $\mathscr{B}'$ are independent of $\hbar$. This yields the conventional 'accelerator physics' form of the Hamiltonian

$$\mathscr{H} = \mathscr{H}_{\rm orb}(\boldsymbol{q}, \boldsymbol{p}) + \boldsymbol{W}(\boldsymbol{q}, \boldsymbol{p}) \cdot \boldsymbol{s}. \tag{4.7}$$

This Hamiltonian describes spin precession in prescribed external fields in the accelerator. Hence, we can now treat $\boldsymbol{s}$ as a classical spin vector, with suitably defined Poisson brackets, etc. We also make further approximations, e.g. to expand the orbital motion around the closed orbit, etc, but such details do not matter here. Also, $\mathscr{H}$ depends explicitly on the azimuth θ.

The accelerator Hamiltonian $\mathscr{H}$ *cannot be quantized*. This is because, to quantize the system, the commutators of a pair of canonically conjugate variables q and p, must satisfy

the relation $[q, p] = \mathrm{i}\hbar$, and the eigenstates of q and p, say $|q'\rangle$ and $|p'\rangle$, respectively, must satisfy relations like $\langle q'|p'\rangle = \mathrm{e}^{\mathrm{i}q'p'/\hbar}$. This requires the eigenvalues q' and p' to span the interval $(-\infty, \infty)$. However, the energy variable H is bounded from below. All of the quantum mechanical (photon emission) calculations must therefore be performed using the Hamiltonian H in (4.4). The results of those calculations (recoils, spin-flips, etc) must then be applied to the orbital and spin trajectories derived from the Hamiltonian $\mathscr{H}$ in (4.7). In other words, there is no single Hamiltonian which does the whole job of calculating semiclassical QED and the accelerator physics betatron oscillations, etc. We are reminded once again that there is a distinction between calculating an individual photon emission matrix element (or cross-section), and the influence of that photon emission on the particle motion.

4.2. Hamiltonian dynamics, perturbations and stochastic interactions

We shall mainly formulate the motion of the orbital and spin motion using the Hamiltonian formalism which is an elegant method. However, it is important to realize that many of the significant theoretical developments in the field were accomplished using other methods.

The characterization of the particle motion via action-angle variables is particularly useful for statistical mechanics, because the actions are, by construction, dynamical invariants of the (unperturbed) motion. The stochastic interactions perturb the values of the actions, i.e. they induce transitions in the values of the actions. This is a particularly elegant way to encapsulate the effects of the stochastic interactions on the orbital motion. In equilibrium, the beam is uniformly distributed over the values of the angles. The beam phase-space density is a function of the actions only. It is, in fact, almost indispensable to employ phase-space to specify the distribution function of a beam of particles.

Very similar concepts also apply to the spin motion. For the spin, one must find a quantization axis such that states quantized along that axis are 'stationary states' of the system. The spin projection along the quantization axis is the spin action variable. The phase of the spin precession around that axis is the conjugate angle variable. In terms of a classical spin model, one must find an axis (we obviously do not call it a 'quantization' axis) such that the spin projection along that axis is a dynamical invariant. In plain language, we must diagonalize the Hamiltonian, not only for the orbit, but also for the spin!

For nonradiative systems, where there are no such stochastic interactions, the use of action-angles (including spin action-angle variables) is still useful if the beams are circulated at a fixed energy for a long time, i.e. in storage rings. The use of dynamical invariants is simply the best way to characterize the long-term phase-space distribution of a beam. The use of action-angles is less useful (useless?) for 'rapid-cycling' machines where a beam is ejected after only a short stay in the accelerator.

We have already alluded to the perturbation theory above. We should be careful to recognize that there are multiple perturbation expansions going on, however. We begin with the orbital motion. By hypothesis, the particles execute bounded oscillations around a central orbit (the closed orbit). We stated above that these oscillations are characterized in terms of action-angle variables. However, despite its formal elegance, the determination of the actions and angles is usually a formidable task. Hence the actions and angles are usually calculated via perturbation theory, in powers of the amplitude of the orbit. (There are actually three amplitudes: two for the transverse oscillations and one for the longitudinal oscillations.) The 'true' actions and angles are therefore known only approximately. On top of this, the stochastic interactions are *another* perturbation. In the case of quantum electrodynamics, the perturbation parameter is the electromagnetic fine-structure constant.

5. Classical spin model

5.1. General remarks

The subsections below are written, more or less, independently. Hence some equations are repeated several times, for self-containedness of the individual subsections. Furthermore, we present derivations of some of the fundamental equations from multiple points of view, and therefore, we deliberately rewrite the equations from scratch, to make the point that they do *not* depend on earlier material.

5.2. Quantum mechanical foundations: Ehrenfest's theorem

Ehrenfest's theorem (Ehrenfest 1927) is a fundamental theorem of quantum mechanics, which is directly relevant to the foundations of much of the work in this paper. Through most parts of this paper we shall work with classical variables and we shall employ carets to denote quantum operators below. Ehrenfest's theorem (actually, a generalization of his original theorem) gives the equation of motion for the expectation value $\langle\hat{A}\rangle = \langle\psi|\hat{A}|\psi\rangle$ of a quantum operator $\hat{A}$, for a system in a state $|\psi\rangle$. The resulting equation of motion describes the time evolution of c-number variables, not q-number operators. The generalized form of Ehrenfest's theorem states that

$$\frac{\mathrm{d}\langle\hat{A}\rangle}{\mathrm{d}t} = \left\langle\frac{\partial\hat{A}}{\partial t}\right\rangle + \frac{1}{\mathrm{i}\hbar}\,\langle[\hat{A},\hat{H}]\rangle. \tag{5.1}$$

Here $\hat{H}$ is the Hamiltonian operator. Ehrenfest's theorem is valid in both, the Schrödinger and Heisenberg pictures of quantum mechanics. We begin with the Heisenberg picture. The Heisenberg equation of motion for $\hat{A}$ is

$$\frac{\mathrm{d}\hat{A}}{\mathrm{d}t} = \frac{\partial\hat{A}}{\partial t} + \frac{1}{\mathrm{i}\hbar}\,[\hat{A},\hat{H}]. \tag{5.2}$$

Since the bracket states do not vary with time in the Heisenberg picture, we take the expectation value of the above equation over the state $|\psi\rangle$, and (5.1) follows immediately.

We now employ the Schrödinger picture. To avoid proliferation of notation, we do not use separate symbols for Schrödinger variables. The Schrödinger equation for a quantum state $|\psi(t)\rangle$ is

$$\mathrm{i}\hbar\frac{\partial}{\partial t}|\psi\rangle = \hat{H}|\psi\rangle. \tag{5.3}$$

Then

$$\begin{aligned}\frac{\mathrm{d}}{\mathrm{d}t}\langle\psi|\hat{A}|\psi\rangle &= \left(\frac{\partial}{\partial t}\langle\psi|\right)\hat{A}|\psi\rangle + \langle\psi|\frac{\partial\hat{A}}{\partial t}|\psi\rangle + \langle\psi|\hat{A}\left(\frac{\partial}{\partial t}|\psi\rangle\right)\\ &= -\frac{1}{\mathrm{i}\hbar}(\langle\psi|\hat{H}^{\dagger})\hat{A}|\psi\rangle + \langle\psi|\frac{\partial\hat{A}}{\partial t}|\psi\rangle + \frac{1}{\mathrm{i}\hbar}\,\langle\psi|\hat{A}\,(\hat{H}|\psi\rangle)\\ &= \left\langle\frac{\partial\hat{A}}{\partial t}\right\rangle + \frac{1}{\mathrm{i}\hbar}\,\langle[\hat{A},\hat{H}]\rangle,\end{aligned} \tag{5.4}$$

which proves the theorem. Note that it is essential to the proof that the Hamiltonian be a Hermitian (self-adjoint) operator. In the Heisenberg picture, it is necessary for the Hamiltonian to be Hermitian, in order to yield a self-consistent equation of motion for $A^{\dagger}$.

5.3. Classical spin model

Let us apply Ehrenfest's theorem to the case of the spin operator $\hat{A} = \hat{s}$. There is then no partial derivative $\partial\hat{A}/\partial t$ term. We begin with a magnetic dipole Hamiltonian

$$\hat{H} = -\hat{\boldsymbol{\mu}} \cdot \hat{\boldsymbol{B}} = \hat{\boldsymbol{\Omega}} \cdot \hat{s}. \tag{5.5}$$

Here $\hat{\boldsymbol{B}}$ is the magnetic field (in principle, also an operator) and $\hat{\boldsymbol{\Omega}}$ is the spin precession vector operator. We do *not* assume $\hat{s}$ is a spin $\frac{1}{2}$ operator. The commutator is

$$[\hat{s}, \hat{H}] = [\hat{s}, \hat{\boldsymbol{\Omega}} \cdot \hat{s}] = \mathrm{i}\hbar\, \hat{\boldsymbol{\Omega}} \times \hat{s}. \tag{5.6}$$

Substitution into (5.1) yields

$$\frac{\mathrm{d}}{\mathrm{d}t}\langle\hat{s}\rangle = \langle\hat{\boldsymbol{\Omega}} \times \hat{s}\rangle. \tag{5.7}$$

If $\hat{\boldsymbol{\Omega}}$ is a constant, say $\hat{\boldsymbol{\Omega}} = \Omega\,\boldsymbol{e}$ where $\boldsymbol{e}$ is a fixed unit vector, we can simplify the above to

$$\frac{\mathrm{d}}{\mathrm{d}t}\langle\hat{s}\rangle = \Omega\boldsymbol{e} \times \langle\hat{s}\rangle. \tag{5.8}$$

This is just the equation of motion for a rigid-body spin precession. The solution, starting from $t = 0$, is

$$\langle\hat{s}\rangle_t = \boldsymbol{e} \cdot \langle\hat{s}\rangle_0\, \boldsymbol{e} + \sin(\Omega t)\, \boldsymbol{e} \times \langle\hat{s}\rangle_0 - \cos(\Omega t)\, \boldsymbol{e} \times (\boldsymbol{e} \times \langle\hat{s}\rangle_0). \tag{5.9}$$

This is simply a rotation through an angle Ωt around the axis $\boldsymbol{e}$. Hence, the evolution of the spin state of a quantum system can be equivalently parametrized by the precession of a classical spin vector $\langle\hat{s}\rangle$. If the spin precession vector (operator) $\hat{\boldsymbol{\Omega}}$ depends on the orbital dynamical variables $\hat{\boldsymbol{x}}$ and $\hat{\boldsymbol{p}}$ (quantum operators), then the equation of motion (5.7) reads

$$\frac{\mathrm{d}}{\mathrm{d}t}\langle\hat{s}\rangle = \langle\hat{\boldsymbol{\Omega}}(\hat{\boldsymbol{x}}, \hat{\boldsymbol{p}}) \times \hat{s}\rangle. \tag{5.10}$$

Since $\hat{\boldsymbol{\Omega}}$ is also a quantum operator, we cannot move it out of the expectation value so easily. To the extent that $\hat{\boldsymbol{\Omega}}$ does not depend on $\hat{s}$, we can write

$$\frac{\mathrm{d}}{\mathrm{d}t}\langle\hat{s}\rangle = \langle\hat{\boldsymbol{\Omega}}\rangle \times \langle\hat{s}\rangle, \tag{5.11}$$

where the expectations are over the orbital and spin states, respectively. This is still an equation of motion for a rigid-body spin rotation of a classical spin vector, under the action of a c-number spin precession vector $\langle\hat{\boldsymbol{\Omega}}\rangle$, which is an expectation over the orbital quantum state of the system.

However, (5.11) is still not useful as it stands. The expectation value $\langle\hat{\boldsymbol{\Omega}}\rangle$ is not simple to calculate, in general. We need an auxiliary condition, a very important one that will underlie all of the work in this paper, namely, the *semiclassical approximation*. We shall approximate that,

$$\langle\hat{\boldsymbol{\Omega}}(\hat{\boldsymbol{x}}, \hat{\boldsymbol{p}})\rangle \simeq \boldsymbol{\Omega}(\langle\hat{\boldsymbol{x}}\rangle, \langle\hat{\boldsymbol{p}}\rangle). \tag{5.12}$$

Here $\langle\hat{\boldsymbol{x}}\rangle$ and $\langle\hat{\boldsymbol{p}}\rangle$ are the c-number expectation values of the position and momentum operators, and can be visualized as specifiying a classical orbital trajectory. We can write, dropping the carets for the classical variables,

$$\boldsymbol{x} \equiv \langle\hat{\boldsymbol{x}}\rangle, \qquad \boldsymbol{p} \equiv \langle\hat{\boldsymbol{p}}\rangle, \qquad \boldsymbol{s} \equiv \langle\hat{s}\rangle. \tag{5.13}$$

For the semiclassical approximation, we write $\boldsymbol{\Omega}_{\mathrm{sc}} \equiv \boldsymbol{\Omega}(\boldsymbol{x}, \boldsymbol{p})$, from which it follows that

$$\frac{\mathrm{d}\boldsymbol{s}}{\mathrm{d}t} \simeq \boldsymbol{\Omega}_{\mathrm{sc}} \times \boldsymbol{s}. \tag{5.14}$$

Hence we have 'proved' that the evolution of the spin motion of a quantum system can be described instead by the precession of a classical spin vector $\boldsymbol{s}$, under the action of a semiclassical spin precession vector $\boldsymbol{\Omega}_{\mathrm{sc}}$. This is true in the semiclassical approximation, even if the spin precession vector depends on the orbital motion. Below, we shall examine the loopholes in the above proof.

5.4. Semiclassical approximation

Ehrenfest's theorem is a general result of quantum mechanics, for a system in an arbitrary quantum state $|\psi\rangle$. The semiclassical approximation is *not* part of Ehrenfest's theorem. However, we do need the semiclassical approximation to proceed further with the analysis of spin dynamics in particle accelerators. Let us examine the validity of the semiclassical approximation.

It helps to illustrate the basic concepts, using the more familiar examples of Ehrenfest's thorem, i.e. the position and momentum operators. For a Hamiltonian

$$\hat{H} = \frac{\hat{\boldsymbol{p}}^2}{2m} + V(\hat{\boldsymbol{x}}), \tag{5.15}$$

Ehrenfest's theorem states, as one can easily derive, that

$$\frac{\mathrm{d}\langle\hat{\boldsymbol{x}}\rangle}{\mathrm{d}t} = \frac{\langle\hat{\boldsymbol{p}}\rangle}{m}, \qquad \frac{\mathrm{d}\langle\hat{\boldsymbol{p}}\rangle}{\mathrm{d}t} = -\langle\boldsymbol{\nabla}_{\hat{\boldsymbol{x}}} V(\hat{\boldsymbol{x}})\rangle. \tag{5.16}$$

These are the usual Newtonian velocity and force laws, which are frequently combined into the second-order differential equation

$$m\frac{\mathrm{d}^2\langle\hat{\boldsymbol{x}}\rangle}{\mathrm{d}t^2} = -\langle\boldsymbol{\nabla}_{\hat{\boldsymbol{x}}} V(\hat{\boldsymbol{x}})\rangle. \tag{5.17}$$

Strictly speaking, Ehrenfest derived his theorem for the evolution of $\langle\hat{\boldsymbol{x}}\rangle$ and $\langle\hat{\boldsymbol{p}}\rangle$ as in (5.16) and/or (5.17). Its use for the expectation value of the spin operator was first remarked upon by Bloch (1946). An excellent discussion of the classical spin model was given by Ford and Hirt (1961), in a regrettably unpublished report. In modern usage, Ehrenfest's theorem is easily seen to apply to the evolution of the expectation value of any quantum operator.

Let us solve the equations of motion explicitly for the case of a one-dimensional harmonic oscillator

$$\hat{H} = \frac{\hat{p}^2}{2m} + \frac{1}{2}m\omega^2\hat{x}^2. \tag{5.18}$$

Then,

$$\frac{\mathrm{d}\langle\hat{x}\rangle}{\mathrm{d}t} = \frac{\langle\hat{p}\rangle}{m}, \qquad \frac{\mathrm{d}\langle\hat{p}\rangle}{\mathrm{d}t} = -m\omega^2\langle\hat{x}\rangle, \tag{5.19}$$

which leads to the familiar simple harmonic equation

$$\frac{\mathrm{d}^2\langle\hat{x}\rangle}{\mathrm{d}t^2} + \omega^2\langle\hat{x}\rangle = 0. \tag{5.20}$$

This has the solution,

$$\langle\hat{x}\rangle_t = \langle\hat{x}\rangle_0 \cos(\omega t) + \frac{\langle\hat{p}\rangle_0}{m\omega}\sin(\omega t), \tag{5.21}$$

which is the familiar classical solution of a simple harmonic oscillator. So far so good. Let us now calculate the classical expectation value of the energy. We obtain

$$E = \langle\hat{H}\rangle = \frac{\langle\hat{p}^2\rangle}{2m} + \frac{1}{2}m\omega^2\langle\hat{x}^2\rangle. \tag{5.22}$$

We need the values of $\langle\hat{x}^2\rangle$ and $\langle\hat{p}^2\rangle$, but we only have solutions for $\langle\hat{x}\rangle$ and $\langle\hat{p}\rangle$. We invoke the semiclassical approximation, for the *first* time in the analysis of the harmonic oscillator, to write $\langle\hat{x}^2\rangle \simeq \langle\hat{x}\rangle^2$ and $\langle\hat{p}^2\rangle \simeq \langle\hat{p}\rangle^2$, to obtain the semiclassical value

$$E_{\mathrm{sc}} \simeq \frac{\langle\hat{p}\rangle^2}{2m} + \frac{1}{2}m\omega^2\langle\hat{x}\rangle^2. \tag{5.23}$$

We now select the quantum state $|\psi\rangle$ to be the nth energy eigenstate $|n\rangle$, for which we know $E_n = (n + \frac{1}{2})\hbar\omega$. For this quantum state, we also know that $\langle\hat{x}\rangle = \langle\hat{p}\rangle = 0$. Then $E_{\rm sc} = 0$. The semiclassical approximation has badly gone wrong. Perhaps the reader was expecting to see an expression for the energy but lacking the zero-point term. Instead we obtain nothing at all.

This simple example illustrates a fundamental limitation of the semiclassical approximation: a semiclassical description of the orbital trajectory is only valid if the spread in the coordinates and momenta is negligible. Introduce the standard deviations $\sigma_x^2 = \langle\hat{x}^2\rangle - \langle\hat{x}\rangle^2$ and $\sigma_p^2 = \langle\hat{p}^2\rangle - \langle\hat{p}\rangle^2$. For a semiclassical description of the orbit to be valid, we require $\sigma_x \ll |\langle\hat{x}\rangle|$, and also $\sigma_p \ll |\langle\hat{p}\rangle|$. The quantum uncertainty in the orbital trajectory must be small. Usually, we tacitly assume this to be the case, because we take the orbital coordinates and momenta to be of 'O(1)', while the standard deviations are relatively of O($\hbar$). To the extent that $\sigma_{\boldsymbol{x}}$ and $\sigma_{\boldsymbol{p}}$ are negligible, we can then approximate, for any function f,

$$\langle\hat{f}(\boldsymbol{x},\boldsymbol{p})\rangle \simeq f(\langle\hat{\boldsymbol{x}}\rangle, \langle\hat{\boldsymbol{p}}\rangle), \tag{5.24}$$

and write

$$f_{\rm sc} \equiv f(\boldsymbol{x},\boldsymbol{p}) = f(\langle\hat{\boldsymbol{x}}\rangle, \langle\hat{\boldsymbol{p}}\rangle). \tag{5.25}$$

This may or may not be justified, depending on circumstances. In the case of a harmonic oscillator, we need the system to be in a superposition of states such that, averaged over time, $\sigma_x \ll |\langle\hat{x}\rangle|$ and $\sigma_p \ll |\langle\hat{p}\rangle|$. A pure energy eigenstate, no matter how highly excited, does not meet this criterion.

On the other hand, a highly localized wavepacket, which is, of course, then not an energy eigenstate, *can* fulfil the semiclassical constraints. This localized wavepacket is then a 'point' particle, and evolves according to a (semi)classical equation of motion. If the wavepacket is composed of eigenstates of highly excited energy levels, the uncertainty in the energy is negligible relative to the average energy, and we can speak of a definite (semiclassical) energy, too.

Throughout this paper, we must interpret terms like 'position', 'momentum', 'energy' and 'angular momentum' in the semiclassical sense. In chapter zero, we discussed the model of a quantum particle in a uniform magnetic field (Landau levels, etc). We pointed out, that for very highly excited energy levels, we could construct a localized wavepacket and consider the position, momentum, energy and angular momentum to have definite values, without violating Heisenberg's Uncertainty Principle. When such a particle circulates in the static electric and magnetic fields of an accelerator, a semiclassical approximation of the orbit is valid. When two such particles collide head on and annihilate each other, as in e^+e^- storage rings, the semiclassical approximation is *not* valid at the instant of collision.

5.5. Failure of the classical spin model

As we pointed out in chapter zero, we cannot construct semiclassical wavepackets for a spin $\frac{1}{2}$. There is no limiting case where the spin states form a continuum. Nevertheless, we have seen from above, that the evolution of the spin state of a quantum system can be described by the precession of a classical spin vector. However, this cannot always be true.

The classical spin model fails when the spin evolution is not deterministic. The most important example for us is, when an electron emits a photon of synchrotron radiation. Recall the full semiclassical QED Hamiltonian for motion in the prescribed external accelerator and the photon radiation fields, in (4.4). The term prescribed 'external' accelerator fields includes the radio-frequency electromagnetic fields in the accelerating (and/or longitudinally focusing) cavities in the accelerator, whose frequency may be 500 MHz or more. A classical

spin model will satisfactorily describe the evolution of a spin under the influence of the external accelerator fields, but will *not* describe the evolution of the spin operator (or spin wavefunction) in an interaction with the radiation electromagnetic fields.

Basically, the classical spin model will fail if an *individual* interaction can change the spin state from 'up' to 'down' in an infinitesimal time interval, along some suitably defined quantization axis. Note that this has nothing to do with the semiclassical treatment of the orbit: Ehrenfest's theorem fails in this case. In terms of the Schrödinger picture, the wavefunction changes discontinuously, and in a nondeterministic manner. The emission of a photon of spin-flip radiation can do this. The action of a time-independent (or slowly varying) accelerator magnetic field (or even a 500 MHz radio-frequency electric field) does not.

The classical spin model also fails in polarimetry measurements. Even for a polarized proton, where photon emission is not relevant, a classical treatment of the spin motion cannot be used to analyse the response of a polarimeter. A hadronic polarimeter requires the proton to interact with some target via a spin-dependent reaction. The left–right or up–down asymmetry in the scattering cross-section is measured. The spin must be treated quantum mechanically.

Hence, the failure of the classical spin model is more tied to the failure of Ehrenfest's theorem, than to the breakdown of the semiclassical approximation, although they do tend to go together.

5.6. Spinor representation

We now take the classical spin model as given. The spin equation of motion is

$$\frac{\mathrm{d}\boldsymbol{s}}{\mathrm{d}t} = \boldsymbol{\Omega} \times \boldsymbol{s}, \tag{5.26}$$

where all the variables are classical dynamical variables, and the orbital motion is treated semiclassically. All carets, subscripts, etc, have been dropped. The above equation of motion can be derived from the semiclassical Hamiltonian

$$H = \boldsymbol{\Omega} \cdot \boldsymbol{s}. \tag{5.27}$$

The Poisson brackets for the components of the classical spin vector are *defined* by analogy with the quantum theory:

$$\{s_i, s_j\} = \sum_k \epsilon_{ijk}\, s_k, \tag{5.28}$$

where the braces denote a Poisson bracket, and ϵ_{ijk} is the isotropic totally antisymmetric tensor. The equation of motion for a classical dynamical variable, in this case $\boldsymbol{s}$, is

$$\frac{\mathrm{d}\boldsymbol{s}}{\mathrm{d}t} = \{\boldsymbol{s}, H\}. \tag{5.29}$$

Use of (5.28) leads to (5.26).

It is more common in accelerator physics to take the independent variable to be the arc-length s along the reference orbit, or the generalized azimuth θ, given by $\theta = 2\pi s/C$, where the ring circumference is C. We write the spin precession equation, using the independent variable θ, as

$$\frac{\mathrm{d}\boldsymbol{s}}{\mathrm{d}\theta} = \boldsymbol{W} \times \boldsymbol{s}. \tag{5.30}$$

We employ $\boldsymbol{W}$ to distinguish the spin precession vector from $\boldsymbol{\Omega}$, which has different dimensions. It is, moreover, a common practice in the literature to represent a *classical* spin not by a vector $\boldsymbol{s}$, but via a spinor Ψ. The relationship between $\boldsymbol{s}$ and Ψ is

$$\boldsymbol{s} = \Psi^\dagger \boldsymbol{\sigma} \Psi, \tag{5.31}$$

where $\boldsymbol{\sigma}$ is a vector of Pauli matrices. Hence, there is not a one-to-one relationship between $\boldsymbol{s}$ and Ψ: the same vector $\boldsymbol{s}$ results if one multiplies Ψ by an arbitrary overall phase factor. The spinor Ψ is complex, and hence has four independent parameters (two real and two imaginary parts). The irrelevance of a global phase factor removes one degree of freedom, hence, Ψ has only three degrees of freedom. The normalization to unity, for both $\boldsymbol{s}$ and Ψ, removes another degree of freedom from both. The equation of motion for Ψ is

$$\frac{\mathrm{d}\Psi}{\mathrm{d}\theta} = -\mathrm{i}H\Psi, \tag{5.32}$$

with the Hamiltonian

$$H = \tfrac{1}{2}\boldsymbol{W}\cdot\boldsymbol{\sigma}. \tag{5.33}$$

Equation (5.32) bears a formal resemblance to the Schrödinger equation, and the Hamiltonian in (5.33) bears a striking formal resemblance to that for a spin $\frac{1}{2}$ particle, with $\hbar = 1$ in both cases. All the standard mathematical manipulations of Pauli matrix and spinor algebra will work for Ψ. Nevertheless, it is important to recognize that Ψ does not necessarily describe a spin $\frac{1}{2}$ particle. The spinor Ψ is *defined* via the classical spin $\boldsymbol{s}$, in (5.31). The equation of motion (5.32) does not refer to quantized operators.

5.7. Normalization

Since (5.26) is homogeneous in $\boldsymbol{s}$, we typically normalize it to unity: $\boldsymbol{s}\cdot\boldsymbol{s} = 1$. However, there are hidden subtleties in doing so. Let us begin with spin $\frac{1}{2}$, and consider an arbitrary spin state $|\psi\rangle = a|\uparrow\rangle + b|\downarrow\rangle$, where $|a|^2 + |b|^2 = 1$. Then, denoting the coordinate basis vectors by $\boldsymbol{e}_1$, $\boldsymbol{e}_2$ and $\boldsymbol{e}_3$, respectively,

$$\langle\psi|\hat{\boldsymbol{s}}|\psi\rangle = \frac{\hbar}{2}\langle\psi|\boldsymbol{\sigma}|\psi\rangle = \frac{\hbar}{2}[(a^*b + ab^*)\boldsymbol{e}_1 + \mathrm{i}(a^*b - ab^*)\boldsymbol{e}_2 + (aa^* - bb^*)\boldsymbol{e}_3]. \tag{5.34}$$

Then, for arbitrary a and b,

$$|\langle\psi|\hat{\boldsymbol{s}}|\psi\rangle|^2 = \frac{\hbar^2}{4}(aa^* + bb^*)^2 = \frac{\hbar^2}{4}. \tag{5.35}$$

Hence, if we normalize the classical spin vector via

$$\boldsymbol{s}_{\mathrm{cl}} = \frac{2}{\hbar}\langle\psi|\hat{\boldsymbol{s}}|\psi\rangle, \tag{5.36}$$

we obtain a unit vector: $|\boldsymbol{s}_{\mathrm{cl}}|^2 = 1$. So far so good.

Normalization problems arise for higher spins. For spin 1, there are three spin states along any quantization axis. Let us employ the standard choice of eigenstates of $\hat{s}_3$, with eigenvalues of $1, 0$ and -1, and denote the states by $|1\rangle$, $|0\rangle$ and $|-1\rangle$, respectively. Then, for any eigenstate $|m\rangle$ of $\hat{s}_3$, we have

$$\langle m|\hat{s}_1|m\rangle = 0, \qquad \langle m|\hat{s}_2|m\rangle = 0, \qquad \langle m|\hat{s}_3|m\rangle = m\hbar. \tag{5.37}$$

We now select the spin state to be $|\psi\rangle = |0\rangle$. This leads to the most unfortunate conclusion

$$\langle\psi|\hat{s}_1|\psi\rangle = \langle\psi|\hat{s}_2|\psi\rangle = \langle\psi|\hat{s}_3|\psi\rangle = 0. \tag{5.38}$$

The classical spin vector vanishes completely. There is no way to normalize this vector to unity. In more generality, if we select an arbitrary spin state $|\psi\rangle = a_+|1\rangle + a_0|0\rangle + a_-|-1\rangle$ with $|a_+|^2 + |a_0|^2 + |a_-|^2 = 1$, we find that, rather than always being unity, the normalization can take *any* fixed value from 0 to 1:

$$\frac{|\langle\psi|\hat{\boldsymbol{s}}|\psi\rangle|^2}{\hbar^2} \in [0, 1]. \tag{5.39}$$

The length of an individual classical spin vector is fixed (for fixed a_+, a_0 and a_-), but different classical spin vectors have different lengths, in general. Similar normalization problems arise for spin $\frac{3}{2}$ particles, etc.

5.8. Polarization and spin

The polarization vector is defined as the statistical average of an ensemble of classical spin vectors

$$\boldsymbol{P} = \langle \boldsymbol{s} \rangle. \tag{5.40}$$

Note that it is possible for an *individual* particle to be unpolarized: the ensemble in this case consists of a single particle, and the polarization is defined via a time-average over many observations of the spin

$$\boldsymbol{P} = \bar{\boldsymbol{s}}. \tag{5.41}$$

In both cases, one has $|\boldsymbol{P}| \leqslant 1$, if the classical spin vectors are normalized to unity. If the *ergodic hypothesis* is applicable, as it is in the case of radiative polarization via the emission of photons of synchrotron radiation, then the two definitions yield the same answer.

However, we are moving too quickly. We need to analyse the classical spin model in more detail. The classical spin vector is an expectation value of the quantum spin operator for a particle in a state $|\psi\rangle$. Hence it cannot be determined by an individual observation of the quantum spin operator. Because the classical spin vector is an average, all of its three components can be specified simultaneously. (This of course cannot be done in an individual observation of a quantum spin.) However, we usually think of the average of several measurements (of the spin operator) as a *polarization*, not a spin. We need to reconcile these statements and clarify the definition of the polarization. To do so, we need to examine pure states and statistical mixtures.

5.9. Pure states and statistical mixtures

The information about a quantum statistical ensemble is specified by a density matrix ρ. Strictly speaking, the concept of a density matrix applies to *any* quantum statistical ensemble, not just the spin and polarization. We write

$$\rho = \sum_i w_i |\psi_i\rangle\langle\psi_i|, \tag{5.42}$$

where the $|\psi_i\rangle$ are a complete orthonormal set of states (a basis set). The weights w_i are nonnegative real numbers which sum to unity; by convention, the trace of the density matrix is normalized to unity and evidently, $0 \leqslant w_i \leqslant 1$. A pure state is defined as a statistical system which can be specified by a single wavefunction. The density matrix of a pure state has the form

$$\rho = |\psi\rangle\langle\psi|, \tag{5.43}$$

i.e. one of the w_i equals unity, and all the others vanish. The expectation of any operator A is given by taking the trace of the product of A with the density matrix:

$$\langle A \rangle = \mathrm{Tr}\{\rho A\} = \sum_i w_i \langle\psi_i|A|\psi_i\rangle. \tag{5.44}$$

In particular, for the spin operator, the polarization vector is given by

$$\boldsymbol{P} = \mathrm{Tr}\{\rho \hat{\boldsymbol{s}}\} = \sum_i w_i \langle\psi_i|\hat{\boldsymbol{s}}|\psi_i\rangle. \tag{5.45}$$

It is immediately obvious that the polarization vector is therefore a *weighted sum* of classical spin vectors

$$\boldsymbol{P} = \sum_i w_i \boldsymbol{s}_i \tag{5.46}$$

and *this* is what we mean by the statement $\boldsymbol{P} = \langle \boldsymbol{s} \rangle$ in (5.40). It is also clear that the classical spin vector $\boldsymbol{s}$ is, by construction, the expectation of the spin operator for a system in a pure state. We have seen previously in (5.11), that a classical spin precesses without change of magnitude. However, $\langle \boldsymbol{\Omega} \rangle_i$ need not be the same for all the classical spins $\boldsymbol{s}_i$, and the magnitude of the polarization vector may not, therefore, be preserved with time.

Ehrenfest's theorem applies only to systems in pure states. The expectation value in the theorem explicitly assumes the existence of a wavefunction, not a statistical mixture.

If the spins are unpolarized, then all the weights w_i are equal, say, to w. Then

$$\rho = w \sum_i |\psi_i\rangle\langle\psi_i|. \tag{5.47}$$

Since, by definition, the states $|\psi_i\rangle$ are a complete orthonormal set (a basis), we invoke the completeness theorem

$$\sum_i |\psi_i\rangle\langle\psi_i| = \mathbb{I}, \tag{5.48}$$

where $\mathbb{I}$ is the identity operator, to deduce $\rho = w\,\mathbb{I}$, i.e. the density matrix of an unpolarized system is simply a unit matrix, normalized to a unit trace. For particles of spin s, there are $2s + 1$ states, hence

$$\rho = \frac{\mathbb{I}}{2s+1}. \tag{5.49}$$

For a system of spin $\frac{1}{2}$ particles, the density matrix is a 2×2 Hermitian matrix, and is related to the polarization vector $\boldsymbol{P}$ via

$$\rho = \tfrac{1}{2}(1 + \boldsymbol{P} \cdot \boldsymbol{\sigma}). \tag{5.50}$$

However, there are subtleties to this. Since we deal with particle *beams*, the particles are not all located at the same space–time point. The states $|\psi_i\rangle$ in the density matrix ρ are not only spin states, but carry an orbital dependence also. It is more accurate to write (for spin $\frac{1}{2}$, and setting $z = (\boldsymbol{x}, \boldsymbol{p})$ for brevity)

$$\rho = w_+(z)|\Psi_+(z)\rangle\langle\Psi_+(z)| + w_-(z)|\Psi_-(z)\rangle\langle\Psi_-(z)|, \tag{5.51}$$

where $|\Psi_+(z)\rangle$ and $|\Psi_-(z)\rangle$ are spin states quantized 'up' and 'down', respectively, in a small phase-space volume element at the orbital point z. The trace of ρ is an integral over the phase-space z. We can extract a purely orbital component $w(z)$ and write

$$\rho = w(z)\{\, u_+(z)|\Psi_+(z)\rangle\langle\Psi_+(z)| + u_-(z)|\Psi_-(z)\rangle\langle\Psi_-(z)|\}, \tag{5.52}$$

where the factorization is such that $u_+(z) + u_-(z) = 1$. Here $w(z)$ is obviously the unpolarized purely orbital phase-space density, and the term in brackets is a *polarization density*, or intrinsic angular momentum density per particle per unit volume of phase-space. This is truly the full mathematical physics expression for the polarization. In section 27, we shall briefly describe how the above expression has been used in a Fokker–Planck type equation for the spin–orbit evolution of a beam.

Most of the time, we shall work with the expression $\boldsymbol{P} = \langle \boldsymbol{s} \rangle$, where we recognize now, that the angular brackets denote an integral over the orbital phase-space *as well as* a sum over the weights of the up and down spin states at each phase-space point. In other words, there are

actually *two* statistical averages: an outer average over the orbital motion, and an inner average over the spin distribution at a particular value of z.

The polarization is a property of the entire beam; it is not attached to an individual particle, nor to a specific point in phase-space (such as the closed orbit). It is one density matrix, or one vector (for spin $\frac{1}{2}$), and is a collective property of the entire statistical ensemble.

As if the above is not enough, the direction of the quantization axis of the spin states need not be same at every phase-space point z: the quantization axis of $|\Psi_{\pm}(z)\rangle$ depends on z. This may sound like unnecessarily heavy formalism, but it is a fact of the utmost significance, as we shall see in great detail in section 27.

The consequences of the above statements are most easily seen by deriving an equation of motion for the polarization. Consider that

$$\frac{\mathrm{d}\boldsymbol{P}}{\mathrm{d}t} =? \sum_i w_i \boldsymbol{\Omega}_i \times \boldsymbol{s}_i =? \boldsymbol{\Omega} \times \sum_i w_i \boldsymbol{s}_i = \boldsymbol{\Omega} \times \boldsymbol{P}. \tag{5.53}$$

Is the above derivation valid? It may be, depending on circumstances, but it is wrong in general. There are two reasons for this:

- the spin precession vector $\boldsymbol{\Omega}$ is *not* always the same for all the particles: there is a distinction between $\boldsymbol{\Omega}$ and $\boldsymbol{\Omega}_i$;
- the weights w_i need not be constant: $\mathrm{d}w_i/\mathrm{d}t \neq 0$.

Unless $\boldsymbol{\Omega}$ is the same for all the particles (as in a uniform $\boldsymbol{B}$ field), and the statistical weights are constant, the polarization does not precess like a rigid-body rotation. This fact is known in MRI work, where a magnetic field gradient is applied across the body, and the spin precession frequency is therefore correlated with the location of the spin in the body. There is a gradient of precession frequencies for the individual spins.

5.10. Tensor polarization

There is increasing interest in the acceleration of polarized spin 1 particles, such as deuterons. An extremely readable account of polarization for spin 1, and of Cartesian and spherical tensors is given by Karpius (2003). We do *not* use the classical spin model below. For spin 1, the polarization density matrix is a 3×3 matrix. It can be written in the form

$$\rho_{ij} = \frac{1}{3}\delta_{ij} + \sum_k \epsilon_{ijk} P_k + P_{ij}. \tag{5.54}$$

The quantity P_k is a polarization vector. The quantity P_{ij} is a symmetric traceless tensor, and describes the 'tensor polarization' of the ensemble. The above tensor polarization is in a Cartesian basis. It is also common practice to describe both the vector and tensor polarizations using spherical tensors. Because of the non-commutativity of the angular momentum operators, spherical tensors are related to, but not exactly the same as, spherical harmonics. We consider Cartesian and spherical bases below. For greater readability, we shall denote the quantum spin operator by $\boldsymbol{S}$, where the spin value is S, so $\boldsymbol{S}^2 = S(S+1)\hbar^2$. Next, the angle brackets below denote an average over an arbitrary statistical mixture of states. To avoid unnecessarily cumbersome notation, we shall assume that the spin states are all quantized along the same axis, independent of the orbital phase-space location z.

We begin with the Cartesian basis. The components of the polarization vector and tensor are given by

$$P_{\mathrm{i}} = \frac{1}{S\hbar}\langle S_i \rangle, \qquad P_{ij} = \frac{3/2\langle S_i S_j + S_j S_i \rangle - \boldsymbol{S}^2 \delta_{ij}}{S(2S-1)\hbar^2}. \tag{5.55}$$

We do not claim that $\langle S_i \rangle$ can be normalized to $\hbar$ or unity, etc, even for a pure state. The polarization tensor is indeed traceless: $\sum_i S_i S_i = \boldsymbol{S}^2$, hence $\sum_i P_{ii} = 0$. For an unpolarized beam, $\langle S_i \rangle = 0$ and $\langle S_i S_j \rangle = (1/3)\boldsymbol{S}^2 \delta_{ij}$, and so the polarization vector and tensor both vanish. For spin 1,

$$P_{\mathrm{i}} = \frac{1}{\hbar}\langle S_i \rangle, \qquad P_{ij} = \frac{3}{2\hbar^2}\langle S_i S_j + S_j S_i \rangle - 2\delta_{ij}. \tag{5.56}$$

The use of spherical harmonics is an elegant alternative parametrization. The spherical tensors up to rank 2, with statistical averages, are given by (see Karpius (2003)),

$$\begin{aligned}
T_{00} &= 1, \\
T_{10} &= \sqrt{\frac{3}{2}}\frac{\langle S_3 \rangle}{\hbar}, \\
T_{1\pm1} &= \mp\frac{\sqrt{3}}{2}\frac{\langle S_1 \pm \mathrm{i}S_2 \rangle}{\hbar}, \\
T_{20} &= \frac{1}{\sqrt{2}}\frac{\langle 3S_3^2 - 2 \rangle}{\hbar^2}, \\
T_{2\pm1} &= \mp\frac{\sqrt{3}}{2}\frac{\langle (S_1 \pm \mathrm{i}S_2)S_3 + S_3(S_1 \pm \mathrm{i}S_2) \rangle}{\hbar^2}, \\
T_{2\pm2} &= \frac{\sqrt{3}}{2}\frac{\langle (S_1 \pm \mathrm{i}S_2)^2 \rangle}{\hbar^2}.
\end{aligned} \tag{5.57}$$

These expressions correct misprints of normalization by Lee (1997). Suppose that a spin 1 particle is in a pure state $|1\rangle$ quantized along polar angles (θ, ϕ). Then,

$$|1\rangle_{\theta,\phi} = \mathrm{e}^{-\mathrm{i}\phi}\cos^2\frac{\theta}{2}\,|1\rangle + \sqrt{2}\cos\frac{\theta}{2}\sin\frac{\theta}{2}\,|0\rangle + \mathrm{e}^{\mathrm{i}\phi}\sin^2\frac{\theta}{2}\,|-1\rangle. \tag{5.58}$$

Clearly,

$$\begin{aligned}
P_3 &= \cos^4\frac{\theta}{2} - \sin^4\frac{\theta}{2} = \cos\theta, \\
P_{33} &= 3\left(\cos^4\frac{\theta}{2} + \sin^4\frac{\theta}{2}\right) - 2 = \frac{1}{2}(3\cos^2\theta - 1).
\end{aligned} \tag{5.59}$$

The values of P_3 and P_{33} thus transform exactly like spherical harmonics of rank 1 and 2, respectively.

Let us consider the expressions for P_3 and P_{33} in terms of the fractional populations of the states. For spin $\frac{1}{2}$, the fractional populations are $N_\pm$ with an obvious notation. Then,

$$P_3 = N_+ - N_-. \tag{5.60}$$

For spin 1, we can write (N_+, N_0, N_-). Then $P_3 = N_+ - N_-$ as before, but note that now, $N_+ + N_0 + N_- = 1$, so $N_+ + N_- < 1$ in general. As for the tensor polarization,

$$P_{33} = 3(N_+ + N_-) - 2(N_+ + N_0 + N_-) = 1 - 3N_0. \tag{5.61}$$

For both spin $\frac{1}{2}$ and 1, the bounds on the vector polarization are

$$-1 \leqslant P_3 \leqslant 1, \tag{5.62}$$

while for spin 1, the bounds on the tensor polarization component P_{33} are

$$-2 \leqslant P_{33} \leqslant 1. \tag{5.63}$$

The foregoing remarks also demonstrate, that *for spin* $\frac{1}{2}$ *only*, the vector polarization of a pure state is $\pm 100\%$ (either $N_+ = 1$ or $N_- = 1$). However for spin 1, the vector polarization can be 100%, 0 or -100%, according as $N_+ = 1$, $N_0 = 1$ or $N_- = 1$.

Equations of motion to track the spherical tensor polarization components $(T_2, T_1, \ldots, T_{-2})$ through an accelerator, for arbitrary initial conditions, were presented by Huang *et al* (1993). The equations track the evolution of the tensor components directly. Naturally, such tracking equations assume that the spin precession vector is the same for all the particles.

5.11. Spin precession equation

We have gone through a good deal of formal theory above. Here, we start from scratch and take the semiclassical approximation and the classical spin model as given *a priori*. Although we wrote formal expressions for the spin precession equation above, we did not specify the form of the spin precession vector in terms of laboratory electric and magnetic fields. We shall do so here. As stated in the introduction, we employ cgs units. For a nonrelativistic spin, the Hamiltonian is

$$H = -\boldsymbol{\mu} \cdot \boldsymbol{B} = -\frac{ge}{2mc} \boldsymbol{s} \cdot \boldsymbol{B}. \tag{5.64}$$

Here $\boldsymbol{\mu}$ is the particle magnetic moment, $\boldsymbol{B}$ is the external magnetic field, g is the g-factor, e and m are the particle charge and mass, respectively, $\boldsymbol{s}$ is the spin vector and c is, of course, the speed of light. The spin precession equation is

$$\frac{\mathrm{d}\boldsymbol{s}}{\mathrm{d}t} = \boldsymbol{\mu} \times \boldsymbol{B} = -\frac{ge}{2mc} \boldsymbol{B} \times \boldsymbol{s}. \tag{5.65}$$

There are several ways to generalize this to the relativistic case. They all, of course, lead to the same answer, but some derivations are more transparent than others. We shall present two derivations, the first based on Lorentz transforms, and later, a derivation based exclusively on four-vectors.

We follow the relativistic generalization of the spin precession equation given by Shatunov (2001) using Lorentz transformations. This derivation follows the approach of Thomas (1927). We follow a particle with relativistic velocity $\boldsymbol{v}$ moving under the actions of laboratory frame electric and magnetic fields $\boldsymbol{E}$ and $\boldsymbol{B}$, respectively, along a trajectory determined by the Lorentz force equation, with $\boldsymbol{\beta} = \boldsymbol{v}/c$

$$\frac{\mathrm{d}\boldsymbol{p}}{\mathrm{d}t} = e\,(\boldsymbol{E} + \boldsymbol{\beta} \times \boldsymbol{B}). \tag{5.66}$$

(Recall that we employ cgs units so $\boldsymbol{E}$ and $\boldsymbol{B}$ have the same dimensions.) From the above equation we deduce that

$$\frac{\mathrm{d}\boldsymbol{\beta}}{\mathrm{d}t} = \frac{e}{mc\gamma}\,(\boldsymbol{E} - \boldsymbol{E} \cdot \boldsymbol{\beta}\boldsymbol{\beta} + \boldsymbol{\beta} \times \boldsymbol{B}). \tag{5.67}$$

The reader should refer to figure 24. In addition to the laboratory frame 'L', we also define two other frames: the particle rest-frame 'C', and an inertial frame 'I' moving with the particle velocity $\boldsymbol{v}_{t=0}$. The coordinate origins of both the frames C and I coincide with the lab frame L at $t = 0$. We need to be more careful when specifying the frames I and C, to render them well-defined. We define that the Lorentz transformation from the lab frame L, to the frames I and C at $t = 0$ be accomplished by a *single* boost, with a Lorentz factor $\gamma = 1/\sqrt{1 - v^2/c^2}$. The spin $\boldsymbol{s}$ is defined with this choice for the 'rest-frame' C. It is otherwise possible to define another rest-frame C', defined as follows. We boost from L, to an intermediate frame F, using a boost with a velocity $\boldsymbol{v}_1$ which is arbitrary, and then perform a second boost with a velocity $\boldsymbol{v}_2$,

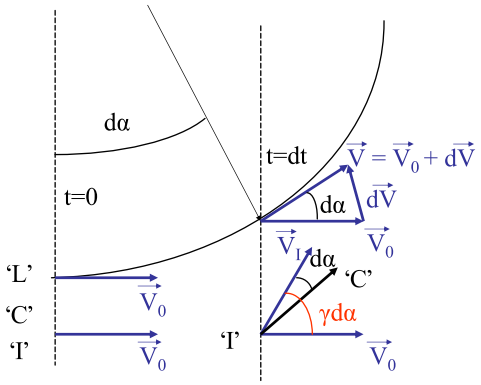

Figure 24. Coordinate systems and inertial frames for spin and orbital motion.

such that under the combined Lorentz boosts $\mathcal{L}(\boldsymbol{v}_2)\mathcal{L}(\boldsymbol{v}_1)$, the final particle velocity is zero: this is the frame C'. However C' does *not* coincide with C. This arises from the structure of the Lorentz group. The (homogeneous) Lorentz group has six generators: three rotations and three boosts, along the x, y and z axes, say. The rotations by themselves form a noncommuting subgroup $SO(3)$, i.e. a combination of two rotations is also a rotation. However, the boosts do not form a subgroup. A combination of two non-parallel Lorentz boosts is, in general, a single boost *plus* a spatial rotation. (This spatial rotation is the Thomas precession.) The 'rest-frame' spin $\boldsymbol{s}$ is not well-defined unless we insist that the Lorentz transformation from the lab frame to the particle rest frame be accomplished by a single boost.

At an infinitesimal time $t = \mathrm{d}t$ later, the particle will rotate through an angle

$$\mathrm{d}\boldsymbol{\alpha} = \frac{\boldsymbol{\beta} \times \mathrm{d}\boldsymbol{\beta}}{\beta^2} = \frac{\boldsymbol{\beta} \times \dot{\boldsymbol{\beta}}}{\beta^2}\,\mathrm{d}t. \tag{5.68}$$

This is a kinematic effect. For motion in prescribed external electric and magnetic fields, we have

$$\frac{\boldsymbol{\beta} \times \dot{\boldsymbol{\beta}}}{\beta^2} = -\frac{e}{mc\gamma}\left[\boldsymbol{B}_\perp - \frac{\boldsymbol{\beta} \times \boldsymbol{E}}{\beta^2}\right]. \tag{5.69}$$

We write

$$\boldsymbol{B}_\parallel = \frac{\boldsymbol{B} \cdot \boldsymbol{\beta}\boldsymbol{\beta}}{\beta^2}, \qquad \boldsymbol{B}_\perp = \boldsymbol{B} - \boldsymbol{B}_\perp = \frac{\boldsymbol{\beta} \times (\boldsymbol{B} \times \boldsymbol{\beta})}{\beta^2}, \tag{5.70}$$

to denote the components of the magnetic field parallel and perpendicular to the velocity $\boldsymbol{v}$, respectively. Under a Lorentz boost, with the relativistic factor γ from the lab frame to the moving frames at $t = 0$, we find

$$\boldsymbol{B}_C = \gamma\,[\boldsymbol{B}_\perp - \boldsymbol{\beta} \times \boldsymbol{E}] + \boldsymbol{B}_\parallel. \tag{5.71}$$

The spin changes in the proper time interval $\mathrm{d}\tau = \mathrm{d}t/\gamma$ according to (5.65), by

$$(\mathrm{d}\boldsymbol{s})_I = -\frac{ge}{mc}\,\boldsymbol{B}_C \times \boldsymbol{s}\,\mathrm{d}\tau. \tag{5.72}$$

To find the change in the rest frame, we have to note that the 'C' frame itself rotates relative to the inertial frame, through an angle $\mathrm{d}\phi$. Subtracting this rotation we get,

$$\mathrm{d}\boldsymbol{s} = (\mathrm{d}\boldsymbol{s})_I - \mathrm{d}\boldsymbol{\phi} \times \boldsymbol{s}. \tag{5.73}$$

The angle $\mathrm{d}\phi$ can be found as follows. First, at time $\mathrm{d}t$ the 'old' rest frame (at $t = 0$) is oriented at an angle $-\mathrm{d}\boldsymbol{\alpha}$ relative to the new velocity $\boldsymbol{v} + \mathrm{d}\boldsymbol{v}$. Second, in the moving inertial

Table 2. Magnetic moment anomalies of particles referenced in this paper. The value for the muon is taken from Bennett *et al* (2004). The mass in MeV and the energy spacing of imperfection resonances is also shown.

Symbol	Anomaly $a = \frac{1}{2}(g-2)$	Accuracy	Mass (MeV)	$\Delta E = mc^2/a$ (MeV)
$e^{\pm}$	$1.159\,652\,1859 \times 10^{-3}$	$\pm 3.8 \times 10^{-12}$	510.9989×10^{-3}	440.65
$\mu^{\pm}$	$1.165\,9208 \times 10^{-3}$	$\pm 6.0 \times 10^{-7}$	105.658	90 622.24
p	1.792 847 351	$\pm 2.8 \times 10^{-8}$	938.272	523.34
d	−0.142 9878	$\pm 5.0 \times 10^{-7}$	1875.613	13 117.30

frame, both these directions are rotating (same as the 'new' velocity) γ times faster than in the laboratory frame. Hence,

$$\mathrm{d}\phi = \gamma \mathrm{d}\boldsymbol{\alpha} - \mathrm{d}\boldsymbol{\alpha} = (\gamma - 1)\mathrm{d}\boldsymbol{\alpha}. \tag{5.74}$$

Thus, we obtain

$$\mathrm{d}\boldsymbol{s} = \left[-\frac{e}{mc\gamma}\boldsymbol{B}_C \times \boldsymbol{s} - \frac{\gamma - 1}{\beta^2}(\boldsymbol{\beta} \times \dot{\boldsymbol{\beta}}) \times \boldsymbol{s}\right]\mathrm{d}t. \tag{5.75}$$

We can write this in the form:

$$\frac{\mathrm{d}\boldsymbol{s}}{\mathrm{d}t} = \boldsymbol{\Omega} \times \boldsymbol{s}. \tag{5.76}$$

The spin precession vector $\boldsymbol{\Omega}$ is given by

$$\boldsymbol{\Omega} = -\boldsymbol{\mu} \cdot \frac{\boldsymbol{B}_C}{\gamma} + \boldsymbol{\omega}_{\mathrm{T}}, \tag{5.77}$$

where the Thomas precession vector $\boldsymbol{\omega}_{\mathrm{T}}$ is given by

$$\boldsymbol{\omega}_{\mathrm{T}} = -\frac{\gamma - 1}{\beta^2}\boldsymbol{\beta} \times \dot{\boldsymbol{\beta}} = -\frac{\gamma^2}{\gamma + 1}\boldsymbol{\beta} \times \dot{\boldsymbol{\beta}}. \tag{5.78}$$

In terms of a Hamiltonian, we have

$$H = -\boldsymbol{\mu} \cdot \frac{\boldsymbol{B}_C}{\gamma} + \boldsymbol{\omega}_{\mathrm{T}} \cdot \boldsymbol{s}. \tag{5.79}$$

The spin precession vector, or the Hamiltonian, contains two terms. The first is a magnetic dipole interaction with the rest-frame magnetic field, time-dilated by a factor γ, and the second is Thomas precession (Thomas 1927) due to the relativistic kinematics. Note that the Thomas precession term is *independent* of the electric and magnetic fields. It would exist even if the acceleration $\dot{\boldsymbol{v}}$ were due to gravitation or other non-electromagnetic causes. It is only that in the cases of interest to us, the acceleration is also electromagnetic in origin, given by the Lorentz force.

We note in passing, that the above form of the Hamiltonian is valid also for neutral particles possessing a magnetic moment, e.g. neutrons. One works directly with the magnetic moment $\boldsymbol{\mu}$ and does not introduce an electric charge, etc. (However, one can use g in conjunction with a Bohr magneton or a nuclear magneton.) For charged particles, by substitution of the expressions for the various terms, we obtain

$$\boldsymbol{\Omega} = -\frac{e}{mc}\left[\left(a + \frac{1}{\gamma}\right)\boldsymbol{B}_{\perp} + \frac{1+a}{\gamma}\boldsymbol{B}_{\parallel} - \left(a + \frac{1}{\gamma+1}\right)\boldsymbol{\beta} \times \boldsymbol{E}\right]. \tag{5.80}$$

Here, we have decomposed g into a sum of 'normal' and 'anomalous' parts, namely, $g = 2(1+a)$, where a is called the *magnetic moment anomaly*. The values of the magnetic moment anomalies of the various particles we treat in this review are shown in table 2. The table also

shows the particle mass and the energy spacing of the so-called 'imperfection resonances' (to be defined later in this paper).

We have expressed the fields in terms of components parallel and perpendicular to the velocity vector. This is a very useful form and we shall make heavy use of it below. An equivalent expression that is also commonly used, and which does not decompose the fields into components, is

$$\boldsymbol{\Omega} = -\frac{e}{mc}\left[\left(a + \frac{1}{\gamma}\right)\boldsymbol{B} - \frac{a\gamma}{\gamma+1}\boldsymbol{\beta}\cdot\boldsymbol{B}\boldsymbol{\beta} - \left(a + \frac{1}{\gamma+1}\right)\boldsymbol{\beta}\times\boldsymbol{E}\right]. \tag{5.81}$$

Before proceeding further, we analyse some of the salient features of the above expressions.

(a) The first and most important point to note is that $\boldsymbol{s}$ is expressed in the *rest frame*, whereas $\boldsymbol{E}$ and $\boldsymbol{B}$ are the fields in the *laboratory frame*. This is a deliberate choice. The spin is an intrinsic property of the particle, and is only truly meaningful in the particle rest frame.

(b) The anomalous part of the magnetic moment couples differently to the electric and magnetic fields than do the other terms. This is a fact of utmost significance, and underlies almost all of the spin manipulations we treat in this paper. This lack of symmetry in the coupling is due to the fact that the anomalous magnetic moment couples only to the rest-frame magnetic field (see (5.79)). The contribution of the normal magnetic dipole moment is mixed with the contribution from the Thomas precession.

(c) *Wien filter:* an important special case is that of a uniform magnetic field and an orthogonal electric field, such that the Lorentz force vanishes: $\boldsymbol{E} + \boldsymbol{\beta}\times\boldsymbol{B} = 0$. For simplicity, suppose that $(\boldsymbol{E}, \boldsymbol{B}, \boldsymbol{\beta})$ form an orthogonal triad: the velocity is orthogonal to both the electric and magnetic fields. Then the acceleration of the particle vanishes: $\dot{\boldsymbol{\beta}} = 0$, and so the Thomas precession vanishes: the particle travels in a straight line, so all the Lorentz boosts commute. The Hamiltonian and spin precession vector are then, simply

$$H = -\boldsymbol{\mu}\cdot\frac{\boldsymbol{B}_C}{\gamma}, \qquad \boldsymbol{\Omega} = -\frac{ge}{mc}(\boldsymbol{B} - \boldsymbol{\beta}\times\boldsymbol{E}) = -\frac{ge}{\gamma^2 mc}\boldsymbol{B}. \tag{5.82}$$

Hence, the orbit moves in a straight line, but the spin precesses around the magnetic field. Such a device is called a Wien filter, and can be used to rotate the spin relative to the particle momentum. The effectiveness of a Wien filter falls off rapidly with energy because of the factor of γ^2 in the denominator. It is also astigmatic because it focuses the orbital motion, but in only one plane.

(d) From (5.80), we see that for longitudinal and transverse magnetic fields of equal magnitude, the ratio of the effect on the spin precession due to the transverse and longitudinal magnetic fields is $(a\gamma + 1)/(a + 1)$. The value of $a\gamma$ greatly exceeds unity at the operating energies of most modern high-energy particle accelerators. Even in accelerators of a few GeV energy, $a\gamma \simeq 2$–5, while $a\gamma \simeq 62.5$ in HERA at 27.5 GeV, and $G\gamma \simeq 200$ in RHIC at 100 GeV. Recall, that for protons it is conventional to write $G = (g-2)/2$. Hence, transverse magnetic fields have a greater effect on the spin precession than do longitudinal magnetic fields. The ratio increases proportionately with energy.

(e) In the important case of a uniform vertical magnetic field with *no* electric field, the orbital revolution frequency for horizontal circular motion is

$$\boldsymbol{\omega}_{\text{rev}} = -\frac{e}{\gamma mc}\boldsymbol{B}, \tag{5.83}$$

whereas the spin precession frequency is

$$\boldsymbol{\Omega} = -\frac{e}{mc}\left(a + \frac{1}{\gamma}\right)\boldsymbol{B} = (a\gamma + 1)\,\boldsymbol{\omega}_{\text{rev}}. \tag{5.84}$$

The ratio of the spin precession frequency to the orbital revolution frequency is called the *spin tune* (we shall make this expression more precise later, for motion on off-axis trajectories). For a planar ring, the value of the spin tune is

$$\nu_{\rm spin} = a\gamma. \tag{5.85}$$

We subtract unity because in the 'accelerator frame', the spin precession is measured relative to the orbit, hence $\nu_{\rm spin} = (\Omega - \omega_{\rm rev})/\omega_{\rm rev}$. Equation (5.85) is, simultaneously, the simplest and most important equation in all of the spin manipulations we shall encounter. Its consequences are profound, and will be seen throughout this paper. We note for future reference, that setting $\Delta(a\gamma) = 1$, i.e. $\Delta E = mc^2/a$, we have (see table 2)

$$(\Delta E)_e \simeq 440.65\,\text{MeV}, \qquad (\Delta E)_p \simeq 523.34\,\text{MeV}. \tag{5.86}$$

Hence, $a\gamma$ or $G\gamma$ increases by one unit for an increase in the beam energy of 0.44 GeV (electrons), or 0.523 GeV (protons). The condition $a\gamma \gg 1$, or $G\gamma \gg 1$ is therefore satisfied by most accelerators, though not all. AmPS, SHR and VEPP-2M operate(d) at around $a\gamma = 1$–2 and the IUCF Cooler ran at $G\gamma \simeq 2$. LEP operated at $a\gamma = 100$–200, while RHIC at top energy will operate at $G\gamma \simeq 450$.

5.12. Resonant depolarization

We interrupt the order of presentation to describe a very important experimental technique. We shall present the derivation of the spin precession using a covariant formulation later. First, however, we now have enough information to understand the supremely important experimental technique of *resonant depolarization*. The use of resonant depolarizers (and also spin-flippers, to be discussed in section 6), helps to exclude systematic errors from experiments with polarized beams. Resonant depolarization also furnishes the most accurate method of calibrating the beam energy in storage rings, and has been utilized with success at many accelerators (see section 30 for precision tests of the Standard Model, etc). These possibilities for resonant depolarization were recognized very early at BINP in 1968, with the development of rf depolarizers (see Baier (1972)).

The basic idea of resonant depolarization is as follows. We saw above, that in a planar ring the value of the spin tune is $\nu_{\rm spin} = a\gamma$. Since the values of a_{e^+} and a_{e^-} are known to great accuracy, by measuring the spin tune, one can deduce the value of γ to a high precision. From a knowledge of the electron mass, one can then calibrate the beam energy to high accuracy.

As a matter of fact, the value of the proton magnetic moment anomaly (or that of many other hadrons) is also known to considerable precision. Hence, resonant depolarization also works in hadron storage rings. The machine must, however, be a storage ring (where the beam energy is fixed), and not a synchrotron, where the beam energy is changing rapidly, because otherwise the value of $a\gamma$ is not constant.

Whether for leptons or hadrons, a radio-frequency magnetic field is applied in the horizontal plane to kick the spins. The kick frequency is aliased with a multiple of the orbital revolution frequency f_c. The frequency for the kicks to act coherently on the spins is one of the two possibilities,

$$f_{\rm rf}^{+} = (a\gamma - k)\, f_c, \qquad f_{\rm rf}^{-} = (k - a\gamma)\, f_c, \tag{5.87}$$

where k is an integer. Although the kick to a spin on an individual pass around the ring is small, when the kicker frequency is close to the resonant frequency (after including aliasing with the revolution frequency), the kicks add up coherently, and the cumulative effect of the kicks is to tilt the spins strongly away from the vertical. The spins decohere, leading to depolarization. We shall treat decoherence mechanisms quantitatively in section 21. The frequency of the

kicker $f_{\rm rf}$ is swept across the resonant value, and the centre of the dip in the polarization is identified. This can generally be done with great accuracy. Note, that if the beam has an rms energy spread σ_E, then this results in a spread of spin tunes $\sigma_\nu = \sigma_E/(mc^2/a)$. However, in the experiment, we measure the spin tune averaged over time (all phases of the synchrotron oscillations) hence, the final accuracy is much higher than the momentum-induced spread of the spin tune. The kicker field can be either longitudinal, i.e. an rf solenoid, or transverse, i.e. a magnetic dipole rf kicker. Both air-core and ferrite-core kickers have been used. It is not always necessary to build a special device; for example, it is possible to feed a high-frequency sinusiodal signal from a signal generator into a stripline kicker normally used for other purposes (betatron tune measurements). The precise engineering details do not matter to the principle of operation.

Complications can arise from the synchrotron oscillations. From (3.3), there can be multiple 'synchrotron sideband' resonances, so that depolarization can occur at any of the frequencies

$$f_{\rm rf}^{+} = (a\gamma - k - mQ_s)\, f_{\rm c}, \qquad f_{\rm rf}^{-} = (k + mQ_s - a\gamma)\, f_{\rm c}, \tag{5.88}$$

where m is an integer. One must therefore be careful to verify that the depolarization is due to the central resonance $m = 0$. This can be done by varying the synchrotron tune: the frequency of the resonance should not change. Such complications were already known in the early work on resonant depolarization: Serednyakov *et al* (1976) employed a depolarizer and observed depolarization from the parent, and $m = \pm 1$ synchrotron sideband resonances at VEPP-2M. See figure 61 later in this paper, for a graph of frequency sweeps and depolarization from the parent resonance and $m = -1$ synchrotron sideband at the SLS. Additional discussions of the complications from synchrotron sidebands will be presented in section 6. Synchrotron sideband resonances will be studied in detail in section 20.

Note that nonplanarities, e.g. the presence of longitudinal magnetic fields, can induce systematic errors in the energy calibration measurement. For example, most high energy e^+e^- colliders are equipped with detector solenoids. The solenoid magnetic fields must either be compensated or switched off.

5.13. Spin precession equation: covariant derivation

Bargmann *et al*'s (1959) covariant formulation is the better-known derivation of the spin precession equation. We denote four-vectors by uppercase letters below. Our metric is $g^{\mu\nu} = \mathrm{diag}(1, -1, -1, -1)$, i.e. a timelike separation is positive. Our derivation follows Bargmann *et al* (1959). It is first necessary to generalize the spin $\boldsymbol{s}$ which is defined only in the particle rest frame. We denote the lab frame by K, and an 'instantaneous rest frame', i.e. an inertial reference frame instantaneously comoving with the particle, by K'. We seek a four-vector $S = (S^0, \boldsymbol{S})$ in the lab frame which reduces to $(0, \boldsymbol{s})$ in the instantaneous rest frame. The velocity four-vector $U = \gamma(c, \boldsymbol{v})$ equals $(c, 0)$ in the rest frame. The vanishing of the time component of S in the instantaneous rest frame is therefore guaranteed by imposing the covariant constraint

$$U \cdot S = 0. \tag{5.89}$$

In the inertial frame K, the time component of the spin four-vector is therefore, not independent, but is related to the space components via $U \cdot S = cS^0 - \boldsymbol{v} \cdot \boldsymbol{S} = 0$, or

$$S^0 = \boldsymbol{\beta} \cdot \boldsymbol{S}. \tag{5.90}$$

We know that the nonrelativistic spin precession equation is

$$\frac{\mathrm{d}\boldsymbol{s}}{\mathrm{d}t} = \frac{ge}{2mc}\, \boldsymbol{s} \times \boldsymbol{B}', \tag{5.91}$$

where the prime denotes evaluation in the rest frame. The time derivative of the spin four-vector must generalize to $\mathrm{d}S/\mathrm{d}\tau$, where τ is the particle's proper time. We demand that the relativistic equation also be linear in the spin four-vector S^α, and the external fields, specified by the electromagnetic four-tensor $F^{\alpha\beta}$, given by

$$F = \begin{pmatrix} 0 & -E_1 & -E_2 & -E_3 \\ E_1 & 0 & -B_3 & B_2 \\ E_2 & B_3 & 0 & -B_1 \\ E_3 & -B_2 & B_1 & 0 \end{pmatrix}. \tag{5.92}$$

We also note that although S^0 vanishes in the instantaneous rest frame, the derivative $\mathrm{d}S^0/\mathrm{d}\tau$ need not vanish. In fact, from (5.90) one has, in the instantaneous rest frame,

$$\frac{\mathrm{d}S^0}{\mathrm{d}\tau} = \boldsymbol{S} \cdot \frac{\mathrm{d}\boldsymbol{\beta}}{\mathrm{d}\tau}. \tag{5.93}$$

The relativistic generalization of (5.91) and (5.93) is

$$\frac{\mathrm{d}S}{\mathrm{d}\tau} = \frac{ge}{2mc}[F \cdot S + (S \cdot F \cdot U)U] - \left(\frac{\mathrm{d}U}{\mathrm{d}\tau} \cdot S\right) U. \tag{5.94}$$

This is a covariant equation by construction, and one can verify that it reduces to the desired result (5.91) by evaluation in the instantaneous rest frame.

If the external electric and magnetic fields $\boldsymbol{E}$ and $\boldsymbol{B}$ are spatially homogeneous (or if Stern–Gerlach forces like $\boldsymbol{\nabla}(\boldsymbol{\mu} \cdot \boldsymbol{B})$ can be neglected) then one can prove that

$$\frac{\mathrm{d}U}{\mathrm{d}\tau} = \frac{e}{mc} F \cdot U. \tag{5.95}$$

Then one obtains the BMT equation (for the four-vector S),

$$\frac{\mathrm{d}S}{\mathrm{d}\tau} = \frac{e}{mc}\left[\frac{g}{2} F \cdot S + \left(\frac{g}{2} - 1\right)(S \cdot F \cdot U)U\right]. \tag{5.96}$$

One can derive that the relation between $\boldsymbol{S}$ and $\boldsymbol{s}$ is

$$s = \boldsymbol{S} - \frac{\gamma}{\gamma + 1} \beta \cdot \boldsymbol{S}\beta \tag{5.97}$$

and the inverse

$$\boldsymbol{S} = \boldsymbol{s} + \frac{\gamma^2}{\gamma + 1} \boldsymbol{\beta} \cdot \boldsymbol{s}\boldsymbol{\beta}, \qquad S^0 = \gamma \boldsymbol{\beta} \cdot \boldsymbol{s}. \tag{5.98}$$

The relativistic spin precession equation for $\boldsymbol{s}$ is

$$\frac{\mathrm{d}\boldsymbol{s}}{\mathrm{d}t} = -\frac{e}{mc}\left[\left(a + \frac{1}{\gamma}\right)\boldsymbol{B} - \frac{a\gamma}{\gamma + 1} \boldsymbol{\beta} \cdot \boldsymbol{B}\boldsymbol{\beta} - \left(a + \frac{1}{\gamma + 1}\right)\boldsymbol{\beta} \times \boldsymbol{E}\right] \times \boldsymbol{s}, \tag{5.99}$$

in agreement with (5.76) and (5.81).

We make some observations on both the Thomas and BMT derivations.

- Although we did not say so in the previous derivation using Lorentz transforms, but in order to carry through the derivation as presented, the electric and magnetic fields must be spatially homogeneous. At the very least, as pointed out above, Stern–Gerlach type gradient forces must be negligible. Otherwise, the acceleration (or change to the orbital trajectory) is not correctly given by the above equations. We tacitly assumed in the Lorentz boosts, etc, that the orbit was not affected by the spin. In practice, the spin precession equation works well in the external electric and magnetic fields encountered in typical modern day accelerators. The spatial variation of the magnetic field in a quadrupole, for example, is not sufficiently steep to invalidate the equation.

- We shall later use this same spin precession equation (or the corresponding Hamiltonian) to calculate the spin-flip photon emission probabilities per unit time, in the semiclassical approximation. The electric and magnetic fields will be photon radiation fields. They can hardly be considered either spatially or temporally homogeneous, yet we shall correctly reproduce the results of calculations based on the Dirac equation for radiative polarization in a planar ring (the Sokolov–Ternov formula). Hence, the equation does work over a large domain of field configurations, provided only that the spin motion does not react back on the orbit.

We close this section with a few remarks on work by other authors. The following statements are by no means intended to be a comprehensive historical review. The BMT derivation of the spin precession equation is by far the most popular, and the equation is most commonly referred to in the literature as the 'BMT equation'. We shall call it the Thomas–BMT equation in this paper. Certainly, the kinematical term in the spin precession is universally acknowledged as 'Thomas precession'. Thomas (1927) himself pointed out, in a note added in the proof of his paper, that shortly after submission of his paper, a similar equation and kinematical conditions were published by Frenkel (1926), who analysed the Zeeman effect and multiplet structure in atoms. Frenkel represented the spin by an antisymmetric four-tensor $S^{\alpha\beta}$, where S^{00}, $S^{0\beta}$ and $S^{\alpha 0}$ vanish in the rest frame. The above mentioned authors all derived a classical spin precession equation valid for arbitrary values of the quantum spin operator. However, special cases have been treated by a number of other authors. Equations for spin $\frac{1}{2}$ were considered by Tolhoek and Groot (1951), Mendlowitz and Case (1955a, 1955b) and Carrassi (1958). The problem was also studied by Kramers (1958), who showed that for a particular choice of the equation of motion, one is led to conclude that the gyromagnetic ratio for a classical particle is the same as the Dirac value for an electron, i.e. $g = 2$. This is a curious conclusion which is now known to be erroneous. Weak points in Kramers' arguments were pointed out by Bargmann *et al* (1959). The use of a four-vector to represent the intrinsic angular momentum, or polarization, was first introduced by Michel and Wightman (1955). An excellent overview of the classical spin precession equation, mentioning the connection to Ehrenfest's theorem, is given by Ford and Hirt (1961). Their report is regrettably unpublished. They show that the two formalisms based on the use of an antisymmetric four-tensor and a four-vector representation of the spin, are equivalent. Fort and Hirt also derive a covariant classical equation of motion including a possible nonzero *electric* dipole moment (EDM). We shall study briefly the EDMs later in this paper; the relevant equation of motion will be presented there. As we have already stated, the above spin precession equation was derived under the assumption that derivatives of the fields are negligible. Good (1961) derived a classical spin precession including also first-order field gradients (spatial derivatives) in the external electric and magnetic fields. (It is assumed that terms of second degree are negligible.) The equation was motivated by the analysis of a composite particle, specifically, a nucleus in its ground state. Good showed that the electric quadrupole moment must also be taken into account. The internal variables of the composite particle are eliminated, leading to coupled differential equations for the position, and intrinsic angular momentum of the composite particle.

5.14. Precession of the longitudinal spin component

Of particular interest is the equation of motion for the precession of the *longitudinal* spin component $s_\parallel = \boldsymbol{s} \cdot \hat{\boldsymbol{\beta}}$. From standard relativity theory and the Lorentz equation,

$$\frac{\mathrm{d}\hat{\boldsymbol{\beta}}}{\mathrm{d}t} = -\frac{e}{mc\beta\gamma}\,\hat{\boldsymbol{\beta}} \times (\hat{\boldsymbol{\beta}} \times \boldsymbol{E} - \beta\,\boldsymbol{B}). \tag{5.100}$$

Then

$$\begin{aligned}\frac{\mathrm{d}(\boldsymbol{s}\cdot\hat{\boldsymbol{\beta}})}{\mathrm{d}t} &= \frac{\mathrm{d}\boldsymbol{s}}{\mathrm{d}t}\cdot\hat{\boldsymbol{\beta}} + \boldsymbol{s}\cdot\frac{\mathrm{d}\hat{\boldsymbol{\beta}}}{\mathrm{d}t} \\ &= (\boldsymbol{\Omega}\times\boldsymbol{s})\cdot\hat{\boldsymbol{\beta}} - \frac{e}{mc\beta\gamma}[\hat{\boldsymbol{\beta}}\times(\hat{\boldsymbol{\beta}}\times\boldsymbol{E} - \beta\boldsymbol{B})]\cdot\boldsymbol{s} \\ &\equiv \boldsymbol{\Omega}_{\mathrm{long}}\cdot(\boldsymbol{s}\times\hat{\boldsymbol{\beta}}). \end{aligned} \tag{5.101}$$

Some algebra yields

$$\boldsymbol{\Omega}_{\mathrm{long}} = -\frac{e}{mc}\Big[a\,\boldsymbol{B} - \Big(a - \frac{1}{\beta^2\gamma^2}\Big)\boldsymbol{\beta}\times\boldsymbol{E}\Big]. \tag{5.102}$$

The precession frequency of the longitudinal spin component is $|\boldsymbol{\Omega}_{\mathrm{long}}|$. Equation (5.102) has important consequences for the operation of experiments to measure the anomalous magnetic moment of muons, as will be reviewed in section 11.

6. Froissart–Stora formula

6.1. General remarks

By 'nonradiative polarization', we mean the acceleration and storage of spin-polarized charged particle beams which do not emit sufficient synchrotron radiation to polarize the beam spontaneously. Muon storage rings are a special case of nonradiative polarization where, additionally, the particles also decay in flight. They will be treated separately. Here we assume that the particles are stable.

Radiative polarization places great restrictions on the accelerator: not even all electron and positron storage rings qualify, because the polarization buildup time may be much longer than the beam storage time. Nonradiative polarization, by contrast, includes a much greater variety of particle species and experimental usage. RHIC, for example, operates as a polarized proton collider. The ZGS delivered (polarized and unpolarized) proton and deuteron beams to external beamlines for fixed-target experiments. ELSA delivers polarized electron beams to external targets. AmPS and SHR circulate(d) nonradiatively polarized electron beams for use with internal targets. SATURNE-II accelerated polarized protons, deuterons and ^{6}Li. The list goes on. The majority of the particle beams which fall into the category of nonradiatively polarized beams are, however, polarized protons.

Broadly speaking, the subject of nonradiative polarization divides into two areas: acceleration of a spin-polarized beam from low to high energy in an accelerator, and long-term storage of a nonradiatively polarized beam. The two topics are not mutually exclusive, as acceleration of a spin-polarized beam from low to high energy may first be required before the beam is stored at the final top energy, e.g. at RHIC. This section treats the first of the above two topics, namely, acceleration (which means 'increase of energy', as opposed to its true meaning as a rate of change of a velocity vector). 'Acceleration' can also mean *de*celeration. The literature on the subject was historically motivated by the acceleration of polarized proton beams, hence, we mainly write $G = (g-2)/2$ below.

6.2. Basic formalism

We treat only rings whose design is planar. The actual closed orbit will contain imperfections, and will not be planar, but the *ideal* paper-design machine will have no spin rotators, etc. The reason for this is simple: the majority of accelerators are planar, and the research developed

accordingly. We discuss later, the application of some of these ideas to a ring with one or a pair of Snakes.

Since the ring is assumed planar by design, the particle spins precess around the vertical axis for orbital motion on the ideal design orbit, i.e. in the absence of any perturbing terms. The principal perturbation to the spin precession comes from *horizontal* magnetic fields, due to the off-axis orbital motion. We employ the classical spin model throughout the calculations below. The polarization vector $\boldsymbol{P}$ is obtained by averaging over all the particle spins $\boldsymbol{s}$, i.e. $\boldsymbol{P} = \langle \boldsymbol{s} \rangle$. In keeping with the standard practice in the field, we shall employ the spinor representation, where $\boldsymbol{s} = \langle \Psi | \boldsymbol{\sigma} | \Psi \rangle$, and $\boldsymbol{\sigma}$ is a vector of Pauli matrices. The independent variable is θ, the generalized azimuth around the ring. Dropping the bracket notation, the equation of motion for Ψ is

$$\frac{\mathrm{d}\Psi}{\mathrm{d}\theta} = -\frac{\mathrm{i}}{2}\, \boldsymbol{W} \cdot \boldsymbol{\sigma}\, \Psi = -\mathrm{i}\, \mathcal{H}\, \Psi, \tag{6.1}$$

where $\boldsymbol{W}$ is the spin precession vector, and where we have employed a Hamiltonian $\mathcal{H} = \frac{1}{2}\boldsymbol{W}\cdot\boldsymbol{\sigma}$. We now divide $\boldsymbol{W}$ into unperturbed and perturbation terms $\boldsymbol{W} = \boldsymbol{W}_0 + \boldsymbol{w}$, where $\boldsymbol{W}_0$ describes motion on the design orbit, and $\boldsymbol{w}$ consists of the (horizontal) perturbing fields. We know that for a planar ring $\boldsymbol{W}_0 = \nu_0\, \boldsymbol{e}_3$ where $\nu_0 = G\gamma_0$, where γ_0 is the Lorentz factor of the reference particle. We discuss the perturbation $\boldsymbol{w}$ later. To begin with, we neglect the energy spread of the beam, so all the particles precess around the vertical axis at the same rate ν_0. Since the beam is being accelerated, the energy of the reference particle increases with θ. We assume that the rate of increase of the beam energy is uniform. Hence ν_0 is not constant, but rather

$$\frac{\mathrm{d}\nu_0}{\mathrm{d}\theta} = \alpha, \tag{6.2}$$

where α is constant, i.e. independent of θ and also of the particle oscillation amplitude, etc. It should not be confused with the electromagnetic fine-structure constant, because there is no quantum electrodynamic perturbation theory below. Hence,

$$\nu_0 = \nu_{00} + \alpha\theta, \tag{6.3}$$

where ν_{00} is a constant which will be specified when solving the model below. We can then write $\mathcal{H} = \mathcal{H}_0 + \mathcal{H}_1$, where

$$\mathcal{H}_0 = \tfrac{1}{2}\, \boldsymbol{W}_0 \cdot \boldsymbol{\sigma} = \tfrac{1}{2}\, \nu_0\, \sigma_3, \qquad \mathcal{H}_1 = \tfrac{1}{2}\, \boldsymbol{w} \cdot \boldsymbol{\sigma} = \tfrac{1}{2}(w_1\sigma_1 + w_2\sigma_2), \tag{6.4}$$

where $w_1 = \boldsymbol{w} \cdot \boldsymbol{e}_1$ and $w_2 = \boldsymbol{w} \cdot \boldsymbol{e}_2$. Hence,

$$\frac{\mathrm{d}\Psi}{\mathrm{d}\theta} = -\frac{\mathrm{i}}{2} \begin{pmatrix} \nu_0 & w_1 - \mathrm{i}w_2 \\ w_1 + \mathrm{i}w_2 & -\nu_0 \end{pmatrix} \Psi. \tag{6.5}$$

The next step is to transform to the 'interaction picture' by defining a new spinor,

$$\Psi_{\mathrm{I}} = \mathrm{e}^{\mathrm{i}\int_0^\theta \mathcal{H}_0\, \mathrm{d}\theta'}\, \Psi = \mathrm{e}^{(\mathrm{i}/2)[\nu_{00}\theta + (1/2)\alpha\theta^2]\sigma_3}\, \Psi. \tag{6.6}$$

Substituting into (6.5), the equation of motion for Ψ_{I} has only off-diagonal terms. Defining

$$m_{21} = (w_1 + \mathrm{i}w_2)\, \mathrm{e}^{-\mathrm{i}[\nu_{00}\theta + (1/2)\alpha\theta^2]}, \tag{6.7}$$

yields

$$\frac{\mathrm{d}\Psi_{\mathrm{I}}}{\mathrm{d}\theta} = -\frac{\mathrm{i}}{2} \begin{pmatrix} 0 & m_{21}^* \\ m_{21} & 0 \end{pmatrix} \Psi_{\mathrm{I}}. \tag{6.8}$$

The standard next step is to expand $w_1 + \mathrm{i}w_2$ in Fourier harmonics.

6.3. *Froissart–Stora formula*

Froissart and Stora (1960) found the exact analytical solution for the depolarization of a spin-polarized beam caused by the crossing of a *single* resonance driving term, i.e. only one Fourier harmonic in the perturbing Hamiltonian. Effectively, the Froissart–Stora formula assumes that the depolarizing resonances are narrow and well-separated. Hence the beam crosses only *one* resonance at a time. This approximation is not always true in practice, and much effort has been expended on finding theoretical formulae to do a better job.

By hypothesis, the beam is initially fully polarized along the vertical axis: $P_\mathrm{i} = P(-\infty) = 1$. The accelerator energy increases at a steady rate, and the spins of the particles are tilted away from the vertical by the horizontal perturbing fields. Far from resonance, on the other side, the spins again precess around the vertical axis. We seek the final asymptotic polarization:

$$P_\mathrm{f} = P(\infty) = \langle s_3 \rangle_{\theta\to\infty}. \tag{6.9}$$

The average is over the particles in the beam. Hence, starting from $s_3(\theta \to -\infty) = 1$, we wish to evaluate $s_3(\theta \to \infty)$. Now the transformation to the interaction picture does not affect the vertical component of $\boldsymbol{s}$:

$$s_3 = \langle \Psi \,|\, \sigma_3 \,|\, \Psi \rangle = \langle \Psi_\mathrm{I} \,|\, \sigma_3 \,|\, \Psi_\mathrm{I} \rangle. \tag{6.10}$$

Hence, we can obtain s_3, thence $\langle s_3 \rangle$, i.e. P_f, directly from the spinor Ψ_I. We can, thus, work exclusively with the interaction picture.

The perturbation contains only one Fourier harmonic:

$$w_1 + \mathrm{i}w_2 = \epsilon\, \mathrm{e}^{\mathrm{i}\phi}, \tag{6.11}$$

where ϵ is the magnitude of the resonance driving term (assumed invariant), and the rate of change of the phase ϕ is

$$\frac{\mathrm{d}\phi}{\mathrm{d}\theta} = Q, \tag{6.12}$$

i.e. $\phi = \phi_0 + Q\theta$, where Q is also a fixed parameter, basically the dimensionless precession frequency of the perturbing term. Evidently ϕ_0 is an initial phase. The beam could, of course, have a spread of values for both ϵ, Q and especially ϕ_0. These are again complications which will be ignored below. Proceeding with the solution,

$$m_{21} = \epsilon\, \mathrm{e}^{\mathrm{i}\phi_0}\, \mathrm{e}^{-\mathrm{i}[\nu_{00}\theta + (1/2)\alpha\theta^2]}\, \mathrm{e}^{\mathrm{i}Q\theta}. \tag{6.13}$$

We set the constant $\nu_{00} = Q$ in the above expression, i.e. we choose the origin of θ to be at the point of crossing the resonant tune. Then,

$$m_{21} = \epsilon\, \mathrm{e}^{\mathrm{i}\phi_0} \mathrm{e}^{-\mathrm{i}\alpha\theta^2/2}. \tag{6.14}$$

Define $\bar{\epsilon} = \epsilon\, \mathrm{e}^{\mathrm{i}\phi_0}$, then,

$$\frac{\mathrm{d}\Psi_\mathrm{I}}{\mathrm{d}\theta} = -\frac{\mathrm{i}}{2} \begin{pmatrix} 0 & \bar{\epsilon}^*\, \mathrm{e}^{\mathrm{i}\alpha\theta^2/2} \\ \bar{\epsilon}\, \mathrm{e}^{-\mathrm{i}\alpha\theta^2/2} & 0 \end{pmatrix} \Psi_\mathrm{I}. \tag{6.15}$$

Froissart and Stora succeeded in solving this equation for Ψ_I. Write

$$\Psi_\mathrm{I} = \begin{pmatrix} \Psi_+ \\ \Psi_- \end{pmatrix} \tag{6.16}$$

with the normalization $|\Psi_+|^2 + |\Psi_-|^2 = 1$. This yields a pair of coupled ordinary differential equations, namely,

$$\frac{\mathrm{d}\Psi_+}{\mathrm{d}\theta} = -\frac{\mathrm{i}}{2}\, \bar{\epsilon}^*\, \mathrm{e}^{\mathrm{i}\alpha\theta^2/2}\, \Psi_-, \qquad \frac{\mathrm{d}\Psi_-}{\mathrm{d}\theta} = -\frac{\mathrm{i}}{2}\, \bar{\epsilon}\, \mathrm{e}^{-\mathrm{i}\alpha\theta^2/2}\, \Psi_+. \tag{6.17}$$

Eliminating Ψ_+ yields

$$\frac{\mathrm{d}^2\Psi_-}{\mathrm{d}\theta^2} + \mathrm{i}\alpha\theta\frac{\mathrm{d}\Psi_-}{\mathrm{d}\theta} + \frac{\epsilon^2}{4}\Psi_- = 0. \tag{6.18}$$

We now change variables to $z = -\mathrm{i}\alpha\theta^2/2$. This yields the equation,

$$z^2\frac{\mathrm{d}^2\Psi_-}{\mathrm{d}z^2} + \left(z - \frac{1}{2}\right)\frac{\mathrm{d}\Psi_-}{\mathrm{d}z} - \mathrm{i}\frac{\epsilon^2}{8\alpha}\Psi_- = 0. \tag{6.19}$$

This equation can be solved in terms of confluent hypergeometric functions using the initial conditions,

$$\begin{aligned} &\Psi_-(-\infty) = 0, \\ &\left|\frac{\mathrm{d}\Psi}{\mathrm{d}\theta}\right|_{\theta\to-\infty} = \frac{\bar{\epsilon}}{2}\,|\Psi_+(-\infty)| = \frac{\bar{\epsilon}}{2}. \end{aligned} \tag{6.20}$$

We shall omit the messy algebra. The asymptotic polarization, starting from $P_\mathrm{i} = P(-\infty) = 1$, is $P_\mathrm{f} = 1 - 2|\Psi_-(\infty)|^2 = 2|\Psi_+(\infty)|^2 - 1$. The answer is known as the Froissart–Stora formula:

$$\frac{P_\mathrm{f}}{P_\mathrm{i}} = 2\,\mathrm{e}^{-\pi\epsilon^2/(2|\alpha|)} - 1. \tag{6.21}$$

We have generalized in order to treat an initial polarization of less than 100%. The Froissart–Stora formula is an elegant, succinct expression. All the details of the accelerator structure are encapsulated in the parameter ϵ. The formula was motivated by the acceleration of polarized proton beams in the 3 GeV SATURNE proton synchrotron at Saclay. This was a weak-focusing synchrotron, later rebuilt as a strong-focusing synchrotron SATURNE-II, functional until 1997. The formula has been used with great success as a theoretical tool to aid in the design of resonance correction schemes, for the acceleration of beams of spin-polarized protons in a number of synchrotrons.

A graph of the ratio $P_\mathrm{f}/P_\mathrm{i}$ as a function of $\sqrt{\epsilon^2/\alpha}$ is shown in figure 25. The same figure also shows a plot of the tensor polarization $P_{33\mathrm{f}}/P_{33\mathrm{i}}$ (for spin 1 particles). We shall discuss tensor polarization later in this paper.

Equation (6.21) is unchanged under a sign reversal $\epsilon \to -\epsilon$. This is intuitively obvious, because a resonance strength of ϵ or $-\epsilon$ is basically the same thing. Similarly it is clear that the asymptotic polarization does not depend on the direction in which the resonance is crossed, hence $P_\mathrm{f}/P_\mathrm{i}$ depends on $|\alpha|$. It is also intuitively obvious that the values of Q_y and ϕ_0 do not appear in the Froissart–Stora formula.

We analyse two important special cases. For $\epsilon^2/\alpha \ll 1$, i.e. small ϵ or large α (weak resonance strength or rapid passage across the resonance), there is negligible depolarization, as should be obvious:

$$\frac{P_\mathrm{f}}{P_\mathrm{i}} \simeq 1 - \frac{\pi\epsilon^2}{|\alpha|}. \tag{6.22}$$

The other extreme case is the 'adiabatic condition' or the 'adiabatic limit' given by $\epsilon^2/|\alpha| \gg 1$, i.e. a strong resonance or very slow (adiabatic) passage across the resonance. There is, again, negligible depolarization, but almost total *reversal* of the polarization:

$$\frac{P_\mathrm{f}}{P_\mathrm{i}} \simeq -1. \tag{6.23}$$

This phenomenon is called 'adiabatic spin-flip'. It is arguably a misnomer, since all the spins in the beam precess smoothly, over a long time interval. This is in contrast to an abrupt change

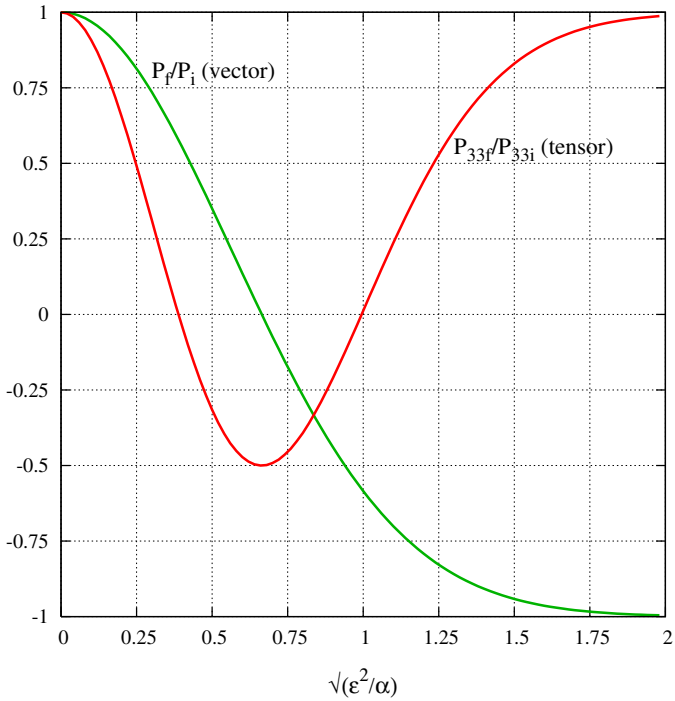

Figure 25. Ratio of the final to initial vector polarization P_f/P_i, and tensor polarization P_{33f}/P_{33i} as a function of $\sqrt{\epsilon^2/\alpha}$, where ϵ is the resonance strength, and α is the crossing speed.

of the spin state of an *individual* spin from up to down, induced by a single event, such as a photon emission.

The concept of adiabatic spin-flip is of the utmost significance. In general, it is difficult and tedious to adjust the accelerator to correct (eliminate) the strength of a resonance driving term. However, it is relatively much easier to *increase* its magnitude. In fact, the modern practice at many accelerators is to deliberately induce a resonance driving term that is so strong that the beam crosses the resonance with reversal of the polarization, but *no* decrease of magnitude. We shall see examples of such work later in this paper. See especially the work with partial Snakes in section 26.

6.4. Resonant spin-flip

The fact that the polarization direction will reverse, with negligible depolarization, when $\epsilon^2/|\alpha| \gg 1$, furnishes the basis for the operation of a *spin-flipper*. Recall, when discussing resonant depolarization earlier in this paper, we pointed out that a radio-frequency horizontal perturbing field could be employed to depolarize the spins by tuning the kicker frequency to a resonant value (see (5.87)). In fact, a radio-frequency horizontal perturbing field can also be used to *flip* the spins *without depolarization*, by sweeping the kicker frequency across the resonant value while satisfying the adiabtic condition $\epsilon^2/|\alpha| \gg 1$. This requires either: (i) a slow passage across the resonant frequency, which may be undesirable because other effects may have time to interfere with the polarization; or (ii) a relatively strong rf kicker field. This means that a transverse magnetic field is preferable at high energies, but both longitudinal and transverse magnetic fields have been used successfully in practice. The overall procedure

is called resonant spin-flip. An early demonstration of a spin-flipper was given by Polunin and Shatunov (1982). In more modern work, a spin-flip efficiency in excess of 99.9% was reported by Leonova *et al* (2004).

Resonant spin-flip aids greatly in eliminating systematic errors in experiments with polarized beams. The directions of the spins are reversed *in situ* in an accelerator, while the 'background' accelerator parameters remain unchanged. Batches of spins of opposite orientations of the polarization (but the *same* magnitude of polarization) are delivered to the experimental target. Typically, the spin direction can be reversed many times during a single experimental run. Resonant spin-flip is a standard experimental technique in experiments using both polarized proton (hadron) and electron beams. It is also a useful idea to selectively depolarize some of the bunches in a storage ring, to compare the data from polarized and unpolarized beams under identical machine conditions. Once again, this aids in reducing the systematic errors in an experiment with polarized beams.

6.5. Beyond the Froissart–Stora formula

The Froissart–Stora formula explicitly treats only one resonance driving term. It is a good approximation when the individual resonances are narrow and do not overlap, so that successive resonances can be crossed in isolation. Much effort has been expended to generalize beyond the Froissart–Stora formula, but there is no convincing formula. Part of the problem is that the situation rapidly fragments into numerous special cases. We consider a few important cases below.

The first important situation is when two resonances overlap, typically an imperfection and an intrinsic resonance. For example, there is overlap at the AGS between the $k = 51$ imperfection resonance and the intrinsic resonance $60 - Q_y$, because $Q_y \simeq 8.75$. (See calculations by Courant and Ruth (1980).) Overlapping resonances are usually treated via numerical simulations. Lee (1997) presents several studies of the problem. Derbenev and Kondratenko (1971) have also studied the problem.

Another very important case is that of synchrotron oscillations. Since the spin tune in a planar ring is proportional to the energy, $\nu_{\rm spin} = a\gamma = a\gamma_0(1+\Delta E/E_0)$, the energy oscillations may, in fact, cause some particles to cross a resonance line multiple times. This problem is especially troublesome during slow passage across a resonance; the synchrotron oscillations spoil the adiabatic condition and lead to depolarization. The effects of synchrotron oscillations on resonance crossing were observed at VEPP-2M in the work with partial Snakes to cross the $a\gamma = 1$ resonance (Derbenev *et al* 1977). Complications from synchrotron oscillations were also observed at SATURNE-II to cross the $G\gamma = 2$ resonance (Aniel *et al* 1985). VEPP-2M accelerated polarized e^+e^- beams and SATURNE-II accelerated polarized proton beams. The VEPP-2M work will be reviewed in section 24, and the SATURNE-II work will be reviewed in section 25. The effects of synchrotron oscillations have, by now, been observed at several synchrotrons. Yokoya (1983c) studied the effects of the synchrotron oscillations in the limit of adiabatic passage across a resonance. The asymptotic polarization is parametrized via $P_{\rm f} = -1+\Delta P$. Basically, there are two contributions to ΔP. The first is because of the energy oscillations due to the synchrotron oscillations. The second, for electron beams, is from the synchrotron radiation, which also causes the particle energy and betatron oscillations to diffuse in the orbital phase-space. This leads to a 'spin diffusion' for the particle spins. We summarize the principal results. We write $\Delta P = \Delta P_1 + \Delta P_2$ for the contributions from the synchrotron oscillations and spin diffusion, respectively. For brevity, we also define $b = \epsilon/\sqrt{\alpha}$. It is assumed that $b \gg 1$. The expression for ΔP_1, after averaging over the phases and amplitudes

of the synchrotron oscillations, is

$$\Delta P = \frac{\pi \nu_0}{2\alpha} \frac{\sigma_E^2}{E_0^2} G\Big(\frac{Q_s}{\sqrt{\alpha}}\Big). \tag{6.24}$$

Here, σ_E^2/E_0^2 is the mean square relative energy spread and $G(\omega)$ is a Fourier transform of a Green function ('response' function). The expression for $G(\omega)$ is given by a contour integral. The contribution from the spin diffusion term is

$$\Delta P_2 = \frac{11}{18} \frac{\tau_{\rm rev}}{\tau_{\rm ST}} \frac{\nu_0^2}{\alpha^{3/2}} K(b), \tag{6.25}$$

where $\tau_{\rm rev}$ is the revolution period, and $\tau_{\rm ST}$ is the Sokolov–Ternov polarization buildup time in a planar ring. Here, $K(b)$ is not a modified Bessel function, but is given by

$$K(b) = \int_{1/b}^{\infty} \frac{{\rm d}\omega}{\omega^2} |G(\omega)|^2. \tag{6.26}$$

For $b \gg 1$, Yokoya shows that a very good approximation is

$$K(b) \simeq \frac{1}{4b}. \tag{6.27}$$

Using this approximation, we deduce

$$\Delta P_2 \simeq \frac{11}{72} \frac{\tau_{\rm rev}}{\tau_{\rm ST}} \frac{\nu_0^2}{\alpha\epsilon}. \tag{6.28}$$

Calculations based on Yokoya's work have been employed to aid design studies for the acceleration of polarized electron beams at ELSA (Steier and Husmann 1998).

Finally, we describe an interesting *empirical* generalization of the Froissart–Stora formula based on the studies of resonant spin-flipping of polarized proton beams at the IUCF Cooler. Blinov *et al* (2000) write

$$\left.\frac{P_{\rm f}}{P_{\rm i}}\right|_{\rm emp} = (1+\eta)\, {\rm e}^{-\pi\epsilon^2/(2\alpha)} - \eta, \tag{6.29}$$

where $0 \leqslant \eta \leqslant 1$. Then, for small ϵ^2/α, we have negligible depolarization $P_{\rm f}/P_{\rm i} \simeq 1$, while at the opposite extreme, we have partial polarization reversal: $P_{\rm f}/P_{\rm i} \simeq -\eta$. The value of η is, effectively, a measure of the 'efficiency' of adiabatic spin-flip. The Froissart–Stora formula corresponds to $\eta = 1$. In practice, the above empirical formula has been tested only for values of η close to unity; it is not known if the expression continues to be valid for small η.

7. Equations of motion in accelerator coordinates

7.1. Coordinate systems

We denote the basis vectors by $\{\boldsymbol{e}_1, \boldsymbol{e}_2, \boldsymbol{e}_3\}$. Here $\boldsymbol{e}_1$ points radially outwards, $\boldsymbol{e}_2$ is longitudinal and counterclockwise and $\boldsymbol{e}_3$ points vertically upwards. Suppose the radius of curvature of the reference orbit is ρ, which is assumed to lie (locally, anyway) in the horizontal plane. The derivatives of the basis vectors are

$$\frac{{\rm d}\boldsymbol{e}_1}{{\rm d}s} = \frac{\boldsymbol{e}_2}{\rho}, \qquad \frac{{\rm d}\boldsymbol{e}_2}{{\rm d}s} = -\frac{\boldsymbol{e}_1}{\rho}, \qquad \frac{{\rm d}\boldsymbol{e}_3}{{\rm d}s} = 0. \tag{7.1}$$

7.2. Orbital equation of motion

The particle location is

$$\boldsymbol{r} = (\rho + x)\,\boldsymbol{e}_1 + y\,\boldsymbol{e}_3. \tag{7.2}$$

After a small increment in the arc-length δs, the new location is

$$\boldsymbol{r} + \delta\boldsymbol{r} \simeq (\rho + x + \delta x)\left(\boldsymbol{e}_1 + \frac{\delta s}{\rho}\boldsymbol{e}_2\right) + (y + \delta y)\,\boldsymbol{e}_3. \tag{7.3}$$

Hence,

$$\delta\boldsymbol{r} = \delta x\,\boldsymbol{e}_1 + (\rho + x)\frac{\delta s}{\rho}\boldsymbol{e}_2 + \delta y\,\boldsymbol{e}_3. \tag{7.4}$$

The derivative with respect to the arc-length is

$$\frac{\mathrm{d}\boldsymbol{r}}{\mathrm{d}s} = \frac{\mathrm{d}x}{\mathrm{d}s}\,\boldsymbol{e}_1 + \left(1 + \frac{x}{\rho}\right)\boldsymbol{e}_2 + \frac{\mathrm{d}y}{\mathrm{d}s}\,\boldsymbol{e}_3 = x'\,\boldsymbol{e}_1 + \left(1 + \frac{x}{\rho}\right)\boldsymbol{e}_2 + y'\,\boldsymbol{e}_3, \tag{7.5}$$

where $x' \equiv \mathrm{d}x/\mathrm{d}s$ and $y' \equiv \mathrm{d}y/\mathrm{d}s$. The velocity is

$$\boldsymbol{v} = \frac{\mathrm{d}\boldsymbol{r}}{\mathrm{d}t} = \frac{\mathrm{d}s}{\mathrm{d}t}\frac{\mathrm{d}\boldsymbol{r}}{\mathrm{d}s}. \tag{7.6}$$

From the expression for $\delta\boldsymbol{r}$ we see that,

$$v = \frac{\mathrm{d}s}{\mathrm{d}t}\sqrt{\left(1 + \frac{x}{\rho}\right)^2 + x'^2 + y'^2}. \tag{7.7}$$

The value of v is a constant for motion in pure magnetic fields. For brevity, we write $v_s = \mathrm{d}s/\mathrm{d}t$ below. If we retain only terms up to the first order in the derivatives we obtain, after some algebra,

$$\boldsymbol{v} \simeq \frac{v}{1 + x/\rho}\frac{\mathrm{d}\boldsymbol{r}}{\mathrm{d}s} \simeq v(x'\,\boldsymbol{e}_1 + \boldsymbol{e}_2 + y'\,\boldsymbol{e}_3) \tag{7.8}$$

and

$$\frac{\mathrm{d}\boldsymbol{v}}{\mathrm{d}t} \simeq v^2\left(1 - \frac{x}{\rho}\right)\left[\left(x'' - \frac{1}{\rho}\right)\boldsymbol{e}_1 + \frac{x'}{\rho}\boldsymbol{e}_2 + y''\boldsymbol{e}_3\right]. \tag{7.9}$$

This can be substituted in the Lorentz equation (5.66) to obtain the equation of motion for the particle orbit in the accelerator coordinate system. We get,

$$\gamma m v^2\left(1 - \frac{x}{\rho}\right)\left[\left(x'' - \frac{1}{\rho}\right)\boldsymbol{e}_1 + \frac{x'}{\rho}\boldsymbol{e}_2 + y''\boldsymbol{e}_3\right] = \frac{ev}{c}(x'\,\boldsymbol{e}_1 + \boldsymbol{e}_2 + y'\,\boldsymbol{e}_3)(B_x\boldsymbol{e}_1 + B_s\boldsymbol{e}_2 + B_y\boldsymbol{e}_3). \tag{7.10}$$

It is common practice to define a symbol '$B\rho$' given by $p/e = \gamma m v/e = -B\rho/c$ (the minus sign is due to our choice of coordinate system). Then,

$$\begin{aligned}
-B\rho\left(1 - \frac{x}{\rho}\right)\left(x'' - \frac{1}{\rho}\right) &= B_y - B_s y', \\
-B\rho\left(1 - \frac{x}{\rho}\right)\frac{x'}{\rho} &= B_x y' - B_y x', \\
-B\rho\left(1 - \frac{x}{\rho}\right)y'' &= B_s x' - B_x.
\end{aligned} \tag{7.11}$$

7.3. Spin equation of motion

Next, we treat the spin precession equation. Recall that $\mathrm{d}\boldsymbol{s}/\mathrm{d}t = \boldsymbol{\Omega} \times \boldsymbol{s}$, and now,

$$\frac{\mathrm{d}\boldsymbol{s}}{\mathrm{d}t} = \frac{\mathrm{d}s}{\mathrm{d}t}\frac{\mathrm{d}\boldsymbol{s}}{\mathrm{d}s} \simeq \frac{v}{1+x/\rho}\frac{\mathrm{d}\boldsymbol{s}}{\mathrm{d}s}. \tag{7.12}$$

We write,

$$\boldsymbol{s} = s_1\boldsymbol{e}_1 + s_2\boldsymbol{e}_2 + s_3\boldsymbol{e}_3. \tag{7.13}$$

Hence,

$$\frac{\mathrm{d}\boldsymbol{s}}{\mathrm{d}s} = \Big(\frac{\mathrm{d}s_1}{\mathrm{d}s} - \frac{s_2}{\rho}\Big)\boldsymbol{e}_1 + \Big(\frac{\mathrm{d}s_2}{\mathrm{d}s} + \frac{s_1}{\rho}\Big)\boldsymbol{e}_2 + \frac{\mathrm{d}s_3}{\mathrm{d}s}\boldsymbol{e}_3. \tag{7.14}$$

Setting $\bar{\boldsymbol{\Omega}} = \boldsymbol{\Omega}/v$, the equations of motion for the individual components are,

$$\begin{aligned}
\frac{\mathrm{d}s_1}{\mathrm{d}s} &= \Big(1+\frac{x}{\rho}\Big)(\bar{\boldsymbol{\Omega}} \times \boldsymbol{s}) \cdot \boldsymbol{e}_1 + \frac{s_2}{\rho},\\
\frac{\mathrm{d}s_2}{\mathrm{d}s} &= \Big(1+\frac{x}{\rho}\Big)(\bar{\boldsymbol{\Omega}} \times \boldsymbol{s}) \cdot \boldsymbol{e}_2 - \frac{s_1}{\rho},\\
\frac{\mathrm{d}s_3}{\mathrm{d}s} &= \Big(1+\frac{x}{\rho}\Big)(\bar{\boldsymbol{\Omega}} \times \boldsymbol{s}) \cdot \boldsymbol{e}_3,
\end{aligned} \tag{7.15}$$

which we can write more compactly in the form

$$\frac{\mathrm{d}\boldsymbol{s}}{\mathrm{d}s} = \Big[\Big(1+\frac{x}{\rho}\Big)\bar{\boldsymbol{\Omega}} - \frac{\boldsymbol{e}_3}{\rho}\Big] \times \boldsymbol{s}. \tag{7.16}$$

In accelerator coordinates, the spin precession equation has either of the equivalent forms,

$$\frac{\mathrm{d}\boldsymbol{s}}{\mathrm{d}s} = \boldsymbol{W}_s \times \boldsymbol{s}, \qquad \frac{\mathrm{d}\boldsymbol{s}}{\mathrm{d}\theta} = R\boldsymbol{W}_s \times \boldsymbol{s} \equiv \boldsymbol{W} \times \boldsymbol{s}, \tag{7.17}$$

where

$$\begin{aligned}
\boldsymbol{W}_s =& -\frac{e}{pc}\Big(1+\frac{x}{\rho}\Big)\Big[(a\gamma+1)\boldsymbol{B}_\perp + (1+a)\boldsymbol{B}_\parallel - \Big(a\gamma + \frac{\gamma}{\gamma+1}\Big)\boldsymbol{\beta}\times\boldsymbol{E}\Big] - \frac{\boldsymbol{e}_3}{\rho}\\
=& -\frac{e}{pc}\Big(1+\frac{x}{\rho}\Big)\Big[(a\gamma+1)\boldsymbol{B} - \frac{a\gamma^2}{\gamma+1}\boldsymbol{\beta}\cdot\boldsymbol{B}\boldsymbol{\beta} - \Big(a\gamma + \frac{\gamma}{\gamma+1}\Big)\boldsymbol{\beta}\times\boldsymbol{E}\Big] - \frac{\boldsymbol{e}_3}{\rho}.
\end{aligned} \tag{7.18}$$

Let us set aside the term in the electric field in $\boldsymbol{W}_s$ and focus our attention on the terms in the magnetic field. Call the resulting vector $\tilde{\boldsymbol{W}}_s$. Then,

$$\begin{aligned}
\tilde{\boldsymbol{W}}_s =& -\frac{e}{pc}\Big(1+\frac{x}{\rho}\Big)\Big\{(a\gamma+1)(B_x\boldsymbol{e}_1 + B_s\boldsymbol{e}_2 + B_y\boldsymbol{e}_3)\\
&-\frac{a\gamma^2}{\gamma+1}\frac{v^2}{c^2}\frac{B_x x' + B_s(1+x/\rho) + B_y y'}{(1+x/\rho)^2 + x'^2 + y'^2}\Big[x'\boldsymbol{e}_1 + \Big(1+\frac{x}{\rho}\Big)\boldsymbol{e}_2 + y'\boldsymbol{e}_3\Big]\Big\} - \frac{\boldsymbol{e}_3}{\rho}.
\end{aligned} \tag{7.19}$$

This is obviously messy. Most authors approximate the expression for $\tilde{\boldsymbol{\Omega}}$ to the first order in the derivatives much earlier than this. However, we display the higher order terms explicitly, basically for reference, just to note their form and existence. Having done so, we *now* drop all terms in x'^2 and $x'y'$, etc. We also use the result

$$a\frac{\gamma^2}{\gamma+1}\frac{v^2}{c^2} = a\frac{\gamma^2-1}{\gamma+1} = a(\gamma-1), \tag{7.20}$$

to obtain

$$\begin{aligned}
\tilde{\boldsymbol{W}}_s \simeq& -\frac{e}{pc}\Big\{\Big(1+\frac{x}{\rho}\Big)[(a\gamma+1)(B_x\boldsymbol{e}_1 + B_y\boldsymbol{e}_3) + (a+1)B_s\boldsymbol{e}_2]\\
&-a(\gamma-1)[B_s x'\boldsymbol{e}_1 + (B_x x' + B_y y')\boldsymbol{e}_2 + B_s y'\boldsymbol{e}_3]\Big\} - \frac{\boldsymbol{e}_3}{\rho}.
\end{aligned} \tag{7.21}$$

Recall the symbol $B\rho$, and with obvious notation write $B\rho_0$ for the value on the reference orbit, i.e. $p_0/e = -B\rho_0/c$, where p_0 is the momentum of the reference particle. Then $p/e = -(B\rho_0/c)(1 + \Delta p/p_0)$. Set $\delta = \Delta p/p_0$ for brevity. We also use $\boldsymbol{W}$ rather than $\boldsymbol{W}_s$. Then, writing $\tilde{\boldsymbol{W}}$ to denote the term in $\boldsymbol{W}$ without the electric field,

$$\tilde{\boldsymbol{W}} \simeq \frac{R}{B\rho_0(1+\delta)}\left\{\left(1+\frac{x}{\rho}\right)[(a\gamma+1)(B_x\boldsymbol{e}_1 + B_y\boldsymbol{e}_3) + (a+1)B_s\boldsymbol{e}_2] - a(\gamma-1)[B_s x'\boldsymbol{e}_1 + (B_x x' + B_y y')\boldsymbol{e}_2 + B_s y'\boldsymbol{e}_3]\right\} - \frac{R}{\rho}\boldsymbol{e}_3. \tag{7.22}$$

Most terms in the above expression actually vanish in standard beamline elements. Such expressions will be given below.

7.4. Dipoles and steering correctors

We shall describe expressions for the spin precession vector $\boldsymbol{W}$ in various standard beamline elements below, but here, we make a simple but important observation pertaining to the curvature of the reference orbit, i.e. the term in $(R/\rho)\boldsymbol{e}_3$ in $\boldsymbol{W}$. In their passage through a dipole magnet (horizontal bend), not only the spin precesses, but the reference orbit also curves. Hence, the net spin precession angle is reduced. Consider motion on the reference orbit through a pure vertical dipole field, so $(e/p)(\boldsymbol{B}_\perp/c) = -\boldsymbol{e}_3/\rho$. On the reference orbit $x = 0$ and also $\boldsymbol{B}_\parallel = 0$. Then,

$$\boldsymbol{W}_{\text{dipole}} = (a\gamma_0 + 1)\frac{R}{\rho}\boldsymbol{e}_3 - \frac{R}{\rho}\boldsymbol{e}_3 = a\gamma_0\frac{R}{\rho}\boldsymbol{e}_3. \tag{7.23}$$

The orbital bend angle is $\theta_{\text{b}} = L_{\text{dipole}}/\rho$, and so the spin precession angle through the dipole, *relative to the reference orbit*, is

$$\psi_{\text{dipole}} = a\gamma_0\,\theta_{\text{b}}. \tag{7.24}$$

However, suppose now that the dipole is a *steering corrector* magnet, with a bend angle θ_{c} and a length L_{c}. Even though a steering corrector is a dipole magnetic field, the reference orbit through it is a *straight* line: it does *not* bend. The coordinate basis vectors $\boldsymbol{e}_{1,2,3}$, do not rotate during passage through the corrector, and so $\rho^{-1} = 0$. Then $e\boldsymbol{B}_\perp/(pc) = -(\theta_{\text{c}}/L_{\text{c}})\boldsymbol{e}_3$, and so now,

$$\boldsymbol{W}_{\text{corr}} = (a\gamma_0 + 1)\frac{R}{L_{\text{c}}}\,\theta_{\text{c}}\,\boldsymbol{e}_3. \tag{7.25}$$

Integrating over the length of the corrector, the spin rotation angle, again relative to the reference orbit, is

$$\psi_{\text{corr}} = (a\gamma_0 + 1)\theta_{\text{c}}. \tag{7.26}$$

The coefficient is $a\gamma_0 + 1$, not $a\gamma$. The same remarks apply to the passage of a spin through a vertical bend/corrector.

7.5. Spin precession vector in standard beamline elements

7.5.1. Multipole expansion. For static magnetic fields in two dimensions (transverse to the reference axis, assumed straight), one can express the magnetic field as a curl of a vector potential $\boldsymbol{A} = A_s(x, y)\hat{\boldsymbol{s}}$, where we shall write $\hat{\boldsymbol{x}} = \boldsymbol{e}_1$, $\hat{\boldsymbol{s}} = \boldsymbol{e}_2$ and $\hat{\boldsymbol{y}} = \boldsymbol{e}_3$ to conform to more common practice. One can expand the potential in a Fourier series

$$A_s = \sum_{n=1}^{\infty}\frac{r^n}{n}[-a_n\,\sin(n\phi) + b_n\cos(n\phi)], \tag{7.27}$$

where $r = \sqrt{x^2 + y^2}$ and $\phi = \tan^{-1}(y/x)$ are polar coordinates. There is no need for a constant $n = 0$ term. (The indices for the harmonics follow the European convention, as opposed to the American convention of writing $a_n \sin((n+1)\phi)$ etc, and starting the indices from $n = 0$.) The terms in $\cos(n\phi)$ are called normal multipoles and the terms in $\sin(n\phi)$ are called skew multipoles. The word 'normal' is universally omitted. The magnetic fields in regular multipoles (quadrupole, sextupole, etc) are

$$\begin{aligned}
\boldsymbol{B}_{\text{quad}} &= b_2\,[x\hat{\boldsymbol{y}} + y\hat{\boldsymbol{x}}] = \frac{\partial B_y}{\partial x}\,[x\hat{\boldsymbol{y}} + y\hat{\boldsymbol{x}}],\\
\boldsymbol{B}_{\text{sext}} &= b_3\,[(x^2 - y^2)\hat{\boldsymbol{x}} + 2xy\hat{\boldsymbol{y}}] = \frac{1}{2}\frac{\partial^2 B_y}{\partial x^2}\,[(x^2 - y^2)\hat{\boldsymbol{x}} + 2xy\hat{\boldsymbol{y}}],\\
&\vdots
\end{aligned} \tag{7.28}$$

and in skew multipoles (skew quadrupole, skew sextupole, etc), they are

$$\begin{aligned}
\boldsymbol{B}_{\text{skew quad}} &= a_2\,[x\hat{\boldsymbol{x}} - y\hat{\boldsymbol{y}}] = \frac{\partial B_x}{\partial x}\,[x\hat{\boldsymbol{x}} - y\hat{\boldsymbol{y}}],\\
\boldsymbol{B}_{\text{skew sext}} &= a_3\,[2xy\hat{\boldsymbol{x}} + (x^2 - y^2)\hat{\boldsymbol{y}}] = \frac{1}{2}\frac{\partial^2 B_x}{\partial x^2}\,[2xy\hat{\boldsymbol{x}} + (x^2 - y^2)\hat{\boldsymbol{y}}],\\
&\vdots
\end{aligned} \tag{7.29}$$

The polynomials in x and y are simply the real and imaginary parts of $(x+\mathrm{i}y)^n$ for $n = 1, 2, \ldots$. A skew quadrupole is that which is rotated through 45° around the longitudinal axis, while a skew sextupole is that rotated through 30° around the longitudinal axis, etc.

The magnetic fields in a horizontal and a vertical dipole are $B_{\text{h-dipole}} = B_y\,\hat{\boldsymbol{y}}$, $B_{\text{v-dipole}} = B_x\,\hat{\boldsymbol{x}}$. The reference axis curves in a dipole (counterclockwise for positive B_y or B_x, for an electron), so the simple Fourier series is only approximate. There are higher order corrections of $\mathrm{O}(h^{-1})$ to the above fields. The leading order correction is typically a sextupole term. A *combined function* magnet has both a dipole and quadrupole field. The magnetic field in a solenoid is parallel to the reference axis, and does not fit into the multipole classification. All the above statements ignore the fringe fields at the magnet entrance and exit. Fringe fields are not treated in this paper.

7.5.2. Horizontal dipoles. We treat only sector dipoles, with pole faces normal to the design orbit. Consider a vertical dipole field $\boldsymbol{B} = B_y\boldsymbol{e}_3$, which we express in the slightly curious form, $B_y = B\rho_0/\rho_x$. Here, ρ_x is the bending radius of the dipole. Since there is no electric field, we can drop the tilde. Then,

$$\boldsymbol{W} = \frac{R}{\rho_x(1+\delta)}\left\{\left(1 + \frac{x}{\rho_x}\right)(a\gamma + 1)\boldsymbol{e}_3 - a(\gamma - 1)\,y'\boldsymbol{e}_2\right\} - \frac{R}{\rho_x}\boldsymbol{e}_3. \tag{7.30}$$

We have seen that on the reference orbit the value is

$$\boldsymbol{W}_0 = \frac{R}{\rho_x}\,a\gamma_0\,\boldsymbol{e}_3. \tag{7.31}$$

For off-axis motion, use the notation $\boldsymbol{w}$ to denote the off-axis component of $\boldsymbol{W}$: this will be standard practice throughout this paper. Decompose $\boldsymbol{w}$ into horizontal betatron, vertical betatron and synchrotron terms via

$$\boldsymbol{w} = \boldsymbol{w}_{x_\beta} + \boldsymbol{w}_{y_\beta} + \boldsymbol{w}_\delta. \tag{7.32}$$

First, consider a horizontal betatron oscillation and set $x = x_\beta$, etc. Then

$$\boldsymbol{w}_{x_\beta} = R\,(a\gamma_0 + 1)\frac{x_\beta}{\rho_x^2}\,\boldsymbol{e}_3. \tag{7.33}$$

For the vertical betatron oscillation, set $y' = y'_\beta$. Then

$$\boldsymbol{w}_{y_\beta} = -R\,a(\gamma_0 - 1)\frac{y'_\beta}{\rho_x}\boldsymbol{e}_2. \tag{7.34}$$

Normally, we think that a horizontally bending dipole rotates only around the vertical axis, but there is a small component of rotation along the reference orbit $\boldsymbol{e}_2$, because the spin precession term $\boldsymbol{\Omega}_\parallel$ is directed along the velocity, not the reference orbit. The synchrotron oscillations are the most complicated. We not only set $\delta \neq 0$, but we also set $x_\delta = D_x\delta$ and $y' = D'_y\delta$. Furthermore, $\gamma = \gamma_0(1 + \beta_0^2\delta)$. Then,

$$\boldsymbol{w}_\delta = R\left\{\left[(a\gamma_0 + 1)\frac{D_x}{\rho_x^2} - \left(\frac{a}{\gamma_0} + 1\right)\frac{1}{\rho_x}\right]\boldsymbol{e}_3 - a(\gamma_0 - 1)\frac{D'_y}{\rho_x}\boldsymbol{e}_2\right\}\delta. \tag{7.35}$$

For ultrarelativistic motion (electron or positron storage rings) where $\gamma \gg 1$, it is usual to employ $\delta\gamma/\gamma_0$ and to write,

$$\boldsymbol{w}_\delta = R\left\{\left[(a\gamma_0 + 1)\frac{D_x}{\rho_x^2} - \frac{1}{\rho_x}\right]\boldsymbol{e}_3 - a\gamma_0\frac{D'_y}{\rho_x}\boldsymbol{e}_2\right\}\frac{\delta\gamma}{\gamma_0}. \tag{7.36}$$

7.5.3. Vertical dipoles. We again treat only sector dipoles, with pole faces normal to the design orbit. The positive sense of rotation is counterclockwise around the outward radial unit vector $\boldsymbol{e}_1$. We have not really treated vertical bends in detail above, but the reader should be able to fill in the details. The bending radius is ρ_y. Then,

$$\begin{aligned}
\boldsymbol{W}_0 &= \frac{R}{\rho_y}\,a\gamma_0\,\boldsymbol{e}_1,\\
\boldsymbol{w}_{x_\beta} &= -R\,a(\gamma_0 - 1)\frac{x'_\beta}{\rho_y}\boldsymbol{e}_2,\\
\boldsymbol{w}_{y_\beta} &= -R\,(a\gamma_0 + 1)\frac{y_\beta}{\rho_y^2}\,\boldsymbol{e}_1,\\
\boldsymbol{w}_\delta &= -R\left\{\left[(a\gamma_0 + 1)\frac{D_y}{\rho_y^2} + \left(\frac{a}{\gamma_0} + 1\right)\frac{1}{\rho_y}\right]\boldsymbol{e}_1 + a(\gamma_0 - 1)\frac{D'_x}{\rho_y}\boldsymbol{e}_2\right\}\delta.
\end{aligned} \tag{7.37}$$

7.5.4. Solenoid. A solenoid is the other standard beamline element where there is nonzero spin precession on the reference orbit, which in a solenoid, coincides with the solenoid axis. We consider only the main body of a solenoid, so $\boldsymbol{B} = B_{\rm sol}\boldsymbol{e}_2$, whence

$$\boldsymbol{W} \simeq R\frac{B_{\rm sol}}{B\rho_0}\frac{1}{1+\delta}\{(a+1)\boldsymbol{e}_2 - a(\gamma - 1)\,(x'\boldsymbol{e}_1 + y'\boldsymbol{e}_3)\}. \tag{7.38}$$

We neglect the betatron oscillations and treat only off-axis motion due to the synchrotron oscillations; even then, we shall assume that the horizontal and vertical dispersions (specifically D'_x and D'_y) vanish. Then

$$\boldsymbol{W}_0 = R(a+1)\frac{B_{\rm sol}}{B\rho_0}\,\boldsymbol{e}_2, \qquad \boldsymbol{w}_\delta = -R(a+1)\frac{B_{\rm sol}}{B\rho_0}\,\delta\,\boldsymbol{e}_2. \tag{7.39}$$

It is common to employ p/e, rather than $B\rho/c$, in which case the spin rotation angle integrated over the solenoid length $L_{\rm sol}$ is

$$\psi_{\rm spin} = -(a+1)\frac{e}{p}\frac{(BL)_{\rm sol}}{c}. \tag{7.40}$$

Written in this way it is immediately obvious that $\psi \propto 1/p$, i.e. the spin rotation angle is simply inversely proportional to the momentum. This is a particularly clear example of 'chromatic aberration' for the spin motion. The spins of particles with different momenta are rotated through different angles.

7.5.5. Quadrupole. There is no spin precession on-axis: $\boldsymbol{W}_0 = 0$. The field in a quadrupole can be written as

$$\boldsymbol{B}_{\text{quad}} = B'(y\boldsymbol{e}_1 + x\boldsymbol{e}_3), \tag{7.41}$$

where $B' = \partial B/\partial x$ is the quadrupole field gradient. Then,

$$\boldsymbol{w} \simeq R\frac{B'}{B\rho_0}\frac{1}{1+\delta}\{(a\gamma+1)(y\boldsymbol{e}_1 + x\boldsymbol{e}_3) - a(\gamma-1)\,(yx' + xy')\,\boldsymbol{e}_2\}. \tag{7.42}$$

This must be simplified to linear order in the orbital variables. Evidently,

$$\begin{aligned}
\boldsymbol{w}_{x_\beta} &= R(a\gamma+1)\frac{B'}{B\rho_0}\,x_\beta\,\boldsymbol{e}_3,\\
\boldsymbol{w}_{y_\beta} &= R(a\gamma+1)\frac{B'}{B\rho_0}\,y_\beta\,\boldsymbol{e}_1,\\
\boldsymbol{w}_\delta &= R(a\gamma+1)\frac{B'}{B\rho_0}\,(D_y\boldsymbol{e}_1 + D_x\boldsymbol{e}_3)\,\delta.
\end{aligned} \tag{7.43}$$

7.5.6. Skew quadrupole. The field in a skew quadrupole can be written as

$$\boldsymbol{B}_{\text{sq}} = B'\,(x\boldsymbol{e}_1 - y\boldsymbol{e}_3), \tag{7.44}$$

where $B' = \partial B/\partial x$ is the skew quadrupole field gradient. Again $\boldsymbol{W}_0 = 0$ and now,

$$\boldsymbol{w} \simeq R\frac{B'}{B\rho_0}\frac{1}{1+\delta}\{(a\gamma+1)(x\boldsymbol{e}_1 - y\boldsymbol{e}_3) - a(\gamma-1)\,(xx' - yy')\boldsymbol{e}_2\}. \tag{7.45}$$

Hence,

$$\begin{aligned}
\boldsymbol{w}_{x_\beta} &= R(a\gamma+1)\frac{B'}{B\rho_0}\,x_\beta\boldsymbol{e}_1,\\
\boldsymbol{w}_{y_\beta} &= -R(a\gamma+1)\frac{B'}{B\rho_0}\,y_\beta\boldsymbol{e}_3,\\
\boldsymbol{w}_\delta &= R(a\gamma+1)\frac{B'}{B\rho_0}\,(D_x\boldsymbol{e}_1 - D_y\boldsymbol{e}_3)\,\delta.
\end{aligned} \tag{7.46}$$

7.5.7. Sextupole. The field in a sextupole can be written as

$$\boldsymbol{B}_{\text{sext}} = \tfrac{1}{2}B''\,[(x^2 - y^2)\boldsymbol{e}_1 + 2xy\boldsymbol{e}_3], \tag{7.47}$$

where $B'' = \partial^2 B/\partial x^2$. The contribution of a sextupole to the spin precession necessarily contains a term of at least quadratic order in the orbital variables. Nevertheless, even if only linear dynamics are used to describe the orbital motion, one can still obtain terms such as

$$\boldsymbol{w} \simeq R(a\gamma+1)\frac{1}{2}\frac{B''}{B\rho_0}[(x_\beta^2 - y_\beta^2)\boldsymbol{e}_1 + 2x_\beta y_\beta\boldsymbol{e}_3], \tag{7.48}$$

which are derived from the linear orbital dynamics. In practice, the major contribution of sextupoles to the spin motion arises from the fact that, in general, the imperfect closed orbit

passes off-centre through the sextupoles; the sextupoles therefore act effectively like (weak) quadrupoles. Hence, instead of x_β, we write $x_{\mathrm{c.o.}} + x_\beta$, so

$$x_\beta^2 - y_\beta^2 \to 2(x_{\mathrm{c.o.}} x_\beta - y_{\mathrm{c.o.}} y_\beta), \qquad x_\beta y_\beta \to x_{\mathrm{c.o.}} y_\beta + y_{\mathrm{c.o.}} x_\beta \tag{7.49}$$

and we obtain an expression like

$$\boldsymbol{w} \simeq R(a\gamma + 1)\frac{B''}{B\rho_0}[(x_{\mathrm{c.o.}} x_\beta - y_{\mathrm{c.o.}} y_\beta)\boldsymbol{e}_1 + (x_{\mathrm{c.o.}} y_\beta + x_\beta y_{\mathrm{c.o.}})\boldsymbol{e}_3]. \tag{7.50}$$

A more important contribution of the sextupoles is via the chromaticity; the momentum offset of a particle changes its betatron tune. The induced tunespread affects the widths of the spin resonances.

7.5.8. Higher multipoles. This simply becomes tedious. It will be left as an exercise for the reader. As a general rule, most accelerators are equipped with dipoles, quadrupoles and sextupoles; not many have higher order multipoles. Even the use of skew quadrupoles is limited; they are only employed in special circumstances.

8. Single particle dynamics

8.1. General remarks

We mainly treat only linear orbital dynamics. The effects of the coupling of nonlinear orbital dynamics to the spin motion are at best poorly understood, except in very specific circumstances. Linear orbital dynamics means, of course, that the orbital equations of motion are approximated by linear differential equations, or, equivalently, the Hamiltonian of the orbital motion contains only terms up to quadratic order in the orbital dynamical variables. Edwards and Syphers (1993) give a good introduction to the orbital dynamics (but do not discuss spin).

8.2. Transverse dynamics

The orbital dynamics basically subdivide into transverse and longitudinal dynamics. The transverse oscillations are called (horizontal and vertical) betatron oscillations, and the longitudinal ones are called synchrotron oscillations. In the approximation of linear orbital dynamics, the horizontal betatron oscillations are solutions of the pseudoharmonic differential equation, known as *Hill's equation*,

$$x'' + G_x(s)\, x = 0, \tag{8.1}$$

where the focusing function G_x depends on the arc-length s, and is related to the magnetic fields in the dipoles and quadrupoles via

$$G_x = \frac{1}{\rho_x^2} + \frac{1}{B\rho_0}\frac{\partial B_y}{\partial x}. \tag{8.2}$$

The function G_x is periodic around the ring: $G_x(s + C) = G_x(s)$, where C is the ring circumference. The above equation can be solved using a WKB (Wentzel–Kramers–Brillouin) approximation. The standard parametrization of a horizontal betatron oscillation is

$$x_\beta(\theta) = \sqrt{2I_x\beta_x(\theta)}\cos(\psi_x(\theta) + \phi_{x0}). \tag{8.3}$$

Note that we shall switch between the use of the arc-length s, and the azimuth θ without change of notation since $\theta = s/R$, simply a proportionality. Here I_x and ϕ_{x0} are independent of the

azimuth θ. Obviously, ϕ_{x0} is an initial phase, while the value of I_x sets the amplitude of the motion. The function β_x is called the (horizontal) *beta function* and depends on the azimuth θ. The beta function sets an envelope for the amplitude of the orbital oscillation and is periodic around the ring: $\beta_x(\theta + 2\pi) = \beta_x(\theta)$. Its value is determined by the focusing structure of the accelerator lattice (the dipoles and quadrupoles). The function ψ_x is called the *betatron phase*, and gives the rate of phase advance of the betatron oscillation around the accelerator. It is related to the beta function via

$$\psi_x(s) = \int_0^s \frac{\mathrm{d}s'}{\beta_x(s')}. \tag{8.4}$$

Unlike the beta function, the betatron phase is *not* periodic around the ring. Instead, it undergoes a phase advance, given by

$$\psi_x(\theta + 2\pi) = \psi_x(\theta) + 2\pi Q_x. \tag{8.5}$$

Here, Q_x is called the (horizontal betatron) *tune*. The betatron tune is a dimensionless oscillation frequency: it is the betatron frequency (in Hz, say) divided by the revolution frequency around the ring.

In addition to the beta function, there are two other periodic functions α and γ, given by $\alpha_x = -\frac{1}{2}\mathrm{d}\beta_x/\mathrm{d}s$ and $\gamma_x = (1 + \alpha_x^2)/\beta_x$, so $\beta_x\gamma_x - \alpha_x^2 = 1$. Writing $\mu_x = 2\pi Q_x$ for the one-turn betatron phase advance, the one-turn map of the betatron motion around the ring is given by the matrix

$$M_{x_\beta} = \begin{pmatrix} \cos\mu_x + \beta_x \sin\mu_x & \alpha_x \sin\mu_x \\ -\gamma_x \sin\mu_x & \cos\mu_x - \beta_x \sin\mu_x \end{pmatrix}. \tag{8.6}$$

It is easily verified that the determinant of this matrix is unity. The trio $(\alpha_x, \beta_x, \gamma_x)$ are called Twiss parameters or Courant–Snyder parameters. Generally, since the orbital equation of motion is linear, the mapping of a betatron oscillation from any initial azimuth θ_i to a final azimuth θ_f is given by a 2×2 matrix. The one-turn matrix is the important special case where $\theta_\mathrm{f} = \theta_\mathrm{i} + 2\pi$. One can easily show that the quantity

$$A_x \equiv \gamma_x x_\beta^2 + 2\alpha_x x_\beta x'_\beta + \beta_x x'^2_\beta \tag{8.7}$$

is an invariant of the motion. It is called the *Courant–Snyder invariant* (Courant and Snyder 1958). In terms of our parametrization for x_β above, $A_x = 2I_x$. If we take a snapshot of the betatron motion at a fixed azimuth θ_* on successive turns around the accelerator (called a *Poincaré section*), the points in (x_β, x'_β) space will map out an ellipse whose area is πA_x or $2\pi I_x$.

In a beam of particles circulating in an accelerator, there will be a statistical distribution of the values of I_x. It is reasonable, in most cases, to assume the beam has no coherent betatron motion, i.e. $\langle x_\beta \rangle = \langle x'_\beta \rangle = 0$. We define the *emittance* of the beam ε_x via

$$\varepsilon_x = \langle A_x \rangle. \tag{8.8}$$

It is important to be clear about our use of the term 'emittance'. Some authors use the term emittance for an individual particle but we do *not*. We define the emittance as a *statistical* average property of the *entire beam*. The invariant associated with an individual trajectory is A_x, the average over all trajectories is ε_x.

Analogously to the horizontal betatron oscillations, there are also vertical betatron oscillations. The equation of motion is

$$y'' + G_y(s)\, y = 0, \tag{8.9}$$

where the focusing function of the vertical oscillations is

$$G_y = \frac{1}{\rho_y^2} - \frac{1}{B\rho_0}\frac{\partial B_y}{\partial x}. \tag{8.10}$$

The curvature term ρ_y^{-2} is zero in a planar ring since all the bending occurs only in the horizontal plane. Most accelerators are planar by design. The vertical quad gradient term has the opposite sign to that in G_x. The parametrization of a vertical betatron oscillation is obviously

$$y_\beta(\theta) = \sqrt{2I_y\beta_y(\theta)}\cos(\psi_y(\theta) + \phi_{y0}), \tag{8.11}$$

where all the symbols are defined by analogy with the horizontal betatron oscillations, so the vertical betatron phase is related to the vertical beta function via

$$\psi_y(s) = \int_0^s \frac{\mathrm{d}s'}{\beta_y(s')}, \tag{8.12}$$

and the vertical betatron tune is given by

$$\psi_y(\theta + 2\pi) = \psi_y(\theta) + 2\pi Q_y. \tag{8.13}$$

There is, correspondingly, a one-turn map for the vertical betatron motion, and a vertical betatron Courant–Snyder invariant

$$A_y \equiv \gamma_y y_\beta^2 + 2\alpha_y y_\beta y'_\beta + \beta_y y'^2_\beta = 2I_y, \tag{8.14}$$

and an rms vertical betatron emittance

$$\varepsilon_y = \langle W_y \rangle. \tag{8.15}$$

8.3. Closed-orbit imperfections

We have tacitly assumed above that the closed orbit coincides with the design orbit. In a real accelerator, the magnets may be misaligned for a variety of reasons, including field and gradient errors, also tilts and rolls of the magnets, settling due to ground motion, etc. In principle, the betatron oscillations, and other functions to be described below, should be referenced to the imperfect closed orbit. We shall not consider the matter in detail here.

8.4. Transverse coupling

In most accelerators, the horizontal and vertical oscillations are uncoupled, and so one can speak of the horizontal and vertical betatron oscillations separately. It is also possible, within the framework of linear orbital dynamics, for the horizontal and vertical orbital oscillations to be coupled. The one-turn map must be parametrized by a full 4×4 matrix instead of a pair of decoupled 2×2 matrices. The normal modes ('Floquet modes') are more complicated. A parametrization of the 4×4 matrix, to handle transverse coupling in the linear dynamical approximation, has been given by Edwards and Teng (1973). In general, we shall treat uncoupled orbital oscillations.

8.5. Canonical variables, phase-space and normalized emittance

The variables $x' = \mathrm{d}x/\mathrm{d}s$ and $y' = \mathrm{d}y/\mathrm{d}s$ are not conjugate to x and y, respectively, and so (x, x') and (y, y') are not pairs of canonical variables. For motion with horizontal bending,

$$x' = \frac{p_x}{p_s}\left(1 + \frac{x}{\rho}\right), \qquad y' = \frac{p_y}{p_s}\left(1 + \frac{x}{\rho}\right). \tag{8.16}$$

The difference between p_s and p_0 is small, where p_0 is the longitudinal momentum of the reference particle. In the approximation of linear orbital dynamics, we can further neglect the products xp_x and xp_y, so

$$x' \simeq \frac{p_x}{p_0}, \qquad y' \simeq \frac{p_y}{p_0}. \tag{8.17}$$

Now p_0 is a fixed quantity, while p_x and p_y are conjugate to x and y, respectively. Then, $(x, p_x/p_0)$ constitutes a phase-space, as does $(y, p_y/p_0)$. For full generality, to include coupling, one should write $(x, p_x/p_0, y, p_y/p_0)$. Many modern accelerator computer codes, to integrate the orbital equations of motion do, in fact, use the variables $(x, p_x/p_0)$ and $(y, p_y/p_0)$. In the linear dynamical approximation, they coincide with (x, x') and (y, y'). However, $(x, p_x/p_0)$ and $(y, p_y/p_0)$ remain canonical when treating higher order terms in the motion, whereas (x, x') and (y, y') do not. We shall require canonical variables throughout most of this paper, to correctly set up the theory of the spin dynamics. Hence, we shall work with the variables $(x, p_x/p_0)$ and $(y, p_y/p_0)$.

Our first example of the use of the variables $(x, p_x/p_0)$ and $(y, p_y/p_0)$ is to analyse the concept of the *normalized emittance*. The statement that p_0 is a fixed quantity is only true if the beam is not accelerated; otherwise the value of p_0 does change. If the beam is accelerated, i.e. the reference energy and momentum are varied, the emittances ε_x and ε_y, as defined above, are not Lorentz invariants. Instead, one must scale them by $\beta_0\gamma_0$, where the reference momentum is $p_0 = mc\beta_0\gamma_0$, i.e. one effectively uses the variables $(x, p_x/(mc))$ and $(y, p_y/(mc))$. The normalized emittances $\varepsilon^N_{x,y}$ are defined via

$$\varepsilon^N_x = \beta_0\gamma_0\,\varepsilon_x, \qquad \varepsilon^N_y = \beta_0\gamma_0\,\varepsilon_y. \tag{8.18}$$

The normalized emittances are Lorentz invariants under boosts along the beam direction $\boldsymbol{p}_0$. The emittances of hadron beams are almost always specified in terms of normalized emittances. This is not true for electron beams, because the synchrotron radiation (recoils from the photon emissions) acts as a stochastic mechanism which randomizes the particle motion and causes the beam to settle down to a self-consistent equilibrium value, which is not invariant under Lorentz boosts.

8.6. Action-angle variables

When the orbital motion is parametrized in terms of a phase-space, i.e. $(x, p_x/p_0)$ and $(y, p_y/p_0)$, the invariants I_x and I_y acquire a new and important significance. They are the *action variables* of the motion. An orbital trajectory can be specified using *action-angle* variables, namely, (I_x, ϕ_x) and (I_y, ϕ_y). Here ϕ_x and ϕ_y are the horizontal and vertical angle variables, respectively. We shall treat the horizontal motion for definiteness. The actions are invariant along a trajectory, but the angles increase according to

$$\frac{\mathrm{d}\phi_j}{\mathrm{d}\theta} = Q_j \qquad (j = x, y), \tag{8.19}$$

so the solution along a trajectory is $\phi_j = Q_j\theta + \phi_{j0}$. Still treating linear orbital dynamics, the parametrization of a betatron oscillation is

$$\begin{aligned} x_\beta(\theta) &\equiv \sqrt{2I_x\beta_x(\theta)}\cos(\phi_x + \Psi_x(\theta)), \\ y_\beta(\theta) &\equiv \sqrt{2I_y\beta_y(\theta)}\cos(\phi_y + \Psi_y(\theta)), \end{aligned} \tag{8.20}$$

where $\Psi_j(\theta) = \psi_j(\theta) - Q_j\theta$ $(j = x, y)$ is periodic in θ. There are several important points to note about action-angle variables:

- The use of action-angle variables is *not* restricted to linear orbital dynamics; it applies in full generality to nonlinear dynamical systems.
- The action-angle variables (I_x, ϕ_x) are dynamical variables in the Hamiltonian sense, as are (x, p_x). One can parametrize the orbital phase-space using (I_x, ϕ_x) rather than (x, p_x), for example. The betatron phase ψ_x is *not* a dynamical variable.

- The actions index a particular trajectory, and the angles parametrize the motion along that trajectory. The set of all trajectories for fixed $\boldsymbol{I} = \boldsymbol{I}_*$ is called an *invariant torus*. The set of invariant torii are said to *foliate* the phase-space. Invariant torii never intersect.
- Action-angle variables only exist if the phase-space manifold is compact. We are therefore making a tacit assumption here, that the orbital oscillations are bounded. Indeed, if the orbital motion is unbounded, the beam will simply be lost from the machine. To yield interesting physics, the accelerator must be set up so that the orbits are stable and bounded. Even then, the existence of action-angle variables is not guaranteed. We are therefore making some restrictive assumptions on the orbital motion.
- The use of action-angle variables is, in most cases, the most elegant way to formulate the statistical mechanics of the system. In equilibrium, the particle distribution has a uniform distribution over the values of the angles. The equilibrium particle distribution is, therefore, a function of the actions only.

8.7. Formal definition of the orbital tunes

The more formally correct definition of an orbital tune is that, it is the *secular rate of phase advance* of the orbital angle variable. By 'secular' we mean that the rate of orbital phase advance does not average to zero over a full oscillation period of ϕ. (This definition must be made more precise when there are multiple angle variables with different, and usually incommensurate, oscillation periods. Consult a textbook on higher classical dynamics.) Equation (8.19) should be considered as the formal definition of the orbital tune. If a system is fully integrable *and* the motion is expressible in action-angle form, then the diagonalized Hamiltonian is a function of only the actions:

$$\mathscr{H} = \mathscr{H}(\boldsymbol{I}). \tag{8.21}$$

Hamilton's equations then read

$$\frac{\mathrm{d}\phi_j}{\mathrm{d}\theta} = \frac{\partial \mathscr{H}}{\partial I_j}, \qquad \frac{\mathrm{d}I_j}{\mathrm{d}\theta} = -\frac{\partial \mathscr{H}}{\partial \phi_j} = 0. \tag{8.22}$$

The I_j are invariants, which is expressed by the fact that the ϕ_j do not appear in $\mathscr{H}$. The angles are so-called *ignorable coordinates*. Since the tune is $Q_j = \mathrm{d}\phi_j/\mathrm{d}\theta$ by definition, we see that

$$Q_j = \frac{\partial \mathscr{H}}{\partial I_j}. \tag{8.23}$$

In the linear dynamical case, the Hamiltonian is simply $\mathscr{H} = \boldsymbol{Q} \cdot \boldsymbol{I}$. The spin tune will later be defined as the secular rate of the spin phase advance, when action-angles for the spin are introduced.

8.8. Synchrotron oscillations and longitudinal phase-space

In addition to the transverse oscillations, i.e. width and height, a bunch of particles in an accelerator also has a length, i.e. a longitudinal extent. Consider a simple model of horizontal circular motion in a uniform vertical magnetic field B. Equating the centripetal acceleration (force) to the Lorentz force,

$$m\gamma \frac{v^2}{r} = e\frac{v}{c}B, \tag{8.24}$$

one obtains for the angular velocity $\omega = v/r$, that

$$\omega = \frac{eB}{mc\gamma}. \tag{8.25}$$

The revolution frequency decreases with the energy. Hence, if a beam of particles with an energy spread circulates in an accelerator—and any beam in a real accelerator will inevitably have an energy spread—the particles will separate longitudinally.

Longitudinal focusing of the orbital motion in particle accelerators is achieved via the use of radio-frequency longitudinal electric fields (TM modes in waveguides called rf cavities) to push the particles longitudinally. As noted in chapter zero, the rf cavities actually perform three, not necessarily mutually exclusive, functions. They supply a differential longitudinal push to the particles based on their time of arrival (at the cavities) relative to the reference particle (also known as the *synchronous particle*). For electron and positron rings, the rf cavities also replenish the energy lost to synchrotron radiation. For synchrotrons of all types, the rf cavities are also used to do work on the particles to ramp up the beam energy ('acceleration') from injection to the top energy.

There is naturally a longitudinal phase-space. There are two sets of variables one can use to parametrize the longitudinal oscillations. One set is the longitudinal offset, and the longitudinal momentum offset, relative to the reference particle, i.e. $(z, \Delta p_s)$. The other is a time-of-arrival and energy offset relative to the reference particle, i.e. $(\tau, \Delta E)$. One can multiply τ by the speed of light to obtain a length $c\tau$. In practice, one employs the relative momentum or energy offset $\Delta p/p_0$ or $\Delta E/E_0$. A longitudinal oscillation can be parametrized via

$$\frac{\Delta p}{p_0} = \sqrt{2I_z}\cos\phi_z, \tag{8.26}$$

where (I_z, ϕ_z) are the longitudinal action-angle variables. There is also obviously a longitudinal emittance ε_z. The longitudinal emittance is measured in units of electronvolt-second, if one employs $(z, \Delta p_s)$, or $(\tau, \Delta E)$ without dividing by p_0 or E_0, as the case may be.

8.9. Dispersion

Return to the model of horizontal circular motion in a uniform vertical magnetic field B. Solve (8.24) as follows: $pc = eBr$. Hence, to the first order in small quantities (for fixed B) $\Delta p/p = \Delta r/r$. If a particle has a momentum offset Δp relative to the reference particle, its orbital radius is slightly larger. The basic idea is the same for more complicated magnetic focusing structures. If a particle has a relative momentum offset $\Delta p/p_0$, we write the horizontal motion as a sum of betatron and 'dispersion' terms

$$x = x_\beta + x_\delta. \tag{8.27}$$

This decomposition, of course, assumes linear orbital dynamics. We also write

$$x_\delta = D_x \frac{\Delta p}{p_0}. \tag{8.28}$$

The function D_x is called the (horizontal) *dispersion* function. Hence, the total horizontal motion in a beam has contributions from both the betatron oscillations and the momentum spread. When averaging over the particle distribution, if there are no coherent betatron or energy oscillations, then

$$\langle x\rangle = \langle x_\beta\rangle + \langle x_\delta\rangle = 0 \tag{8.29}$$

and the second moment (rms beam width) is

$$\langle x^2\rangle = \langle (x_\beta + x_\delta)^2\rangle = \langle x_\beta^2\rangle + 2\langle x_\beta x_\delta\rangle + \langle x_\delta^2\rangle = \beta_x\langle I_x\rangle + D_x^2\langle I_z\rangle. \tag{8.30}$$

The two contributions are usually of comparable magnitude. It is assumed that there is no correlation between the betatron and the synchrotron oscillations, so $\langle x_\beta x_\delta\rangle = 0$.

There is, correspondingly, a vertical dispersion function D_y, where

$$y = y_\beta + y_\delta, \qquad y_\delta = D_y \frac{\Delta p}{p_0}. \tag{8.31}$$

In a planar ring, the vertical dispersion is zero. If a ring contains vertical bending, or if there are imperfections or misalignments in the ring, then the vertical dispersion will be nonzero, but small. The equations satisfied by the horizontal and vertical dispersions are

$$D_x'' + G_x(s) D_x = \frac{1}{\rho_x}, \qquad D_y'' + G_y(s) D_y = -\frac{1}{\rho_y}. \tag{8.32}$$

In a planar ring, $\rho_y^{-1} = 0$ everywhere, hence in the ideal design, $D_y = 0$.

8.10. Momentum compaction factor

We saw that both the revolution frequency around the ring and also the orbit radius vary with the fractional momentum offset of a particle. Let us formalize this relationship. First, from $\omega = v/r$ we have, to the first order in small quantities,

$$\frac{\Delta\omega}{\omega} = \frac{\Delta v}{v} - \frac{\Delta r}{r}. \tag{8.33}$$

From the elementary relativity theory

$$\frac{\Delta v}{v} = \frac{1}{\gamma^2}\frac{\Delta p}{p}. \tag{8.34}$$

What about the relation of $\Delta r/r$ to $\Delta p/p$? We define the *momentum compaction factor* α_c via

$$\frac{\Delta C}{C} = \frac{\Delta r}{r} = \alpha_c \frac{\Delta p}{p}. \tag{8.35}$$

Then, for either the revolution frequency f, or the angular frequency ω,

$$\frac{\Delta f}{f} = \frac{\Delta\omega}{\omega} = \left(\frac{1}{\gamma^2} - \alpha_c\right)\frac{\Delta p}{p}. \tag{8.36}$$

It is easily worked out that $\alpha_c = 1$ for motion in a uniform vertical magnetic field. In general, $\alpha \ll 1$, for example, $\alpha_c \simeq 1.86 \times 10^{-4}$ at LEP. The momentum compaction factor is related to the (horizontal) dispersion via

$$\alpha_c = \left\langle \frac{D_x}{\rho_x} \right\rangle = \frac{1}{C} \oint \frac{D_x}{\rho_x}\, \mathrm{d}s. \tag{8.37}$$

At higher orders, one expands in a series

$$\frac{\Delta f}{f} = \frac{1}{\gamma^2}\frac{\Delta p}{p} - \alpha_{c1}\frac{\Delta p}{p} - \alpha_{c2}\left(\frac{\Delta p}{p}\right)^2 + \cdots. \tag{8.38}$$

Basically, there are two competing contributions to the fractional change in the revolution frequency $\Delta f/f$. The first is that particles with higher momentum have a higher speed, and hence, a higher revolution frequency. The second is that particles with higher momentum travel in orbits of larger radius, and hence a lower revolution frequency. Equation (8.36) describes the competition between these two effects. In ultrarelativistic rings, we can neglect γ^{-2}, and furthermore, approximate $\Delta p/p \simeq \Delta E/E$, so that it is typical to write

$$\frac{\Delta f}{f} = -\alpha_c \frac{\Delta E}{E}. \tag{8.39}$$

This is done, for example, by Sands (1970).

8.11. Chromaticity

The values of the betatron tunes can be affected by higher-order nonlinear terms in the orbital focusing, but a more important contribution is, in fact, from the momentum offset. The focusing by a quadrupole is slightly weaker for higher momentum particles. Hence, the betatron tunes depend on the fractional momentum offset $\Delta p/p_0$. The (horizontal and vertical) *chromaticity* ξ_x and ξ_y, respectively, is defined to the first order in small quantities via

$$Q_x = Q_{x0} + \xi_x \frac{\Delta p}{p_0}, \qquad Q_y = Q_{y0} + \xi_y \frac{\Delta p}{p_0}. \tag{8.40}$$

Sextupole magnets can affect the value of the chromaticity. Chromaticity control is, in fact, one of the principal uses of sextupole magnets in modern accelerators. To do this, the dispersion must be nonzero at the location of a sextupole.

The chromaticity will provide us with one of the clearest examples of the effects on nonlinear orbital dynamics on the spin/polarization in experimental work at the KEK-PS, to be reviewed later in this paper.

9. Orbital beam emittances

9.1. General remarks

In the previous section we mainly discussed the orbital motion of individual particles, although we did mention the Courant–Snyder invariant and the orbital emittances. Here, we discuss the determination of the orbital beam emittances. We shall mainly review the statistical mechanics of the effects of the synchrotron radiation on the orbital motion. The treatment will be regrettably brief. We also include only a very short discussion of nonradiative beams.

Holt (1984) presents an excellent exposition on equilibration via stochastic fluctuations and damping mechanisms in the context of electron and stochastic cooling. Jowett (1987) gives an excellent lecture on the statistical mechanics of electron storage rings. (The above authors do not discuss spin.) Jowett reminds the reader of the important fact that, the term 'statistical mechanics' is *not* synonymous with 'thermodynamic equilibrium'. Instead, an electron beam in a storage ring receives energy from rf cavities and emits photons, leading to overall energy loss and 'random walks' in response to the recoils from the photon emissions, etc, ultimately establishing a *nonthermal* steady-state phase-space distribution for the electrons.

9.2. Nonradiative beams

The emittance of a nonradiative beam, i.e. not emitting synchrotron radiation (i.e. a hadron beam or a muon beam), is generally determined at injection into a machine. Consequently, the emittance is really determined at the source where the particles are created. In most modern accelerator complexes, the beam is then transported to the final accelerator via a cascaded chain of intermediate 'booster' accelerators. During the transport process, the normalized beam emittances remain invariant. By Liouville's theorem, the beam emittance remains invariant during storage of the beam, as long as the beam is acted upon only by Hamiltonian forces. This is an approximation which is violated in several ways.

The beam emittances may increase for various reasons ('beam blowup') during the transport process. One obvious process is that the optics of one machine (the beta functions and dispersion, etc) may not be matched to the next. Other sources of emittance blowup are intrabeam scattering, because the particles all have the same sign of charge and hence, repel one another, and also, beam–gas scattering with residual gas molecules or ions in the beam

vacuum chamber. Such processes also apply to electron beams. We shall not discuss these mechanisms in detail. These are non-Hamiltonian processes in the sense that they are random stochastic interactions.

There are also two important mechanisms which are used to *decrease* the emittances of nonradiative beams. The process of emittance reduction is called *cooling*. The two mechanisms are called stochastic cooling and electron cooling. They are important in many modern accelerator complexes. We briefly discuss electron cooling below.

The original idea of electron cooling was invented by Budker (1967) as a method to cool *antiproton* beams, because the production of antiprotons, by scattering high-energy protons onto a target, produces an antiproton beam with a very large emittance. Gersh Budker was the pioneer of many innovative accelerator physics ideas. The Budker Institute of Nuclear Physics (BINP) at Novosibirsk is named after him. Electron cooling also works for beams of protons and heavy ions, and is used today for that purpose. Basically, proton beams are 'hot' in the sense that they have a large transverse momentum and a large transverse emittance. To cool the proton beam, i.e. to reduce its transverse emittance, a 'cool' beam of electrons, with the same longitudinal velocity as the protons, but a much lower transverse momentum, is injected collinearly with the protons in a straight section of the ring. The electron beam is matched to the proton beam width and height. The basic idea is that of mixing a hot and a cold gas—the gas molecules collide (via Coulomb scattering) and the hot gas (in this case, the protons) cools down, and the cold gas (the electrons) heats up. The electrons are dumped at the end of the straight section. A fresh batch of electrons is injected into the ring on the next pass of the protons around the ring. In this way, the proton beam emittance is reduced.

The Coulomb potential is spin-independent, so the electron cooling process *per se* has little effect on the proton spins. However, the presence of a (strong) solenoid in the ring (especially if not fully compensated) can cause a possibly significant spin rotation. In fact, the overall combination of the toroidal magnetic field and the vertical steering magnets in the electron cooling section of the IUCF Cooler *did* lead to a significant (and initially unsuspected) spin rotation in that ring. This caused a systematic error in the measurement of the spin tune at the IUCF Cooler. The matter is reviewed in MSY1.

9.3. Synchrotron radiation formulae

The emission of photons induces recoils in the particle motion. This is a stochastic randomizing mechanism which mixes up the particles in the orbital phase-space, and leads to a self-consistent equilibrium emittance. The problem of radiative equilibrium is viewed in this review as an application of fundamental statistical mechanical principles to the motion of particle beams in accelerators.

We treat only the simplest case of synchrotron radiation in dipole magnets, i.e. the particle motion is locally a circular arc of radius ρ in a locally uniform magnetic field B. The basic formulae for classical synchrotron radiation were worked out in Schwinger's (1949) classic paper. We use formulae which are expressed in forms more directly suitable for 'accelerator coordinates' from sources such as Sands (1970) below. The classical synchrotron radiation power output, for motion at energy E in a circular arc of radius ρ, is

$$P_\gamma = \frac{2}{3}\frac{e^2 c}{\rho^2}\beta^4\gamma^4 = \frac{2}{3}\frac{e^2 c\beta^4}{(mc^2)^4}\frac{E^4}{\rho^2}, \tag{9.1}$$

where all the symbols have their usual meanings. The spectral density of the synchrotron radiation (the radiated power per unit frequency interval) is, say, $\mathscr{P}(\omega)$, where

$$P_\gamma = \int_0^\infty \mathscr{P}(\omega)\,\mathrm{d}\omega. \tag{9.2}$$

One can write

$$\mathscr{P}(\omega) = \frac{9\sqrt{3}}{8\pi}\frac{P_\gamma}{\omega_c}\frac{\omega}{\omega_c}\int_{\omega/\omega_c}^{\infty} K_{5/3}(x)\,\mathrm{d}x, \tag{9.3}$$

where $K_{5/3}$ is a modifed Bessel function of the second kind. The radiated power spectrum per unit frequency exhibits a broad maximum around a 'critical frequency' ω_c, given by

$$\omega_c = \frac{3}{2}\,\omega_{\rm rev}\gamma^3 = \frac{3}{2}\frac{c\gamma^3}{\rho}, \tag{9.4}$$

where $\omega = c/\rho$ is the revolution frequency for ultrarelativistic motion. It was pointed out in section 2, in connection with the Sokolov–Ternov work, that the perturbation expansion parameter for calculating the synchrotron radiation power spectrum is

$$\xi = \frac{\hbar\omega_c}{E} = \frac{3}{2}\frac{\hbar}{mc\rho}\gamma^2 = \frac{3}{2}\frac{\lambda_c}{\rho}\gamma^2. \tag{9.5}$$

Here, λ_c is the Compton wavelength. In present-day storage rings $\xi \ll 1$, i.e. a typical photon takes away only a small fraction of the electron energy. In the 'quantum regime' $\xi \geqslant 1$, and a semiclassical approximation cannot be used.

The number of photons in the frequency interval $(\omega, \omega + \mathrm{d}\omega)$ is $n(\omega) = \mathscr{P}(\omega)/(\hbar\omega)$, hence, the total rate of emission of photons is

$$\mathscr{N} = \int_0^\infty \mathscr{P}(\omega)\frac{\mathrm{d}\omega}{\hbar\omega} = \frac{15\sqrt{3}}{8}\frac{P_\gamma}{u_c}, \tag{9.6}$$

where the critical energy is $u_c = \hbar\omega_c$. The mean photon energy is

$$\langle u\rangle = \frac{1}{\mathscr{N}}\int_0^\infty u n(u)\,\mathrm{d}u = \frac{P_\gamma}{\mathscr{N}} = \frac{8}{15\sqrt{3}}\,u_c, \tag{9.7}$$

writing $u = \hbar\omega$ and $n(u)\mathrm{d}u$ for $\mathscr{P}(\omega)\,\mathrm{d}\omega/(\hbar\omega)$. Also relevant is the mean square photon energy, which is $\langle u^2\rangle = (11/27)\,u_c^2$ and the product

$$\mathscr{N}\langle u^2\rangle = \int_0^\infty u^2 n(u)\,\mathrm{d}u = \frac{55}{24\sqrt{3}}\,u_c\,P_\gamma. \tag{9.8}$$

Since the emission of a photon, of course, reduces the electron energy, it is quite common to denote the relative energy change by $\delta\gamma/\gamma = -\hbar\omega/E$. The average time rate of change of the second moment $(\delta\gamma/\gamma)^2$, is given by

$$\frac{\mathrm{d}(\delta\gamma/\gamma)^2}{\mathrm{d}t} = \mathscr{N}\left\langle\frac{u^2}{E^2}\right\rangle = \frac{55}{24\sqrt{3}}\frac{e^2\hbar\gamma^5}{m^2c^2}\frac{1}{|\rho|^3}. \tag{9.9}$$

It is also standard to express the above formulae in terms of the so-called *quantum constant*, which is proportional (and very nearly equal) to the electron Compton wavelength

$$C_q = \frac{55}{32\sqrt{3}}\frac{\hbar}{mc} \simeq 0.992\frac{\hbar}{mc} = 3.84\times10^{-13}\,\mathrm{m}. \tag{9.10}$$

9.4. Beam parameters for radiative equilibrium

The next step is to calculate the contribution of the fluctuation terms, and to take suitable statistical averages over the photon emissions, to derive the equilibrium beam width, energy spread, etc in a synchrotron or storage ring. We merely state the results. Consult Sands (1970) for the detailed derivations. The equilibrium relative energy spread is given by

$$\sigma_\epsilon^2 = \frac{\sigma_E^2}{E_0^2} = \langle I_z\rangle = \frac{C_q}{J_s}\frac{\oint(1/|\rho_x|^3)\,\mathrm{d}s}{\oint(1/\rho_x^2)\,\mathrm{d}s}\,\gamma_0^2. \tag{9.11}$$

Here, $C_{\rm q}$ is the quantum constant and J_s is a so-called 'partition number'. The rms absolute energy spread σ_E is therefore proportional to the square of the beam energy. As for the bunch length (time-of-arrival),

$$\sigma_\tau = \frac{\alpha}{\omega_{\rm s}}\,\sigma_\epsilon, \tag{9.12}$$

where α is the momentum compaction factor, and $\omega_{\rm s}$ is the synchrotron oscillation frequency. The expression for the equilibrium horizontal betatron actions is

$$\langle I_x\rangle = \frac{C_q}{J_x}\,\frac{\oint (1/|\rho_x|^3)\,\mathscr{H}_x^D\,{\rm d}s}{\oint (1/\rho_x^2)\,{\rm d}s}\,\gamma_0^2. \tag{9.13}$$

Here, J_x is another partition number and

$$\mathscr{H}_x^D \equiv \gamma_x D_x^2 + 2\alpha_x D_x D_x' + \beta_x D_x'^2. \tag{9.14}$$

It is analogous to the Courant–Snyder invariant with D_x and D_x' substituted for x_β and x_β', respectively; however $\mathscr{H}_x^D$ is not an invariant. The mean-square horizontal betatron beam size is given by

$$\sigma_{x\beta}^2(\theta) = \beta_x(\theta)\langle I_x\rangle \tag{9.15}$$

and the overall total mean-square beam size is

$$\sigma_x^2 = \beta_x\langle I_x\rangle + D_x^2\sigma_\epsilon^2. \tag{9.16}$$

The average beam size varies with the azimuth. Typically, the value of β_x is minimized and D_x is made to vanish at the interaction points of a collider (both electron and hadron), so as to increase the beam luminosity.

Note that both $\langle I_x\rangle$ and σ_ϵ^2 are proportional to E_0^2, so the two contributions to the beam size scale identically with the beam energy, and are of comparable magnitude at any beam energy. Since $\langle I_x\rangle \propto E_0^2$, etc, one does not define a normalized emittance for a beam in radiative equilibrium.

Multiplying by $p_0 = mc\beta_0\gamma_0$ gives the corresponding average value in the $(x,\,p_x)$ phase-space, which is

$$p_0\langle I_x\rangle = \hbar\,\frac{55}{32\sqrt{3}}\,\frac{1}{J_x}\,\frac{\oint (1/|\rho_x|^3)\,\mathscr{H}_x^D\,{\rm d}s}{\oint (1/\rho_x^2)\,{\rm d}s}\,\gamma_0^3. \tag{9.17}$$

Roughly taking ρ_x as uniform and estimating $\mathscr{H}_x^D \simeq \rho$, and approximating $J_x \simeq 1$ and $55/(32\sqrt{3}) \simeq 1$, yields $p_0\langle I_x\rangle \simeq \hbar\,\gamma_0^3$. This number is far in excess of $\hbar$ in present-day storage rings.

The equilibrium value for the vertical betatron actions would depend on the quantity

$$\mathscr{H}_y^D \equiv \gamma_y D_y^2 + 2\alpha_y D_y D_y' + \beta_y D_y'^2. \tag{9.18}$$

There is an obvious difficulty with the above expression, which is that $D_y = D_y' = 0$ in a perfectly aligned planar ring. Hence, $\mathscr{H}_y^D = 0$, and so $\langle I_y\rangle = 0$: the vertical beam size would vanish. In practice, the vertical beam size is not zero, but it is small. Most e^+e^- beams in high-energy accelerators are 'flat beams', which is another way of saying that $\langle I_x\rangle \gg \langle I_y\rangle$, possibly $\langle I_x\rangle \gtrsim 100\langle I_y\rangle$. Note the following important points:

- The nonzero value of the vertical betatron emittance results from such things as misalignments and imperfections in the machine, including (small) transverse x–y betatron coupling, which causes the vertical betatron oscillations to couple into the horizontal plane. Hence, the value of the vertical betatron emittance is determined by machine imperfections.

- In some machines such as modern synchrotron light sources, a certain amount of betatron coupling is deliberately induced to increase the vertical emittance. This is because the particle density is otherwise so high that the rate of beam loss from intrabeam scattering becomes too high, and the beam lifetime is unacceptably reduced.
- Another factor, which is not important for real machines but is, nevertheless, a valid theoretical point, is that the direction of an emitted photon is not exactly parallel to the particle momentum. The photon does carry away a small transverse momentum, and this does make a small, but nonzero, contribution to $\langle I_y \rangle$. The influence of such vertical recoils on the electron *spins* was studied by Bell and Leinaas (1987) for a model weak-focusing ring. The Bell–Leinaas work is reviewed in section 27.12.

The orbital damping time constants are typically a few milliseconds (in rings with bending radii of a few metres, and energies of a few GeV), up to a few seconds in a very large high-energy ring like LEP. A reasonable order-of-magnitude estimate is 1–100 ms. The polarization buildup time constant, by contrast, can be several hours. Hence, the orbital beam distribution can be considered to be already in equilibrium when deriving the formula for the equilibrium radiative polarization of the spins.

10. Maps and other basic concepts of spin dynamics

10.1. Maps and Poincaré sections

Obviously, the transformation of a spin vector from an initial azimuth θ_i to a final azimuth θ_f is a rotation. If we employ a spinor (vector) representation, the map of the spin motion is an element of the Lie group $SU(2)$ or $SO(3)$, respectively. Frequently, the map of greatest interest is the *one-turn map* (OTM) around the ring circumference. The starting and ending azimuths are the same: $\theta_\mathrm{f} = \theta_\mathrm{i} + 2\pi$. The one-turn map, say M_OTM, is, in general, a function of θ_i, and also of the initial orbital phase-space point z_i, where we employ z to collectively denote all the orbital dynamical variables. Instead of solving differential equations for the orbital and spin motion continuously around the ring, we examine it on successive passes around the ring, at a fixed azimuth, say θ_*. This technique of analysing the motion is called a *Poincaré section*. Note that a map is more general than a Poincaré section. A map can apply to a single-pass system, such as a linear accelerator. A Poincaré section is a specialized use of maps, for systems with a period in the motion (2π in the aximuth θ in our case).

An important special case is the spin map for particle motion on the *closed orbit*, i.e. $z = 0$. Note that for the orbital motion this is trivial; the orbital map is just the identity, but for the spin, the map is a nontrivial rotation even on the closed orbit. Let us employ the spinor representation. One can parametrize the one-turn map on the closed orbit via

$$M(\theta_*, \theta_* + 2\pi) = \mathrm{e}^{-\mathrm{i}\pi\nu_\mathrm{c.o.}\boldsymbol{\sigma}\cdot\boldsymbol{n}_0}. \tag{10.1}$$

The vector $\boldsymbol{n}_0$ is the spin rotation axis of the one-turn spin map at the azimuth θ_*. We shall discuss the other parameter, $\nu_\mathrm{c.o}$, shortly. The vector $\boldsymbol{n}_0(\theta)$ is the solution of the spin motion on the closed orbit which repeats after one turn, and therefore, repeats after *every* turn. In general, the long-term polarization of the beam points along $\boldsymbol{n}_0$. This is actually not strictly true, one must solve for the spin motion on all the off-axis orbital trajectories and take a statistical average, and it is possible that the answer might not point along $\boldsymbol{n}_0$. Mane (2003b) has given an example of a model accelerator, where the average spin direction does not point along $\boldsymbol{n}_0$. However, for all practical purposes, we may take $\boldsymbol{n}_0(\theta)$ to be the long-term polarization direction, also called the 'stable polarization direction', at the azimuth θ.

The other parameter, $\nu_{\text{c.o.}}$, is the spin tune on the closed orbit. In general, on any orbital trajectory, the spin tune is defined as the *secular* rate of the spin phase advance per turn, around the ring circumference. This is completely analogous to the orbital motion, where the orbital tunes are defined as the secular rates of the phase advances of the orbital oscillation modes. However, in the case of the spin motion, there is a rate of spin phase advance even on the closed orbit $z = 0$. The spin phase advance over one turn around the closed orbit, is the spin rotation angle of the one-turn map, and the closed orbit spin tune is this angle divided by 2π. We shall generally drop the subscript on $\nu_{\text{c.o.}}$, and just write ν. The reader should be able to deduce from the context whether ν refers to the closed orbit, or to an off-axis orbital trajectory.

10.2. Uniqueness of solutions

Note that the solution pair $(-\boldsymbol{n}_0, -\nu_{\text{c.o.}})$ would yield exactly the same one-turn map for the spin motion. This is also true for off-axis trajectories, as long as the trajectory is not on a spin–orbit resonance. However, for the spin tune, a Poincaré section cannot, in general, distinguish between ν and $1 - \nu$. We drop the subscript on $\nu_{\text{c.o.}}$ because the preceding statement applies to all orbits, not just the closed orbit. A Poincaré section also cannot yield the integer part of the spin tune. Hence, there is considerable ambiguity in deciding what 'the' value of the spin tune is. Only the fractional part $[\nu]$ can be meaningfully defined, and even then, there are two possibilities, namely, $[\nu]$ and $1 - [\nu]$.

10.3. Design and closed orbit

We now address an important issue which is frequently not addressed clearly in the literature, causing different authors to use the same notation and terminology to mean different things. We need to distinguish between the *closed orbit* and the *design orbit* of a ring. The design orbit is a theoretical construct, for a paper design of a machine where all the magnets are perfectly aligned. In a real accelerator, due to inevitable tolerances of manufacture and surveying, etc, the closed orbit will differ from the design orbit by small imperfections. Most theoretical treatments of map techniques, etc, assume that the orbital motion due to the imperfections has already been solved, and so the phase-space point $z = 0$ refers to the imperfect closed orbit, not the design orbit. Otherwise, when treating simple model systems, e.g. in textbooks, the imperfections are taken as zero. If the origin of the map were not referred to the imperfect closed orbit, then there would be *two* perturbation expansions to deal with simultaneously, namely, powers of the amplitude of the imperfections, as well as powers of the amplitudes of the orbital oscillations.

As we shall see below, some of the depolarizing spin resonances are driven by closed orbit imperfections, and others by the orbital oscillations, and some by a combination of both. Hence, the imperfections are frequently not negligible when treating the spin motion. In writing the one-turn spin map above, our use of $\boldsymbol{n}_0$ and $\nu_{\text{c.o.}}$ refers to the imperfect closed orbit. We shall describe several formalisms below, to calculate the spin quantization axis $\boldsymbol{n}$ and the spin tune ν, as functions of the orbital phase-space variables. In all of those formalisms, it will be assumed that the point $z = 0$ refers to the imperfect closed orbit, and the spin motion on the imperfect closed orbit has already been solved, before proceeding to $z \neq 0$. We shall see one example later in this paper, of a so-called 'hybrid spin resonance', where the spin precessions resonate with a combination of both the orbital oscillations and the closed orbit imperfections.

10.4. Spin tune for a planar ring

We now write down and solve the equation of motion on the design orbit of a planar ring with a uniform bending radius, so $R = \rho$ and $x = 0$, etc. We have discussed this problem on more than one occasion already. Then, $(e/p)(\boldsymbol{B}_\perp/c) = -\boldsymbol{e}_3/\rho$ and $R = \rho$ and so

$$\boldsymbol{W} = R\,(a\gamma_0 + 1)\frac{\boldsymbol{e}_3}{\rho} - \frac{R}{\rho}\,\boldsymbol{e}_3 = a\gamma\boldsymbol{e}_3, \tag{10.2}$$

where γ_0 is the Lorentz factor of the reference particle. The spin precession equation in the accelerator coordinates is thus

$$\frac{\mathrm{d}\boldsymbol{s}}{\mathrm{d}\theta} = a\gamma_0\,\boldsymbol{e}_3 \times \boldsymbol{s}. \tag{10.3}$$

The value of the spin tune is $\nu_0 = a\gamma_0$. The above conclusion holds for *any* planar ring, e.g. with reverse bends, as long as the overall orbital bend angle is 360° (i.e. no figure of eight machines). The solution for $\boldsymbol{n}_0$ is clearly $\boldsymbol{n}_0 = \boldsymbol{e}_3$. The expression for the spin tune in a planar ring is so important that we denote it by the special symbol ν_0.

The spin tune in a perfectly aligned planar ring is *proportional to the average beam energy*. The consequences of this simple fact are profound. It implies (among other things) that, if a spin-polarized beam is injected into an accelerator at a low energy and accelerated to a high energy, the spins will cross resonances whenever the value of ν_0 equals an integer (see (3.3), with $\nu_0 = m_0$). Such resonances will occur at regular energy intervals, spaced by $\Delta(a\gamma) = 1$, i.e. $\Delta E = mc^2/a$. We saw earlier that this implies that a resonance is crossed for every 440.65 MeV increase in the beam energy for electrons, while for protons, a resonance is crossed every 523.34 MeV. (There are also other resonances, of course, whose locations depend on the values of the orbital tunes.)

10.5. Resonance crossing in a planar ring

Almost all synchrotrons are 'fast-cycling', which means that the rate of beam energy increase is fairly rapid, and the beam is not stored at the top energy flattop for very long. Instead, it is delivered to an external beamline, and a fresh batch of particles is injected and accelerated. Under such circumstances, there is usually sufficient time for a coherence to develop between the spin precession and only the first-order combinations of the orbital oscillations. The resonance spectrum for acceleration in a planar synchrotron is given by

$$\nu_0 = m_0 \pm m_x Q_x \pm m_y Q_y \qquad (m_{x,y} \in \{0, 1\},\ |m_x| + |m_y| = 1). \tag{10.4}$$

In addition to the above, the synchrotron oscillations (energy oscillations) are also important. This is because $\nu = a\gamma$, and since the value of γ has a spread (energy spread of the beam), the spin tunes also have a spread of values.

In the present subsection, we shall treat only rings where the unperturbed spin direction (direction of $\boldsymbol{n}_0$) is vertical in the arcs. There are important modifications to the statements below if $\boldsymbol{n}_0$ is not vertical, as can happen in a ring with one or more partial Snakes. Since we have have not discussed (partial) Snakes yet, we shall revisit this topic in section 13.4, after we have introduced the concept of partial Snakes. However, to understand why partial Snakes are useful, we must first understand the simpler case of rings *without* such devices.

If, then, the spins precess around the vertical axis on the design orbit, the contribution of additional vertical magnetic fields from perturbations does not change the spin precession axis, and thus, does not decohere the spins (thereby depolarizing the beam). Hence, at the leading order, the leading sources of depolarizing perturbations are due to *horizontal* magnetic fields. The horizontal magnetic fields can arise from either of two sources: motion on the

vertical component of the imperfect closed orbit, caused by magnet errors or misalignments, and from the vertical component of the orbital oscillations. The latter can be due to the vertical betatron oscillations, or to coupling between the horizontal and vertical orbital motion, so that the horizontal betatron oscillations couple into the vertical plane.

We speak of the vertical component of the orbital motion, because the principal source of the perturbations is from the orbital motion through the quadrupoles, and the quadrupole magnetic field is $\boldsymbol{B}_{\mathrm{quad}} \propto y\boldsymbol{e}_1 + x\boldsymbol{e}_3$. Hence, the vertical orbital motion induces horizontal (in fact radial) perturbations in the spin precession vector $\boldsymbol{W}$.

The resonances where the spins couple to the perturbations from an imperfect closed orbit are called, not surprisingly, 'imperfection' resonances. The resonances where the spins couple to the betatron oscillations are called 'intrinsic' resonances, because they exist even in a machine without misalignments, and are intrinsic to the accelerator.

The horizontal betatron oscillations can also drive depolarizing spin resonances, but in a planar ring as we have defined it here, such resonances typically arise via coupling of the transverse (x, y) orbital motion, so that the horizontal betatron oscillations can drive radial perturbing terms in the spin precession vector. Intrinsic resonances driven by the horizontal betatron oscillations are frequently called 'coupling' resonances for this reason. However, we shall see in section 13.4, that in a ring equipped with one or more partial Snakes, the horizontal betatron oscillations can drive intrinsic resonances even if there is no transverse x–y coupling in the ring.

In the acceleration of polarized proton beams in the AGS for injection into RHIC, the spin tune crosses a total of 42 imperfection resonances, 4 strong and 3 weak intrinsic resonances (due to the vertical betatron oscillations) and 4 coupling resonances.

10.6. Resonances for stored beams

In a storage ring, where the particles circulate at a fixed energy for long periods, higher-order resonances can also be important. For example, numerous higher-order spin resonances are visible in the SPEAR polarization data shown in figure 6. Note also, in that figure, that the horizontal betatron spin resonance is *wider* than the vertical betatron spin resonance.

10.7. Symplecticity and unitarity

10.7.1. Phase-space flows. For a dynamical system whose equations of motion are derived from a Hamiltonian, the phase-space trajectories $(\boldsymbol{q}(t), \boldsymbol{p}(t))$ lie on a so-called *symplectic manifold*. Two good and reasonably modern texts on the subject are by José and Saletan (1998) and Goldstein *et al* (2002). Basically, the values of Poisson brackets are preserved on a symplectic manifold. The transformation of the phase-space variables, from an initial azimuth θ_{i}, to a final azimuth θ_{f}, is then canonical, as required by Hamilton's equations. In the simplest case of only one coordinate and conjugate momentum, the symplectic condition implies that the phase-space area of an infinitesimal phase-space element $(\mathrm{d}q, \mathrm{d}p)$ is preserved along a trajectory. In higher dimensions, the symplectic conditions are more restrictive than just simple area (or volume) preservation.

For the spin motion, the corresponding concept is unitarity. Essentially, unitarity means the length of a (classical) spin vector does not change during the evolution of the system. The most general spin transformation is a change of direction (rotation).

10.7.2. Symplectic matrices. Consider the important special case of linear orbital dynamics. The origin is at the closed orbit. The mapping of the phase-space flows of a linear dynamical

Hamiltonian system is described by a *symplectic matrix*. Recall that a square matrix M is called *orthogonal*, if it satisfies the condition $M^{\mathrm{T}} I M = I$, where I is the unit matrix and M^{T} is the transpose of M. We usually write this more simply as $M^{\mathrm{T}} M = I$. A symplectic matrix is defined analogously. A symplectic matrix is always even-dimensional, say $2n$, because it describes n coordinates and n conjugate momenta. Define the $(2n) \times (2n)$ skew-symmetric matrix

$$J = \begin{pmatrix} 0 & I \\ -I & 0 \end{pmatrix}. \tag{10.5}$$

Then M is a symplectic matrix if it satisfies the condition

$$M^{\mathrm{T}} J M = J. \tag{10.6}$$

A symplectic matrix has unit determinant. In addition, for stable particle motion, the eigenvalues of a symplectic matrix must lie on the unit circle. Hence, they must come in complex conjugate pairs, $\mathrm{e}^{\pm \mathrm{i}\mu}$, where μ is real. For our purposes, we parametrize the orbital motion as a 6-dimensional column vector

$$X = \begin{pmatrix} x \\ p_x/p_0 \\ y \\ p_y/p_0 \\ z \\ \delta \end{pmatrix}, \tag{10.7}$$

where $\delta = \Delta p/p_0$ is the relative momentum offset (and p_0 is the momentum of the reference particle). Here, we group the coordinates and momenta in pairs. We redefine the skew-symmetric J in 2×2 blocks via

$$J = \begin{pmatrix} 0 & 1 & & & & \\ -1 & 0 & & & & \\ & & 0 & 1 & & \\ & & -1 & 0 & & \\ & & & & 0 & 1 \\ & & & & -1 & 0 \end{pmatrix}, \tag{10.8}$$

where blanks denote zeros in the above matrix. Then, an orbital mapping $M(\theta_{\mathrm{i}}, \theta_{\mathrm{f}})$, in the approximation of linear dynamics, is described by a symplectic matrix with the above definition of J.

Much of the formalism below, for the use of eigenvectors of symplectic matrices for use in accelerator dynamics, was developed by Chao (1979). The map of principal interest to us is the one-turn map $M_{\mathrm{otm}} = M(\theta_{\mathrm{i}}, \theta_{\mathrm{i}} + 2\pi)$. We parametrize the orbital motion using the 6-dimensional eigenvectors of the one-turn map E_j with corresponding eigenvalues $\mathrm{e}^{\mathrm{i}\mu_j}$:

$$M_{\mathrm{otm}} E_j = \mathrm{e}^{\mathrm{i}\mu_j} E_j. \tag{10.9}$$

The eigenvalues come in complex conjugate pairs, $j = \pm 1, \pm 2, \pm 3$, where $\mu_{-j} = -\mu_j$, $j = 1, 2, 3$. Note that $E_{-j} = E_j^*$. It is easily seen that if the horizontal, vertical and longitudinal motions are uncoupled, that $\mu_1 = 2\pi Q_x$, $\mu_2 = 2\pi Q_y$ and $\mu_3 = 2\pi Q_s$, where $Q_{x,y,s}$ are the horizontal betatron, vertical betatron and synchrotron tunes, respectively. The symplectic eigenvector formalism can accomodate coupling between the orbital planes without

any change of notation. The orthonormality relation between the eigenvectors is

$$\begin{aligned} E_j^\dagger J E_j &= \mathrm{i} \qquad j > 0, \\ E_j^\dagger J E_j &= -\mathrm{i} \qquad j < 0, \\ E_j^\dagger J E_k &= 0 \qquad j \neq k. \end{aligned} \tag{10.10}$$

We can then decompose the column vector X into a sum of eigenvectors $X = \sum_j a_j E_j$. In the absence of coherent orbital motion, i.e. $\langle a_{\pm j} \rangle = 0$, the statistical average values of the second moments $\langle |a_{\pm j}|^2 \rangle$ are proportional to $\langle I_j \rangle$.

Of particular interest, is the case where the orbit is perturbed by the emission of a photon of synchrotron radiation. This occurs only for ultrarelativistic motion, hence we may approximate $\delta = \Delta\gamma/\gamma_0$. In the approximation of point photon emission, the difference $\delta X = X_\mathrm{f} - X_\mathrm{i}$ between the initial and final orbital motion is zero except for the final component δ, i.e.

$$\delta X \simeq -\frac{\hbar\omega_\mathrm{ph}}{E} \begin{pmatrix} 0 \\ 0 \\ 0 \\ 0 \\ 0 \\ 1 \end{pmatrix}. \tag{10.11}$$

In the case of nonlinear orbital dynamics, δX would depend on the initial phase-space point X_i, but for linear dynamics, it does not. This has led some authors to commit the mistake of oversimplifying by saying 'without loss of generality, we can assume $X_\mathrm{i} = 0$ before a photon emission'. This is not so; a particle can be *anywhere* in the phase-space just prior to a photon emission, not necessarily on the closed orbit. It is a subtle but important point. With an obvious notation, we can define a partial derivative

$$\gamma \frac{\partial X}{\partial \gamma} = \begin{pmatrix} 0 \\ 0 \\ 0 \\ 0 \\ 0 \\ 1 \end{pmatrix}, \tag{10.12}$$

and write

$$\delta X \simeq -\frac{\hbar\omega_\mathrm{ph}}{E} \left(\gamma \frac{\partial X}{\partial \gamma} \right). \tag{10.13}$$

We decompose $\gamma(\partial X/\partial\gamma)$ into eigenvectors. This will be important below. Using the orthonormality relations, the answer is

$$\gamma \frac{\partial X}{\partial \gamma} = \sum_j \gamma \frac{\partial a_j}{\partial \gamma} E_j, \tag{10.14}$$

where

$$\begin{aligned} \gamma \frac{\partial a_j}{\partial \gamma} &= -\mathrm{i} E_{5j}^* \qquad j > 0, \\ \gamma \frac{\partial a_j}{\partial \gamma} &= \mathrm{i} E_{5j}^* \qquad j < 0. \end{aligned} \tag{10.15}$$

10.7.3. Lie algebraic formalism. The use of Lie algebra for accelerator physics was pioneered by Dragt (see, e.g., Dragt and Finn (1976)). The Poisson brackets of two operators f and g are denoted by $\{f, g\} =: f : g$. We seek the phase-space variables z at time t, starting from z_0 at $t = 0$. The equation of motion for the map M is

$$\frac{\mathrm{d}M}{\mathrm{d}t} = M : -H(z_0) : . \tag{10.16}$$

The formal solution is

$$M = \exp(t : -H(z_0) :). \tag{10.17}$$

An operator of the form $\exp(: f :)$ is called a *Lie transformation*. The exponential is defined by its power series expansion

$$\exp(: f :) \equiv \sum_{j=0}^{\infty} \frac{: f :^j}{j!}. \tag{10.18}$$

Here the powers mean the following, when acting on a function $g(z)$

$$: f :^0 g = g, \qquad : f :^2 g = \{f, \{f, g\}\}, \tag{10.19}$$

etc. For brevity, we drop explicit mention of t and z_0 in (10.17) and write just $\mathrm{e}^{-:H:}$. In practice, $H(z)$ is usually expressed as a power series in z. Then $\mathrm{e}^{-:H:}$ can be decomposed into the form

$$\mathrm{e}^{-:H:} = \cdots \mathrm{e}^{-:H_3:} \mathrm{e}^{-:H_2:} \mathrm{e}^{-:H_1:}, \tag{10.20}$$

where H_j contains terms of order z^j. For practical usage, the series is truncated at some suitable order. The term H_1 causes a closed orbit distortion, and the term H_2 determines the linear orbital dynamics. By a suitable redefinition of the location of the origin, we can 'complete the square' and eliminate the linear terms in H_1, so it is conventional to express (10.20) starting from H_2. We concatenate the Lie transformations of all the beamline elements from $\theta = 0$ to 2π, and decompose the map into a product to obtain

$$\bar{z} = \cdots \mathrm{e}^{-:H_3:} \mathrm{e}^{-:H_2:} \mathrm{e}^{-:H_1:} z = \mathrm{e}^{-:H:} z. \tag{10.21}$$

The convergence of the resulting series in z is not guaranteed.

Dragt and Finn (1976) treated only the orbital motion, but even though the spin variables do not come in canonically conjugate pairs (because there are three of them), the Lie algebraic formalism is affected *not in the least*. The extension to include spin was published by Yokoya (1987). We follow Yokoya (1987) below. We write the Hamiltonian in a beamline element in the form

$$H = H_{\mathrm{orb}}(z) + \boldsymbol{W}(z) \cdot \boldsymbol{s}. \tag{10.22}$$

We denote the spin precession vector by $\boldsymbol{W}$. Then,

$$\bar{z}_i = \mathrm{e}^{-:H_{\mathrm{orb}} + \boldsymbol{W}\cdot\boldsymbol{s}:} z_i, \qquad \bar{\boldsymbol{s}}_i = \mathrm{e}^{-:H_{\mathrm{orb}} + \boldsymbol{W}\cdot\boldsymbol{s}:} \boldsymbol{s}_i. \tag{10.23}$$

As we have already stated, we neglect the effect of the spin on the orbit, so one can simplify

$$\bar{z}_i = \mathrm{e}^{-:H_{\mathrm{orb}}:} z_i, \qquad \bar{\boldsymbol{s}}_i = \mathrm{e}^{-:H_{\mathrm{orb}} + \boldsymbol{W}\cdot\boldsymbol{s}:} \boldsymbol{s}_i. \tag{10.24}$$

Expanding the solution for $\bar{\boldsymbol{s}}_i$, the first term is $\boldsymbol{s}_i$, and the second is $\boldsymbol{W} \times \boldsymbol{s}$ because $: \boldsymbol{s} :$ and H_{orb} commute. At the next order one has

$$\{\boldsymbol{W} \cdot \boldsymbol{s}, \boldsymbol{W} \times \boldsymbol{s}\} = \boldsymbol{W} \times (\boldsymbol{W} \times \boldsymbol{s}) + \sum_j s_j \{W_j, \boldsymbol{W}\} \times \boldsymbol{s}. \tag{10.25}$$

The second term on the rhs will be ignored because it is proportional to $O(\hbar^2)$. Hence, Planck's constant does lurk in the background, in the classical spin model. The Lie transformation for the one-turn spin–orbit map T can be expressed as

$$T = \cdots e^{-:\boldsymbol{W}_3\cdot\boldsymbol{s}:} e^{-:\boldsymbol{W}_2\cdot\boldsymbol{s}:} e^{-:\boldsymbol{W}_1\cdot\boldsymbol{s}:} e^{-:\boldsymbol{W}_0\cdot\boldsymbol{s}:} \cdots e^{-:H_3:} e^{-:H_2:} e^{-:H_1:}. \tag{10.26}$$

Note that the orbital part starts from H_1 (the closed orbit distortions, which can be removed by a change of origin), but the spin terms start with $\boldsymbol{W}_0 \cdot \boldsymbol{s}$. This is simply an expression of the fact that there is a nontrivial spin rotation on the accelerator closed orbit. We shall develop the Lie algebra formalism later in this review.

10.7.4. Symplectic and unitary integrators. Generally it is essential to preserve the symplecticity of the motion during numerical integration of the equations of motion. At the simplest level, a violation of symplecticity will lead to nonconservation of probability in the phase-space. Note that it is, in general, impossible to create an integrator which is both symplectic and conservative. Generally, a symplectic integrator conserves the energy of a 'nearby' Hamiltonian which is close, in some sense, to the original Hamiltonian.

Consider a mapping for a timestep t, say $M(t)$. An nth order symplectic integrator is defined to be a symplectic approximation to $M(t)$, say $T_n(t)$, which equals $M(t)$ up to error terms of $O(t^{n+1})$, i.e.

$$T_n(t) = M(t) + O(t^{n+1}) \equiv \exp(t : -H : +t^{n+1} R_n), \tag{10.27}$$

where R_n is a remainder term whose detailed form is not important. Ruth (1983) derived an example of a fourth order symplectic integrator. Forest (1992) has given examples of symplectic integrators up to $n = 6$. In a beautiful paper, Yoshida (1990) showed how to construct higher even-order symplectic integrators starting from only a second-order symmetric symplectic integrator $T_2(t)$, such as the symmetric integrator that we presented above. It is essential that the integrator must be symmetric, i.e. one must have

$$T_{2n}(-t) T_{2n}(t) = 1 \tag{10.28}$$

exactly, not merely to some degree of approximation. Given $T_{2n}(t)$, Yoshida defined

$$T_{2n+2}(t) = T_{2n}(at) T_{2n}(bt) T_{2n}(at), \tag{10.29}$$

subject to the conditions

$$2a + b = 1, \qquad 2a^{2n+1} + b^{2n+1} = 0. \tag{10.30}$$

This has the solutions

$$a = \frac{1}{2 - 2^{1/(2n+1)}}, \qquad b = -\frac{2^{1/(2n+1)}}{2 - 2^{1/(2n+1)}}. \tag{10.31}$$

Then $T_{2n+2}(t)$ is a symmetric symplectic integrator of order $2n + 2$. A significant feature of the above symplectic integrators is that the value of b is *negative*. It can be shown that, beyond the second order, an explicit symplectic integrator must necessarily contain negative intermediate timesteps.

Mane (1993) extended Yoshida's procedure to include the spin. In the case of spin, the map is unitary. The spin equation of motion can be expressed in the form

$$\frac{\mathrm{d}\boldsymbol{s}}{\mathrm{d}t} = \boldsymbol{W}(z) \times \boldsymbol{s} =: -\boldsymbol{W} \cdot \boldsymbol{s} : \boldsymbol{s}, \tag{10.32}$$

where the Poisson brackets of the spin variables are

$$\{s_i, s_j\} =: s_i : s_j = \sum_k \epsilon_{ijk} s_k. \tag{10.33}$$

Given an orbital second order symmetric symplectic integrator, one can construct two possible symmetric second order spin–orbit integrators, namely

$$\begin{aligned} S_2^a &= \exp\left(\frac{t}{2} : -\boldsymbol{W}\cdot\boldsymbol{s} :\right) T_2(t) \exp\left(\frac{t}{2} : -\boldsymbol{W}\cdot\boldsymbol{s} :\right), \\ S_2^b &= T_2\left(\frac{t}{2}\right) \exp(t : -\boldsymbol{W}\cdot\boldsymbol{s} :) T_2\left(\frac{t}{2}\right). \end{aligned} \tag{10.34}$$

Yoshida's procedure can be used to build up higher order spin–orbit integrators. The integrator S_2^b is precisely the case of $k = 2$ by Balandin and Golubeva (1993). Their integrator has been coded in a programme VasiLIE (Balandin and Golubeva 1992). The above authors have written a detailed paper on the use of Hamiltonian methods for nonradiative, spin $\frac{1}{2}$ beam dynamics (Balandin and Golubeva 1997).

Other second-order symmetric symplectic–unitary spin–orbit integrators are possible. Let us add a spin term to the Hamiltonian:

$$H = T(\boldsymbol{p}) + V(\boldsymbol{q}) + \boldsymbol{W}(\boldsymbol{q},\boldsymbol{p})\cdot\boldsymbol{s}. \tag{10.35}$$

The integration scheme is now

$$S_2 = \begin{cases} \boldsymbol{q}_{i+1/2} = \boldsymbol{q}_i + \dfrac{\epsilon}{2}\nabla_{\boldsymbol{p}} T(\boldsymbol{p}_i), \\ \boldsymbol{p}_{i+1/2} = \boldsymbol{p}_i - \dfrac{\epsilon}{2}\nabla_{\boldsymbol{q}} V(\boldsymbol{q}_{i+1/2}), \\ \boldsymbol{s}_{i+1} = \mathrm{e}^{\epsilon : -\boldsymbol{W}(\boldsymbol{q}_{i+(1/2)},\boldsymbol{p}_{i+1/2})\cdot\boldsymbol{s}_i :}\boldsymbol{s}_i, \\ \boldsymbol{p}_{i+1} = \boldsymbol{p}_{i+1/2} - \dfrac{\epsilon}{2}\nabla_{\boldsymbol{q}} V(\boldsymbol{q}_{i+1/2}), \\ \boldsymbol{q}_{i+1} = \boldsymbol{q}_{i+1/2} + \dfrac{\epsilon}{2}\nabla_{\boldsymbol{p}} T(\boldsymbol{p}_{i+1}). \end{cases} \tag{10.36}$$

The spin tracking code SPINK, used for studies at RHIC (Luccio *et al* 1999), employs an integrator of the form S_2 above, i.e. the full spin rotation is applied in the middle of a beamline element, as a 'kick' to the spin, while the kick to the orbit is split into two equal pieces. Note, however, that SPINK was developed independently of Mane's work.

11. Muon storage rings

11.1. General remarks

One can proceed with yet more theory, but we now have enough material to examine in depth the spin dynamics of a real storage ring, i.e. experimental work in full, not merely isolated illustrations of specific points of theory. Curiously enough, our first detailed description of actual rings, as opposed to formal theory, is for neither electrons nor protons, but instead, for muon storage rings. These are nonradiative leptonic systems. The absence of synchrotron radiation simplifies the accelerator dynamics. We consider three examples below. The first is an actual ring, built at BNL to measure the anomalous magnetic moment of the muon to high precision (experiment E821). The purpose of the ring was, therefore, explicitly to carefully analyse the spin precessions of the particles. The experiment has recently been completed, and the results are of great interest to the scientific community because they reveal a slight discrepancy between theory and experiment. Already, mistakes have been found in earlier theoretical work, in reanalysis of calculations motivated by the new experimental results. The second muon storage ring is a high-energy ($50 \times 50\,\mathrm{GeV}$) $\mu^+\mu^-$ collider. Our analysis will be much more cursory, and mainly limited to a brief statement of the physics goals of such

a machine, and the use of spin dynamics to calibrate the beam energy of the ring. The third muon storage ring is also a proposed machine, once again, to perform a high-precision test of the Standard Model. The goal is to measure the muon *electric* dipole moment.

11.2. BNL muon g − 2 ring

11.2.1. Background. One of the most important applications of spin dynamics in accelerators (or otherwise), is to perform precision tests of the Standard Model. Many experiments have been performed over the years to measure the anomalous magnetic moments of the leptons: the electron, positron and the positive and negative muons. The anomalous magnetic moments of the electron and positron are essentially pure QED effects. Because of its higher mass, however, the muon has stronger non-QED couplings, hence the value of the anomalous magnetic moment of the muon contains significant additional contributions from the strong and weak interactions. There is also the possibility of contributions from physics beyond the Standard Model. In general, the sensitivity of the magnetic moment anomaly to couplings to other particles goes as the square of the mass, so

$$\frac{\Delta a}{a} \propto \frac{m^2}{M^2}, \tag{11.1}$$

where m is the lepton mass and M is the mass scale of 'new physics'. Since $m_\mu/m_\mathrm{e} \simeq 206$, it follows that the magnetic moment anomaly of the muon is roughly 40 000 times more sensitive to contributions from new physics.

The first theoretical calculation of the anomalous magnetic moment of the electron was by Schwinger (1948), who found

$$a_\mathrm{Schwinger} = \frac{\alpha}{2\pi}, \tag{11.2}$$

where α is the electromagnetic fine-structure constant. This is usually called the Schwinger term. Schwinger's result applies to any Dirac particle; it is also the leading order contribution to the anomalous magnetic moment of the muon. At higher orders, nonelectromagnetic (weak and hadronic) processes also contribute measurably to a_μ. Since perturbative QCD calculations are difficult, the relevant hadronic cross-sections are measured experimentally, in an $\mathrm{e}^+\mathrm{e}^-$ collider, and the results are used to estimate the hadronic contribution to a_μ. Such measurements were carried out at the VEPP-2M collider as a contrbution to the muon $g - 2$ determination. See, for example, Akhmetshin *et al* (2002).

Muons are not stable particles, hence they cannot be stored in modified Penning traps. Their rest frame decay lifetime is approximately 2.2 μs. All experiments to measure the $\mu^\pm$ anomalous magnetic moments have circulated muons in a magnetic field, to measure the spin precession frequency. In fact, prior to the modern Penning trap work for electrons (e.g. see Dehmelt (1986)), the previous best measurements of the e^+ and e^- anomalous magnetic moments also circulated electrons and positrons in a magnetic field. The review by Rich and Wesley (1972) describes this earlier work on electrons and positrons, including early experiments on the lepton g factors.

An experiment has recently been concluded at BNL to measure the anomalous magnetic moment of the positive and negative muons. The experiment consisted of a custom-built storage ring, with an extremely homogeneous, uniform magnetic field, specifically designed to circulate muons (Danby *et al* 2001). It was an improved version of an earlier CERN experiment which also consisted of a custom-built muon storage ring (Bailey *et al* 1979, Combley 1981). The value of the magnetic moment anomaly of the positive muon is (Bennett *et al* 2002)

$$a_{\mu^+} = 0.001\,165\,9204(7)(5)\ (0.7\,\mathrm{ppm}), \tag{11.3}$$

where the first error is statistical, and the second is systematic. A recently announced value for the negative muon is (Bennett *et al* 2004)

$$a_{\mu^-} = 0.001\,165\,9214(8)(3)\ (0.7\,\text{ppm}), \tag{11.4}$$

giving a world average value of

$$a_\mu(\text{exp}) = 0.001\,165\,9208(6)\ (0.5\,\text{ppm}). \tag{11.5}$$

Roberts (2004) gives an up-to-date review of the lepton (magnetic *and* electric) dipole moments.

Our main interest here is the spin dynamics involved in the operation of the BNL experiment. It was, arguably, the closest approximation of a real machine to the theoretically ideal model of a pure vertical magnetic field. It was a nonradiative system, thereby avoiding the complications of synchrotron radiation. It operated at an energy (actually, Lorentz factor) called the 'magic gamma' which is an interesting feature described briefly earlier. It was also a superconducting magnet, although that is not relevant to this paper. We shall examine the spin dynamics issues of the BNL experiment below.

To date, there have been three high-precision experiments at CERN to measure the anomalous magnetic moment of the muon (Charpak *et al* 1961, Bailey *et al* 1972, 1979). An experiment was also performed at Berkeley by Henry *et al* (1969). The Berkeley experiment precessed the muon spins in a solenoid, similar to the electron $g-2$ experiments, and measured a_μ to an accuracy of $\pm 5.7\%$. All the other experiments have used dipole magnetic fields. The first CERN experiment circulated muons inside a 6 m long bending magnet. The second and third CERN experiments as well as the BNL experiment operated storage rings custom-built to circulate muons to measure a_μ. Both the third CERN experiment and the BNL experiment operated at the 'magic gamma'. A recent detailed review of all the muon $g-2$ experiments is given by Farley and Semertzidis (2004). Their review quotes heavily from an earlier review by Farley and Picasso (1990).

11.2.2. Spin precession. The basic spin precession equations were written earlier in this paper, but we repeat the relevant equations to keep the discussion self-contained. To avoid needless complications, we assume here that the momentum and spin vectors lie in the horizontal plane, and are hence orthogonal to the magnetic field, which is vertical. The orbital revolution frequency (cyclotron frequency) in a uniform vertical magnetic field $\boldsymbol{B}$, for a particle of mass m and charge e, is given by solving the equation

$$\frac{\mathrm{d}\boldsymbol{p}}{\mathrm{d}t} = e\,\boldsymbol{\beta} \times \boldsymbol{B}. \tag{11.6}$$

The cyclotron (angular) frequency vector is

$$\boldsymbol{\Omega}_\mathrm{c} = -\frac{e}{mc\gamma}\boldsymbol{B}. \tag{11.7}$$

The spin precession (angular) frequency is given by the equation

$$\frac{\mathrm{d}\boldsymbol{s}}{\mathrm{d}t} = -\frac{e}{mc}\left(a + \frac{1}{\gamma}\right)\boldsymbol{B} \times \boldsymbol{s} \tag{11.8}$$

and is

$$\boldsymbol{\Omega}_\mathrm{s} = -\frac{e}{mc}\left(a + \frac{1}{\gamma}\right)\boldsymbol{B}. \tag{11.9}$$

The precession frequency of the spin, in a frame rotating with the orbit, is the difference

$$\boldsymbol{\Omega}_\mathrm{diff} = \boldsymbol{\Omega}_\mathrm{s} - \boldsymbol{\Omega}_\mathrm{c} = -a\frac{e}{mc}\boldsymbol{B}. \tag{11.10}$$

In particular, this is the spin precession frequency of the longitudinal spin component $s_\parallel \equiv \boldsymbol{s} \cdot \hat{\boldsymbol{\beta}}\hat{\boldsymbol{\beta}}$. Significantly, $\Omega_{\rm diff}$ is proportional to a itself. Hence, there is no need to measure two large quantities $\Omega_{\rm s}$ and $\Omega_{\rm c}$ individually, and to subtract them to determine the value of a. A measurement of the precession frequency of the longitudinal spin component yields the value of a directly. This is the basis of the experiment to measure the muon anomalous magnetic moment. Note that the fact that the longitudinal polarization remains constant if $g = 2$ exactly, was known a long time ago, even before the publication of the spin precession equation by Bargmann *et al* (1959) (although not before the work of Thomas (1927)). It was noted in the 1957 parity violation experiment by Garwin *et al* (1957). Of course the goal of their experiment, which measured the spin precession of stopped muons, was to prove the nonconservation of parity in the weak interactions, a major crisis of physics in 1957, and not to measure the anomalous magnetic moment of the muon. As a subsidiary finding of their experiment, they reported that $g_{\mu^+} = 2.00 \pm 0.10$, and, with limited accuracy, that $g_{\mu^-} = g_{\mu^+}$.

The fundamental challenge of the BNL experiment then, was to measure $\omega_\parallel$ very accurately. The magnetic field $\boldsymbol{B}$ had to be made as homogeneous as possible, and its value had to be accurately measured. In the BNL experiment, this meant calibrating the value of B to one part in 10^7. The magnetic field was calibrated using NMR probes to measure the proton spin precession frequency, $\omega_{\rm p}$, in the magnetic field. The result was converted to the muon spin precession frequency (for muons at rest) $\omega_\mu = geB/(2mc)$ using the ratio $\lambda = \omega_\mu/\omega_{\rm p} = \mu_\mu/\mu_{\rm p}$, where μ_μ and $\mu_{\rm p}$ are the magnetic moments of the muon and proton, respectively. The value of λ is known to 28 ppb from the hyperfine structure of muonium (Particle Data Book, Eidelman *et al* (2004)), namely, $\lambda = 3.183\,345\,118(89)$. Muonium is a bound state of a positive muon and an electron, a 'leptonic atom'. It should not be confused with a 'muonic atom' which is the bound state of a proton and a negative muon.

Most accelerators consist of lumped elements, but this was not possible for the muon $g-2$ ring. A uniform magnetic field implies continuous coverage around the circumference. Hence, the particles entered the storage volume through the fringe field of the main magnet via an 'inflector' channel (superconducting magnet) which nulled the local field, but without leaking flux into the storage region. Consequently, there was no phase-space matching of the incoming beam to the storage ring optics. The mismatch of the inflector and storage ring acceptances reduced the injection efficiency of the incoming muon beam to about 8.3%. A good, albeit brief, summary of the accelerator physics of the muon $g-2$ ring is given by Roberts (2002).

As the muons circulate in the ring, they decay into electrons (for μ^-) or into positrons (for μ^+), plus neutrinos. It is a three-body decay, hence, the decay electrons have an angular and energy distribution. For brevity, we shall omit saying 'electrons or positrons'. The angular distribution of the decay electrons in the muon rest frame (centre-of-mass of the decay products) is (Barr *et al* 1989)

$$\frac{{\rm d}^2 N}{{\rm d}x\,{\rm d}\cos\theta} = N[x^2(3-2x) - \hat{P}x^2(1-2x)\cos\theta]. \tag{11.11}$$

Here, N denotes the number of muon decays, x is the ratio of the electron energy $E_{\rm e}$ to its maximum possible energy ($\simeq m_\mu c^2/2$), θ is the angle of the electron in the muon rest frame with respect to the direction $\hat{\boldsymbol{v}}$ of the muon in the lab frame and $\hat{P}$ is the product of the muon charge (in units of the positron charge) and the $\hat{\boldsymbol{v}}$ component of the muon polarization. From the above, one can deduce that the count rate at a detector, for electrons or positrons with energies greater than a threshold E in the lab frame, varies like (Bennett *et al* 2002)

$$N(t) = N_0(E)\,{\rm e}^{-t/(\gamma\tau)}[1 + A(E)\cos(\omega_a\, t + \psi_0(E))], \tag{11.12}$$

where N_0 is a normalization constant, A an asymmetry parameter and ψ_0 an initial phase. The above is a sinusoidal function with an exponential decay envelope. By fitting to the above

profile, one can extract the value of ω_a. It is tacitly assumed above, that ψ_0 is the same for all the particles, and depends only on the threshold energy E. Note that if ψ_0 were uniformly distributed over the interval $[0, 2\pi]$, then the asymmetry term would average to zero and it would not be possible to determine ω_a from $N(t)$. The incoming muon beam must, therefore, be polarized.

11.2.3. Orbital focusing. A uniform vertical magnetic field is not sufficient, on its own, to store particles, since it does not constrain the vertical velocity components of the particles. Vertical focusing of the particle orbits is required. Normally, quadrupole magnets are employed to accomplish the task. This cannot be done in the present case, because the magnetic field *must* be homogeneous, and cannot contain a quadrupole component. Hence *electric* fields were used to focus the particles, via electrostatic quadrupoles. When an electric field $\boldsymbol{E}$ is present, the equation for $\boldsymbol{\Omega}_{\rm long}$ acquires some extra terms:

$$\boldsymbol{\Omega}_{\rm long} = -\frac{e}{mc}\left[a\boldsymbol{B} - \left(a - \frac{1}{\beta^2\gamma^2}\right)\boldsymbol{\beta}\times\boldsymbol{E}\right]. \tag{11.13}$$

As we saw earlier, this expression is valid in general, for arbitrary $\boldsymbol{B}$ and $\boldsymbol{E}$, but it applies *only* to the precession of the longitudinal spin component, hence, the notation $\boldsymbol{\Omega}_{\rm long}$. This expression leads to a significant conclusion: if the value of the particle energy is chosen such that $\gamma = \gamma_*$, where

$$a - \frac{1}{\beta_*^2\gamma_*^2} = 0, \tag{11.14}$$

then the electric field will have *no* effect on $\boldsymbol{\Omega}_{\rm long}$. The value γ_* is called the 'magic' gamma. Its value is $\gamma_* \simeq 29.3$ for muons. Since the muon lifetime in its rest frame is approximately 2.2 μs, the time-dilated lifetime of the stored muon beam was approximately 64.4 μs. Since the value of a_μ is already known approximately from previous experiments, we can solve the above equation to deduce that the value of the 'magic' muon momentum is

$$p_* = mc\beta_*\gamma_* = \frac{mc}{\sqrt{a_\mu}} \simeq 3.094\,{\rm GeV\,c^{-1}}. \tag{11.15}$$

The above value was thus chosen to be the design momentum of the ring. For off-momentum particles, the contribution of the electric field to $\boldsymbol{\Omega}_{\rm long}$ was less than one part in a million (Semertzidis *et al* 2003). The strength of the magnetic field in the ring was $B \simeq 1.45\,{\rm T}$, leading to an orbit radius of $R_0 = 7112\,{\rm mm}$ (Danby *et al* 2001).

However, the quadrupoles could not span the entire circumference of the ring, because space must be available to inject the particles, etc. Hence, there was some azimuthal nonuniformity in the focusing, i.e. $\beta_{x,y}$ depended on θ, also the dispersion D_x. To minimize such dependence on θ, the quadrupoles were arranged so as to have four-fold superperiodicity around the ring. Then

$$\left(\frac{\beta_x^{\rm max}}{\beta_x^{\rm min}}\right)^{1/2} \simeq 1.04, \qquad \left(\frac{\beta_y^{\rm max}}{\beta_y^{\rm min}}\right)^{1/2} \simeq 1.03. \tag{11.16}$$

Hence the horizontal and vertical beam sizes were almost uniform around the ring. The fiducial volume of the beam was a circle of 45 mm radius around the central (design) orbit. Apertures were placed to constrain the maximum beam width and height to this limit. An excellent description of the design and operation of the BNL muon storage ring quadrupoles is given by Semertzidis *et al* (2003), which gives the actual values of the betatron tunes used in the operation of the ring, the strengths of the higher order multipoles, and a listing of the principal orbital resonances

There was no longitudinal focusing in the ring. The injected beam, therefore, decohered longitudinally during storage. This did not compromise the accuracy of the experiment.

11.2.4. Particle injection. In the earlier CERN muon storage ring, and also in the early experimental runs of the BNL muon storage ring, pions were injected into the ring. The principal decay mode of a charged pion is into a muon and (anti)neutrino, via the decay reactions $\pi^+ \rightarrow \mu^+ + \nu_\mu$ and $\pi^- \rightarrow \mu^- + \bar{\nu}_\mu$, with a mean lifetime of 2.6033×10^{-8} s in the pion rest frame. Other decay modes have negligible branching ratios. For a ring radius of $R_0 = 7112$ mm, the pions travelled approximately halfway around the ring before decaying into muons. The muons were, therefore, born *in situ* in the ring. Note that because the above pion decay is a *two-body* decay, the muon is produced with a definite helicity. However, note also, that in the pion rest frame, the direction of the emitted muon is *isotropic*. Thus, although every *individual* muon in the beam was born with the same helicity, the muon *beam* as a whole was *unpolarized*.

However, the motion of the muons is *not* ergodic. The muon spin and momentum are correlated. Boosting from the pion rest frame to the lab (storage ring) frame, the muons that are emitted in the forward direction will have the highest longitudinal momentum, *and* will be longitudinally polarized. The experiment was configured so that only those muons for which $|\boldsymbol{s}_\parallel| > 0.95$ were accepted by the storage ring aperture. The fiducial volume of the ring was a circle of radius 45 mm around the beam axis. Setting $x_\delta = 45$ mm and $D_x = R_0/Q_x^2$, where $Q_x \simeq 0.93$, gives a maximum momentum acceptance for the ring of $(\Delta p/p_*)_{\max} \simeq 0.005$. The momentum of the injected pions was chosen such that only those muons with the highest longitudinal momentum fell into this acceptance. The emittance of the secondary muon beam far exceeded the acceptance of the ring. The vast majority of the decay muons was lost. For all practical purposes, the phase-space density of the stored muon beam was uniform across the acceptance of the ring.

The other scenario from which the bulk of the experimental data was derived, was to inject muons into the ring. A beam of pions decayed in a transfer line upstream of the ring, and a spin-polarized muon beam was injected into the ring. The earlier CERN experiments used only pion injection. The muons entered the BNL ring in the horizontal plane at an angle to the ring's design orbit. (A few unwanted pions also managed to enter the ring.) A horizontal kicker was installed in the ring, to kick the muon beam onto the closed orbit. The kicker was a dynamic device to place the muons onto the closed orbit (or approximately so). More details on the kicker are given by Efstathiadis *et al* (2003). To properly align the centroid of the muon beam onto the closed orbit, one must set *both* $\langle x \rangle$ and $\langle p_x \rangle$ to zero, where the angle brackets denote an average over the injected muons. Since there was only enough space for one kicker, it was placed roughly one quarter of a betatron oscillation downstream of the inflector, i.e. where $\langle x \rangle$ crossed zero. The kicker was configured to render $\langle x' \rangle = 0$. Since the horizontal betatron tune was approximately unity, the kicker was placed roughly one-quarter of the circumference of the ring downstream from the inflector. Even so, it was not possible to set $\langle x \rangle$ and $\langle x' \rangle$ exactly to zero. Hence, the injected muon beam had a residual coherent betatron oscillation (denoted 'CBO' by the E821 collaboration). Such a coherent betatron oscillation did not exist in the pion injection scenario, where the beam is uniformly distributed across the orbital phase-space.

In the muon injection scenario, the phase-space density of the injected beam was not uniform across the acceptance of the ring. Since the motion of the muons is not ergodic, the muons do not spread out in the orbital phase-space. Nonlinear terms in the betatron motion can potentially decohere the beam in the betatron phase-space, but the quadrupoles were designed to minimize the magnitudes of such nonlinear terms (Semertzidis *et al* 2003). Hence, the coherent betatron oscillation persisted during the beam storage time.

The presence of a coherent betatron oscillation meant that the 'average' direction of motion of the muon beam did not coincide with the design axis of the storage ring. However, the beam energy had been configured to lie at the 'magic gamma' so that the effect of the electric fields

on the beam cancel out between $\boldsymbol{\Omega}_s$ and $\boldsymbol{\Omega}_c$ (recall (11.13)), so the effect on the longitudinal spin component was minimized. Nevertheless, the coherent betatron oscillation had to be accounted for in the fits of the experimental data. The detailed theory and measurements of the coherent betatron oscillation are given by Orlov *et al* (2002).

In addition to the centroid, the injected beam also has an emittance, and the tails of the beam distribution were too large to fit into the acceptance of the ring. The beam had to be 'scraped' to eliminate these tails. Otherwise, for example, the particles in the tails would enter regions where the magnetic field was not of sufficient quality, and would spoil the measurement. Beam scraping was also required in the pion injection scenario.

11.2.5. Further remarks. Notice how we switched from the quantum to the classical spin model and back again without missing a beat. We employed quantum mechanics to quantify the muon spin orientation, in the birth of a muon from pion decay via the weak interaction. We seamlessly switched over to a classical spin model to calculate the subsequent precession of the muon spin in the magnetic field (and electric field—the magic gamma) of the storage ring. The above details are never discussed in the particle physics literature, but they are significant to us because the equations of motion such as (11.6) and (11.8) *were* derived in a fixed inertial reference frame, not in the accelerator frame. Usually, in accelerator physics, we derive the equations of motion in the accelerator reference frame, and we then speak of the 'spin tune', in addition to the orbital (betatron) tunes. We have seen that for spin precession along the design orbit of a planar ring, the value of the spin tune is $\nu_{\text{spin}} = a\gamma$. Although we mentioned the orbital betatron tunes, we always worked with the spin precession *frequency*. We never mentioned the spin *tune* in the context of the muon spin precession. Had the experiment measured the spin tune, i.e. the value of $a\gamma$, it would then be necessary to divide by γ, i.e. a number not very accurately known.

The E821 experiment achieved an overall accuracy of 0.54 ppm for a_μ, of which 0.46 ppm was the statistical error. One can, therefore, likely do better with a larger sample of muons. It has recently been proposed to extend the experiment using various enhancements, to achieve an accuracy of 0.2 ppm (proposal P969), with a statistical error of 0.14 ppm and a systematic error of 0.1 ppm. The proposal has received scientific approval and is awaiting funding approval (as of mid-2005). To attain the improved accuracy would require a factor of ten larger muon sample. A factor of five is expected to be achieved by a combination of factors, including a higher proton beam intensity in the AGS and more numerous and stronger quadrupoles in the pion decay channel. In addition, data taking would begin sooner by eliminating the pion flash. This would be done by using the *backward* decay muons, so the pion momentum would be $5.32\,\text{GeV}\,\text{c}^{-1}$ (recall the muon magic momentum is $3.094\,\text{GeV}\,\text{c}^{-1}$). With such a large difference in momentum, no pions would make it past the final bend magnet in the injection beamline and the inflector, thereby eliminating the pion flash. Ideas are also proposed to reduce or eliminate the coherent betatron oscillation. The detector electronics would also require improvement.

11.3. Muon collider

As stated above, the muon collider is a proposed idea, not an actual machine. See Alsharo'a *et al* (2003) for a report on the design. A schematic layout of the muon collider complex was shown in figure 18. The physics motivation for such a machine is partly due to the exciting recent results establishing the existence of neutrino oscillations, as well as the desire to probe physics at higher energy scales, e.g. to search for the Higgs particle, or physics beyond the Standard Model. (The concept of a muon collider automatically carries with it the concept of a

Table 3. Basic parameters of a muon collider. Reprinted with permission from Raja and Tollestrup (1998). Copyright (1998) by the American Physical Society.

Parameter	Value
Muon energy	50 GeV
γ	473.22
Spin precession in one turn	3.4667 rad
Magnetic field	4.0 T
Radius of ring	41.666 666 m
Beam circulation time	$0.873\,27 \times 10^{-3}$ s
Dilated muon lifetime	$0.103\,97 \times 10^{-2}$ s
Turn by turn decay constant	0.8399×10^{-3}

neutrino factory.) Electron–positron colliders emit copious synchrotron radiation and become prohibitively expensive to operate, and are also very large in circumference. A $\mu^+\mu^-$ collider offers the promise of a more compact lepton collider with the reach to probe new physics. The idea of a muon collider is, in fact, not new; it was originally suggested by Budker (1970), one of Budker's many contributions to accelerator physics (electron cooling was another one).

The basic problem with muons, of course, is that they decay, with a rest-frame lifetime of 2.2 μs, so they must be accelerated to high energy rapidly, to time-dilate their lifetime. The muon beam emittance must also be reduced so as to achieve a reasonable luminosity for particle physics experiments. These are serious technical challenges, and some very innovative ideas have been developed to address them. However, as appealing as all of the above work is, it does not directly pertain to the spin dynamics in storage rings. We only note one aspect of the design, which is, to employ the muon spin precession to calibrate the energy of the muon storage ring. A detailed analysis of the issues involved is given by Raja and Tollestrup (1998). Essentially, the procedure is the reverse of that employed in the BNL or CERN muon $g-2$ rings: the decay electrons are measured, thereby yielding a value for the frequency of the muon spin precession. We use (11.6) and (11.8) in reverse: we measure the orbital revolution frequency ω_c and the spin precession frequency ω_s, and divide to obtain (for horizontal motion in a planar ring with no electric field) $\omega_s/\omega_c = a\gamma + 1$. Given an accurate value for a_μ (from the muon $g-2$ experiment), one uses the above equation to deduce the value of γ, thence the muon beam energy. The basic parameters of relevance to us are tabulated in table 3.

Most of the analysis by Raja and Tollestrup (1998) is devoted to the statistical and systematic errors in determining the value of ω_s. We omit the particle physics issues such as detecting the electrons and understanding the backgrounds, detector efficiencies, etc. We focus our attention more on the accelerator physics issues. First, note that there are no resonance crossing issues in a muon collider. Unlike an electron synchrotron, where the value of the spin tune equals an integer every 440 MeV (equate $\Delta E = m_e c^2/a$), for muons, the value of $a_\mu\gamma$ equals unity for $\gamma = 1/a_\mu \simeq 857.691$, corresponding to a muon energy of 90.622 GeV, using (11.5) for a_μ (see table 2). Hence, a (50 × 50) GeV collider will not cross any such depolarizing spin resonances. Depolarizing resonances due to betatron oscillations can be avoided by designing the machine lattice appropriately.

Note that the muon collider does not operate at the 'magic gamma', but it also does not employ electrostatic quadrupole focusing, because electrostatic quadrupoles cannot generate a sufficiently strong focusing gradient at the design energy of a muon collider. The electric fields in the ring will be for longitudinal focusing (and also acceleration to high energy), and so, to the leading order, the cross product vanishes: $\boldsymbol{\beta} \times \boldsymbol{E} = 0$. Furthermore, the electric fields will be localized to only a few rf cavities in the ring. Hence, any systematic errors from the electric fields will likely be negligible. A potentially more serious concern is that the focusing

of the betatron orbits will necessarily be accomplished using magnetic quadrupoles. This means that the magnetic field in the ring will be vertical only on the design orbit. The principal perturbations to the spin precession arise from radial magnetic fields, because such fields tilt the spins away from the vertical, and are the principal source of perturbations to the spin motion. The effect is proportional to the amplitude of the vertical closed orbit imperfections. The effects were analysed (for LEP, but applicable more generally to other rings) by Assmann and Koutchouk (1994) (see also Arnaudon *et al* (1995b)). There is both a net spin tune shift and a spread in the value of the spin tune. The average spin tune shift is

$$\langle \delta\nu \rangle = \frac{\cot(\pi\nu_0)}{8\pi}\,\nu_0^2[n_{\rm Q}(Kl_{\rm Q})^2\sigma_y^2 + n_{\rm CV}\sigma_{\theta\,{\rm CV}}^2]. \tag{11.17}$$

Here, $\nu_0 = a\gamma$, $n_{\rm Q}$ is the number of quadrupoles, with integrated gradient $Kl_{\rm Q}$, σ_y the rms vertical misalignment spread of the closed orbit at the quadrupoles, $n_{\rm CV}$ the number of vertical correction dipoles and $\sigma_{\theta\,{\rm CV}}$ the rms bend angle in the vertical correctors. The spin tune spread is given by

$$\sigma_{\delta\nu} = \frac{\langle \delta\nu \rangle}{\cos(\pi\nu_0)}. \tag{11.18}$$

The numerical values for the muon collider have been analysed by Raja and Tollestrup (1998), and are negligible. For conservative parameter values, the results are that, the spin tuneshift corresponds to an energy calibration shift of $(m_\mu c^2/a_\mu)\langle\delta\nu\rangle \simeq -0.24\,{\rm keV}$ and the spin tunespread corresponds to an energy calibration spread of $(m_\mu c^2/a_\mu)\sigma_{\delta\nu} \simeq 1.46\,{\rm keV}$, both of which are negligible. The smallness of these numbers is because: (i) they depend on ν_0^2, and the value of ν_0 is 206 times smaller for muons than for electrons (although the beam energy is approximately 50 GeV in both LEP and the muon collider); and (ii) there are fewer quadrupoles in the muon collider because of the shorter circumference.

Another source of concern is the presence of longitudinal magnetic fields from solenoids in the experimental detectors of the muon collider. If a solenoid rotates the spins around the longitudinal axis through an angle $\psi_{\rm sol}$, then the spin rotation matrix around the ring is given by

$$M = {\rm e}^{-{\rm i}\pi\nu_0\sigma_3}\,{\rm e}^{-{\rm i}\psi_{\rm sol}\sigma_2/2}. \tag{11.19}$$

We equate this to the standard parametrization $M = {\rm e}^{-{\rm i}\pi\nu_{\rm co}\boldsymbol{\sigma}\cdot\boldsymbol{n}_0}$, where $\nu_{\rm co}$ is the closed-orbit spin tune. Writing $\nu_{\rm co} = \nu_0 + \delta\nu$, we take the trace of the two expressions for M to obtain

$$\cos(\pi(\nu_0 + \delta\nu)) = \cos(\pi\nu_0)\cos\frac{\psi_{\rm sol}}{2}. \tag{11.20}$$

Parameter values of a solenoid field of 1.5 T, and a solenoid length of 6 m are assumed, yielding (at a beam energy of 50 GeV) a spin tune shift of $\delta\nu = -1.901\times10^{-5}$, or a fractional spin tune shift of $\delta\nu/\nu = -3.45\times10^{-5}$, or a shift in energy calibration of $-1.72\,{\rm MeV}$. The effect here, is bigger than an electron ring such as LEP because of the fact that the spin tune ν_0 being smaller by a factor of 206 works *against* the muon collider, in this case. The spin tuneshift cannot be neglected in this case. The most effective solution for a muon collider, is to place 'anti-solenoids' of reverse polarity on either side of the main detector solenoid, to cancel out the overall spin precession.

It remains to be seen if the proposal will be funded. A $\mu^+\mu^-$ collider will provide an exceptionally clean probe of physics at the high-energy frontier, free of many of the backgrounds found in hadron colliders.

11.4. Muon electric dipole moment

It should be noted that *spin* dynamics does not exclusively mean *magnetic* dipole moments. It is also possible for an elementary particle to possess an electric dipole moment (EDM).

For a nonrelativistic particle, the Hamiltonian is given by a straightforward analogy with the magnetic dipole term:

$$H = -(\boldsymbol{d}\cdot\boldsymbol{E} + \boldsymbol{\mu}\cdot\boldsymbol{B}) = -(d\boldsymbol{E} + \mu\boldsymbol{B})\cdot\frac{\boldsymbol{s}}{|\boldsymbol{s}|}, \tag{11.21}$$

where d and μ are the electric and magnetic dipole moments, respectively. Note that an EDM for an elementary particle, if it exists, must be parallel to the magnetic dipole moment. Basically, the angular momentum of any internal charge distribution would cause the EDM to average to zero except along the direction of the particle spin. Furthermore, if a nonzero EDM were to exist not parallel to the magnetic dipole moment, it would supply a new quantum number to the particle. The degeneracy of the ground state of an electron in a hydrogen atom would then be four, not two, for example. The absence of such extra degeneracies is experimental evidence that the EDM is parallel to the magnetic dipole moment.

The search for nonzero EDMs began with the seminal paper of Purcell and Ramsey (1950). Because the electric field is a polar vector, whereas the magnetic field and the spin are axial vectors, the existence of a permanent EDM for a fundamental particle violates both parity (P) and time-reversal (T) symmetries. Nowadays, using CPT invariance, we usually write CP violation, rather than T violation. Nevertheless, they pointed out that the issue should really be settled by experiments. Today, we know that both P and CP are violated in the Standard Model, hence the theoretical arguments have been invalidated. Nevertheless, no nonzero EDMs have been found. The Standard Model is unusual in that it allows for CP violation, via a CP-violating phase in the Cabibbo–Kobayashi–Maskawa matrix, but at the same time, predicts only small values for any EDMs of fundamental particles. Many theories of CP violation also imply large EDMs, and have been ruled out by experiments (see the review by Ramsey (1982)). Measurements of electric dipole moments, or bounds on their values, therefore, place stringent constraints on theoretical extensions beyond the Standard Model.

If there is an EDM of magnitude $d = \eta e\hbar/(4mc)$, in addition to the magnetic dipole moment $\mu = ge\hbar/(4mc)$, the spin-dependent part of the Hamiltonian becomes

$$\begin{aligned} H &= -\frac{ge}{2mc}\frac{\boldsymbol{B}'}{\gamma}\cdot\boldsymbol{s} - \frac{\eta e}{2mc}\frac{\boldsymbol{E}'}{\gamma}\cdot\boldsymbol{s} + \boldsymbol{\omega}_{\mathrm{T}}\cdot\boldsymbol{s} \\ &= -\left\{\frac{ge}{2mc}\left[\frac{\boldsymbol{B}_{\parallel}}{\gamma} + \boldsymbol{B}_{\perp} - \boldsymbol{\beta}\times\boldsymbol{E}\right] + \frac{\eta e}{2mc}\left[\frac{\boldsymbol{E}_{\parallel}}{\gamma} + \boldsymbol{E}_{\perp} + \boldsymbol{\beta}\times\boldsymbol{B}\right] + \frac{\gamma^2}{\gamma+1}(\boldsymbol{\beta}\times\dot{\boldsymbol{\beta}})\right\}\cdot\boldsymbol{s}, \end{aligned} \tag{11.22}$$

where $\boldsymbol{B}'$ and $\boldsymbol{E}'$ are the rest-frame magnetic and electric fields, respectively, and $\boldsymbol{\omega}_{\mathrm{T}}$ is the Thomas precession vector. We have seen previously how the terms in the magnetic moment and the Thomas precession combine to yield $\boldsymbol{\Omega}_{\mathrm{long}}$ for the precession of the longitudinal spin component. Now, there are some extra terms, namely

$$\boldsymbol{\Omega}_{\mathrm{long}} = -\frac{e}{mc}\left[a\boldsymbol{B} - \left(a - \frac{1}{\beta^2\gamma^2}\right)\boldsymbol{\beta}\times\boldsymbol{E} + \frac{\eta}{2}(\boldsymbol{E} + \boldsymbol{\beta}\times\boldsymbol{B})\right], \tag{11.23}$$

where, just like $\boldsymbol{B}_{\parallel}$, the terms in $\boldsymbol{E}_{\parallel}$ do not contribute. There is an extra contribution to the spin precession vector of

$$\boldsymbol{\Omega}_{\mathrm{e}} = -\frac{\eta}{2}\frac{e}{mc}(\boldsymbol{E} + \boldsymbol{\beta}\times\boldsymbol{B}). \tag{11.24}$$

This combination of electric and magnetic fields is the same as that in the Lorentz force.

The third CERN experiment to measure the muon $g-2$, also performed a side experiment to search for a muon EDM, obtaining a limit of $|d_\mu| < (3.7 \pm 3.4)\times 10^{-19}$ e—(cm)

(Bailey *et al* 1978). This value corresponds to $|\omega_e/\omega_a| < 10^{-2}$. (The current best limit for the electron EDM is $|d_e| < 1.6 \times 10^{-27}$ e—(cm) (Regan *et al* 2002).) A proposal to perform a new experiment to measure the muon EDM, using a new storage ring, has recently been put forth (Farley *et al* 2004).

12. Polarimetry

12.1. General remarks

The subject of polarimetry is vast, and lies outside the domain of 'spin dynamics' proper. However, we can hardly ignore the matter, since the results of the experiments described in this paper have to be measured *somehow*. Muon rings have inbuilt polarimeters, via the energy spectrum of the electrons in the muon decay. For other types of accelerators, explicit polarimeters are required. We shall present only a brief description of a few selected methods of polarimetry. We treat only vector polarization below. The polarization along a certain direction is given by

$$P = \frac{N_\uparrow - N_\downarrow}{N_\uparrow + N_\downarrow}, \tag{12.1}$$

where $N_\uparrow$ and $N_\downarrow$ are the number of particles, with spins parallel and antiparallel to the chosen direction, respectively. Typically one selects some spin-dependent reaction (or interaction), and what one obtains is

$$P = \frac{1}{A}\frac{n_\uparrow - n_\downarrow}{n_\uparrow + n_\downarrow}, \tag{12.2}$$

where $n_\uparrow$ and $n_\downarrow$ are the number of scattered particles, properly normalized, with the beam polarization up or down, respectively. This method assumes that one can reverse the beam polarization without any other changes to the environment. The quantity A is called the 'analysing power' of the reaction, and relates the measured asymmetry to the true polarization. It is a number between -1 and 1. (Recall that the polarization itself can lie between -1 and 1. It is also possible for the analysing power to be negative.) Similarly, an apparatus which can measure the number of scattered particles n_L and n_R, to the right and left, respectively, can also determine the degree of vertical beam polarization. (It is then not necessary to reverse the beam polarization.) This is an independent type of measurement, and one can obtain P by substituting $n_{L,R}$ instead, into (12.2). One can also combine both methods to reduce systematic errors and potential dependences on geometrical effects:

$$P = \frac{1}{A}\frac{\sqrt{n_{L\uparrow}n_{R\downarrow}} - \sqrt{n_{L\downarrow}n_{R\uparrow}}}{\sqrt{n_{L\uparrow}n_{R\downarrow}} + \sqrt{n_{L\downarrow}n_{R\uparrow}}}. \tag{12.3}$$

The associated statistical error in the polarization measurement depends on both the analysing power A, and the total number of events n, where $n = n_\uparrow + n_\downarrow$ or $n = n_L + n_R$, or a sum of all four if a combined measurement is performed. The statistical error is

$$\Delta P = \frac{1}{A\sqrt{n}}. \tag{12.4}$$

Hence one tries to optimize the value of $A^2 n$. The number of data events required increases quadratically as the analysing power decreases.

The subject of polarimetry broadly divides into lepton (electron and positron) and hadron polarimetry. Lepton polarimetry is greatly aided by the fact that spin-dependent QED reactions, which are calculable to high accuracy, are available for use, e.g. the Compton

scattering of polarized electrons against circularly polarized photons. Note that by 'lepton polarimetry', we mean only electrons and positrons, not muons. The paper on electron polarimetry by Tolhoek (1956) is nearly 50 years old now but is still a classic in the field. Two excellent relatively modern papers are by Sinclair (1998) on electron (positron) polarimetry, and Makdisi (1998) on proton polarimetry. Grames *et al* (2004) has a recent comparison of the analysing powers of five different electron polarimeters, of four different types. The comparison was possible because at the Thomas Jefferson Laboratory, the CEBAF facility can deliver a beam of the same polarization to all the polarimeters simultaneously. Hadron polarimetry is handicapped by the lack of suitable accurately calculable spin-dependent reactions. The cross-sections for QED processes such as Compton scattering are simply too small to be practical. Basically, one determines the analysing power of a polarimeter by using a beam of known polarization to calibrate the asymmetry. The polarimeter is then used to measure the polarization of a beam in an accelerator. Hadron polarimetry is, therefore, much more phenomenological. We confine our review of hadron polarimetry to proton polarimetry at RHIC.

As a general comment on experiments with polarized beams, it is very useful to selectively depolarize some of the particle bunches in a ring and/or to reverse the direction of the polarization during the course of an experiment. This aids greatly in reducing systematic errors in an experiment. For example, in the 2003 polarized proton run at RHIC, the bunch polarizations in the two RHIC rings had a pattern of $(++--)$ in one ring, and $(+-+-)$ in the other ring. This ensured that all four helicity combinations were delivered to the experiments under identical machine conditions during a single RHIC run. Another possibility that is used in practice, is to reverse the polarization direction of successive bunches from the polarized particle source, possibly using a pseudorandom number generator to avoid any correlations of the polarization direction with the machine's operational periodicities. Another idea that has been employed in e^+e^- rings with radiatively polarized beams, is to let the bunches polarize, then depolarize (some of) the bunches during storage, and compare the results for polarized and unpolarized particle bunches under the same machine conditions. It is also possible to let a bunch polarize, take measurements, depolarize it, make more measurements with the *same* bunch, then let it repolarize, etc. It is also possible to reverse the polarization direction of a particle bunch *during storage*—this can, and has been done for both polarized hadron (proton and deuteron) beams and polarized electron and positron beams.

12.2. Lepton polarimetry

12.2.1. Touschek effect: Møller scattering. The earliest observations of polarization in electron storage rings were made using large-angle intrabeam scattering (known as the Touschek effect), at ACO (Orsay Storage Ring Group 1971) and VEPP-2 (Baier 1972). The actual collision process is Møller scattering (elastic electron–electron scattering). The scattering cross-section is spin-dependent, hence the particle loss rate depends on the beam polarization. In modern synchrotron light sources, the electron beam emittances are so small (especially the vertical emittance), and the particle density so high, that the beam lifetime (particle loss rate) is dominated by large-angle intrabeam scattering. In fact, at the ALS, the vertical emittance is deliberately increased by inducing transverse x–y coupling, to reduce the Touschek effect, and thereby, increase the beam lifetime (Byrd 2004).

Ford and Mullin (1957, 1958) give a calculation of the particle loss rate for one-dimensional transverse betatron oscillations. In practice, cases are possible where the vertical rms divergence $\sigma_{y'}$ may not be negligible relative to the radial rms divergence $\sigma_{x'}$. A calculation treating two-dimensional transverse betatron oscillations was published by

Serednyakov *et al* (1976). This work had some errors of algebra; the corrected formula was published soon after by Baier *et al* (1978). The full formula is complicated, and depends on the beam divergences, machine acceptance, momentum cutoff for 'large angle' scattering, etc. The essential feature is that, the particle loss rate is linear in P^2:

$$\dot{N} = -\frac{N^2 c}{\sqrt{2} V \gamma^2 \sigma_{x'} \sigma_{y'}} (a + bP^2). \tag{12.5}$$

Here N is the total number of particles in the beam, V the volume of the beam and a and b are suitably defined functions. What really matters is that, the loss rate is a linear function of P^2. Note that $b < 0$, so a higher polarization means a smaller particle loss rate. The contribution of the polarization to the number of elastic scatterings per unit time can be conveniently characterized by the ratio

$$\Delta = \Delta_{\max} P^2 = \frac{\dot{N}_0 - \dot{N}_P}{\dot{N}_0}, \tag{12.6}$$

where $\dot{N}_0$ and $\dot{N}_P$ are the scattering rates for unpolarized and polarized beams, respectively.

The overall particle loss rate is lower if the beam is polarized (recall $b < 0$). Hence, measurements of the particle loss rate, especially, changes in the *relative* loss rate, can serve as a quick and efficient method of measuring *relative* changes in the beam polarization level. The sign of the polarization cannot be determined by this method, but is not required for beam energy calibration measurements, in any case. The analysing power is not particularly relevant. Changes in the particle loss rate, as the frequency of an rf kicker is swept across a depolarizing resonance line, are immediately visible. Depending on the parameters of the setup, the beam may or may not suffer total depolarization during such a frequency sweep. If it does, then one must wait for the synchrotron radiation to build up the polarization again. Frequently, all that is required, is to detect a measureable *change* in the Touschek loss rate, not to depolarize the beam completely.

Note, that because the Touschek effect depends on two-body scattering, the lifetime does not follow a simple exponential law. Instead, the exponential 'lifetime' is given by

$$\tau_{ts}^{-1} = -\frac{1}{N}\frac{dN}{dt} \propto N. \tag{12.7}$$

Hence, one defines and measures a 'normalized' lifetime, given by

$$\tau_N^{-1} = -\frac{1}{N^2}\frac{dN}{dt} = \frac{1}{N\tau_{ts}} = \text{const}, \tag{12.8}$$

where 'const' actually depends on the momentum acceptance of the ring and the beam divergences, etc, and also the polarization, as is evident from (12.5), hence, in actuality

$$\tau_N^{-1} \propto a + bP^2. \tag{12.9}$$

A large loss of polarization, i.e. a sharp increase in the normalized loss rate, is observed if resonant depolarization is used, and the kicker frequency matches the spin resonance frequency (aliased with the revolution frequency). An example of such a procedure is shown in figure 26. The frequency at which the count rate increases suddenly is clearly identifiable. This procedure was carried out as part of a high-precision experiment to determine the masses of the J/ψ and ψ' vector mesons. Precision measurements using polarized beams will be reviewed in more detail in section 30.

Since the normalized lifetime depends on the degree of the polarization via P^2, it is technically insensitive to the sign of the polarization. In practice, however, it may be possible to determine also the sign of P, because we know that for radiatively polarized beams,

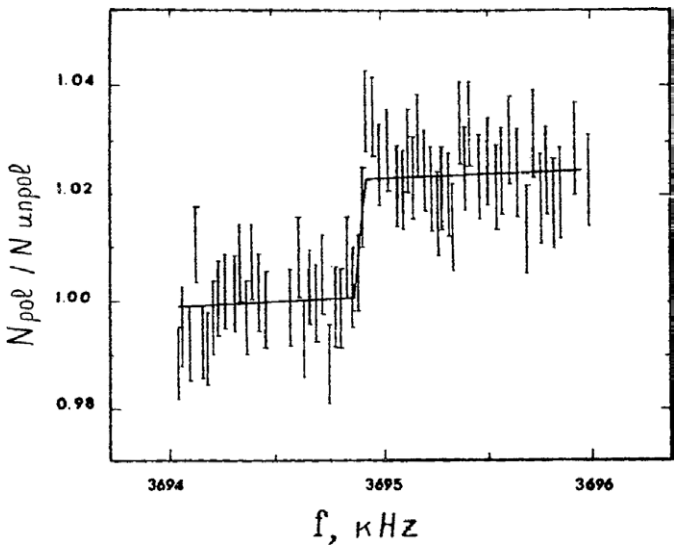

Figure 26. Step increase in Touschek normalized counting rate due to resonant depolarization of the beam.

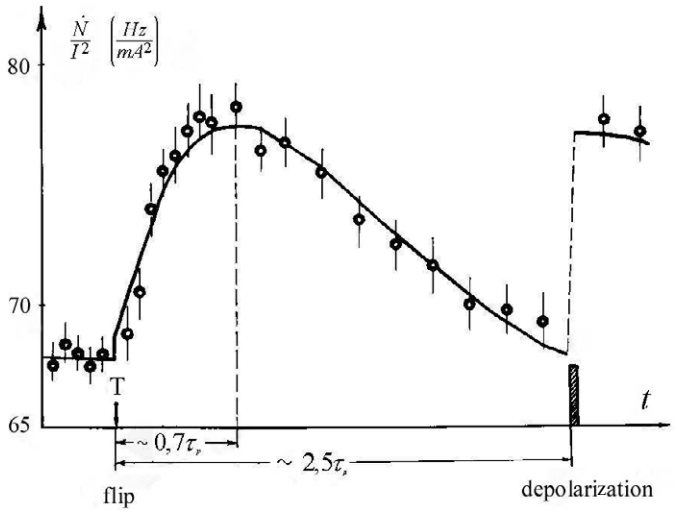

Figure 27. Touschek normalized counting rate for a polarized beam after a spin-flip.

the polarization builds up to an asymptotic level, starting from any arbitrary initial value. The direction of the asymptotic Sokolov–Ternov polarization (sign of asymptotic value of P) is calculable. Hence, if the polarization time constant τ is not too large, one can observe τ_N^{-1} change with time as the polarization builds up. One can use the rate of change, coupled with a knowledge of the asymptotic Sokolov–Ternov polarization, to determine the sign of P.

A beautiful illustration of the above idea, from studies at VEPP-2M, is given by Polunin and Shatunov (1982). A graph of the normalized loss rate as a function of time is shown in figure 27. The beam in the VEPP-2M storage ring was first allowed to polarize for about 1.5 h, to

reach its asymptotic level. As can be seen in figure 27, the normalized loss rate was initially not changing with time. The polarization direction was then rapidly *reversed* by a spin-flipper. The study by Polunin and Shatunov (1982) was, in fact, an early demonstration of the spin-flipper concept (see section 6). Since the normalized Touschek loss rate depends on P^2, immediately after the spin-flip, *nothing* happened to the normalized loss rate. The evolution of the polarization, taking $t = 0$ as the instant of spin-flip, was

$$P(t) = P_\infty(1 - 2\mathrm{e}^{-t/\tau}), \tag{12.10}$$

where P_∞ is the asymptotic polarization level. Hence, the polarization increased from $-P_\infty$ to P_∞, which meant that its magnitude initially *decreased*, then crossed zero and subsequently *increased*. The loss rate, therefore, initially increased as the beam depolarized. After the polarization crossed zero, the normalized loss rate decreased, as the magnitude of the polarization began to increase. Note that the time to depolarize fully (to reach $P = 0$ from $-P_\infty$) was 0.7τ, but the time to repolarize (to reach P_∞ from 0) was longer, about 1.8τ. This is obvious from the slope of an exponential curve, but should be verified by the reader. The *rate of change* of the normalized loss rate can, therefore, serve to indicate the sign of the polarization. Eventually, the beam repolarized to its initial value, after about 2.5τ, as indicated in the figure. The beam was then immediately and fully depolarized using resonant depolarization, and the loss rate immediately increased, in a step, to its maximum ($P = 0$) value. Overall, figure 27 is a striking demonstration of the polarization dependence of the Touschek effect, coupled with the spin-flipper concept.

For the Touschek lifetime technique to work, it is necessary that the particle loss rate be dominated by the intrabeam scattering. Other sources of particle loss are, for example, elastic collisions against residual gas molecules in the beam vacuum chamber (beam–gas scattering) and bremsstrahlung on nuclei. These are single particle processes and follow an exponential law. A lucid analysis is given by Streun (2001). The contributions from elastic (beam–gas) scattering, bremsstrahlung and the Touschek effect add up, giving a total loss rate of

$$\frac{1}{\tau} = \frac{1}{\tau_{\mathrm{el}}} + \frac{1}{\tau_{\mathrm{bs}}} + \frac{1}{\tau_{\mathrm{ts}}} \tag{12.11}$$

with an obvious notation. The dominance of τ_{ts}^{-1} must be verified on a case-by-case basis at each accelerator. Streun presents experimental evidence that $\tau_{\mathrm{ts}}^{-1} \propto I_{\mathrm{sb}}$ (the single bunch current) at the SLS.

12.2.2. Compton backscattering. The most common technique to measure the polarization of high-energy $\mathrm{e}^\pm$ beams is that of Compton backscattering. A beam of circularly polarized laser photons is shot at the electron (or positron) beam, and the backscattered photons are detected. Compton backscattering was first employed at SPEAR2 (Gustavson *et al* 1979). (Note that radiative polarization *per se* was first observed at SPEAR1 by Camerini *et al* (1975), but this earlier work did not employ Compton backscattering.) Compton backscattering polarimeters have since been operated in almost all major high-energy $\mathrm{e}^+\mathrm{e}^-$ colliders. A nonexhaustive listing is VEPP-4 (Artamonov *et al* 1982), DORIS (Barber *et al* 1983a), PETRA (Barber *et al* 1983b), CESR (MacKay *et al* 1984), TRISTAN (Nakajima *et al* 1991) and LEP (Badier *et al* 1991b). A schematic of a Compton backscattering polarimeter setup (the LEP polarimeter) is shown in figure 28. In all of the above rings, the $\mathrm{e}^\pm$ beams were polarized vertically, i.e. transverse to the particle momentum. HERA is equipped with both transverse (Barber *et al* 1990) and longitudinal (Beckmann *et al* 2002) Compton backscattering polarimeters. A longitudinal Compton backscattering polarimeter was employed at AmPS (Passchier *et al* 1998), and now at SHR (Franklin 2000, Franklin *et al* 2003). A Compton

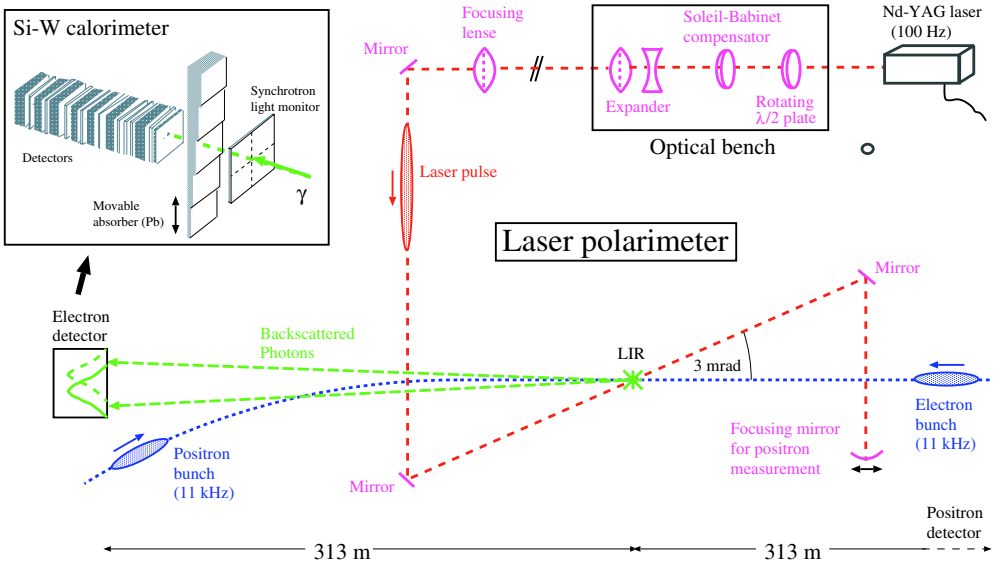

Figure 28. Schematic of the LEP polarimeter. Courtesy of Wenninger (private communication) and CERN.

backscattering transverse polarimeter has also been employed at the BESSY I synchrotron light source (Klein *et al* 1997, 1998). The SLC employed a longitudinal Compton backscattering polarimeter (Shapiro *et al* 1993, Woods *et al* 1997). A unique feature was that it detected the scattered *electrons*, not the photons, although other detectors were later installed to also detect the photons (Berridge *et al* 1999).

A laser Compton backscattering polarimeter can be constructed to operate in either 'single-photon' mode or 'multiphoton' mode. The single-photon mode uses a laser of relatively low peak power and a high repetition rate. There is a maximum of one backscattered photon per interaction of the laser pulse and the electron beam. The multiphoton mode uses a laser of higher peak power, and there are multiple backscattered photons per interaction. Both types of polarimeters have been successfully operated.

When an electron is vertically polarized and the incident photon is circularly polarized, the backscattering Compton cross-section is asymmetric above and below the median plane. The maximum asymmetry occurs when the incident photon energy equals the electron rest energy $m_e c^2$ in the electron rest frame. We can define an asymmetry

$$A_L = \left(\frac{N_+ - N_-}{N_+ + N_-}\right)_L, \tag{12.12}$$

where $N_\pm$ are the photon counts above and below the median plane, respectively. We correspondingly define an asymmetry A_R for right-handed incident photons, and define the overall asymmetry as $A = (A_R - A_L)/2$. The asymmetry A is free of most systematic errors, and is proportional to the electron polarization $\boldsymbol{P}$. The analysing power is a few per cent for electron beam energies of a few GeV. To avoid systematic errors, it is essential that the incident photon beam have a very high degree of circular polarization. The presence of linear photon polarization can generate a false asymmetry.

To measure the longitudinal beam polarization using Compton backscattering, we measure the energy distribution of the backscattered photons. Suppose a photon with circular polarization ξ_2, and energy E_λ, is incident upon an electron with polarization $\boldsymbol{P}_e$ and energy E_e.

If the polarization lies in the horizontal plane, it will rotate around the vertical axis around the ring circumference, and so the polarization vector will not, in general, be longitudinal at the photon–electron interaction point. This is the case in SHR at MIT-Bates, where there is a dipole with an orbital bend angle of 22.5° between the polarimeter location and the BLAST detector. Since the polarization must be longitudinal at the BLAST detector, the angle between the polarization vector and the longitudinal direction depends on the beam energy. (At the SHR, the value of $a\gamma$ varies from less than 1 to approximately 2.3.) Suppose the longitudinal component of the polarization vector is $P_2\boldsymbol{e}_2$. Then the Compton backscattering differential cross-section can be expressed as (here E_γ is the energy of the backscattered photon)

$$\frac{\mathrm{d}\sigma}{\mathrm{d}E_\gamma} = \frac{\mathrm{d}\sigma_0}{\mathrm{d}E_\gamma}\,[1 + \xi_2 P_2 \alpha_2(E_\gamma)], \tag{12.13}$$

where α_2 is a function of E_e and E_λ. Here $\mathrm{d}\sigma_0/\mathrm{d}E_\gamma$ is the cross-section for unpolarized electrons and photons, and $\xi_2 = \pm 1$ is the photon helicity. For a given value of E_λ and E_e, we can define an asymmetry via

$$A_\mathrm{long} = \frac{N_\mathrm{R}(E_\gamma) - N_\mathrm{L}(E_\gamma)}{N_\mathrm{R}(E_\gamma) + N_\mathrm{L}(E_\gamma)} = \Delta\xi_2\, P_2\, \alpha_2(E_\gamma), \tag{12.14}$$

where $N_{\mathrm{L,R}}(E_\gamma)$ are the photon counts for left-handed and right-handed incident circularly polarized photons, and $\Delta\xi_2$ is one-half the difference between the two photon polarization states, so $\Delta\xi_2 = -1$ for $\xi_2 = 1$ and -1. The analysing power is again small, a few per cent, for beam energies of a few GeV or less than a GeV.

In both cases of Compton backscattering measurements of the transverse and longitudinal beam polarization, the technique is fast, and results of a few per cent accuracy can be obtained in a few seconds. The method is nondestructive to the electron or positron beam. Actually, the electron or positron struck by a photon is lost from the beam, but this is a very small percentage of the number of particles in the beam. Note that the above statement implicitly assumes that the polarization is uniform across the beam; else we would not obtain an accurate sampling of the polarization. The polarization can be monitored continuously, which is especially important in situations where the polarization cannot be assumed to remain constant over the lifetime of the stored beam.

However, a Compton backscattering polarimeter takes a fair amount of setup and maintenance. It takes careful effort to deliver a high degree of circular photon polarization at the photon–electron interaction point. The laser and electron beams are not automatically guaranteed to collide—the position of the electron beam can fluctuate and must be monitored, possibly requiring a feedback loop. Hot spots can develop when the laser beam is reflected off mirrors or in prisms, using total internal reflection.

12.2.3. Helical undulator. This is really an innovative accelerator physics experiment to measure the polarization of colliding e^+e^- beams. A helical undulator was placed at one of the e^+e^- interaction points of the VEPP-2M ring (Vorobyov *et al* 1986, Kezerashvili *et al* 1992). VEPP-2M is an e^+e^- collider with a beam energy of 180–700 MeV (0.36–1.4 GeV centre-of-mass energy). A schematic layout of the VEPP-2M ring and preaccelerator complex was shown in figure 2. The electrons (positrons) emitted circularly polarized photons upon passage through the undulator, which then impinged on the oppositely moving positron (electron) beam. The degree of circular photon polarization was essentially 100% (Stokes parameter of $\xi_2 = \pm 1$). Hence, the e^- and e^+ beams themselves generated the circularly polarized photons for use in Compton backscattering. This yielded a Compton backscattering polarimeter for both beams together. The more usual laser Compton backscattering setup only measures the polarization

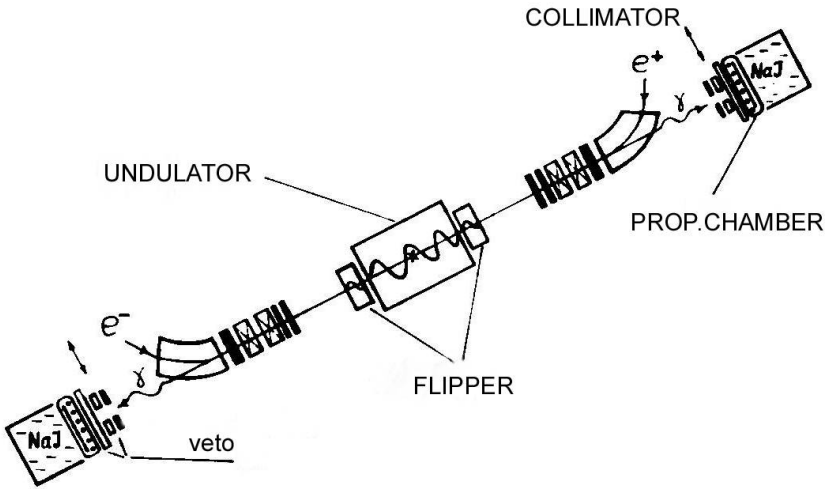

Figure 29. Schematic of helical undulator at VEPP-2M. Reprinted from Kezerashvili *et al* (1992). Copyright (1992) with permission from Elsevier.

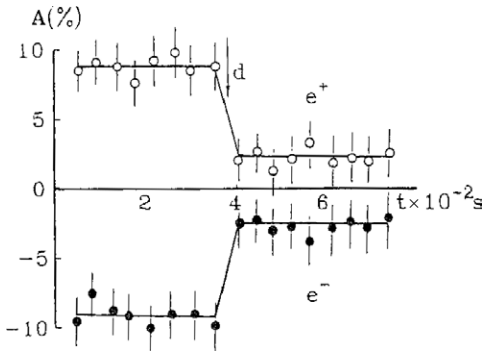

Figure 30. Simultaneous resonant depolarization of the e^+e^- beams at VEPP-2M. Reprinted from Kezerashvili *et al* (1992). Copyright (1992) with permission from Elsevier.

of one of the two beams circulating in the storage ring. A schematic figure of the setup is shown in figure 29. The measured polarization degree of the beams was (Kezerashvili *et al* 1992)

$$P = 0.83 \pm 0.07 \pm 0.08, \tag{12.15}$$

where the first error is statistical and the second is systematic. The beams had equal degree of polarization. The experiment also demonstrated simultaneous resonant depolarization of the e^+ and e^- beams, as shown in figure 30. In this case, the polarizations of the two beams were measured using the asymmetries of the backscattered photon distributions. Hence, the plotted variable has the opposite sign for the two beams. This is, as opposed to what one would obtain from a Touschek normalized count rate.

The undulator design is significant, because it foreshadowed the later design of helical magnetic fields for the Siberian Snakes and spin rotators at RHIC. The superconducting undulator was made up of two halves, one on either side of the e^+e^- interaction point. Each half consisted of four full helix periods (four full 360° twists of the helical magnetic field). The helical-field Snake and spin rotator design is reviewed in detail in MSY1.

12.3. Hadron polarimetry: proton polarimetry at RHIC

12.3.1. General remarks. Polarimetry for polarized hadron beams is more difficult than for lepton beams, because the cross-sections of QED processes such as Compton backscattering are too small and, therefore, cannot be used. One must rely on hadronic interactions, for which there are no theoretically calculable asymmetries. The analysing power of the polarimeter must, therefore, be determined phenomenologically. Consult the review by Makdisi (1998). A list of reactions which have been employed for proton polarimetry, the kinematic regions where they are useful, and the analysing powers, is given by Roser (2002).

We consider only the polarimeters employed at RHIC. An overview of polarized proton polarimetry in the BNL complex, from the injector linac through to RHIC, is given by Spinka (2003). There are two types of devices in RHIC, a fast relative polarimeter (pC CNI polarimeter) based on proton–carbon elastic scattering in the Coulomb nuclear interference (CNI) region, and an absolute polarimeter using elastic proton–proton scattering, also in the CNI region. The successful commissioning of the RHIC CNI polarimeter is described by Huang *et al* (2001). The design of the absolute *pp* polarimeter is described by Bravar (2003). It was installed in RHIC in Spring 2004. The results of commissioning tests should be available soon, but unfortunately, not in time for this review. An idea for absolute calibration of the pC polarimeter, by circulating a beam of carbon nuclei in RHIC, is described by Igo and Tanihata (2003).

12.3.2. Absolute pp polarimeter. The absolute polarimeter consists of a hydrogen gas jet that is squirted across the path of the circulating proton beam. Most of the information below is taken from Bravar (2003). The chosen reaction is elastic *pp* scattering at very small momentum transfer t, in the CNI region $0.001 < |t| < 0.02$ $(\mathrm{GeV\,c^{-1}})^2$. Here t is a Mandelstam variable. We explain the concept of Coulomb nuclear interference more fully (but still briefly) in the description of the pC CNI polarimeter below. One contribution to the left–right asymmetry for elastic *pp* scattering cross-section, with one proton transversely polarized relative to the incident momentum direction, arises from the interference of the (real) electromagnetic spin-flip amplitude, due to the anomalous magnetic moment of the proton, with the (pure imaginary) hadronic spin-nonflip amplitude. This effect is, in fact, fully calculable within QED. However, there is also a contribution to the asymmetry from the (real) hadronic spin-flip amplitude. This is a nonperturbative QCD effect and is not presently calculable. The analysing power of the elastic *pp* reaction reaches a maximum in the CNI region of about $A \simeq 0.045$ (Buttimore *et al* 1999). The precision of the present knowledge of the analysing power is, however, not adequate for RHIC; a new measurement will be required. The *pp* polarimeter was installed and commissioned in 2004, thereby allowing an absolute calibration of the RHIC polarization at the flattop of 100 GeV. Unfortunately the information of the analysing power will not be available in time for this review.

A *self-calibration* technique can be performed with the polarimeter, at any beam energy, and free of theoretical assumptions. The idea goes as follows. The transverse spin asymmetry of elastic *pp* scattering of a polarized beam on an unpolarized target is equal in magnitude, but opposite in sign, to the transverse spin asymmetry of an unpolarized beam incident on a polarized target, in the same kinematical region (same value of momentum transfer t). Hence, at first, a gas jet of known degree of polarization is injected across the path of an unpolarized proton beam. The asymmetry in the differential cross-section is recorded; this yields the analysing power. Next, an unpolarized gas jet is injected across the path of a circulating polarized proton beam (of unknown degree of polarization). The asymmetry in the elastic *pp* differential scattering cross-section is compared to the (negative of the) previously measured analysing power; this yields the degree of polarization of the circulating beam.

Unfortunately, the luminosity of the polarized gas jet target is too low to offer a fast measurement of the polarization; data must be accumulated over 24 h to obtain sufficient statistics for a measurement. However, because of the low density of the gas jet, it can be operated continuously without disrupting the emittance of the circulating beam, or reducing the beam lifetime.

12.3.3. CNI polarimeter. A significant experimental challenge for proton polarimetry is that suitable hadronic interactions for polarized proton beams with energies above about 30 GeV are difficult to find. We have seen that elastic pp scattering can be used, but is slow. One candidate reaction with suitable properties is the elastic scattering of polarized protons against carbon nuclei, in the Coulomb nuclear interference (CNI) region. The CNI polarimeter is the 'workhorse' polarimeter in RHIC. For scattering very close to the forward direction, i.e. very small values of $|t|$, the interaction is dominated by the Coulomb potential, which is a QED effect, and is calculable (and spin-independent). At larger scattering angles, the Coulomb and hadronic (nuclear) forces overlap, leading to maximal interference. At large scattering angles (large $|t|$), the hadronic interaction dominates and the cross-section falls off exponentially with $|t|$. The CNI region is the interval of intermediate scattering angles where a maximal asymmetry in the elastic scattering cross-section can be observed. A study of the pC analysing power at the AGS is reported by Tojo *et al* (2002), who state that the hadronic spin-flip term is not negligible.

The scheme is to place a thin carbon filament in the path of the beam, and to measure the proton–carbon scattering cross-section. The carbon filament can be swung in and out of the path of the beam in RHIC. The final proton travels very close to the forward direction. To detect it would require placing detectors so close to the beam, that it would constrict the accelerator beam pipe unacceptably. Hence, the scattered protons are not detected and only the scattered carbon nuclei are detected. The kinetic energy of a scattered carbon nucleus is very low and hence, easily stopped, in particular if the carbon filament itself is too thick. In the RHIC CNI polarimeter, the filament is only about 100 atoms thick. In the events of interest, the carbon nuclei are scattered through about 90° to the beam direction. A pair of detectors located at either side of the filament (i.e. not the main experimental detectors of RHIC), measure the left–right asymmetry of the scattered carbon nuclei. This yields a measure of the vertical polarization of the proton beam. At RHIC, it is also important to measure the horizontal polarization component, so there are also two pairs of detectors at $\pm 45^\circ$ relative to the horizontal plane. These detectors measure the radial component of the polarization.

The CNI polarimeter is fast, and gives results in a few minutes. Its analysing power cannot be determined by a self-calibration method like the elastic pp polarimeter. Up to 2003 the analysing power of the CNI polarimeter had only been calibrated at the RHIC injection energy of 24 GeV (Spinka 2003). With the installation of the pp gas jet polarimeter in 2004, the CNI polarimeters could be calibrated at 100 GeV. However, even without an absolute calibration, the CNI polarimeter can be used to determine *relative* changes in the proton beam polarization during a store. The measurement technique is destructive to the carbon filaments, which are only about 100 atoms thick, and so cannot be left in place during the whole beam storage period. The polarization is measured as needed, every few hours.

12.3.4. Further remarks. Both the gas jet and CNI polarimeters only measure the transverse components of the polarization, i.e. vertical and/or radial. To measure the longitudinal polarization in a RHIC arc, two polarimeters are required at different azimuthal locations. The value of the radial polarization is measured at both polarimeters, and the longitudinal

polarization is calculated by solving a matrix equation. We are tacitly assuming that the spins rotate around a vertical axis between the two polarimeters, which is the case in the RHIC arcs. To verify that the polarization is longitudinal at the STAR and PHENIX detectors at RHIC, the CNI polarimeter measures the degree of the vertical polarization in a RHIC arc, while the detectors are equipped with local polarimeters which verify that the transverse asymmetry in the polarized *pp* cross-section is zero. The combination of both sets of measurements establishes the degree of polarization in the ring, and that it is longitudinal at the detectors. The use of particle detectors as polarimeters has a long history. Recall that in e^+e^- colliders, the particle detectors were used as polarimeters for some of the early observations of radiative polarization.

13. Siberian Snakes and spin rotators

13.1. General remarks

The companion paper MSY1 reviewed Siberian Snakes and spin rotators in detail. Specifically, we presented the theoretical definitions of such devices: why they were necessary/useful in accelerators, and also, several explicit designs of Snakes and rotators. This paper, therefore, presents only a *very* brief summary.

A Siberian Snake is theoretically defined as a device which rotates the particle spin through 180° around an axis in the horizontal plane, while leaving the orbital motion unaffected. The original idea was proposed nearly thirty years by Derbenev and Kondratenko (1976). Mathematically, a Siberian Snake is usually modelled as a δ-function point object, which rotates a spin through 180°, but is an identity map for the orbital motion.

A solenoid with the appropriate field integral can function as a Siberian Snake. This is/was the case at the IUCF Cooler, AmPS and SHR. At AmPS and SHR, the Snake consists of two solenoids in series. At RHIC the Snakes are built using transverse fields. The field pattern in each RHIC Snake consists of four full-twist helical magnetic fields. The RHIC Snakes and spin rotators are described by Alekseev *et al* (2003). They employ a design by the VEPP-2M design team from BINP (see, e.g., Ptitsyn and Shatunov (1995), (1997)). The designs are reviewed in detail in MSY1.

A spin rotator is an insertion device which rotates the spin direction without perturbing the orbital motion. Spin rotators were also reviewed in MSY1. They are of interest, because most particle physics experiments require longitudinal polarization at the interaction point, whereas the polarization is vertical in the arcs. In general, a pair of spin rotators is required, one to rotate the spins from the vertical to the longitudinal (upstream of the interaction point), and another to restore the spins to the vertical downstream of the interaction point. There are some caveats to the above statements which will be described in the next paragraph, and are reviewed in detail in MSY1. Spin rotators have been successfully operated at RHIC and HERA. The RHIC spin rotators employ four full-twist helical magnets (see the statements about the RHIC Snakes above). The HERA spin rotator employs interleaved transverse (horizontal and vertical) dipole fields, the so-called 'Buon–Steffen minirotator' (Buon and Steffen 1986).

It is not strictly true that a spin rotator rotates a spin from the vertical to the longitudinal (or vice-versa), or that there is no bending of the design orbit. At RHIC, there is a horizontal bend of ± 3.675 mrad between a spin rotator and the collision point. Since the spin precession angle through a horizontal bend is energy dependent, a RHIC spin rotator must actually rotate the spins from the vertical to an energy-dependent direction in the horizontal plane, to attain longitudinal polarization at the collision point (and vice-versa downstream of the interaction point). In the case of HERA, the minirotator design contains an overall horizontal bend of the

design orbit, so the HERA lepton ring geometry changes depending on the energy of the lepton ring. The minirotator magnets are moved and locked into place. (A RHIC spin rotator does not impart an overall bend to the design orbit, so the RHIC geometry does not vary with energy.) However, a HERA minirotator does rotate the spins from the vertical to the longitudinal and vice-versa.

A 'partial Snake' is one whose spin rotation angle is less than 180°. MSY1 reviewed only full-strength Snakes. The partial Snake strength is usually expressed as a percentage, e.g. a 5% partial Snake is one whose spin rotation angle is $0.05 \times 180^\circ = 9^\circ$. This paper will review the usefulness of partial Snakes, and their use for the correction of depolarizing resonances. Obviously, a solenoid can function as a partial Snake, and was so employed at VEPP-2M, and later at the AGS. Other designs using transverse fields will be reviewed below.

13.2. One-turn spin rotation matrix

Let the spin rotation axis of a Siberian Snake be at an angle ξ relative to $\boldsymbol{e}_1$. The overall spin rotation can be decomposed into a 180° rotation around the radial axis $\boldsymbol{e}_1$, followed by a rotation through an angle 2ξ around the vertical axis $\boldsymbol{e}_3$:

$$\begin{aligned} M_{\text{Snake}} &= \mathrm{e}^{-\mathrm{i}\pi\boldsymbol{\sigma}\cdot(\boldsymbol{e}_1\cos\xi+\boldsymbol{e}_2\sin\xi)/2} \\ &= -\mathrm{i}(\sigma_1\cos\xi+\sigma_2\sin\xi) = \mathrm{e}^{-\mathrm{i}\xi\sigma_3}\,(-\mathrm{i}\sigma_1) = (-\mathrm{i}\sigma_1)\,\mathrm{e}^{\mathrm{i}\xi\sigma_3}. \end{aligned} \tag{13.1}$$

The last line shows that we can also rotate clockwise through 2ξ around the vertical, and then, by 180° around the radial axis. We can call ξ the 'Snake axis angle', although this is not standard terminology. For a partial Snake, with a spin rotation angle $\lambda_s\pi$, the spin rotation matrix is

$$M_{\text{partial}} = \mathrm{e}^{-\mathrm{i}\lambda_s\pi\boldsymbol{\sigma}\cdot(\boldsymbol{e}_1\cos\xi+\boldsymbol{e}_2\sin\xi)/2} = \cos\frac{\lambda_s\pi}{2} - \mathrm{i}\sin\frac{\lambda_s\pi}{2}\,\mathrm{e}^{-\mathrm{i}\xi\sigma_3}\,\sigma_1. \tag{13.2}$$

For a partial Snake, one tacitly assumes that $0 \leqslant \lambda_s \leqslant 1$.

We calculate the one-turn spin rotation matrix for a ring with one Snake. We place the origin at the point diametrically opposite the Snake. The spin rotation angle in an arc is written as $\pi\nu_0$, where $\nu_0 = a\gamma$ or $\nu_0 = G\gamma$. The spin rotation matrix of an arc is

$$M_{\text{arc}} = \mathrm{e}^{-\mathrm{i}\pi\nu_0\sigma_3/2}, \tag{13.3}$$

hence, the overall one-turn spin rotation matrix on the design orbit is

$$\begin{aligned} M_{\text{ring}} &= M_{\text{arc}}\,M_{\text{Snake}}\,M_{\text{arc}} \\ &= \mathrm{e}^{-\mathrm{i}\pi\nu_0\sigma_3/2}\,\mathrm{e}^{-\mathrm{i}\xi\sigma_3}\,(-\mathrm{i}\sigma_1)\,\mathrm{e}^{-\mathrm{i}\pi\nu_0\sigma_3/2} \\ &= \mathrm{e}^{-\mathrm{i}\xi\sigma_3}(-\mathrm{i}\sigma_1). \end{aligned} \tag{13.4}$$

We equate this to the closed-orbit spin tune and spin rotation axis via

$$M_{\text{ring}} \equiv \mathrm{e}^{-\mathrm{i}\pi\nu_{\text{c.o.}}\boldsymbol{\sigma}\cdot\boldsymbol{n}_0}. \tag{13.5}$$

Hence, we deduce that the value of the spin tune on the design orbit is simply

$$\nu_{\text{c.o.}} = \tfrac{1}{2}. \tag{13.6}$$

The vector $\boldsymbol{n}_0$ is the spin rotation axis, and is also the direction of the stable long-term polarization. We deduce that the spin rotation axis (polarization direction) at the origin is parallel to the spin rotation axis of the Snake, namely

$$\boldsymbol{n}_0 = \boldsymbol{e}_1\cos\xi + \boldsymbol{e}_2\sin\xi. \tag{13.7}$$

Hence, the use of a Siberian Snake in a ring makes the value of the spin tune *independent* of the beam energy. In addition, the stable polarization direction lies in the horizontal plane all around the circumference.

We now calculate the one-turn spin rotation matrix for a planar ring equipped with two Siberian Snakes. The Snakes are placed at diametrically opposite points of the ring, say, at $\theta = 0$ and $\theta = \pi$. The Snake spin rotation axes are also orthogonal: say at ξ and $\xi + \pi/2$ (both axes lie in the horizontal plane). The Snake spin rotation matrices are

$$M_{s1} = \mathrm{e}^{-\mathrm{i}\xi\sigma_3}(-\mathrm{i}\sigma_1), \qquad M_{s2} = \mathrm{e}^{-\mathrm{i}\xi\sigma_3}(-\mathrm{i}\sigma_2). \tag{13.8}$$

We place the origin just after the exit of the first Snake. The one-turn spin rotation matrix is

$$\begin{aligned} M_{2\ \mathrm{Snakes}} &= M_{s1}\, M_{\mathrm{arc}}\, M_{s2}\, M_{\mathrm{arc}} \\ &= \mathrm{e}^{-\mathrm{i}\xi\sigma_3}\,(-\mathrm{i}\sigma_1)\,\mathrm{e}^{-\mathrm{i}\pi\nu_0\sigma_3/2}\mathrm{e}^{-\mathrm{i}\xi\sigma_3}\,(-\mathrm{i}\sigma_2)\,\mathrm{e}^{-\mathrm{i}\pi\nu_0\sigma_3/2} \\ &= -\mathrm{i}\sigma_3 \\ &= \mathrm{e}^{-\mathrm{i}\pi\sigma_3/2}. \end{aligned} \tag{13.9}$$

This is a spin rotation of 180° around the vertical axis. Hence, once again, the value of the spin tune is

$$\nu_{\mathrm{c.o.}} = \tfrac{1}{2}, \tag{13.10}$$

independent of the beam energy. The spin rotation axis is given by

$$\boldsymbol{n}_0 = \begin{cases} \boldsymbol{e}_3 & \text{for } \theta \in (0, \pi), \\ -\boldsymbol{e}_3 & \text{for } \theta \in (\pi, 2\pi). \end{cases} \tag{13.11}$$

The stable polarization direction is vertically up in one arc of the ring, and vertically down in the other arc.

The fact that the value of the spin tune is independent of the beam energy means that a polarized beam can be accelerated to arbitrarily high energies without crossing any depolarizing resonances. However, as explained in MSY1, depolarizing resonances can, and do, exist in rings with Siberian Snakes. They are called 'Snake resonances'. As explained in MSY1, Snake resonances actually play a useful beam physics role at RHIC, to help calibrate the currents in the RHIC Snake magnets.

13.3. Partial Snakes

Up to 2003, all rings which employed partial Snakes used only one partial Snake, which was a solenoid in all cases. A partial Snake with transverse magnetic fields (a variable-pitch helical field design) was operated at the AGS during the 2004 polarized proton run at BNL (Huang *et al* 2003b). The design of Snakes using helical fields was reviewed in MSY1.

We calculate the one-turn spin rotation matrix for a planar ring with one solenoidal Snake, of fractional strength λ. We place the origin just before the Snake. The one-turn spin rotation matrix is

$$\begin{aligned} M &= \mathrm{e}^{-\mathrm{i}\pi\nu_0\sigma_3}\mathrm{e}^{-\mathrm{i}\pi\lambda\sigma_2/2} \\ &= \cos(\pi\nu_0)\cos\frac{\pi\lambda}{2} + \mathrm{i}\sigma_1\sin(\pi\nu_0)\sin\frac{\pi\lambda}{2} \\ &\quad - \mathrm{i}\sigma_2\cos(\pi\nu_0)\sin\frac{\pi\lambda}{2} - \mathrm{i}\sigma_3\sin(\pi\nu_0)\cos\frac{\pi\lambda}{2}. \end{aligned} \tag{13.12}$$

Equating this to $\mathrm{e}^{-\mathrm{i}\pi\nu_{\mathrm{c.o.}}\boldsymbol{\sigma}\cdot\boldsymbol{n}_0}$ yields

$$\cos(\pi\nu_{\mathrm{c.o.}}) = \cos(\pi\nu_0)\cos\frac{\pi\lambda}{2} \tag{13.13}$$

for the spin tune. The components of $\boldsymbol{n}_0$ are given by

$$\begin{aligned} n_1 &= -\frac{\sin(\pi\nu_0)\sin(\pi\lambda/2)}{\sin(\pi\nu_{\text{c.o.}})}, \\ n_2 &= \frac{\cos(\pi\nu_0)\sin(\pi\lambda/2)}{\sin(\pi\nu_{\text{c.o.}})}, \\ n_3 &= \frac{\sin(\pi\nu_0)\cos(\pi\lambda/2)}{\sin(\pi\nu_{\text{c.o.}})}. \end{aligned} \tag{13.14}$$

One can, therefore, deduce the value of λ from (13.13). The magnitude of the horizontal component of $\boldsymbol{n}_0$ is $n_\perp = \sin(\pi\lambda/2)/\sin(\pi\nu_{\text{c.o.}})$. If the value of ν_0 is close to an integer, and $|\lambda| \ll 1$, then $\cos(\pi\nu_{\text{c.o.}}) \simeq 1$, and also $\sin(\pi\nu_0) \simeq 0$, in which case $n_3 \ll 1$ and $n_\perp \simeq 1$, i.e. the polarization can be strongly tilted away from the vertical.

A demonstration of the above tilt of the polarization direction was one of the first spin dynamics studies performed at the IUCF Cooler (Krisch *et al* 1989). The polarimeter in the IUCF Cooler could measure only the radial and vertical polarization components, i.e. the transverse polarization. The beam energy was held fixed (i.e. fixed ν_0), and the partial Snake strength λ, was varied. According to theory, the radial polarization should be an odd function of λ and hence, change sign across $\lambda = 0$, while the vertical polarization component should be an even function of λ, and display a maximum at $\lambda = 0$. Let us define ϕ via

$$n_3 = \cos\phi, \qquad n_\perp = \sin\phi. \tag{13.15}$$

Hence, ϕ is related to the partial Snake strength λ via

$$\tan\phi = \frac{\tan(\pi\lambda/2)}{\sin(\pi\nu_0)}. \tag{13.16}$$

A vertically polarized beam (say, with polarization P_0) was injected into the IUCF Cooler. The projection of the initial polarization along $\boldsymbol{n}_0$ is $P_0\cos\phi$. The long-term polarization, at an azimuth θ around the ring, where the partial Snake is at $\theta = \pi$, and using subscripts (r, l, v) for (radial, longitudinal, vertical), was then

$$P_{\text{r}} = -P_0\sin(\nu_0\theta)\sin\phi, \qquad P_{\text{l}} = P_0\cos(\nu_0\theta)\sin\phi, \qquad P_{\text{v}} = P_0\cos^2\phi. \tag{13.17}$$

The polarimeter was located at $\theta = 2\pi/3$. Note that we are equating the polarization to the components of $\boldsymbol{n}_0$. This is permissible, since the experiment was simply measuring the spin precession, and not any depolarizing resonances. A graph of the vertical and radial polarization for 120 MeV polarized protons is shown in figure 31. The curve is a theoretical fit given by (13.17).

Figure 32 shows a graph of the radial and vertical polarization at the IUCF Cooler with *synchrotron sideband resonances* on either side of the central peak of P_{v}, also in the graph of the radial component P_{r}. These sidebands represent true depolarization: both P_{r} and P_{v} vanish together. Section 20 reviews synchrotron sideband resonances.

13.4. Intrinsic resonances driven by horizontal betatron oscillations

We remarked earlier in section 10.5, that the principal intrinsic resonances in a planar ring are driven by the vertical betatron resonances, and that intrinsic resonances driven by the horizontal betatron resonances typically arise due to transverse betatron coupling. This is because the unperturbed spin direction (direction of $\boldsymbol{n}_0$) is usually vertical in the arcs of a planar ring.

The above statements must be modified for rings with partial Snakes, because in such rings, $\boldsymbol{n}_0$ usually has a radial component. (One can define such rings to be 'nonplanar' but that is beside the point.) For example, the AGS has been equipped for several years with a

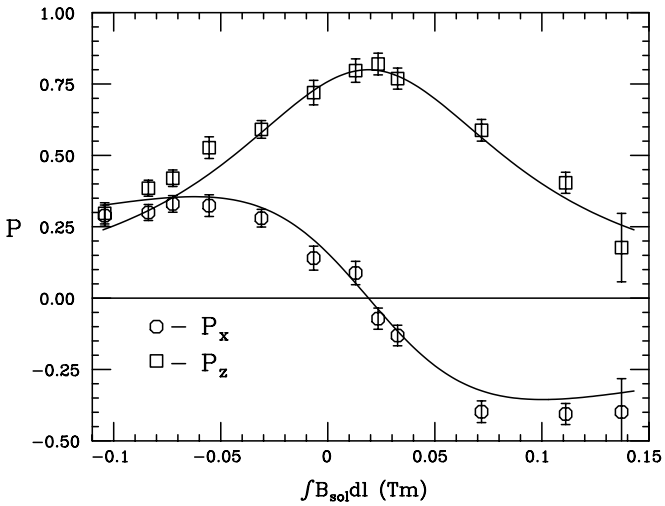

Figure 31. Graphs of the vertical and radial polarization components in the IUCF Cooler as a function of the integrated field in the compensating solenoids, at a kinetic energy of 120 MeV. The solid curves are a theoretical fit. Reprinted with permission from Lee and Berglund (1996). Copyright (1996) by the American Physical Society.

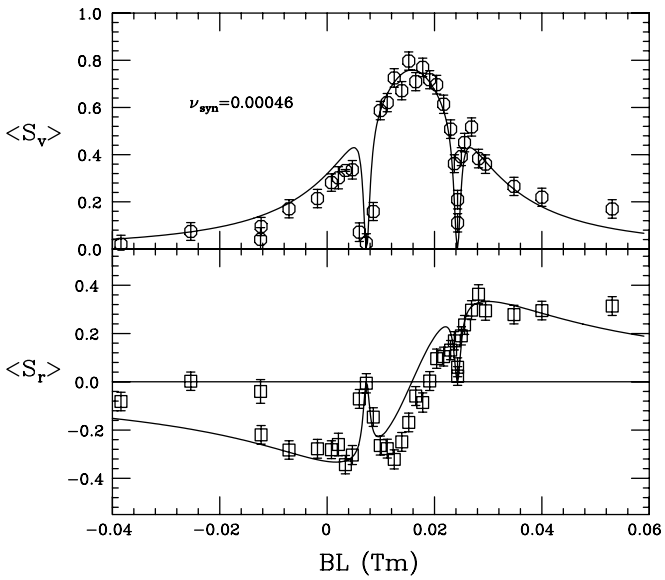

Figure 32. Graphs of the vertical and radial polarization components in the IUCF Cooler as a function of the integrated field in the compensating solenoids, at a kinetic energy of 104.5 MeV. Synchrotron sideband resonances are also visible. The solid curves are a theoretical fit. Reprinted with permission from Lee and Berglund (1996). Copyright (1996) by the American Physical Society.

solenoid partial Snake (Huang *et al* 1994), and now contains two partial Snakes (the second partial Snake is a helical-field device, see Huang *et al* (2003b) for details). The horizontal betatron oscillations drive variations in the vertical component of the spin precession vector, which perturb (and decohere) the radial components of the particle spins. Such intrinsic spin

resonances driven by the horizontal betatron oscillations can exist even if there is no x–y betatron coupling in the ring.

13.5. Siberian Snakes in very high-energy electron rings

In this subsection, we consider (pairs of) Siberian Snakes in very *high* energy e^+e^- storage rings. At first blush, this seems like a peculiar idea. The polarization direction would reverse in each arc, for a ring equipped with a pair of Siberian Snakes (or several pairs of Snakes). Hence the Snakes would kill the radiative polarization. Nevertheless, the idea to insert pairs of Snakes in very high-energy e^+e^- storage rings—we are talking here of several hundred GeV, much beyond the highest LEP beam energy of about 100 GeV—was proposed by no less than the masters in the field, Derbenev and Kondratenko (1978).

Basically, in three papers Derbenev *et al* (1979a, 1979b, 1982) explored the idea of polarizing the beam *in situ* at high energy, by using circularly polarized electromagnetic waves. The basic idea is that the (circularly polarized) photons are used to selectively *knock out* electrons in one of the two (vertically polarized) spin states. To obtain sufficiently hard photons, one might even consider a free-electron laser as the photon source, or for super-high energy rings, to use the coherent synchrotron radiation from the oppositely circulating beam (the positron beam) as the source of photons, by passing the positrons through a helical undulator, just prior to an e^+e^- interaction point.

14. Vector field of spin quantization axes

14.1. Quantum theory

It will clarify matters if we begin with the quantum theory. The Heisenberg equation of motion for an arbitrary operator A (for *a*rbitrary) is

$$i\hbar\frac{dA}{dt} = [A, H] + i\hbar\frac{\partial A}{\partial t}. \tag{14.1}$$

Our interest is in dynamical variables, which are those operators whose dynamics is generated *solely* by the Hamiltonian. A variable such as $A = at + bt^2$, with no connection to the dynamics of the system, is of no interest. A dynamical variable D has no explicit time dependence ($\partial D/\partial t = 0$), and its Heisenberg equation of motion is

$$i\hbar\frac{dD}{dt} = [D, H]. \tag{14.2}$$

This is the equation of motion for all standard textbook variables such as $\boldsymbol{r}$, $\boldsymbol{p}$, $\boldsymbol{L} = \boldsymbol{r} \times \boldsymbol{p}$, $\boldsymbol{J}$, etc, and in particular, $\boldsymbol{s}$. We are further interested in *i*nvariants of the motion I (more formally, *first integrals of the motion*), which are dynamical variables that are furthermore constant in time:

$$\frac{dI}{dt} = \frac{\partial I}{\partial t} = 0, \tag{14.3}$$

from which it follows, from the Heisenberg equation of motion, that I commutes with the Hamiltonian $[I, H] = 0$. *This* is why quantum mechanics textbooks place such emphasis on finding a complete set of commuting observables: the sought-for operators are dynamical invariants, and the corresponding eigenstates are, thus, stationary states of the system.

The three components of a quantum spin operator do not commute, so only one of them will, in general, commute with the Hamiltonian (unless the Hamiltonian is spin-independent, in which case, there will be no polarization). We seek a quantization axis, call it $\boldsymbol{n}$, such that

the spin projection $\boldsymbol{s}\cdot\boldsymbol{n}$—we are treating $\boldsymbol{s}$ as a quantum operator here—will be a dynamical invariant. This requires two conditions:

$$\frac{\partial}{\partial t}\boldsymbol{s}\cdot\boldsymbol{n}=0, \qquad \frac{\mathrm{d}}{\mathrm{d}t}\boldsymbol{s}\cdot\boldsymbol{n}=0. \tag{14.4}$$

From these, it will follow that $\boldsymbol{s}\cdot\boldsymbol{n}$ commutes with the Hamiltonian: $[\boldsymbol{s}\cdot\boldsymbol{n},\ H]=0$. We already know that $\boldsymbol{s}$ is a dynamical variable: $\partial\boldsymbol{s}/\partial t=0$. Hence, it is merely necessary to demand that $\boldsymbol{n}$ also be explicitly time-independent:

$$\frac{\partial\boldsymbol{n}}{\partial t}=0, \tag{14.5}$$

which means that $\boldsymbol{n}$ is a function of the coordinates and momenta only: $\boldsymbol{n}=\boldsymbol{n}(\boldsymbol{q},\boldsymbol{p})$. As for the second condition, we know that

$$\frac{\mathrm{d}\boldsymbol{s}}{\mathrm{d}t}=\boldsymbol{\Omega}\times\boldsymbol{s}. \tag{14.6}$$

This is an equation for a quantum operator $\boldsymbol{s}$. Up to now, all of our manipulations have been exact, even if formal. This is where the semiclassical approximation enters. We demand that $\boldsymbol{n}$ also satisfy the equation

$$\frac{\mathrm{d}\boldsymbol{n}}{\mathrm{d}t}=\boldsymbol{\Omega}\times\boldsymbol{n}. \tag{14.7}$$

Here, $\boldsymbol{n}$ is a classical variable, not a quantum operator, but in the semiclassical approximation, the orbital motion is not quantized. More rigorously, we should write

$$\frac{\mathrm{d}\boldsymbol{n}}{\mathrm{d}t}=\langle\boldsymbol{\Omega}\rangle\times\boldsymbol{n}, \tag{14.8}$$

where $\langle\boldsymbol{\Omega}\rangle$ denotes the classical expectation value of the quantum operator $\boldsymbol{\Omega}$. Then,

$$\frac{\mathrm{d}}{\mathrm{d}t}\boldsymbol{s}\cdot\boldsymbol{n}=\frac{\mathrm{d}\boldsymbol{s}}{\mathrm{d}t}\cdot\boldsymbol{n}+\boldsymbol{s}\cdot\frac{\mathrm{d}\boldsymbol{n}}{\mathrm{d}t}=(\boldsymbol{\Omega}\times\boldsymbol{s})\cdot\boldsymbol{n}+\boldsymbol{s}\cdot(\langle\boldsymbol{\Omega}\rangle\times\boldsymbol{n})\simeq 0. \tag{14.9}$$

In the semiclassical approximation, the difference between the terms is of a higher order in $\hbar$, and can be neglected.

Hence, overall, the axis $\boldsymbol{n}$ that we seek is not a fixed axis, but is a dynamical variable, a function of the orbital phase-space variables $\boldsymbol{q}$ and $\boldsymbol{p}$ (treated in the semiclassical approximation). It is, moreover, an explicitly time-independent solution of the spin precession equation. In appendix A, it will be shown that the solution for $\boldsymbol{n}$ is unique, provided that the orbit does not lie on a spin resonance.

Note in passing, that the above procedure is a general prescription to diagonalize the spin motion of any semiclassical quantum system. At no time did we ever say that the Hamiltonian was that for a particle accelerator.

Consider a uniform magnetic field, say $\boldsymbol{B}=B\hat{\boldsymbol{z}}$. Then $H=-\boldsymbol{\mu}\cdot\boldsymbol{B}=-geB/(2mc)\boldsymbol{s}\cdot\hat{\boldsymbol{z}}$. In that case, we simply set $\boldsymbol{n}$ to the direction of the magnetic field: $\boldsymbol{n}=\hat{\boldsymbol{z}}$, in which case, trivially $\partial\boldsymbol{n}/\partial t=0$, and also

$$\frac{\mathrm{d}\boldsymbol{n}}{\mathrm{d}t}=\cdots\hat{\boldsymbol{z}}\times\boldsymbol{n}=0, \tag{14.10}$$

this being the well-known fact that, for a uniform field, the spin component quantized along the direction of the field commutes with the Hamiltonian.

14.2. Classical mechanics

We now express the above ideas using classical mechanics. We also employ map techniques; this is not strictly necessary, but is, by far, the most elegant formulation. The evolution of the spin, starting from an initial azimuth θ_*, to that one turn later $\theta_* + 2\pi$, is given by a one-turn map $M(z; \theta_*)$. On the closed orbit ($z = 0$), we have called the solution $\boldsymbol{n}_0$, which is a function only of θ_*. Now select some initial phase-space point, say, z_i, and suppose that after one turn, it maps to z_f, in general, a different point (the special case $z = 0$ is a fixed point). Then $\boldsymbol{n}(z; \theta)$ is defined in the following way. First, on any orbital trajectory, $\boldsymbol{n}$ satisfies the spin precession equation

$$\frac{\mathrm{d}\boldsymbol{n}}{\mathrm{d}\theta} = \boldsymbol{W}(z; \theta) \times \boldsymbol{n}. \tag{14.11}$$

Next, we want the vector $\boldsymbol{n}(z_\mathrm{i}; \theta_*)$, after integrating to $(z_\mathrm{f}, \theta_* + 2\pi)$, to equal the vector $\boldsymbol{n}(z_\mathrm{f}; \theta_*)$ at the original azimuth θ_* (because θ_* and $\theta_* + 2\pi$ denote the same phase-space). This condition makes $\boldsymbol{n}$ a vector field over the orbital phase-space. The more formal statement is that, if the one-turn orbital map is $\mathscr{M}$, then

$$\mathscr{M}\boldsymbol{n}(z; \theta_*) = \boldsymbol{n}(\mathscr{M}z; \theta_*). \tag{14.12}$$

The formal canonical transformation theory to diagonalize the spin–orbit Hamiltonian will be presented in appendix A. Note that the concept of spin eigenstates is useful only if the beam is stored at constant energy for many turns, i.e. a storage ring. If the beam is being accelerated to high energy, as in a synchrotron, then the phase-spaces at θ_* and $\theta_* + 2\pi$ are *not* identical, and one cannot meaningfully define $\boldsymbol{n}$. One can, however, still define the solution $\boldsymbol{n}_0$ on the closed orbit.

We return to stored beams. It is most convenient, for the formal theory, to characterize the orbital motion using action-angle variables $(\boldsymbol{I}, \phi)$. The actions are invariant along an orbital trajectory. By definition the points ϕ_j and $\phi_j + 2\pi$ represent the same phase-space point, for $j = 1, 2, 3$. Then, the above constraints imply that $\boldsymbol{n}$ satisfies the relations,

$$\begin{aligned}\boldsymbol{n}(\boldsymbol{I}, \phi_1, \phi_2, \phi_3; \theta) &= \boldsymbol{n}(\boldsymbol{I}, \phi_1 + 2\pi, \phi_2, \phi_3; \theta) \\ &= \boldsymbol{n}(\boldsymbol{I}, \phi_1, \phi_2 + 2\pi, \phi_3; \theta) \\ &= \boldsymbol{n}(\boldsymbol{I}, \phi_1, \phi_2, \phi_3 + 2\pi; \theta) \\ &= \boldsymbol{n}(\boldsymbol{I}, \phi_1, \phi_2, \phi_3; \theta + 2\pi).\end{aligned} \tag{14.13}$$

15. Formal solution for the spin quantization axis

We shall present some useful and important basic results about the effects of perturbations to the spin motion in the next section. First, we derive a solution for the spin quantization axis, $\boldsymbol{n}$. This section will present two formal solutions, both of which are useful as starting points for perturbation theory later in this paper. As we have already done, we decompose the spin precession vector $\boldsymbol{W}$ into a closed-orbit and off-axis terms: $\boldsymbol{W} = \boldsymbol{W}_0 + \boldsymbol{w}$. In keeping with the remarks earlier about the distinction between the closed orbit and design orbit, it may be necessary occasionally to write $\boldsymbol{W}_{00}$ to denote a vector on the design orbit. In general, $\boldsymbol{W}_0$ will denote the spin precession vector on the imperfect closed orbit.

We already know that the solution on the closed orbit is $\boldsymbol{n}_0$ (by definition):

$$\frac{\mathrm{d}\boldsymbol{n}_0}{\mathrm{d}\theta} = \boldsymbol{W}_0 \times \boldsymbol{n}_0 \tag{15.1}$$

and $\boldsymbol{n}_0$ is periodic around the ring:

$$\boldsymbol{n}_0(\theta + 2\pi) = \boldsymbol{n}_0(\theta). \tag{15.2}$$

The spin tune on the closed orbit is denoted by $\nu_{\text{c.o.}}$, as already stated. Since the spin precession equation is three-dimensional, there are two other linearly independent solutions on the closed orbit. Let us denote them by $\boldsymbol{l}_0$ and $\boldsymbol{m}_0$, with obvious notation. Hence,

$$\frac{\mathrm{d}\boldsymbol{l}_0}{\mathrm{d}\theta} = \boldsymbol{W}_0 \times \boldsymbol{l}_0, \qquad \frac{\mathrm{d}\boldsymbol{m}_0}{\mathrm{d}\theta} = \boldsymbol{W}_0 \times \boldsymbol{m}_0. \tag{15.3}$$

A convenient vector to use in calculations is

$$\boldsymbol{k}_0 \equiv \boldsymbol{l}_0 + \mathrm{i}\boldsymbol{m}_0. \tag{15.4}$$

It is straightforward to show, not just on the closed orbit but on *any* orbit, that the angle between any pair of solutions $\boldsymbol{s}_1$ and $\boldsymbol{s}_2$ of the spin precession is invariant:

$$\frac{\mathrm{d}}{\mathrm{d}\theta}\boldsymbol{s}_1 \cdot \boldsymbol{s}_2 = \frac{\mathrm{d}\boldsymbol{s}_1}{\mathrm{d}\theta} \cdot \boldsymbol{s}_2 + \boldsymbol{s}_1 \cdot \frac{\mathrm{d}\boldsymbol{s}_2}{\mathrm{d}\theta} = (\boldsymbol{W} \times \boldsymbol{s}_1) \cdot \boldsymbol{s}_2 + \boldsymbol{s}_1 \cdot (\boldsymbol{W} \times \boldsymbol{s}_2) = 0. \tag{15.5}$$

Hence, if $\boldsymbol{s}_1 \cdot \boldsymbol{s}_2 = 0$, then they will remain orthogonal. Specifically, on the closed orbit, we can therefore choose $(\boldsymbol{l}_0, \boldsymbol{m}_0, \boldsymbol{n}_0)$ to be an orthonormal triad.

Note that $\boldsymbol{l}_0$ and $\boldsymbol{m}_0$ are *not* periodic around the ring. Since the spin rotation angle after one turn (on the closed orbit) is by definition, $\mu_0 \equiv 2\pi\,\nu_{\text{c.o.}}$, we have

$$\begin{pmatrix} \boldsymbol{l}_0 \\ \boldsymbol{m}_0 \end{pmatrix}_{\theta+2\pi} = \begin{pmatrix} \cos\mu_0 & \sin\mu_0 \\ -\sin\mu_0 & \cos\mu_0 \end{pmatrix} \begin{pmatrix} \boldsymbol{l}_0 \\ \boldsymbol{m}_0 \end{pmatrix}_{\theta}. \tag{15.6}$$

In general, the value of $\nu_{\text{c.o.}}$ is not an integer, e.g. for a planar ring it is $\nu_{\text{c.o.}} = a\gamma$. A convenient way of stating the periodicities is also,

$$\boldsymbol{k}_0(\theta + 2\pi) = \mathrm{e}^{-\mathrm{i}2\pi\nu_{\text{c.o.}}}\boldsymbol{k}_0(\theta). \tag{15.7}$$

We then express $\boldsymbol{n}$, off the closed orbit, using $\boldsymbol{l}_0$, $\boldsymbol{m}_0$ and $\boldsymbol{n}_0$ as a basis, i.e.

$$\boldsymbol{n} = n_1\boldsymbol{l}_0 + n_2\boldsymbol{m}_0 + n_3\boldsymbol{n}_0. \tag{15.8}$$

Clearly, on the closed orbit $n_1 = n_2 = 0$ and $n_3 = 1$. For brevity, define $w_1 = \boldsymbol{w} \cdot \boldsymbol{l}_0$, $w_2 = \boldsymbol{w} \cdot \boldsymbol{m}_0$ and $w_3 = \boldsymbol{w} \cdot \boldsymbol{n}_0$. The equations of motion for the components (n_1, n_2, n_3) are

$$\frac{\mathrm{d}}{\mathrm{d}\theta}\begin{pmatrix} n_1 \\ n_2 \\ n_3 \end{pmatrix} = \begin{pmatrix} 0 & -w_3 & w_2 \\ w_3 & 0 & -w_1 \\ -w_2 & w_1 & 0 \end{pmatrix}\begin{pmatrix} n_1 \\ n_2 \\ n_3 \end{pmatrix} = -\mathrm{i}(\boldsymbol{w} \cdot \boldsymbol{J})\begin{pmatrix} n_1 \\ n_2 \\ n_3 \end{pmatrix}, \tag{15.9}$$

where $\boldsymbol{J}$ is a vector of spin 1 angular momentum matrices. The formal solution for the components is then,

$$\begin{pmatrix} n_1 \\ n_2 \\ n_3 \end{pmatrix} = \mathrm{T}\left\{\exp\left(-\mathrm{i}\int_{-\infty}^{\theta} \boldsymbol{w} \cdot \boldsymbol{J}\,\mathrm{d}\theta'\right)\right\}\begin{pmatrix} 0 \\ 0 \\ 1 \end{pmatrix}, \tag{15.10}$$

where 'T' denotes a θ-ordered product of operators. A θ-ordered product of two noncommuting operators $A(\theta_1)$ and $B(\theta_2)$, is defined such that the operator at a higher value of θ is always placed on the left:

$$\mathrm{T}\{A(\theta_1)B(\theta_2)\} = \begin{cases} A(\theta_1)B(\theta_2) & \text{if } \theta_1 > \theta_2, \\ B(\theta_2)A(\theta_1) & \text{if } \theta_2 > \theta_1. \end{cases} \tag{15.11}$$

The expression is not well-defined for $\theta_1 = \theta_2$. The θ-ordering concept generalizes in the obvious way, to products of more than two noncommuting operators.

Equation (15.10) is in a Cartesian basis, which is not the most convenient for manipulating angular momentum matrices. Later in this paper, we shall express the θ-ordered exponential using spherical harmonics.

Another very important idea is to note, that since $\boldsymbol{n}$ is a unit vector, it really has only two independent degrees of freedom. Hence, it can be parametrized by a complex variable ζ via

$$\boldsymbol{n} = \sqrt{1 - |\zeta|^2}\,\boldsymbol{n}_0 + \Re(\zeta \boldsymbol{k}_0^*). \tag{15.12}$$

Obviously, $\zeta = 0$ on the closed orbit. The equation of motion for ζ is

$$\frac{\mathrm{d}\zeta}{\mathrm{d}\theta} = -\mathrm{i}\boldsymbol{w}\cdot\boldsymbol{k}_0\sqrt{1-|\zeta|^2} + \mathrm{i}\boldsymbol{w}\cdot\boldsymbol{n}_0\,\zeta. \tag{15.13}$$

The solution for ζ, no matter how approximate, always yields a unit vector for $\boldsymbol{n}$, but unfortunately, the equation is nonlinear. In practice, (15.13) is too difficult to solve to arbitrary orders. It is truncated to either first-order perturbation theory,

$$\frac{\mathrm{d}\zeta}{\mathrm{d}\theta} \simeq -\mathrm{i}\boldsymbol{w}\cdot\boldsymbol{k}_0, \tag{15.14}$$

or approximated to include only a subset of the higher-order terms:

$$\frac{\mathrm{d}\zeta}{\mathrm{d}\theta} \simeq -\mathrm{i}\boldsymbol{w}\cdot\boldsymbol{k}_0 + \mathrm{i}\boldsymbol{w}\cdot\boldsymbol{n}_0\,\zeta. \tag{15.15}$$

These approximations can yield solutions such that, sometimes $|\zeta| > 1$. The solution is then no longer unitary. Both (15.14) and (15.15) are very important. To first order, the solution for ζ is,

$$\zeta \simeq -\mathrm{i}\int_{-\infty}^{\theta} \boldsymbol{w}\cdot\boldsymbol{k}_0\,\mathrm{d}\theta'. \tag{15.16}$$

To go beyond first order, the most common approximation is to neglect the term in $|\zeta|^2$ in the square root (see (15.15)). The differential equation for ζ is then again linear, and can be formally solved in closed form. The solution is

$$\zeta \simeq -\mathrm{i}\mathrm{e}^{-\mathrm{i}\chi(\theta)}\int_{-\infty}^{\theta} \mathrm{e}^{\mathrm{i}\chi(\theta')}\,\boldsymbol{\omega}\cdot\boldsymbol{k}_0\,\mathrm{d}\theta', \tag{15.17}$$

where

$$\chi(\theta) = -\int_{-\infty}^{\theta} \boldsymbol{w}\cdot\boldsymbol{n}_0\,\mathrm{d}\theta'. \tag{15.18}$$

The above approximate solutions for ζ will be heavily used in this paper.

16. Single resonance model

16.1. General remarks

In general, the theoretical analysis of the spin dynamics in accelerators can take one of two paths. One is to develop sophisticated numerical formalisms and computer programs to solve the spin precession equation. Such programs are essential to design modern high-energy accelerators with complicated structures. Nevertheless, the programs *are* complicated. The alternative path is to develop (very) simple models of accelerators which are analytically tractable. The behaviour of the spin and the polarization in such models can be calculated exactly. Frequently, such models can provide useful estimates even for complicated machines. The single resonance model (SRM) is the most important nontrivial exactly solvable model.

In the single resonance model, only one term is retained in the perturbing term of the spin precession vector $\boldsymbol{w}$. With only one Fourier harmonic in $\boldsymbol{w}$, the model has only one spin resonance, hence its name. Despite its simplicity, or more likely, because of it, the SRM is an important pedagogical model, and underlies much of the analytical work on spin dynamics

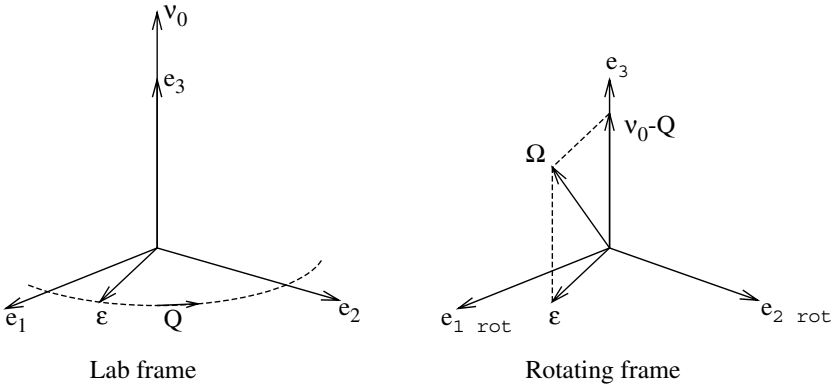

Figure 33. Schematic of spin precession vector for the single resonance model in the lab and rotating frames.

in accelerators. In MSY1, we reviewed the solution of the single resonance model with one, or a pair, of Siberian Snake(s), in terms of so-called 'sine-Bessel' functions. Models based on the single resonance model have historically played an important role in many theoretical analyses of the spin dynamics in accelerators.

The single resonance model is clearly related to the Froissart–Stora formula. The model for the spin precession vector is the same. However, in the SRM we assume the beam energy is *fixed*, and the problem is to determine the quantization axis of the spin eigenstates. The formulation of the single resonance model in terms of an action-angle formalism, and the recognition that the solution for the spin rotation axis is an example of the $\boldsymbol{n}$ axis, was pointed out by Mane (1988b). Many others have since elaborated on the model, e.g. see the review of the SRM by Vogt (2000).

16.2. Notation and basic formalism

The spin precession vector of the single resonance model is

$$\boldsymbol{W}_{\mathrm{SRM}} = \nu_0\,\boldsymbol{e}_3 + \epsilon(\boldsymbol{e}_1\cos\phi + \boldsymbol{e}_2\,\sin\phi). \tag{16.1}$$

The motion on the design orbit is a spin precession around the vertical, while the perturbing term, proportional to ϵ, lies in the horizontal plane. The choice of terminology is perhaps slightly unfortunate, because the solution below is nonperturbative, and is valid for arbitrary ϵ. Nevertheless, the tacit assumption is that $\epsilon = 0$ on the design orbit. Here, ϵ is called the 'resonance strength' for reasons that become clear, below. Also, ϕ is a phase, which evolves according to

$$\frac{\mathrm{d}\phi}{\mathrm{d}\theta} = Q. \tag{16.2}$$

We can write $\phi = Q\theta + \phi_0$. If the resonance driving term is due to a vertical betatron oscillation, then Q is the vertical betatron tune (plus or minus an integer), while if $\boldsymbol{w}$ is due to a vertical closed orbit imperfection, then the value of Q is an integer. The formalism below is the same either way; it is only that in the case of a betatron oscillation, there will be a statistical distribution of values of ϕ_0, and also, a statistical distribution of the values of ϵ.

A simple way to solve for the spin motion is to transform to a frame rotating around $\boldsymbol{e}_3$ at tune Q. The basic vectors in the lab frame and the rotating frame are shown in figure 33.

In the rotating frame the spin precession vector is

$$\boldsymbol{W}'_{\rm SRM} = (\nu_0 - Q)\boldsymbol{e}_3 + \epsilon\,(\boldsymbol{e}_1\cos(\phi - Q\theta) + \boldsymbol{e}_2\sin(\phi - Q\theta)), \tag{16.3}$$

where we use a prime to denote quantities in the rotating frame. Note that $\boldsymbol{W}'_{\rm SRM}$ is a *fixed* vector because $\mathrm{d}\boldsymbol{W}'_{\rm SRM}/\mathrm{d}\theta = 0$. Then the spin $\boldsymbol{s}'$ rotates around $\boldsymbol{W}'_{\rm SRM}$,

$$\frac{\mathrm{d}\boldsymbol{s}'}{\mathrm{d}\theta} = \boldsymbol{W}'_{\rm SRM} \times \boldsymbol{s}'. \tag{16.4}$$

Since $\boldsymbol{W}'_{\rm SRM}$ is a fixed vector, the solution for $\boldsymbol{n}'$ is simply a unit vector in the direction of $\boldsymbol{W}'_{\rm SRM}$,

$$\boldsymbol{n}' = \frac{\boldsymbol{W}'_{\rm SRM}}{|\boldsymbol{W}'_{\rm SRM}|}, \tag{16.5}$$

while the spin tune is just the magnitude of $\boldsymbol{W}'_{\rm SRM}$,

$$\nu' = |\boldsymbol{W}'_{\rm SRM}|. \tag{16.6}$$

Now, define the vector $\boldsymbol{\Omega}$ and its magnitude Ω:

$$\boldsymbol{\Omega} = (\nu_0 - Q)\,\boldsymbol{e}_3 + \epsilon(\boldsymbol{e}_1\cos\phi + \boldsymbol{e}_2\,\sin\phi), \qquad \Omega = \sqrt{(\nu_0 - Q)^2 + \epsilon^2}. \tag{16.7}$$

We take the positive root for Ω. Note that $\boldsymbol{\Omega}$ as defined in (16.7) should not be confused with the previous usage of $\boldsymbol{\Omega}$ to denote the spin precession vector using the time t as the independent variable. In the original reference frame, one possible solution for $\boldsymbol{n}$ and ν is

$$\boldsymbol{n} = \frac{\boldsymbol{\Omega}}{\Omega}, \qquad \nu = \Omega + Q = Q + \sqrt{(\nu_0 - Q)^2 + \epsilon^2}. \tag{16.8}$$

The expressions for both n_3 and ν are continuous functions of ν_0, for fixed Q and ϵ. The graph for ν, as a function of $\nu_0 - Q$ for fixed ϵ, is a hyperbola.

The above solutions are correct but have some curious (but *not* erroneous) properties. Consider the limiting behaviour as $\epsilon \to 0$, for fixed $\nu_0 - Q \neq 0$. Then $|\nu_0 - Q| \gg |\epsilon|$, for sufficiently small $|\epsilon|$, so $\Omega \simeq |\nu_0 - Q|$. If $\nu_0 - Q > 0$, we have,

$$\boldsymbol{n} \simeq \boldsymbol{n}_3, \qquad \nu \simeq \nu_0. \tag{16.9}$$

This is the expected closed-orbit behaviour for $\epsilon \to 0$. However, if $\nu_0 - Q < 0$, then

$$\boldsymbol{n} \simeq -\boldsymbol{e}_3, \qquad \nu \simeq 2Q - \nu_0. \tag{16.10}$$

Exactly at $\nu_0 = Q$, we cannot have $|\nu_0 - Q| \gg |\epsilon|$. In this case $\Omega = \epsilon$ (assuming $\epsilon > 0$). Then,

$$\boldsymbol{n} = \boldsymbol{e}_1\cos\phi + \boldsymbol{e}_2\,\sin\phi, \qquad \nu = Q + \epsilon. \tag{16.11}$$

However, we would like $\boldsymbol{n}$ to always point up when $\epsilon \to 0$ for $\nu_0 - Q \neq 0$, and correspondingly, for the spin tune to reduce to the closed-orbit value ν_0, i.e. to the expressions in (16.9). An alternative solution for $\boldsymbol{n}$ and ν is

$$\begin{aligned} \boldsymbol{n}_{\rm SRM} &= \mathrm{s}_{\nu_0 - Q}\,\frac{\boldsymbol{\Omega}}{\Omega}, \\ \nu_{\rm SRM} &= Q + \mathrm{s}_{\nu_0 - Q}\,\Omega = Q + \mathrm{s}_{\nu_0 - Q}\sqrt{(\nu_0 - Q)^2 + \epsilon^2}. \end{aligned} \tag{16.12}$$

Here, s_x is the sign function, and equals ± 1 according to $x > 0$ or $x < 0$, respectively. Exactly at $\nu_0 = Q$, we can accept either sign in (16.12). The expressions in (16.12) are our official solutions for $\boldsymbol{n}$ and ν for the SRM below, which explains the suffix 'SRM' on the solutions. They reduce to the desired solutions $\boldsymbol{n} \to \boldsymbol{e}_3$ and $\nu \to \nu_0$ when $\epsilon \to 0$, for any $\nu_0 - Q \neq 0$. Exactly at $\nu_0 = Q$, we have

$$\boldsymbol{n}_{\rm SRM} = \pm(\boldsymbol{e}_1\cos\phi + \boldsymbol{e}_2\,\sin\phi), \qquad \nu_{\rm SRM} = Q \pm \epsilon. \tag{16.13}$$

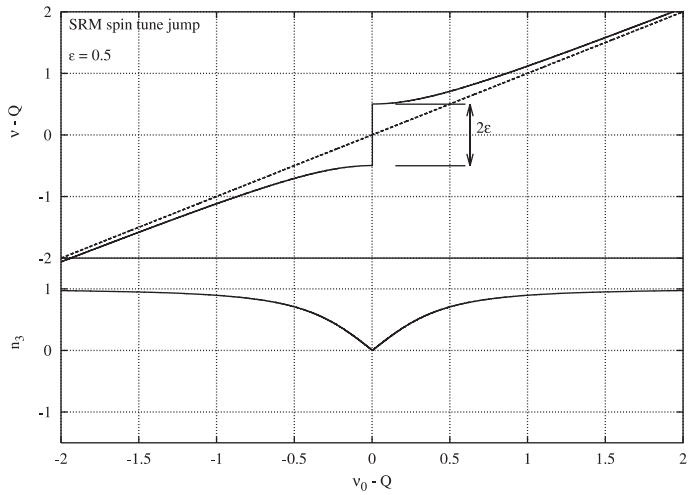

Figure 34. Graphs of the spin tune (actually $\nu - Q$), and the vertical component n_3, as a function of $\nu_0 - Q$, for the single resonance model. The dashed line is the closed-orbit solution, i.e. ν_0. There is a jump in the graph of the spin tune.

If $\nu - Q \to 0^+$ through positive values, then we obtain the solutions with the plus sign, while if $\nu_0 - Q \to 0^-$ through negative values, then we obtain the solutions with the minus sign. Hence, both $\boldsymbol{n}_{\mathrm{SRM}}$ and ν_{SRM} are discontinuous at the tune line $\nu_0 = Q$.

We stated that when $\epsilon = 0$, the solution is $\boldsymbol{n} = \boldsymbol{e}_3$, and obviously the direction of $\boldsymbol{n}$ approaches the horizontal plane for $|\epsilon| \gg |\nu_0 - Q|$. Basically, $\boldsymbol{n}$ starts off vertical on the design orbit and tilts towards the horizontal as the magnitude of the driving term increases. However, consider what happens when $\nu_0 = Q$. In that case, $\boldsymbol{n}$ is *horizontal* for all $\epsilon \neq 0$ (see (16.13)). The spin tilts into the horizontal plane as soon as ϵ is even infinitesimally nonzero. This is characteristic of a resonance: extreme variation of the direction of the spin eigenstates in response to small changes in the model parameters. We graph the value of $\nu - Q$ and the vertical component n_3 as a function of $\nu_0 - Q$, for the expressions in (16.12). The graph is shown in figure 34.

16.3. Adiabatic spin-flip

Consider what happens if the beam energy (value of ν_0) is increased adiabatically from far below Q, to far above Q. Since we are treating an *adiabatic* variation of the parameter ν_0, the relevant solution for $\boldsymbol{n}$ is given by (16.8). Evidently, $\boldsymbol{n}$ starts vertically up (say) and evolves smoothly, and ends up pointing vertically *down*. The value of $\boldsymbol{s} \cdot \boldsymbol{n} = 1$ is an adiabatic invariant, so if $\boldsymbol{s} \cdot \boldsymbol{n} = 1$ initially, it will remain so during acceleration. The spin follows $\boldsymbol{n}$, and ends up pointing downwards. This is the adiabatic spin-flip of the the Froissart–Stora formula. If the acceleration is not adiabatic, the value of $\boldsymbol{s} \cdot \boldsymbol{n}$ will not remain invariant, and depolarization can result.

16.4. Spin tune jump

An alternative idea which has been suggested to identify the locations and widths of depolarizing spin resonances, is to search for jumps in the value of the spin tune, as in (16.12). This idea is explored by Vogt (2000), for example. As displayed in figure 34, the graph for the

spin tune does, indeed, exhibit a jump at the location of the resonance $\nu_0 = Q$. Furthermore, the magnitude of the jump is 2ϵ, as indicated in the figure.

This is an elegant idea, but it does have its limitations. Even using the single resonance model, though, we have seen from (16.8) and (16.12), that there is more than one possible solution for the spin tune, and not all the solutions have jumps, e.g. the expression in (16.8) is continuous. Evidently, we must select the solution for the spin tune ν, which reduces to the closed-orbit value $\nu_{\text{c.o.}}$, as the resonance strength ϵ goes to zero. It may not always be clear what this solution is for a more complicated model, e.g. with multiple resonance driving terms, and also, especially, if one is performing a purely numerical calculation for the spin tune. Other pitfalls are that the location of the spin tune jump may not be exactly at the location of the resonance. In addition, the spin tune may not suffer a jump at all across a depolarizing spin resonance, e.g. for the single resonance model with a single Snake, or a pair of diametrically opposed orthogonal Snakes, as was shown in MSY1.

17. SMILE

17.1. Solution for the vector field of spin quantization axes

The SMILE algorithm (Mane 1987b) was, historically, the first general formalism for the spin quantization axes, which treated all the orbital oscillation modes to arbitrary orders. Other formalisms had been published earlier, but they all treated only a subset of the betatron and synchrotron oscillations, or were restricted to low orders of perturbation theory (typically first order). We review the SMILE formalism briefly below.

We summarize a few basic definitions. We decompose the spin precession vector $\boldsymbol{W}$ into a closed orbit and off-axis terms: $\boldsymbol{W} = \boldsymbol{W}_0 + \boldsymbol{w}$. The spin tune on the closed orbit is denoted by $\nu_{\text{c.o.}}$. We denote the solutions for the spin motion on the closed orbit by $\boldsymbol{l}_0$, $\boldsymbol{m}_0$ and $\boldsymbol{n}_0$, where the one-turn periodicities of the vectors are

$$\boldsymbol{n}_0(\theta + 2\pi) = \boldsymbol{n}_0(\theta), \qquad (\boldsymbol{l}_0 \pm \mathrm{i}\boldsymbol{m}_0)_{\theta+2\pi} = \mathrm{e}^{-\mathrm{i}2\pi\nu_{\text{c.o.}}}(\boldsymbol{l}_0 \pm \mathrm{i}\boldsymbol{m}_0)_\theta. \tag{17.1}$$

We then express $\boldsymbol{n}$, off the closed orbit, using $\boldsymbol{l}_0$, $\boldsymbol{m}_0$ and $\boldsymbol{n}_0$ as a basis, i.e.

$$\boldsymbol{n} = n_1\boldsymbol{l}_0 + n_2\boldsymbol{m}_0 + n_3\boldsymbol{n}_0. \tag{17.2}$$

Clearly, on the closed orbit $n_1 = n_2 = 0$ and $n_3 = 1$. For brevity, define $w_1 = \boldsymbol{w}\cdot\boldsymbol{l}_0$, $w_2 = \boldsymbol{w}\cdot\boldsymbol{m}_0$ and $w_3 = \boldsymbol{w}\cdot\boldsymbol{n}_0$. The formal solution for n_1, n_2 and n_3 was given in (15.10). It is more elegant to make use of angular momentum theory and to employ spherical harmonics. Define

$$V_{\pm1} = \mp\frac{n_1 \pm \mathrm{i}n_2}{\sqrt{2}}, \qquad V_0 = n_3. \tag{17.3}$$

Also define $w_\pm = w_1 \pm \mathrm{i}w_2$. Define a vector of spin 1 angular momentum matrices $\boldsymbol{J}$:

$$J_3 = \begin{pmatrix} 1 & 0 & 0 \\ 0 & 0 & 0 \\ 0 & 0 & -1 \end{pmatrix}, \qquad J_+ = \begin{pmatrix} 0 & \sqrt{2} & 0 \\ 0 & 0 & \sqrt{2} \\ 0 & 0 & 0 \end{pmatrix}, \qquad J_- = \begin{pmatrix} 0 & 0 & 0 \\ \sqrt{2} & 0 & 0 \\ 0 & \sqrt{2} & 0 \end{pmatrix}. \tag{17.4}$$

Then,

$$\boldsymbol{w}\cdot\boldsymbol{J} = w_3J_3 + \tfrac{1}{2}(w_+J_- + w_-J_+). \tag{17.5}$$

The equation of motion for (V_1, V_0, V_{-1}) is

$$\frac{\mathrm{d}}{\mathrm{d}\theta}\begin{pmatrix} V_1 \\ V_0 \\ V_{-1} \end{pmatrix} = \mathrm{i}\,(\boldsymbol{w}\cdot\boldsymbol{J})^{\mathrm{T}}\begin{pmatrix} V_1 \\ V_0 \\ V_{-1} \end{pmatrix}, \tag{17.6}$$

where T denotes a transpose. Here,

$$(\boldsymbol{w}\cdot\boldsymbol{J})^{\mathrm{T}} = \begin{pmatrix} w_3 & w_+/\sqrt{2} & 0 \\ w_-/\sqrt{2} & 0 & w_+/\sqrt{2} \\ 0 & w_-/\sqrt{2} & -w_3 \end{pmatrix}. \tag{17.7}$$

The solution with the appropriate periodicities, and which reduces to $V_{\pm 1} = 0$ and $V_0 = 1$ when $\boldsymbol{w} = 0$, is

$$\begin{pmatrix} V_1 \\ V_0 \\ V_{-1} \end{pmatrix} = \mathrm{T}\left\{\exp\left(\mathrm{i}\int_{-\infty}^{\theta}(\boldsymbol{w}\cdot\boldsymbol{J})^{\mathrm{T}}\mathrm{d}\theta'\right)\right\}\begin{pmatrix} 0 \\ 1 \\ 0 \end{pmatrix}. \tag{17.8}$$

Here, 'T' denotes a θ-ordered product of operators. To evaluate the θ-ordered product, one expands the exponential in a power series, and evaluates the integrals term by term:

$$\begin{pmatrix} V_1 \\ V_0 \\ V_{-1} \end{pmatrix} = \left\{1 + \mathrm{i}\int_{-\infty}^{\theta}(\boldsymbol{w}\cdot\boldsymbol{J})^{\mathrm{T}}\,\mathrm{d}\theta' - \int_{-\infty}^{\theta}\int_{-\infty}^{\theta'}(\boldsymbol{w}(\theta')\cdot\boldsymbol{J})^{\mathrm{T}}\,(\boldsymbol{w}(\theta'')\cdot\boldsymbol{J})^{\mathrm{T}}\,\mathrm{d}\theta'\mathrm{d}\theta'' + \cdots\right\}\begin{pmatrix} 0 \\ 1 \\ 0 \end{pmatrix}. \tag{17.9}$$

The operators are always placed in descending order of θ', θ'', etc, as we read from left to right. Note that $V_{-1} = -V_1^*$, hence it is only necessary to solve for V_1 and V_0. This is the SMILE solution for $\boldsymbol{n}$. It is a perturbative algorithm, in powers of the orbital oscillation amplitudes. The convergence of the series is not guaranteed.

Let us discuss the lower limit of integration of $-\infty$ briefly. It has the same origin as the lower limit of $-\infty$ in the integrals in (15.16)–(15.18). Basically, it is a formal device to satisfy the periodicity conditions on $\boldsymbol{n}$ listed in (14.13). The SMILE integrals can be rendered well-defined by the use of a convergence factor, or by analysing the structure of the integrals analytically, as will be done below.

In practice, SMILE was actually implemented (in a computer programme) only for linear orbital dynamics, i.e. $\boldsymbol{w}$ is linear in the orbital modes. As one can see, the above formal series applies to any expression for $\boldsymbol{w}$, but in normal parlance, SMILE is taken to imply linear orbital dynamics. The algorithm goes further, to explain how to evaluate the integrals numerically.

With the restriction to linear orbital dynamics, one can express the orbital motion as a linear combination of six-dimensional eigenvectors $X = \sum_j a_j E_j$. Similarly, one can decompose $\boldsymbol{w}$ into an eigenvector sum,

$$\boldsymbol{w} = \sum_j a_j \boldsymbol{w}_j, \tag{17.10}$$

where $\boldsymbol{w}_j$ is the spin–orbit coupling due to the eigenvector E_j. One then has $\boldsymbol{w}_j(\theta + 2\pi) = \mathrm{e}^{\mathrm{i}2\pi Q_j}\boldsymbol{w}_j(\theta)$, or

$$\begin{aligned} w_{j+}(\theta + 2\pi) &= \mathrm{e}^{\mathrm{i}2\pi(Q_j - \nu_{\mathrm{c.o.}})}w_{j+}(\theta), \\ w_{j-}(\theta + 2\pi) &= \mathrm{e}^{\mathrm{i}2\pi(Q_j + \nu_{\mathrm{c.o.}})}w_{j-}(\theta), \\ w_{j3}(\theta + 2\pi) &= \mathrm{e}^{\mathrm{i}2\pi Q_j}w_{j3}(\theta). \end{aligned} \tag{17.11}$$

17.2. First order solution

The zeroth-order solutions for V_1 and V_0 are $V_0^{(0)} = 1$ and $V_{\pm 1}^{(0)} = 0$, by definition. The first-order solutions for V_1 and V_0, say $V_1^{(1)}$ and $V_0^{(1)}$, are given by integrating

$$\frac{\mathrm{d}}{\mathrm{d}\theta}\begin{pmatrix} V_1^{(1)} \\ V_0^{(1)} \\ V_{-1}^{(1)} \end{pmatrix} = \mathrm{i}\,(\boldsymbol{w}\cdot\boldsymbol{J})^{\mathrm{T}}\begin{pmatrix} 0 \\ 1 \\ 0 \end{pmatrix}. \tag{17.12}$$

The solution is

$$V_0^{(1)} = 0, \qquad V_{\pm 1}^{(1)} = \frac{\mathrm{i}}{\sqrt{2}}\int_{-\infty}^{\theta} w_{\pm}\,\mathrm{d}\theta'. \tag{17.13}$$

The above expressions express the well-known fact that the leading-order perturbations to the spin motion are driven by terms *orthogonal to* $\boldsymbol{n}_0$. Hence, there is no first-order contribution to V_0. This fact was already implicit in the formulation of the single resonance model: the resonance driving term (the perturbation $\boldsymbol{w}$) was assumed to lie in the horizontal plane, i.e. orthogonal to $\boldsymbol{n}_0$.

In a ring with a single Siberian Snake, $\boldsymbol{n}_0$ lies in the horizontal plane. In such a case, the leading order perturbations in $\boldsymbol{w}$ have components in both the horizontal and vertical directions.

At higher orders, both terms parallel and orthogonal to $\boldsymbol{n}_0$ (in the off-axis spin precession vector $\boldsymbol{w}$) will contribute to the solution for $\boldsymbol{n}$. The terms in $\boldsymbol{w}$ parallel to $\boldsymbol{n}_0$ are, in fact, usually the most important ones at higher orders, e.g. for synchrotron sideband resonances.

As we have pointed out, it is only necessary to solve for V_1, and not both $V_{\pm 1}$. We can decompose the solution for V_1 into a sum of eigenvector terms:

$$V_1^{(1)} = \frac{\mathrm{i}}{\sqrt{2}}\sum_j a_j \int_{-\infty}^{\theta} w_{j+}\,\mathrm{d}\theta' \equiv \sum_j a_j\, V_1^j, \tag{17.14}$$

with obvious notation. Then,

$$V_1^j(\theta + 2\pi) = \mathrm{e}^{\mathrm{i}2\pi(Q_j - \nu_{\mathrm{c.o.}})} V_1^j(\theta). \tag{17.15}$$

This can be used to express the solution for V_1^j in a compact form suitable for numerical evaluation:

$$V_1^j(\theta) = \frac{\mathrm{i}}{\sqrt{2}}\int_{-\infty}^{\theta} w_{j+}\,\mathrm{d}\theta' = \frac{1}{\mathrm{e}^{\mathrm{i}2\pi(Q_j - \nu_{\mathrm{c.o.}})} - 1}\frac{\mathrm{i}}{\sqrt{2}}\int_{\theta}^{\theta+2\pi} w_{j+}\,\mathrm{d}\theta'. \tag{17.16}$$

Hence, the value of $V_1^j(\theta)$ is obtained by an integral around the circumference, based at θ, multiplied by a so-called 'resonance denominator'. The resonance denominator vanishes when $\nu_{\mathrm{c.o.}} = Q_j + k$, where k is an integer: this is a first-order spin resonance. For future reference, the one-turn integrals around the ring are known as (first-order) 'spin integrals'.

17.3. Higher-order spin integrals

At the second order, a sample term, say the expression for V_1, is

$$V_1^{(2)} = -\frac{1}{\sqrt{2}}\int_{-\infty}^{\theta}\int_{-\infty}^{\theta'} w_3(\theta')w_+(\theta'')\,\mathrm{d}\theta'\,\mathrm{d}\theta''. \tag{17.17}$$

This can be decomposed into a double sum over the orbital modes,

$$\begin{aligned} V_1^{(2)} &= -\frac{1}{\sqrt{2}} \sum_{j_1,j_2} a_{j_1} a_{j_2} \int_{-\infty}^{\theta} \int_{-\infty}^{\theta'} w_{j_1\,3}(\theta') w_{j_2\,+}(\theta'')\,\mathrm{d}\theta'\,\mathrm{d}\theta'' \\ &= \mathrm{i} \sum_{j_1,j_2} a_{j_1} a_{j_2} \int_{-\infty}^{\theta} w_{j_1\,3}(\theta') V_1^{j_2}(\theta')\,\mathrm{d}\theta' \\ &\equiv \sum_{j_1,j_2} a_{j_1} a_{j_2} V_1^{j_1 j_2}. \end{aligned} \tag{17.18}$$

This can further be telescoped into a set of one-turn integrals with resonance denominators:

$$V_1^{j_1 j_2} = \frac{\mathrm{i}}{\mathrm{e}^{\mathrm{i}2\pi(Q_{j_1}+Q_{j_2}-\nu_{\mathrm{c.o.}})} - 1} \int_{\theta}^{\theta+2\pi} w_{j_1\,3}(\theta') V_1^{j_2}(\theta')\,\mathrm{d}\theta'. \tag{17.19}$$

(Of course, $V_1^{j_2}$ contains a first-order resonance denominator already.) The new resonance denominator diverges at the second-order resonance

$$\nu_{\mathrm{c.o.}} = Q_{j_1} + Q_{j_2} + k. \tag{17.20}$$

The above expression is significant, because it depends only on the *sum* $Q_{j_1} + Q_{j_2}$, and *not* on the order of terms: the integral $V_1^{j_2 j_1}$ has the same resonance denominator.

This is a significant finding. The terms $V_1^{j_1 j_2}$ and $V_1^{j_2 j_1}$ need *not* be stored separately. Similar statements apply to the terms in V_0 and V_{-1}. Overall, this means that the number of terms to store only increases polynomially, not exponentially, with the order of perturbation theory.

Further details of the formalism, to keep track of all the higher-order terms, are given by Mane (1987b), with important additional refinements by Mane (1992b). Furthermore, it is obvious from (17.9), that the calculation of the higher-order integrals can be formulated recursively.

17.4. Higher-order versus nonlinear spin resonances

The SMILE solution for $\boldsymbol{n}$, using only linear orbital dynamics, demonstrates an important point about the higher-order spin resonances: *all* of the higher-order resonances can, in principle, be driven by purely *linear* orbital dynamics. This clarified a fallacy in the literature pertaining to that point: many authors called the first-order spin resonances 'linear' resonances, and the higher-order ones 'nonlinear' resonances, with the tacit (or sometimes explicit) claim that nonlinear orbital dynamics was required to explain the 'nonlinear' resonances. SMILE showed that this is not so: the linear orbital dynamics can do it all. In fact, nonlinear orbital dynamics can drive even the first-order resonances. It is more common now, to classify the spin resonances as 'first-order' and 'higher-order'.

17.5. Quadrupoles versus higher multipoles

The SMILE algorithm also shows why quadrupoles are the dominant sources of the perturbations to the spin motion when compared with the higher-order multipoles such as sextupoles, etc. Consider a second-order spin resonance of the form $\nu = Q_x + Q_y + k$. Such a resonance can be driven, in first-order perturbation theory, by a sextupole via the xy term in the sextupole field. The relevant first-order integral is

$$V_1^{\mathrm{sext}} \sim \int_{-\infty}^{\theta} w_+(\theta')\,\mathrm{d}\theta'. \tag{17.21}$$

The quadrupoles can also drive such a resonance, but only at the second order of perturbation theory via an integral such as,

$$V_1^{\text{quad}} \sim \int_{-\infty}^{\theta} w_3(\theta') \int_{-\infty}^{\theta'} w_+(\theta'')\, \mathrm{d}\theta'\, \mathrm{d}\theta''. \tag{17.22}$$

From the expressions for w_+ and w_0 in a quadrupole and a sextupole, the magnitudes of the driving terms are roughly,

$$\begin{aligned} w_+^{\text{sext}} &\propto (a\gamma + 1)\, xy, \\ w_+^{\text{quad}} &\propto (a\gamma + 1)\, y, \\ w_0^{\text{quad}} &\propto (a\gamma + 1)\, x. \end{aligned} \tag{17.23}$$

Let N_{quad} and N_{sext} be the numbers of quadrupoles and sextupoles in the ring. Glossing over the detailed structure of the integrands (the accelerator lattice), it follows that the magnitudes of the quadrupole and sextupole contributions are

$$V_1^{\text{quad}} \propto (a\gamma + 1)^2\, N_{\text{quad}}\, xy, \qquad V_1^{\text{sext}} \propto (a\gamma + 1)\, N_{\text{sext}} xy. \tag{17.24}$$

Hence, even though the quadrupoles contribute at only the second order of perturbation theory, their contribution is of $\mathrm{O}((a\gamma{+}1)^2)$, whereas the sextupole contribution is only to the first power $\mathrm{O}((a\gamma + 1))$. For $a\gamma \gg 1$, e.g. $a\gamma > 100$ at both RHIC and LEP, the quadrupoles dominate completely. Even in lower energy rings, e.g. $a\gamma \simeq$ 1–5, in machines such as VEPP-2M, SHR or the IUCF Cooler, the number of sextupoles is relatively small, hence, barring some feature of the accelerator lattice, the contribution of sextupoles to the resonance driving terms is dominated by the quadrupoles. The situation is even more extreme for octupoles, where the ratio is

$$V_1^{\text{quad}} \propto (a\gamma + 1)^3\, N_{\text{quad}}, \qquad V_1^{\text{oct}} \propto (a\gamma + 1)\, N_{\text{oct}}. \tag{17.25}$$

Indeed, many accelerators are not even equipped with octupoles, so $N_{\text{oct}} = 0$. Similar arguments apply to higher multipoles such as decapoles. Hence, the driving terms of the spin resonances are typically dominated by the quadrupoles (plus a smaller contribution from the dipoles) in all the accelerators of interest in this paper. Solenoids and Snakes may also contribute.

The sextupoles can, however, exert an influence on the spin resonances indirectly, via the chromaticity; this is really the major mechanism whereby sextupoles influence the spin motion. In other words, the sextupoles affect the spin dynamics, not so much via the amplitudes of the driving terms (the orbital actions), but rather via the tunes (the orbital angle variables). We shall see some examples of the effects of the chromaticity on the spin motion later in this paper.

17.6. Concluding remarks

SMILE was the first formalism to treat all the orbital oscillations systematically, to all orders. It demonstrated that the calculation of the higher-order terms was a problem of *polynomial*, not exponential, complexity. Note that because $\boldsymbol{n}$ is a *unit* vector, it has only two independent degrees of freedom, but SMILE treats all three components of $\boldsymbol{n}$ on an equal footing. This leads to a linear matrix equation for V_1, V_0 and V_{-1} (note that $\boldsymbol{w}$ is assumed to be already known as a function of θ). However, the resulting solution is *not* guaranteed to be unitary: if the θ-ordered exponential is truncated at any finite order of perturbation theory, the resulting approximate solution is, in general, *not* a unit vector. Many earlier formalisms to solve for $\boldsymbol{n}$ made use of unitarity to parametrize $\boldsymbol{n}$, using a complex variable ζ as in (15.12). This leads to a nonlinear

equation of motion (15.13) which is difficult to solve to arbitrary orders. Other formalisms, such as SLIM (Chao 1981), treated only first-order perturbation theory.

Yokoya (1987) published a formalism using Lie algebra, which treated all the orbital modes to all orders (via perturbation theory in powers of $|\boldsymbol{w}|$), preserved unitarity, and included nonlinear orbital dynamics in principle. The Lie algebra formalism was also derived by Eidelman and Yakimenko (1994, 1995), and coded into a programme SpinLIE (Eidelman and Yakimenko 1993). Yokoya later developed the nonperturbative algorithms (and coded into programs) SODOM (Yokoya 1992) and SODOM2 (Yokoya 1999), which will be reviewed in section 23.

18. Convergence of perturbation theory

A general analysis of the convergence of perturbation theory is difficult, if not impossible. We treat only the single resonance model. Consider the solution for $(\boldsymbol{n}\cdot\boldsymbol{n}_0)^2$, i.e. n_3^2, in the SRM. The solution is

$$n_3^2 = \frac{(\nu_0 - Q)^2}{(\nu_0 - Q)^2 + \epsilon^2}. \tag{18.1}$$

The notation has been defined previously. The perturbative expansion in powers of ϵ is

$$V_0^2 = 1 - \frac{\epsilon^2}{(\nu_0 - Q)^2} + \frac{\epsilon^4}{(\nu_0 - Q)^4} - \frac{\epsilon^6}{(\nu_0 - Q)^6} + \cdots. \tag{18.2}$$

This is what SMILE would yield. The series converges if $|\epsilon| < |\nu_0 - Q|$, i.e. the 'distance' to the resonance.

The convergence of a Taylor series expansion in powers of the orbital amplitudes was investigated further by other authors, e.g. see Hoffstaetter *et al* (1999) or Vogt (2000). When there are multiple resonance driving terms, the convergence is dominated by the nearest strong resonance. Suppose this resonance is at a tune ν_*, and its resonance strength is ϵ_*, then a Taylor series expansion in powers of the orbital amplitudes around the closed orbit is 'useful' if $|\epsilon_*/(\nu_{\text{c.o.}} - \nu_*)| < 1$. By 'useful', we mean there may be weaker higher-order resonances in the vicinity, so that the resonance denominators in the perturbation series will, eventually, encounter a 'small denominator' division by a small quantity, but the corresponding numerator may be so small as to render the divergence harmless.

Let us average the solution for n_3^2 for the SRM over the phase-space. We employ a Gaussian distribution in the orbital phase-space. Let us write $\langle\epsilon^2\rangle = \sigma^2$. For a Gaussian beam,

$$\langle\epsilon^{2n}\rangle = n!\,\sigma^{2n}. \tag{18.3}$$

Hence,

$$\langle n_3^2\rangle_{\text{pert}} = 1 - \frac{\sigma^2}{(\nu_0 - Q)^2} + 2!\frac{\sigma^4}{(\nu_0 - Q)^4} - 3!\frac{\sigma^6}{(\nu_0 - Q)^6} + \cdots. \tag{18.4}$$

The average of the exact solution is

$$\langle n_3^2\rangle_{\text{exact}} = \int_0^\infty \frac{(\nu_0 - Q)^2}{(\nu_0 - Q)^2 + \epsilon^2}\, 2\epsilon\, \mathrm{e}^{-\epsilon^2/\sigma^2}\frac{\mathrm{d}\epsilon}{\sigma^2}. \tag{18.5}$$

Defining $t = \epsilon^2/\sigma^2$ and $x = (\nu_0 - Q)^2/\sigma^2$, the above integral is

$$\mathcal{I}(x) = x\int_0^\infty \frac{\mathrm{e}^{-t}}{t + x}\,\mathrm{d}t = x\mathrm{e}^x\int_x^\infty \frac{\mathrm{e}^{-t}}{t}\,\mathrm{d}t. \tag{18.6}$$

This is related to standard mathematical integrals. The *en-integrals* are defined via

$$E_n(x) = \int_1^\infty \frac{\mathrm{e}^{-xt}}{t^n}\,\mathrm{d}t, \tag{18.7}$$

while the *exponential integral* is defined as

$$\mathrm{Ei}(x) = -\int_{-x}^{\infty} \frac{\mathrm{e}^{-t}}{t}\,\mathrm{d}t. \tag{18.8}$$

The overall minus sign and the integration limit of $-x$ are historical. One sees that,

$$E_1(x) = -\mathrm{Ei}(-x) = \int_{x}^{\infty} \frac{\mathrm{e}^{-t}}{t}\,\mathrm{d}t. \tag{18.9}$$

Hence, $\mathcal{I}(x) = x\mathrm{e}^x E_1(x)$. We follow Bleistein and Handelsman (1986) below. The exponential integral is difficult to expand in a power series. It has a logarithmic singularity at $x = 0$, hence it cannot be Taylor expanded around $x = 0$. In our case, we wish to expand in powers of $\sigma^2/(\nu_0 - Q)^2$, i.e. in powers of $1/x$ around $1/x = 0$. The answer is, as in the SMILE solution,

$$\mathcal{I}(x) = \sum_{k=0}^{\infty} (-1)^k \frac{k!}{x^k}. \tag{18.10}$$

The radius of convergence of this series, in powers of $1/x$, is zero: the ratio of the $(k+1)$th term to the kth term is

$$\lim_{k\to\infty} \frac{a_{k+1}}{a_k} = -\lim_{k\to\infty} \frac{k+1}{x} \to \infty, \tag{18.11}$$

which diverges for any fixed $1/x \neq 0$. It is well-known that the above power series expansion for the exponential integral, or, in our case, for $\mathcal{I}(x)$, is an *asymptotic series*. It converges for terms up to $k \leqslant k_*$, where $k_* x \simeq 1$, and then the addition of more terms causes the sum to diverge. Hence, even if the SMILE perturbation series converges, i.e. $|\epsilon/(\nu_0 - Q)| < 1$, a term-by-term average followed by a sum over the terms yields only an asymptotic series.

Let us briefly analyse the problem using Lie algebra. We shall not spell out the full details of Yokoya's (1987) formalism. All that matters here is that, to the first order in ϵ, the solution for $\boldsymbol{n}$ is given by

$$\boldsymbol{n}_{\mathrm{Lie},1} = \boldsymbol{e}_3 \cos\chi_1 + \sin\chi_1 (\boldsymbol{e}_1 \cos\phi + \boldsymbol{e}_2 \sin\phi), \tag{18.12}$$

where

$$\chi_1 = \left| -\mathrm{i} \int_{-\infty}^{\theta} w_+\,\mathrm{d}\theta' \right| = \left| \frac{\epsilon}{\nu_0 - Q}\,\mathrm{e}^{\mathrm{i}(\phi - \nu_0\theta)} \right| = \frac{\epsilon}{\nu_0 - Q}. \tag{18.13}$$

This evidently agrees with the Taylor series solution to the first and second orders in ϵ. Note that the solution, though approximate, is *exactly* unitary:

$$|\boldsymbol{n}_{\mathrm{Lie},1}|^2 = 1, \tag{18.14}$$

even though χ_1 diverges at a resonance. Although χ_1 is only of the first power in ϵ, and the solution for $\boldsymbol{n}$ is technically accurate only to $\mathrm{O}(\epsilon^2)$, the actual expression for $\boldsymbol{n}_{\mathrm{Lie},1}$ contains all powers of ϵ. Once again, let us examine the expression for $(\boldsymbol{n}\cdot\boldsymbol{n}_0)^2$. The answer is

$$(\boldsymbol{n}_{\mathrm{Lie},1}\cdot\boldsymbol{n}_0)^2 = \cos^2\chi_1 = 1 - \chi_1^2 + \frac{\chi_1^4}{3} + \cdots, \tag{18.15}$$

as compared to the exact result,

$$(\boldsymbol{n}\cdot\boldsymbol{n}_0)^2 = 1 - \chi_1^2 + \chi_1^4 + \cdots \tag{18.16}$$

so, although the value of $\cos^2\chi_1$ is guaranteed to lie between 0 and 1 for any value of χ, the solution is approximate and differs from the exact answer at $\mathrm{O}(\epsilon^4)$. The average over the orbital distribution is given by

$$\langle (\boldsymbol{n}_{\mathrm{Lie},1}\cdot\boldsymbol{n}_0)^2 \rangle = \int_0^{\infty} \cos^2\chi_1\, 2\epsilon\, \mathrm{e}^{-\epsilon^2/\sigma^2} \frac{\mathrm{d}\epsilon}{\sigma^2}. \tag{18.17}$$

This is a finite integral, basically a Fresnel-type integral. If one calculates the solution to higher orders, the higher-order solution will have the symbolic form,

$$\boldsymbol{n}_{\rm Lie} = \boldsymbol{e}_3 \cos\chi + \sin\chi\,(\boldsymbol{e}_1\cos\phi + \boldsymbol{e}_2\sin\phi\,), \tag{18.18}$$

where $\chi = \chi_1 + \chi_3 + \chi_5 + \cdots$, and $\chi_k \propto \epsilon^k$, and we know from the exact solution that only the odd powers will appear. The solution for $\boldsymbol{n}_{\rm Lie}$ is always unitary, even if the sum for χ is truncated at any finite order.

Hence, the inclusion of higher-order terms causes the expression for $\boldsymbol{n}_{\rm Lie}$ to change in a way that cannot be expressed as a simple addition to a lower-order solution. For example, the integral in (18.17) must be reworked as each new order in the Lie series is calculated. This is both a strength and a weakness of the Lie algebraic formalism: the perturbative solution is always unitary, but the inclusion of high-order terms requires previously calculated expressions (e.g. statistical averages) to be recalculated.

The above analyses highlight some of the strengths, and also the limitations of various perturbation series. A formalism such as SMILE, which treats all three components of $\boldsymbol{n}$ as independent variables on an equal footing, can be formulated recursively to arbitrary orders. However, the resulting approximate solution is not exactly unitary, the perturbation series may not converge, and a term-by-term statistical average over the orbital phase-space may yield an asymptotic series, even for such a simple case as the single resonance model.

The use of formalisms which preserve the unitarity of $\boldsymbol{n}$ exactly, all suffer from the problem that they cannot be coded recursively; this means that solving to high orders is difficult. The statistical averages over the orbital phase-space are also not simple to calculate, in general.

19. First-order perturbations to the spin precession

19.1. General remarks

We now examine the off-axis spin precessions. Naturally, the subject of the off-axis spin motion covers many topics, so in this section, we shall treat only the first-order perturbations. The principal aim of this section is to introduce some simple notions, which form the basis for many of the underlying approximations when treating more complicated systems. This is one of those sections where it is necessary to carefully distinguish between the spin basis vectors referenced to the design orbit and the imperfect closed orbit. By default, the spin basis vectors in the section will be referenced to the *imperfect closed orbit*. We shall try to write the basic formulae in a general notation which does not require one to break down the equations into special cases prematurely.

19.2. Spin basis vectors

Recall the spin basis $\{\boldsymbol{l}_0, \boldsymbol{m}_0, \boldsymbol{n}_0\}$, which are the solutions for the spin motion on the closed orbit, and also recall $\boldsymbol{k}_0 = \boldsymbol{l}_0 + \mathrm{i}\boldsymbol{m}_0$. In a perfectly aligned planar ring, without Snakes, $\boldsymbol{W}_0 \parallel \boldsymbol{e}_3$, say $\boldsymbol{W}_0 = W_0\boldsymbol{e}_3$, and $\boldsymbol{n}_0 = \boldsymbol{e}_3$ is everywhere vertical. For brevity define

$$\psi_0 = \int_0^\theta W_0(\theta')\,\mathrm{d}\theta'. \tag{19.1}$$

Then, $\psi_0(\theta + 2\pi) - \psi_0(\theta) = 2\pi\,\nu_{\rm c.o.}$. Then one can write,

$$\begin{aligned} \boldsymbol{l}_0 &= \cos\psi_0\,\boldsymbol{e}_1 + \sin\psi_0\,\boldsymbol{e}_2, \\ \boldsymbol{m}_0 &= -\sin\psi_0\,\boldsymbol{e}_1 + \cos\psi_0\,\boldsymbol{e}_2, \\ \boldsymbol{k}_0 &= (\boldsymbol{e}_1 + \mathrm{i}\boldsymbol{e}_2)\,\mathrm{e}^{-\mathrm{i}\psi_0}. \end{aligned} \tag{19.2}$$

The above vectors obviously lie in the horizontal plane. In the simplest case, we can just set $W_0 = \nu_0$, a constant, in which case $\psi_0 = \nu_0\theta$, which is what we did in the idealized models earlier in this paper. For a ring with two diametrically opposite Snakes, we have to apply the above expressions in each arc, with suitable matching conditions across the Snakes.

For a perfectly aligned planar ring with *one* Snake, $\boldsymbol{n}_0$ precesses in the horizontal plane, all around the ring. The only example of a single Snake that we shall treat is a solenoid. Let the Snake be located at $\theta = \pi$, diametrically opposite to the origin. Then,

$$\boldsymbol{n}_0 = -\sin\psi_0\,\boldsymbol{e}_1 + \cos\psi_0\,\boldsymbol{e}_2, \qquad \theta \in (-\pi, \pi), \tag{19.3}$$

with a discontinuity in $\boldsymbol{n}$ across the Snake for a pointlike solenoid spin rotation. The spin tune is $\nu_{\text{c.o.}} = \frac{1}{2}$. The other two spin basis vectors can be chosen to be, for $-\pi < \theta < \pi$,

$$\boldsymbol{l}_0 = \boldsymbol{e}_3, \qquad \boldsymbol{m}_0 = \cos\psi_0\,\boldsymbol{e}_1 + \sin\psi_0\,\boldsymbol{e}_2, \tag{19.4}$$

with $\boldsymbol{l}_0(\theta + 2\pi) = -\boldsymbol{l}_0(\theta)$ and $\boldsymbol{m}_0(\theta + 2\pi) = -\boldsymbol{m}_0(\theta)$ on successive turns. In this model, the vector $\boldsymbol{k}_0$ has nonzero components along all three axes.

19.3. Resonance driving terms: Fourier harmonics

We now derive expressions for the driving strengths of the first-order resonances. It is simplest to work with the parametrization of $\boldsymbol{n}$ using a complex variable ζ (see (15.12)). To first order, the solution for ζ is (see (15.16))

$$\zeta \simeq -\mathrm{i}\int_{-\infty}^{\theta} \boldsymbol{w}\cdot\boldsymbol{k}_0\,\mathrm{d}\theta'. \tag{19.5}$$

The problem, therefore, reduces to identifying the components of $\boldsymbol{w}$ parallel to $\boldsymbol{k}_0$. In a perfectly aligned planar ring with no Snakes, only the horizontal components of $\boldsymbol{w}$ will contribute. In a ring with a single Snake, all three components of $\boldsymbol{w}$ will contribute, even if the ring is perfectly aligned.

To proceed further, we expand $\boldsymbol{w}\cdot\boldsymbol{k}_0$ in Fourier harmonics. This is not strictly necessary, but is by far the clearest exposition of the underlying physics. Because of the generality of our formalism, we can treat both planar rings, and rings with a single Snake on the same footing. Also, because of the generality of our formalism, we can treat closed-orbit imperfections using the same formalism. For now, we say that $\boldsymbol{w}$ is due to some orbital mode $\boldsymbol{w}_j$, where $j = \pm1, \pm2, \pm3$ and $Q_{-j} = -Q_j$. The 'mode' can be extended to include closed-orbit imperfections, which we can absorb into our notation by writing $j = 0$, in which case the 'tune' Q_j is just unity. If $\boldsymbol{w}$ is due to closed-orbit imperfections, then the vectors $\boldsymbol{n}_0$ and $\boldsymbol{k}_0$ are of course referenced to the ideal design orbit. We then write, with a fairly self-explanatory notation,

$$\boldsymbol{w}_j\cdot\boldsymbol{k}_0 = \sum_k w_{jk}\,\mathrm{e}^{\mathrm{i}(\phi_j + k\theta - \nu_{\text{c.o.}}\theta)}. \tag{19.6}$$

The full expression is just a sum over j:

$$\boldsymbol{w}\cdot\boldsymbol{k}_0 = \sum_j\sum_k w_{jk}\,\mathrm{e}^{\mathrm{i}(\phi_j + k\theta - \nu_{\text{c.o.}}\theta)}, \tag{19.7}$$

where the sum over j could be over all six orbital oscillation modes and the closed-orbit imperfections. To avoid unnecessary clutter, we shall just treat one value of j at a time, below.

Strictly speaking, the concept of a Fourier series applies to a function $f(\theta)$ which is *periodic* in θ, namely, $f(\theta + 2\pi) = f(\theta)$. However the integrand $\boldsymbol{w}_j\cdot\boldsymbol{k}_0$ is *not* periodic in θ. In general, one has

$$\boldsymbol{w}_j\cdot\boldsymbol{k}_0(\theta + 2\pi) = \mathrm{e}^{\mathrm{i}2\pi(Q_j - \nu_{\text{c.o.}})}\,\boldsymbol{w}_j\cdot\boldsymbol{k}_0(\theta). \tag{19.8}$$

Consequently, we define a periodic function $f(\theta)$ via

$$f(\theta) = \mathrm{e}^{-\mathrm{i}(\phi_j - \nu_{\mathrm{c.o.}}\theta)}\, \boldsymbol{w}_j \cdot \boldsymbol{k}_0. \tag{19.9}$$

This periodic function is expanded in Fourier harmonics. The exponential $\mathrm{e}^{-\mathrm{i}(\phi_j - \nu_{\mathrm{c.o.}}\theta)}$ is then brought over to the other side; this is how we obtain the Fourier sum in (19.6).

The solution for ζ is, assuming the validity of interchanging sums and integrals, etc,

$$\begin{aligned}
\zeta_j &= -\mathrm{i}\int_{-\infty}^{\theta} \boldsymbol{w}\cdot\boldsymbol{k}_0\,\mathrm{d}\theta' \\
&= -\mathrm{i}\sum_k w_{jk}\int_{-\infty}^{\theta} \mathrm{e}^{\mathrm{i}(\phi'_j + k\theta' - \nu_{\mathrm{c.o.}}\theta')}\,\mathrm{d}\theta' \\
&= \sum_k \frac{w_{jk}}{\nu_{\mathrm{c.o.}} - Q_j - k}\,\mathrm{e}^{\mathrm{i}(\phi_j + k\theta - \nu_{\mathrm{c.o.}}\theta)}.
\end{aligned} \tag{19.10}$$

We remark in passing on a subtle point when evaluating integrals such as the above. The argument is presented by Yokoya (1983a). The exponent ϕ'_j is actually a dynamical variable (not explicitly a function of θ'), whereas the integral is over θ'. The integral is properly evaluated using the following trick: by the definition of action-angle variables, $\phi - Q\theta$ is independent of θ, hence

$$\phi' = \phi - Q\theta + Q\theta'. \tag{19.11}$$

We can pull $\phi - Q\theta$ out of the integral, to obtain an expression of the form

$$I = \int_{-\infty}^{\theta} \mathrm{e}^{\mathrm{i}\phi'} g(\theta')\,\mathrm{d}\theta' = \mathrm{e}^{\mathrm{i}(\phi - Q\theta)}\int_{-\infty}^{\theta} \mathrm{e}^{\mathrm{i}Q\theta'} g(\theta')\,\mathrm{d}\theta', \tag{19.12}$$

where g is some function of θ'. The integrand is now purely a function of θ'. The above technique will be used without comment throughout this paper, when evaluating integrals over dynamical variables.

19.4. Planar rings

19.4.1. General remarks. By a planar ring we mean one with no Siberian Snakes. The spin basis vectors, $\boldsymbol{n}_0$ and $\boldsymbol{k}_0$, are here referenced to the ideal design orbit, i.e. $\boldsymbol{n}_0 = \boldsymbol{e}_3$, etc (see (19.2)). Then $\boldsymbol{w}$ contains two terms: one from the closed orbit imperfections, and another from the orbital oscillations. Symbolically, with obvious notation,

$$\boldsymbol{w} = \boldsymbol{w}_{\mathrm{c.o.}} + \boldsymbol{w}_{\mathrm{osc}}. \tag{19.13}$$

We shall treat the closed-orbit imperfections first, then the orbital oscillations.

19.4.2. Closed-orbit imperfections. Evidently, by a 'planar' ring we really mean a ring whose design is planar. Consider the terms in $\boldsymbol{w}$ which pertain to the perturbations due to motion on the imperfect closed orbit. As already noted, $\boldsymbol{k}_0$ lies in the horizontal plane, and only the horizontal components of $\boldsymbol{w}$ will, therefore, contribute. The most important contributions to $\boldsymbol{w}$ come from horizontal dipoles and quadrupoles, in fact, mainly the quadrupoles in high-energy accelerators, recall the statements in section 7. There could also be a contribution to $\boldsymbol{w}$ from solenoids, which we shall discuss below. In dipoles and quadrupoles, $\boldsymbol{w}$ is linear in the orbital motion. For example, in a quadrupole (see (7.42))

$$\boldsymbol{w}_{\mathrm{quad}} = R(a\gamma + 1)\frac{B'}{B\rho_0}\,(y\boldsymbol{e}_1 + x\boldsymbol{e}_3). \tag{19.14}$$

For a horizontal dipole, from (7.33) and (7.34), dropping the subscript for the betatron motion,

$$\boldsymbol{w}_{\text{hbend}} = R\left[(a\gamma_0 + 1)\frac{x}{\rho_x^2}\,\boldsymbol{e}_3 - a(\gamma_0 - 1)\frac{y'}{\rho_x}\boldsymbol{e}_2\right]. \tag{19.15}$$

Hence, it is the *vertical* component of the imperfect closed orbit which contributes to the first-order perturbation to the spin precession. The vertical component includes both y and y' terms from the quads and dipoles, respectively. The contribution from the quadrupoles is usually much larger, especially in large rings, where the bend radius ρ_x is large.

If the ring contains solenoids, then $\boldsymbol{w}\cdot\boldsymbol{k}_0$ could contain both x' and y' terms, i.e. a contribution from the horizontal orbital motion. However, solenoids generate transverse x–y coupling, and so the ring is then not 'planar', by our definition here. For the vast majority of accelerators, the vertical component of the closed-orbit imperfections dominates the first-order perturbation to the spin precession.

19.4.3. Orbital oscillations. It is still the case that the value of $\boldsymbol{w}$ is dominated by the horizontal dipoles and the quadrupoles. The quadrupole contribution is

$$\boldsymbol{w}_{\text{quad}} = R(a\gamma + 1)\frac{B'}{B\rho_0}\,(y_\beta\boldsymbol{e}_1 + x_\beta\boldsymbol{e}_3). \tag{19.16}$$

The horizontal dipole contribution is ((7.33) ff)

$$\begin{aligned}\boldsymbol{w}_{\text{hbend}} = {} & R\,(a\gamma_0 + 1)\frac{x_\beta}{\rho_x^2}\,\boldsymbol{e}_3 - R\,a(\gamma_0 - 1)\frac{y'_\beta}{\rho_x}\boldsymbol{e}_2 \\ & + R\left\{\left[(a\gamma_0 + 1)\frac{D_x}{\rho_x^2} - \left(\frac{a}{\gamma_0} + 1\right)\frac{1}{\rho_x}\right]\boldsymbol{e}_3 - a(\gamma_0 - 1)\frac{D'_y}{\rho_x}\boldsymbol{e}_2\right\}\delta.\end{aligned} \tag{19.17}$$

Since the vertical dispersion vanishes in a perfectly aligned planar ring, $D_y = D'_y = 0$, once again, the only terms which contribute to $\boldsymbol{w}\cdot\boldsymbol{k}_0$ are from the vertical orbital motion, i.e. the vertical betatron oscillations.

The dominant contribution to $\boldsymbol{w}\cdot\boldsymbol{k}_0$ is from the vertical betatron oscillations. The presence of transverse x–y coupling can cause the horizontal betatron oscillations to also contribute, but this is typically a weaker effect. Furthermore, if the closed orbit imperfections (or magnet misalignments) are sufficiently large to tip $\boldsymbol{n}_0$ substantially away from the vertical, then, the horizontal betatron oscillations can also drive spin resonances. A resonance of this type is called a 'hybrid resonance', because it involves a combination of intrinsic and imperfection resonance driving terms. A hybrid resonance has been observed at the AGS, and will be reviewed in section 22.4.

19.5. Planar electron accelerators

We have made some tacit assumptions in the preceding subsections, which are *false* for ultrarelativistic electron accelerators. This is because the synchrotron radiation has a profound effect on the perturbations to the spin. In this subsection, the vectors $\boldsymbol{n}_0$ and $\boldsymbol{k}_0$ are referenced to the imperfect closed orbit. Hence, $\boldsymbol{k}_0$ is no longer exactly horizontal, and $\boldsymbol{n}_0$ is no longer exactly vertical, although close. The contribution to $\boldsymbol{w}$ is still, principally, from the horizontal

dipoles and the quadrupoles. It is still the case that,

$$\boldsymbol{w}_{\text{quad}} = R(a\gamma + 1)\frac{B'}{B\rho_0}\,(y_\beta \boldsymbol{e}_1 + x_\beta \boldsymbol{e}_3),$$

$$\boldsymbol{w}_{\text{hbend}} = R\,(a\gamma_0 + 1)\frac{x_\beta}{\rho_x^2}\,\boldsymbol{e}_3 - R\,a(\gamma_0 - 1)\frac{y'_\beta}{\rho_x}\boldsymbol{e}_2 \tag{19.18}$$

$$+R\left\{\left[(a\gamma_0 + 1)\frac{D_x}{\rho_x^2} - \left(\frac{a}{\gamma_0} + 1\right)\frac{1}{\rho_x}\right]\boldsymbol{e}_3 - a(\gamma_0 - 1)\frac{D'_y}{\rho_x}\boldsymbol{e}_2\right\}\delta.$$

The fundamental point to note for electron accelerators is that the vertical betatron emittance vanishes in a perfectly aligned planar ring because the vertical dispersion vanishes: $D_y = D'_y = 0$. Hence, in a perfectly aligned planar ring where $\boldsymbol{k}_0$ is horizontal, *all* of the terms in $\boldsymbol{w} \cdot \boldsymbol{k}_0$ vanish: there are *no* perturbations to the spin motion in a perfectly aligned electron accelerator.

When the ring is not perfectly aligned, i.e. there are closed-orbit imperfections, the analysis for the closed-orbit imperfections is the same as before, i.e. the vertical component of the closed-orbit imperfections dominates. As for the orbital oscillations, the vertical emittance is not exactly zero, although small. Hence, the contributions of the horizontal betatron, vertical betatron and synchrotron oscillations can all be of *comparable* magnitude.

19.6. Nonplanar accelerators

We treat only a ring with a single Siberian Snake (solenoid). We know that in such a ring, the vector $\boldsymbol{k}_0$ has nonzero components along all three axes. Furthermore, because the spin tune is $\frac{1}{2}$, $\boldsymbol{k}_0$ simply reverses sign at every turn. Under these conditions, the closed orbit imperfections contribute negligibly to $\boldsymbol{w} \cdot \boldsymbol{k}_0$. The closed orbit imperfections repeat every turn, hence in the integral $\int_{-\infty}^{\theta} \boldsymbol{w} \cdot \boldsymbol{k}_0\, \mathrm{d}\theta'$, the integral sums to zero every two turns. The integral, therefore, never builds up coherently to achieve a spin resonance. We are, of course, assuming that the magnitudes of the resonance driving terms are small, because if $|w_{jk}|$ is large, then there could be a serious perturbation to the spin even under nonresonant conditions. In fact, we shall encounter precisely this circumstance, when we examine work with partial Siberian Snakes, later in this paper.

We now assume that the ring is perfectly aligned. Evidently, all the horizontal betatron, vertical betatron and synchrotron oscillation modes can contribute to $\boldsymbol{w} \cdot \boldsymbol{k}_0$. The contribution to $\boldsymbol{w} \cdot \boldsymbol{k}_0$ from the solenoid cannot be neglected. Recall we pointed out earlier that the spin rotation angle in a solenoid is inversely proportional to the momentum (see (7.40)). From (7.39),

$$\boldsymbol{w}_{\text{sol}} = -R(a + 1)\frac{B_{\text{sol}}}{B\rho_0}\,\delta\,\boldsymbol{e}_2, \tag{19.19}$$

where we have retained only the terms in the momentum offset (synchrotron oscillations).

In the case of electron rings, the vertical betatron emittance may or may not be much smaller than the horizontal betatron emittance, depending on the compensation of the x–y coupling induced by the solenoid. In any case, the other orbital oscillation modes can contribute to $\boldsymbol{w} \cdot \boldsymbol{k}_0$.

19.7. Planar ring with two Snakes

The only ring with two Snakes, to date, is RHIC. Once again, the spin tune is $\frac{1}{2}$ if the Snakes are at full strength, so the closed orbit imperfections contribute negligibly. Their main effect is to cause the horizontal betatron oscillations to couple into the vertical plane, and vice versa, etc. In a perfectly aligned storage ring with two orthogonal Snakes, the vertical betatron oscillations

will generate the principal contribution to $\boldsymbol{w}\cdot\boldsymbol{k}_0$. In practice, RHIC has observed depolarizing spin resonances from *both* the vertical betatron and the horizontal betatron oscillations (Ptitsyn *et al* 2003, 2004, Ranjbar *et al* 2003). Closed orbit imperfections do influence the spin resonance structure at RHIC.

19.8. Resonance structure of $\boldsymbol{w}\cdot\boldsymbol{n}_0$

Although the function $\boldsymbol{w}\cdot\boldsymbol{n}_0$ does not contribute to the first-order solution for $\boldsymbol{n}$, it does contribute importantly at higher orders. Hence, it makes sense to discuss the resonance structure of $\boldsymbol{w}\cdot\boldsymbol{n}_0$, alongside with that of $\boldsymbol{w}\cdot\boldsymbol{k}_0$. It is also relevant to consider the integral (see (15.18))

$$\chi = -\int_{-\infty}^{\theta} \boldsymbol{w}\cdot\boldsymbol{n}_0\,\mathrm{d}\theta'. \tag{19.20}$$

First, note that $\boldsymbol{n}_0$ is periodic in θ, hence the Fourier sum is of the form

$$\boldsymbol{w}_j\cdot\boldsymbol{n}_0 = \sum_k w'_{jk}\,\mathrm{e}^{\mathrm{i}(\phi_j+k\theta)}. \tag{19.21}$$

Obviously, we begin with a planar ring. We also begin with a perfectly aligned planar ring, so $\boldsymbol{n}_0$ is vertical. The principal sources for $\boldsymbol{w}$ are, of course, the dipoles and the quadrupoles. We now find that it is the *horizontal* components of the closed-orbit imperfections, and the horizontal betatron oscillations and the synchrotron oscillations, which contribute to $\boldsymbol{w}\cdot\boldsymbol{n}_0$. The vertical betatron oscillations couple to $\boldsymbol{w}\cdot\boldsymbol{n}_0$ only when the ring has imperfections, or when there is transverse x–y betatron coupling, so that the resonance driving terms from the vertical betatron oscillations couple into the vertical direction. This is the exact opposite pattern that we obtained for $\boldsymbol{w}\cdot\boldsymbol{k}_0$. We note for future reference that the most important contribution to $\boldsymbol{w}\cdot\boldsymbol{n}_0$ is usually that from the synchrotron oscillations.

Next, we treat nonplanar rings, i.e. rings with a single (solenoid) Siberian Snake. Here, $\boldsymbol{n}_0$ precesses in the horizontal plane in the arc, and, in general, $\boldsymbol{n}_0$ has a nonzero longitudinal component in the solenoid (Snake). Because the Snake is a solenoid, there will necessarily be some transverse x–y betatron coupling, but we assume this is fully compensated by skew quadrupoles, etc, outside the 'Snake system'. However, there will be nonzero betatron coupling inside the Snake system. Since $\boldsymbol{n}_0$ precesses in the horizontal plane in the arc, the horizontal betatron oscillations do not couple to $\boldsymbol{n}_0$ there. However, the horizontal betatron oscillations do couple to $\boldsymbol{n}_0$ in the Snake system. The vertical betatron oscillations couple to $\boldsymbol{n}_0$ in the arc. The synchrotron oscillations do not couple to $\boldsymbol{n}_0$ in the arc, unless the vertical dispersion is nonzero in the arc. We have noted that $\boldsymbol{w}$ is longitudinal in the solenoid, for an off-momentum particle (see (7.39) and also above). Since $\boldsymbol{n}_0$ has a nonzero longitudinal component in the solenoid, the synchrotron oscillations couple to $\boldsymbol{n}_0$ in the solenoid.

The AmPS and SHR both had full-strength solenoid Siberian Snakes, and the x–y coupling was fully compensated outside the Snake system (by a set of quadrupoles and skew quadrupoles). The AmPS and SHR Snake designs and compensation schemes were reviewed in MSY1. The AGS was equipped with a 5% solenoid partial Snake, but the x–y coupling was too large to be compensated by the skew quadrupoles in the AGS. A major motivation to install a transverse-field (helical field) partial Snake in the AGS (Huang *et al* 2003b), was to reduce the x–y coupling. The AGS work with partial Snakes will be reviewed in section 26.

19.9. Scaling with energy

Note that, except for solenoids and some small terms from the dipoles, the first-order perturbation terms in the off-axis spin precession vector $\boldsymbol{w}$ are all proportional to $a\gamma + 1$.

The contributions to $\boldsymbol{w}$ are dominated by the quadrupoles. Other things being equal, at high energies where $a\gamma \gg 1$, the magnitudes of the perturbations, therefore, increase proportionately with the beam energy. Note in practice, that the 'other things' are not equal. In e^+e^- rings, the beam emittances, for example, also increase with energy, which only makes matters worse. Nevertheless, it is true to say the strengths of the depolarizing resonances are stronger in higher energy rings, which is a serious problem for the attainment of a high degree of polarization at high energies.

The energy scaling laws will be derived in more detail later in this paper, when treating radiative and nonradiative systems separately. Furthermore, the above scaling is based on the *first-order* terms only. Evidently, if the first-order terms are not small, then perturbation theory will not be valid, and the higher-order terms will play a significant role. This is correct. We shall develop the formalism to treat the higher-order terms later in this paper.

20. Synchrotron sideband spin resonances

20.1. General remarks

By far the most important of the higher-order spin resonances are due to the synchrotron oscillations. We have noted that early work on resonant depolarization by Serednyakov *et al* (1976) observed synchrotron sideband resonances. Shatunov (1969) had earlier observed depolarization at VEPP-2, which was explained as being from synchrotron sidebands, but the work was regrettably unpublished. See Khoze (1971) for a graph of polarization calculations at VEPP-2 (figure 56), later in this paper. The principal formulae for synchrotron sideband resonances were presented by Derbenev *et al* (1979c). This is not to say that the results were not known earlier, but the above paper was an easily accessible English-language paper. A detailed derivation based on Hamiltonian dynamics was given by Yokoya (1983a). The material below follows Yokoya's paper closely.

20.2. Summary of basic formulae

Recall from section 19, that the off-axis spin precession vector was expanded in Fourier harmonics via (see (19.6))

$$\boldsymbol{w}_j \cdot \boldsymbol{k}_0 = \sum_k w_{jk}\, \mathrm{e}^{\mathrm{i}(\phi_j + k\theta - \nu_{\mathrm{c.o.}}\theta)}. \tag{20.1}$$

Parametrizing $\boldsymbol{n}$ by a complex variable ζ via (see (15.12)),

$$\boldsymbol{n} = \sqrt{1 - |\zeta|^2}\, \boldsymbol{n}_0 + \Re(\zeta \boldsymbol{k}_0^*), \tag{20.2}$$

the solution for ζ (for the mode j) is (see (19.10))

$$\zeta_j = -\mathrm{i} \sum_k w_{jk} \int_{-\infty}^{\theta} \mathrm{e}^{\mathrm{i}(\phi_j' + k\theta' - \nu_{\mathrm{c.o.}}\theta')}\, \mathrm{d}\theta'. \tag{20.3}$$

The value of the integral is

$$\zeta_j = \sum_k \frac{w_{jk}}{\nu_{\mathrm{c.o.}} - Q_j - k}\, \mathrm{e}^{\mathrm{i}(\phi_j + k\theta - \nu_{\mathrm{c.o.}}\theta)}. \tag{20.4}$$

We shall now extend the solution to higher orders, by neglecting $|\zeta|$ in the square root in (15.13). This yields a linear differential equation (see (15.15)):

$$\frac{\mathrm{d}\zeta}{\mathrm{d}\theta} \simeq -\mathrm{i}\boldsymbol{w} \cdot \boldsymbol{k}_0 + \mathrm{i}\boldsymbol{w} \cdot \boldsymbol{n}_0\, \zeta. \tag{20.5}$$

The formal solution is (see (15.17)):

$$\zeta \simeq -\mathrm{i}\mathrm{e}^{-\mathrm{i}\chi(\theta)} \int_{-\infty}^{\theta} \mathrm{e}^{\mathrm{i}\chi(\theta')}\, \boldsymbol{\omega} \cdot \boldsymbol{k}_0 \, \mathrm{d}\theta', \tag{20.6}$$

where (see (15.18))

$$\chi(\theta) = -\int_{-\infty}^{\theta} \boldsymbol{w} \cdot \boldsymbol{n}_0 \, \mathrm{d}\theta'. \tag{20.7}$$

We have already expanded $\boldsymbol{w} \cdot \boldsymbol{k}_0$ in Fourier harmonics earlier and obtained the first-order solution. Now we employ the Fourier harmonics of $\boldsymbol{w} \cdot \boldsymbol{n}_0$ to analyse the higher orders. We can write, for an arbitrary mode j,

$$\chi_j = -\int_{-\infty}^{\theta} \boldsymbol{w}_j \cdot \boldsymbol{n}_0 \, \mathrm{d}\theta' = -\frac{1}{\mathrm{e}^{\mathrm{i}2\pi Q_j} - 1} \int_{\theta}^{\theta+2\pi} \boldsymbol{w}_j \cdot \boldsymbol{n}_0 \, \mathrm{d}\theta'. \tag{20.8}$$

In general, the betatron tunes greatly exceed unity, $Q_{x,y} \gg 1$, i.e. the betatron oscillations complete many periods in one circumference. In that circumstance, the one-turn integral in (20.8) averages closely to zero. On the other hand, the synchrotron tune is much *less* than unity, $Q_s \ll 1$ in most rings. Hence, for synchrotron oscillations, the one-turn integral in (20.8) does not average to zero.

Note that the first-order term arising from $\boldsymbol{w} \cdot \boldsymbol{k}_0$, could itself be from a synchrotron oscillation. To avoid complications, we shall first consider the case where the first-order term in $\boldsymbol{w} \cdot \boldsymbol{k}_0$ is from a betatron oscillation. We shall treat the case of the synchrotron oscillation modifications to a parent first-order synchrotron resonance, afterwards.

Before proceeding further, note that a weak point of the above solution for ζ is that it diverges at a resonance, whereas, we know that one must have $|\zeta| \leqslant 1$. An alternative method of treating the synchrotron sideband resonances is to employ the single resonance model to solve for the parent resonance, and then to perform additional rotations of the reference frames to incorporate the effects of the synchrotron oscillations (effectively a different formulation of perturbation theory). This formulation does, of course, presuppose isolated parent resonances from the outset, but it also has the merit that the solutions for the spin vector are always finite. This point of view is explored by Lee and Berglund (1996) and Lee (1997).

20.3. Planar ring: tune modulation

There is a very simple way to derive the contribution of the synchrotron oscillations in a planar ring, which is sufficiently accurate for most practical purposes. In (20.3), note that the spin tune is given by $\nu_{\mathrm{c.o.}} = \nu_0 = a\gamma_0$. We now introduce an energy offset into γ, i.e. we write

$$\nu = \nu_0 \left(1 + \frac{\Delta E}{E}\right) = \nu_0 \left(1 + \beta_0^2 \frac{\Delta p}{p}\right). \tag{20.9}$$

We next say that the value of $\Delta p/p$ oscillates: this is a synchrotron oscillation. We write

$$\frac{\Delta p}{p} = \sqrt{2I_z} \cos\phi_z. \tag{20.10}$$

Then,

$$\nu = \nu_0 + \nu_0 \beta_0^2 \sqrt{2I_z} \cos\phi_z. \tag{20.11}$$

Applying the appropriate conditions for a solution for $\boldsymbol{n}$, the phase in the exponent is

$$\nu_{\mathrm{c.o.}}\theta \to \nu_0\theta + u\sqrt{2I_z}\, \sin\phi_z, \tag{20.12}$$

where

$$u = \frac{a\gamma_0\beta_0^2}{Q_s}. \tag{20.13}$$

Then, treating only one Fourier harmonic w_{jk},

$$\zeta_{jk} = -\mathrm{i}w_{jk}\int_{-\infty}^{\theta} \mathrm{e}^{\mathrm{i}(\phi_j'+k\theta'-\nu_0\theta'-u\sqrt{2I_z}\sin\phi_z')}\,\mathrm{d}\theta'. \tag{20.14}$$

As stated above, we first consider the case where mode j is a betatron oscillation, not a synchrotron oscillation. To evaluate the integral, we employ the following Bessel function identity

$$\mathrm{e}^{\mathrm{i}r\sin\phi} = \sum_{m=-\infty}^{\infty} J_m(r)\,\mathrm{e}^{\mathrm{i}m\phi}, \tag{20.15}$$

where J_m is a Bessel function. Hence,

$$\zeta_{jk} = -\mathrm{i}w_{jk}\sum_m J_m(u\sqrt{2I_z})\int_{-\infty}^{\theta}\mathrm{e}^{\mathrm{i}(\phi_j'+k\theta'-\nu_0\theta')}\,\mathrm{e}^{-\mathrm{i}m\phi_z'}\,\mathrm{d}\theta'. \tag{20.16}$$

The same trick employed to treat ϕ_j' is played with ϕ_z', to obtain the solution

$$\zeta_{jk} = w_{jk}\sum_m J_m(u\sqrt{2I_z})\frac{\mathrm{e}^{\mathrm{i}(\phi_j-m\phi_z+k\theta-\nu_0\theta)}}{\nu_0-k-Q_j+mQ_s}. \tag{20.17}$$

Each parent first-order resonance is surrounded by a set of satellite resonances, equally spaced at the synchrotron tune. These satellite resonances are called *synchrotron sideband resonances*. The strength of a synchrotron sideband is equal to that of the parent, multiplied by a Bessel function. The interpretation of the resonances as satellites, or sidebands, of a parent resonance is reasonable, because the synchrotron tune is small (recall $Q_s \ll 1$), so the sidebands are clustered around a central resonance, which is usually the strongest.

20.4. Formal Hamiltonian dynamics

We follow Yokoya (1983a). We assume the ring contains no Snakes or spin rotators. Using (20.8) and (20.10), and writing $\boldsymbol{w}_\delta = \boldsymbol{w}_s\,(\Delta p/p)$ for the synchrotron oscillation term, we obtain (dropping any subscript on χ)

$$\chi = -u_\delta\sqrt{2I_z}\,\sin(\phi_z+v_\delta), \tag{20.18}$$

where

$$u_\delta \mathrm{e}^{\mathrm{i}v_\delta\theta} = \frac{\mathrm{i}\mathrm{e}^{-\mathrm{i}Q_s\theta}}{\mathrm{e}^{\mathrm{i}2\pi Q_s}-1}\int_{\theta}^{\theta+2\pi}\boldsymbol{w}_s\cdot\boldsymbol{n}_0\,\mathrm{e}^{\mathrm{i}Q_s\theta'}\,\mathrm{d}\theta'. \tag{20.19}$$

In the limit $Q_s \to 0$, v_δ vanishes and, approximately

$$u_\delta = \frac{1}{2\pi Q_s}\int_{\theta}^{\theta+2\pi}\boldsymbol{w}_s\cdot\boldsymbol{n}_0\,\mathrm{d}\theta'. \tag{20.20}$$

From (7.35), the value of $\boldsymbol{w}_\delta\cdot\boldsymbol{n}_0$ in a perfectly aligned planar ring is

$$\boldsymbol{w}_s\cdot\boldsymbol{n}_0 = R\Big[(a\gamma_0+1)G_xD_x - \left(\frac{a}{\gamma_0}+1\right)\frac{1}{\rho_x}\Big], \tag{20.21}$$

where recall $G_x(s)$ is the focusing function (see (8.2)) in the quadrupoles and horizontal dipoles,

$$G_x = \frac{1}{\rho_x^2} + \frac{1}{B\rho_0}\frac{\partial B_y}{\partial x}. \tag{20.22}$$

Using the differential equation for the horizontal dispersion (see (8.32)),

$$D_x'' + G_x(s) D_x = \frac{1}{\rho_x}. \tag{20.23}$$

We can equivalently write

$$\boldsymbol{w}_s \cdot \boldsymbol{n}_0 = R\Big[-(a\gamma_0 + 1)\, D_x'' + \Big(a\gamma_0 - \frac{a}{\gamma_0}\Big)\frac{1}{\rho_x}\Big] = R\Big[-(a\gamma_0 + 1) D_x'' + \frac{a\gamma_0\beta_0^2}{\rho_x}\Big]. \tag{20.24}$$

Substituting into (20.20), the integral of D_x'' over a full circumference vanishes, while $R \oint \rho_x^{-1}\, \mathrm{d}\theta' = 2\pi$ by definition, so

$$u_\delta = \frac{1}{2\pi\, Q_s} \int_\theta^{\theta+2\pi} \boldsymbol{w}_s \cdot \boldsymbol{n}_0\, \mathrm{d}\theta' = \frac{a\gamma_0\beta_0^2}{Q_s}. \tag{20.25}$$

This coincides with the tune modulation expression derived in (20.13). We shall write u_δ in the argument of the Bessel functions from now on.

Hence, the tune modulation argument yields the correct result for $Q_s \ll 1$ (technically, in the limit $Q_s \to 0$). In practice, the extra level of detail offered by the formal Hamiltonian theory is not important, and the tune modulation derivation is adequate for practical purposes.

The quantity that actually appears in the final polarization formulae is the mean-square $u_\delta^2(\sigma_p/p_0)^2$, generally called the 'tune modulation index' (see below for a more general definition). Its value can become very large in very high-energy $\mathrm{e}^+\mathrm{e}^-$ storage rings, $u_\delta^2(\sigma_p/p_0)^2 \gg 1$, leading to serious depolarization. Yokoya (1983b) suggests some ideas, modifying the ring lattice using vertical bends, to cause the contribution of the D_x'' term to not vanish in u_δ, and thereby reduce the value of the tune modulation index. However, such ideas have never been implemented in practice.

There is, however, a significant difference between the tune modulation solution for ζ_{jk} (see (20.17)), and the solution from Hamiltonian dynamics, which is

$$\zeta_{jk} = \mathrm{e}^{-\mathrm{i}\chi(\theta)}\, w_{jk} \sum_m J_m(u\sqrt{2I_z}) \frac{\mathrm{e}^{\mathrm{i}(\phi_j - m\phi_z + k\theta - \nu_0\theta)}}{\nu_0 - k - Q_j + mQ_s}, \tag{20.26}$$

i.e. there is an extra factor of $\mathrm{e}^{-\mathrm{i}\chi(\theta)}$. If, therefore, we calculate the average of ζ_{jk} over ϕ_z, then the tune modulation solution in (20.17) vanishes except for the parent term ($m = 0$), whereas, the expression in (20.26) does *not* vanish:

$$\begin{aligned}
\langle \zeta_{jk} \rangle &= \Big\langle \mathrm{e}^{-\mathrm{i}\chi(\theta)}\, w_{jk} \sum_m J_m(u\sqrt{2I_z}) \frac{\mathrm{e}^{\mathrm{i}(\phi_j - m\phi_z + k\theta - \nu_0\theta)}}{\nu_0 - k - Q_j + mQ_s} \Big\rangle \\
&= w_{jk} \Big\langle \sum_{mn} J_m(u\sqrt{2I_z}) J_n(u\sqrt{2I_z}) \mathrm{e}^{\mathrm{i}(n-m)\phi_z} \frac{\mathrm{e}^{\mathrm{i}(\phi_j + k\theta - \nu_0\theta)}}{\nu_0 - k - Q_j + mQ_s} \Big\rangle \\
&= w_{jk} \sum_m J_m^2(u\sqrt{2I_z}) \frac{\mathrm{e}^{\mathrm{i}(\phi_j + k\theta - \nu_0\theta)}}{\nu_0 - k - Q_j + mQ_s}.
\end{aligned} \tag{20.27}$$

There are contributions from all the synchrotron sidebands. This is a subtlety not yielded by the tune modulation derivation. Obviously, the tune modulation and Hamiltonian dynamics formalisms yield the same result for $\langle |\zeta_{jk}|^2 \rangle$, since the factor of $\mathrm{e}^{-\mathrm{i}\chi(\theta)}$ cancels out.

20.5. Planar ring: parent synchrotron resonance

Suppose now, that the first-order term is itself due to a synchroton oscillation. We employ the tune modulation derivation. Then, we need to evaluate an integral of the form

$$\zeta_s = -\mathrm{i} \int_{-\infty}^{\theta} \boldsymbol{w}_\delta \cdot \boldsymbol{k}_0\, \mathrm{e}^{-\mathrm{i}u_\delta\sqrt{2I_z}\sin\phi_z'}\, \mathrm{d}\theta', \tag{20.28}$$

where

$$\boldsymbol{w}_\delta \cdot \boldsymbol{k}_0 \propto \frac{\Delta p}{p} = \sqrt{2I_z}\cos\phi_z. \tag{20.29}$$

We can express the integral in the following form, retaining only one Fourier harmonic k in the first order term:

$$\zeta_{sk} = -\mathrm{i}w_{sk}\sqrt{2I_z}\int_{-\infty}^{\theta} \mathrm{e}^{\mathrm{i}(k-\nu_0)\theta'}\ \mathrm{e}^{-\mathrm{i}u_\delta\sqrt{2I_z}\sin\phi_z'}\cos\phi_z'\ \mathrm{d}\theta'. \tag{20.30}$$

To separate the wheat from the chaff, what really matters is the term $\exp\{-\mathrm{i}u_\delta\sqrt{2I_z}\sin\phi_z\}\cos\phi_z$. To process this term, we employ the Bessel function identity

$$\mathrm{e}^{\mathrm{i}r\sin\phi}\cos\phi = \frac{1}{r}\sum_{m=-\infty}^{\infty} m J_m(r)\,\mathrm{e}^{\mathrm{i}m\phi}, \tag{20.31}$$

which can be obtained by differentiating the previous identity in (20.15) with respect to ϕ. Then,

$$\begin{aligned}\zeta_{sk} &= -\mathrm{i}\frac{w_{sk}}{u_\delta}\sum_{m=-\infty}^{\infty} m J_m(u_\delta\sqrt{2I_z})\int_{-\infty}^{\theta}\mathrm{e}^{\mathrm{i}(k\theta'-\nu_0\theta'-m\phi_z')}\,\mathrm{d}\theta' \\ &= \frac{w_{sk}}{u_\delta}\sum_{m=-\infty}^{\infty} m J_m(u_\delta\sqrt{2I_z})\frac{\mathrm{e}^{\mathrm{i}(k\theta-\nu_0\theta-m\phi_z)}}{\nu_0-k+mQ_s}.\end{aligned} \tag{20.32}$$

The difference between a parent synchrotron and a parent betatron spin resonance is that, the first-order synchrotron resonances come in *pairs*, basically $\nu = k \pm Q_s$. Hence, the locations of the synchrotron sidebands of the $\nu = k + Q_s$ spin resonance coincide with those of the $\nu = k - Q_s$ spin resonance. It is therefore not valid to treat the parent resonances in isolation. Thus, the derivation of the synchrotron sideband resonance strengths proceeds somewhat differently. Ultimately, however, the resonance strengths still depend on the Bessel functions J_m, with argument $u_\delta\sqrt{2I_z}$.

20.6. Chromaticity tune modulation

Let us return to the case of a parent first-order betatron resonance and examine the exponent in more detail. Treating a horizontal betatron parent resonance, the exponent is basically $\phi_x - a\gamma_0\theta$. We applied the tune modulation argument to say $a\gamma_0 \to a\gamma_0(1 + \Delta E/E)$. However, note that the betatron tune Q_x is also modulated by the synchrotron oscillations, via the chromaticity. Hence, the exponent should really be modified as follows:

$$Q_x - a\gamma_0 \to Q_{x0} + \xi_x\frac{\Delta p}{p} - a\gamma_0\Big(1+\frac{\Delta E}{E}\Big) = Q_{x0} - a\gamma_0 + (\xi_x - a\gamma_0\beta_0^2)\frac{\Delta p}{p}. \tag{20.33}$$

Using $\Delta p/p = \sqrt{2I_z}\cos\phi_z$, etc the exponent is modified according to

$$\phi_x - a\gamma_0\theta \to \phi_{x0} - a\gamma_0\theta + (\xi_x - a\gamma_0\beta_0^2)\frac{\sqrt{2I_z}}{Q_s}\sin\phi_z. \tag{20.34}$$

A similar derivation applies to the sidebands of the vertical betatron resonances. The argument of the Bessel functions is thus modified to

$$u_\delta \to \frac{a\gamma_0\beta_0^2 - \xi_{x,y}}{Q_s}. \tag{20.35}$$

This is the first explicit example of nonlinear orbital dynamics that we have encountered in the spin dynamics of polarized beams in particle accelerators.

The value of the chromaticity can be adjusted by tuning the sextupoles. If it is set such that

$$\xi_{x,y} - a\gamma_0\beta_0^2 = 0, \tag{20.36}$$

then the synchrotron oscillations will modulate the spin tune and the betatron oscillations *identically* and there will be no net effect on the spin precession. The two tune modulations cancel and the synchrotron sideband resonances *vanish*. However, for the stability of a storage ring, the chromaticity needs to be positive above transition and negative below transition, so that the above idea may not always be workable.

The above cancellation of the orbit and spin tune modulations was first pointed out by Hiramatsu *et al* (1989) who performed an actual experiment to verify the above cancellation at the KEK-PS Booster ring. Mane (1990) independently derived the same cancellation, but his work was purely theoretical. We shall review the excellent work on spin polarized beams at the KEK-PS complex in section 25.

There are also resonances where the exponent is $-\phi_{x,y} - \nu_0\theta$. For these resonances, the tune modulation yields

$$u_\delta \to \frac{a\gamma_0\beta_0^2 + \xi_{x,y}}{Q_s}. \tag{20.37}$$

Since $a\gamma_0\beta_0^2 > 0$ if $a > 0$ (true for electrons and protons) then the chromaticity must be negative to cancel the tune modulation. Hence, there is no single setting of the orbital chromaticities which cancels the tune modulation of all of the parent resonances simultaneously.

20.7. Spin chromaticity

The only nonplanar model we shall treat is a planar ring with a single solenoidal Siberian Snake. The basic formulae for the synchrotron tune modulation in such a ring were derived by Phelps and Anferov (1998). We report on it below. It is simplest to derive the basic result in the following way. Let the fractional Snake strength be λ, where $\lambda = 1$ corresponds to a full-strength Snake. On the design orbit, the one-turn spin map is

$$M = \mathrm{e}^{-\mathrm{i}\pi\nu_0\sigma_3}\,\mathrm{e}^{-\mathrm{i}\lambda\pi\sigma_2/2}, \tag{20.38}$$

and the spin tune is given by equating this matrix to $\mathrm{e}^{-\mathrm{i}\pi\nu_{\mathrm{c.o.}}\boldsymbol{\sigma}\cdot\boldsymbol{n}_0}$. Taking the trace yields

$$\cos(\pi\nu_{\mathrm{c.o.}}) = \cos(\pi\nu_0)\cos\left(\frac{\lambda\pi}{2}\right). \tag{20.39}$$

Recall that for a solenoid, the spin rotation angle, say ψ_{sol}, is inversely proportional to the momentum, so

$$\lambda = -\frac{e(1+a)}{pc}\int B_{\mathrm{sol}}\,\mathrm{d}\ell. \tag{20.40}$$

The solenoid field and length are, of course, independent of the particle momentum. Hence, for a particle with a small relative momentum offset $\Delta p/p$, there are two modifications to the one-turn spin precession angle. One is from the arc, namely, $a\gamma = a\gamma_0(1 + \Delta E/E)$ with $\Delta E/E = \beta_0^2\Delta p/p$, as we have already seen. The other is from the solenoid:

$$\lambda = \frac{\lambda_0}{1 + \Delta p/p} \simeq -\lambda_0\frac{\Delta p}{p}. \tag{20.41}$$

Hence, for small $\delta = \Delta p/p$,

$$\cos(\pi\nu) = \cos(\pi\nu_0(1 + \beta_0^2\delta))\cos\frac{\lambda_0\pi}{2(1+\delta)}. \tag{20.42}$$

Note that this argument applies only if the relative momentum offset $\Delta p/p$ is static, i.e. in the limit of vanishing synchrotron tune $Q_s \to 0$. The spin tune for an off-axis trajectory is, not otherwise, given by the trace of a one-turn map. As we saw above, in connection with the formal Hamiltonian theory, the tune modulation approximation works in the limit $Q_s \to 0$. The tune modulation approximation is adequate for present-day accelerators.

This line of reasoning is also called an *adiabatic approximation* because we can visualize the change in the accelerator as slow, i.e. an adiabatic change to the particle momentum (or energy).

We can express the basic idea in the form of a *spin chromaticity* ξ_{spin}

$$\nu = \nu_{\text{c.o.}} + \xi_{\text{spin}} \frac{\Delta p}{p} \tag{20.43}$$

or

$$\xi_{\text{spin}} = \frac{\partial \nu}{\partial \delta}. \tag{20.44}$$

The spin tune is also defined for off-axis trajectories, so that the above definition is somewhat restricted; it pertains only to a relative momentum offset from the design orbit. We can either differentiate the expression for ν or expand to small quantities in δ. Let the change in the spin tune be $\Delta\nu$. Then to first order in small quantities,

$$\sin(\pi\,\nu_{\text{c.o.}})\,\Delta\nu = -\Big[-\nu_0\beta_0^2\,\sin(\pi\,\nu_0)\cos\left(\frac{\lambda_0\pi}{2}\right) + \frac{\lambda_0}{2}\cos(\pi\,\nu_0)\sin\left(\frac{\lambda_0\pi}{2}\right)\Big]\,\delta. \tag{20.45}$$

Then

$$\frac{\partial \nu}{\partial \delta} = \frac{1}{\sin(\pi\,\nu_{\text{c.o.}})}\Big[\nu_0\beta_0^2\,\sin(\pi\,\nu_0)\cos\left(\frac{\lambda_0\pi}{2}\right) - \frac{\lambda_0}{2}\cos(\pi\,\nu_0)\sin\left(\frac{\lambda_0\pi}{2}\right)\Big]. \tag{20.46}$$

Another way to derive this is

$$\frac{\partial \nu}{\partial \delta} = \Big[\frac{\partial \nu}{\partial \nu_{\text{arc}}}\frac{\partial \nu_{\text{arc}}}{\partial \delta} + \frac{\partial \nu}{\partial \lambda}\frac{\partial \lambda}{\partial \delta}\Big]_{\text{c.o.}}, \tag{20.47}$$

which leads to the same result. Equations (20.46) and (20.47) were derived by Phelps and Anferov (1998). The first contribution to $\partial\nu/\partial\delta$ comes from the arc via the direct dependence of the spin precession on the momentum. The second contribution to $\partial\nu/\partial\delta$ comes from the dependence of the spin precession on the solenoid field. This term would change for a different design of the partial Snake. (For example, the RHIC helical field Snakes are energy independent.) Neglecting any tune modulation contribution from the betatron oscillations, etc, the solution for ζ is still

$$\zeta_{jk} = -\mathrm{i}w_{jk}\int_{-\infty}^{\theta} \mathrm{e}^{\mathrm{i}(\phi_j' + k\theta' - \nu_{\text{c.o.}}\theta' - u_\delta\sqrt{2I_z}\sin\phi_z')}\,\mathrm{d}\theta', \tag{20.48}$$

where now

$$u_\delta = \frac{\xi_{\text{spin}}}{Q_s} = \frac{1}{Q_s}\frac{\partial \nu}{\partial \delta}. \tag{20.49}$$

Each parent resonance is surrounded by a set of synchrotron sidebands given by Bessel functions with arguments $u_\delta\sqrt{2I_z}$ with a more general value for u_δ. The derivation proceeds exactly along the same lines as before:

$$\zeta_{jk} = w_{jk}\sum_m J_m(u_\delta\sqrt{2I_z})\frac{\mathrm{e}^{\mathrm{i}(\phi_j - m\phi_z + k\theta - \nu_{\text{c.o.}}\theta)}}{\nu_{\text{c.o.}} - k - Q_j + mQ_s}. \tag{20.50}$$

The details of the accelerator structure are buried in the value of the Fourier coefficient w_{jk}. The pattern for the synchrotron sidebands is formally exactly the same with just a simple generalization of the definition of u_δ.

For a full-strength Snake, i.e. $\lambda = 1$, the design-orbit spin tune is $\nu_{\text{c.o.}} = \frac{1}{2}$ and so

$$\frac{\partial \nu}{\partial \delta} = -\frac{1}{2}\cos(\pi \nu_0). \tag{20.51}$$

The entire contribution to the spin chromaticity comes from the solenoid. We pointed out earlier, when discussing the structure of $\boldsymbol{w} \cdot \boldsymbol{n}_0$, that for a ring with a full-strength Snake the synchrotron oscillations would not couple to $\boldsymbol{n}_0$ in the arc.

We now derive the spin chromaticity using the Hamiltonian dynamics formalism. The claim is

$$u_\delta = \frac{1}{2\pi Q_s}\int_\theta^{\theta+2\pi} \boldsymbol{w}_s \cdot \boldsymbol{n}_0 \, \mathrm{d}\theta'. \tag{20.52}$$

We treat only a full-strength Snake because it is, otherwise, tedious to work out the expression for $\boldsymbol{n}_0$ all around the ring. We know that $\boldsymbol{w}_s$ is vertical in the arc, hence $\boldsymbol{w}_s \cdot \boldsymbol{n}_0 = 0$ in the arc. In the solenoid we have from above

$$\boldsymbol{w}_s = -\lambda\pi \, \delta_p(\theta - \theta_{\text{sol}}) \, \boldsymbol{e}_2, \tag{20.53}$$

where now $\lambda = 1$. We have previously seen that for a ring with a single full-strength solenoid Snake, $\boldsymbol{n}_0 \cdot \boldsymbol{e}_2 = \cos(\pi \nu_0)$ in the solenoid. Hence,

$$u_\delta = -\frac{1}{2\pi Q_s}\lambda\pi\cos(\pi\nu_0) = -\frac{1}{2Q_s}\cos(\pi\nu_0) = -\frac{1}{Q_s}\frac{\partial\nu}{\partial\delta}, \tag{20.54}$$

which is precisely the desired result. The Hamiltonian theory gives the answer, but the adiabatic tune modulation approximation is easier to apply; it gives us the answer for a partial solenoid Snake of arbitrary strength with relatively little effort.

20.8. Statistical averages

We only average over the synchrotron oscillations below; this brings out the essential physics of what we wish to discuss. It merely complicates matters to average over the betatron oscillations as well; the resulting formulae have too many different emittances. The averages will be over ζ and $|\zeta|^2$ obviously. We need the two formulae

$$\begin{aligned} \langle J_m(u_\delta\sqrt{2I_z})\rangle &= \int_0^\infty \frac{\mathrm{d}I_z}{\langle I_z\rangle}\, \mathrm{e}^{-I_z/\langle I_z\rangle}\, J_m(u_\delta\sqrt{2I_z}) = \mathrm{e}^{-\sigma^2/2} I_m(\sigma^2), \\ \langle J_m^2(u_\delta\sqrt{2I_z})\rangle &= \cdots \qquad\qquad\qquad\qquad = \mathrm{e}^{-\sigma^2} I_m(\sigma^2), \end{aligned} \tag{20.55}$$

where I_m is a modified Bessel function and

$$\sigma = u_\delta\sqrt{\langle I_z\rangle} = \frac{1}{Q_s}\frac{\partial\nu}{\partial\delta}\frac{\sigma_p}{p}. \tag{20.56}$$

It is more common to write this in terms of a derivative with respect to the energy offset $\Delta\gamma/\gamma$ and the relative energy spread,

$$\sigma = \frac{1}{Q_s}\gamma\frac{\partial\nu}{\partial\gamma}\frac{\sigma_E}{E}. \tag{20.57}$$

The derivative $\gamma\,(\partial\nu/\partial\gamma)$ is simply the change $\Delta\nu$ for a small relative energy offset $\Delta\gamma/\gamma$ rather than a relative momentum offset. The quantity

$$x = \sigma^2 \tag{20.58}$$

is called the *tune modulation index*. There is no standard notation; the simplest is to just write x.

Let us average over $|\zeta|^2$ which is typically more relevant for physics. For a betatron parent resonance, the average of $|\zeta|^2$ as given by (20.17), with a generalized definition of u_δ, is

$$\langle|\zeta_{jk}|^2\rangle = \langle|w_{jk}|^2\rangle \sum_m \frac{\mathrm{e}^{-\sigma^2} I_m(\sigma^2)}{(\nu_{\mathrm{c.o.}} - k - Q_j + mQ_s)^2}. \tag{20.59}$$

For a parent synchrotron resonance, the average over ζ also vanishes, though in a different way. The average over the synchrotron oscillation phase kills all the terms in (20.32), except the $m = 0$ term, because $\langle \mathrm{e}^{\mathrm{i}m\phi_z}\rangle = 1$ for $m = 0$ and zero otherwise. However, the $m = 0$ term is $mJ_m = 0$ for $m = 0$. Hence, $\langle\zeta_{sk}\rangle = 0$. From (20.32) the average over $|\zeta|^2$ is

$$\langle|\zeta_{sk}|^2\rangle = \frac{|w_{sk}|^2}{u_\delta^2} \sum_{m=-\infty}^{\infty} \frac{m^2 \mathrm{e}^{-\sigma^2} I_m(\sigma^2)}{(\nu_{\mathrm{c.o.}} - k + mQ_s)^2}. \tag{20.60}$$

20.9. Correlated and uncorrelated resonance crossings

Despite the calculations of the statistical averages above, we are far from done with the statistical mechanics. As should be evident by now, we must investigate the fundamental assumptions under which the above results were derived.

First, there is a tacit assumption in the above derivations that the particles complete many synchrotron oscillation periods (in principle infinite) as they circulate around the ring. Although we did make the approximation $Q_s \to 0$ in some parts of our calculation above, this was a mathematical approximation to simplify certain formulae. It was always assumed that the particles would complete many synchrotron periods when circulating around the ring.

This assumption may not be true. It is possible, at least for proton accelerators, for the rf cavities to be switched off in which case there is no longitudinal focusing and $Q_s = 0$. There should then be no synchrotron sidebands. We begin with the sidebands of a betatron parent term. In the relation

$$\nu = \nu_{\mathrm{c.o.}} + \xi_{\mathrm{spin}} \frac{\Delta p}{p}, \tag{20.61}$$

it is not valid to substitute $\Delta p/p = \sqrt{2I_z}\cos\phi_z$ etc. For simplicity, let us employ the relative energy offset below

$$\nu = \nu_{\mathrm{c.o.}} + \gamma \frac{\partial \nu}{\partial \gamma} \frac{\Delta\gamma}{\gamma} = \nu_{\mathrm{c.o.}} + \Delta\nu \tag{20.62}$$

by a slight overuse of the notation $\Delta\nu$. Then (20.14) should instead be (we generalize to nonplanar rings):

$$\zeta_{jk} = -\mathrm{i}w_{jk} \int_{-\infty}^{\theta} \mathrm{e}^{\mathrm{i}(\phi_j' + k\theta' - (\nu_{\mathrm{c.o.}} + \Delta\nu)\theta')}\, \mathrm{d}\theta' = w_{jk} \frac{\mathrm{e}^{\mathrm{i}(\phi_j + k\theta - (\nu_{\mathrm{c.o.}} + \Delta\nu)\theta)}}{\nu_{\mathrm{c.o.}} + \Delta\nu - k - Q_j}. \tag{20.63}$$

The value of $\Delta\nu$ is a statistical variable because the beam has an energy spread. Hence, instead of a set of synchrotron sideband resonances, there is only one resonance line at the central (parent) location, but the line is broadened. The exact vanishing of the denominator takes place not at one value of $\nu_{\mathrm{c.o.}}$ but over a spread of values. There is, effectively, a spin tunespread.

For a parent synchrotron oscillation, i.e. a pair of first-order resonances centred on $\nu = k \pm Q_s$, the resonance at the integer $\nu = k$ is broadened by the spin tunespread. The spin tunespread is particularly simple to calculate for a planar ring:

$$\nu = \nu_0\Big(1 + \frac{\Delta E}{E}\Big). \tag{20.64}$$

Hence, the rms spin tunespread is proportional to the rms relative energy spread:

$$\sigma_\nu = \nu_0 \frac{\sigma_E}{E}. \tag{20.65}$$

Let us return to the case of a nonzero synchrotron tune. To begin with, treat a planar ring. By virtue of the synchrotron oscillations, the energy (momentum) of the particle—hence, in a planar ring, the spin tune—oscillates up and down as the particle circulates around the ring. The spin tune, therefore, sweeps across the various synchrotron sideband resonance lines rather than remaining fixed at a particular value. The crossings of the value of the spin tune across a particular sideband $m = m_*$ (i.e. $\nu = \nu_{\text{parent}} + m_* Q_s$) may or may not be correlated. Successive passages across a resonance are said to be *correlated* (Derbenev *et al* 1979c) if

$$\frac{(a\gamma_0)^2}{Q_s^2}\left(\frac{\sigma_E}{E}\right)^2 \ll Q_s. \tag{20.66}$$

In more generality, we would write

$$\frac{1}{Q_s^2}\left(\gamma\frac{\partial\nu}{\partial\gamma}\right)^2\left(\frac{\sigma_E}{E}\right)^2 \ll Q_s. \tag{20.67}$$

The lhs is the tune modulation index, so we can also write

$$\sigma^2 \ll Q_s. \tag{20.68}$$

Basically, the lhs is the width of a sideband resonance and the resonance crossings are correlated if this width is much less than the sideband resonance spacing, which is the synchrotron tune Q_s. The mental picture is that if the crossings of a particular resonance line $m = m_*$ are *un*correlated then the depolarization is not tied to that resonance line. In this case, the resonances are broad and overlap significantly—there are no well-discernible individual sideband resonances. When the spin tune crossings (successive passages across a particular resonance line $m = m_*$) are correlated, then a resonance develops only in the narrow vicinity of that line. The mental picture is that the individual sidebands are well-separated distinct resonances.

The criterion for correlated resonance crossings is quite restrictive. Synchrotron sideband resonances are visible in the SPEAR polarization data in figure 6. The value of the tune modulation index was $\sigma^2 \simeq 0.03$ for the SPEAR data but the value of the synchrotron tune was roughly $Q_s \simeq 0.04$. Hence, the criterion for correlated crossings is on the threshold of being satisfied.

20.10. Experimental data

As pointed out above, synchrotron sideband resonances are visible in the SPEAR polarization data, as shown in figure 6. However, the SPEAR data are an example of a radiatively polarized beam, and additional formalism developed so far beyond that is required to calculate those resonances.

Synchrotron sideband resonances along the lines we have described have been observed in proton storage rings, i.e. nonradiatively polarized beams. All the measurements we report below were made at the IUCF Cooler ring. The measurements of synchrotron sideband resonances are some of the most beautiful data taken in the IUCF spin dynamics studies. Measurements of the synchrotron sideband resonances at the IUCF Cooler were made both with and without a (solenoid) Siberian Snake. A superconducting solenoid was used to achieve a full-strength Snake. For partial Snake experiments a weaker warm solenoid was used.

A graph of synchrotron sidebands measured at the IUCF Cooler is displayed in figure 35. The resonances were induced via resonant depolarization by stepping the frequency of an rf solenoid magnet. A 4% partial Snake was used in the study. The plotted quantity was the total

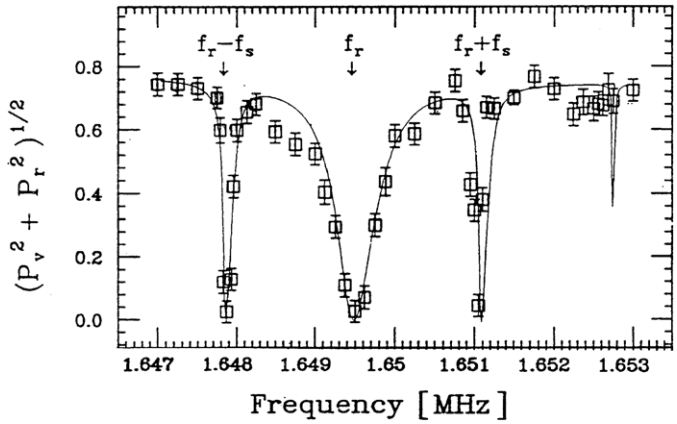

Figure 35. Synchrotron sideband resonances at the IUCF Cooler, with theoretical fit. From Mane (1992a).

transverse polarization $(P_v^2 + P_r^2)^{1/2}$ (vertical and radial polarization components) as a function of the rf solenoid frequency. Two narrow synchrotron sideband resonances are clearly visible, one on either side of the central parent resonance. The data were reported by Anferov *et al* (1992) and fitted theoretically by Mane (1992a). The value of the tune modulation index was $\sigma^2 \simeq 0.1$.

Next we consider the synchrotron sidebands for a vertically polarized beam in the IUCF Cooler (no Snakes). Synchrotron sideband resonances were observed at the IUCF Cooler by Goodwin *et al* (1990). Lee and Berglund (1996) studied the problem of synchrotron sideband resonances theoretically. Their calculation took into account the presence of a systematic error (shift in the value of the spin tune) in the Cooler. The combination of the toroidal magnetic field and the vertical steering magnets in the electron cooling section of the IUCF Cooler netted to an overall spin rotation around the vertical axis, yielding a shift in the value of the spin tune (Pollock 1991). (See MSY1 for a detailed review of this effect.) Since the existence of such a systematic error was not suspected in 1990, the values of the relevant experimental parameters were not recorded in the measurements. Lee and Berglund used the data to retrofit the systematic error to the spin tune and deduced a shift of $\delta\nu \simeq 0.0035$. The value they obtained for the tune modulation index was $\sigma^2 \simeq 0.1$, the same value obtained above by Mane (1992a). This is to be expected, since the beam energy and energy spread were about the same in both experiments, and a 4% partial Snake would not affect the spin chromaticity much.

Many more examples of synchrotron sideband resonances were obtained in the spin dynamics studies at the IUCF Cooler. Chu *et al* (1998) reported the observation of unexpectedly wide synchrotron sideband resonances, wider than would be expected from the theory we have developed above. In addition to the central resonance and the two synchrotron sidebands, the studies also observed narrow resonances very close to the parent resonance. The weak resonances were tentatively identified by the authors as being due to additional weak rf beam structure at $f^* = 1080$ Hz. The 1080 Hz harmonic was later found in the IUCF Cooler rf spectrum. This clearly shows that the theory we have presented above is only a simple linear dynamical theory with a simple model for the synchrotron oscillations. Modern experiments are capable of resolving more detailed structures than present day theory can explain. The large width of the sideband resonances is tentatively explained by the experimenters in the following way. Earlier studies at the IUCF Cooler used single-turn injection, but the measurements by Chu *et al* (1998) were made using multiturn injection with so-called rf

stacking in the longitudinal phase-space. In the latter case, the beam filled a much larger fraction of the rf buckets: at high beam intensities the IUCF Cooler ring was found to have a large synchrotron frequency spread (Nagaitsev 1997). The theory we have presented does not treat nonlinear dynamical synchrotron oscillations with a synchrotron tunespread. Once again, further theoretical work is required on the subject.

Finally, measurements of synchrotron sideband resonances with a (nearly) full-strength Siberian Snake were also made at the IUCF Cooler (Blinov *et al* 1999). The resonances were induced again using an rf solenoid. Note that resonant depolarization and resonant spin-flipping can work not only in planar rings but also in rings equipped with Snakes. With a nearly full strength Siberian Snake (superconducting solenoid), the spin tune was almost, but not exactly, $\frac{1}{2}$. The Snake strength was $\lambda = 1 + \Delta\lambda$ with $\Delta\lambda = (1.996 \pm 0.004)\%$. Hence, $\lambda > 1$ and $\nu_{\rm spin} > \frac{1}{2}$. The two possible locations for the central resonance were ($f_{\rm c}$ is the revolution frequency)

$$f_{\rm r}^{-} = f_{\rm c}(2 - \nu_{\rm spin}), \qquad f_{\rm r}^{+} = f_{\rm c}(1 + \nu_{\rm spin}). \tag{20.69}$$

Measurements of the synchrotron sidebands were made at the higher of the two frequencies, namely, $f_{\rm r}^{+}$.

21. Decoherence and spin tunespread

21.1. General remarks

Most of the theory, so far, has focused on the long-term polarization. It is worthwhile to digress briefly to also consider the spin components *orthogonal* to the direction of the long-term polarization or for practical calculations to $\boldsymbol{n}_0$. In particular, how rapidly do such orthogonal spin components decohere or perhaps are there circumstances where they do not decohere? We treat various models of increasing sophistication below.

21.2. Static energy spread

Consider a planar ring, so $\nu = a\gamma$, and write

$$\nu = \nu_0\Big(1 + \frac{\Delta E}{E}\Big). \tag{21.1}$$

We assume $\Delta E/E$ is static and not a synchrotron oscillation. The spin components in the horizontal plane, therefore, spread out in proportion to $\Delta E/E$,

$$S_{\perp} \sim {\rm e}^{{\rm i}\nu_0\theta}\, {\rm e}^{{\rm i}\nu_0(\Delta E/E)\theta}. \tag{21.2}$$

Let the spin precession angle of the spins be Ψ_N after N turns. The rms spread in the directions of the spins, say σ_{Ψ_N}, is given by

$$\sigma_{\Psi_N} = 2\pi\, N\, \nu_0 \frac{\sigma_E}{E}. \tag{21.3}$$

The decoherence time is given by $\Delta\Psi_N \approx 2\pi$, so

$$N_{\rm decoh} = \frac{1}{\nu_0}\frac{E}{\sigma_E}. \tag{21.4}$$

A typical value for σ_E/E is 10^{-4}–10^{-3}. Let us estimate $\sigma_E/E \simeq 5 \times 10^{-4}$. Let us estimate $\nu_0 \simeq 10$ (the values in modern rings go from 1–100). Then

$$N_{\rm decoh} \approx 200. \tag{21.5}$$

The circulation period for a ring of 300 m circumference is $\tau_c = C/c \simeq 10^{-6}$ s. Then the decoherence time is

$$\tau_{\text{decoh}} = N_{\text{decoh}}\,\tau_c \simeq 200\,\mu\text{s}. \tag{21.6}$$

So the orthogonal spin components do, in fact, decohere rapidly. However, the model treated $\Delta E/E$ as static and not a synchrotron oscillation.

21.3. Synchrotron oscillations

Next, we say that $\Delta E/E$ oscillates and averages to zero (synchrotron oscillation). Hence, taking into account the synchrotron oscillations we write with a fairly obvious notation

$$\frac{\Delta E}{E} = \sqrt{2I_z}\cos\phi_z, \qquad \phi_z = Q_s\theta + \phi_{z0}, \tag{21.7}$$

and the rate of spin phase advance as

$$\nu = \nu_0 + \gamma\frac{\partial\nu}{\partial\gamma}\sqrt{2I_z}\cos\phi_z, \tag{21.8}$$

so the spin phase is

$$\int^{\theta}\nu\,\mathrm{d}\theta' = \nu_0\theta + u_\delta\sqrt{2I_z}\,\sin\phi_z. \tag{21.9}$$

Then

$$S_\perp \sim \mathrm{e}^{\mathrm{i}\nu_0\theta}\,\mathrm{e}^{\mathrm{i}u_\delta\sqrt{2I_z}\,\sin\phi_z} = \mathrm{e}^{\mathrm{i}\nu_0\theta}\sum_{m=-\infty}^{\infty}\mathrm{e}^{\mathrm{i}m\phi_z}\,J_m\bigl(u_\delta\sqrt{2I_z}\bigr), \tag{21.10}$$

using the Bessel function identity (20.15). Averaging uniformly over the initial synchrotron phase ϕ_z, only the $m = 0$ term survives:

$$\langle S_\perp\rangle_{\phi_z} = \mathrm{e}^{\mathrm{i}\nu_0\theta}\Bigl\langle J_0\bigl(u_\delta\sqrt{2I_z}\bigr)\Bigr\rangle. \tag{21.11}$$

Now average over the amplitudes using a Gaussian distribution. The integral over the Bessel function was stated earlier, so

$$\langle S_\perp\rangle = \mathrm{e}^{\mathrm{i}\nu_0\theta}\,\mathrm{e}^{-\sigma^2/2}\,I_0(\sigma^2), \tag{21.12}$$

where recall

$$\sigma^2 = \frac{1}{Q_s^2}\Bigl(\gamma\frac{\partial\nu}{\partial\gamma}\Bigr)^2\frac{\sigma_E^2}{E^2}. \tag{21.13}$$

In this model, the spin spread actually approaches an equilibrium angle given by

$$|\langle S_\perp\rangle| = \mathrm{e}^{-\sigma^2/2}\,I_0(\sigma^2). \tag{21.14}$$

The same conclusion based on work using a Fokker–Planck equation for the evolution of the spin–orbit distribution, was reported by Heinemann (1997) who obtained in terms of the above notation,

$$|\langle S_\perp\rangle|_H = \mathrm{e}^{-\sigma^2/2}. \tag{21.15}$$

The modified Bessel function was not obtained. The use of a Fokker–Planck equation is so complicated that one is usually forced to make simplifying approximations in the beam

distribution, leading to Gaussian expressions. Numerical estimates for a planar HERA-like ring (no spin rotators) indicate that

$$\begin{aligned} &\frac{\sigma_E}{E} \approx 5 \times 10^{-4}, \\ &a\gamma_0 \approx 10^2, \\ &Q_s \approx 0.05, \\ &\sigma^2 \approx 25 \times 10^{-8} \frac{10^4}{25 \times 10^{-4}} \approx 1. \end{aligned} \tag{21.16}$$

Hence, σ^2 is of order unity and so the synchrotron oscillations cannot be neglected.

21.4. Betatron oscillations

Next, we consider the effects of betatron oscillations. We treat a planar ring. The horizontal betatron oscillations cause the spins to see an additional vertical magnetic field

$$\boldsymbol{n}_0 \cdot \boldsymbol{\omega}_\beta \propto (1 + a\gamma_0)\, A_x \cos\phi_x \approx a\gamma_0\, A_x \cos\phi_x. \tag{21.17}$$

We approximate $a\gamma_0 \gg 1$ for simplicity. We are also neglecting many features of the betatron oscillations and treating the beta function as uniform around the circumference and so we neglect the betatron phase. Next $\phi_x = Q_x\theta + \phi_{x0}$. Then the vertical component of the spin precession vector is

$$W_y = \nu_0 + a\gamma_0\, A_x \cos\phi_x. \tag{21.18}$$

The spin phase is now

$$\nu\theta = \nu_0\theta + a\gamma_0 \frac{A_x}{Q_x} \sin\phi_x. \tag{21.19}$$

This is very similar to the synchrotron oscillation model so we simply repeat the calculations. We get

$$S_\perp \sim \mathrm{e}^{\mathrm{i}\nu_0\theta}\, \mathrm{e}^{\mathrm{i}a\gamma_0(A_x/Q_x)\,\sin\phi_x} = \mathrm{e}^{\mathrm{i}\nu_0\theta} \sum_{m=-\infty}^{\infty} \mathrm{e}^{\mathrm{i}m\phi_x}\, J_m\Big(\frac{a\gamma_0 A_x}{Q_x}\Big). \tag{21.20}$$

Average uniformly over the initial phase ϕ_{x0}:

$$\langle S_\perp \rangle = \mathrm{e}^{\mathrm{i}\nu_0\theta}\, J_0\Big(\frac{a\gamma_0 A_x}{Q_x}\Big). \tag{21.21}$$

Average over the amplitudes (Gaussian distribution):

$$|\langle S_\perp \rangle| = \mathrm{e}^{-\sigma_x^2/2} I_0(\sigma_x^2). \tag{21.22}$$

Here

$$\sigma_x^2 = \langle I_x \rangle \frac{(a\gamma_0)^2}{Q_x^2}. \tag{21.23}$$

A simple numerical estimate for a high-energy ring is $\langle I_x \rangle \simeq 10^{-8}$ and $Q_x \simeq 100$, which leads to

$$\sigma_x^2 \simeq 10^{-8} \frac{10^4}{10^4} = 10^{-8} \ll 1. \tag{21.24}$$

Changing the parameter values by a factor of 2 (or perhaps even 10) does not alter the fact that $\sigma_x^2 \ll 1$. Hence, the spin spread (decoherence) caused by the horizontal betatron oscillations

is negligible. Note that we have neglected the quadrupole focusing gradient in the expression for $\boldsymbol{n}_0 \cdot \boldsymbol{\omega}_\beta$ above. It contributes to σ_x^2 but does not change the fact that $\sigma_x^2 \ll 1$. Hence, the betatron oscillations induce negligible decoherence. The particles complete many betatron periods in one pass around the ring and the effect of the betatron oscillations on the spin phase averages very nearly to zero.

21.5. Synchrotron oscillations without stochastic fluctuations

There are some hidden assumptions in the second model above. Recall the synchrotron oscillations

$$\frac{\Delta E}{E} = A_z \cos\phi_z, \qquad \phi_z = Q_s\theta + \phi_{z0}. \tag{21.25}$$

We said the rate of spin phase advance is

$$\nu = \nu_0(1 + A_z \cos\phi_z). \tag{21.26}$$

Let us be more careful to integrate to obtain the spin phase. What really happens is

$$\int_0^\theta \nu \,\mathrm{d}\theta' = \nu_0 \int_0^\theta (1 + A_z \cos\phi_z)\,\mathrm{d}\theta' = \nu_0\theta + \frac{A_z}{Q_s}(\sin\phi_z - \sin\phi_{z0}). \tag{21.27}$$

We neglected the initial phase previously, but we must be more careful. When stochastic fluctuations and damping are present, then the beam settles down to a self-consistent equilibrium distribution which is independent of the initial conditions. Then we can neglect the initial term $\sin\phi_{z0}$. Then we get the previous expression

$$\nu\theta \to \nu_0\theta + \frac{A_z}{Q_s}\sin\phi_z. \tag{21.28}$$

We did this without justification above but now we say so explicitly. One must stress the importance of understanding the underlying asumptions, especially the statistical mechanics, in all these calculations. When there are no stochastic fluctuations, then

$$\begin{aligned} S_\perp &= \mathrm{e}^{\mathrm{i}\nu_0\theta}\,\mathrm{e}^{\mathrm{i}\nu_0\,(A_z/Q_s)\,\sin\phi_z}\,\mathrm{e}^{-\mathrm{i}\nu_0\,(A_z/Q_s)\,\sin\phi_{z0}} \\ &= \mathrm{e}^{\mathrm{i}\nu_0\theta} \sum_{m=-\infty}^{\infty} \mathrm{e}^{\mathrm{i}m\phi_z}\, J_m\Big(\frac{A_z\nu_0}{Q_s}\Big) \sum_{m'=-\infty}^{\infty} \mathrm{e}^{-\mathrm{i}m'\phi_{z0}}\, J_{m'}\Big(\frac{A_z\nu_0}{Q_s}\Big). \end{aligned} \tag{21.29}$$

It is still justified to uniformly average over the initial synchrotron phase ϕ_{z0}. The diagonal terms $m = m'$ survive the average, so

$$\langle S_\perp\rangle_{\phi_{z0}} = \mathrm{e}^{\mathrm{i}\nu_0\theta} \sum_{m=-\infty}^{\infty} \mathrm{e}^{\mathrm{i}mQ_s\theta}\, J_m^2\Big(\frac{A_z\nu_0}{Q_s}\Big). \tag{21.30}$$

This is *not* the same as (21.10). It is an explicit function of θ. It obviously beats with a frequency Q_s, i.e. the spins recohere every synchrotron period (when $\mathrm{e}^{\mathrm{i}Q_s\theta} = 1$). We can further average over the amplitudes using a Gaussian distribution. The integral over the Bessel function was also given earlier. Then

$$\langle S_\perp\rangle = \mathrm{e}^{\mathrm{i}\nu_0\theta} \sum_{m=-\infty}^{\infty} \mathrm{e}^{\mathrm{i}mQ_s\theta}\,\mathrm{e}^{-\sigma^2} I_m(\sigma^2). \tag{21.31}$$

We do not offer numerical estimates here. Readers should be able to make their own numerical estimates of the relevant parameters and sum the modified Bessel functions, if desired.

21.6. Vertically polarized beam and single Snake

In all of the above models, we assumed a fully polarized beam was injected orthogonal to $\boldsymbol{n}_0$. Akchurin *et al* (1992) injected a *vertically* polarized beam into the IUCF Cooler with a full-strength Snake. Since the spin tune is $\frac{1}{2}$, in the absence of decoherence, the polarization should return to its original value after every two turns. The detector was gated to measure the scattering asymmetry every second turn. The authors reported that the vertical polarization did survive for the storage time of about 10 s. Synchrotron sidebands could also be observed.

21.7. Nonlinear dynamical spin tunespread

In all of the above models, we expanded the change to the spin tune only to the first order in the relative energy offset $\Delta E/E$ and we treated the synchrotron oscillations using only linear orbital dynamics.

In a detailed theoretical analysis, backed by experimental studies to confirm the calculations, the change to the spin precession frequency was calculated to the *second* order $(\Delta E/E)^2$. This is another example of the contribution of nonlinear orbital dynamics to the spin motion. The initial theory and experiments were reported by Lysenko *et al* (1986). Further theory and experiments were presented by Koop *et al* (1989). We use material from both the sources below. The authors treat only planar rings and ultrarelativistic particles, i.e. electrons and positrons. Consider first that the spin precession frequency (*not* tune) is

$$\Omega = (1 + a\gamma)\,\omega, \tag{21.32}$$

where ω is the revolution frequency around the ring. For a particle with energy $E = E_0 + \Delta E$, where E_0 is the reference energy, the revolution frequency is

$$\omega = \omega_0\Big[1 - \alpha_1\frac{\Delta E}{E_0} - \alpha_2\Big(\frac{\Delta E}{E_0}\Big)^2 + \cdots\Big]. \tag{21.33}$$

Terms beyond the second order will be neglected below. Here $\alpha_{1,2}$ are the first and second order momentum compaction factors. The spin precession frequency is then written as an offset from the spin precession frequency Ω_0 of the reference particle via $\Omega = \Omega_0 + \Delta\Omega$. Then

$$\Omega = (1 + a\gamma_0)\,\omega \simeq \Big[1 + a\gamma_0 + a\gamma_0\frac{\Delta E}{E_0}\Big]\Big[1 - \alpha_1\frac{\Delta E}{E_0} - \alpha_2\Big(\frac{\Delta E}{E_0}\Big)^2\Big]\omega_0. \tag{21.34}$$

Expanding to the second order,

$$\Delta\Omega = \omega_0\Big\{[a\gamma_0 - (1 + a\gamma_0)\alpha_1]\frac{\Delta E}{E_0} - [(1 + a\gamma_0)\alpha_2 + a\gamma_0\alpha_1]\Big(\frac{\Delta E}{E_0}\Big)^2\Big\}. \tag{21.35}$$

The rest of the calculations are somewhat involved, for example, one must express the horizontal motion up to second order via

$$x = x_\beta + D_{x1}\frac{\Delta E}{E_0} + D_{x2}\Big(\frac{\Delta E}{E_0}\Big)^2. \tag{21.36}$$

The final result is (assuming $\alpha_1 \gg \alpha_2$) (Lysenko *et al* 1986)

$$\langle\Delta\Omega\rangle = \frac{\nu_0\omega_0}{2\alpha_1}\Big[\langle I_x\rangle\langle B''D_{x1}\beta_x\rangle + \Big(\frac{\sigma_E}{E_0}\Big)^2\langle B''D_{x1}^3\rangle\Big], \tag{21.37}$$

where $B'' = \partial^2 B_y/\partial x^2$ is the sextupole field gradient. The analysis by Koop *et al* (1989) calculated terms beyond those in (21.37), but for strong-focusing rings, the extra terms are very small. In practice, in strong-focusing rings the first of the terms in (21.37) is much more important than the second. Writing the formula in terms of the horizontal chromaticity,

$$\langle\Delta\Omega\rangle \simeq \omega_0\frac{\nu_0\langle I_x\rangle}{2\alpha_1}\,\xi_x. \tag{21.38}$$

The value of $\langle\Delta\Omega\rangle$ is minimized when the horizontal chromaticity ξ_x vanishes.

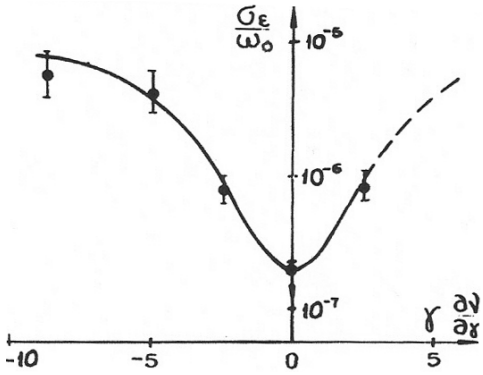

Figure 36. Spin tunespread of the electron beam at VEPP-2M as a function of the horizontal chromaticity. From Koop *et al* (1989). Copyright (1989) by the American Institute of Physics.

An experiment to test the above theory was performed at VEPP-2M (Koop *et al* 1989). The spin tunespread $\langle \Delta\Omega \rangle$ was measured from the residual polarization after the adiabatic (i.e. slow) crossing of the resonance line $\nu = 2$, for various settings of the sextupole strengths. We have not yet discussed the acceleration of spin-polarized beams across depolarizing resonances, for that the reader must consult section 24. The beam was polarized radiatively *in situ* to $P \simeq 80\%$ by the synchrotron radiation; for a review of the theory of radiative polarization, including depolarizing effects, the reader must consult section 27. In any case, the results are plotted in figure 36. The horizontal axis is the chromaticity, written using the notation $\xi_x = \gamma(\partial \nu_x/\partial\gamma)$. On the vertical axis is plotted the value of σ_ϵ/ω_0, where $\omega_\epsilon = \sqrt{\langle \Delta\Omega^2 \rangle}$. Evidently the value of ω_ϵ reaches a minimum (not exactly zero) at vanishing horizontal chromaticity $\gamma(\partial \nu_x/\partial\gamma) = 0$.

22. Higher order resonances

22.1. General remarks

The title of this section is somewhat unfortunate because we have already discussed the most important higher-order spin resonances, namely, the synchrotron sideband resonances, in an earlier section. Here we shall discuss the higher orders of perturbation theory, where the higher-order terms are *not* due to synchrotron oscillations. In general, the resonances described below are weak. However, they have been observed experimentally.

One of the resonances below will be that of a parent vertical betatron intrinsic resonance coupled with a horizontal closed-orbit imperfection. Hence, the first-order term is driven by a vertical betatron oscillation and the higher-order contribution is driven by the horizontal (not vertical) closed-orbit imperfection. However, the final resonance occurs at a spin tune of $\nu = k \pm Q_y$, which is conventionally designated as a first-order resonance. In this case, it is crucial to realize that the spin basis vectors are referenced to the design orbit and the 'second-order' perturbation theory is a joint perturbation expansion in both the closed-orbit imperfections and the orbital oscillations simultaneously. It is important to clearly recognize the perturbation expansion parameter(s) of every calculation.

22.2. Basic formulae

The notation will follow that in section 20. Once again we parametrize $\boldsymbol{n}$ via (15.12)

$$\boldsymbol{n} = \sqrt{1 - |\zeta|^2}\, \boldsymbol{n}_0 + \Re(\zeta \boldsymbol{k}_0^*). \tag{22.1}$$

The solution for ζ to the level of approximation required here is (see (15.17))

$$\zeta \simeq -\mathrm{i}\mathrm{e}^{-\mathrm{i}\chi(\theta)} \int_{-\infty}^{\theta} \mathrm{e}^{\mathrm{i}\chi(\theta')}\, \boldsymbol{\omega} \cdot \boldsymbol{k}_0 \, \mathrm{d}\theta', \tag{22.2}$$

where once again (see (15.18))

$$\chi(\theta) = -\int_{-\infty}^{\theta} \boldsymbol{w} \cdot \boldsymbol{n}_0 \, \mathrm{d}\theta'. \tag{22.3}$$

To the second order, the Taylor series approximations for ζ are

$$\begin{aligned} \zeta^{(1)} &= -\mathrm{i} \int_{-\infty}^{\theta} \boldsymbol{\omega} \cdot \boldsymbol{k}_0 \, \mathrm{d}\theta', \\ \zeta^{(2)} &= \int_{-\infty}^{\theta} \mathrm{d}\theta' \, \boldsymbol{\omega} \cdot \boldsymbol{n}_0(\theta') \int_{-\infty}^{\theta'} \mathrm{d}\theta'' \, \boldsymbol{\omega} \cdot \boldsymbol{k}_0(\theta'') = \mathrm{i} \int_{-\infty}^{\theta} \mathrm{d}\theta' \, \boldsymbol{\omega} \cdot \boldsymbol{n}_0(\theta') \, \zeta^{(1)}(\theta'). \end{aligned} \tag{22.4}$$

We have already explained how at the second order, the integral yields terms which diverge at the second order spin resonances $\nu = k \pm Q_x \pm Q_y$, or $\nu = k \pm 2Q_{x,y}$, etc. Since the higher-order betatron resonances are weak, there is reason to believe that a Taylor series calculation will yield a satisfactory approximation for the strengths of such resonances.

It is also possible for sextupoles to contribute to the second order resonances via the term $\boldsymbol{w} \cdot \boldsymbol{k}_0$ in $\zeta^{(1)}$, though such contributions are weak in general. It was explained earlier that at high energies, where $a\gamma \gg 1$, the contribution of the quadrupoles completely dominates that of the sextupoles and other higher-order multipoles. The presence, or absence, of Siberian Snakes or spin rotators in the ring does not affect these observations.

22.3. Second order betatron spin resonance

A second order betatron spin resonance was observed in studies at the IUCF Cooler (Ohmori *et al* 1995). The measurements were part of the series of excellent studies of spin dynamics with polarized proton beams at the IUCF Cooler. Note that higher order spin resonances had been observed earlier at other rings such as SPEAR (Johnson *et al* 1983), e.g. see figure 6, but always under uncontrolled machine conditions. The work by Ohmori *et al* (1995) was the first direct observation of a second order (or higher order) betatron spin resonance with controlled accelerator parameters. During studies of the intrinsic resonance $\nu = 7 - Q_y$ with a 20% partial Siberian Snake, a second and narrow resonance was observed. Its location was consistent with the assignment $\nu = 1 + Q_y - Q_x$. This was confirmed by changing the value of the horizontal betatron tune without altering the value of the vertical betatron tune. The location (and width) of the vertical betatron intrinsic resonance $\nu = 7 - Q_y$ did not change, but the location of the narrow resonance shifted exactly as expected from the above assignment.

22.4. Hybrid spin resonance

During the acceleration of polarized proton beams at the AGS, a resonance was observed which was due to the joint influence of the vertical betatron oscillations and the *horizontal* closed-orbit imperfections (Bai *et al* 2000). The authors termed it a 'hybrid resonance'. The spin basis vectors $\boldsymbol{n}_0$ and $\boldsymbol{k}_0$ are referenced to the *design orbit*, since we are now treating a joint perturbation of closed orbit imperfections and betatron orbital oscillations. The study by Bai *et al* (2000) also employed a 5% partial Snake (solenoid) in the ring, but this does not seriously affect the analysis below. It is adequate to take $\boldsymbol{n}_0$ to be vertical (the AGS is planar).

The first-order parent resonance is due to the vertical betatron oscillations; there is no need to comment on the matter further. The quantity of interest is χ, i.e. the integrand $\boldsymbol{w}\cdot\boldsymbol{n}_0$. Since $\boldsymbol{n}_0$ is vertical, it is the *horizontal* orbital motion which contributes to $\boldsymbol{w}\cdot\boldsymbol{n}_0$. We can write, with obvious notation,

$$x = x_{\text{c.o.}} + x_\beta + D_x\frac{\Delta p}{p_0}. \tag{22.5}$$

The term of interest here is the first, namely, the horizontal closed-orbit distortions. We decompose $x_{\text{c.o.}}$ into Fourier harmonics

$$x_{\text{c.o.}} = \sum_m \hat{x}_m \cos(m\theta + \kappa_m), \tag{22.6}$$

where κ_m is some phase and the $\hat{x}_m$ are the Fourier harmonic amplitudes. In general, the harmonic with the largest magnitude is given by the value of m closest to the horizontal betatron tune. The tunes were $Q_x \simeq 8.755$ and $Q_y \simeq 8.700$ at the AGS. Hence, the principal harmonic was given by $m_* = 9$. Let us, therefore, retain only the largest Fourier harmonic in $x_{\text{c.o.}}$:

$$x_{\text{c.o.}} \simeq \hat{x}_{m_*}\cos(m_*\theta + \kappa_{m_*}). \tag{22.7}$$

Then we can also Fourier decompose

$$\boldsymbol{w}\cdot\boldsymbol{n}_0 = \sum_m \hat{w}_m \cos(m\theta + \upsilon_m), \tag{22.8}$$

where the υ_m are phases and the $\hat{w}_m$ are the amplitudes. We retain only the principal Fourier harmonic:

$$\boldsymbol{w}\cdot\boldsymbol{n}_0 \simeq \hat{w}_{m_*}\cos(m_*\theta + \upsilon_{m_*}). \tag{22.9}$$

Then

$$\chi \simeq -\int_{-\infty}^{\theta} \hat{w}_{m_*}\cos(m_*\theta' + \upsilon_{m_*})\,\mathrm{d}\theta' = -\frac{\hat{w}_{m_*}}{m_*}\sin(m_*\theta + \upsilon_{m_*}). \tag{22.10}$$

This again leads to a Bessel-function comb of sidebands, this time of the form

$$\zeta_{jk} \simeq w_{jk}\sum_m J_m\left(\frac{\hat{w}_{m_*}}{m_*}\right)\frac{\mathrm{e}^{\mathrm{i}(\phi_j - m(m_*\theta+\upsilon_{m_*})+k\theta-\upsilon_0\theta)}}{\upsilon_0 - k - Q_j + mm_*}, \tag{22.11}$$

where $Q_j = \pm Q_y$ in the present case. The strength of the higher-order resonance is proportional to that of the parent resonance and the function $J_m(\hat{w}_{m_*}/m_*)$.

The parent resonance was $G\gamma = 60 - Q_y \simeq 51.3$. The vertical chromaticity was set to zero by using the ring sextupoles, so as to obtain an accurate value for the vertical betatron tune, free of uncertainties due to the momentum spread of the beam. Because of the narrowness of the resonance width it was important to measure the value of the vertical betatron tune accurately and to identify the location of the polarization loss precisely. The horizontal chromaticity was not set to zero, in fact, it was about $\xi_x \simeq -22.0$. A precise value for the horizontal betatron tune was less critical since the Fourier harmonic of the horizontal closed-orbit distortion was known to be $m_* = 9$. The higher-order resonance was observed at $G\gamma \simeq 42.3$, which corresponds to the $m = 1$ sideband:

$$G\gamma = 60 - Q_y - m_* = 60 - 8.700 - 9 \simeq 42.3. \tag{22.12}$$

Since $J_m(z) \propto z^m$ for small values of $|z|$ and $m = 1$ in this case, the higher-order resonance width should be proportional to the parent resonance width and also the first power of the amplitude of the Fourier harmonic of the horizontal closed-orbit distortion $\hat{x}_{m_*}$. The study

verified that this was so. A 9θ Fourier harmonic of the horizontal closed orbit was deliberately induced by using a set of 32 corrector dipoles, suitably phased, to generate $(\cos(9\theta), \sin(9\theta))$ terms in the horizontal closed orbit. In this way, the value of $\hat{x}_{m_*}$ was varied under controlled conditions. It was also noted by Bai *et al* (2000) that the sextupoles can contribute to the strength of this resonance, though the contribution is likely to be negligible. This was confirmed by noting that the resonance strength did not change for different settings of the sextupole currents. Bai *et al* (2000) calculated the resonance strength using a model of the AGS lattice with the corrector dipoles set to zero. Denoting the resonance strength by ϵ, the results are

$$\epsilon_{\text{th}} = (6.02 \pm 1.17) \times 10^{-4}, \qquad \epsilon_{\text{ex}} = (5.70 \pm 0.87) \times 10^{-4}, \tag{22.13}$$

which is a good match to the data.

23. Nonperturbative algorithms for the vector field of spin quantization axes

23.1. General remarks

We shall now describe three state-of-the-art *nonperturbative* formalisms and also one nonperturbative numerical algorithm to calculate the vector field of spin quantization axes. All of the formalisms employ map methods. The analytical formalisms in order of presentation below are MILES (Mane 2003a), SODOM2 (Yokoya 1999) and SODOM (Yokoya 1992). The purely numerical algorithm is called stroboscopic averaging (Heinemann and Hoffstätter 1996). It is coded into the programme SPRINT. Modern versions of SPRINT now also include the SODOM2 algorithm.

SODOM was used to aid in the analysis of depolarizing spin resonances at LEP (Assmann *et al* 1994a). SODOM2 and SPRINT have been used for design work for Siberian Snakes at HERA. MILES was used to derive the exact analytical solution for the single resonance model with one Siberian Snake and a pair of diametrically opposed Siberian Snakes (the 'sine-Bessel functions'). The solutions were displayed in MSY1.

23.2. MILES

The name MILES (Mane 2003a) is simply an anagram of the name of the earlier formalism SMILE by Mane (1987b). There is, otherwise, no connection between the two formalisms. The fact that $\boldsymbol{n}$ is a vector field over the orbital phase-space means that its transformation is given by

$$\boldsymbol{\sigma} \cdot \boldsymbol{n}(z_{\text{f}}) = M\, \boldsymbol{\sigma} \cdot \boldsymbol{n}(z_{\text{i}})\, M^{-1}, \tag{23.1}$$

where z denotes a point in the orbital phase-space and we have used the spin $\frac{1}{2}$ representation of $SU(2)$ for the matrices. Here

$$\boldsymbol{\sigma} \cdot \boldsymbol{n} = \begin{pmatrix} n_3 & n_1 - \mathrm{i}n_2 \\ n_1 + \mathrm{i}n_2 & -n_3 \end{pmatrix}. \tag{23.2}$$

We shall employ the definitions $n_\pm = n_1 \pm \mathrm{i}n_2$ below. It is simplest to employ the action-angle representation for the orbital motion. Let the orbital angles at the base azimuth θ_* be ϕ_*. Let the one turn orbital phase advances be denoted by $\boldsymbol{\mu} = 2\pi\boldsymbol{Q}$. The orbital tunes $\boldsymbol{Q}$ could depend on the orbital actions—we allow nonlinear dynamics and aberrations, etc. The one-turn mapping for the orbital motion is then

$$(\boldsymbol{I}_*, \boldsymbol{\phi}_*) \mapsto (\boldsymbol{I}_*, \boldsymbol{\phi}_* + \boldsymbol{\mu}). \tag{23.3}$$

The mapping for $\boldsymbol{n}$ is then

$$\boldsymbol{\sigma} \cdot \boldsymbol{n}(\boldsymbol{\phi}_* + \boldsymbol{\mu}) = M\boldsymbol{\sigma} \cdot \boldsymbol{n}(\boldsymbol{\phi}_* + \boldsymbol{\mu})M^{-1}, \tag{23.4}$$

dropping explicit mention of the actions, which are held at fixed values, and also of the base azimuth θ_*. The above relation provides a complete, nonperturbative technique to calculate the vector field of spin quantization axes $\boldsymbol{n}$. An arbitrary $SU(2)$ matrix M can be parametrized as follows:

$$M = \begin{pmatrix} f & -g^* \\ g & f^* \end{pmatrix}, \tag{23.5}$$

where $ff^* + gg^* = 1$. In terms of f and g, we deduce that

$$\begin{aligned} n_3(\phi_* + \boldsymbol{\mu}) &= (ff^* - gg^*)n_3(\phi_*) - f^*g^*n_+(\phi_*) - fgn_-(\phi_*), \\ n_+(\phi_* + \boldsymbol{\mu}) &= 2f^*gn_3(\phi_*) + f^{*2}n_+(\phi_*) - g^2n_-(\phi_*). \end{aligned} \tag{23.6}$$

We now expand f and g, and also n_3 and $n_\pm$, as Fourier series in ϕ_* and equate terms. This is the MILES algorithm. It is nonperturbative and treats nonlinear orbital dynamics.

The above procedure yields the solution at one azimuth θ_*. The solution at other points in the ring can be obtained by particle tracking.

23.3. SODOM2

In the SODOM2 (Yokoya 1999) algorithm the spin is represented by a spinor. The one-turn map equation for a spinor ψ representing $\boldsymbol{n}$ is

$$M\psi(\phi_*) = \mathrm{e}^{-\mathrm{i}v(\phi_*)/2}\psi(\phi_* + \boldsymbol{\mu}). \tag{23.7}$$

Here v is a periodic function of ϕ_*, i.e. $v(\phi_* + 2\pi) = v(\phi_*)$. Once again the values of the orbital actions are held fixed and we do not mention them nor the base azimuth θ_*. We find another function $u(\phi_*)$, also periodic in ϕ_*, such that

$$v(\phi_*) + u(\phi_* + \boldsymbol{\mu}) - u(\phi_*) = \mu_\mathrm{s}, \tag{23.8}$$

where μ_s is independent of ϕ_* and θ_*, and depends, therefore, only on the actions $\boldsymbol{I}$. Then we define a new spinor

$$\Psi = \mathrm{e}^{\mathrm{i}u(\phi_*)/2}\,\psi. \tag{23.9}$$

Then

$$M\Psi(\phi_*) = \mathrm{e}^{-\mathrm{i}\mu_\mathrm{s}/2}\Psi(\phi_* + \boldsymbol{\mu}). \tag{23.10}$$

We now expand M (actually the functions f and g, see the MILES algorithm above) and Ψ as Fourier series in ϕ_*, namely,

$$M = \sum_{\boldsymbol{m}} M_{\boldsymbol{m}}\,\mathrm{e}^{\mathrm{i}\boldsymbol{m}\cdot\phi_*}, \qquad \Psi = \sum_{\boldsymbol{m}} \Psi_{\boldsymbol{m}}\,\mathrm{e}^{\mathrm{i}\boldsymbol{m}\cdot\phi_*}. \tag{23.11}$$

Then (23.10) can be re-expressed as

$$\mathrm{e}^{-\mathrm{i}\boldsymbol{m}\cdot\boldsymbol{\mu}} \sum_{\boldsymbol{m}'} M_{\boldsymbol{m}-\boldsymbol{m}'}\,\Psi_{\boldsymbol{m}'} = \mathrm{e}^{-\mathrm{i}\mu_\mathrm{s}/2}\,\Psi_{\boldsymbol{m}}. \tag{23.12}$$

This can be visualized as an infinite-dimensional matrix eigenvalue problem for $\mathrm{e}^{-\mathrm{i}\mu_\mathrm{s}/2}$. The eigenvector elements are the Fourier harmonics $\Psi_{\boldsymbol{m}}$. The solution for $\boldsymbol{n}$ is

$$\boldsymbol{n} = \Psi^\dagger\boldsymbol{\sigma}\Psi \tag{23.13}$$

and is the same for all the eigenvector solutions of (23.12). The spin tune is given by $\nu = \mu_\mathrm{s}/(2\pi)$. The solutions for the spin tune are not unique up to $\mu_\mathrm{s} \mapsto \mu_\mathrm{s} + \boldsymbol{m}\cdot\boldsymbol{\mu}$, or $\nu \mapsto \nu + \boldsymbol{m}\cdot\boldsymbol{Q}$. However, this is a known ambiguity in the formal canonical transformation theory and not a flaw in the SODOM2 formalism.

In practice, the matrix M must be truncated to a finite number of Fourier harmonics, which generates some numerical error in the solution, and the eigenvalue calculation must also be performed numerically. The bulk of the computation time is spent, not surprisingly, in the eigenvalue/eigenvector solver.

23.4. SODOM

SODOM (Yokoya 1992, 1993) means *S*pin *O*rbit *D*ynamics from the *O*ne-turn *M*ap. Recall that the one-turn map equation for a spinor ψ representing $\boldsymbol{n}$ is

$$M\psi(\phi_*) = \mathrm{e}^{-\mathrm{i}\upsilon(\phi_*)/2}\psi(\phi_* + \boldsymbol{\mu}), \tag{23.14}$$

where υ is a periodic function of ϕ_*. One expresses the spinor via the parametrization

$$\psi(\phi_*) = \frac{1}{\sqrt{1+|\zeta|^2}}\begin{pmatrix}1\\ \zeta\end{pmatrix}. \tag{23.15}$$

Recall also the parametrization for the map

$$M = \begin{pmatrix} f & -g^* \\ g & f^* \end{pmatrix}, \tag{23.16}$$

where $ff^* + gg^* = 1$. This notation is different from that employed by Yokoya (1992), but is used here for uniformity of presentation with MILES, etc. Then

$$\begin{aligned} f - g^*\zeta(\phi_*) &= \mathrm{e}^{-\mathrm{i}\upsilon/2}\Big[\frac{1+|\zeta(\phi_*)|^2}{1+|\zeta(\phi_*+\boldsymbol{\mu})|^2}\Big]^{1/2}, \\ g + f^*\zeta(\phi_*) &= \mathrm{e}^{-\mathrm{i}\upsilon/2}\,\zeta(\phi_*+\boldsymbol{\mu})\Big[\frac{1+|\zeta(\phi_*)|^2}{1+|\zeta(\phi_*+\boldsymbol{\mu})|^2}\Big]^{1/2}. \end{aligned} \tag{23.17}$$

Cross-multiplying and rearranging terms yields

$$g + f^*\zeta(\phi_*) - f\zeta(\phi_*+\boldsymbol{\mu}) + g^*\zeta(\phi_*)\zeta(\phi_*+\boldsymbol{\mu}) = 0. \tag{23.18}$$

This is a nonlinear equation to be solved for ζ. We expand f, g and ζ in Fourier harmonics in ϕ_* and solve for the Fourier coefficients of ζ.

Notice that υ has dropped out of the final equation. SODOM does not calculate the spin tune. Both MILES and SODOM yield only the vector $\boldsymbol{n}$ (or a spinor equivalent). SODOM2 yields in addition the spin tune ν. This has both advantages and disadvantages: there is more output of information, but it also means that two distinct calculations are linked together. It may be easier to solve only for $\boldsymbol{n}$ without the encumbrance of a spin tune calculation.

23.5. Stroboscopic averaging

Stroboscopic averaging (Heinemann and Hoffstätter 1996) is an elegant numerical technique to calculate $\boldsymbol{n}$. It has been implemented in the programme SPRINT. The key idea is this: we know that on any trajectory in the orbital phase-space, the vector $\boldsymbol{n}(z;\theta)$ is the quantization axis for the stationary spin states. Hence, in the long term, only the component $\boldsymbol{s}\cdot\boldsymbol{n}$ of any spin vector $\boldsymbol{s}$ on that trajectory will survive; the components of $\boldsymbol{s}$ orthogonal to $\boldsymbol{n}$ will average to zero. This, of course, presumes that the orbit is not on a spin resonance.

We, therefore, determine $\boldsymbol{n}$ in the following way. We first select a base azimuth θ_*. We parametrize the orbital motion using action-angle variables $(\boldsymbol{I}, \phi_*)$ as already described above. We, of course, hold the actions $\boldsymbol{I}$ at fixed values and do not mention them explicitly below. We then launch a particle at the point $(\phi_* - j\boldsymbol{\mu}, \theta_* - 2\pi j)$ with the spin $\boldsymbol{s}_j$ oriented along $\boldsymbol{n}_0$ and track for j turns. The particle will end up at the phase-space point (ϕ_*, θ_*) for any j. We perform this procedure for N spins, setting $j = 1, 2, \ldots, N$, i.e. one particle is tracked for one turn, another is tracked for two turns, the next for three turns, etc. It is possible with some caching of information to make the computational complexity $\mathrm{O}(N)$ not $\mathrm{O}(N^2)$.

At the end, we will have a set of N spins $\boldsymbol{s}_j$, $j = 1, 2, \ldots, N$, all at the location (ϕ_*, θ_*). We now *average* the spins to obtain

$$\bar{\boldsymbol{s}} \equiv \frac{1}{N} \sum_{j=1}^{N} \boldsymbol{s}_j. \tag{23.19}$$

The key idea here is that the (unknown) components orthogonal to $\boldsymbol{n}$ will average to zero for sufficiently large N. However, the (also unknown) components $\boldsymbol{s}_j \cdot \boldsymbol{n}$ will be invariant during the tracking and will sum up to a nonzero average value. Hence, for sufficiently large N and *if* the average converges then $\bar{\boldsymbol{s}} \parallel \boldsymbol{n}$. The term 'stroboscopic' arises from the Poincaré sections in the tracking: we observe the spins only at discrete intervals, and not continuously. In common with MILES and SODOM, stroboscopic averaging yields only the quantization axis $\boldsymbol{n}$ and not the spin tune.

Note that the sum might not converge if $\boldsymbol{n}_0 \perp \boldsymbol{n}$ or the convergence may be poor, if the orbit is close to a resonance. The choice of launching the spins pointing along $\boldsymbol{n}_0$ is merely a simple convention and a good choice if the orbit is far from resonance in which case most likely one has $\boldsymbol{n} \simeq \boldsymbol{n}_0$. However, another initial vector could be used.

23.6. Summary

All of the above nonperturbative formalisms are map-based techniques, i.e. they all use Poincaré sections. They all yield the solution for $\boldsymbol{n}$ at a fixed pre-determined azimuth θ_*. The solution for the $\boldsymbol{n}$ at other azimuths is obtained by tracking around the ring. The formalisms all assume the orbital motion is expressed in terms of action-angle variables. SODOM, SODOM2 and MILES were formulated as analytical algorithms which can be coded into computer programs. Stroboscopic averaging was conceived from the outset as a numerical algorithm based on particle tracking.

SODOM, SODOM2 and MILES all yield $\boldsymbol{n}(\boldsymbol{I}, \phi_*)$ or a spinor over a whole invariant torus, i.e. all values of ϕ_*. Stroboscopic averaging, by contrast, yields the value for $\boldsymbol{n}$ at only *one* value of ϕ_*. To obtain $\boldsymbol{n}$ over a whole invariant torus, one must repeat the stroboscopic averaging at multiple values of ϕ_* over the surface of the torus. If we track N particles and want information at M values of ϕ_*, the computational complexity is $\mathrm{O}(MN)$. Nevertheless, stroboscopic averaging is a fast and efficient technique. The algorithm is simple to understand and easy to programme. The description by Heinemann and Hoffstätter (1996) is particularly lucid.

Notice, especially, that all of the algorithms are formulated at a high level. We described four state-of-the-art formalisms to calculate $\boldsymbol{n}$, and did not even write down any detailed expressions for the spin precession vector in individual beamline elements, such as a dipole or quadrupole. However, the very fact that the formalisms are nonperturbative also means that they do not immediately reveal important features, such as the importance of synchroton sideband resonances.

24. Acceleration of nonradiatively polarized beams I

24.1. Basic formalism

In this section, we shall review the practical usage of the Froissart–Stora formula. We begin with a planar ring. The particle spins precess around the vertical axis for orbital motion on the ideal design orbit, i.e. in the absence of any perturbing terms. Some of the material below has been presented earlier; here we recapitulate and elaborate. The principal perturbation to

the spin precession comes from *horizontal* magnetic fields due to motion off the design orbit. These perturbations can be due to either of two sources:

- The actual closed orbit is imperfect due to misalignment errors of the actual magnets. The imperfect closed orbit is the same for all the particles in the beam, so there is no average over the orbital phase-space. At the leading order, it is only the vertical component of the closed orbit imperfections which drives the depolarizing resonances. Depolarizing resonances arising from an imperfect (vertical component of the) closed orbit are, therefore, called 'imperfection resonances'.
- The particles execute betatron oscillations and traverse off-axis magnetic fields. These can be due to the vertical betatron oscillations or by transverse coupling effects causing the horizontal betatron oscillations to have a vertical component. Both of these are 'intrinsic resonances' because the betatron oscillations are intrinsic to a machine and even exist in a perfectly aligned ring. However, the resonances driven by the horizontal betatron oscillations are known as 'coupling resonances'. They are relatively weaker and less common than the resonances driven by the vertical betatron oscillations. Here we consider only the resonances due to the vertical betatron oscillations which exist and can be strong in all the synchrotrons. Hence, the term 'intrinsic resonances' will refer only to the vertical betatron oscillations below. For both the intrinsic and coupling resonances, a statistical average over the particle distribution is required.

The standard theoretical formalisms also expand the orbital motion to only the first order in the orbital amplitude (first order in the vertical closed orbit imperfections or first order in the vertical betatron amplitude). However, the effects of the synchrotron oscillations (energy oscillations) can also be significant, because the spin tune is proportional to a particle's energy. Evidence of the influence of synchrotron oscillations has been observed.

Before proceeding further, recall the statements earlier about the use of $\boldsymbol{n}_0$ to denote the spin precession axis on the closed orbit versus the design orbit. We see from above that we shall be dealing with closed orbit imperfections for some of the resonances. Throughout this section, therefore, the spin basis vectors and spin tune are referenced to the *design* orbit. However, we shall continue to use $\boldsymbol{n}_0$ below, to maintain contact with the literature. In all of the calculations below, we shall deal with either an intrinsic resonance or an imperfection resonance, but not both simultaneously.

We employ the classical spin model throughout the calculations below. In a facility such as ELSA, which accelerates polarized electron beams, the particles emit synchrotron radiation throughout the acceleration process. However, there is negligible spin-flip radiation and so a classical treatment of the spin is permissible. For an accelerated spin-polarized electron beam, we may consider the orbital beam emittances to be in quasi-equilibrium at each energy because the orbital damping time is short.

To simplify the exposition, we consider only the perturbation terms due to motion in the quadrupoles of the accelerator. This is, generally, the major contribution to the resonance driving terms. The magnetic field in a quadrupole is

$$\boldsymbol{B}_{\text{quad}} = B'(y\boldsymbol{e}_1 + x\boldsymbol{e}_3), \tag{24.1}$$

where $B' = \partial B/\partial x$ is the gradient of the quadrupole magnetic field. Then the perturbation $\boldsymbol{w}$ has the form

$$\boldsymbol{w} = -\frac{e}{pc}(G\gamma + 1)B'(\theta)\, y(\theta)\, \boldsymbol{e}_1. \tag{24.2}$$

There can also be perturbation terms proportional to y' and terms parallel to $\boldsymbol{e}_2$ which we do not treat here. Courant and Ruth (1980) offer a detailed discussion of the perturbations. We begin

with the imperfection resonances. Then $y = y_{\text{c.o.}}$ and is periodic in θ by the definition of a closed orbit:

$$y_{\text{c.o.}}(\theta + 2\pi) = y_{\text{c.o.}}(\theta). \tag{24.3}$$

Obviously $B'(\theta)$ is periodic in θ. Hence, $\boldsymbol{w}$ is also periodic in θ and can be Fourier expanded as follows:

$$w_1 + \mathrm{i}w_2 = \sum_{k=-\infty}^{\infty} \epsilon_k \, \mathrm{e}^{\mathrm{i}k\theta}. \tag{24.4}$$

The Fourier harmonics ϵ_k are known as the imperfection resonance strengths. Note that they are complex, in general. Their magnitudes are proportional to the amplitude of the closed orbit imperfection.

If y is due to a vertical betatron oscillation, it is not periodic in θ but has the form, as we have seen earlier,

$$y_\beta = \sqrt{2I_y\beta_y}\cos(\phi_y - Q_y\theta + \psi_y(\theta)), \tag{24.5}$$

where

$$\phi_y = Q_y\theta + \phi_{y0}. \tag{24.6}$$

Recall that ψ_y is a (vertical) betatron phase. In this circumstance, we can expand as follows

$$w_1 + \mathrm{i}w_2 = \sum_{k=-\infty}^{\infty} (\epsilon_k^+ \, \mathrm{e}^{\mathrm{i}\phi_y} + \epsilon_k^- \, \mathrm{e}^{-\mathrm{i}\phi_y}) \, \mathrm{e}^{\mathrm{i}k\theta}. \tag{24.7}$$

The Fourier harmonics $\epsilon_k^\pm$ are called the intrinsic resonance strengths. They are also complex and their amplitudes are proportional to the vertical betatron amplitude. If the ring has a superperiodicity P, all the Fourier harmonics in (24.7) *vanish* except those for which k is a multiple of P. We can re-express the sum as

$$w_1 + \mathrm{i}w_2 = \sum_{k=-\infty}^{\infty} (\epsilon_{kP}^+ \, \mathrm{e}^{\mathrm{i}\phi_y} + \epsilon_{kP}^- \, \mathrm{e}^{-\mathrm{i}\phi_y}) \, \mathrm{e}^{\mathrm{i}kP\theta}. \tag{24.8}$$

For example, $P = 12$ for the AGS and 2 for ELSA. The superperiodicity of RHIC (without Snakes) is $P = 3$. In the case of an imperfect closed orbit there is no such symmetry by the nature of imperfections. All integer values of k are allowed. The spectrum of the imperfection and intrinsic resonances is

$$G\gamma = k, \qquad G\gamma = kP \pm Q_y, \tag{24.9}$$

respectively, where in both cases k is an integer. Since we have seen that the value of $G\gamma_0$ increases as the beam is accelerated, this means that the particles cross one resonance after another during the acceleration process, i.e. the Froissart–Stora formula comes into play. In addition to the imperfection resonances, the beam must also cross the intrinsic resonances. A high superperiodicity therefore reduces the number of intrinsic resonances, but in practice there may be other, more important, considerations which constrain the design of the accelerator.

Additional sources which can contribute to the resonance driving terms in a planar ring, merely change the detailed expressions for the Fourier harmonics ϵ_k or $\epsilon_{kP}^\pm$, e.g. see Courant and Ruth (1980). However, the formal structure of the Fourier spectrum is unchanged. If the ring contains transverse x–y betatron coupling, then there are additional resonances driven by the horizontal betatron oscillations. These can be dealt with by an extension of the present formalism.

Formally, we can think of the imperfection terms as a special case of the intrinsic, by setting $P = 1, \phi_y = 0$ and $\epsilon_{kP}^- = 0$ (and the amplitudes of the ϵ_k do not have a statistical distribution). Hence, we employ (24.8) in (6.7), and do not subdivide into special cases. However, note, that this is contrary to the standard practice, which *does* fragment the calculation into special cases. We prefer to keep the formula unified for as long as possible. Then

$$m_{21} = \mathrm{e}^{-\mathrm{i}[\nu_{00}\theta + (1/2)\alpha\theta^2]} \sum_{k=-\infty}^{\infty} (\epsilon_{kP}^+ \mathrm{e}^{\mathrm{i}\phi_y} + \epsilon_{kP}^- \mathrm{e}^{-\mathrm{i}\phi_y})\, \mathrm{e}^{\mathrm{i}kP\theta}. \tag{24.10}$$

Each Fourier harmonic will drive a depolarizing resonance, unless the Fourier coefficient vanishes.

24.2. DEPOL

Courant wrote the programme DEPOL to calculate the imperfection and intrinsic resonance strengths (Courant and Ruth 1980). We review the formalism briefly. Let K denote the spin resonance tune ($K = k$ for an imperfection resonance or $K = kP \pm Q_y$ for an intrinsic resonance). Then DEPOL calculates the integral

$$\epsilon_K = \frac{1}{2\pi} \oint \frac{\zeta(s)}{\rho(s)}\, \mathrm{e}^{\mathrm{i}K\theta(s)}\, \mathrm{d}s, \tag{24.11}$$

where

$$\zeta(s) = -(G\gamma + 1)(\rho y'' + \mathrm{i}y') + \mathrm{i}\rho(G + 1)(y/\rho)'. \tag{24.12}$$

In the case of no betatron coupling, y'' satisfies Hill's equation and the integral can be evaluated in closed form for motion through dipoles and quadrupoles; this was done in the original DEPOL programme. The programme was extended to treat x–y betatron coupling (Ranjbar *et al* 2001) because of the need to treat the coupling induced by a solenoid partial Snake at the AGS, and also for the analysis of RHIC without Snakes. Since for an intrinsic resonance the value of K is not an integer, the value of ϵ_K is obtained by integrating over several turns:

$$\epsilon_K \simeq \frac{1}{2\pi N} \int_0^{NC} \frac{\zeta(s)}{\rho(s)}\, \mathrm{e}^{\mathrm{i}K\theta(s)}\, \mathrm{d}s, \tag{24.13}$$

where the value of N is a user-settable parameter. In principle one takes the limit $N \to \infty$. More recently, it has been recognized (Ranjbar *et al* 2002a) that one can express the resonance strengths for an intrinsic resonance using the type of Fourier analysis presented in (24.7). It is then only necessary to evaluate single-turn integrals around the circumference.

Notice that the integral in DEPOL (see (24.11)) is basically the same as that in the algorithms to calculate the spin quantization axis $\boldsymbol{n}$. It has historically been the case that the literature on radiative and nonradiative polarization have developed more or less separately, with different notations and terminologies for essentially the same concepts. It is also only fair to point out that DEPOL (written in 1980) preceded the publicly available formalisms for $\boldsymbol{n}$ reviewed earlier.

24.3. Statistical averages

If the resonance driving term is from a closed orbit imperfection, then ϵ will have the same value for all the particles. For an intrinsic resonance the value of ϵ varies with the betatron oscillation amplitude.

$$\epsilon^2 = \epsilon_{\mathrm{rms}}^2 \frac{I_y}{I_{\mathrm{rms}}}, \tag{24.14}$$

where $I_{\rm rms}$ is the root-mean-square vertical betatron action (i.e. the vertical betatron unnormalized emittance). Froissart and Stora (1960) showed that for a Gaussian beam distribution

$$\left\langle \frac{P_{\rm f}}{P_{\rm i}} \right\rangle = \frac{1 - (\pi \epsilon_{\rm rms}^2/\alpha)}{1 + (\pi \epsilon_{\rm rms}^2/\alpha)}. \tag{24.15}$$

However, a simpler approximation which is often used, is to employ an 'effective' resonance strength which is given by using the 95% beam emittance value in (6.21) instead. Basically, $\epsilon_{95\%}^2 = 6\epsilon_{\rm rms}^2$ and so

$$\left\langle \frac{P_{\rm f}}{P_{\rm i}} \right\rangle \simeq 2\,{\rm e}^{-\pi \epsilon_{95\%}^2/(2\alpha)} - 1. \tag{24.16}$$

There is some merit to this simpler approach. The majority of the applications of these formulae is to polarized proton (or other hadron) beams. It is important to realize that the motion of polarized protons is not ergodic. The use of a Gaussian beam distribution is an idealization.

24.4. Scaling laws

It is a good approximation to say that the resonance driving terms are principally caused by the vertical orbital motion in the quadrupoles. Roughly speaking, then, for an imperfection resonance

$$\epsilon_k^{\rm imp} \simeq -(G\gamma_0 + 1) \oint \frac{eB'(\theta)}{p_0}\, y_{\rm c.o.}(\theta) {\rm e}^{-{\rm i}k\theta} \frac{{\rm d}\theta}{2\pi}, \tag{24.17}$$

where $B' = \partial B/\partial x$ and p_0 is the momentum of the reference particle. The value of the integrand is independent of the beam energy, to a good approximation. Hence, for $G\gamma_0 \gg 1$, the magnitude of the strength of an imperfection resonance is proportional to the beam energy

$$|\epsilon_k^{\rm imp}| \propto \gamma_0. \tag{24.18}$$

For an intrinsic resonance of the form $G\gamma_0 = kP \pm Q_y$, the corresponding expression is, $K = kP \pm Q_y$,

$$\begin{aligned} \epsilon_k^{\rm int} &\simeq -(G\gamma_0 + 1) \oint \frac{eB'(\theta)}{p_0}\, y_\beta(\theta) {\rm e}^{-{\rm i}K\theta} \frac{{\rm d}\theta}{2\pi} \\ &\simeq -(G\gamma_0 + 1) \oint \frac{eB'(\theta)}{p_0} \sqrt{2\beta_y I_y} {\rm e}^{\pm {\rm i}\psi_y(\theta) + \phi_{y0}}\, {\rm e}^{-{\rm i}K\theta} \frac{{\rm d}\theta}{2\pi}. \end{aligned} \tag{24.19}$$

For a particle at the rms betatron amplitude, using the normalized emittance (recall $\varepsilon_{Ny} = \beta_0\gamma_0\varepsilon_y$), we have

$$\epsilon_k^{\rm int} \simeq (G\gamma_0 + 1) \sqrt{\frac{\varepsilon_{Ny}}{\beta_0\gamma_0}} \oint \frac{eB'(\theta)}{p_0} \sqrt{\beta_y}\, {\rm e}^{\pm {\rm i}\psi_y(\theta) + \phi_{y0}}\, {\rm e}^{-{\rm i}K\theta} \frac{{\rm d}\theta}{2\pi}. \tag{24.20}$$

The integrand is again approximately independent of the beam energy. Hence, for $G\gamma \gg 1$ and $\beta_0 \simeq 1$, the magnitude of the strength of an intrinsic resonance scales as the square root of the beam energy:

$$|\epsilon_k^{\rm int}| \propto \sqrt{\gamma_0}. \tag{24.21}$$

The use of the normalized emittance for the beam size is, of course, meant for nonradiative systems. For polarized electron beams accelerated in synchrotrons to energies of a few GeV, the radiation damping time of the beam emittances is a few milliseconds, so the orbital beam emittances are in radiative equilibrium during acceleration. For electron beams,

the (unnormalized) emittances scale with the energy, $\varepsilon_{x,y,s} \propto E^2$. Hence, for electron rings in radiative (orbital) equilibrium,

$$|\epsilon_k^{\rm int}| \propto \gamma_0^2. \tag{24.22}$$

Hence, for an electron synchrotron, the magnitudes of the intrinsic resonances scale more rapidly with energy than the magnitudes of the imperfection resonances.

The above scaling laws apply to *separated function* accelerators, where the bending and focusing take place in distinct magnets. It has been noted by Anferov (1999) that a different scaling law can be obtained for accelerators which use combined-function magnets, where an individual magnet contains both a dipole and a quadrupole field. The strength of the intrinsic resonances can scale as $1/\sqrt{\gamma}$ rather than $\sqrt{\gamma}$. This is basically because the tilts induced by the radial quadrupole fields rapidly average to a small value, because of the simultaneous precession around the vertical dipole field. However, this cancellation requires a specific design of the accelerator.

In general, the number of intrinsic resonances encountered during the acceleration of a polarized beam is fewer than the number of the imperfection resonances, especially for machines with a high superperiodicity, e.g. $P = 12$ at the AGS. In proton (hadron) synchrotrons, the intrinsic resonances are usually stronger than the imperfection resonances. This is to be expected since the imperfection resonances are, by definition, caused by random small misalignments of the magnets, and are zero by design. The intrinsic resonances exist even in a perfectly aligned machine, and their strengths depend on the vertical betatron emittance, which may be large, depending on the properties of the polarized beam source. By contrast, in an electron synchrotron, the value of the vertical emittance is self-consistently determined, and is proportional to the vertical dispersion. Furthermore, the vertical dispersion is *zero* in a perfectly aligned planar ring. In a real ring, the vertical dispersion arises from misalignments, or from deliberately induced transverse x–y coupling. Hence, in an electron synchrotron, the magnitudes of the driving terms of *both* the imperfection and intrinsic depolarizing resonances are proportional to the misalignments.

A graph of the magnitudes of the strengths of the intrinsic resonances for a RHIC lattice without Snakes is shown in figure 37. A normalized vertical emittance of 10π mm mrad was assumed. A RHIC lattice with $\beta_* = 10$ m at the interaction points was used in the calculations. Notice that the $\sqrt{\gamma}$ scaling of the intrinsic resonance strengths with the beam energy is only approximately satisfied. Many other factors, such as the detailed structure of the accelerator lattice, also contribute to the values of the spin integrals. The scaling law should thus be taken as a rough guide. In particular, there are peaks in figure 37—certain resonances are clearly much stronger than the rest. The locations of the strongest intrinsic resonances are given by

$$G\gamma = kP \pm Q_y \simeq mPM \pm Q_{\rm B}, \tag{24.23}$$

where k and m are integers, $P = 3$ is the superperiodicity of RHIC, $M = 27$ is the number of effective FODO cells per superperiod (including 'dispersion suppressors') and $2\pi Q_{\rm B} = 2\pi(Q_y - 12)$ is the accumulated betatron phase advance of all the FODO cells which contain bending dipoles. The locations of the three strongest intrinsic resonances are given by

$$G\gamma = \begin{cases} 3 \times 81 + (Q_y - 12) & (\gamma = 145), \\ 5 \times 81 - (Q_y - 12) & (\gamma = 216), \\ 5 \times 81 + (Q_y - 12) & (\gamma = 235). \end{cases} \tag{24.24}$$

For the imperfection resonances, the strengths must be estimated using a model of closed-orbit imperfections. A graph of the estimated magnitudes of the imperfection resonance strengths for the above RHIC lattice without Snakes is shown in figure 38, with application

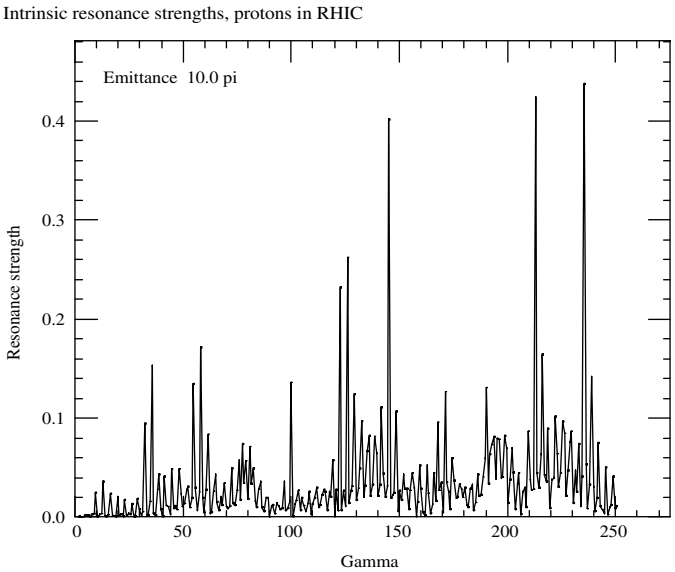

Figure 37. Intrinsic resonance strengths in a RHIC lattice without Snakes, for a 95% normalized vertical emittance of 10π mm mrad. Reprinted from Alekseev *et al* (2003). Copyright (2003) with permission from Elsevier.

of a simulated orbit correction scheme. The initial imperfections were calculated using an uncorrected closed orbit from a random sample of magnet misalignments with an rms spread of ± 0.5 mm, dipole roll angles with a spread of ± 1 mrad, dipole field errors of $\pm 5 \times 10^{-4}$ and position monitor errors of ± 0.5 mm. Present alignment data from RHIC show that the above tolerances are all met or exceeded. After the use of a simulated closed-orbit correction scheme, the vertical closed orbit was corrected to 0.155 mm (rms). The resulting imperfection resonance strengths are displayed in figure 38. The envelope bounding the strengths of the imperfection resonances is roughly linear with the beam energy, as expected from the scaling law, and is given by

$$\epsilon_{\text{imp}} = 0.25 \frac{\gamma}{250} \sigma_y, \tag{24.25}$$

where σ_y is the rms value of the residual closed orbit amplitude in mm. The imperfection resonance strengths, after closed orbit correction, do not exceed 0.04 at any RHIC energy.

24.5. Resonance correction/jumping

Many ideas have been devised to correct (eliminate) the resonance driving terms. We begin with the imperfection resonances. One idea, which is desirable for many reasons having nothing to do with the spin, is to improve the survey and positioning of all the beamline elements, to reduce the closed orbit imperfections. In addition to surveys, the technique of beam-based alignment (BBA) is also employed, where beam position monitors (BPMs) are used to obtain feedback on the beam centroid as it traverses the ring, and this information is used to help with the correction of the closed orbit imperfections. In addition to the above techniques (which are independent of whether the beams are polarized or not), additional orbit corrections are also performed to eliminate specific resonance driving terms. This technique is called 'harmonic orbit correction'.

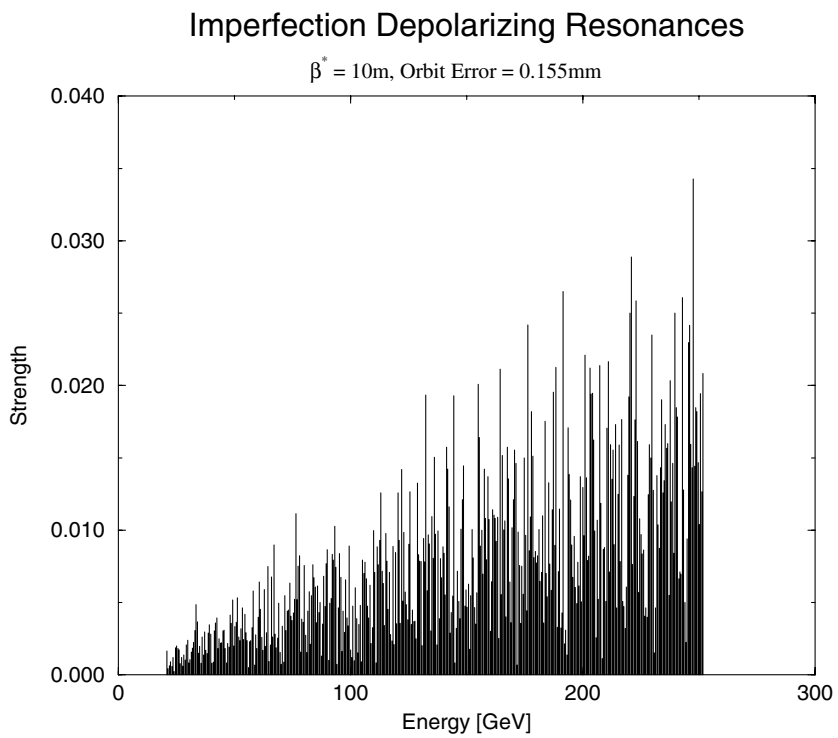

Figure 38. Estimated imperfection resonance strengths in a RHIC lattice without Snakes, with application of a simulated orbit correction scheme. Reprinted from Alekseev *et al* (2003). Copyright (2003) with permission from Elsevier.

For harmonic orbit correction, a set of corrector dipoles are placed around the ring. They are powered so as to generate a Fourier harmonic ϵ_k^{c} (c for 'correction') of a controlled magnitude *and* phase. Recall that the imperfection resonance strength ϵ_k is complex, and has both a real and imaginary part; both must be corrected to eliminate the resonance. A set of 95 corrector dipoles was employed at the AGS to generate the required Fourier harmonics (Khiari *et al* 1989). Harmonic orbit correction is applied to one resonance at a time. In other words, it is a dynamic procedure. We do not attempt to correct all of the harmonics ϵ_k simultaneously, only the one currently being crossed. The beam is extracted at an energy just below the imperfection resonance, and its polarization is measured. Subsequent proton beams are accelerated across the imperfection resonance, and the corrector settings are empirically adjusted to minimize the depolarization. The optimal corrector settings are then saved. The entire procedure is repeated for the next imperfection resonance. As one can imagine, this is a tedious effort. A total of 39 imperfection resonances in the AGS had to be crossed in this way, to accelerate the polarized proton beam to 22 GeV c^{-1}.

The strengths of the fields in the corrector dipoles, for harmonic orbit correction, are usually too small to have a noticeable impact on the beam emittances. The correction of the spin resonances is at a level too small to be detected in the orbital motion. The sensitivity of the spin to the machine parameters, especially for $G\gamma \gg 1$, is much greater than that of the orbital motion. To implement harmonic orbit correction in practice, in the first run of the accelerator, a 'table' of corrector settings is determined empirically, by correcting the imperfection resonances one at a time. These settings are then saved and used for the rest

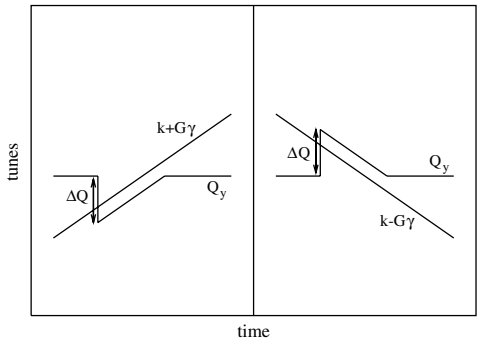

Figure 39. Symbolic plot of tune jumps across the resonances $k \pm G\gamma = Q_y$.

of the running time of the accelerator, on the assumption that the machine parameters do not change. Periodically, the settings may be reviewed and updated. The settings must obviously be reset if the machine is shut down for maintenance and then restarted.

It is fairly clear that harmonic orbit correction is an arduous, time-consuming task, and becomes impractical as one pushes to higher energies, e.g. at RHIC. It is relatively much simpler to *increase* the resonance strength. This is not as foolish as it sounds; it is in fact a very clever idea. The imperfection resonance strengths are deliberately increased to the point where adiabatic spin-flip can be performed at every imperfection resonance. The polarization direction reverses without decrease of magnitude. One, then simply accelerates without correction of the resonances; the polarization merely reverses across each imperfection resonance, which does not matter. This is the essence of the idea behind a partial Siberian Snake, and is the method of choice today for polarized proton acceleration at the AGS. We shall review the partial Snake idea below.

As for the intrinsic resonances, if they are sufficiently weak then no correction is necessary, one accelerates across the resonance sufficiently rapidly, so that $\epsilon^2/\alpha \ll 1$. However, in many cases the strengths of the intrinsic resonances are too large for the resonances to be crossed sufficiently rapidly. Recall, also, that the 'strength' of an intrinsic resonance is a statistical average; the tails of the beam will experience stronger fields and may suffer greater depolarization. One can try the opposite idea, namely, adiabatic spin-flip. This runs into the difficulty that it is not so simple to ensure that $\epsilon^2/\alpha \gg 1$ for particles in the core of the beam, where $\epsilon \to 0$. However, there is also an alternative idea that is commonly used, namely, to *circumvent* the intrinsic resonances by employing the so-called 'tune jump' quadrupoles. A current is rapidly pulsed through a set of quadrupoles (typically air-core rather than ferrite quadrupoles, to enable fast response), to change the vertical betatron tune. Hence, as the spin tune approaches the resonant value during the energy ramp, the value of the vertical betatron tune is changed rapidly ('tune jump') and the value of the spin tune (i.e. $G\gamma$) is suddenly on the *other side* of the resonance. Hence the spin tune, in principle, never equals the intrinsic resonance tune. A symbolic graph of the variation of the spin tune and the betatron tune during a tune jump is indicated in figure 39.

The tune jump technique was pioneered, successfully, at the ZGS (Khoe *et al* 1975). The tune jump technique has since been employed in almost every synchrotron, where nonradiatively polarized beams (electrons and hadrons) have been accelerated. However, a rapid change of the vertical betatron tune is not an adiabatic process. The tune jump technique results in an increase of the normalized vertical betatron emittance, for polarized hadron beams.

An alternative idea to cross the resonances, by jumping the *spin tune* using a spin tune shifter, was proposed by Golubeva *et al* (1994). In principle, the idea would apply to both imperfection and intrinsic resonances. The proposed scheme employed a sequence of radial and longitudinal spin rotations:

$$-\tfrac{1}{2}\mathrm{V}\text{–}\mathrm{L}\text{–}(-\mathrm{V})\text{–}(-\mathrm{L})\text{–}\tfrac{1}{2}\mathrm{V}\text{–}.$$

In the linear dynamical approximation, the orbital deflection cancels internally, and the design does not induce coupling of the horizontal and vertical betatron oscillations. The spin rotation matrix is

$$\begin{aligned} M &= \mathrm{e}^{-\mathrm{i}\phi_x\sigma_1/4}\mathrm{e}^{\mathrm{i}\phi_z\sigma_2/2}\mathrm{e}^{\mathrm{i}\phi_x\sigma_1/2}\mathrm{e}^{-\mathrm{i}\phi_z\sigma_2/2}\mathrm{e}^{-\mathrm{i}\phi_x\sigma_1/4} \\ &= 1 - 2\sin^2\frac{\phi_x}{2}\sin^2\frac{\phi_z}{2} - \mathrm{i}\sigma_1\,\sin\phi_x\sin^2\frac{\phi_z}{2} + \mathrm{i}\sigma_3\sin\frac{\phi_x}{2}\sin\phi_z. \end{aligned} \tag{24.26}$$

Using the small angle approximation $\phi_x \ll 1$, $\phi_z \ll 1$ yields

$$M \simeq 1 - \frac{\phi_x^2\phi_z^2}{8} + \mathrm{i}\sigma_3\frac{\phi_x\phi_z}{2}, \tag{24.27}$$

which is a spin rotation around the vertical and a spin tuneshift of

$$\Delta\nu \simeq \frac{\phi_x\phi_z}{2\pi}. \tag{24.28}$$

One can hold the longitudinal fields fixed and pulse the radial fields. However, this idea has never been used in practice.

One can also *increase* the strength of an intrinsic resonance, and employ adiabatic spin-flip. An innovative idea, which has been successfully employed at the AGS, is to deliberately induce a large-amplitude *coherent betatron oscillation*, using an rf dipole (Bai *et al* 1998). As opposed to our earlier comments that adiabatic spin-flip is problematic because $\epsilon \to 0$ in the core of the beam, in a coherent betatron oscillation *all* the particles share a common, large value of ϵ. The amplitude of the coherent betatron oscillation is relaxed to zero after crossing the intrinsic resonance. This is the modern method of choice to cross intrinsic resonances at the AGS. We shall review this elegant idea when presenting the modern work on polarized beam acceleration in the AGS in section 26.

The above techniques are clearly not mutually exclusive. Different techniques are employed for the various resonances one encounters during the acceleration process. Whether or not one can make $|\epsilon|^2/\alpha \ll 1$ depends, for example, on the maximum value of α that the rf system can deliver.

Obviously, the number of resonances to be crossed depends on the difference between the initial low energy and the final top energy. For a machine such as RHIC, where polarized protons have been accelerated to a momentum of 100 GeV c^{-1} and the top momentum is 250 GeV c^{-1}, the number of resonances to be crossed makes the above ideas impractical. The companion paper MSY1 reviewed the clever idea of Siberian Snakes to render the spin tune independent of the beam energy. This allows one to accelerate polarized beams to high energies without crossing any depolarizing resonances. For now, we confine our attention to the resonance crossing techniques. Problems arise if two resonances overlap, and cannot be crossed individually. Also, sometimes the available rf power is insufficient to accelerate quickly enough across a resonance. We consider a few theoretical ideas to deal with these issues below.

24.6. Resonant spin-flip in nonplanar rings

Note that for resonant spin-flip to work, it is *not* necessary for the ring to be planar. For example, the ring can contain Siberian Snakes. Spin flipping has been accomplished with

beams of polarized protons at the IUCF Cooler in the presence of a nearly full-strength Siberian Snake. Early work employed an rf solenoid spin flipper, achieving a spin-flip efficiency of $(97 \pm 1)\%$ (Blinov *et al* 1998). An rf dipole kicker was used in later work, initially achieving a spin-flip efficiency of $(86.5 \pm 0.5)\%$ (Blinov *et al* 2000), which later improved to 99.6% (Blinov *et al* 2002) and more recently to 99.9% (Morozov *et al* 2003a).

RHIC is also equipped with an rf dipole, but it has not been used much. Some limited studies to use the rf dipole as a spin-flipper were reported by Bai *et al* (2002). The rf dipole is located at a point in RHIC where the stored polarization direction is vertical. (See figure 1, where the device is labelled 'ac dipole'.) The spin-flipper is in a region common to both RHIC rings, but can be configured to flip the spins in the two beams independently. We have seen that for a ring with two Snakes the spin tune is $\frac{1}{2}$. Basically, the spin tune in one ring is moved slightly away from $\frac{1}{2}$, and the spin-flipper is made to resonate with the spins in that beam only. The spins in the other beam merely experience non-resonant high-frequency kicks. The spin-flip efficiency reported was 66%, but this is still preliminary work.

Spin-polarized deuteron beams have also been circulated in the IUCF Cooler, where the first resonant spin-flipping of a vertically polarized deuteron beam was reported (Morozov *et al* 2003b), achieving a spin-flip efficiency of $(94.2 \pm 0.3)\%$. The spins were flipped using an rf solenoid.

Resonant spin-flipping has also been performed using a beam of polarized electrons, at the SHR at MIT-Bates, with an efficiency of $(94.5 \pm 2.5)\%$ (Morozov *et al* 2001). This work employed an air-core rf dipole. The spins were horizontally polarized, because the SHR is equipped with one Siberian Snake, consisting of two solenoids in series. It is expected that the use of more powerful ferrite core rf dipole kickers will improve the spin-flip efficiency.

Resonant spin-flipping in a ring with one Snake is particularly interesting, since the design polarization lies in the *horizontal* plane. Basically, the Froissart–Stora formula was derived on the assumption that the asymptotic polarization direction (far from resonance) is vertical, and that the resonance driving term lies in the horizontal plane, i.e. orthogonal to the direction of the asymptotic polarization. For a ring with one Snake, the asymptotic polarization direction and the perturbing resonance driving term both lie in the horizontal plane. Nevertheless, with some caveats, the Froissart–Stora formula is still applicable.

The basic theory of resonant spin-flipping in a ring with a single approximately full-strength Snake was presented by Koop and Shatunov (1995). Recall that the frequency of the spin flipper $f_{\rm rf}$ can be tuned to either $f_{\rm rf}^{+} = f_{\rm c}(\nu - 1)$ or the mirror frequency $f_{\rm rf}^{-} = f_{\rm c}(1 - \nu)$, where, for simplicity, we treat only the fractional part of the spin tune in the above expressions. The first caveat is that for spin-flip to work it is necessary for the adiabatic condition to be satisfied, namely, $\epsilon^2/|\alpha| \gg 1$. However, in a ring with a full-strength Snake, $\nu = \frac{1}{2}$ and the resonant frequency and its mirror coincide. The adiabatic condition cannot be maintained for both resonance driving terms simultaneously. Hence, one employs a *nearly* full-strength Siberian Snake, so that the spin tune is not exactly $\frac{1}{2}$, so that the resonant frequency is separated from its mirror. Recall in section 20, when citing the measurements of synchrotron sidebands in a ring with a single Snake, it was stated that the measurements were made with a *nearly* full-strength Siberian Snake.

The next caveat is that, for resonant spin-flip to work, what is really required is that the rf perturbing field have a component orthogonal to the direction of the asymptotic polarization. Obviously, the two types of kickers used in practice provide either radial or longitudinal kicks. For either a radial or a longitudinal rf kicker, we decompose the kick into components parallel and perpendicular to the stable spin direction (i.e. $\boldsymbol{n}_0$) at the location of the kicker. The component orthogonal to $\boldsymbol{n}_0$ will accomplish the spin-flip. The Froissart–Stora formula is therefore applicable, except that instead of $|\epsilon|^2$, the amplitude square of the resonance driving

strength should be the orthogonal component

$$|\boldsymbol{\epsilon} \times \boldsymbol{n}_0|^2 = \boldsymbol{\epsilon} \cdot \boldsymbol{\epsilon}^* - (\boldsymbol{\epsilon} \cdot \boldsymbol{n}_0)\,(\boldsymbol{\epsilon}^* \cdot \boldsymbol{n}_0). \tag{24.29}$$

The Froissart–Stora formula is modified to

$$\frac{P_\mathrm{f}}{P_\mathrm{i}} = 2\,\mathrm{e}^{-\pi\,|\boldsymbol{\epsilon}\times\boldsymbol{n}_0|^2/(2|\alpha|)} - 1. \tag{24.30}$$

Of course, the kicks do have a time varying component, parallel to the stable spin direction $\boldsymbol{n}_0$, which will necessarily have an effect close to the moment of resonance passage. However, as evidenced from the work by Blinov *et al* (2002) and Morozov *et al* (2003a) this is not significant, and one can achieve a spin-flip efficiency in excess of 99%. The Froissart–Stora formula was so employed for work at the IUCF Cooler by Blinov *et al* (1998, 2000, 2002) and Morozov *et al* (2003a) and at SHR by Morozov *et al* (2001), in all cases to analyse the performances of spin-flippers.

24.7. Spin response function

It is possible for a spin-flipper to excite *orbital* oscillations, e.g. vertical betatron oscillations in a planar ring, and the perturbing fields induced by those oscillations then tip the spins, leading to decoherence. This is an indirect coupling of the spin-flipper to the spins. The overall function which relates the rotation of a spin to the field of the rf kicker is called the *spin response function*. The basic theory was worked out by Kondratenko (1982) in the same paper which showed that a helical wiggler could act as a Snake. Under suitable circumstances, when the rf kicker frequency is close to the vertical betatron frequency (or some multiple thereof), the indirect coupling can greatly enhance the effect of an rf kicker on the spins.

The indirect term in the spin response function is, however, a double-edged sword. In the initial attempts to employ a spin-flipper to induce resonant depolarization at LEP (Arnaudon *et al* 1992), it was found that the rf kicker could indeed excite the vertical betatron oscillations, but this caused large fluctuations in the electron beam position, distorting the readings at the polarimeter. The excitation of the vertical betatron oscillations can, therefore, have unwanted side-effects.

24.8. Ergodicity

For a polarized proton beam, the orbital motion is *not* ergodic. Hence, if two resonances are crossed in succession (and one or both are intrinsic resonances, with a distribution of particle amplitudes), it is possible in some cases for the polarization to *increase* upon crossing the second resonance. We believe that cases where the polarization was partially restored after passage through a second resonance have been observed, although we cite no examples.

24.9. Partial Snakes

24.9.1. General remarks. The companion paper MSY1 reviewed full-strength Snakes. However, partial Snakes are also useful devices. Consider a solenoid in a synchrotron, with a spin rotation angle of $\lambda_\mathrm{s}\pi$, where $0 < \lambda_\mathrm{s} < 1$. The solenoid is effectively a δ-function longitudinal spin rotator, because its length is very short, when compared with the circumference of the synchrotron. Its spin precession vector is

$$\boldsymbol{W}_\mathrm{sol} \equiv W_\mathrm{sol}\,\boldsymbol{e}_2 = \lambda_\mathrm{s}\pi\;\delta_\mathrm{p}(\theta - \theta_\mathrm{s})\,\boldsymbol{e}_2, \tag{24.31}$$

where θ_s is the azimuthal location of the solenoid and δ_p is the periodic δ-function. We have stated all of the above, earlier in this paper, but here we consider the specific application of these

ideas to the acceleration of nonradiatively polarized beams—this was in fact the motivation to use partial Snakes in accelerators in the first place. Decomposing $W_{\rm sol}$ into Fourier harmonics yields

$$W_{\rm sol} = \frac{\lambda_{\rm s}}{2} \sum_{k=-\infty}^{\infty} {\rm e}^{{\rm i}k(\theta-\theta_{\rm s})}. \tag{24.32}$$

This is, effectively, a sum of imperfection resonance driving terms, all with the same imperfection resonance strength $\lambda_{\rm s}/2$, at every integer k. Adding this to the imperfection resonance strengths already present in the machine, the Froissart–Stora formula for crossing the resonance line $G\gamma = k$ becomes

$$\frac{P_{\rm f}}{P_{\rm i}} = 2\exp\left\{-\frac{\pi}{2\alpha}\left|\frac{\lambda_{\rm s}}{2}\,{\rm e}^{-{\rm i}k\theta_{\rm s}} + \epsilon_k\right|^2\right\} - 1, \tag{24.33}$$

where ϵ_k is the (complex) strength of the imperfection resonance due to the rest of the machine. Recall, α is the rate of increase of $G\gamma$ per turn. Roser (1989) showed that if

$$\lambda_{\rm s} \gg 2|\epsilon_k| + \sqrt{\frac{8\alpha}{\pi}} \tag{24.34}$$

then there would be a reversal of the polarization with negligible loss of polarization.

The implications of this observation are profound: it is *not* necessary to employ complicated resonance correction and crossing schemes; one just installs a partial Snake and accelerates *without* correction. Of course, the intrinsic resonances must still be corrected. A partial Snake does not generate Fourier harmonics at the frequencies (tunes) of the intrinsic resonances.

The above example of a solenoid partial Snake is a working, practical idea, but not the only possibility. A helical field (transverse field) partial Snake was recently installed and operated at the AGS in spring 2004.

24.9.2. Resonance correction at VEPP-2M. Historically, the initial recognition of the partial Snake idea, and experimental usage thereof, was made in 1976 at VEPP-2M (Derbenev *et al* 1977). VEPP-2M is an e^+e^- collider with an operating beam energy of 180–700 MeV. The partial Snake strength was about 5%. The imperfection resonance in question was at $a\gamma = 1$ ($E = 440$ MeV). The Novosibirsk team demonstrated the safe crossing of the resonance with the partial Snake on and full depolarization with the partial Snake off. The ring contained one detector, CMD-2 with a solenoidal field of 1 T, and two compensating solenoids with 3.5 T (see figure 2). In the initial experiment, a room-temperature air core solenoid was installed in the ring. After the first experiment, the partial Snake technique was employed many times to avoid depolarization from the $a\gamma = 1$ imperfection resonance. In that later work, to arrange the partial Snake option, the compensating solenoids of the CMD-2 detector were detuned for the resonance crossing and then returned. There were problems with intrinsic betatron resonances (the values of the betatron tunes were $Q_x = 3.06$ and $Q_y = 3.09$) at $a\gamma = Q_y - 2$ and $a\gamma = 4 - Q_y$. The intrinsic resonances were crossed by two methods: (i) a quick change in the gradient steering coils in the quadrupoles (to 'jump' the betatron tunes) and (ii) fast energy change by a pulse switch of a shunt to the dipoles power supply (energy jump about 20 MeV in 0.05 s), i.e. rapid crossing of a resonance.

The use of partial Snakes is not so simple, however. Note that when we wrote in (24.34) that the Fourier harmonic from the partial Snake has to be much greater than that from the ring, we tacitly assumed that the ring's imperfection harmonic ϵ_k was *one* entity. As we know by now, each central resonance is in fact surrounded by a set of synchrotron sidebands, whose strengths

are given by Bessel functions. If the partial Snake strength is not large enough, the adiabatic condition may not be satisfied at some of the sideband frequencies. In that case, the beam will suffer depolarization during passage across those sideband resonances. The partial Snake strength must therefore be large enough, so that the resonance width from the Fourier harmonic of the partial Snake, i.e. λ_s, covers all the relevant low-order sidebands. The first sideband which is not covered by the partial Snake-induced resonance should be so weak that it does not cause serious depolarization.

In the work at VEPP-2M, we stated that the partial Snake strength was 5%. Hence, the sidebands had to be compensated (weakened) by adjusting the rf system. A specific dip of the rf-voltage was done to decrease the synchrotron tune to 0.007, aiming that only the 7th order sideband could appear ($\lambda_s = 0.05$, $7 \times Q_s = 0.049$), and its resonant harmonic was 10^{-4} less than the main imperfection resonance strength.

24.9.3. Partial snakes for polarized proton beams. The first successful demonstration of the use of a partial Siberian Snake to accelerate a polarized proton beam through a depolarizing resonance, was that of a 10% Snake (a solenoid) at the IUCF Cooler (Blinov *et al* 1994). A beam of polarized protons was accelerated through the $G\gamma = 2$ imperfection resonance without loss of polarization. Increasing the Snake strength to 20% or 30%, however, also shifted the location of the intrinsic resonance $G\gamma = 7 - Q_y$ into the energy range of the beam, causing some depolarization.

Arguably the most extensive, and most successful, use of partial Snakes has been at the AGS. A 5% solenoid partial Snake (9° spin rotation) was installed in the AGS (Huang *et al* 1994) and was used to successfully cross 18 imperfection resonances, although there was some depolarization due to intrinsic resonances. This was a warm solenoid, whose field was ramped during the AGS energy ramp to maintain a 5% partial Snake strength at all energies. If the solenoid were run at a fixed field (to achieve a 5% strength at top energy) it could be as much as a 25% partial Snake at low energy in the AGS. However, a solenoid induces transverse x–y betatron coupling and at a partial Snake strength of 25%, the solenoid induced too much betatron coupling in the AGS. We shall review the use of partial Snakes at the AGS in more detail in section 26.

As for synchrotron sidebands, when crossing imperfection resonances at the IUCF Cooler or the AGS, we have not found evidence in the literature, and via personal communications, that the synchrotron sidebands matter. The synchrotron tune in proton synchrotrons is much smaller than in electron synchrotrons, and so the sidebands are evidently clustered so closely to the parent that a 5% partial Snake (e.g. at the AGS) is able to satisfy the adiabatic condition without special consideration for the sidebands. For example, $Q_s \lesssim 0.001$ at the IUCF Cooler. The value of the synchrotron tune is similar at the AGS. A 5% or a 10% partial Snake would cover all the sidebands up to the fiftieth order or more.

24.10. Polarized deuterons: tensor polarization

The spectrum of the depolarizing resonances (imperfection and intrinsic) is the *same* for both polarized protons and deuterons. This is because depolarization is caused by a decoherence of the *spins*, and it does not matter if the spin value is $\frac{1}{2}$ or 1 or higher. The magnetic moment anomaly of a deuteron is $G_d \simeq -0.1427$, hence the value of $G\gamma$ is negative. This is of course completely irrelevant to the resonance spectrum. What is significant is that $G_p/G_d \simeq -12.5$ and also $m_p/m_d \simeq 1/2$, hence the energy spacing of the imperfection resonances is roughly a factor of 25 greater for deuterons. This greatly reduces the number of imperfection resonances which must be crossed, when accelerating polarized deuterons.

The asymptotic vector and tensor polarizations, after crossing an isolated resonance, are

$$\begin{aligned}\frac{P_{3\mathrm{f}}}{P_{3\mathrm{i}}} &= 2\mathrm{e}^{-\pi\epsilon^2/(2|\alpha|)} - 1,\\ \frac{P_{33\mathrm{f}}}{P_{33\mathrm{i}}} &= \frac{3}{2}(2\mathrm{e}^{-\pi\epsilon^2/(2|\alpha|)} - 1)^2 - \frac{1}{2}.\end{aligned} \tag{24.35}$$

Perhaps more clearly than in the case with protons and electrons, the acceleration of deuterons illustrates the wisdom of writing $|\alpha|$ rather than α in the exponent. Note that

$$-\frac{1}{2} \leqslant \frac{P_{33\mathrm{f}}}{P_{33\mathrm{i}}} \leqslant 1. \tag{24.36}$$

Starting from a tensor polarization of $P_{33\mathrm{i}} = 1$, it is impossible to obtain $P_{33\mathrm{f}} = -2$. However, starting from $P_{33\mathrm{i}} = -2$, it *is* possible to obtain $P_{33\mathrm{f}} = 1$.

This raises the question: starting from $P_{33\mathrm{i}} = -2$, why can we not run the system forward to obtain $P_{33\mathrm{f}} = 1$, and then run it in reverse through the same resonance, to recover $P_{33} = -2$? In principle, we could. The spins evolve under a Hamiltonian system, and the spin motion is reversible. Even for the vector polarization, we could run the system backwards and recover the full initial polarization. All of the above formulae, for both the vector and tensor polarizations, assume implicit statistical averages. In the absence of a true stochastic mechanism, we are slapping statistical averages on top of a Hamiltonian system, which may be reasonable but it is not guaranteed to always be valid.

The first acceleration of a polarized deuteron beam was at the ZGS (Parker *et al* 1979). We briefly review the acceleration of polarized deuterons at the KEK-PS (Booster and Main Ring) below (Sato *et al* 1997). There are no depolarizing resonances for deuterons in the KEK-PS Booster. There is one intrinsic resonance $G\gamma = -8 + Q_y$ and one imperfection resonance $G\gamma = -1$ at the KEK-PS Main Ring. The polarized deuteron beam was injected and accelerated in two patterns:

- First, the beam was injected at 294 MeV and accelerated up to 10.2 GeV and then decelerated to 2 GeV, extracted and the vector and tensor polarizations measured at 2 GeV. (All energies are kinetic energies.) The beam, therefore, crossed the weak intrinsic resonance $G\gamma = -8 + Q_y$ twice, on the way up and again on the way down, without any resonance corrections being applied.
- Second, the beam was injected at 294 MeV and accelerated up to 2 GeV and extracted and the vector and tensor polarizations were measured as above. Hence, no resonances were crossed.

The results indicate that there was no difference in polarization between the two scenarios (for either the vector or the tensor polarization), indicating that the depolarization from the intrinsic resonance $G\gamma = -8 + Q_y$ was indeed small.

The first reported resonant spin-flip of a polarized deuteron beam was claimed by Morozov *et al* (2003b), in studies at the IUCF Cooler. The experimenters displayed graphs of the values of the vector and tensor polarizations $P_{3\mathrm{f}}$ and $P_{33\mathrm{f}}$. The data agree with (24.35), with use of an empirical modification. Morozov *et al* (2003b) write

$$\begin{aligned}\left.\frac{P_{3\mathrm{f}}}{P_{3\mathrm{i}}}\right|_{\mathrm{emp}} &= (1+\eta_{\mathrm{v}})\mathrm{e}^{-\pi\epsilon_{\mathrm{v}}^2/(2|\alpha|)} - \eta_{\mathrm{v}},\\ \left.\frac{P_{33\mathrm{f}}}{P_{33\mathrm{i}}}\right|_{\mathrm{emp}} &= \frac{3}{2}[(1+\eta_{\mathrm{t}})\mathrm{e}^{-\pi\epsilon^2/(2|\alpha|)} - \eta_{\mathrm{t}}]^2 - \frac{1}{2},\end{aligned} \tag{24.37}$$

where ϵ_{v} and η_{v} are the vector polarization resonance strength and spin-flip efficiency, respectively, and ϵ_{t} and η_{t} denote the corresponding quantities for the tensor polarization.

The measurements indicate that a single value of ϵ, and also a single value of η, fit the spin-flipping of both the vector and tensor polarizations of the deuteron beam at the IUCF Cooler. In fact, the structure of the angular momentum operators dictates that this must be so. Nevertheless, such details must be tested. Whatever mechanism originates the resonance ϵ and/or the spin-flip efficiency η, it applies to the *spins* and not to a specific spherical harmonic.

24.11. Figure-of-eight ring

We remark, in passing, on an alternative idea which has been proposed to avoid resonance crossing. A new Cooler Synchrotron has been proposed at the Research Center for Nuclear Physics (RCNP) in Osaka (Sato 1997). The synchrotron will accelerate beams of polarized protons to a maximum momentum of $5.86\,\mathrm{GeV\,c^{-1}}$, for use in nuclear physics experiments. The ring geometry will be a figure-of-eight, so that the overall spin precession angle after a complete circuit will be zero, independent of the beam energy. This will avoid all the intrinsic resonances and all of the imperfection resonances, except for $\nu_{\mathrm{spin}} = 0$ (it does not make sense to write '$G\gamma = 0$'). It is, therefore, only necessary to correct the one imperfection resonance. It has been planned to rectify the above resonance using a partial Siberian Snake. Spin tracking studies have indicated that the design looks promising (Hatanaka *et al* 1997).

25. Acceleration of nonradiatively polarized beams II

25.1. General remarks

This section describes some of the experimental work to accelerate polarized beams in synchrotrons. The list of accelerators below is by no means exhaustive. Furthermore, the partial Snake work at the AGS is discussed separately, in section 26. We begin with a brief description of some of the early experimental work, from the 1970s and 1980s, on the acceleration of polarized proton beams at four facilities, namely, the ZGS, AGS, SATURNE-II and KEK-PS, in that order. See also the (very brief) listing of the early experimental work on the acceleration of polarized proton beams to high energy in section 6.

The ZGS demonstrated the first acceleration of polarized proton beams to high energy in a synchrotron. The maximum proton momentum was $12.5\,\mathrm{GeV\,c^{-1}}$. The tune jumping technique was used to cross the intrinsic resonances (imperfection resonances were negligible in the ZGS). The second machine is the AGS. Being a strong-focusing synchrotron, the quadrupole field gradients (hence the strengths of the depolarizing resonances) were much stronger at the AGS than at the ZGS. In particular, although the imperfection resonances were negligible in the ZGS, they were not in the AGS, hence there were many more resonances to cross when accelerating polarized protons in the AGS. The third machine is SATURNE-II. Recall that the Froissart–Stora formula was motivated by the crossing of depolarizing resonances in the original weak-focusing SATURNE synchrotron. The ring was later rebuilt as a strong-focusing synchrotron SATURNE-II. A polarized proton programme at SATURNE-II was envisaged from the outset, as well as the acceleration of other polarized species such as deuterons. This is one of the rare examples where the machine lattice was designed with the requirements of polarized beams in mind. The spin dynamics at SATURNE-II displayed some noteworthy features which will be reviewed below. The fourth is the KEK-PS, also a strong focusing synchrotron, where the first acceleration and transfer of a polarized proton beam in a cascaded system was accomplished (Booster to PS Main Ring). Note that a Booster synchrotron was later constructed as a pre-accelerator to the AGS, making

it also a cascaded system, but this was done later, in the 1990s (see figure 1). In its own turn the AGS is now an injector to RHIC.

To avoid repeating all the same ideas on tune jumping and resonance correction, for every machine, we present a case study of the resonance crossings at *one* synchrotron. We also select it to be a modern facility, where the use of polarized beams is an active part of the experimental physics programme. The complex is ELSA, the Electron Stretcher Accelerator at the University of Bonn. ELSA accelerates polarized *electrons* to a maximum energy of 3.5 GeV. The presence of synchrotron radiation has important consequences not found in proton synchrotrons. In addition, a particularly nice accelerator physics study was carried out at the KEK-PS, on the effects of the orbital chromaticity on the synchrotron sidebands of an intrinsic resonance. This is a direct demonstration of the effects of nonlinear orbital motion on the spin motion (the betatron oscillations of an intrinsic resonance are linear dynamical orbital motion). To our knowledge, the chromaticity study has not been repeated at other accelerators.

25.2. Early work at selected high energy proton synchrotrons

25.2.1. ZGS. The ZGS was a weak-focusing synchrotron. Polarized protons were accelerated at the ZGS until the machine ceased operations in 1979 (Khoe *et al* 1975, Cho *et al* 1976). The imperfection resonances in the ZGS were fairly weak and could be ignored. However, the intrinsic resonances were strong, and almost total depolarization resulted if the intrinsic resonances were not corrected. The ZGS had a fourfold symmetry (superperiodicity $P = 4$), with a partial eightfold symmetry. Hence, the intrinsic resonances of the form $G\gamma = 8k \pm Q_y$ were stronger than those of the form $G\gamma = 8k + 4 \pm Q_y$. There were a total of 11 intrinsic resonances up to the full momentum of the ZGS of 12.5 GeV c^{-1}. The intrinsic resonances were crossed via the tune jump technique. The tune jump technique was pioneered at the ZGS (contemporaneously with tune jumps for intrinsic resonances at VEPP-2M by Derbenev *et al* (1977) mentioned earlier in section 24). Two pulsed quadrupoles were used to shift the value of the vertical betatron tune rapidly (rise time of 20 μs), relaxing to the unperturbed value after several ms. The polarized proton source delivered a polarization level of 75–80%. Khoe *et al* (1975) reported that a polarization level of $(73 \pm 8)\%$ was delivered at a momentum of 6 GeV c^{-1}, and about $(55 \pm 15)\%$ polarization at a momentum of 8.5 GeV c^{-1}. A later paper (Spinka *et al* 1983) gives information which was used to correct the beam polarization values used in experiments after the fact. In particular, it indicates that there was some depolarization at 1.2 and 1.75 GeV, when previously it was thought there would be none below 3 GeV.

The ZGS complex also demonstrated, in 1978, the first ever acceleration of a high-energy polarized deuteron beam (Parker *et al* 1979). By 1979, polarized deuterons had been accelerated to the ZGS top momentum of 12 GeV c^{-1}. Crabb *et al* (1979) reported the results of an elastic polarized n–p scattering experiment, using a beam of 6 GeV c^{-1} polarized *neutrons* (obtained by the breakup of the 12 GeV c^{-1} polarized deuterons from the ZGS) incident on a fixed polarized proton target. The neutron polarization was 53% and the fixed-target proton polarization was 75%. Both spins were oriented perpendicular to the n–p scattering plane.

25.2.2. AGS. After the ZGS ceased operations, a polarized proton programme was initiated at the AGS. Being strong focusing, the quadrupole focusing gradients were larger in the AGS, and the imperfection resonances were too strong to be ignored. Theoretical calculations of the resonance strengths and development of correction techniques were performed (Courant and Ruth 1980). Most of the results below are taken from Khiari *et al* (1989), who reported the successful acceleration of polarized protons to a momentum of 22 GeV c^{-1}. Consult that work for references to earlier work on polarized proton acceleration in the AGS. The paper

also discussed the experimental measurements of spin-flip effects in elastic pp scattering using the extracted polarized proton beam, as well as the polarized proton source, but our interest is in accelerator physics. The AGS has a superperiodicity of $P = 12$. A total of 95 correction dipoles were employed to correct the strengths of the imperfection resonances (8 dipoles per superperiod with one dipole missing). This was an arduous task. The beam was accelerated just before a resonance, extracted and its polarization measured. The beam energy was then increased to cross the imperfection resonance and the corrector settings adjusted to optimize the final polarization level. For acceleration up to 22 GeV c^{-1}, a total of 39 imperfection resonances had to be crossed; the above procedure had to be performed for each one. Six intrinsic resonances also had to be crossed during the energy ramp. The intrinsic resonances were crossed using pulsed quadrupoles to induce tune jumps. There were 12 pulsed quadrupoles, one in each superperiod. However, the requisite power supplies were expensive and only 10 could be purchased at the time of the work reported by Khiari *et al* (1989), hence 2 pulsed quadrupoles were unused.

The polarized proton source delivered approximately 75% polarization. Approximately 10% was lost between injection and 13.3 GeV c^{-1}, where $P = (65 \pm 3)\%$. There was a depolarization of about 20% near 14 GeV c^{-1}, attributed to an interference between the $G\gamma = 36 - Q_y$ intrinsic resonance and the $G\gamma = 27$ imperfection resonance ($Q_y \simeq 8.75$ in the AGS). The polarization at 16.5 GeV c^{-1} was $(44 \pm 4)\%$ and at 18.5 GeV c^{-1} it was $(47 \pm 4)\%$. There was no evidence of significant polarization loss from 14 GeV c^{-1} to 22 GeV c^{-1}, where the polarization was $(42 \pm 4)\%$.

It was only after some ten odd years that new ideas of partial Snakes and adiabatic excitation of coherent betatron oscillations, to be discussed in section 26, were able to overcome the arduousness of the above resonance correction and jumping procedures.

The intrinsic resonance $G\gamma = 60 - Q_y$ is very strong. Note that the AGS superperiodicity is $P = 12$ but there is a weaker symmetry of $P = 60$. That resonance overlaps with the imperfection resonance $G\gamma = 51$ (recall $Q_y \simeq 8.75$). The above intrinsic resonance occurs at an energy of roughly 26.8 GeV and sets an effective upper limit on the maximum energy of the polarized proton acceleration in the AGS. The extraction and delivery of polarized protons to RHIC is performed at $G\gamma = 46.5$, below the energy of this resonance.

The AGS has not, to date, accelerated polarized ion species other than protons. There are plans to accelerate polarized deuterons as well as polarized ^{3}He for delivery to RHIC.

25.2.3. SATURNE-II. The material below is mainly from Aniel *et al* (1985) and Maggiora (1995). (See also Grorud *et al* (1982).) Polarized protons were accelerated at SATURNE-II starting around 1980. The ring also accelerated polarized deuterons and ^{6}Li. Polarized neutrons were produced by the breakup of polarized deuterons on a Be target. We shall only discuss the acceleration of polarized protons and, very briefly, polarized deuterons. The operating range of SATURNE-II spanned the six imperfection resonances $G\gamma = 2$–7 (maximum proton kinetic energy of about 3 GeV). The ring superperiodicity was 4 so there were two intrinsic resonances in this spin tune interval, namely,

$$G\gamma = Q_y, \qquad G\gamma = 8 - Q_y. \tag{25.1}$$

The value of the vertical betatron tune was $Q_y = 3.6$. As already stated, SATURNE-II was a strong-focusing synchrotron, and so the depolarizing resonance strengths were much stronger than in a weak-focusing synchrotron like the ZGS. Because of this fact, the imperfection and intrinsic resonances were mainly crossed using the adiabatic spin-flip technique. The delivered proton polarization level was as much as 80% up to the top energy. Polarization levels of 90% were also recorded on some occasions (basically the minimum extraction energy).

In fact, SATURNE-II had two extraction channels so that beams could be delivered at two different energies to two different experiments. From the point of view of this paper, the acceleration of the polarized proton beams at SATURNE-II was notable for three features. To phrase the matter in a positive manner, the polarization was a sensitive probe of the machine structure:

- Depolarization was observed from the betatron resonances $G\gamma = 7 - Q_y$ and $G_\gamma = 1 + Q_y$. These resonances were 'unpredictable' in the sense that they were due to lattice imperfections, which broke the perfect superperiodicity of the machine. Hence, the resonance strengths were not reproducible on startup after a machine shutdown. Empirical correction methods had to be applied to overcome the depolarization from these resonances.
- After acceleration to the desired top energy, the beam was held at 'flattop' (i.e. a constant energy) for so-called 'slow extraction'. Most experiments prefer the beam to be dribbled out more or less continuously (with a concomitant lower peak current) over a period of one to a few seconds, rather than to receive the whole proton bunch in one pulse. During the flattop, weaker resonances have sufficient time to act in concert with the spin precession, leading to depolarization. In particular, the *horizontal* betatron tune was set to $Q_x = 11/3$ for slow extraction at SATURNE-II. Depolarization from the resonance $G\gamma = Q_x$ was clearly observed if the beam was extracted at a kinetic energy of (980 ± 5) MeV. The observation of the resonance $G\gamma = Q_x$ at flattop at SATURNE-II is a counterpart to the resonances in the polarization of stored e^+e^- beams, which are held at a fixed energy for several hours.
- The crossing of the lowest energy imperfection resonance $G\gamma = 2$ displayed unexpected behaviour. The Froissart–Stora formula failed badly for this resonance. Theory and simulations eventually demonstrated that synchrotron oscillations were responsible for the deviations from the Froissart–Stora formula. Because of the synchrotron oscillations and the maximum achievable rate of acceleration, some particles crossed this resonance line multiple times. Adiabatic spin-flip could not be used to cross this resonance. Instead the resonance driving term was cancelled using corrector magnets.

As for polarized deuterons, recall that SATURNE-II was designed with the acceleration of polarized beams in mind. Hence, the ring was designed so that the resonance strengths would be strong enough for the complete spin-flip of polarized protons but weak enough to avoid any depolarization for deuterons. Hence, there were no strong depolarizing resonances for deuterons in the operating range of SATURNE-II. The first resonance $G\gamma = Q_y - 4$ was out of the energy range of the machine for the standard operating tune of $Q_y = 3.607$. The delivered tensor polarization was in the range of 90–75% (minimum and maximum extracted beam energy, respectively) and about 60% for the vector polarization.

25.2.4. KEK-PS. The KEK-PS was actually a cascaded system of two strong-focusing synchrotrons, a Booster and a Main Ring, and depolarizing resonances had to be overcome in each one. Furthermore, the polarized beam had to be transferred from the Booster to the Main Ring without suffering losses in the transfer process. A schematic view of the accelerator layout was shown in figure 12.

Most of the material below is from Sato (1988) and Sato *et al* (1988). In the Booster, two pulsed quadrupoles were installed to jump the intrinsic resonances, and two pulsed dipoles to correct the closed orbit imperfections. The superperiodicities are $P = 8$ for the Booster and $P = 4$ for the Main Ring. The beam was accelerated to a kinetic energy of $T_{\max} = 500$ MeV in the Booster. One imperfection resonance $G\gamma = 2$ at $T = 108$ MeV and three intrinsic

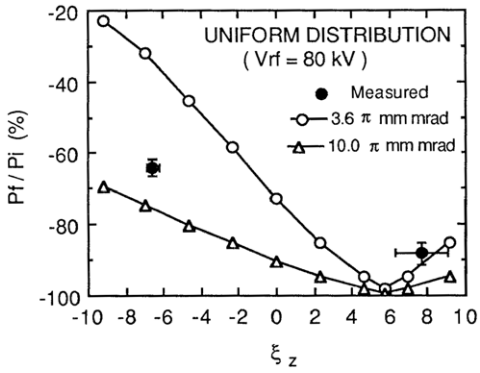

Figure 40. Dependence of the ratio of the final to the initial polarization on the vertical chromaticity at the KEK-PS Booster, for crossing of the $G\gamma = Q_y$ intrinsic resonance. From Toyama *et al* (1989).

resonances were crossed. One of the intrinsic resonances is a coupling resonance given by the horizontal betatron tune $G\gamma = Q_x$ at $T = 190$ MeV. Approximately 8% relative polarization loss was expected in crossing this resonance as opposed to negligible polarization loss from the crossing of the other resonances. This demonstrates that the horizontal betatron oscillations cannot always be ignored during polarized beam acceleration. The resonance strengths in the Booster are tabulated by Sato *et al* (1988). Because the Booster was a combined-function strong-focusing synchrotron, which included a strong sextupole field component to correct the chromaticity, some depolarization arose from higher order resonances (not reviewed here).

In the KEK-PS Main Ring, 4 pulsed quadrupoles were used to jump the intrinsic resonances and 28 corrector dipoles were used to correct the imperfection resonances. There were several strong intrinsic resonances in the Main Ring; however, there were no coupling resonances.

This brings us to some beautiful accelerator physics. The effects of the synchrotron oscillations could not be ignored, when using an adiabatic spin-flip to cross the intrinsic resonance $\nu = Q_y$, in the KEK-PS Booster. Reducing the rf voltage, to reduce the synchrotron tune, led to approximately 50% beam loss which was unacceptable. A clever observation was made, which was to utilize the *chromaticity* to correct the effects of the synchrotron oscillations, presented first at a conference (Hiramatsu *et al* 1989) and later published formally (Toyama *et al* 1990).

We reviewed the basic formulae of synchroton sideband resonances in section 20 (see (20.33) etc). The basic idea is to use the orbital tune modulation, via the chromaticity, to cancel that from the spin tune. The relevant criterion was given in (20.36):

$$\xi_{x,y} - G\gamma_0\beta_0^2 = 0. \tag{25.2}$$

The value of the vertical chromaticity can be adjusted by tuning the sextupoles. As we pointed out, this is an explicit example of nonlinear orbital dynamics influencing the spin dynamics. A study was performed to test the above idea. The results are shown in figure 40. The value of the vertical betatron tune used in the studies was $Q_y \simeq 6.25$, the resonance was $G\gamma_0 = Q_y$ and $\beta_0 \simeq 1$. The horizontal axis shows the value of the vertical chromaticity (the authors employed the notation ξ_z). The curves are theoretical calculations of $P_\mathrm{f}/P_\mathrm{i}$ (final to initial polarization) for two different values of the vertical betatron emittance, showing that one can achieve $P_\mathrm{f}/P_\mathrm{i} = -1$ at $\xi_y = G\gamma_0\beta_0^2 \simeq 6.25$. Two experimental data points are shown. Unfortunately, due to lack of time more data could not be taken and the experiment was never repeated.

The polarization attained at the KEK-PS Booster and Main Ring was reported by Sato (1988). The quoted values supersede those by Sato *et al* (1988), because of an

improvement in the calibration of the analysing power of the polarimeter. As we have explained, hadron polarimetry is phenomenological and is hampered by the lack of accurately calculable interactions. The polarized proton source delivered a polarization level of about $(55 \pm 5)\%$. Approximately 75% of the polarization was preserved in the Booster, with a polarization of $(44.2 \pm 2)\%$ at a kinetic energy of 500 MeV. The maximum energy of the KEK-PS Main Ring was 12 GeV. A polarization level of 25% was achieved at 5 GeV and 5% in a study up to 7.6 GeV. The particle physics experiments were performed at an energy of 3.5 GeV, where the polarization was $(38.4 \pm 1.5)\%$.

We reviewed the acceleration of polarized deuterons at the KEK-PS earlier (Sato *et al* 1997), when discussing the extension of the Froissart–Stora formula to the tensor polarization of spin 1 particles.

25.3. Case study: ELSA

ELSA is the *EL*ectron *S*tretcher *A*ccelerator at the University of Bonn. The term ELSA denotes the whole facility consisting of an electron gun (thermionic or polarized), linac, booster and stretcher ring. It is a University facility, and University students participated in the design and construction of the accelerator and experimental facilities. ELSA differs from most of the other synchrotrons, which accelerate nonradiatively polarized beams, in that it accelerates polarized *electrons*. The electron beam emits synchrotron radiation throughout the acceleration process. The stretcher ring receives electron bunches (500 MHz structure) from a booster synchrotron and accelerates them to an energy of 0.5–3.5 GeV. After acceleration, this bunched beam is extracted over several seconds leading to a continuous beam (i.e. on a timescale larger than a few nanoseconds, because the 500 MHz structure still exists) for delivery to fixed target experiments for nuclear physics. ELSA also operates part-time as a dedicated synchrotron light source, but our interest is in its use as a synchrotron. A schematic figure of the ring and associated complex was shown in figure 13. Since 1997/98, experiments using polarized electrons have been carried out there. Indeed, the future nuclear physics programme at ELSA will rely mainly on polarized beams. A recent example achievement is the first measurement of the Gerasimov–Drell–Hearn sum rule for ^{1}H from 0.7 to 2.9 GeV (Dutz *et al* 2003). (The energy range below 800 MeV had previously been investigated elsewhere.) The GDH sum rule links the anomalous magnetic moment of the proton to the difference of the integrated cross-sections for the absorption of circularly polarized photons with spins parallel and antiparallel to that of the (longitudinally polarized) proton. Circularly polarized photons were produced by bremsstrahlung from longitudinally polarized electrons in a thin metal radiator foil (Cu 15 μm), at six electron beam energy settings of 1.0, 1.4, 1.9, 2.4, 2.9 and 3.0 GeV. The GDH experiment ran from 1998 to 2002. More recent experiments, which we shall not describe in detail, are the Crystal Barrel and TAPS (studies of photoproduction of meson resonances).

A polarized electron source is used when operating the ELSA facility in a synchrotron mode. In the study we report below, which took place in 1997/8, polarized electrons were injected at 1.2 GeV and accelerated to 2.1 GeV (Nakamura *et al* 1998, Steier *et al* 1998). We shall describe more recent work (after 1998) later in this review. It had previously been found that the imperfection resonances $a\gamma = 1$ and $a\gamma = 2$ in the booster ring are weak, but strong depolarization occurs in the booster at the resonance $a\gamma = 3$ at 1.32 GeV (recall that for electrons $a\gamma$ increases by one unit every 440 MeV). There was not enough space in the booster to install equipment for resonance correction. Hence, the injection energy into the stretcher ring of ELSA had to be kept below 1.32 GeV. A total of five depolarizing resonances must be crossed in this energy interval: two imperfection resonances ($a\gamma = 3$ and 4) and three intrinsic resonances ($a\gamma = Q_y - 2$, $8 - Q_y$ and Q_y). The stretcher ring superperiodicity is $P = 2$.

Table 4. Resonance strengths at the ELSA stretcher ring up to 2.1 GeV. Reprinted from Nakamura *et al* (1998). Copyright (1998) with permission from Elsevier.

Resonance	E (GeV)	$\lvert\epsilon\rvert \times 10^5$ (calculated)	$\lvert\epsilon\rvert \times 10^5$ (measured)
$Q_y - 2$	1.14	6.8	4 ± 1
3	1.32	100	108 ± 3
$8 - Q_y$	1.5	3.9	9.4 ± 1
4	1.76	160	150 ± 20
Q_y	2.0	87	60 ± 20

The value of the vertical betatron tune used in the studies was $Q_y = 4.57$. (In later work, a value of 4.431 was used (Hoffmann *et al* 2001).) The resonances are tabulated in table 4.

The resonances are identified, along with their energies, including the experimentally observed and theoretically calculated resonance strengths. The value of the vertical betatron tune was also only approximately constant during the ramp. The imperfection resonance strengths were calculated using measured closed orbit values determined from beam based alignment. Note that the first resonance occurs at an energy of 1.14 GeV, which is below the normal injection energy of 1.2 GeV. The beam was injected at a lower energy of 1.1 GeV during some studies, thereby crossing this resonance. The experimental data were obtained by fitting to the Froissart–Stora formula. The theoretical values were also calculated without including synchrotron oscillations. There is good agreement between the experimental and theoretical numbers.

The actual experimental study was carried out in several steps. First, the beam was injected at 1.2 GeV and extracted at 1.27 GeV (to stay below the imperfection resonance at 1.32 GeV). No resonances are crossed in this small energy interval, hence no depolarization is expected, *if* the polarization direction is vertical at injection. In the first study, the final polarization was measured as a function of the spin orientation at the source. The direction of the injected polarization can be controlled by a solenoid in front of the linac, from which it enters the booster ring, before entering the stretcher ring. In later work, the solenoid was adjusted to ensure that the polarization direction was vertical at injection into the stretcher ring.

The electron beam polarization was measured after extraction from the ring as follows. The spins were rotated into the horizontal plane by a solenoid (superconducting, with a maximum integrated field of 12.5 T m), and then precessed to the longitudinal direction via two downstream bending magnets. The polarization was measured using a Møller polarimeter, to determine the counting rate asymmetry from collision against a target foil containing polarized electrons. The dipole magnets downstream of the solenoid rotate the spins through an energy-dependent angle, hence the polarization is not exactly longitudinal at the polarimeter. A matrix inversion is performed to determine the actual degree of polarization in the stretcher ring from the value measured at the polarimeter. A detailed description of the Møller polarimeter is given by Speckner *et al* (2004). The stretcher ring is also equipped with a Compton backscattering polarimeter (Doll *et al* 2002).

The next study was to accelerate the beam to an energy of 1.37 GeV so that only the imperfection resonance $a\gamma = 3$ was crossed during acceleration. The crossing speed was varied in the study. The ratio of the final to the initial polarization is plotted against $\epsilon/\sqrt{\alpha}$ in figure 41, where ϵ is the resonance strength and α is the (dimensionless) crossing speed. The ramping speed varied between 0.1 and 7 GeV s^{-1}. Note that there are two sets of data shown in the figure, one without any orbit correction of the resonance strength (ϵ_1, in the spin-flip domain) and one where harmonic orbit correction was employed to reduce the resonance strength (ϵ_2, non-flip domain). These data are an excellent validation of the Froissart–Stora formula in both regimes. By 1997/8 the Froissart–Stora formula had, of course, been validated

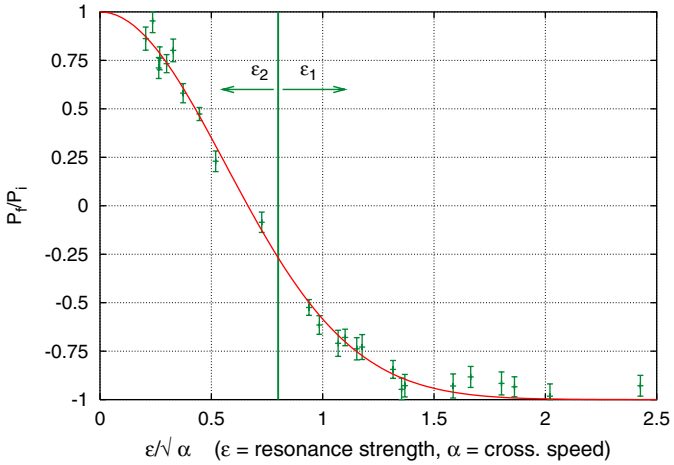

Figure 41. Ratio of the polarization before and after crossing the imperfection resonance $a\gamma = 3$, at the ELSA stretcher ring, as a function of the resonance strength and crossing speed. Reprinted from Nakamura *et al* (1998). Copyright (1998) with permission from Elsevier.

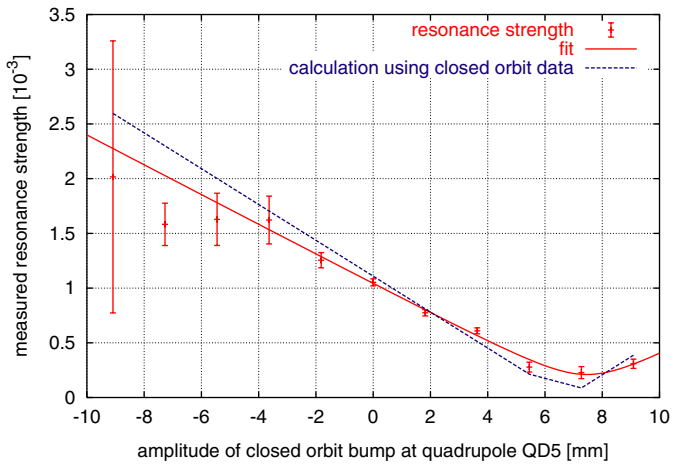

Figure 42. Measured and calculated resonance strength, as a function of the amplitude of the closed orbit bump, at the ELSA stretcher ring. Reprinted from Nakamura *et al* (1998). Copyright (1998) with permission from Elsevier.

many times at other accelerators, but figure 41 is a particularly clean demonstration. The harmonic correction was applied using two localized vertical closed orbit bumps. The phase of one of the bumps was coincidentally in phase with the imperfection resonance driving term. The amplitude of that bump is plotted on the horizontal axis of figure 42, while the vertical axis shows the calculated and measured imperfection resonance strengths. The theory and the data agree closely. In later work, nearly all the correctors in the ring were employed for harmonic orbit correction, to avoid saturation effects in the corrector dipoles (Hoffmann 2001).

The situation was different when crossing the imperfection resonance $a\gamma = 4$ at 1.76 GeV; it was not possible to fit the Froissart–Stora formula without also including significant

contributions from the synchrotron oscillations and synchrotron radiation. However, once that was done, the strength of the 'parent' term did agree with the theory. The experimental results were modelled, using the spin tracking programme called SPINDANCE, which was developed in-house (Hoffmann 2001). Because of the synchrotron radiation, transfer maps for each individual dipole in the ELSA stretcher ring were calculated, and the energy loss due to synchrotron radiation was calculated between the dipole maps. Using SPINDANCE gave results in good agreement with the measurements for the depolarization observed in the crossing of the imperfection resonance at 1.76 GeV ($a\gamma = 4$). To obtain agreement between the simulations and the data to this level of accuracy, a coherent synchrotron oscillation with an amplitude of about twice the equilibrium energy spread had to be included in the tracking. Such a coherent synchrotron oscillation has, in fact, been observed in the ELSA stretcher ring (Steier *et al* 1998). The amplitude used in the simulations is in approximate agreement with the amplitude measured in the longitudinal bunch spectrum. Coherent synchrotron oscillations have not been treated in the formal theory that we have presented in this paper. Even in the best case, about 15% polarization loss (25% relative polarization loss) was observed upon crossing this resonance. Overall, the injected polarization was 63% at 1.3 GeV and 45% was preserved in going up to a beam energy of 1.9 GeV.

The intrinsic resonance $a\gamma = Q_y$ at 2.0 GeV is very strong. Nearly two-thirds of the polarization was lost crossing this resonance. It is not possible to accelerate sufficiently and rapidly across this resonance. Adiabatic spin-flip (very slow crossing speed) also does not work because of the very strong spin diffusion due to the synchrotron radiation. Recall the work by Yokoya (1983c), reported in section 6, on modifications to the Froissart–Stora formula due to the effects of synchrotron radiation.

The above represents the status of polarized beam acceleration at ELSA up to 1997/8. In later work, two tune jumping quadrupoles were installed to jump across this resonance, and also all of the other intrinsic resonances (Steier *et al* 1999). The depolarization from the $a\gamma = Q_y$ resonance was reduced to less than 1%.

Hoffmann *et al* (2001) report the progress on the acceleration of polarized beams at ELSA since 1997/8. A new polarized electron source was installed, delivering a polarization of 80% with a quantum efficiency of 0.4% and a current of 100 mA. About 5% polarization is lost in the booster. The closed orbit imperfections in the stretcher ring were measured with a beam position monitor system at 28 observation points, and corrected using 19 vertical and 21 horizontal corrector magnets. The resulting imperfections were less than 0.2 mm (rms). The closed orbit was measured and corrected at the energy of each imperfection resonance and the corrector settings recorded. Hence, a total of five sets of settings were stored. Between the resonances a linear interpolation of the kick angles was performed. To achieve a good final polarization, it was also necessary to apply additional, empirically determined harmonic corrections. 'Empirically determined' means that the polarization of the extracted beam was measured with the Møller polarimeter for different settings of the harmonic corrections. In this way, a dynamic correction of all the imperfection resonances was achieved, resulting in negligible depolarization. The intrinsic resonances were all crossed via tune jumps using the pulsed quadrupoles. (It was not possible to increase the acceleration rate at ELSA to a sufficiently high value to cross the resonances without depolarization.) The tune jump was $\Delta Q_y = 0.1$ (maximum) with a rise time of 4–14 μs, and returned to its original value within 4–20 ms, before the next resonance was crossed. In practice, if good polarization could be obtained using a tune jump of less than 0.1 then the smaller value was used to minimize the risk of beam loss due to crossing a betatron resonance. With these improvements, a polarization level of 72% can be delivered up to 2 GeV, 65% at 2.55 GeV and 55% at 3.2 GeV (see figure 14). The figure also displays the progress in the delivered polarization level since 1997.

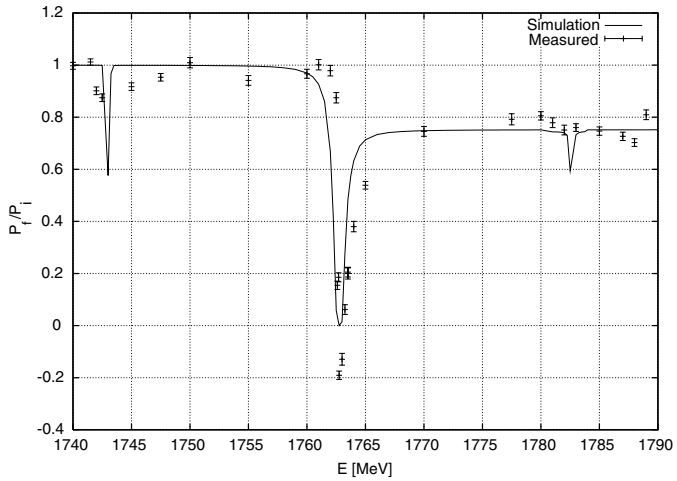

Figure 43. Beam energy calibration at the ELSA stretcher ring using resonant depolarization. From Hoffmann (2001).

We close with a mention of one additional study carried out before the above improvements were implemented. This was to calibrate the beam energy of ELSA using resonant depolarization (Hoffmann 2001). A polarized beam was accelerated to a preset final energy, and the polarization of the extracted beam was measured. The energy was incremented by a small step and the process repeated. The data are displayed in figure 43. The above measurements were carried out across the energy of the $a\gamma = 4$ imperfection resonance at 1.76 GeV. (Similar energy calibrations have also been performed for the $a\gamma = 2$, 3, 5, 6 and 7 imperfection resonances.) The sharp dip in the extracted polarization at the location of the resonance is clearly visible. The 25% relative polarization loss upon crossing the resonance, mentioned earlier, is also visible on the high energy side. The theoretical fit also includes the two synchrotron sidebands of the parent resonance, namely, $a\gamma = 4 \pm Q_s$. The experimental data do not resolve the synchrotron sidebands very clearly because the value of the synchrotron tune was only approximate and not accurately constant during the ramp. The determination of the centre of the parent depolarizing resonance yielded an energy calibration of $\Delta E/E = 2 \times 10^{-4}$, which was better than expected.

25.4. Concluding remarks

Clearly, the Froissart–Stora formula has been verified experimentally in great detail at several synchrotrons, both for polarized protons and electrons. A number of innovative ideas have been successfully implemented to overcome (or circumvent) the various types of depolarizing resonances. There are, of course, yet more ideas to come.

We are grateful to Frommberger (2004) for generously sharing information about the ELSA facility and copies of experimental data. We are also grateful to Sato (2004) for news and publications of the activities of the polarized proton and deuteron beam group at KEK. Sato was also a member of the team who discovered the second-order betatron spin resonance in the IUCF Cooler mentioned in section 22 and, in fact, he suggested that the narrow resonance observed in the studies (Ohmori *et al* 1995) was a higher-order betatron spin resonance, which as we saw was confirmed by varying the horizontal betatron tune (keeping the vertical tune fixed).

26. The BNL complex: RHIC, AGS and the transfer line

26.1. General remarks

Many ideas for the acceleration of nonradiatively polarized beams were pioneered at BNL. The early work at the AGS was reviewed in section 25. Here we review more modern work at BNL. A special issue of *Nuclear Instruments and Methods* A was devoted to 'The Relativistic Heavy-Ion Collider Project: RHIC and its Detectors' (2003 **499** issues 2–3, 235–880). This volume contains detailed information about all aspects of RHIC (of which polarized protons are just one part). A second review titled 'The RHIC Accelerator' and devoted to the accelerator physics (including the spin physics) was written by Harrison *et al* (2002). The two reviews given above were major sources of information for the material below.

Polarized protons were first accelerated and collided (at 100 GeV) at RHIC in the run from December 2001 to January 2002 (Roser *et al* 2003). The Snakes performed successfully. The spin rotators were not in place yet; they were commissioned later (MacKay *et al* 2003b). Roser (2003) gives a recent overview of the RHIC status and plans, while MacKay *et al* (2003a) gives an overview of the spin dynamics at the AGS and RHIC. A schematic layout of the BNL complex for polarized proton acceleration was shown in figure 1.

Since RHIC is a heavy ion (or a polarized proton–proton) collider, the particle species have the same sign of charge. Hence, RHIC consists of two rings, called the Blue and Yellow rings. Polarized protons circulate clockwise in the Blue ring and counterclockwise in the Yellow ring. The rings lie side-by-side and intersect at six points. See figure 44 for a description of the RHIC clock numbering system for the interaction points. Four of the six interaction points of RHIC house experimental detectors: the large detectors STAR at 6 o'clock and PHENIX at 8 o'clock, and the smaller detectors BRAHMS at 2 o'clock (also the pp2pp detector to measure the elastic pp scattering cross-section) and PHOBOS at 10 o'clock. The pC CNI polarimeters (also the gas jet polarimeter) are at 12 o'clock and the spin-flipper (ac dipole) is at 4 o'clock.

Although RHIC is a planar ring, it does not lie in the same plane as the AGS, hence the transfer line connecting the AGS to RHIC contains a vertical drop (RHIC is at a lower elevation than the AGS). This raises some issues of spin matching, to avoid depolarization during the transfer process, as we shall describe below.

With the advent of RHIC, it became essential that polarized proton acceleration at the AGS become a robust turnkey operation. Old-style resonance correction and jumping is too laborious. We shall review the new ideas employed at the AGS to accelerate polarized proton beams.

26.2. Accelerator chain

We begin with a highly condensed summary of all the components which will *not* be reviewed in detail below. The material below is mainly from Huang *et al* (2003c). Polarized protons (H^- ions) are produced from a new 'Optically Pumped Polarized Ion Source' (Zelensky 1999). The H^- ions are accelerated in an RFQ (radio-frequency quadrupole) and a linac to a kinetic energy of 200 MeV ($\gamma = 1.21$). The beam is then stripped and injected into a Booster. The beam crosses two imperfection resonances in the Booster, namely, $G\gamma = 3$ and 4, which are crossed by increasing the amplitude of the vertical closed orbit imperfections so as to induce adiabatic spin-flips. The protons are extracted from the Booster before they encounter the first intrinsic resonance at $G\gamma = Q_y = 4.9$. Before 2004 the protons were extracted at an energy corresponding to $G\gamma = 4.7$, but starting in 2004 the value used is $G\gamma = 4.5$ (Huang 2005). The change in extraction energy was made to optimize the polarization transfer to the AGS. In the AGS, the beam is accelerated to approximately 24.3 GeV total energy ($\gamma = 25.94$), but it is more pertinent to write $G\gamma = 46.5$ because the spins are transferred to RHIC at this value

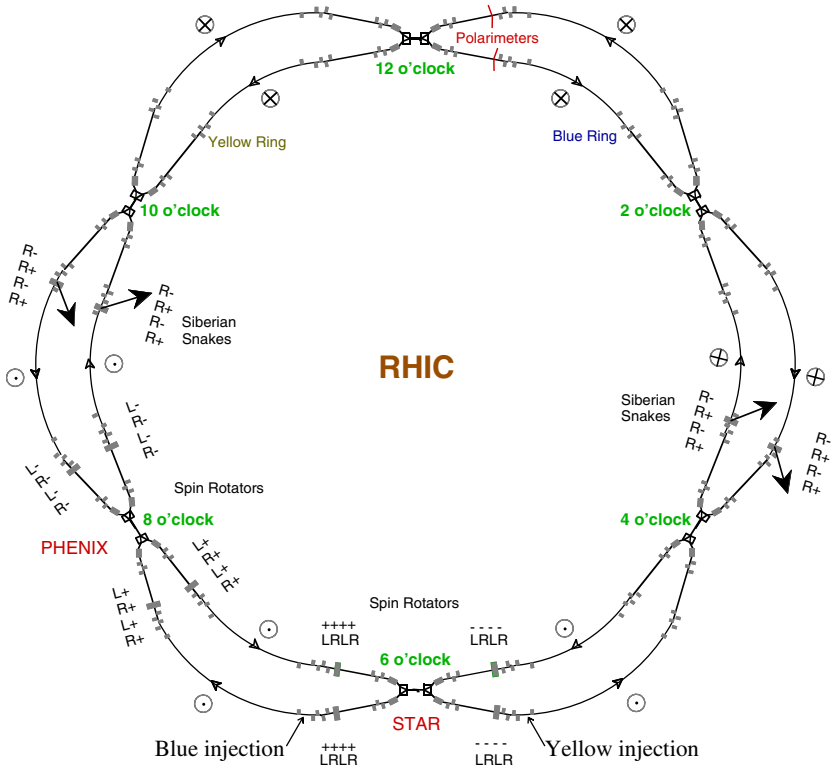

Figure 44. Schematic plan view of RHIC, greatly exaggerating the arcs. This figure corrects some misprints in Alekseev *et al* (2003). Courtesy of MacKay (private communication) and BNL Collider Accelerator Department.

of $G\gamma$. The values $G\gamma = 47.5$ and 48.5 have also been considered (but not used). Once in RHIC, the polarized protons have been accelerated to 100 GeV, as of the time of the writing of this paper. The eventual RHIC top energy is 250 GeV.

The polarization at the end of the linac is about 80%. There are polarimeters at several points in the chain: one at the source, another at the end of the linac, others in the AGS and in each of the RHIC rings. There are also local polarimeters at the STAR and PHENIX experimental detectors at RHIC. The PHENIX local polarimeter was used, for example, to commission the RHIC spin rotators.

26.3. RHIC

26.3.1. Snake placement. As stated earlier, RHIC consists of two side-by-side intersecting rings. The rings cross each other in the interaction regions, although the beams collide head-on at the actual interaction points (IPs). The shape of each RHIC ring is nominally a hexagon, but because the rings cross each other, each ring actually consists of three inner arcs and three outer arcs. Each RHIC ring, therefore, has a superperiodicity of $P = 3$ and not 6. A schematic layout of RHIC, which greatly exaggerates the inner and outer arcs, is shown in figure 44. Both the Snakes and the spin rotators are indicated in figure 44, as well as the direction of the polarization in the two rings, assuming the polarization is vertically up at the injection point. The injection points and direction of propagation of the beams are marked in the figure.

The geometry of the inner and outer arcs raises an important point about the placement of the Siberian Snakes at RHIC. We stated earlier, when deriving the stable polarization direction and spin tune for Snakes in an idealized model of a planar ring, that the Snakes must be at 'diametrically opposite' points of the ring. Because RHIC has inner and outer arcs, the Snakes must in fact be placed such that the beam direction is *parallel* at the locations of the two Snakes; only then will the orbital bending in each half add up to 180°. This implies an *unequal* path length in the two halves connecting the Snakes. This is a subtlety hidden in the term 'diametrically opposite' when applied to a real machine.

26.3.2. Spin rotators: helicity combinations. In 2003, RHIC ran with 55 polarized proton bunches in each ring at an energy of 100 GeV. The bunches were injected with vertical polarization with a pattern of $(++--)$ in one ring and $(+-+-)$ in the other ring. This pattern ensures that all four helicity combinations are automatically delivered to the experiments, during a single RHIC run, which helps to minimize systematic errors. This is an important distinguishing feature as compared to a ring with a radiatively polarized beam such as HERA. The HERA spin rotators can offer independent choices of lepton helicity at different interaction points, but the helicity at a given IP cannot be changed during a run; the spin rotators must instead be reconfigured for a new run.

RHIC is also equipped with a spin-flipper which has undergone preliminary commissioning tests (Bai *et al* 2002). The spin-flipper can be used to selectively reverse the directions of the spins in one ring only, thereby further reducing the systematic errors in the experiments.

26.3.3. Snake calibration. Suppose the Snake spin rotation axis points at an angle ϕ to the longitudinal, and the four-helix combination rotates the spins through an angle μ. The question arises as to how to calibrate the helical fields so that the spin rotation axis points in the desired direction and the spin rotation is $\mu = \pi$. If the Snakes are perfectly set, the spin tune should be $\frac{1}{2}$ at all energies, but in practice a variation in the spin tune of 0.01 was observed during the RHIC energy ramp from $\gamma = 25.9364$ to $\gamma = 107.0922$. This variation was small enough so that the currents in the Snake helices were held fixed during the ramp.

Ranjbar *et al* (2002b) describes the Snake calibration procedure. Field maps of the helices, and the orbit and spin dynamics through each Snake, taking into account higher-order field components, have previously been generated. The RHIC spin flipper was used to measure the spin tune and to verify the spin tune predictions against the measured values. First, one can easily show by Pauli matrix multiplication that given angles (ϕ_1, μ_1) and (ϕ_2, μ_2) in the two helical dipole modules (which we want to act as Snakes),

$$\cos(\nu\pi) = \cos\frac{\mu_1}{2}\cos\frac{\mu_2}{2}\cos(\pi G\gamma) - \sin\frac{\mu_1}{2}\sin\frac{\mu_2}{2}\cos(\phi_2 - \phi_1). \tag{26.1}$$

For RHIC, the desired settings are $\phi_2 = -\phi_1 = \pi/4$ and $\mu_1 = \mu_2 = \pi$. To calibrate the RHIC Snakes, a set of μ and ϕ values for a range of input currents was generated. From this a fourth order polynomial was generated. This was compared to the theoretical calculations.

The RHIC Blue ring was detuned to a theoretical value of $\nu = 0.48$. Partial spin-flip was observed, using the spin-flipper, for driving frequencies in the interval $\nu = 0.47$ to 0.49. Either the spin tune was not exactly 0.48 or else the spin tune distribution exceeded ± 0.01. It was also noticed that partial spin flipping took place in the Yellow ring, although that ring should have been insensitive to the spin-flipper.

A possible explanation is as follows. The design of a RHIC Snake consists of four full-twist helices. Helices 1 and 4 are powered in series, as are helices 2 and 3, hence a RHIC Snake

contains two nested helix pairs. The design of the RHIC Snakes and spin rotators is reviewed in detail in MSY1. According to calculations, the desired current values are 325 A for the inner helices and 100 A for the outer helices. After more detailed investigations of one Snake in the Yellow ring, it was found that the above current settings yielded $\mu = 179.956\,475^\circ$ and $\phi = -44.085\,3423^\circ$ instead of ideal values of 180° and -45°, respectively. This 1° offset of the Snake spin rotation axis can account for a ± 0.01 variation in the value of the spin tune, which might explain the spin detuning in the Yellow ring.

Snake resonances are also used to calibrate the RHIC Snakes (Roser 2005). The fractional part of the vertical betatron tune $[Q_y]$ is set to 0.24, i.e. close but not equal to 0.25. The currents in the RHIC Snake helices are adjusted until depolarization is observed (a second-order Snake resonance $\nu_{\text{spin}} - 2[Q_y] = 0$). From this information one can calculate the currents required to achieve a spin tune of 0.5.

26.3.4. Spin rotator calibration. The spin rotators were calibrated as follows. To measure the direction of the polarization at the interaction points, both the PHENIX and STAR detectors are equipped with local polarimeters, which can measure the transverse polarization components at the interaction point. When the polarization at the IP is longitudinal, the polarimeters show no asymmetry, but the pC CNI polarimeter in the arcs show a nonzero vertical polarization. The PHENIX local polarimeter, for example, was based on the observation from a test experiment which revealed a left–right asymmetry in very forward neutron production from collisions of protons with one transversely polarized beam.

First, both spin rotators were turned off. The asymmetry in the PHENIX polarimeter response indicated that the vertical polarization was indeed of the opposite sign from that at the pC CNI polarimeter, which was on the other side of the Snakes. After successful commissioning, the PHENIX polarimeter registered a left–right asymmetry close to zero.

Actually, on the first try, a sign error in the spin rotation angles caused all the spin rotators to be connected with the leads of the power supplies reversed (Mackay *et al* 2003b). This resulted in an almost *radial* polarization at the PHENIX local polarimeter. Fortunately, the design of the spin rotators was such that the error could be rectified by simply reversing the leads to the power supplies. Although it was a mistake, the incident built confidence in both the PHENIX polarimeter and the overall theoretical model of the spin rotators.

26.4. AGS

26.4.1. Partial Snakes. We have seen that a partial Snake effectively makes the imperfection resonances stronger, so that adiabatic spin-flip is induced at every imperfection resonance. It is much easier to increase the resonance strengths deterministically, via the use of a partial Snake, than to correct the individual random terms to zero. Furthermore, after a machine shutdown and startup, there is no need to recalibrate all the corrector settings for the imperfection resonances.

The set of imperfection resonances at the AGS span the interval $G\gamma = 5$–46 inclusive. Transfer to RHIC, typically, occurs at $G\gamma = 46.5$ (the value of 47.5 has also been considered as a future possibility). The initial AGS partial Snake was a warm solenoid. The solenoid field was ramped with the beam momentum to act as a 5% partial Snake at all beam energies (Huang *et al* 1994). A partial Snake strength of about 5% is adequate to overcome the imperfection resonances at the AGS. The alternative scenario would be to run the solenoid at full current throughout the energy ramp. At low energies (injection), this would mean that the solenoid would be a 25% partial Snake. However, this induced too much transverse betatron coupling in the AGS.

In spring 2004, a double-pitch helical-field partial Snake was installed and operated in the AGS. The old solenoid was still in the ring, but the two partial Snakes were not run simultaneously. The design of the helical-field device was described by Huang *et al* (2003b). The helical magnet partial Snake induces much less transverse betatron coupling, although the precise degree of coupling is not yet quantitatively known. The reduction of the betatron coupling is expected to reduce or eliminate the coupling resonances, which depend on the horizontal betatron tune. Since the helical-field partial Snake has transverse magnetic fields, the fields are not ramped with the beam energy. The partial Snake strength is then proportional to $G\gamma/p \propto 1/\beta$. The variation of particle speed is noticeable at the AGS, hence the helical-field partial Snake strength is about 8% at low momentum, decreasing to about 5% at top momentum. With the use of partial Snakes, almost all of the problems of the crossing of the imperfection resonances at the AGS have been effectively solved.

26.4.2. Intrinsic resonances. The use of partial Snakes does not overcome the intrinsic resonances. A partial Snake introduces Fourier harmonics at integer tune values only in the spin precession vector (or in the Hamiltonian). This was already noted experimentally in the initial work with a partial Snake at the AGS (Huang *et al* 1994). The magnitude of polarization is preserved when crossing the imperfection resonances (integer values if $G\gamma$), but drops in steps as successive intrinsic resonances are crossed ($G\gamma = Q_y$, $20 - Q_y$ and $12 + Q_y$), yielding a final polarization of $P \simeq 20\%$. Hence, additional ideas are required to deal with the intrinsic resonances. *Without* a partial Snake, there is almost a total loss of polarization during acceleration.

Studies with the solenoid partial Snake were performed to investigate the crossing of a strong intrinsic resonance at $G\gamma = 0 + Q_y$ (Huang *et al* 2003a). At this lower energy, the solenoid was powered to a higher current so that it acted as an 11.4% partial Snake. This value was a compromise between increasing the partial Snake strength and avoiding too much betatron coupling. Huang *et al* (2003a) found that the beam was successfully accelerated across the $G\gamma = 0 + Q_y$ intrinsic resonance with no detectable depolarization.

However, the modern technique to cross intrinsic resonances at the AGS does not use a partial Snake. To overcome the intrinsic resonances, the same basic idea of increasing the resonance strength is employed. This must be done carefully, however. A *coherent* betatron oscillation is induced when crossing an intrinsic resonance. Then ϵ will have a large value for all the particles and the adiabatic spin-flip condition can be satisfied for all the particles simultaneously. The intrinsic resonance can then be crossed via adiabatic spin-flip. Such an idea was tried in the IUCF Cooler (Crandell *et al* 1996) and it did work. However, there were side-effects. The beam was kicked to have a large coherent vertical betatron amplitude. This changed the orbital phase-space distribution from a circle into an annulus (after decoherence of the betatron oscillations), which resulted in the undesirable effect of increasing the vertical betatron emittance.

Instead, at the AGS, an rf dipole is employed to increase the coherent betatron oscillation amplitude *adiabatically* and to decrease it back to zero after the intrinsic resonance has been crossed; this results in no loss of polarization *and* no increase of the vertical betatron emittance. The principle of exciting, sustaining and de-exciting a coherent vertical betatron oscillation, with no resultant increase in the emittance, was tested by Bai *et al* (1997). The application of the idea to the crossing of intrinsic resonances was reported by Bai *et al* (1998). The use of coherent betatron oscillations to cross intrinsic resonances is now standard at the AGS. It is possible that when a coherent betatron oscillation is excited, the beam scrapes against apertures in the ring resulting in a loss of intensity, albeit without depolarization. Such matters are ongoing issues of research.

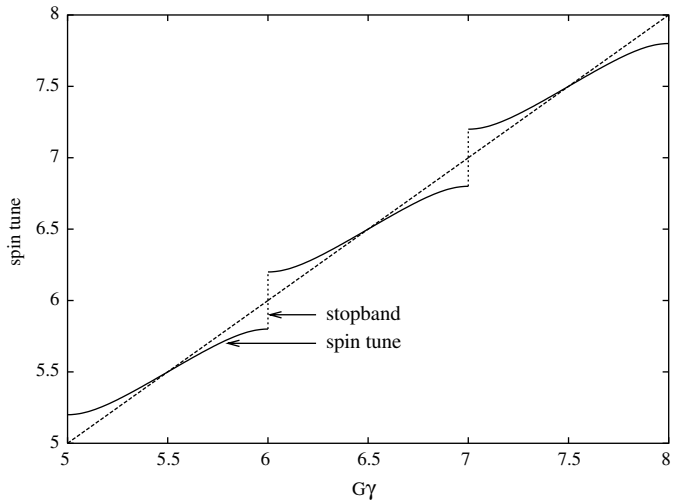

Figure 45. Spin tune and stopbands as a function of $G\gamma$ for a planar ring and a partial Siberian Snake.

In practice, the ac dipole is not operated at all of the intrinsic resonances. The ac dipole is used to cross the strong intrinsic resonances $0 + Q_y$, $12 + Q_y$ and $36 \pm Q_y$. The ac dipole is not used at the weaker intrinsic resonances $24 \pm Q_y$ and $48 - Q_y$; instead the crossing speed (rate of energy increase) is made as large as possible (no tune jump is employed). There are also coupling resonances at $0 + Q_x$, $12 + Q_x$ and $36 \pm Q_x$. The crossing speed is again made as high as possible. There is some loss of polarization from crossing the intrinsic resonances. The imperfection resonances do not seem to result in any polarization loss.

Essentially, the full polarization of 80% was delivered from the source to the AGS in the 2004 run. The polarization was about 40–50% at AGS extraction and transfer to RHIC. The successful acceleration and storage of the polarized proton beams at RHIC was reviewed in the companion paper MSY1.

We briefly remark that the use of a coherent betatron oscillation to cross the intrinsic resonances was also considered at ELSA. A study of the ac dipole and other resonance crossing schemes for use at ELSA is given by Steier (1999). For electron beams, because of synchrotron oscillations and the stochastic nature of the synchrotron radiation, one gets multiple/stochastic resonance crossings. Calculations indicated that, at higher energies at ELSA, the effect was strong enough so that there is never a complete spin-flip, independent of how strong one makes the intrinsic resonances with the ac dipole. As we saw earlier, tune jumps are employed at ELSA to cross the intrinsic resonances. Tune jumps induce emittance growth in a proton ring, but this is not the case in electron rings because the synchrotron radiation damping quickly restores the emittance.

26.4.3. Stronger partial Snake. It is planned (for 2005) to install a cold, i.e. superconducting, double-pitch helical magnet partial Snake into the AGS. (The warm and cold helical partial Snakes may be operated together.) The reasoning is, at least partly, as follows. The spin tune for a planar ring with a partial Snake of strength λ_s was worked out in (13.13) and is given by $\cos(\pi\nu) = \cos(\pi\nu_0)\cos(\lambda_s\pi/2)$. A graph of the spin tune ν against $\nu_0 = G\gamma$, for $\lambda_s = 0.4$, is shown in figure 45. This graph is very similar to figure 34 for the single resonance model, except here the spin tune jumps not just once but at every integer value of ν_0.

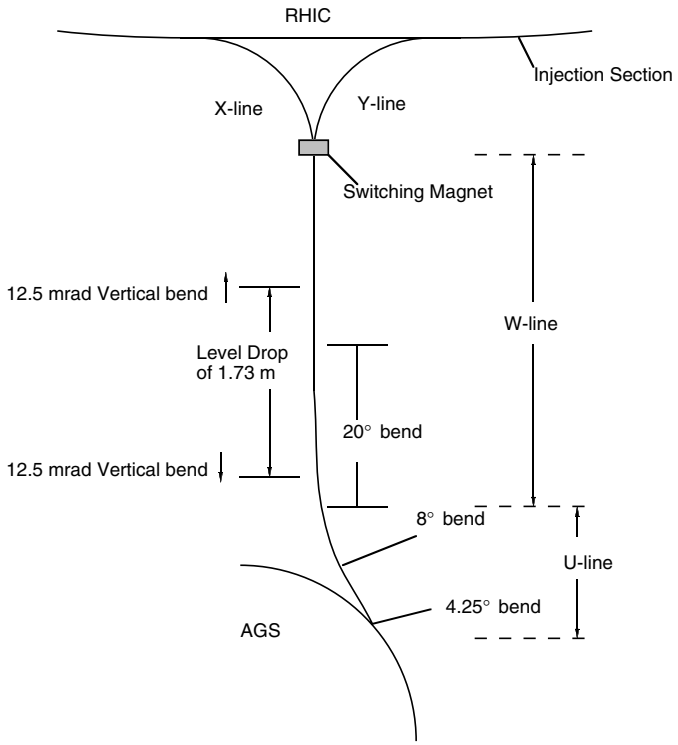

Figure 46. Schematic plan view of the ATR line connecting the AGS to RHIC. Reprinted from Alekseev *et al* (2003). Copyright (2003) with permission from Elsevier.

If the stopbands, i.e. the gaps or jumps in the spin tune, are sufficiently large, the vertical betatron tune Q_y can be placed *in the stopband*, in which case the spin tune will never cross an intrinsic resonance and the adiabatic excitation of coherent betatron oscillations, etc will become unnecessary. This idea has not been used with the current partial Snake because the stopband is too small. The vertical betatron tune would be too close to an integer leading to beam instabilities.

26.5. AGS–RHIC transfer line

In most cascaded systems, the individual accelerators are planar, and moreover the different machines lie in the same plane. The stable polarization is vertical in all the components of the accelerator chain. In the BNL complex, the linac, Booster and AGS all lie in the same plane. The polarization is vertical at injection ($G\gamma = 2.18$) and extraction ($G\gamma = 4.5$) in the Booster ring, and subsequent transfer to the AGS. Because of the 5% solenoid partial Snake in the AGS (i.e. 9° spin rotation around the longitudinal axis), the stable spin direction is tilted at 4.5° from the vertical. The above analysis is for a solenoid partial Snake; the angle is different for a double-pitch helical partial Snake. Furthermore, the plane of the AGS is 1.7 m higher than that of RHIC. The transfer line connecting the AGS to RHIC (known as ATR) contains interleaved horizontal and vertical bends. The beams are injected vertically into RHIC (and the polarization is also vertical). A schematic view of the ATR transfer line is shown in figure 46. The 12.5 mrad vertical bend is located in the region of the 20° horizontal bend. The level of

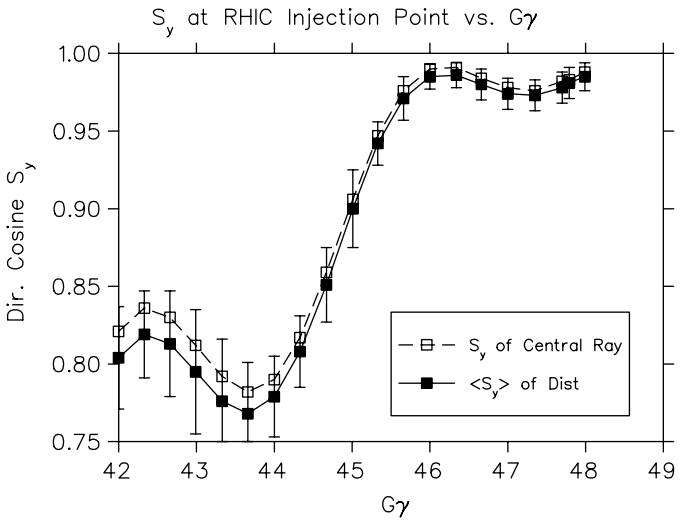

Figure 47. Vertical spin component at the RHIC injection point as a function of $G\gamma$, assuming vertical polarization at extraction from the AGS. Reprinted from Alekseev *et al* (2003). Copyright (2003) with permission from Elsevier.

the ATR drops by 1.73 m in this section. The first vertical bend angle is 12.5 mrad, but the second is −12.46 mrad, to correct for the Earth's curvature over the length of this section of the ATR.

The beams are injected into RHIC vertically. From the end of the ATR, the beam is directed into one of two arcs (see figure 46). The beam passes off-centre through two quadrupoles in the RHIC ring which, therefore, also act as dipoles. This reduces the required strength of the final kicker into RHIC to 1.73 mrad.

We have seen that for a ring equipped with a pair of Snakes, the stable spin direction is vertical. Hence, there will be a loss of polarization if the injected polarization into RHIC does not point vertically. The AGS–RHIC transfer line must, therefore, be 'spin-matched' to deliver vertically polarized beams into the RHIC rings. The transfer line is optimized to operate at the value of $G\gamma = 46.5$ and this is the current value of $G\gamma$ for RHIC injection. The higher value of 47.5 has also been considered. In practice, because the interleaved horizontal and vertical bends lead to noncommuting spin rotations, and also because of the partial Snake in the AGS, the spin match in the ATR is not perfect. A further complication is that because the transfer line divides into two (for injection into the Blue and Yellow rings of RHIC, respectively), the polarization direction can in fact be different in the two rings. A sketch of the vertical spin component at the RHIC injection point as a function of $G\gamma$, assuming vertical polarization at extraction from the AGS (i.e. no partial Snake), is shown in figure 47. The value of the vertical spin component is highest at $G\gamma = 46.5$ since the ATR is optimized to operate at this energy.

27. Radiative polarization I

27.1. General remarks

The Sokolov–Ternov formula was basically a QED calculation. To understand the behaviour of the polarization in actual storage rings, it is also necessary to pay attention to the statistical mechanics of the electron (positron) beam dynamics. This is very much at the heart of the

Derbenev–Kondratenko formula (Derbenev and Kondratenko 1973) and also later work by Mane (1987a). This section presents the in-depth quantum-statistical-mechanical derivation of the equilibrium radiative polarization.

27.2. Radiated intensity for $g \neq 2$

The Sokolov–Ternov formula was derived assuming $g = 2$. In fact, the values of the asymptotic polarization and the buildup time depend on g. The generalization to arbitrary g was given by Derbenev and Kondratenko (1973) using semiclassical QED. The expressions below follow Jackson (1976) (with an additional function F_4). Define

$$\begin{aligned}
F_1(a) &= 1 + \frac{41}{45}a - \frac{23}{18}a^2 - \frac{8}{15}a^3 + \frac{14}{15}a^4 - \frac{8}{5\sqrt{3}}\frac{a}{|a|}\left(1 + \frac{11}{12}a - \frac{17}{12}a^2 - \frac{13}{24}a^3 + a^4\right),\\
F_2(a) &= \frac{8}{5\sqrt{3}}\left(1 + \frac{14}{3}a + 8a^2 + \frac{23}{3}a^3 + \frac{10}{3}a^4 + \frac{2}{3}a^5\right),\\
F_3(a) &= \frac{1}{18}\left(7 - 2a + \frac{13}{5}a^2\right),\\
F_4(a) &= F_1(a)\mathrm{e}^{-\sqrt{12}|a|} + \frac{a}{|a|}F_2(a),
\end{aligned} \tag{27.1}$$

where $a = (g-2)/2$. Suppose the direction of the equilibrium polarization direction is not vertical, but is oriented at a polar angle θ_0 to the vertical, and at an azimuthal angle ϕ_0 relative to the beam direction. Then the polarization buildup is still exponential, as in (2.2), but the new expressions for the time constant and the equilibrium degree of the polarization are

$$\begin{aligned}
\frac{\tau_{\mathrm{ST}}}{\tau_{\mathrm{pol}}} &= F_4(a) + (2F_3(a) - F_4(a))\sin^2\theta_0\cos^2\phi_0,\\
P_{\mathrm{eq}} &= \frac{F_2(a)\cos\theta_0}{F_4(a) + (2F_3(a) - F_4(a))\sin^2\theta_0\cos^2\phi_0}.
\end{aligned} \tag{27.2}$$

This corrects a misprint by Jackson (1976). For the important and special case of $\theta_0 = 0$, i.e. polarization buildup in the vertical direction, the above expressions simplify to

$$\frac{\tau_{\mathrm{ST}}}{\tau_{\mathrm{pol}}} = F_4(a), \qquad P_{\mathrm{eq}} = \frac{F_2(a)}{F_4(a)}. \tag{27.3}$$

There are some notable points in the above expressions:

- The equilibrium polarization and the buildup time depend *only on* a and *not* on $a\gamma$. We have seen previously that for motion in transverse magnetic fields, the value of a contributes to quantities such as the spin tune via the combination $a\gamma$. That is not the case in the expressions for the spin-flip photon emission matrix elements.
- A graph of the equilibrium degree of polarization as a function of g is shown in figure 48. A graph of the ratio of τ/τ_{ST}, as a function of g, is shown in figure 49. If $g \to \pm\infty$ then $P_{\mathrm{eq}} \to \pm 1$, as a simple two-level system would suggest. Note, however, that if $0 \leqslant g \lesssim 1.2$, then P_{eq} is *negative* even though the value of g is *positive*. Hence, $P_{\mathrm{eq}} < 0$ although the magnetic moment is positive, i.e. the energetically *unfavourable* state is preferentially populated. This is due to the contribution of the Thomas precession. In particular, there is a nonzero polarization of $P_{\mathrm{eq}} \simeq -0.98$ even at $g = 0$, i.e. no magnetic moment. The graph of τ/τ_{ST} is also not an even function of g.

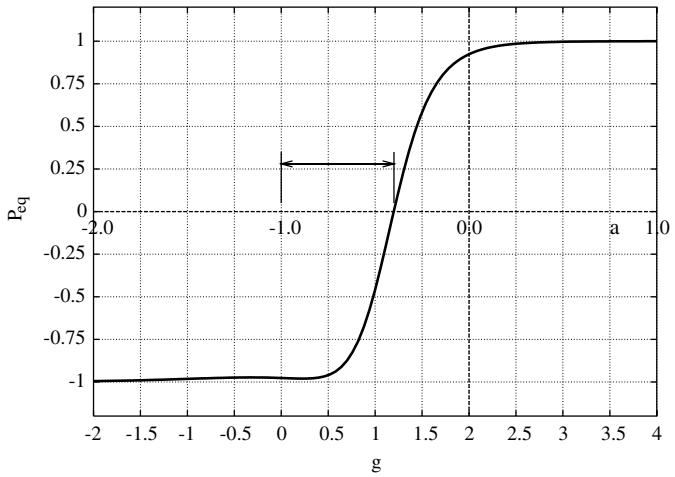

Figure 48. Graph of the equilibrium radiative polarization in a uniform magnetic field as a function of the g-factor for a positively charged particle.

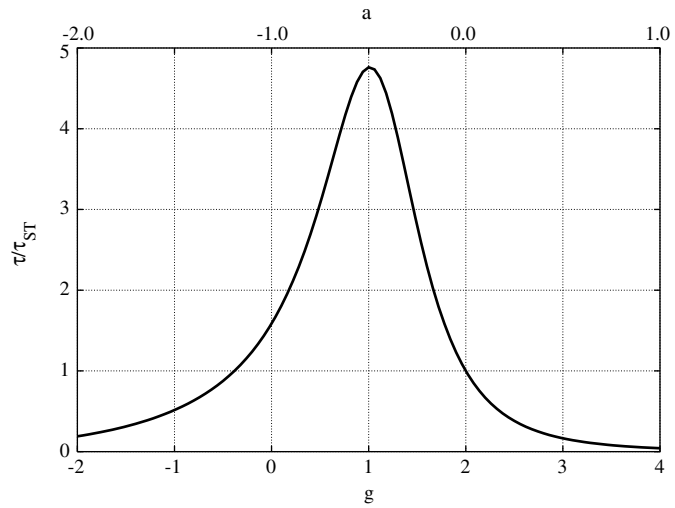

Figure 49. Graph of the buildup time τ of the radiative polarization in a uniform magnetic field, as a function of the g-factor, and expressed as a ratio to the Sokolov–Ternov value τ_{ST}.

27.3. Two-level system: magnetic dipole M1 transition

Since the polarization arises as a result of transitions between spin states, it is possible to understand the phenomenon at a 'simple' level as a magnetic dipole M1 transition in a two-level spin system. Such an approach was first published by Lyboshitz (1967). Jackson (1976) has analysed this model in detail. We summarize the principal findings. Essentially, one boosts to the instantaneously comoving frame, and treats a magnetic dipole M1 transition in a nonrelativistic two-level system. One then boosts back to the lab frame. We begin with the magnetic moment

$$\boldsymbol{\mu} = \frac{ge}{2mc}\frac{\hbar\boldsymbol{\sigma}}{2}, \tag{27.4}$$

where we write $\hbar\boldsymbol{\sigma}/2$ for the quantum spin operator, since we have used $\boldsymbol{s}$ to denote the classical spin vector. Then, in a frame instantaneously comoving with the particle, the frequency splitting of the two spin states is

$$\Delta\omega' = \left|\frac{g}{2}\right| \gamma^2\, \omega_{\rm c}, \tag{27.5}$$

where we employ primes to denote quantities in the instantaneously comoving frame. Recall that, $\omega_{\rm c} = v/\rho \simeq c/\rho$ is the revolution (cyclotron) frequency. The spin-flip transition probability per unit time, for a magnetic dipole transition, from the up to the down state is

$$w' = \frac{4}{3\hbar}\left(\frac{\Delta\omega'}{c}\right)^3 |\langle\downarrow |\boldsymbol{\mu}| \uparrow\rangle|^2 = \frac{2}{3}\left|\frac{g}{2}\right|^5 \frac{e^2\hbar\gamma^6}{m^2c^2\rho^3}. \tag{27.6}$$

The time dilation in boosting to the lab frame reduces the transition rate by one power of γ, so

$$\tau^{-1} = \frac{2}{3}\left|\frac{g}{2}\right|^5 \frac{e^2\hbar\gamma^5}{m^2c^2\rho^3}. \tag{27.7}$$

This is an even function of g and vanishes for $g = 0$. Since the system is at essentially zero temperature, all the particles fall to the 'ground' state (lower energy state), leading to an asymptotic polarization of 100%. A simple check verifies that the polarization has the correct sign for electrons and positrons. Comparing to $\tau_{\rm ST}$, we see that for $g \simeq 2$ the results are almost the same. Clearly, certain parameters must appear simply on dimensional grounds. But the powers of dimensionless quantities, such as γ, are also correctly given by the simple two-level model. This shows that the naive model correctly describes the overall kinematics of the polarization process. The naive model also shows, that for $g \neq 2$, the value of $\tau_{\rm pol}$ is a function of g itself or $a = (g-2)/2$ and not $a\gamma$. The more sophisticated calculations, leading to the expressions in (27.3), are in agreement with this finding. The corrections for $g \neq 2$ are given simply by functions of a, not $a\gamma$, and with *no* additional terms in γ and ρ, etc. The naive model obviously fails for $g = 0$, and cannot explain the negative polarization for $0 < g \lesssim 1.2$. Hence, the simple model gives a good qualitative understanding of the radiative polarization kinetics for charged ultrarelativistic particles. Lyboshitz (1967) pointed out that the naive model is, in fact, exact for radiative polarization of *uncharged* particles possessing a magnetic moment. For such particles, one must not write g and e, etc. One must use μ, etc. For ultrarelativistic neutral particles the radiation is pure spin light.

27.4. Nonvertical asymptotic polarization

Up to now we have treated only a planar ring with a uniform magnetic field. The polarization direction is obviously vertical. The case where the polarization does not build up in the vertical direction was first addressed by Baier and Katkov (1967). Let us denote the direction of the polarization buildup by $\boldsymbol{n}_0$, i.e. the one-turn periodic orbit of the spin motion along the design orbit. Baier and Katkov (1967) obtained the following expressions for the asymptotic polarization and buildup time:

$$\begin{aligned} P_{\rm eq} &= \frac{8}{5\sqrt{3}}\frac{\oint (\mathrm{d}\theta/|\rho|^3)\,\hat{\boldsymbol{b}}\cdot\boldsymbol{n}_0}{\oint (\mathrm{d}\theta/|\rho|^3)\,[1-(2/9)(\boldsymbol{n}_0\cdot\hat{\boldsymbol{v}})^2]}, \\ \tau_{\rm BK}^{-1} &= \tau_{\rm ST}^{-1}\oint\left(\frac{\mathrm{d}\theta}{|\rho|^3}\right)[1-\left(\frac{2}{9}\right)(\boldsymbol{n}_0\cdot\hat{\boldsymbol{v}})^2]. \end{aligned} \tag{27.8}$$

Here $\hat{\boldsymbol{v}}$ is a unit vector parallel to the local velocity vector (tangent to the particle orbit), $\dot{\boldsymbol{v}}$ the time derivative of $\boldsymbol{v}$, with $\hat{\dot{\boldsymbol{v}}} = \dot{\boldsymbol{v}}/|\dot{\boldsymbol{v}}|$ (normal to the particle orbit) and $\hat{\boldsymbol{b}} = \boldsymbol{v}\times\dot{\boldsymbol{v}}/(|\boldsymbol{v}\times\dot{\boldsymbol{v}}|)$ the binormal vector. For motion in a locally uniform magnetic field, $\hat{\boldsymbol{b}}$ is a unit vector in the

direction of the local magnetic field, hence the notation. The functions $F_{1,2,3,4}(a)$ defined above are in agreement with the Baier–Katkov results, setting $a = 0$.

The Baier–Katkov formulae are little-used. For a planar ring, especially to obtain simple 'back of the envelope' estimates, the Sokolov–Ternov formula is more popular. For more complicated storage ring models, the Derbenev–Kondratenko formula to be presented below supersedes the above formula.

Baier *et al* (1970) also worked out a formula for the time evolution of the polarization vector, assuming motion in external magnetic fields only:

$$\frac{\mathrm{d}\boldsymbol{P}}{\mathrm{d}t} = \boldsymbol{\Omega} \times \boldsymbol{P} - \frac{1}{\tau_{\mathrm{ST}}}\Big[\boldsymbol{P} - \frac{2}{9}(\boldsymbol{P}\cdot\hat{\boldsymbol{v}})\hat{\boldsymbol{v}} + \frac{8}{5\sqrt{3}}\hat{\boldsymbol{b}}\Big]. \tag{27.9}$$

This is known as the Baier–Katkov–Strakhovenko formula. It is also relatively little-used. Essentially, the equation says that the polarization vector rotates like a rigid body (the $\boldsymbol{\Omega} \times \boldsymbol{P}$ term) and the individual components of $\boldsymbol{P}$ relax to their equilibrium values, all with the same time constant τ_{ST}, which is not true. There is no point in pursuing the matter further.

27.5. Equilibrium radiative polarization

We now embark on the principal intellectual adventure of this section, i.e. the derivation of the equilibrium radiative polarization, namely, the Derbenev–Kondratenko formula (Derbenev and Kondratenko 1973). First note that the polarization vector is defined as the average of the individual spin vectors $\boldsymbol{P} = \langle \boldsymbol{s} \rangle$. The angle brackets denote a sum over all the particles. The above is a general formula. It is *not* restricted to equilibrium. It is always valid, but as it stands, it is of little use. We now restrict ourselves to equilibrium. In that case, we need the spin projections along $\boldsymbol{n}$, at each point in the orbital phase-space. Recall that $\boldsymbol{n}$ is the quantization axis of the spin eigenstates of the Hamiltonian at each point in the orbital phase-space. In the case of a planar ring as treated by Sokolov and Ternov (1964), the spin quantization axis was the same for all the particles, but we are now embarking on a much more general formulation. We do *not* specify any particular restriction on the structure of the accelerator. The expression for the equilibrium polarization is

$$\boldsymbol{P}_{\mathrm{eq}} = \langle\langle \boldsymbol{s}\cdot\boldsymbol{n}\rangle\boldsymbol{n}\rangle. \tag{27.10}$$

Note very carefully that there are *two* statistical averages. For brevity, denote a point in the orbital phase-space by $z \equiv (\boldsymbol{q}, \boldsymbol{p})$. The inner angle brackets denote an average over the spin projection along $\boldsymbol{n}(z)$, i.e. a sum of spins (actually $\boldsymbol{s}\cdot\boldsymbol{n}(z)$) in an infinitesimal phase-space volume element centred at a *particular* value of z. The outer angle brackets denote a sum (or integral) over the orbital phase-space, i.e. over all values of z.

The picture to bear in mind is this. At each orbital phase-space point z, there is a subpopulation of spins, in an infinitesimal volume element $\mathrm{d}z$ centred on z. In addition, there is of course a population density in the orbital phase-space. Note also that the statistical averages in (27.10) are now *equilibrium* statistical averages (for both the orbit and spin).

We have previously remarked that because $\tau_{\mathrm{pol}} \gg \tau_{\mathrm{orbit}}$, the magnitude of the equilibrium polarization density is uniform across the orbital phase-space. An individual particle carries its spin all across the orbital phase-space many times before undergoing a spin-flip. What this means, in the above formula, is that the value of $\langle \boldsymbol{s}\cdot\boldsymbol{n}(z)\rangle$ is *independent* of the value of z. Although the notation is rather compressed, we can factorize

$$\boldsymbol{P}_{\mathrm{eq}} \simeq \langle\langle \boldsymbol{s}\cdot\boldsymbol{n}\rangle\rangle\langle\boldsymbol{n}\rangle. \tag{27.11}$$

The notation $\langle\langle \boldsymbol{s}\cdot\boldsymbol{n}\rangle\rangle$ denotes an average over the spins (based on spin-flip transition rates), and averaged over the full orbital phase-space. We shall discuss this in a moment. The term $\langle\boldsymbol{n}\rangle$ is

an average over a cone of quantization axes. The opening angle of this cone is negligible, for all practical purposes, i.e. $|\langle \boldsymbol{n} \rangle| \simeq 1$. (We have not proved the above statement here, but simple calculations for sample models show that it is an excellent approximation.) Hence, we can further approximate that the equilibrium degree of the polarization is simply

$$P_{\rm eq} \simeq \langle\langle \boldsymbol{s} \cdot \boldsymbol{n} \rangle\rangle. \tag{27.12}$$

We must now calculate this average. To do so, we must balance the spin-flip transition rates. The answer is similar to before, for the Sokolov–Ternov formula, but with an important twist:

$$P_{\rm eq} = \frac{\langle p_+ - p_- \rangle}{\langle p_+ + p_- \rangle}. \tag{27.13}$$

This is the key to the notation $\langle\langle \cdots \rangle\rangle$: the spin-flip transition probabilities per unit time $\langle p_+ \rangle$ and $\langle p_- \rangle$ are *averaged over the orbital phase-space*. One does *not* calculate 'local' spin-flip transition rates, at a particular phase-space point z to obtain a 'local' polarization, followed by an average over z. One averages the rates over z *first*, and *then* deduces a polarization for the *whole* beam.

We now make a further simplifying approximation—an excellent one in practice. We note that a synchrotron radiation photon is emitted almost entirely in the forward direction, at an angle of $\mathrm{O}(1/\gamma)$, relative to the particle momentum. We know that for ultrarelativistic electrons $1/\gamma \ll 1$. Hence, it is satisfactory to assume that the principal effect of the particle's recoil is simply a loss of longitudinal momentum, i.e. a loss of energy.

We now come to one of the most important parts of the polarization calculation: the proper characterization of the term 'spin-flip'. This is one of the most important sections of this review. Now we shall see why it is so important that $\boldsymbol{n}$ depends on the phase-space location z.

Because the particle loses energy during a photon emission and because $\boldsymbol{n}$ depends on z, the orbital trajectory, and hence the value of $\boldsymbol{n}$, is *not* the same before and after a photon emission. Let us write $\boldsymbol{n} = \boldsymbol{n}(z', E)$, where z' denotes all of the other orbital variables. It is important to note that E here is the energy of an *individual* particle and *not* the average energy of the whole beam. Then, after a photon emission, the orbital trajectory has the same value for z' (we assume 'point' photon emission) but a lower energy $E + \delta E$, where $\delta E = -\hbar\omega_{\rm ph}$. A spin 'flip' is then not a transition from an 'up' state $|\boldsymbol{n}\rangle$ to a 'down' state $|-\boldsymbol{n}\rangle$ along the same axis, but to a down state *along a different axis* $|-\boldsymbol{n}(z', E + \delta E)\rangle$. A schematic diagram displaying the quantization axes before and after a spin-flip photon emission is shown in figure 50. The symbol $\gamma(\partial \boldsymbol{n}/\partial\gamma)$ will be explained soon.

This was Derbenev and Kondratenko's great insight: photon emission spin-flip is *not* a 180° reversal of the spin direction. The spin-flip photon emission matrix elements are actually

$$M_{\mp} = \langle \mp \boldsymbol{n}(z', E + \delta E) | \, \mathrm{H}_{\rm int} \, | \pm \boldsymbol{n}(z', E) \rangle, \tag{27.14}$$

where recall

$$H_{\rm int} = -e\,(\boldsymbol{\beta} \cdot \boldsymbol{A}_{\rm rad} - \Phi_{\rm rad}) + \boldsymbol{\Omega}_{\rm rad} \cdot \boldsymbol{s}_{\rm op}. \tag{27.15}$$

We now dispose of a minor technicality that was not handled correctly in the original works by Derbenev and Kondratenko (1973) and Mane (1987a). The interaction Hamiltonian $H_{\rm int}$ above is the semiclassical quantum electrodynamic Hamiltonian, with time t as the independent variable. The vectors $\boldsymbol{n}(z', E)$ and $\boldsymbol{n}(z', E + \delta E)$ are specified in terms of orbital trajectories using the 'accelerator coordinates' with the arc-length θ as the independent variable. The above expression for the spin-flip matrix elements, therefore, mixes quantities based on different independent variables. In fact, Derbenev and Kondratenko (1973) recognized this difficulty, but did not solve it. In an earlier paper, Derbenev and Kondratenko (1972) introduced a phase-space dependent spin quantization axis, where it was denoted by $\boldsymbol{m}$ and defined using θ as the

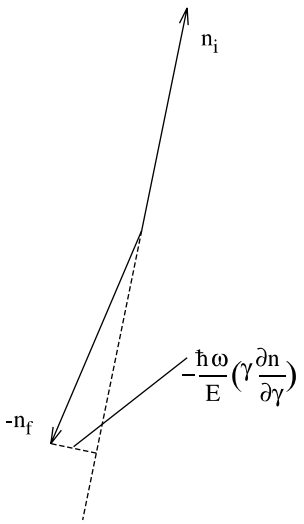

Figure 50. Symbolic depiction of radiative spin-flip.

independent variable. However, by the time of their definitive 1973 paper, they had realized that the photon emission interaction Hamiltonian must be based on time t as the independent variable. Hence, $\boldsymbol{n}$ was defined by Derbenev and Kondratenko (1973) using t not θ. They glossed over this change of definition. Mane (1987a) treated $\boldsymbol{n}$ as a function of t and then θ at different points in his paper without comment.

What should really be done is to calculate the photon emission matrix elements using the time t as the independent variable and between two *arbitrarily oriented* spin states (also specified as functions of t), i.e. a general spin-dependent matrix element. It is adequate to treat the particle motion as a locally circular arc, just as for ordinary synchrotron radiation. Then, just as for ordinary synchrotron radiation one expresses the recoil in terms of a change to the betatron and synchrotron oscillations, so also one expresses the change of spin state in terms of the spin trajectories given by $\boldsymbol{n}(z', E)$ and $\boldsymbol{n}(z', E + \delta E)$. The above discussion is really a technicality, just to clear up a theoretical nicety, which has gone uncorrected in literature for 30 years. The reader may safely skip the above statements as pedantic details.

What *is* of the utmost importance is the following. Because the initial and final spin states are not exactly antiparallel, i.e. they are not exactly orthogonal states, the spin-independent term in H_{int}, namely the term $-e\,(\boldsymbol{\beta}\cdot\boldsymbol{A}_{\text{rad}} - \Phi_{\text{rad}})$, can and does contribute to the spin-flip matrix element. This term is normally considered to produce the classical synchrotron radiation, i.e. nonflip radiation, because it does not couple to the spin operator. We see now, however, that this term which mainly produces nonflip radiation, can and does contribute to the spin-flip process, because of the change in the spin state induced by the particle recoil. It is a subtle but important effect. In practice, because the value of $\delta E/E$ is very small, the angle between $\boldsymbol{n}(z', E)$ and $\boldsymbol{n}(z', E + \delta E)$ is also very small. However, because the magnitude of the spin-independent term $-e\,(\boldsymbol{\beta}\cdot\boldsymbol{A}_{\text{rad}} - \Phi_{\text{rad}})$ is $\mathrm{O}(\hbar^0) = \mathrm{O}(1)$, it is enormously greater than that of the spin-dependent term $\boldsymbol{\Omega}_{\text{rad}}\cdot\boldsymbol{s}_{\text{op}}$ (which is $\mathrm{O}(\hbar)$). Hence, the two sets of contributions to the spin-flip matrix element are of *comparable* magnitude.

To summarize, spin-flip can occur via *two* mechanisms. One is the direct coupling of a photon to the particle's spin operator. This mechanism is easily understood. The other mechanism is indirect. It proceeds via a change to the orbital trajectory, causing a change to

the spin quantization axis, and thereby allowing the initial spin state to have a nonzero overlap with the opposite final spin state. Because of quantum mechanics, the contributions of the two mechanisms must be added in the matrix element, before squaring to calculate a cross-section. The mechanisms can, therefore, interfere with each other. We shall see this below.

Since $\delta E \ll E$, we can write to the first order in small quantities,

$$\boldsymbol{n}(z', E + \delta E) \simeq \boldsymbol{n}(z', E) + \delta E \frac{\partial \boldsymbol{n}}{\partial E} \simeq \boldsymbol{n}(z', E) + \frac{\delta E}{E}\left(\gamma \frac{\partial \boldsymbol{n}}{\partial \gamma}\right). \tag{27.16}$$

In the last line, the various factors are written in dimensionless form, which is more elegant and is the universal practice in the field. This introduces the very important phase-space derivative $\gamma(\partial \boldsymbol{n}/\partial\gamma)$ of $\boldsymbol{n}$. For brevity many authors write $\boldsymbol{d} \equiv \gamma(\partial \boldsymbol{n}/\partial\gamma)$.

The partial derivative is taken at a point in the orbital phase-space by varying the particle energy and assuming point photon emission. The definition of the partial derivative should be understood carefully. As noted, when discussing the effect of a photon emission on the orbital motion (much earlier in this review), the values of x' and y' do not change appreciably under the approximation of 'point photon emission'. The momenta p_x, p_y and p_z on the other hand, *do* change: they all suffer a fractional recoil $\boldsymbol{p} \to \boldsymbol{p}(1 - (\hbar\omega_{\rm ph}/E))$. It is also clear that the particle coordinates do not change during a point photon emission. Hence, the partial derivative is taken with respect to fixed x' and y'

$$\gamma \frac{\partial \boldsymbol{n}}{\partial \gamma} = \gamma \frac{\partial \boldsymbol{n}}{\partial \gamma}\bigg|_{x,x',y,y',\Delta t}, \tag{27.17}$$

where Δt is the time-of-arrival offset which is conjugate to the energy E. In general, the notation $\gamma(\partial \boldsymbol{n}/\partial\gamma)$ is employed without subscripts, because it is tedious to retain all the subscripts, but it is important to understand which variables are held fixed when taking the partial derivative. Since $\boldsymbol{n} \cdot \boldsymbol{n} = 1$, a partial differentiation reveals that

$$\gamma \frac{\partial \boldsymbol{n}}{\partial \gamma} \cdot \boldsymbol{n} = 0, \tag{27.18}$$

i.e. the two vectors are orthogonal at every phase-space point (or rather the two vector *fields* are orthogonal). The magnitude of $\gamma(\partial \boldsymbol{n}/\partial\gamma)$ is not constrained by any upper limit and it can become large at the locations of depolarizing spin resonances.

We can now proceed in one of two directions. Derbenev and Kondratenko (1973) attach $\boldsymbol{n}$ to an individual particle and follow it around in the orbital phase-space, and take suitable time averages over the orbital and spin motion. Mane (1987a) calculates spin-flip transition rates, etc, in an infinitesimal phase-space volume element, and takes suitable averages over the orbital and spin phase-spaces. By the hypothesis that the particle motion is ergodic, the two formalisms yield the same answer. Either way, one needs to evaluate the spin-flip transition probabilities per unit time via

$$\begin{aligned} p_{\mp} = \int_{-\infty}^{\infty} {\rm d}\tau \frac{{\rm d}^3\boldsymbol{k}}{(2\pi)^3}\frac{2\pi}{\hbar\omega} \langle \pm\boldsymbol{n}(z', E) \left| H_{\rm int}\left(t + \frac{\tau}{2}\right)\right| \mp \boldsymbol{n}(z', E - \hbar\omega)\rangle \\ \times \langle \mp\boldsymbol{n}(z', E - \hbar\omega) \left| H_{\rm int}\left(t - \frac{\tau}{2}\right)\right| \pm \boldsymbol{n}(z', E)\rangle, \end{aligned} \tag{27.19}$$

where the energy and momentum of the emitted photon are $\hbar\omega$ and $\hbar\boldsymbol{k}$, respectively. The limits of integration can safely be approximated by $\pm\infty$ because the integrands fall off rapidly for large τ and $|\boldsymbol{k}|$. This is a standard practice in synchrotron radiation calculations. To evaluate the spin-flip matrix elements, we write

$$\boldsymbol{D} = \frac{\hbar\omega}{E}\left(\gamma \frac{\partial \boldsymbol{n}}{\partial \gamma}\right). \tag{27.20}$$

We then note that to the leading order in $\hbar$,

$$|-\boldsymbol{n}(z',\,E-\hbar\omega)\rangle \simeq \mathrm{e}^{\mathrm{i}(\boldsymbol{n}\times\boldsymbol{D})\cdot\boldsymbol{s}_{\mathrm{op}}/\hbar}|-\boldsymbol{n}(z',\,E)\rangle \tag{27.21}$$

and so

$$\begin{aligned}\langle -\boldsymbol{n}(z',\,E-\hbar\omega)|H_{\mathrm{int}}|\boldsymbol{n}(z',\,E)\rangle \\ &\simeq \langle -\boldsymbol{n}|\mathrm{e}^{-\mathrm{i}(\boldsymbol{n}\times\boldsymbol{D})\cdot\boldsymbol{s}_{\mathrm{op}}/\hbar}H_{\mathrm{int}}|\boldsymbol{n}\rangle \\ &\simeq \Big\langle -\boldsymbol{n}\Big|\Big[-\frac{\mathrm{ie}}{\hbar}(\boldsymbol{n}\times\boldsymbol{D})\cdot\boldsymbol{s}_{\mathrm{op}}(\Phi_{\mathrm{rad}}-\boldsymbol{\beta}\cdot\boldsymbol{A}_{\mathrm{rad}})+\boldsymbol{\Omega}_{\mathrm{rad}}\cdot\boldsymbol{s}_{\mathrm{op}}\Big]\Big|\boldsymbol{n}\Big\rangle.\end{aligned} \tag{27.22}$$

The term in $\boldsymbol{\Omega}_{\mathrm{rad}}\cdot\boldsymbol{s}_{\mathrm{op}}$ yields the Sokolov–Ternov polarization, obviously. The term in $\boldsymbol{n}\times\boldsymbol{D}$ yields the additional Derbenev–Kondatenko contributions. Note that the two terms appear in the matrix element, hence, there is quantum-mechanical interference between them.

To dispose of another theoretical nicety, to express the above matrix element using proper quantum field theory, we should point out that the initial and final states have zero and one photons, respectively: the state $|\pm\boldsymbol{n}_{\mathrm{i}},0\rangle$ goes to $|\mp\boldsymbol{n}_{\mathrm{f}},\gamma\rangle$, with a symbolic notation 'γ' for the emitted photon. We have emphasized the electron spin state and omitted explicit mention of the photon, but it should not be overlooked.

One substitutes the above expression for the spin-flip matrix element in (27.22) into (27.19) to obtain the spin-flip transition probability per unit time. The quantities $p_{\pm}$ are then averaged over the orbital phase-space as in (27.13). We omit the details of the calculations of the matrix elements and of the spin-flip transition rates. We obtain the Derbenev–Kondratenko formula for the equilibrium degree of the radiative polarization (Derbenev and Kondratenko 1973)

$$P_{\mathrm{eq}}=\frac{8}{5\sqrt{3}}\frac{\langle\oint(\mathrm{d}\theta/|\rho|^3)\hat{\boldsymbol{b}}\cdot[\boldsymbol{n}-\gamma(\partial\boldsymbol{n}/\partial\gamma)]\rangle}{\langle\oint(\mathrm{d}\theta/|\rho|^3)[1-(2/9)(\boldsymbol{n}\cdot\hat{\boldsymbol{v}})^2+(11/18)|\gamma(\partial\boldsymbol{n}/\partial\gamma)|^2]\rangle}. \tag{27.23}$$

The vectors $\hat{\boldsymbol{v}}$ and $\hat{\boldsymbol{b}}$ were defined earlier in connection with the Baier–Katkov formula (see the statements after (27.8)). The integral over θ is around the circumference of the ring and the angle brackets are over the orbital phase-space. The term in $\gamma(\partial\boldsymbol{n}/\partial\gamma)$ in the numerator is the result of quantum mechanical interference between the terms $-e\,(\boldsymbol{\beta}\cdot\boldsymbol{A}_{\mathrm{rad}}-\Phi_{\mathrm{rad}})$ and $\boldsymbol{\Omega}_{\mathrm{rad}}\cdot\boldsymbol{s}_{\mathrm{op}}$ of the interaction Hamiltonian H_{int}, in the spin-flip photon emission matrix elements. The corresponding expression for the polarization buildup time is

$$\tau_{\mathrm{eq}}^{-1}=\tau_{\mathrm{ST}}^{-1}\Big\langle\oint\frac{\mathrm{d}\theta}{|\rho|^3}\Big[1-\frac{2}{9}(\boldsymbol{n}\cdot\hat{\boldsymbol{v}})^2+\frac{11}{18}\Big|\gamma\frac{\partial\boldsymbol{n}}{\partial\gamma}\Big|^2\Big]\Big\rangle. \tag{27.24}$$

The derivative $\gamma(\partial\boldsymbol{n}/\partial\gamma)$ vanishes for a planar ring, because $\boldsymbol{n}=\hat{\boldsymbol{b}}$ on all orbits, hence for a planar ring the above expression reduces to the Sokolov–Ternov result.

The above formulae were derived by setting $g=2$ in the photon emission matrix elements. Mane (1986) calculated the first order corrections in a to the terms in $\gamma(\partial\boldsymbol{n}/\partial\gamma)$ in (27.23) and (27.24). The results are of academic interest only. They are insignificant for real rings.

Very significantly, the Derbenev–Kondratenko formula is a completely abstract formula, based purely on fundamental physical principles of higher classical dynamics (the definition of $\boldsymbol{n}$), statistical mechanics (the numerous averages and most especially the proper characterization of the concept of spin-flip) and semiclassical quantum electrodynamics (the actual interaction Hamiltonian and matrix elements). We never, at any stage, wrote down a beta function or assumed decoupled betatron oscillations, or anything about nonlinear orbital dynamics, etc. All of the details of the accelerator structure are encapsulated in the vector field $\boldsymbol{n}$ and its partial derivative $\gamma(\partial\boldsymbol{n}/\partial\gamma)$.

This is the great power of the Derbenev–Kondratenko formulation: it cleanly separates the quantum electrodynamic perturbation theory from the accelerator physics perturbation theory

(expansion in powers of the amplitudes of the orbital oscillations). To actually evaluate the above formula for a (model of a) real accelerator, we need to calculate both $\boldsymbol{n}$ and $\gamma(\partial\boldsymbol{n}/\partial\gamma)$, as functions of the orbital phase-space variables. This usually entails the use of perturbation theory, although modern nonperturbative algorithms do now exist, and have been reviewed above. The expressions for $\boldsymbol{n}$ and $\gamma(\partial\boldsymbol{n}/\partial\gamma)$ depend heavily on the product $a\gamma$, and $a\gamma \gg 1$ in modern machines such as LEP and HERA. But a perturbation expansion in the orbital oscillation amplitudes is distinct from perturbation theory in the quantum electrodynamics.

The Derbenev–Kondratenko formula assumes that the photon emission takes place in a locally uniform magnetic field, i.e. the synchrotron radiation is assumed to be emitted from dipole magnets. It does not take into account synchrotron radiation from more complicated devices such as undulators or free-electron lasers, etc.

27.6. Useful approximate formula

A good approximation to the Derbenev–Kondratenko formula (27.23) is the following. Since almost all storage rings are planar, $\boldsymbol{b}\cdot\boldsymbol{n} \simeq 1$, and also $\boldsymbol{b}\cdot\gamma(\partial\boldsymbol{n}/\partial\gamma) \simeq 0$ to a good approximation. The denominator term $(\boldsymbol{n}\cdot\hat{\boldsymbol{v}})^2$ also vanishes to a good approximation. Hence, all that is left is the term in $|\gamma(\partial\boldsymbol{n}/\partial\gamma)|^2$. We then approximate (27.23) via

$$P_{\text{eq}} \simeq \frac{8}{5\sqrt{3}}\left(1+\frac{\tau_{\text{ST}}}{\tau_{\text{depol}}}\right)^{-1}, \tag{27.25}$$

where τ_{ST} is the Sokolov–Ternov polarization buildup time and τ_{depol} is a 'depolarizing' time, given by

$$\frac{\tau_{\text{ST}}}{\tau_{\text{depol}}} = \frac{11}{18}\frac{\langle \oint(\mathrm{d}\theta/|\rho|^3)|\gamma(\partial\boldsymbol{n}/\partial\gamma)|^2\rangle}{\oint(\mathrm{d}\theta/|\rho|^3)}. \tag{27.26}$$

Equation (27.25) has an immediate interpretation as a competition between a Sokolov–Ternov 'polarizing rate' and a 'depolarizing rate' (leading to a lower asymptotic level), arising from resonance driving terms. It is a good approximation in practice. Indeed, (27.25) is quoted far more widely than (27.23). See the discussion of spin diffusion below.

27.7. Spin diffusion

The term 'spin diffusion' is widely used in the literature on radiative polarization. It is an alternative way of visualizing the depolarization induced by the stochastic fluctuations. It has the merit of being simple to visualize. The concept of spin diffusion is actually older than the Derbenev–Kondratenko formula. In fact, one year before their definitive 1973 paper, they published a paper with the title 'Diffusion of Particle Spins in Storage Rings' (Derbenev and Kondratenko 1972). Theoretical calculations of the depolarizing resonances in the VEPP-2 storage ring were carried out using the spin diffusion model (Shatunov 1969). See figure 56 for a graph of the polarization rate in the VEPP-2 storage ring (Khoze 1971). The review by Baier (1972) cites Baier and Orlov (1966) for the development of the spin diffusion model. The 1966 paper treated spin diffusion based on a parent intrinsic resonance. The later spin diffusion work by Derbenev and Kondratenko (1972) is more general.

As with the semiclassical quantum derivation, spin diffusion also does require a recognition that the spin quantization axis depends on the orbital phase-space location; this fact is explicitly noted by Baier (1972). An alternative way to view the photon emission process is to consider that, during a photon emission, a classical spin vector $\boldsymbol{s}$ does *not* change, just as the orbital position vector $\boldsymbol{r}$ also does not change (point photon emission). However, the quantization axis $\boldsymbol{n}$ changes, as we have noted. Hence, the spin projection $\boldsymbol{s}\cdot\boldsymbol{n}$ changes slightly by virtue

of the change in $\boldsymbol{n}$. Note that when we say the spin vector 'does not change' during a photon emission, we are tacitly neglecting the Sokolov–Ternov spin-flip terms. Indeed, to discuss spin diffusion, let us for the moment neglect the Sokolov–Ternov spin-flip terms.

We follow the derivation by Shatunov (2001). Also consult figure 50 for the vectors $\boldsymbol{n}$ and $\delta\boldsymbol{n}$ before and after a photon emission. Denote the average spin projection along $\boldsymbol{n}$ by S_n, and neglect the Sokolov–Ternov terms. Then

$$\delta S_n = (\boldsymbol{S}_n \cdot \delta\boldsymbol{n}) = S_n(\boldsymbol{n} \cdot \delta\boldsymbol{n}) + S_\perp \Im(\boldsymbol{k}^* \cdot \delta\boldsymbol{n}). \tag{27.27}$$

Here $\boldsymbol{k}$ is the generalization of the vector $\boldsymbol{k}_0 = \boldsymbol{l}_0 + \mathrm{i}\boldsymbol{m}_0$, i.e. a solution of the spin precession equation and orthogonal to $\boldsymbol{n}$. Because the radiation does not depend on the spin phase, the term in $S_\perp$ averaged over many photon emissions yields zero. The resulting change to S_n is diffusive: it is of the second order in the fluctuations, i.e.

$$\delta S_n \simeq -\tfrac{1}{2}(\delta\boldsymbol{n})^2 S_n, \tag{27.28}$$

which yields

$$\frac{\mathrm{d}S_n}{\mathrm{d}t} = -\frac{1}{2}\, S_n \left\langle \left|\gamma \frac{\partial \boldsymbol{n}}{\partial \gamma}\right|^2 \frac{\mathrm{d}(\delta\gamma/\gamma)^2}{\mathrm{d}t} \right\rangle_\theta \equiv -\alpha_+ S_n, \tag{27.29}$$

where recall $\delta\boldsymbol{n} \simeq -(\hbar\omega_{\mathrm{ph}}/E)\gamma\,(\partial\boldsymbol{n}/\partial\gamma)$. Equation (27.29) is identical to equation (4.46) in Baier (1972), with appropriate changes of notation. Recall also from (9.9) that

$$\frac{\mathrm{d}(\delta\gamma/\gamma)^2}{\mathrm{d}t} = \frac{55}{24\sqrt{3}} \frac{e^2\hbar\gamma^5}{m^2c^2} \frac{1}{|\rho|^3}. \tag{27.30}$$

Hence

$$\alpha_+ = \frac{5\sqrt{3}}{8} \frac{e^2\hbar\gamma^5}{m^2c^2} \frac{11}{18} \left\langle \oint \frac{\mathrm{d}\theta}{|\rho|^3} \left|\gamma \frac{\partial \boldsymbol{n}}{\partial \gamma}\right|^2 \right\rangle. \tag{27.31}$$

This is the $(11/18)|\gamma\,(\partial\boldsymbol{n}/\partial\gamma)|^2$ term in (27.23). This is spin diffusion: the value of the average spin projection S_n evolves diffusively due to terms of second order in the fluctuations (the first-order fluctuations average to zero).

This is the most common way to view the term in $|\gamma\,(\partial\boldsymbol{n}/\partial\gamma)|^2$ in the polarization buildup time and in the denominator of the equilibrium radiative polarization level. It is at the heart of the approximate polarization formula we described above, namely, a competition between a Sokolov–Ternov 'polarizing rate' and a spin diffusion 'depolarizing rate'. One can compare them to damping and fluctuation terms, although in the case of spin the 'damping' term is not the average of the synchrotron radiation, nor is the fluctuation, a zero-mean term, centred on the damping contribution.

Note that there is also another diffusive contribution to the polarization level, namely, $P_{\mathrm{eq}} \propto |\langle\boldsymbol{n}\rangle|$, where the equilibrium distribution of the spin quantization axes is *also* established by the diffusion of the orbital motion over the orbital phase-space. This is also a diffusion in a very real sense and the value of this term is also calculated by Baier (1972), but it is not what is meant by the term 'spin diffusion'. The value of $|\langle\boldsymbol{n}\rangle|$, as we have explained earlier, is very close to unity and can usually be ignored.

The equation for the polarization buildup can be written as

$$\frac{\mathrm{d}P}{\mathrm{d}t} = \alpha_- - \alpha_+ P. \tag{27.32}$$

In terms of the spin-flip probabilities per unit time,

$$\alpha_- = \langle p_\uparrow - p_\downarrow \rangle, \qquad \alpha_+ = \langle p_\uparrow + p_\downarrow \rangle. \tag{27.33}$$

The equilibrium polarization is $P_{\rm eq} = \alpha_-/\alpha_+$ and the solution for $P(t)$, starting from $P = 0$ at $t = 0$ is

$$P(t) = \frac{\alpha_-}{\alpha_+}(1 - {\rm e}^{-\alpha_+ t}). \tag{27.34}$$

Hence, α_+ is a damping rate: the polarization degree relaxes exponentially to its equilibrium value at the rate α_+. Now note that the spin diffusion term $|\gamma\ (\partial \boldsymbol{n}/\partial\gamma)|^2$ enters the polarization formula via a contribution to α_+ only. In other words, the spin *diffusion* contributes to the polarization *damping* rate. For the above reason, the term 'diffusion' as used in the context of spin dynamics must be interpreted with some care.

Spin diffusion does not directly address the linear term in $\boldsymbol{d} = \gamma\ (\partial \boldsymbol{n}/\partial\gamma)$ in the numerator of (27.23). A marriage of classical and quantum spin models is used to derive the linear term in $\boldsymbol{d}$, e.g. see Shatunov (2001). Later in this section, the Derbenev–Kondratenko formula will be extended to also include the $O(1/\gamma)$ effects of the transverse recoils to the orbital motion. *Nobody* has come up with a classical–quantum spin diffusion model for the extra terms which appear. All of the derivations are quantum-mechanical.

27.8. Calibration of polarimeters

Let us set aside the abstract statistical-mechanical theory and consider a practical usage of the spin diffusion model. Equation (27.25) is used to calibrate the polarimeters in high-energy storage rings. The asymptotic value of the polarization is experimentally determined in the following way. From the parametrization, in terms of a polarizing and depolarizing rate, the asymptotic polarization is related to the buildup time via (writing $x = \tau_{\rm ST}/\tau_{\rm d}$)

$$P(t) = \frac{P_{\rm ST}}{1 + x}\ (1 - {\rm e}^{-(1+x)t/\tau_{\rm ST}}). \tag{27.35}$$

By measuring the buildup rate τ, and by calculating the Sokolov–Ternov term $\tau_{\rm ST}$, one can equate

$$P_\infty = \frac{P_{\rm ST}}{1 + x}. \tag{27.36}$$

If $x \gg 1$, which also implies a low asymptotic polarization level, then the polarization equilibrates quickly and one can simply observe the polarization settle to equilibrium. By measuring the polarization rise time, one can deduce the asymptotic polarization level. This is in fact the standard practice. Most graphs of experimental data of radiative polarization measurements display the *extrapolated* asymptotic polarization level.

27.9. Correlation of polarization rate and asymptotic level

Mechanisms which speed up the rate of the polarization buildup also tend to decrease the asymptotic polarization level. This is because the mechanisms for speeding up the rate of the polarization buildup are usually *isotropic*. They increase the rate of spin-flip in both the directions equally. Hence, the value of α_+ increases while that of α_- does not change.

One idea to speed up the polarization buildup, without decreasing the asymptotic polarization level, is to employ asymmetric wigglers. An asymmetric wiggler has a short sharp positive bend and a long gentle negative bend, with a total field integral of zero, as described in the work on spin light in section 2. The asymmetric wiggler is placed in a region of zero dispersion so as not to excite quantum fluctuations which would increase the beam size. Then the rate of synchrotron radiation, including spin-flip radiation, increases so that the polarization buildup speeds up.

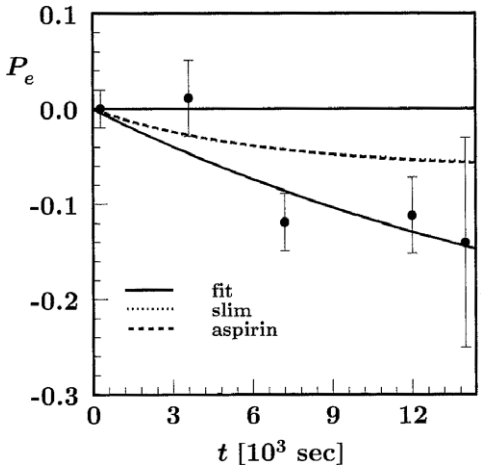

Figure 51. Measurement of the kinetic polarization at AmPS. An empirical fit to the data is shown as well as the theoretical curves using the codes SLIM and ASPIRRIN (the figure mislabels the code as 'aspirin'). The SLIM and ASPIRRIN curves lie on top of each other. From Passchier (2000).

The use of asymmetric wigglers was suggested for LEP, because otherwise at a beam energy of 45.6 GeV (the so-called LEP1) the Sokolov–Ternov polarization buildup time was in excess of 5 h. A set of so-called 'polarization wigglers' were, therefore, installed at LEP. They turned out to be successful for applications having nothing to do with the spin, and *not* successful for polarization work. The LEP polarization wigglers increased the energy spread of the beam; this enhanced the strength of the depolarizing resonances (basically the synchrotron sideband resonances), thereby reducing the asymptotic polarization to a low level. Ultimately, they were not used for polarization work. Nevertheless, the name 'polarization wigglers' was retained. The polarization wigglers were extremely useful for LEP2, enabling much higher beam currents and luminosities to be attained.

Ultimately, it remains the case for all known machines that an increase in the polarization buildup rate is accompanied by a reduction in the asymptotic polarization level.

27.10. Kinetic polarization

The linear term in $\hat{\boldsymbol{b}} \cdot \gamma(\partial \boldsymbol{n}/\partial\gamma)$ in (27.23) is called the 'kinetic polarization' term. It has never been observed. In general, $\boldsymbol{n}$ is almost vertical in the arcs, and so $\hat{\boldsymbol{b}} \cdot \boldsymbol{n} \simeq 1$ and so $\hat{\boldsymbol{b}} \cdot \boldsymbol{d} \simeq 0$ in most machines. One needs $\hat{\boldsymbol{b}} \cdot \boldsymbol{n} = 0$ on the design orbit and also $\hat{\boldsymbol{b}} \cdot \boldsymbol{d} \neq 0$ to truly observe the kinetic polarization. Such is the case in an electron ring with a single Siberian Snake (AmPS and SHR). Figure 51 is, from an attempted measurement, the kinetic polarization at AmPS (Passchier 2000). The data are limited. The theoretical fits were performed using the codes SLIM (Chao 1981b) and ASPIRRIN (Perevedentsev *et al* 2003). The theoretical fits are preliminary, and do not really fit the data. A direct observation of the kinetic polarization term would spectacularly verify the Derbenev–Kondratenko formula.

27.11. Statistical-mechanical evolution equation for spin–orbit distribution

The Derbenev–Kondratenko formula (27.23) is to this day the definitive formula to calculate the equilibrium radiative polarization in high-energy electron and positron storage rings. Further

work in the field has been to mainly develop formalisms to evaluate the formula for models of actual storage rings (e.g. as opposed to the idealized case of a purely planar ring). In most cases, these formalisms are numerical algorithms, and have been coded into computer programs. We have already seen many of the formalisms, although we discussed only $\boldsymbol{n}$ and not the derivative $\gamma(\partial \boldsymbol{n}/\partial\gamma)$.

As for formal theory, note that the Sokolov–Ternov and Derbenev–Kondratenko formulae all describe the equilibrium or asymptotic polarization. They do not describe the evolution of the polarization as a function of the time, or, in accelerator coordinates, the azimuth, other than to say that the polarization of an initially unpolarized beam builds up exponentially. The formalisms do not treat decoherence (of the spins), for example. An important equation to describe the transport and diffusion of a beam distribution in phase-space is the Fokker–Planck equation. Jowett (1987) gives an account of the stochastic processes and statistical mechanics for the orbital motion in high-energy electron storage rings. Barber and co-workers have pursued the idea of extending the Fokker–Planck equation to also include spin transport and diffusion (Heinemann and Barber 2001a, 2001b). As before, we denote a point in the orbital phase-space by z and the azimuth by θ. Let the orbital phase-space density of the particles be $\psi(z, \theta)$. The Fokker–Planck equation for ψ is

$$\frac{\partial \psi}{\partial \theta} = \mathcal{L}_{\mathrm{FP,orb}}\, \psi(z, \theta), \tag{27.37}$$

where the orbital Fokker–Planck operator $\mathcal{L}_{\mathrm{FP,orb}}$ can be written as

$$\mathcal{L}_{\mathrm{FP,orb}} = \mathcal{L}_{\mathrm{Ham}} + \mathcal{L}_0 + \mathcal{L}_1 + \mathcal{L}_2. \tag{27.38}$$

Here, $\mathcal{L}_{\mathrm{Ham}}$ simply contains a Poisson bracket with the orbital Hamiltonian and would lead to a nonradiative equation of motion. The other operators $\mathcal{L}_{0,1,2}$ are terms due to the radiation damping and noise. Explicit expressions for the operators are given by Jowett (1987). In this formulation, the photon emission is modelled as a Gaussian white noise process (with zero mean) plus continuous radiation damping. The operators $\mathcal{L}_{0,1,2}$ contain the zeroth, first and second order derivatives, respectively, for the components of z. The key idea, to derive a corresponding equation for the polarization, is to introduce the notion of a phase-space polarization density $\boldsymbol{\mathcal{P}}$ of the form

$$\boldsymbol{\mathcal{P}}(z, \theta) = \boldsymbol{P}_{\mathrm{loc}}(z, \theta)\, \psi(z, \theta), \tag{27.39}$$

where $\boldsymbol{P}_{\mathrm{loc}}$ is the 'local' polarization in an infinitesimal phase-space volume element centred on z. It is essential to note that a Fokker–Planck equation cannot be written for $\boldsymbol{P}_{\mathrm{loc}}$ itself. One must work with $\boldsymbol{\mathcal{P}}$, which contains a joint spin–orbit density. See Heinemann and Barber (2001a) for details. The final equation is

$$\frac{\partial \boldsymbol{\mathcal{P}}}{\partial \theta} = \mathcal{L}_{\mathrm{FP,orb}}\, \boldsymbol{\mathcal{P}} + \boldsymbol{W} \times \boldsymbol{\mathcal{P}}, \tag{27.40}$$

where recall $\boldsymbol{W} = \boldsymbol{W}(z, \theta)$ is the spin precession vector at a particular point in the orbital phase-space. This equation is much more comprehensive than the Baier–Katkov–Strakhovenko formula (27.9). The polarization of the whole beam, at an azimuth θ, is given by

$$\boldsymbol{P}(\theta) = \int \boldsymbol{\mathcal{P}}(z, \theta)\, \mathrm{d}z. \tag{27.41}$$

The evolution equation is for the joint spin–orbit distribution. There is no simple evolution equation for only the polarization $\boldsymbol{P}$ itself. Heinemann (1997) has applied (27.40) to various simple exactly solvable models, e.g. to calculate the decoherence of the spins of a spin-polarized beam after injection into an accelerator (see section 21).

27.12. Transverse momentum recoils

27.12.1. General remarks. We now extend the theory to include the momentum recoil in both the transverse and longitudinal directions. The contribution from the transverse recoils is much smaller, by roughly $O(1/\gamma)$, than from the longitudinal recoils. They have no significance in present-day storage rings. They are of theoretical interest, however, because they connect to some interesting work on the coupling of the Unruh effect to the electron spin in ultrarelativistic accelerators. We discuss the Unruh effect below.

27.12.2. Unruh effect. Unruh (1976) showed that an observer in a uniformly accelerated reference frame would observe the vacuum electromagnetic fluctuations to have a thermal (blackbody) spectrum with a temperature

$$T = \frac{\hbar a_*}{2\pi c k_B}. \tag{27.42}$$

Here, a_* is the proper acceleration of the observer (the acceleration in an inertial reference frame instantaneously comoving with the observer) and k_B is Boltzmann's constant. This followed from an earlier finding by Hawking (1974) that the effects of a strong gravitational field on the quantum fluctuations of the vacuum would cause a black hole to radiate with a temperature $T' = (\hbar g_*)/(2\pi c k_B)$, where g_* is the acceleration due to gravity at the surface of the black hole. We append subscript asterisks to the accelerations, to avoid confusion with the quantities a and g for a particle spin. The fact that the vacuum has a nonzero temperature in an accelerated reference frame is called the Unruh effect, and the temperature T is called the Unruh, or Hawking–Unruh, temperature. Some years later, the late John Bell (of Bell's theorem fame), in collaboration with various co-workers, investigated the possibility of using the coupling of an electron's spin to the vacuum fluctuations of the electromagnetic field as a possible detector of the Unruh effect (Bell and Leinaas 1983, 1987, Bell *et al* 1985). The latest of those works is the most definitive and supersedes the previous ones, and will be reviewed below. Note that Leinaas (2002) has also written a summary of the Bell–Leinaas work.

First, the Unruh temperature mentioned above is for an observer undergoing *linear* acceleration. For all realizable accelerations in a laboratory, the Unruh temperature is too small to be observable. However, the centripetal acceleration in ultrarelativistic circular motion in an orbit of radius ρ is c^2/ρ, and for values of ρ in present-day accelerators, this acceleration is very much larger than any achievable linear acceleration. The possibility of detecting the Unruh effect is, therefore, much more promising in a circularly accelerated reference frame. Hence, Bell *et al* were led to study the vacuum fluctuations of the electromagnetic field in a circularly accelerated reference frame. This is known as the circular Unruh effect. In this case, Bell and Leinaas (1987) reported an effective temperature of

$$T = \frac{13}{96}\sqrt{3}\,\frac{\hbar a_*}{c k_B} \tag{27.43}$$

for the vacuum fluctuations which couple to the particle spin. This is a higher effective temperature than in the linear case. Hacyan and Sarmiento (1989) calculated the energy–stress–momentum tensor of the vacuum electromagnetic field, for both linearly and circularly uniformly accelerated observers. Another paper on the subject is by Hirayama and Hara (1999). The Hacyan–Sarmiento and Hirayama–Hara papers do not treat the coupling to a particle spin, and so they are not directly relevant to this paper, but they did find that for circular acceleration, the vacuum fluctuations do not have a thermal spectrum. Unruh (1998) re-examined his original calculation and also the case of circular acceleration and confirmed the Bell–Leinaas finding. Unruh (1998) reported that the higher effective temperature is due

to the details of the spin–orbit coupling, rather than the nonthermal nature of the vacuum fluctuations.

Bell *et al* investigated the coupling of the vacuum electromagnetic fields to the spin of a particle, where the spin is at rest (say at the origin), of a uniformly circularly accelerated reference frame. The motivating idea is that the vacuum fluctuations might polarize the spin. The value of the polarization, as a function of suitably defined parameters, might have a unique signature which could signal the Unruh effect. Bell and Leinaas (1987) calculated the polarization for particle motion in a planar ring. As we know, in addition to inducing spin-flip, the vacuum fluctuations also induce recoils in the particle motion. They considered the effect of the transverse momentum recoils on the *vertical momentum* of the particle, i.e. the vertical betatron emittance induced by the transverse momentum recoils. This effect is small and is neglected in most practical calculations for real rings. The previous Derbenev–Kondratenko formalism treated only the longitudinal recoils (energy loss), as noted earlier. Bell and Leinaas (1987) treated a perfectly aligned planar ring (zero vertical dispersion) with weak focusing of the vertical betatron oscillations. ('Weak' focusing just to simplify the theoretical analysis. Strong focusing will also prove their point. See below.) They found that, at a suitable energy, the polarization would exhibit a resonance, and the maximum value of the polarization is approximately 99.2%. Far away from the resonance, the polarization approached the Sokolov–Ternov value of $8/(5\sqrt{3}) \simeq 92.4\%$. The Bell–Leinaas expression for the equilibrium degree of the polarization in a planar weak-focusing ring is

$$P_{\rm BL} = \frac{8}{5\sqrt{3}} \frac{1 - (f_{\rm BL}/6)}{1 - (f_{\rm BL}/18) + (13/360) f_{\rm BL}^2}, \tag{27.44}$$

where

$$f_{\rm BL} = \frac{2}{\gamma} \frac{Q_y^2 \nu}{Q_y^2 - \nu^2} = \frac{2a}{1 - (\nu/Q_y)^2}. \tag{27.45}$$

Here, $\nu = a\gamma$ and recall $a = (g-2)/2$ and γ is the Lorentz factor of the beam energy. Finally, Q_y is the vertical betatron tune. For a weak-focusing machine $0 < Q_y < 1$. At $\nu = Q_y$ the term in (27.45) diverges, i.e. there is a resonance. A graph of $P_{\rm BL}$ as a function of ν/Q_y is plotted in figure 52. The polarization actually drops to a negative value on the low energy side of the resonance, with a minumum value of approximately -0.169, and climbs to a high value, with a maximum of approximately 0.992, on the high energy side. Far from resonance, $f_{\rm BL} \to 0$ and the degree of the polarization is the Sokolov–Ternov value of $8/(5\sqrt{3}) \simeq 0.924$. Obviously, an infinity in $f_{\rm BL}$ is an artifact of the perturbation theory.

The above finding of a high polarization, and a possible detectable signal of the circular Unruh effect, aroused considerable interest. The most obvious question is, of course, how/why is this result different from that of quantum electrodynamics? The answer is that it is not. We review the quantum electrodynamic formulation of this problem in the next section.

27.12.3. QED formulation. Bell and Leinaas (1987) treated a model of a planar ring and included the effects of the vertical transverse recoils due to the photon emissions (they did not treat the horizontal transverse recoils). Sokolov and Ternov (1964) included only the longitudinal recoils (energy loss) in their treatment of a planar ring. The Derbenev–Kondratenko formalism treats spin resonances, but their formula also only treats longitudinal recoils. Barber and Mane (1988) extended Derbenev and Kondratenko's formalism to treat both longitudinal recoils and transverse recoils, parallel to the local magnetic field. Their generalized formula reproduces the Bell–Leinaas findings. Hence, we can conclude that the circular Unruh effect calculations provide an independent confirmation of the semiclassical

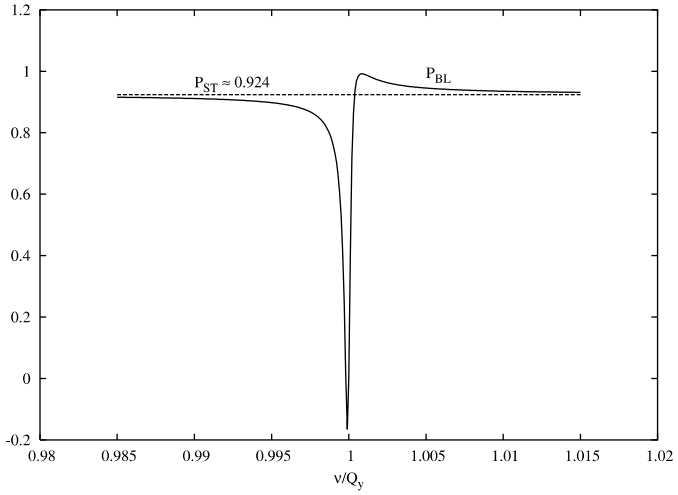

Figure 52. Graph of the Bell–Leinaas polarization $P_{\rm BL}$ as a function of the ratio ν/Q_y, where ν is the spin tune and Q_y is the vertical betatron tune. The Sokolov–Ternov polarization $P_{\rm ST} = 8/(5\sqrt{3}) \simeq 0.924$ is also indicated by a dashed line.

QED radiative polarization calculations. We describe the Barber–Mane calculation briefly below.

Recall the coordinate system for motion in a locally circular arc, namely, $(\hat{\boldsymbol{v}}, \dot{\hat{\boldsymbol{v}}}, \hat{\boldsymbol{b}})$, defined earlier. Denote the momentum of the particle by $\boldsymbol{p}$ and its dimensionless velocity vector by $\boldsymbol{\beta} = \boldsymbol{v}/c$. The component of $\boldsymbol{\beta}$ parallel to $\hat{\boldsymbol{b}}$ is denoted by $\beta_b = \boldsymbol{\beta}\cdot\hat{\boldsymbol{b}}$. Then define the additional partial derivative $\partial\boldsymbol{n}/\partial\beta_b$. The polarization formula, taking into account both longitudinal recoils and those along $\hat{\boldsymbol{b}}$, is then (Barber and Mane 1988)

$$
\begin{aligned}
P_{\rm BM} &= \frac{8}{5\sqrt{3}}\frac{\alpha_-^{\rm BM}}{\alpha_+^{\rm BM}},\\
\alpha_-^{\rm BM} &= \Big\langle \oint \frac{{\rm d}\theta}{|\rho|^3}\Big[\boldsymbol{n}\cdot\hat{\boldsymbol{b}} - \gamma\frac{\partial\boldsymbol{n}}{\partial\gamma}\cdot\hat{\boldsymbol{b}} + \frac{1}{3\gamma}\frac{\partial\boldsymbol{n}}{\partial\beta_b}\cdot\hat{\boldsymbol{v}}\Big]\Big\rangle,\\
\alpha_+^{\rm BM} &= \Big\langle \oint \frac{{\rm d}\theta}{|\rho|^3}\Big[1 - \frac{2}{9}(\boldsymbol{n}\cdot\hat{\boldsymbol{v}})^2 + \frac{11}{18}\Big|\gamma\frac{\partial\boldsymbol{n}}{\partial\gamma}\Big|^2 + \frac{1}{9\gamma}\dot{\hat{\boldsymbol{v}}}\cdot\Big(\boldsymbol{n}\times\frac{\partial\boldsymbol{n}}{\partial\beta_b}\Big) + \frac{13}{90\gamma^2}\Big|\frac{\partial\boldsymbol{n}}{\partial\beta_b}\Big|^2\Big]\Big\rangle.
\end{aligned}
\tag{27.46}
$$

The above formula is quite general and is applicable to both strong and weak focusing accelerators. We now specialize to the case of a planar ring with vertical (not necessarily weak) focusing. It can be shown that $\gamma(\partial\boldsymbol{n}/\partial\gamma)$ vanishes in this model, just as it does in the Sokolov–Ternov model, although we do not prove it here. Then define a new vector

$$
\boldsymbol{f}_{\rm BM} = -\frac{2}{\gamma}\frac{\partial\boldsymbol{n}}{\partial\beta_b}. \tag{27.47}
$$

The equilibrium polarization in a planar ring with vertical focusing is

$$
P'_{\rm BM} = \frac{8}{5\sqrt{3}}\frac{\langle \oint ({\rm d}\theta/|\rho|^3)[\hat{\boldsymbol{b}}\cdot\boldsymbol{n} - (1/6)\hat{\boldsymbol{v}}\cdot\boldsymbol{f}_{\rm BM}]\rangle}{\langle \oint ({\rm d}\theta/|\rho|^3)[1 - (2/9)(\boldsymbol{n}\cdot\hat{\boldsymbol{v}})^2 - (1/18)\dot{\hat{\boldsymbol{v}}}\cdot(\boldsymbol{n}\times\boldsymbol{f}_{\rm BM}) + (13/360)|\boldsymbol{f}_{\rm BM}|^2]\rangle}. \tag{27.48}
$$

We must evaluate $\boldsymbol{n}$ and $\boldsymbol{f}_{\rm BM}$ for this model, in the special case of weak focusing. The reader is directed to Barber and Mane (1988) for the explicit calculations. The answer is

$$\boldsymbol{f}_{\rm BM} = \Big[\frac{2}{\gamma} + \frac{2a}{1-(\nu/Q_y)^2}\Big]\hat{v}. \tag{27.49}$$

Hence, define

$$f_{\rm BM} = \frac{2}{\gamma} + \frac{2a}{1-(\nu/Q_y)^2} = f_{\rm BL} + \frac{2}{\gamma}. \tag{27.50}$$

We obtain

$$P_{\rm BM} = \frac{8}{5\sqrt{3}}\frac{1-(f_{\rm BM}/6)}{1-(f_{\rm BM}/18)+(13/360)f_{\rm BM}^2}, \tag{27.51}$$

which is basically the same as (27.44). The difference between $f_{\rm BL}$ and $f_{\rm BM}$ is a nonresonant term, and hence is not important. We can, therefore, claim that the Barber–Mane and the Bell–Leinaas expressions agree.

We can also solve for $\boldsymbol{n}$, for a planar ring with strong focusing, and substitute the results into (27.48). There is still a resonance.

This demonstrates that lab-frame QED can indeed explain the Bell–Leinaas result. The modern view is that the radiative polarization of the particle spins in a storage ring is, therefore, a manifestation of the circular Unruh effect. There is no 'extra' contribution to the polarization beyond that of lab-frame QED, but there is, rather, an independent confirmation of QED.

27.13. Transverse momentum recoils in all planes

Mane (1987c) extended the polarization formula to include transverse recoils in all planes. Hand and Skuja (1987, 1989) also published a formalism to calculate the equilibrium radiative polarization, treating recoils in all planes. The slight differences of detail in some of the transverse recoil terms between the Mane and Hand–Skuja formulae have never been resolved; the terms in question are simply too small to be of any practical significance.

28. Radiative polarization II

28.1. Spin–orbit coupling vector

The quantity $\gamma(\partial\boldsymbol{n}/\partial\gamma)$ is called the *spin–orbit coupling function* or the *spin–orbit coupling vector*. It is, of course, a vector field, but no matter. Shatunov (2001) employs the designation 'vector of spin–orbit coupling' in his lecture. The origin of the name is historical, basically a compromise to clarify certain confusions. As far as we can trace the matter, the term 'spin–orbit coupling vector' was suggested by Kondratenko at the 1982 Workshop on Polarized Electron Acceleration and Storage at Hamburg, available as DESY Report M-82/09. Many non-Soviet authors designated $\gamma(\partial\boldsymbol{n}/\partial\gamma)$ by names such as the 'spin dispersion' or the 'spin chromaticity' but all such names are now obsolete. The term 'spin–orbit coupling vector', although a bit vague, is the universal modern name.

In recent years, the term 'spin chromaticity' has resurfaced, with the correct interpretation as the variation of the *spin tune* for an off-axis particle with a momentum offset $\Delta p/p$. Analogously to the orbital chromaticity, one can write, starting from the closed-orbit spin tune,

$$\nu = \nu_{\rm c.o.} + \xi_{\rm spin}\frac{\Delta p}{p}. \tag{28.1}$$

We have in fact discussed the spin chromaticity, defined in this way, earlier in this review.

In this section, we review some of the formalisms which have been developed to evaluate the theoretical formulae for actual accelerators. Most of the formalisms below are analytical. There is one formalism which is purely numerical, i.e. it tracks particles and their spins via numerical integration of the equations of motion, with Monte Carlo simulations of stochastic fluctuations, damping and spin-flip, etc. That programme is SITROS (Kewisch *et al* 1989). It will not be reviewed in detail below.

28.2. Solution of simple model

We treat a planar ring with a single solenoid, which we take to be a full-strength Siberian Snake. We assume ultrarelativistic motion so the spin precession angle in the solenoid is proportional to $1/\gamma$. The model was solved by Korostelev and Shatunov (2001). They included the contribution of both the betatron and synchrotron oscillations, and gave the solution for $\boldsymbol{d}_0$ at all azimuths around the ring. The derivation below is a special case of theirs, treating only the synchrotron oscillations, and we give the solution only at the origin. We place the origin just before the solenoid. The spin precession vector is

$$\boldsymbol{W} = a\gamma \boldsymbol{e}_3 + \pi \frac{\gamma_0}{\gamma}\, \delta_p(\theta - 0^+)\, \boldsymbol{e}_2. \tag{28.2}$$

The one-turn map is

$$\begin{aligned} M &= \mathrm{e}^{-\mathrm{i}\pi a\gamma\sigma_3}\, \mathrm{e}^{-\mathrm{i}\pi(\gamma_0/\gamma)\sigma_2/2} \\ &= \cos(\pi a\gamma)\cos\left(\frac{\pi}{2}\frac{\gamma_0}{\gamma}\right) + \mathrm{i}\sigma_1 \sin(\pi a\gamma)\sin\left(\frac{\pi}{2}\frac{\gamma_0}{\gamma}\right) \\ &\quad - \mathrm{i}\sigma_2 \cos(\pi a\gamma)\sin\left(\frac{\pi}{2}\frac{\gamma_0}{\gamma}\right) - \mathrm{i}\sigma_3 \sin(\pi a\gamma)\cos\left(\frac{\pi}{2}\frac{\gamma_0}{\gamma}\right) \\ &\equiv \cos(\pi\nu) - \mathrm{i}\sin(\pi\nu)\boldsymbol{\sigma}\cdot\boldsymbol{n}. \end{aligned} \tag{28.3}$$

The design-orbit map is of course

$$M_0 = \mathrm{i}\sigma_1 \sin(\pi\nu_0) - \mathrm{i}\sigma_2 \cos(\pi\nu_0), \tag{28.4}$$

with $\nu_0 = a\gamma_0$, Then $\nu_{\mathrm{c.o.}} = \frac{1}{2}$ and

$$\boldsymbol{n}_0 = -\boldsymbol{e}_1 \sin(\pi\nu_0) + \boldsymbol{e}_2 \cos(\pi\nu_0). \tag{28.5}$$

Now

$$\cos(\pi\nu) = \cos(\pi a\gamma)\cos\left(\frac{\pi}{2}\frac{\gamma_0}{\gamma}\right). \tag{28.6}$$

Hence,

$$-\pi\gamma\frac{\partial\nu}{\partial\gamma}\,\sin(\pi\nu) = -\pi a\gamma\,\sin(\pi a\gamma)\cos\left(\frac{\pi}{2}\frac{\gamma_0}{\gamma}\right) + \frac{\pi}{2}\frac{\gamma_0}{\gamma}\cos(\pi a\gamma)\sin\left(\frac{\pi}{2}\frac{\gamma_0}{\gamma}\right). \tag{28.7}$$

Evaluating on the design orbit,

$$\gamma\frac{\partial\nu}{\partial\gamma}\bigg|_{\mathrm{c.o.}} = -\frac{1}{2}\frac{\cos(\pi\nu_0)}{\sin(\pi\nu_0)}, \tag{28.8}$$

which is finite as long as $\sin(\pi\nu_0) \neq 0$. As for $\boldsymbol{n}$,

$$\gamma\frac{\partial}{\partial\gamma}(\sin(\pi\nu)\boldsymbol{\sigma}\cdot\boldsymbol{n}) = \pi\gamma\frac{\partial\nu}{\partial\gamma}\cos(\pi\nu)\boldsymbol{\sigma}\cdot\boldsymbol{n} + \sin(\pi\nu)\boldsymbol{\sigma}\cdot\boldsymbol{d}, \tag{28.9}$$

writing $\boldsymbol{d}$ for $\gamma\,(\partial\boldsymbol{n}/\partial\gamma)$. Evaluating on the design orbit, $\cos(\pi\nu_{\mathrm{c.o.}}) = 0$ and $\sin(\pi\nu_{\mathrm{c.o.}}) = 1$, hence

$$\left[\gamma\frac{\partial}{\partial\gamma}(\sin(\pi\nu)\boldsymbol{\sigma}\cdot\boldsymbol{n})\right]_{\mathrm{c.o.}} = \boldsymbol{\sigma}\cdot\boldsymbol{d}_0. \tag{28.10}$$

From the one-turn map,

$$\gamma\frac{\partial}{\partial\gamma}(\sin(\pi\nu)\boldsymbol{\sigma}\cdot\boldsymbol{n}) = -\sigma_1\Big[\pi a\gamma\cos(\pi a\gamma)\sin\Big(\frac{\pi}{2}\frac{\gamma_0}{\gamma}\Big) - \frac{\pi}{2}\frac{\gamma_0}{\gamma}\sin(\pi a\gamma)\cos\Big(\frac{\pi}{2}\frac{\gamma_0}{\gamma}\Big)\Big]$$
$$-\sigma_2\Big[\pi a\gamma\sin(\pi a\gamma)\sin\Big(\frac{\pi}{2}\frac{\gamma_0}{\gamma}\Big) + \frac{\pi}{2}\frac{\gamma_0}{\gamma}\cos(\pi a\gamma)\cos\Big(\frac{\pi}{2}\frac{\gamma_0}{\gamma}\Big)\Big]$$
$$+\sigma_3\Big[\pi a\gamma\cos(\pi a\gamma)\cos\Big(\frac{\pi}{2}\frac{\gamma_0}{\gamma}\Big) + \frac{\pi}{2}\frac{\gamma_0}{\gamma}\sin(\pi a\gamma)\sin\Big(\frac{\pi}{2}\frac{\gamma_0}{\gamma}\Big)\Big]. \tag{28.11}$$

Evaluating on the design orbit,

$$\boldsymbol{d}_0 = -\pi\nu_0[\boldsymbol{e}_1\cos(\pi\nu_0) + \boldsymbol{e}_2\,\sin(\pi\nu_0)] + \boldsymbol{e}_3\frac{\pi}{2}\sin(\pi\nu_0). \tag{28.12}$$

Evidently, $\boldsymbol{n}_0\cdot\boldsymbol{d}_0 = 0$. Depending on the value of ν_0, the magnitude of $\boldsymbol{d}_0$ can be arbitrarily large.

28.3. Smile

The Smile algorithm was reviewed earlier in this paper, in section 17. The solution for $\boldsymbol{n}$ was expressed as a θ-ordered exponential of noncommuting angular momentum operators, which was evaluated using a Taylor expansion in powers of the orbital amplitudes around the closed orbit. Consult section 17 for the details. Treating only linear orbital dynamics, one can express the orbital trajectory X as a sum of eigenvector modes $X = \sum_j a_j\,E_j$, where $j = \pm1, \pm2, \pm3$. Furthermore,

$$\gamma\frac{\partial X}{\partial\gamma} = \sum_j \gamma\frac{\partial a_j}{\partial\gamma}\,E_j, \tag{28.13}$$

where from (10.15)

$$\gamma\frac{\partial a_j}{\partial\gamma} = \begin{cases} -\mathrm{i}E^*_{5j} & j > 0 \\ \mathrm{i}E^*_{5j} & j < 0. \end{cases} \tag{28.14}$$

All of this is directly applicable to the Smile algorithm. One can expand V_1, say, into a sum of spin integrals over orbital eigenvector modes

$$V_1 = \sum a_1^{m_1}a_{-1}^{m_{-1}}a_2^{m_2}a_{-2}^{m_{-2}}a_3^{m_3}a_{-3}^{m_{-3}}V_1^{m_1m_{-1}m_2m_{-2}m_3m_{-3}}. \tag{28.15}$$

Then

$$\gamma\frac{\partial V_1}{\partial\gamma} = \sum\gamma\frac{\partial}{\partial\gamma}(a_1^{m_1}a_{-1}^{m_{-1}}a_2^{m_2}a_{-2}^{m_{-2}}a_3^{m_3}a_{-3}^{m_{-3}})V_1^{m_1m_{-1}m_2m_{-2}m_3m_{-3}}, \tag{28.16}$$

i.e. a term-by-term sum of phase-space derivatives, assuming of course that the whole thing converges, which as we have seen (for $\boldsymbol{n}$) it may not. The phase-space derivative of an individual term is given by

$$\gamma\frac{\partial}{\partial\gamma}(a_1^{m_1}a_{-1}^{m_{-1}}a_2^{m_2}a_{-2}^{m_{-2}}a_3^{m_3}a_{-3}^{m_{-3}}) = m_1\left(\gamma\frac{\partial a_1}{\partial\gamma}\right)a_1^{m_1-1}a_{-1}^{m_{-1}}a_2^{m_2}a_{-2}^{m_{-2}}a_3^{m_3}a_{-3}^{m_{-3}}$$
$$+m_{-1}\left(\gamma\frac{\partial a_{-1}}{\partial\gamma}\right)a_1^{m_1}a_{-1}^{m_{-1}-1}a_2^{m_2}a_{-2}^{m_{-2}}a_3^{m_3}a_{-3}^{m_{-3}} + \cdots. \tag{28.17}$$

The same ideas apply also to V_0 and V_{-1}. The statistical averages required are $\langle\boldsymbol{n}\rangle$, $\langle\gamma(\partial\boldsymbol{n}/\partial\gamma)\rangle$, $\langle(\boldsymbol{n}\cdot\hat{\boldsymbol{v}})^2\rangle$ and $\langle|\gamma(\partial\boldsymbol{n}/\partial\gamma)|^2\rangle$. The one over $|\gamma(\partial\boldsymbol{n}/\partial\gamma)|^2$ is typically the most important.

28.4. SLIM

Historically, before a general Taylor series expansion to all orders in all the orbital modes was developed, there was, for several years, a solution to the first order in the orbital amplitudes only. This was the SLIM algorithm, developed by Chao (1981a). It is an important formalism. We shall ignore any sociological issues concerning the fact that previous Soviet theoretical solutions may have existed for $\boldsymbol{n}$ and $\boldsymbol{d}$ to the first order in the orbital amplitudes, e.g. see equation (3.7) of Derbenev *et al* (1979c). Chao (1981a) formulated the SLIM algorithm using the so-called 'generalized matrices' but we shall employ a different derivation to avoid introducing yet more formalism. Recall from (15.12) that the solution for $\boldsymbol{n}$ can be parametrized as $\boldsymbol{n} = \boldsymbol{n}_0\sqrt{1-|\zeta|^2} + \Re(\zeta \boldsymbol{k}_0^*)$ and to the first order in the orbital amplitudes, the solution for ζ is (see (15.16))

$$\zeta \simeq -\mathrm{i}\int_{-\infty}^{\theta} \boldsymbol{w}_+ \,\mathrm{d}\theta'. \tag{28.18}$$

All of the notation has been explained in sections 15 and 17. In terms of the orbital symplectic eigenvector formalism, we write

$$\zeta \simeq -\mathrm{i}\sum_j a_j \int_{-\infty}^{\theta} \boldsymbol{w}_{j+} \,\mathrm{d}\theta'. \tag{28.19}$$

The $\boldsymbol{w}_{j+}$ are proportional to the orbital oscillation modes E_j. To calculate $\boldsymbol{d}$, we want the derivative $\gamma(\partial\zeta/\partial\gamma)$. To this level of approximation $\boldsymbol{d} \simeq \boldsymbol{d}_0$, with obvious notation. Then

$$\boldsymbol{d}_0 = \Re\left\{\gamma\frac{\partial\zeta}{\partial\gamma}\boldsymbol{k}_0^*\right\}. \tag{28.20}$$

To the first order, using (10.15),

$$\begin{aligned}\gamma\frac{\partial\zeta}{\partial\gamma} &= -\mathrm{i}\sum_j \gamma\frac{\partial a_j}{\partial\gamma}\int_{-\infty}^{\theta}\boldsymbol{w}_{j+}\,\mathrm{d}\theta' \\ &= -\sum_{j>0} E_{5j}^*\int_{-\infty}^{\theta}\boldsymbol{w}_{j+}\,\mathrm{d}\theta' + \sum_{j<0} E_{5j}^*\int_{-\infty}^{\theta}\boldsymbol{w}_{j+}\,\mathrm{d}\theta'.\end{aligned} \tag{28.21}$$

This is, of course, the type of expression which SMILE later generalized to higher orders, but it not easily visualizable in terms of the machine lattice parameters (the beta and dispersion functions, etc).

A more transparent expression was given by Yokoya (1982), in terms of the accelerator lattice functions. We follow the above paper, with small changes of notation to conform to the definitions in this paper, and write

$$\boldsymbol{d}_0 = \tfrac{1}{2}\,\Im\{\boldsymbol{k}_0^*(\Delta_{x\beta} + \Delta_{-x\beta} + \Delta_{y\beta} + \Delta_{-y\beta} + \Delta_{z\beta} + \Delta_{-z\beta})\}. \tag{28.22}$$

Yokoya (1982) employed the (x, y, z) coordinate basis, where z points clockwise around the ring. Hence, the expressions for $\Delta_{\pm x\beta}$ contain some $\pm$ sign differences relative to what one would obtain using the $\boldsymbol{e}_{1,2,3}$ basis. Furthermore, the subscripts on $\Delta_{\pm x\beta}$ suggest (correctly) that the orbital motion is decomposed into uncoupled horizontal and vertical betatron oscillations and synchrotron oscillations. By contrast, the orbital eigenvector modes E_j above are fully general symplectic solutions, which include arbitrary linear x–y coupling. The orbital motion in most accelerators can be described by uncoupled betatron and synchrotron oscillations, the $\Delta_{\pm x\beta}$. Then define

$$\boldsymbol{k}_0 = k_x\hat{\boldsymbol{x}} + k_y\hat{\boldsymbol{y}} + k_z\hat{\boldsymbol{z}} \tag{28.23}$$

and also the focusing functions

$$G_x = \frac{1}{\rho_x^2} + \frac{1}{B\rho}\frac{\partial B_y}{\partial x}, \qquad G_y = \frac{1}{\rho_y^2} - \frac{1}{B\rho}\frac{\partial B_y}{\partial x}. \tag{28.24}$$

To write down the expressions for $\Delta_{\pm x}$, we actually follow Yokoya (1983a) which presents more general expressions than does Yokoya (1982). The expressions for $\Delta_{\pm x}$ are

$$\begin{aligned}
\Delta_{\pm x\beta}(s) &= \frac{a\gamma + 1}{\mathrm{e}^{\mathrm{i}2\pi(\nu_{\mathrm{c.o.}} \pm Q_x)} - 1} \\
&\quad \times \left\{ \frac{\mathrm{e}^{\mp \mathrm{i}\psi_x}}{\sqrt{\beta_x}} [-D_x \pm \mathrm{i}(\beta_x D_x' + \alpha_x D_x)] \right\}_s \int_s^{s+C} [k_y G_x \sqrt{\beta_x}\, \mathrm{e}^{\pm \mathrm{i}\psi_x}]_{s'}\, \mathrm{d}s', \\
\Delta_{\pm y\beta}(s) &= \frac{a\gamma + 1}{\mathrm{e}^{\mathrm{i}2\pi(\nu_{\mathrm{c.o.}} \pm Q_y)} - 1} \\
&\quad \times \left\{ \frac{\mathrm{e}^{\mp \mathrm{i}\psi_y}}{\sqrt{\beta_y}} [-D_y \pm \mathrm{i}(\beta_y D_y' + \alpha_y D_y)] \right\}_s \int_s^{s+C} [k_x G_y \sqrt{\beta_y}\, \mathrm{e}^{\pm \mathrm{i}\psi_y}]_{s'}\, \mathrm{d}s', \\
\Delta_{\pm z\beta}(s) &= \frac{1}{\mathrm{e}^{\mathrm{i}2\pi(\nu_{\mathrm{c.o.}} \pm Q_z)} - 1}\, \mathrm{e}^{\mp \mathrm{i}\psi_z(s)} \\
&\quad \times \int_s^{s+C} \left\{ \left[(a\gamma + 1) G_x D_x - \frac{1}{\rho_x} \right] k_y - \left[(a\gamma + 1) G_y D_y - \frac{1}{\rho_y} \right] k_x \right\}_{s'} \mathrm{e}^{\pm \mathrm{i}\psi_z(s')}\, \mathrm{d}s'.
\end{aligned} \tag{28.25}$$

Here, $\alpha_{x,y}$ and $\beta_{x,y}$ are the Twiss functions and $\psi_{x,y,z}$ are the betatron phases, and $D_{x,y}$ are the horizontal and vertical dispersions. ($D_y = D_y' = 0$ in a perfectly aligned planar ring.) Note that, just like $\boldsymbol{n}_0$, the vector $\boldsymbol{d}_0$ is also periodic around the ring:

$$\boldsymbol{d}_0(\theta + 2\pi) = \boldsymbol{d}_0(\theta). \tag{28.26}$$

Inspection of the individual Δ_j reveals that

$$\Delta_j(\theta + 2\pi) = \Delta_j(\theta) \qquad j = \pm x, \pm y, \pm z. \tag{28.27}$$

The same periodicity could also have been derived using the general orbit eigenvector formalism.

To summarize, the vector $\boldsymbol{d}_0$ is the value of $\boldsymbol{d}$ on the closed orbit. It does not depend on the orbital action-angles (or the beam emittances, when averaging over the beam), because the orbital action-angles disappeared when taking the partial derivative $\gamma(\partial\zeta/\partial\gamma)$. Hence, when the Derbenev–Kondratenko formula is evaluated using only $\boldsymbol{n}_0$ and $\boldsymbol{d}_0$, the statistical average over the orbital phase-space is trivial.

Since the SLIM formalism only treats the orbital motion to the first order, the approximate solution for $\boldsymbol{d}$, namely, $\boldsymbol{d}_0$, only diverges at the first order resonances. This fact unfortunately led workers in the field to conclude that the higher-order resonances require nonlinear orbital dynamics. We now know that this is not so: linear orbital dynamics can drive all of the higher-order spin resonances.

28.5. Spin integrals

The numerators of the Δ_j in (28.25), without the resonance denominators, are called the *Chao spin integrals* (Chao 1981a) or also the Chao–Yokoya spin integrals (Chao and Yokoya 1981). We ignore the sociological fact that these integrals were known in Soviet papers long before Chao and Yokoya's work. Buon (1981) also found the same functions. We shall just write 'spin integrals' or 'first-order spin integrals' below. In more detail, let us write

$$\Delta_j(s) = \frac{\tilde{\Delta}_j(s)}{\mathrm{e}^{\mathrm{i}2\pi(\nu_{\mathrm{c.o.}} \pm Q_j)} - 1}. \tag{28.28}$$

The numerators $\tilde{\Delta}_j$ are the spin integrals. It is more usual not to employ a complex notation and to express the integrals using real integrands. A very important point to be noted is that in a perfectly aligned planar ring all the first-order spin integrals *vanish*. This is because:

- for $\Delta_{\pm x\beta}$, the vector $\boldsymbol{k}_0$ lies in the horizontal plane and so $k_y = 0$ and so the integrand in (28.25) is zero.
- for $\Delta_{\pm y\beta}$, the integrand is nonzero because k_x is nonzero, but the multiplier in (28.25) vanishes because the vertical dispersion is zero in a perfectly aligned planar ring: $D_y = D'_y = 0$.
- the vanishing of $\Delta_{\pm z\beta}$ is due to a combination of two effects. One is that $k_y = 0$, so $D_x k_y = 0$ and the other is that $D_y = 0$ and also $\rho_y^{-1} = 0$, so the whole integrand also vanishes.

Hence, in a planar ring, which most accelerators are by design, the nonvanishing of the spin integrals, i.e. of $\boldsymbol{d}_0$, is actually entirely due to lattice imperfections. Note that the spin basis vectors $\boldsymbol{l}_0$, $\boldsymbol{m}_0$ and $\boldsymbol{n}_0$ are referenced to the closed orbit, and *not* the design orbit. The presence of imperfections does not cause the vertical dispersion to vanish identically, and also causes the horizontal betatron oscillations to couple into the vertical plane. Similarly, the contribution from the synchrotron oscillations also does not vanish.

At higher orders (the SMILE perturbation series), the higher order integrals are all proportional to the values of the first-order spin integrals, and so, in a perfectly aligned planar ring, all of the spin integrals also vanish. The nonvanishing of the individual terms is due to the lattice imperfections.

28.6. Imperfection resonance driving terms

The six first-order integrals in the solution for $\boldsymbol{n}$ diverge at the first-order spin resonances $\nu = k \pm Q_j$ (k = integer). What about the integer resonances, or 'imperfection resonances' $\nu = k$? For nonradiatively polarized beams, the imperfection resonance driving terms arise from the closed-orbit imperfections. The situation is more subtle for radiatively polarized beams. For radiatively polarized beams, the contributions of the (vertical *and* horizontal) closed-orbit imperfections are built into the values of the closed-orbit vectors $\boldsymbol{l}_0$, $\boldsymbol{m}_0$ and $\boldsymbol{n}_0$. In particular, if the value of the spin tune is close to an integer, then the direction of $\boldsymbol{n}_0$ can be strongly tilted away from the vertical. Given the 'imperfect' vectors $\boldsymbol{n}_0$ and $\boldsymbol{k}_0$, the values of the Chao–Yokoya first-order spin integrals are then strongly nonzero, and so the value of the equilibrium polarization is strongly reduced.

Hence, in algorithms to calculate the equilibrium radiative polarization, the effects of the closed-orbit imperfections are implicit in the values of the spin basis vectors and do not appear as explicit resonance driving terms. For this reason it is important to recognize that the spin basis vectors are referenced to the imperfect closed orbit, not the ideal design orbit.

28.7. Scaling with energy

An important feature of $\boldsymbol{d}_0$ in a planar ring is that $|\boldsymbol{d}_0| \propto (a\gamma + 1)$, as is evident from the expressions for the Δ_j in (28.25). There are also terms of order $\mathrm{O}(1/\rho_{x,y})$, but for most machines these terms are of lesser magnitude. Since $|\boldsymbol{d}|^2$ appears in the denominator of the Derbenev–Kondratenko formula, and $a\gamma \gg 1$ for energies of several GeV, this means that at high energies, the equilibrium polarization level scales according to

$$P_{\mathrm{eq}} \simeq \frac{8}{5\sqrt{3}} \frac{1}{1 + \alpha^2 E^2}, \tag{28.29}$$

where α is some function of the ring lattice. As far as we can trace the matter, this scaling was first pointed out by Buon (1982). The scaling law is of course based on first-order perturbation theory, and as the magnitude of the first-order terms increases so will that of the higher-order terms. Eventually the degree of the equilibrium polarization will drop off even faster than the rate given by (28.29). As we shall see for LEP, later in this paper, the above scaling worked up to about 46 GeV (LEP1), but the degree of polarization fell off more rapidly with energy for beam energies going up from 46 GeV to over 60 GeV (Assmann *et al* 2001), due to higher order resonances.

28.8. Strong spin matching

Naturally, one wants to reduce the magnitude of $|\boldsymbol{d}|^2$ in a storage ring, to improve the equilibrium polarization level. In particular, the installation of spin rotators in a ring, such as at HERA, makes a ring nonplanar, hence $\boldsymbol{d}$ will be nonzero even in a perfect design. This will seriously reduce the achievable radiative polarization in a storage ring, potentially. Strong spin matching consists of designing the accelerator lattice so that all the first-order spin integrals vanish: $\tilde{\Delta}_j(s) = 0$ at *every* point around the ring circumference. A ring which is spin matched is said to be *spin transparent*.

Since there are six orbital modes (six values of j), and each $\tilde{\Delta}_j$ is complex, this implies twelve conditions at each value of s. In practice, because the synchrotron tune is small, $Q_s \ll 1$, it is usual to approximate $Q_s \simeq 0$ in the spin integrals, in which case there are ten conditions which must be satisfied at each value of s.

The strong spin matching conditions must be satisfied at *every* value of s, because the overall polarization is determined by the entire structure of the accelerator. This makes strong spin matching a very restrictive constraint on the design of an accelerator. One typically employs some symmetry to reduce the number of constraints, but even then, strong spin matching is very difficult to achieve. In practice, one attempts to reduce the value of $|\boldsymbol{d}|^2$ integrated around the circumference. More precisely, one attempts to minimize the value of $\oint |\rho|^{-3}|\boldsymbol{d}|^2\,\mathrm{d}s'$. Most of the effort in the design of the Buon–Steffen minirotator of HERA (Buon and Steffen 1986) was devoted to the spin-matching of the minirotators to the HERA lattice.

28.9. Harmonic spin matching

Evidently, strong spin matching is almost impossible to achieve in practice. It may also be unnecessary for practical applications. The related and important technique of harmonic spin matching addresses this issue. The notion of harmonic spin matching is described by Rossmanith and Schmidt (1985). See also the earlier work by Derbenev *et al* (1977). Froissart and Stora (1960) also described ideas for correction of the Fourier harmonics of the imperfect closed orbit (for nonradiatively polarized beams). Harmonic spin matching is based on two observations: first, it is known that the major perturbations to the spins in a planar ring arise from vertical orbital motion in the quadrupoles. Second, the major driving terms of the depolarizing spin resonances (to first order, anyway) are the integer harmonics (what would be called imperfection resonances for nonradiatively polarized beams). We decompose $\boldsymbol{d}$ into Fourier harmonics, and write, approximately (noting that $|\boldsymbol{d}| \propto (a\gamma + 1)$),

$$|\boldsymbol{d}|^2 \propto (a\gamma + 1)^2 \sum_k \frac{|c_k|^2}{(\nu_0 - k)^2}, \tag{28.30}$$

where k is an integer and recall $\nu_0 = a\gamma$. The above expression assumes that the Fourier harmonics (the resonance driving terms) are uncorrelated. It is a reasonable starting

approximation. The task is then to identify the harmonics which contribute the most to the depolarization, i.e. to $|\boldsymbol{d}|^2$. If the harmonics are of roughly equal magnitude (again a reasonable working hypothesis), then the relevant harmonic will be the one closest to the spin tune ν_0. In the case where the fractional part of ν_0 is close to $\frac{1}{2}$, the two nearest harmonics have to be corrected.

The correction procedure uses a technique similar to that employed for nonradiatively polarized beams. A set of vertical corrector dipoles, distributed around the ring, are employed to generate Fourier harmonics to counter those from the machine imperfections. As we have seen with nonradiatively polarized beams, localized vertical closed orbit bumps can also be used, instead of correctors distributed around the whole circumference. Although nominally the quantity being corrected is $|\boldsymbol{d}|^2$, in practice the driving terms of both $\boldsymbol{n}$ and $\boldsymbol{d}$ are the Fourier harmonics in the off-axis spin precession vector $\boldsymbol{w}$.

Harmonic spin matching is usually implemented empirically. One adjusts the values of the correctors (or vertical closed orbit bumps) to optimize the measured polarization. The corrector settings are saved for future reference. In some machines, such as LEP, where the detector solenoids induced reproducible perturbations to the spin motion, a 'deterministic' harmonic spin matching technique was implemented, where the settings of the vertical closed orbit bumps could be calculated as a function of the solenoid fields and lattice parameters. We shall review the harmonic spin matching work at LEP in section 31.

Harmonic spin matching is an important technique and has been successfully employed at a number of high-energy electron storage rings. It is much simpler to implement than strong spin matching (which requires a (re)design of the accelerator lattice), and can easily be modified as the machine operating point changes, or upgrades to a machine are implemented.

28.10. Nonplanar rings

We treat only one example of a nonplanar ring, namely, a storage ring with a single Siberian Snake, and we take the Snake to be a solenoid, since that is the only Snake design which has ever been used in real rings. We have shown previously that, when solving for $\boldsymbol{n}$, the first-order integral $\int_{-\infty}^{\theta} \boldsymbol{w}_+ \cdot \boldsymbol{k}_0 \, \mathrm{d}\theta'$ did *not* vanish in a perfectly aligned ring with a single Snake. Similarly, the value of $\boldsymbol{d}_0$ also does not vanish in a perfectly aligned ring with a single Snake. Examining the spin integrals in (28.25), we see that $k_y \neq 0$. Furthermore, with a solenoid in the ring, there may be transverse betatron coupling, so D_y may not vanish.

The Sokolov–Ternov radiative polarization vanishes in a ring with a single Snake. Hence, the principal interest in $\boldsymbol{d}$, for a ring with a single Snake, is to observe the kinetic polarization term. As mentioned earlier, attempts to observe the kinetic polarization have been inconclusive. It is stated by Korostelev and Shatunov (2001) that a maximum polarization level of about 80% may be achievable for $|\boldsymbol{d}| \simeq 1.2$. If confirmed, this would be a spectacular triumph of spin dynamics in accelerators.

Calculations of $\gamma(\partial \boldsymbol{n}/\partial\gamma)$ to first order have been carried out for AmPS (de Jager *et al* 1997) and SHR (Korostelev and Shatunov 2001). The calculations are basically the same and will be reviewed as one. In both rings the Snake system consists of two solenoids in series and one pair of quadrupoles and two pairs of skew quadrupoles. The schematic design is (not to scale)

$$\text{SQ1–SQ2–SOL–Q–Q–SOL–}(-\text{SQ2})\text{–}(-\text{SQ1}).$$

The notation $(-\text{SQ}n)$ means that the skew quad is rotated in the opposite sense to SQn, for $n = 1, 2$. We follow Korostelev and Shatunov (2001). They write $\boldsymbol{d}_0 = \Re(\mathrm{i}D\boldsymbol{\eta}^*)$, which we have written as $\boldsymbol{d}_0 = \Im(\Delta \boldsymbol{k}_0^*)$, so $\Delta = -D$ and $\boldsymbol{\eta} = \boldsymbol{k}_0$. The origin is just after the Snake.

The solution for $\boldsymbol{n}_0$ is, for $\theta \in (0, 2\pi)$,

$$\boldsymbol{n}_0(\theta) = \sin(\nu_0\Theta)\,\boldsymbol{e}_1 + \cos(\nu_0\Theta)\,\boldsymbol{e}_2, \tag{28.31}$$

where

$$\Theta(\theta) = \pi - \int_0^{s(\theta)} \frac{\mathrm{d}s'}{\rho_x(s')}. \tag{28.32}$$

The closed-orbit spin precession vector in the arcs is not necessarily uniform around the circumference. We further recognize that at both AmPS and SHR the horizontal and vertical dispersions both vanish at the location of the Snake ($D_x = D_y = 0$ at $\theta = \pi$). We also note that the quadrupole and skew quadrupoles fully compensate the transverse betatron coupling outside the Snake region. Then, there are two contributions to Δ, written as $\Delta = \Delta_\gamma + \Delta_\beta$. The term Δ_γ arises from the direct dependence of $\boldsymbol{n}$ on the particle energy, while Δ_β results from the jump of the betatron amplitudes during the emission of photons. Then,

$$\begin{aligned}
\Delta_\gamma &= \frac{\pi}{2}\sin(\pi\nu_0) - \mathrm{i}\nu_0\Theta, \\
\Delta_\beta &= \frac{\pi\nu_0}{4\cos(\pi Q_x)}[\cos(\pi\nu_0)\Im(\mathrm{e}^{\mathrm{i}\pi Q_x} J(\theta) G_{1x}^*) + \mathrm{i}\Im(\mathrm{e}^{\mathrm{i}\pi Q_x} J(\theta) G_{1y}^*)].
\end{aligned} \tag{28.33}$$

The expression for $\boldsymbol{d}_0$ in (28.12) is a special case of Δ_γ, setting $\theta = 2\pi$ (i.e. $\Theta = -\pi$). Here,

$$G_{1x,y} = f'_{1x,y(\mathrm{out})} - f'_{1,x,y(\mathrm{in})} \tag{28.34}$$

is the difference between the derivative of the first-mode Floquet functions $f_{1x,y}$ at the exit of the solenoid ('out') and the entrance ('in'). At both AmPS and SHR 'the' solenoid consists of two solenoids in series, so 'in' means the entrance of the first solenoid and 'out' means the exit of the second solenoid. The function $J(\theta)$ is given by

$$J(\theta) = f_{1x} D'_x - f'_{1x} D_x. \tag{28.35}$$

Although the betatron modes are fully decoupled *outside* the Snake system there is nonzero x–y betatron coupling inside the Snake system, hence, one must express the orbital motion in terms of Floquet modes.

The real parts of Δ_γ and Δ_β couple to $\boldsymbol{e}_3$, and therefore contribute to the $\hat{\boldsymbol{b}} \cdot \boldsymbol{d}$ kinetic polarization term. Treating only Δ_γ, the contribution is, assuming a uniform bending radius $\rho_x(s) = \rho$,

$$\oint \frac{\mathrm{d}s}{|\rho_x^3|}\hat{\boldsymbol{b}} \cdot \boldsymbol{d} = \frac{\pi^2}{2\rho^2}\sin(\pi\nu_0). \tag{28.36}$$

28.11. Synchrotron sidebands

28.11.1. Enhancement factors. We pointed out earlier that the most important higher-order spin resonances are the synchrotron sidebands of the parent resonances. Obviously $\gamma(\partial\boldsymbol{n}/\partial\gamma)$ also contributes to such sidebands. We shall treat only planar rings, since we are studying radiative polarization. Many important papers exist on the subject of the synchrotron sideband spin resonances for radiatively polarized beams. A short list is Derbenev *et al* (1979c), Yokoya (1983a), Biscari *et al* (1984), Buon (1989) and Mane (1990, 1992b).

We follow Yokoya (1983a) and Mane (1990) below. Actually Mane (1990) is a correction of some errors of algebra in Yokoya (1983a). Once again, the formulae below were derived using an (x, y, z) coordinate basis, where z propagates clockwise around the ring. The vector $\boldsymbol{n}$ is again parametrized via complex ζ: $\boldsymbol{n} = \boldsymbol{n}_0\sqrt{1 - |\zeta|^2} + \Re(\zeta\boldsymbol{k}_0^*)$, with the approximate equation of motion (15.15). The solution is (see (15.18))

$$\zeta \simeq -\mathrm{i}\mathrm{e}^{-\mathrm{i}\chi(\theta)}\int_{-\infty}^{\theta} \mathrm{e}^{\mathrm{i}\chi(\theta')}\,\boldsymbol{\omega} \cdot \boldsymbol{k}_0\,\mathrm{d}\theta', \tag{28.37}$$

where

$$\chi(\theta) = -\int_{-\infty}^{\theta} \boldsymbol{w}\cdot\boldsymbol{n}_0\,\mathrm{d}\theta'. \tag{28.38}$$

All of this was worked out earlier and is completely general. In principle, all the orbital oscillation modes contribute to χ, but the betatron oscillations average almost to zero because $Q_{x,y} \gg 1$. Only the synchrotron oscillations add up coherently to a large total, because $Q_s \ll 1$. This was explained earlier in this paper. Hence, only the synchrotron oscillations are retained in χ below. For a planar ring, we define $u_\epsilon = a\gamma/Q_s$ and then integrate to obtain

$$\chi = \sqrt{2I_z}\,u_\epsilon\,\sin\phi_z, \tag{28.39}$$

which yields

$$\zeta = \mathrm{e}^{-\mathrm{i}\chi}\sum_{m=-\infty}^{\infty}\Big[\frac{m}{u_\epsilon}A_m(\theta) + \sum_{\pm}\sqrt{2I_x\beta_x}\,\mathrm{e}^{\pm\mathrm{i}(\phi_x+\tilde{\psi}_x)}B_{m,\pm x}(\theta)\Big]\mathrm{e}^{\mathrm{i}m\phi_z}\,J_m(\sqrt{2I_z}\,u_\epsilon), \tag{28.40}$$

where

$$\begin{aligned}
A_m(\theta) &= -\mathrm{i}\frac{\mathrm{e}^{-\mathrm{i}mQ_s\theta}}{\mathrm{e}^{\mathrm{i}2\pi(\nu 0+mQ_s)}-1}\int_\theta^{\theta+2\pi}\mathrm{e}^{\mathrm{i}mQ_s\theta'}\boldsymbol{\omega}_\epsilon\cdot\boldsymbol{k}_0\,\mathrm{d}\theta',\\
B_{m,\pm x}(\theta) &= -\frac{\mathrm{i}}{2}\frac{\mathrm{e}^{\mp\mathrm{i}(\tilde{\psi}_x+Q_x\theta)-\mathrm{i}mQ_s\theta}}{(\mathrm{e}^{\mathrm{i}2\pi(\nu 0\pm Q_x+mQ_s)}-1)\sqrt{\beta_x}}\int_\theta^{\theta+2\pi}\mathrm{e}^{\pm\mathrm{i}(\tilde{\phi}_x+Q_x\theta')+\mathrm{i}mQ_s\theta'}\sqrt{\beta_x}\,\boldsymbol{\omega}_x\cdot\boldsymbol{k}_0\,\mathrm{d}\theta'.
\end{aligned} \tag{28.41}$$

All of this was also worked out before and the notation explained there. The term in A_m describes the synchrotron sidebands of a parent synchrotron resonance and the terms in $B_{m,\pm x}$ describe the synchrotron sidebands of a parent horizontal betatron resonance, and there is correspondingly a term for the synchrotron sidebands of a parent vertical betatron resonance. To solve for $\gamma\,(\partial\boldsymbol{n}/\partial\gamma)$, we need the phase-space derivative $\gamma(\partial\zeta/\partial\gamma)$. From Yokoya (1983a)

$$\begin{aligned}
\gamma\frac{\partial}{\partial\gamma}\big[\sqrt{2I_x\beta_x}\,\mathrm{e}^{\pm\mathrm{i}(\phi_x+\tilde{\psi}_x)}\big] &= -D_x \pm \mathrm{i}(\alpha_x D_x + \beta_x D_x'),\\
\gamma\frac{\partial}{\partial\gamma}\big[J_m(\sqrt{2I_z}\,u_\epsilon)\,\mathrm{e}^{\mathrm{i}m\phi_z}\big] &= \frac{u_\epsilon}{2}\big[J_{m-1}(\sqrt{2I_z}\,u_\epsilon)\,\mathrm{e}^{\mathrm{i}(m-1)\phi_z} + J_{m+1}(\sqrt{2I_z}\,u_\epsilon)\,\mathrm{e}^{\mathrm{i}(m+1)\phi_z}\big],
\end{aligned} \tag{28.42}$$

with a similar expression for the vertical betatron oscillations. Then, omitting much algebra,

$$\gamma\frac{\partial\zeta}{\partial\gamma} = \mathrm{e}^{-\mathrm{i}\chi}\sum_{m=-\infty}^{\infty}C_m(\theta)\,J_m(\sqrt{2I_z}\,u_\epsilon)\,\mathrm{e}^{\mathrm{i}m\phi_z}, \tag{28.43}$$

where

$$\begin{aligned}
C_m(\theta) = {}& \tfrac{1}{2}\left[(m+1)A_{m+1}(\theta) - (m-1)A_{m-1}(\theta)\right]\\
&+\sum_{\pm}\Big\{[-D_x \pm \mathrm{i}(\alpha_x D_x + \beta_x D_x')]B_{m,\pm x}(\theta)\\
&+\sqrt{2I_x\beta_x}\,\mathrm{e}^{\pm\mathrm{i}(\phi_x+\tilde{\psi}_x)}\frac{u_\epsilon}{2}(B_{m+1,\pm x}(\theta) - B_{m-1,\pm x}(\theta))\Big\}\\
&+\sum_{\pm}\Big\{[-D_y \pm \mathrm{i}(\alpha_y D_y + \beta_y D_y')]B_{m,\pm y}(\theta)\\
&+\sqrt{2I_y\beta_y}\,\mathrm{e}^{\pm\mathrm{i}(\phi_y+\tilde{\psi}_y)}\frac{u_\epsilon}{2}(B_{m+1,\pm y}(\theta) - B_{m-1,\pm y}(\theta))\Big\}.
\end{aligned} \tag{28.44}$$

To calculate $\langle \boldsymbol{d} \rangle$ we need $\langle \gamma(\partial\zeta/\partial\gamma)\rangle$, which is not important. Of far greater interest is the quadratic term $\langle |\boldsymbol{d}|^2 \rangle$. For this we need $\langle |\gamma(\partial\zeta/\partial\gamma)|^2\rangle$. The average over the synchrotron oscillations is given by

$$\begin{aligned}\left\langle \left| \gamma \frac{\partial \zeta}{\partial \gamma} \right|^2 \right\rangle &= \sum_{m=-\infty}^{\infty} |C_m(\theta)|^2 \int_0^{\infty} \frac{\mathrm{d}I_z}{\langle I_z \rangle} \mathrm{e}^{-I_z/\langle I_z\rangle} J_m^2(\sqrt{2I_z}\, u_\epsilon) \\ &= \sum_{m=-\infty}^{\infty} |C_m(\theta)|^2 \, \mathrm{e}^{-\sigma^2} I_m(\sigma^2), \end{aligned} \tag{28.45}$$

where we recall the tune modulation index is

$$\sigma^2 = \langle I_z \rangle u_\epsilon^2 = \left(\frac{\sigma_E}{E}\right)^2 \frac{(a\gamma)^2}{Q_s^2}. \tag{28.46}$$

The physics is most clearly illuminated if we expand $\boldsymbol{w}$ in Fourier harmonics. Then

$$\begin{aligned} \boldsymbol{w}_\epsilon \cdot \boldsymbol{k}_0 &= \sum_{n=-\infty}^{\infty} a_n \mathrm{e}^{\mathrm{i}(\nu_0+n)\theta}, \\ \mathrm{e}^{\pm \mathrm{i}(\tilde{\psi}_x + Q_x\theta)} \beta_x^{1/2} \boldsymbol{w}_x \cdot \boldsymbol{k}_0 &= \sum_{n=-\infty}^{\infty} b_{n,\pm x} \mathrm{e}^{\mathrm{i}(\pm Q_x + \nu_0 + n)\theta}. \end{aligned} \tag{28.47}$$

The vertical betatron oscillations will be omitted to avoid cluttering the exposition. They can be worked out by analogy with the horizontal betatron oscillations. Then

$$\begin{aligned} A_m(\theta) &= -\sum_n \frac{a_n}{\nu_0 + n + m Q_s} \mathrm{e}^{\mathrm{i}(\nu_0+n)\theta}, \\ B_{m,\pm x}(\theta) &= -\frac{1}{2} \sum_n \frac{b_{n,\pm x}}{\nu_0 + n \pm Q_x + m Q_s} \frac{\mathrm{e}^{\mp \mathrm{i}\tilde{\psi}_x + \mathrm{i}(\nu_0+n)\theta}}{\sqrt{\beta_x}}. \end{aligned} \tag{28.48}$$

The case of greatest interest is the sidebands of an isolated parent resonance, i.e. to select a single term a_n or $b_{n,\pm x}$. Let us begin with the sidebands of a pair of first-order synchrotron resonances centred on an integer, i.e. a_n. We define $\Delta\nu = \nu_0 + n$. Then, omitting the calculations of all the averages

$$\left\langle \left| \gamma \frac{\partial \zeta}{\partial \gamma} \right|^2 \right\rangle = |a_n|^2 F_{n,z}. \tag{28.49}$$

It is conventional to express the strengths of the synchrotron sidebands as a ratio relative to the strength of the parent resonance, i.e. when $\sigma^2 = 0$. In this case the parent resonance strength is $|a_n|^2$. Hence, the ratio is

$$F_{n,z} = \sum_{m=-\infty}^{\infty} \frac{(\Delta\nu)^2 \, \mathrm{e}^{-\sigma^2} I_m(\sigma^2)}{[(\Delta\nu + m Q_s)^2 - Q_s^2]^2}. \tag{28.50}$$

This formula was derived by Derbenev *et al* (1979c). It is an important formula, and has been (re)derived by several authors, e.g. Yokoya (1983a), Biscari *et al* (1984), Buon (1989) and Mane (1989a).

As for the synchrotron sidebands of a horizontal betatron resonance, set $\Delta\nu = \nu_0 + n \pm Q_x$, and recall the symbol $\mathscr{H}_x^D$ from (9.14). One then has

$$\left\langle \left| \gamma \frac{\partial \zeta}{\partial \gamma} \right|^2 \right\rangle = \frac{\mathscr{H}_x^D}{4} \frac{|b_{n,\pm x}|^2}{(\Delta\nu)^2} F_{n,x}, \tag{28.51}$$

where the ratio relative to the strength of the parent resonance (i.e. when $\sigma^2 = 0$) is now (Buon 1989, Mane 1989a)

$$F_{n,x} = \sum_{m=-\infty}^{\infty} \frac{(\Delta\nu)^2}{(\Delta\nu + mQ_s)^2} \, \mathrm{e}^{-\sigma^2} \Big[\Big(1 + \frac{J_s}{J_x}\Big) I_{|m|}(\sigma^2) + \frac{J_s}{J_x} \, \sigma^2 \, I_{|m|+1}(\sigma^2) \Big]. \tag{28.52}$$

Here J_x and J_s are the partition numbers mentioned in section 9.4.

28.11.2. Chromaticity modulation. We pointed out earlier, in connection with experimental studies at the KEK-PS Booster, that if one has a spin integral of the form

$$\zeta = -\mathrm{i} \int f(\theta) \mathrm{e}^{\mathrm{i}(\nu_0\theta' - \phi'_x)} \, \mathrm{d}\theta', \tag{28.53}$$

where f is a function of no interest to the current discussion, then the betatron phase advance would also display tune modulation, via the chromaticity. Treating only the ultrarelativistic case, we can write

$$Q_x \to Q_{x0} + \xi_x \frac{\Delta\gamma}{\gamma_0}. \tag{28.54}$$

Hence, with an obvious notation,

$$\nu_0\theta - \phi_x \to \nu_0\theta - \phi_{x0} + (\nu_0 - \xi_x) \frac{\sqrt{2I_z}}{Q_s} \sin\phi_z. \tag{28.55}$$

Then the tune modulation index should read

$$\sigma^2 = \Big(\frac{\sigma_E}{E}\Big)^2 \frac{(a\gamma - \xi)^2}{Q_s^2}. \tag{28.56}$$

In particular, if $a\gamma = \xi_x$, the modulations of the spin tune and the betatron tune cancel and there are no synchrotron sideband resonances. This was derived in section 20 for nonradiative beams. Evidently, the same reasoning applies for radiatively polarized beams (Mane 1990).

29. Radiatively polarized stored beams

29.1. General remarks

In this section, we shall review some experimental measurements of radiative polarization at several storage rings. We include both modern work and important historical work, but there are many measurements that are omitted for reasons of space. This section focuses on purely 'accelerator physics' issues. Subsequent sections will describe the uses of radiative polarization for precision measurements, e.g. tests of the Standard Model.

29.2. HERA: longitudinal radiative polarization

HERA is the Hadron Elektron Ring Anlage at DESY, Hamburg. It is a two-ring lepton–hadron collider. The proton ring HERA-p originally operated at 820 GeV, and now has been upgraded to 920 GeV (so-called HERA2). The lepton ring HERA-e was designed to operate at 27–35 GeV and usually runs at 27.5 GeV. HERA-e has circulated both electrons and positrons.

The collision of leptons and hadrons (protons, and possibly other species at a later date) provides a deep-inelastic leptonic probe of hadronic structure at momentum transfers not available at other facilities. For such physics, it is natural to demand longitudinal polarization

of the lepton beam at the interaction point. HERA was therefore designed at the outset to utilize the Sokolov–Ternov radiative polarization of the lepton beam, with spin rotators to provide longitudinal lepton polarization at the interaction points. The Buon–Steffen minirotator (Buon and Steffen 1986) was reviewed in detail in MSY1. HERA has to date operated with unpolarized protons, but see MSY1 for a review of design studies for Siberian Snakes to accelerate and store polarized protons in HERA-p.

HERA was the first high-energy storage ring to attain *longitudinal* radiative polarization of a stored electron beam. HERA has also stored longitudinally polarized high-energy *positron* beams, something no other accelerator has ever done. The SLC, to be discussed briefly later in this paper, collided longitudinally polarized electrons against unpolarized positrons at a higher beam energy of 45.6 GeV, but the SLC was a linear collider, not a ring, and so required a polarized electron source.

The first observation of electron spin polarization at HERA (in the transverse direction) took place in November 1991, and was at about the 8% level (Barber *et al* 1993). Steps to improve the polarization level were taken via orbit correction and also the technique of harmonic spin-matching to eliminate the driving terms of specific spin resonances. By 1994 the asymptotic vertical polarization had been increased to about 60% (Barber *et al* 1994).

The first pair of spin rotators was installed in the HERA East Hall in May 1994 (Barber 1995a). The asymptotic vertical polarization was about 65% with the rotators off. After activating the spin rotators, and without further orbit correction, an asymptotic polarization of about 56% was recorded (Barber *et al* 1995b). The longitudinal polarization (asymptotic) level was increased to about 65% in the next few days. In November 1994, longitudinal positron polarization was observed, also with an asymptotic level of about 65%. The lepton and proton beams do not collide in the HERA East Hall. Instead HERMES, an internal gas jet experiment, colliding a gas jet of protons against longitudinally polarized electrons/positrons, operates there. A sample result from the HERMES experiment, of asymmetry measurements in deeply virtual Compton scattering, using a longitudinally polarized positron beam and an unpolarized hydrogen gas jet target, is shown by Airapetian *et al* (2001).

The HERA West Hall has a transverse Compton backscattering polarimeter (Barber *et al* 1990), which measures the vertical polarization, and a longitudinal Compton backscattering polarimeter (Beckmann *et al* 2002) in the HERA East Hall, just upstream of the HERMES experiment. Zetsche (1997) reported on resonance depolarization measurements (using the transverse polarimeter) to calibrate the HERA-e beam energy. Note that the spin rotators had to be turned off for this work, because the spin rotators induce small spin tuneshifts (so then $\nu \neq a\gamma$).

In 2003, mini-rotator pairs were installed at the interaction points of the H1 and ZEUS high-energy physics detectors. A recent report on the status of HERA-e is given by Barber *et al* (2004). The delivered (not asymptotic) longitudinal positron polarization level, in the presence of e^+p collisions, is about 40%, increasing to about 50% at the end of a run. The data also indicate that the asymptotic polarization level itself increases with time (Barber *et al* 2004).

During the time interval of nine years from 1994 to 2003 between the installation of the first mini-rotator pair and the others, HERA underwent a luminosity and energy upgrade (increase of proton beam energy to 920 GeV), becoming HERA2. The upgrade had some serious consequences for the attainment of longitudinal polarization. In particular, the anti-solenoids, which had been compensating the main detector solenoids in the North and South interaction regions, were removed. The quadrupoles in the interaction regions also became stronger. Details of the lepton orbital dynamics are given by Hoffstätter and Willeke (1999). (Note that the above authors do not discuss the spin dynamics.) The effects on the polarization

were studied, and a more sophisticated model of the spin motion with the new HERA optics was developed (Berglund *et al* 1998). In particular, the polarization direction is not always parallel to the solenoid field direction in the H1 detector. A more accurate solenoid representation was tested using a parametrization of the measured field (especially the fringe fields at the H1 solenoid entrance and exit). A later review, describing the success of HERA polarization operations after the upgrade, is given by Barber and Gianfelice (2002).

All the theory presented in this paper has been for noncolliding beams. In practice, the beam–beam interaction is frequently a limiting factor in the performance of modern high-energy colliders. Over the years, HERA has naturally undergone improvements to increase the proton current and the specific luminosity (= luminosity/current). A definite correlation between the luminosity and the lepton polarization has been observed, but by careful tuning of the machine optics it has been possible to deal with the beam–beam interaction and to deliver a high degree of longitudinal polarization (Gianfelice 2003).

29.3. SPEAR polarization data

29.3.1. General remarks. The SLAC–Wisconsin collaboration (Johnson *et al* 1983) measured the polarization of the positron beam at SPEAR (see figure 6). Although the official publication of the measurements is dated 1983, the data were taken several years earlier (by 1979). Several spin resonances, including both first-order and higher-order, are visible. The SPEAR polarization data remain to this day the best example of an energy scan displaying the spin resonances of a radiatively polarized stored electron or positron beam. SPEAR was run in a single-beam mode and the positron polarization was measured in the studies. The beam energy was above 3.5 GeV so that the polarization buildup time would be $\lesssim$15 min, to allow numerous points to be scanned in a reasonable time. Note that the measurements in figure 6 were not performed in a single energy scan. The polarization was measured parasitically over several machine shifts. The machine tunes, etc, were not held fixed in the scans. A rudimentary effort was made to shift the energy (i.e. spin tune) to a common baseline, and this is how the data in figure 6 were compiled.

In fact the SLAC–Wisconsin collaboration did take limited data with colliding e^+e^- beams. Some of those data were published by Johnson *et al* (1983). The results are rather limited, and are not presented here. To this day the effects of the beam–beam interaction on the polarization of stored colliding beams are poorly understood.

The curve through the data in figure 6 is a guide to the eye, not a theoretical fit. Four theoretical fits to the SPEAR data were published:

- Chao (1981b)—first order resonances
- Mane (1988a)—all resonances
- Buon (1989)—synchrotron sideband resonance
- Lee and Berglund (1996)—synchrotron sideband resonances

The fits by Chao and Mane were *ab initio* calculations which constructed a model for the resonance strengths using the SPEAR machine lattice. The other two calculations (by Buon and Lee and Berglund), fit the *ratios* of resonance widths. The machine lattice-dependent quantities cancel out in the ratio. The fits by Chao, Mane and Buon employ the Derbenev–Kondratenko formula, while the Lee–Berglund formalism does *not*. We shall discuss this surprising fact below.

29.3.2. Theoretical fit 1: Chao. Chao (1981a) fitted the SPEAR polarization data using the SLIM algorithm (Chao 1981b), which he developed. The SLIM programme calculates

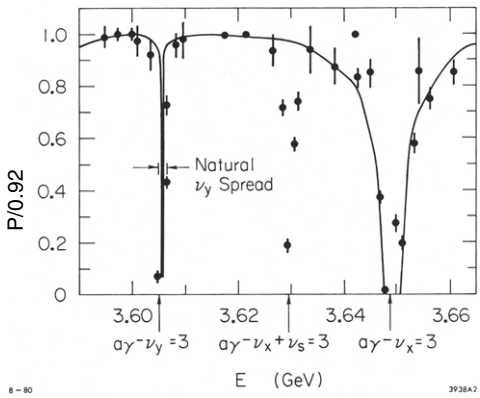

Figure 53. Theoretical fit of the SPEAR polarization data using SLIM. From Chao (1981b). Copyright (1981) by the American Institute of Physics.

the vectors $\boldsymbol{n}_0$ and $\boldsymbol{d}_0$ on the closed orbit only, and yields only first-order spin resonances. As explained earlier, all the resonance strengths vanish in a perfectly aligned planar ring (SPEAR was planar). Hence, a Monte Carlo simulation of the machine imperfections was required, to fit the data theoretically. A fit to the data, using SLIM, is shown in figure 53. The program exhibits depolarization at the first-order resonances $\nu = \nu_x + 3$ and $\nu = \nu_y + 3$ (the notation used was $\nu_{x,y,s}$ for the orbital tunes). The higher-order resonance $\nu = 3 + \nu_x - \nu_s$, also visible in the graph, is not fitted by the theory.

Notice that in marked contrast to the situation in hadron synchrotrons, where the dominant intrinsic resonances are due to the vertical betatron oscillations, in SPEAR the *horizontal* betatron resonance $\nu = \nu_x + 3$ is much wider than the vertical betatron resonance $\nu = \nu_y + 3$. Note also from figure 53 that the theoretical fit to the vertical betatron resonance is narrower than the experimental data. We shall comment on this below.

29.3.3. Theoretical fit 2: Mane. Mane (1988a) fitted the SPEAR polarization data using his programme SMILE (Mane 1987b). See also Mane (1989b) for more details. The fit to the data was shown in figure 7. The SMILE formalism was explained earlier, and can go to arbitrarily high orders in principle, hence, it fits many more resonances than did SLIM. Figure 7 remains to this day the most extensive fit of the spin resonances of a radiatively polarized beam. There are several notable features in the fit.

(a) As with SLIM, it was necessary to generate a model of the SPEAR lattice imperfections. To calibrate the magnitude of the imperfections, the theoretical model was fitted to the width of the first-order horizontal betatron resonance $\nu = \nu_x + 3$ at 3.65 GeV. Hence, the width of this resonance was an input to the theory.

(b) As Chao (1981a) found, when fitting the vertical betatron resonance $\nu = \nu_y + 3$ using SLIM, the SMILE theoretical fit was narrower than the observed resonance width. Since SMILE calculated the resonance widths using linear dynamics of high orders, this showed that the width of the first-order spin resonance $\nu = \nu_y + 3$ was due to nonlinear orbital dynamics. The experimenters (Johnson *et al* 1983) stated that the width of the $\nu = \nu_y + 3$ was determined by the tune spread of the vertical betatron oscillations. The vertical betatron resonance $\nu = \nu_y + 3$ at 3.605 GeV in the SPEAR data is, therefore, an example of a *first*-order *nonlinear* spin resonance. It is not true that the higher-order resonances are due to nonlinear orbital dynamics, nor that the first-order resonances are purely due to linear orbital dynamics.

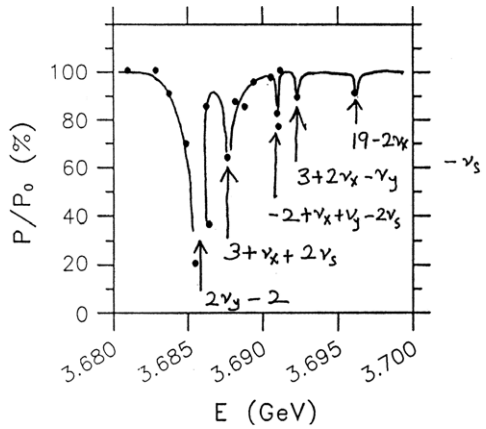

Figure 54. Theoretical interpretation of the cluster of closely spaced resonances in the SPEAR polarization data near 3.688 GeV. From Mane (1988a).

(c) The horizontal betatron resonance $\nu = \nu_x + 3$ at 3.65 GeV is surrounded by several clearly visible synchrotron sidebands (up to $m = \pm 2$). The widths of the synchrotron sidebands were fitted *without* further adjustment of the theoretical inputs, once the tunes and the lattice imperfections had been fixed. The *second* order synchrotron sidebands $\nu = 3 + \nu_x \pm 2\nu_s$ at 3.61 GeV ($m = -2$) and 3.688 GeV ($m = 2$) are particularly interesting. According to theory, these two resonances should have equal width, but according to the guide to the eye in figure 6, the $m = 2$ sideband at 3.688 GeV is considerably wider than the $m = -2$ sideband at 3.61 GeV. Why was this? The answer is as follows. Note that there are many data points in the vicinity of the resonance at 3.688 GeV, some with quite high polarization ($P/P_0 > 80\%$). There is another resonance $\nu = 2\nu_y - 2$ very close to the $m = 2$ synchrotron sideband $\nu = 3 + \nu_x + 2\nu_s$ at 3.688 GeV. The SMILE fit to the data showed two narrow resonances at 3.688 GeV. The points of high polarization in the middle of the 'resonance' are *real*, not noise. The polarization drops, rises, then drops again, as one sweeps the beam energy. The $m = \pm 2$ synchrotron sideband resonances are indeed of equal width. Mane (1988) interpolated the SPEAR data 'by hand' to denote a cluster of five resonances, indicated in the inset in figure 7 and displayed in detail in figure 54. No other theoretical formalism has explained the experimental SPEAR data near 3.688 GeV in figure 6.

29.3.4. Theoretical fit 3: Buon. Buon (1989, 1990) independently derived formulae to fit the *ratio* of the synchrotron sideband resonance widths to that of a parent betatron resonance $\nu = n + Q_{x,y}$, or a doublet of synchrotron resonances $\nu = n \pm Q_s$. The formulae were displayed in (28.50) and (28.52). Buon also stated that there was only definitive data to quantitatively fit the $m = -1$ synchrotron sideband $\nu = 3 + \nu_x - \nu_s$ (at 3.63 GeV) of the parent horizontal betatron spin resonance $\nu = 3 + \nu_x$ (at 3.65 GeV). The energy spread of SPEAR was a known quantity, as was the synchrotron tune and the value of $a\gamma$. From this information, one could deduce that the value of the tune modulation index was $\sigma^2 \simeq 0.03$. Buon did not attempt to explain the disparity between the widths of the $m = \pm 2$ synchrotron sidebands at 3.61 and 3.688 GeV, nor any of the other resonances in the SPEAR data.

29.3.5. Theoretical fit 4: Lee and Berglund. The fourth (and final, to date) theoretical fit of the SPEAR data was by Lee and Berglund (1996), with more details by Lee (1997). We review

their work briefly. Their formalism is considerably different from the first three fits reviewed above. Mari Berglund (2004) kindly brought to our attention her PhD thesis (Berglund 2001), in which she addressed many details not adequately discussed in the above references. Lee (2005) kindly explained to us that the basic idea is a phenomenological fit, to see what information one can extract from the data with a minimum of theoretical inputs. It is not a 'fundamental' derivation like the earlier works.

Basically, Lee and Berglund (1996) parametrized the resonances using Lorentzians (as one obtains from the single resonance model, see section 16)

$$P_{\rm eq}^{\rm LB} \simeq \frac{8}{5\sqrt{3}} \frac{\delta^2}{\delta^2 + |\epsilon|^2}, \tag{29.1}$$

where $\delta = \nu - \nu_{\rm res}$ is the distance to the resonance and ϵ is the resonance strength. Note that in the close vicinity of a resonance, one can show that $|\gamma(\partial \boldsymbol{n}/\partial\gamma)| \propto |\epsilon/\delta|$, e.g. as in the harmonic spin matching technique. Then, neglecting factors of $11/18$, etc, the spin-diffusion approximation to the Derbenev–Kondratenko formula yields

$$P_{\rm eq} \simeq \frac{8}{5\sqrt{3}} \frac{1}{1 + |\epsilon|^2/\delta^2}, \tag{29.2}$$

which is equivalent to (29.1). Hence, the Lee–Berglund parametrization is basically valid close to a resonance, with a phenomenological value for ϵ. For brevity we define $\lambda = \sqrt{\delta^2 + |\epsilon|^2}$. When there are multiple parent resonances, indexed by i, they express the overall magnitude of the polarization by

$$P_{\rm eq}^{\rm LB} = P_{\rm ST} \prod_i \frac{\delta_i^2}{\lambda_i^2}, \tag{29.3}$$

i.e. a product of single resonance terms. They retrofitted the widths of the parent resonances $\nu = \nu_x + 3$, $\nu = \nu_y + 3$ and $\nu = 8 + \nu_x - \nu_y$ from the experimental data. The synchrotron sideband resonances were added using a Bessel-function 'comb' as derived earlier for the single resonance model, with the tune modulation index $\sigma^2 = (\sigma_E/E)^2(a\gamma/\nu_s)^2$. They wrote the Bessel functions as $J_m(g)$ (i.e. before an average over the beam distribution), where $g = \beta^2\, \nu_0\, \hat{a}/\nu_s$. They employed a '95% emittance' value $\hat{a} = \sqrt{6}\sigma_{\rm p}/p$, and obviously $\beta^2 \simeq 1$. For SPEAR, they obtained $g \simeq 0.42$. Comparing with the value found by Buon earlier, we find that $\frac{1}{6}g^2 \simeq 0.0294$, in agreement with Buon's finding $\sigma^2 \simeq 0.03$ reported above. Lee and Berglund (1996) only fit up to 3.66 GeV and thus covered only the lower ($m = -1$ and $m = -2$) synchrotron sidebands of the horizontal betatron resonance $\nu = \nu_x + 3$ at 3.65 GeV. Therefore, they do not explain the discrepancy in the observed widths of the $m = \pm 2$ sidebands.

29.4. VEPP-4

A spin resonance scan as a function of beam energy was performed at VEPP-4. The data are shown in figure 55. The data span the energy interval from roughly $a\gamma \simeq 10.5$ to $a\gamma \simeq 12$. The values of the orbital tunes are indicated in the figure. Several integer and first-order betatron spin resonances are visible. No synchrotron sideband resonances are indicated, possibly because the synchrotron tune was too small to resolve distinct sideband resonances. No theoretical fit to the VEPP-4 data was published.

The data were taken as part of the effort to measure the masses of the vector mesons Υ, Υ' and Υ''. Precision measurements of the masses of vector mesons produced by e^+e^- will be reviewed in section 30. There is substantial polarization at the beam energies $\frac{1}{2}M_\Upsilon c^2$ and $\frac{1}{2}M_{\Upsilon''}c^2$, but relatively little at $\frac{1}{2}M_{\Upsilon'}c^2$, because of the proximity to various first-order

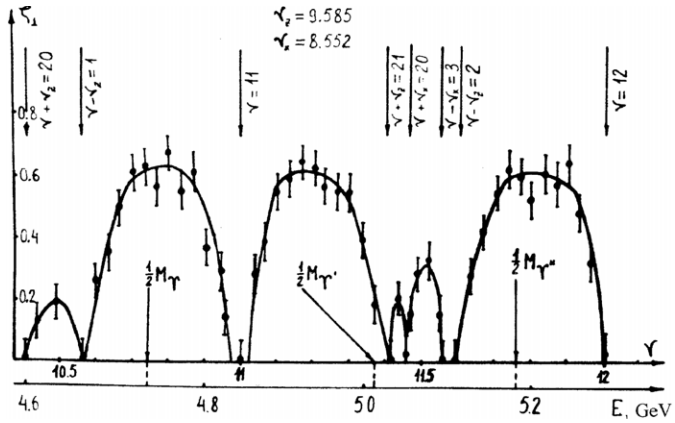

Figure 55. Resonance scan at VEPP-4 in the energy range of the Υ, Υ' and Υ'' mesons.

betatron depolarizing resonances due to the values of the betatron tunes. Hence, the beam energy calibration was performed at a point offset by 30 MeV from the peak of the Υ' resonance (60 MeV centre-of-mass) and the energy at the operating point for the experiment was obtained by extrapolation using magnetic field calibrations. The beam energy calibrations were performed both below and above the $e^+e^- \to \Upsilon' \to$ hadrons resonance peak.

The energy of the VEPP-4 ring was initially 3 GeV, before an upgrade to reach the mass of the Υ. In its earlier version, VEPP-4 was also used to measure the masses of the charmed mesons J/ψ and ψ' (Zholents *et al* 1981). Since the polarization buildup time strongly depends on the beam energy, at the lower beam energy of 1.6 GeV, the Sokolov–Ternov polarization buildup time at VEPP-4 was over 100 h. Hence, the electrons were radiatively polarized in the VEPP-3 booster ring, where $\tau_{\rm pol} \simeq 1.5$ h and the polarized beam was transferred to VEPP-4. The principal concern, then, was not polarization but *depolarization*. The depolarization time in VEPP-4 at $E \simeq 1.6$ GeV was estimated theoretically by Zholents *et al* (1981); consult that paper for a graph of the theoretical calculations. Although there are depolarizing resonances present in the vicinity of $E = \frac{1}{2}M_{\psi'}c^2$, the polarization survived long enough to make accurate measurements.

29.5. VEPP-2M

Earlier in this review, we showed a graph of the buildup of the polarization in VEPP-2M (see figure 3). It was one of the early observations of radiative polarization in storage rings (Serednyakov *et al* 1976). In that same paper, the authors also calculated (estimated) the strength of the depolarizing resonances in the ring. It is a calculation of first-order resonances, some with sidebands. The paper, unfortunately, does not contain a graph of a comparison of theory with data.

29.6. VEPP-2

VEPP-2 was a weak-focusing storage ring (the later ring VEPP-2M was strong-focusing). Some of the earliest observations of radiative polarization were made at VEPP-2. We have cited those measurements earlier in this review (Baier 1972). A beautiful theoretical estimation of the depolarizing resonances is available. The function plotted was the overall polarization buildup rate τ^{-1} as a function of the beam energy. The graph is shown in figure 56. Several features

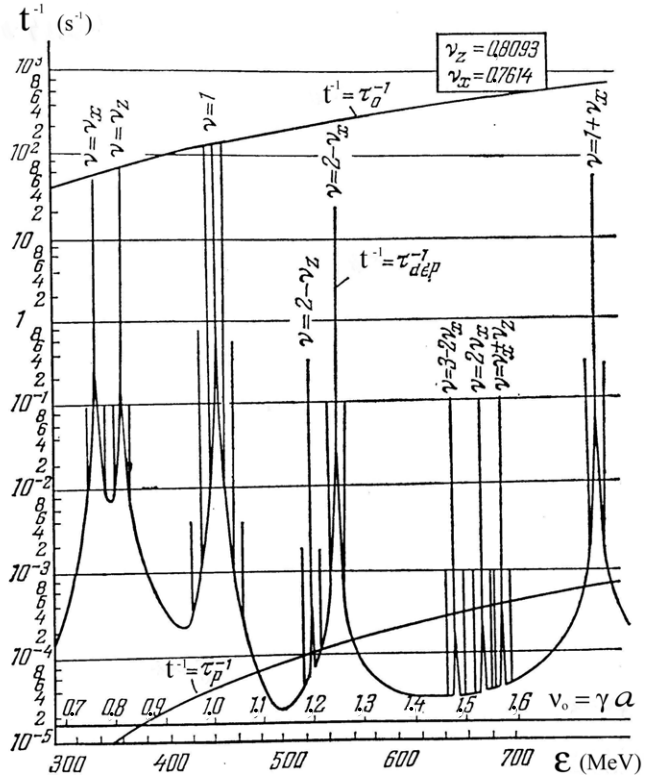

Figure 56. Theoretical estimate of polarization rate at VEPP-2, including higher-order resonances. From Khoze (1971).

of the calculation are notable:

- The calculation employed the spin diffusion model. The calculation assumed a vertical unperturbed axis (planar ring). The Derbenev–Kondratenko formula (dated 1973) was the eventual formal general formula, but approximate techniques for both synchrotron and betatron spin resonances, and sufficiently powerful for application to actual rings, were already known as the INP at Novosibirsk before then. Regrettably, these ideas remained unknown to the outside world for many years. The techniques to calculate the higher-order resonances were not formally published as an algorithm, unlike SLIM and SMILE, etc.
- Note that figure 56 depicts *second-order betatron spin resonances*, plus synchrotron sidebands, in the vicinity of 660 MeV. We follow the notation in the figure and write $\nu_{x,z}$. The first-order resonances in a planar ring all arise from imperfection terms. We also know that in a planar ring, $\boldsymbol{w} \cdot \boldsymbol{n}_0$ vanishes for the vertical betatron oscillations, but is nonzero for the horizontal betatron oscillations. Hence, the strongest second-order betatron spin resonances will be $k \pm 2\nu_x$ and $\nu_x \pm \nu_z$. The resonances $k \pm 2\nu_z$ will be weak. This is exactly what the resonance calculations in figure 56 indicate: three second-order betatron spin resonances are shown, at approximately 660 MeV, and they are $3 - 2\nu_x$, $2\nu_x$ and $\nu_x + \nu_z$. Note from the figure that $\nu_x = 0.7614$ and $\nu_z = 0.8093$, so the three resonances are close together in energy. The resonance $2\nu_z$ should appear at a slightly higher energy, but it is too weak.

30. Precision measurements I

30.1. General remarks

In this section we review some high-precision physics measurements using polarized beams. All the experiments below used radiatively polarized beams; for high-precision work one requires stable machine operating conditions, i.e. storage rings and not synchrotrons, and this basically implies radiative polarization. By far the most important use of radiatively polarized stored beams is the calibration of the beam energy, which is usually accomplished by the technique of resonant depolarization, but we shall also describe some other techniques below. The basic ideas of resonant depolarization and resonant spin-flip were described earlier in this review. In all the particle-physics experiments below, we employ 'natural units' and put $c = 1$ ($\hbar$ will not appear below).

The resonant depolarization of polarized beams in e^+e^- annihilation (electro- hadro-production) experiments provides, in many cases, the most accurate measurements of the masses of vector mesons with assignment $J^{PC} = 1^{--}$. The machine is operated at the peak of the resonance cross-section of the vector meson, and resonant depolarization is employed to calibrate the beam energy. Resonant depolarization is not limited to measurements of the masses of vector *mesons*. The mass of the Z^0 intermediate vector boson, which carries the weak neutral current, was measured to an accuracy of 2.1 MeV using resonant depolarization at LEP. The whole of section 31 will be devoted to the excellent work with polarized beams at LEP.

Note that, if the only interest in polarized beams is to calibrate the beam energy via resonant depolarization, it is *not* necessary for the spins to have a high level of polarization. It is only necessary to be able to identify the centre of the depolarizing resonance accurately. This is especially important in cases where the Sokolov–Ternov polarization buildup time may be long, or the presence of depolarizing resonances limits the asymptotic degree of polarization to a value much less than the Sokolov–Ternov limit of 92.4%. For example, a polarization level of as little as 10% will suffice.

An rf kicker may resonate with a synchrotron sideband rather than the central resonance. This is a source of experimental error in the energy calibration measurements. One must justify that the kicker frequency is aliased to the central line. This can be done by varying the value of the synchrotron tune, e.g. by varying the rf voltage, and verifying that the location of the resonance does not vary with changes in the synchrotron tune.

30.2. Measurements of particle masses

We do not give an exhaustive list of the mass measurements of all the vector mesons. We consider below two experiments to measure the mass of the Υ (officially $\Upsilon(1S)$). MacKay *et al* (1984) reported the value of the Υ mass to be

$$M_\Upsilon = 9459.97 \pm 0.11 \pm 0.07\,\text{MeV}, \tag{30.1}$$

where the first error is statistical and the second is systematic. The measurement was made at CESR using the nonmagnetic CUSB detector. The solenoid in the other particle detector (CLEO) was switched off, to avoid systematic errors in the spin precession formula caused by the presence of longitudinal fields in the ring. The positron beam energy was measured using laser Compton backscattering. The above value is combined with that from Artamonov *et al* (2000), who obtained

$$M_\Upsilon = 9460.51 \pm 0.09 \pm 0.05\,\text{MeV}. \tag{30.2}$$

This gives a world average value in the Particle Data Book (Eidelman *et al* 2004) of

$$M_\Upsilon = 9460.30 \pm 0.26\,\text{MeV}. \tag{30.3}$$

There is an interesting twist to one of the experiments. The value quoted by Artamonov *et al* (2000) is from a reanalysis of two earlier experiments at VEPP-4 (Baru *et al* 1992 and Artamonov *et al* 1984), using a revised value for the electron mass. The latter experiment subsumes an earlier experiment reported by the same group (Artamonov *et al* 1982). The 1982 experiment is particularly interesting from an accelerator physics standpoint. The beam polarization was measured using two techniques. One method was laser Compton backscattering. The other method is unusual, developed in-house at Novosibirsk, and never tried up to that time in particle accelerators. As far as we are aware it has not been tried in other e^+e^- colliders.

It is well-known that classical synchrotron radiation (which dominates the emitted photon intensity) is strongly linearly polarized in the median plane of the beam orbit. However, the out-of-plane radiation, above and below the median plane, contains a circular polarization component. Hence, the electron and positron beams in VEPP-4 were separated *vertically*, and the circularly polarized photons from the out-of-plane synchrotron radiation of one beam were used to scatter against the particles in the oppositely moving beam. The optimal vertical beam separation in the experiment was 120 μm and the rms vertical beam size was 30 μm. The beam polarization at VEPP-4 was about 80%. Using the synchrotron radiation, the Compton backscattering asymmetry was 5%, for both the electron and positron beams. Using laser Compton backscattering, the asymmetry was 1.3%, where the laser was fired against the electron beam only. The higher asymmetry was because the synchrotron radiation photons had an energy of 100 eV, whereas the laser photons had an energy of only 2 eV. The depolarization was performed using a radially directed rf magnetic field. The experiment reported a value of (Artamonov *et al* 1982)

$$M_\Upsilon = 9459.6 \pm 0.6\,\text{MeV}. \tag{30.4}$$

As stated above, this value has been superseded by more accurate measurements by the same group, and by other groups also using VEPP-4.

In conjunction with e^+e^- annihilation, resonant depolarization has been used to calibrate the masses of many vector mesons from the $\omega(782)$ on up. Such measurements fall into the field of metrology. Many of these measurements were made using the VEPP-2M and VEPP-4 e^+e^- storage rings at Novosibirsk, and many are still current in the Particle Data Book (Eidelman *et al* 2004). The masses of the ω, ϕ, $K^\pm$ and K^0 were measured at VEPP-2M and the masses of the J/ψ, ψ', Υ, Υ' and Υ'' were measured at VEPP-4. Precision mass measurements were also made at other accelerators, e.g. at DORIS for the Υ' (Barber *et al* 1984) and, of course, at CESR for the Υ (MacKay *et al* 1984). A comprehensive review of the precision mass measurements at the VEPP-2M and VEPP-4 rings was given by Skrinsky and Shatunov (1989). We review here some noteworthy results pertaining to the $\phi(1020)$ meson and also the kaons. In particular, kaons are *spin zero* pseudoscalar mesons—how can e^+e^- annihilation be used to measure their mass?

The measurement of the mass of the $\phi(1020)$ in 1975 was historically the first precision mass measurement at Novosibirsk (Aul'chenko *et al* 1975). The experiment was conducted at the VEPP-2M storage ring using the OLYA detector. The information below is from Bukin *et al* (1978) and the review by Skrinsky and Shatunov (1989). At such a low beam energy (510 MeV), the radiative polarization buildup time at VEPP-2M is too long. Hence, the beam was stored at the maximum energy of the ring (700 MeV), where the polarization time was approximately 50 min and a polarization level of about 80% was attained. One sees that precision mass measurements are not always as simple as simply placing the beam at the peak

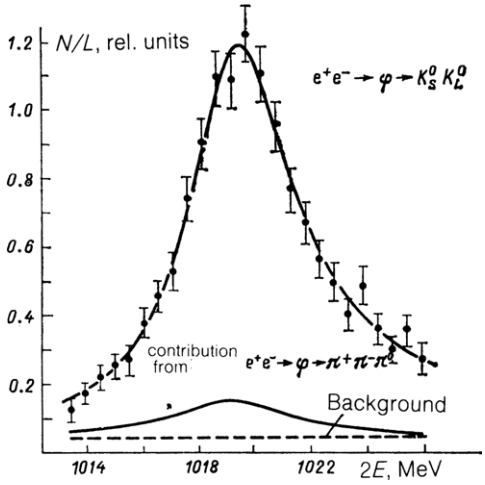

Figure 57. Annihilation cross-section at the $\phi(1020)$ resonance peak for the two decay channels $e^+e^- \to \phi \to K_L^0 K_S^0$ and $e^+e^- \to \phi \to \pi^+\pi^-\pi^0$ and the background event level. Reprinted with permission from Bukin *et al* (1978). Copyright (1978) by the American Institute of Physics.

of the resonance cross-section. After the beams had polarized, the beam energy was lowered through several weak depolarizing spin resonances to the ϕ meson region. The spin precession frequency was measured by observing a jump in the intrabeam scattering loss rate (Touschek effect) upon sweeping the frequency of a depolarizer. The beam energy measured in this way was calibrated againt the frequency of an NMR probe. This was done at several energy points. In this way, a calibration of the beam energy against the NMR probe frequency was determined. The experiment then proceeded as follows. The beam energy in the vicinity of the ϕ peak was calibrated via the NMR frequency at the beginning of the experiment and also at the end. The accuracy of the energy calibration was

$$\frac{\Delta E_{\rm cm}}{E_{\rm cm}} \simeq 1.0 \times 10^{-4}. \tag{30.5}$$

The ϕ resonance peak was measured in the two decay channels $e^+e^- \to \phi \to K_L^0 K_S^0$ and $e^+e^- \to \phi \to \pi^+\pi^-\pi^0$. The energy distribution of the events is shown in figure 57. The data in figure 57 are plotted taking account of the radiative corrections and also the $\omega - \phi$ interference. The ϕ meson mass and width from the data in figure 57 are

$$M_\phi = (1019.52 \pm 0.13)\,\text{MeV}, \qquad \Gamma_\phi = (4.36 \pm 0.19)\,\text{MeV}. \tag{30.6}$$

The above results were published by Bukin *et al* (1978). The result is still competitive with more modern measurements. The current world average value from the Particle Data Book (Eidelman *et al* 2004) is

$$M_\phi = (1019.456 \pm 0.02)\,\text{MeV}, \qquad \Gamma_\phi = (4.26 \pm 0.05)\,\text{MeV}. \tag{30.7}$$

We now briefly discuss the measurement of the masses of the kaons. Most of the current best measurements of the charged kaon mass come from kaonic atoms. Only one is from e^+e^- annihilation. For the K^0 the e^+e^- annihilation experiments are still quite competitive. The fundamental question, however, is how can one employ e^+e^- annihilation to measure the masses of *kaons*? The kaons are after all spin zero pseudoscalar mesons, and cannot be produced as a resonance (like the ϕ or Υ, etc) in e^+e^- annihilation.

We begin with the neutral K^0 meson. The information below is taken from Barkov *et al* (1987). The results from this experiment are still a major component of the world average in the Particle Data Book. Basically, the measurement technique for kaons proceeds indirectly via the ϕ resonance. The reaction studied was $e^+e^- \to \phi \to K_L^0 K_S^0$, where the K_S^0 subsequently decayed into charged pions via $K_S^0 \to \pi^+\pi^-$. The kaons produced from the decay of a ϕ at rest moved slowly and the K_S^0 decayed in the detector. Furthermore, being produced via resonant e^+e^- annihilation (the ϕ), the $K_L^0 K_S^0$ production cross-section is large resulting in a large data sample. The decay $\pi^+\pi^-$ were observed in the CMD detector. The high resolution of the detector permitted one to reconstruct, from the vector sum of the momenta of the π^+ and π^-, the momentum of the K_S^0 which produced them. One can also measure the opening angle ϕ between π^+ and π^-, in particular the minimum value ψ_0. At this minimum opening angle, the pions are emitted in the K_S^0 rest frame in a direction perpendicular to the lab-frame K_S^0 momentum. The kaon mass is calculated from the formula

$$M_{K^0} = \left[E_{\mathrm{K}}^2 \sin^2 \frac{\psi_0}{2} + 4m_\pi^2 \cos^2 \frac{\psi_0}{2} \right]^{1/2}. \tag{30.8}$$

Here E_{K} is the kaon energy, which up to radiative corrections is equal to half the total energy of the colliding e^+e^- beams—measured via resonant depolarization, remember—and m_π is the pion mass, which must be determined independently.

According to Barkov *et al* (1987), the e^+e^- beam was set on the left-hand slope of the ϕ resonance peak, at $2E = (1018.64 \pm 0.3)$ MeV. By 1987 the beam lifetime at VEPP-2M had improved to the point where it was feasible to allow the beams to polarize radiatively at the energy of the ϕ resonance itself ($\tau_{\mathrm{pol}} \simeq 3$ h). The beams were held at the above energy for 3–4 h, yielding a polarization level of 50–60%. The average beam energy was measured to be constant to an accuracy of 15 keV. The result reported by Barkov *et al* (1987) was

$$M_{K^0} = (497.661 \pm 0.033)\,\mathrm{MeV}. \tag{30.9}$$

As stated above, this value is still current, and contributes to the world average.

For charged kaons, five of the six experiments for $M_{K^\pm}$ used to compute the world average in the Particle Data Book are from kaonic atoms. The sixth is via annihilation $e^+e^- \to \phi \to K^+K^-$ near the peak of the ϕ resonance (Barkov *et al* 1979). It is that experiment which we review below. The principle of the experiment is simple. One employs the energy–momentum relationship $E^2 = p^2 + m^2$. Since the kaons are produced in the ϕ rest frame, one has $E_{K^\pm} = \frac{1}{2}E_{\mathrm{cm}}$, the value of which is measured via resonant depolarization of the e^+e^- beams. The kaon momentum was determined via range measurements in a detector of five layers of photoemulsion. The result was (Barkov *et al* 1979)

$$\tfrac{1}{2}(M_{K^+} + M_{K^-}) = (493.670 \pm 0.029)\,\mathrm{MeV}. \tag{30.10}$$

Note that the kaonic atom experiments give the mass of only the *negative* kaon M_{K^-}. The above experiment can be used to deduce a value for M_{K^+}, with practically the same accuracy as that quoted above, since the value of M_{K^-} is well-known from the kaonic atoms. Indeed, of all the experiments listed in the Particle Data Book, the one by Barkov *et al* (1979) is the only one which gives a mass for the K^+.

A new set of high-precision measurements of meson masses has recently been completed at VEPP-2M, using the CMD2 detector (see also Akhmetshin *et al* (2004) for a reanalysis of earlier data). A new round of precision mass measurements at the upgraded VEPP-4M storage ring was announced by Blinov *et al* (2002), including the τ-lepton as well as vector mesons. New results for the masses of the J/ψ and ψ' were published by Aul'chenko *et al* (2003).

30.3. CPT invariance

We now turn to other measurements, not connected with the particle masses. Experiments were conducted at VEPP-2M to compare the ratio of the values of the anomalous magnetic moments of the electron and the positron to high accuracy. Note that the experiments measured the *ratio*; the actual magnetic moment anomalies were not measured to the same degree of accuracy. The equality of the anomalous magnetic moments of the electron and positron provides a precision test of CPT invariance. In two earlier experiments, Serednyakov *et al* (1977) and Vasserman *et al* (1987a), resonant depolarization was used to establish the equality of the spin tunes of the electron and positron beams. A different and innovative technique was used in a later work by Vasserman *et al* (1987b). This is the experiment described below.

The Sokolov–Ternov radiation caused the electron and positron spins to polarize vertically with equal and opposite values. Now recall the Froissart–Stora formula, from section 6. If the adiabatic condition is satisfied, i.e. $\epsilon^2/|\alpha| \gg 1$, then there will be complete reversal of the spin direction with negligible loss of polarization. However, suppose we stop *halfway*, i.e. when the value of $a\gamma$ crosses the tune of the resonance driving term. Then the spins will be rotated into the horizontal plane with negligible loss of polarization. This was done by Vasserman *et al* (1987b). Define $\omega_\mathrm{r} = \omega_\mathrm{rev}(1 + a\gamma)$ as the resonant frequency. A horizontal radio-frequency field was applied, starting from some initial value $\omega_\mathrm{i} \ll \omega_\mathrm{r}$ and increasing in value slowly so as to satisfy the adiabatic condition $\epsilon^2/\alpha \gg 1$. The radio-frequency field was switched off at the resonant frequency ω_r and the spins were allowed to precess freely in the horizontal plane. After a time, the spins were rotated back to the vertical, by reapplying the radio-frequency field starting at the frequency ω_r and sweeping backwards to the initial value ω_i. Note that the *same* radio-frequency kicker sufficed to rotate the spins of *both* beams. This can be seen by the consideration of signs of the particle charges, and the velocities and initial spin orientations. The magnitude of the restored polarization was

$$P_\mathrm{f} = P_0\,\mathrm{e}^{-(\delta\psi)^2/2}. \tag{30.11}$$

Here, $\delta\psi$ is the angle of the spread of the spins (while precessing in the horizontal plane). The rotation of the spins back to the vertical cancels the first-order spread in the spin directions, but cannot cancel the second order spread $\frac{1}{2}(\delta\psi)^2$; this leads to (30.11). The spins were allowed to polarize again, via Sokolov–Ternov radiation. The whole process was repeated several times during a machine fill. While the spins were in the horizontal plane, the difference in the spin rotation angle in a time interval T was

$$\Delta\psi = \int_0^\mathrm{T} (\Omega_{\mathrm{e}^+} - \Omega_{\mathrm{e}^-})\,\mathrm{d}t, \tag{30.12}$$

with obvious notation. The angle $\Delta\psi$ should not be confused with the spread $\delta\psi$. The value of T was limited by the depolarization time of the spins. If the spin precession angles were equal then the restored polarization ratios should be equal:

$$\frac{P_\mathrm{f}^+}{P_0^+} = \frac{P_\mathrm{f}^-}{P_0^-}, \tag{30.13}$$

with an obvious notation. Hence, the e^+ and e^- polarizations were measured before and after the rotation of the spins to the horizontal plane. An example of such a measurement is shown in figure 58. The variables plotted are (the authors use S not P)

$$\frac{S^+}{S_0} = S\cos\psi, \qquad \frac{S^-}{S_0} = S\cos(\psi + \Delta\psi), \tag{30.14}$$

where $S = \mathrm{e}^{-(\delta\psi)^2/2}$ is the remanent polarization ratio after the free precession and restoration to the vertical. If the spin precession frequencies were equal, then the graph would be exactly

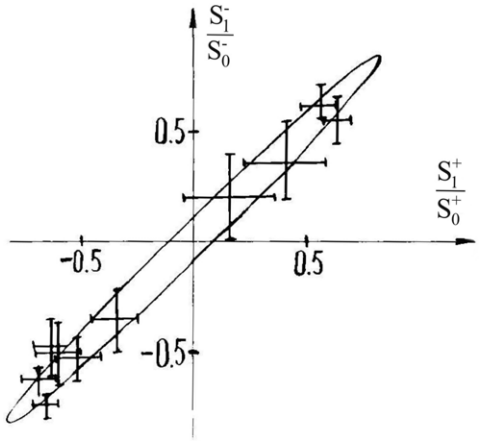

Figure 58. Comparison of the restored vertical polarization of the electron and positron beams (after free precession in the horizontal plane) at VEPP-2M. Reprinted from Vasserman *et al* (1987b). Copyright (1987) with permission from Elsevier.

a straight line. To obtain a better calibration of the value of S, a radial static electric field was applied in one part of the ring, while the spins were precessing in the horizontal plane to cause a separation of the spin precession frequencies. From (5.81), one finds that the frequency split is

$$\Delta = \Omega^+ - \Omega^- = 2a\frac{e}{mc}\langle E\rangle = 2a\gamma\frac{\langle E\rangle}{\langle B_y\rangle}\,\omega_{\rm rev}, \tag{30.15}$$

which evaluated to 2.5 Hz for this experiment. In other measurements, the electric field was increased by a factor of 2.5. The graphs of S^-/S_0 against S^+/S_0, for the various settings of the electric field, are essentially Lissajous figures. The same value of S was used to fit all the data. The overall conclusion for the case of zero electric field was that the phase difference was $|\Delta\psi| < 5^\circ$, which implied, assuming $m_{e^+} = m_{e^-}$ (Vasserman *et al* 1987b)

$$\frac{\Omega_{e^+} - \Omega_{e^-}}{\Omega_{\rm avg}} = \frac{a_{e^+} - a_{e^-}}{a_{\rm avg}} \leqslant 1 \times 10^{-8}. \tag{30.16}$$

The above result was for a time the best limit on CPT invariance for leptons, but is now obsolete, having been superseded by more accurate measurements using Penning traps. Multiplying by $(g-2)/g \simeq 1.2 \times 10^{-3}$ to compare to other results, the above bound is (Particle Data Book, Eidelman *et al* 2004)

$$\frac{g_{e^+} - g_{e^-}}{g_{\rm avg}} \leqslant 12 \times 10^{-12}, \tag{30.17}$$

as compared to the current best limit using Penning traps (Dyck *et al* 1987)

$$\frac{g_{e^+} - g_{e^-}}{g_{\rm avg}} \leqslant -0.5 \times 10^{-12}. \tag{30.18}$$

However, note that the trap experiments measure the value of g (or $g-2$). The accelerator experiment measured the difference in spin precession frequencies, so that the experiment really demonstrated the equality of $ea_e/(mc^2)$, in principle a different combination of fundamental constants.

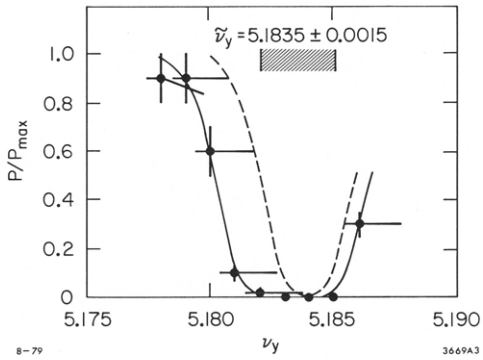

Figure 59. Measurement of the SPEAR positron beam polarization in the vicinity of the vertical betatron spin resonance $\nu_y + 3$. From Fischer *et al* (1979).

30.4. SPEAR: energy calibration via betatron spin resonance

The measurements at SPEAR (Fischer *et al* 1979) were the first use of resonant depolarization to calibrate the beam energy *using a laser Compton backscattering polarimeter*. Previous energy calibrations using resonant depolarization (e.g. at VEPP-2M and VEPP-4) employed Touschek scattering for the polarimetry. Also note that in contrast to other experiments, the SPEAR beam energy was calibrated by measuring the (vertical) betatron tune, and not by sweeping the frequency of an rf kicker.

The (noncolliding, positron) beam energy was held fixed at $E \simeq 3.6061\,\mathrm{GeV}$ and the polarization was plotted against the vertical betatron tune (the other machine tunes were held fixed). The resonance $\nu = \nu_y + 3$ was chosen because it was narrow, thereby permitting a precise determination of its centre (see figure 6 and the discussion in section 29). The data are shown in figure 59. The error bars indicate the polarization uncertainty and also the betatron tunespread. From the measurement $\nu_y^{\mathrm{exp}} = 5.1838 \pm 0.0015$, the energy was calibrated to be

$$E = \frac{m_e c^2}{a_e}(\nu_y^{\mathrm{exp}} + 3) = 3.6061 \pm 0.0007\,\mathrm{GeV}, \tag{30.19}$$

a relative accuracy of $\pm 0.02\%$. Magnetic field measurements could achieve only $\pm 0.1\%$. We were informed (Sinclair 2004) that the technique was used later to measure the mass of the ψ' meson (although not formally published).

30.5. CESR and the B-factories

A study of the feasibility of longitudinal polarization at CESR has been reported by Wang (2001). Otherwise (other than the measurement of the Υ mass), little or nothing has been done with polarized beams at CESR and the PEP-II and KEK-B B factories.

30.6. TRISTAN

Radiative polarization was observed at TRISTAN (Mizumachi *et al* 1990) before the ring was converted into a part of KEK-B. The material below is mainly from Nakajima *et al* (1991) and Nakajima (1993). A laser Compton backscattering polarimeter was used. Initially, a single-photon Compton backscattering polarimeter was employed. The polarimeter could simultaneously measure both the vertical and longitudinal polarization components of the

electron beam. According to Nakajima *et al* (1991), a vertical polarization of 33% and a longitudinal polarization of 18% was observed at a beam energy of 29 GeV, corresponding to a total polarization of 37% and tilted at an angle of 29° to the vertical. The degree of the longitudinal polarization was also found to be correlated with the strength of the solenoid fields in the particle detectors during colliding-beam operations. The tilt of the polarization by 29° is surprising. Unfortunately, the measurements were not pursued in greater detail. At TRISTAN, the Sokolov–Ternov polarization time at a beam energy of 29 GeV was only 140 s. Later, the polarization was measured at 14.76 GeV and an asymptotic polarization level of 70% was recorded (Nakajima 1993). The Sokolov–Ternov polarization time at a beam energy of 14.76 GeV was 68.5 min, as expected from the E^{-5} dependence of the polarization buildup time. Resonant depolarization was also employed at TRISTAN to calibrate the electron beam energy during colliding-beam operation, yielding a measurement of (Nakajima 1993)

$$E = 28\,887.639 \pm 0.022\,\text{MeV}, \tag{30.20}$$

which is a relative accuracy of 10^{-6}. Later, a multi-photon Compton backscattering polarimeter was employed, which had less error from background but could only measure the transverse polarization.

30.7. Synchrotron radiation light sources

30.7.1. General remarks. This is a somewhat peripheral topic, but deserves a brief mention. The use of polarized beams for precision measurements is not restricted to high-energy particle physics. Synchrotron radiation light sources are important research facilities for materials science, diffraction studies of biological molecules, etc. An overview is given by Margaritondo (2002). Modern light sources are equipped with excellent beam position monitoring and orbit correction feedback systems. The beams have very small emittances to supply photon beams of high brightness and brilliance. Hence, the depolarizing spin resonances are weak.

It is desirable for the machine operation to have an accurately calibrated beam energy. In practice, the *absolute* energy calibration is not necessarily critical; what is of much greater importance, is to have a *stable* beam energy during machine operations. For this reason, it is typically more important to record changes in the beam energy. The polarization buildup time may or may not be much shorter than the beam storage time. When the BESSY I light source operated at its top energy of 800–850 MeV, the Sokolov–Ternov buildup time was roughly 3 h (Klein *et al* 1997). When the ring operated in a lower energy mode at 340 MeV, the use of radiative polarization was impractical. Nevertheless, a laser Compton backscattering system was installed at BESSY I to measure the electron beam polarization and resonant depolarization measurements were carried out at the energy of 800 MeV (Klein *et al* 1997, 1998). At the newer light source, BESSY II, the use of resonant depolarization energy calibration helped to improve the stability of the beam energy from $\pm 7 \times 10^{-4}$ to $\pm 3 \times 10^{-4}$ (Kuske and Goergen 2000).

In many modern synchrotron light sources, but not all, the beam emittances are so small and the particle density, therefore, so high that the beam loss lifetime is dominated by the Touschek effect. At the ALS, SLS and BESSY II, the Touschek lifetime measurement was employed as the polarimeter. BESSY I had a Compton polarimeter, as stated above.

At the ALS (see figure 16), the beam energy is 1.5–1.9 GeV and the relative accuracy of the resonant depolarization measurements is 1×10^{-5}, which is an order of a magnitude better than alternative techniques. Note, however, the principal method of correcting energy variations at the ALS is to record the changes in the orbit position in dispersive regions and feedback on the rf frequency. The use of resonant depolarization is an additional tool.

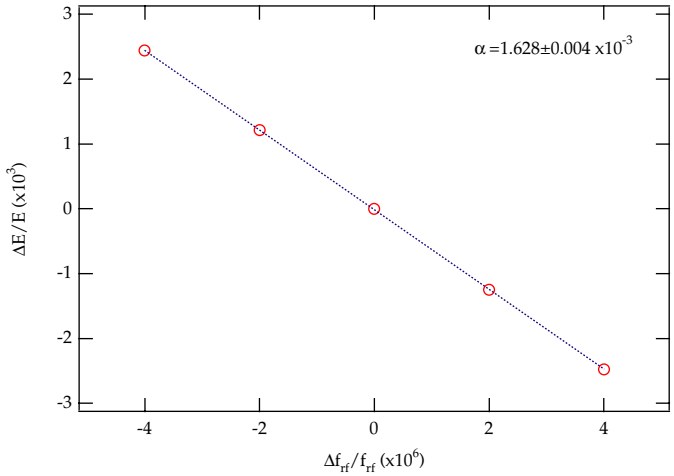

Figure 60. Measurement of the beam energy variation as a function of the rf frequency at the ALS. The slope is the negative inverse of the momentum compaction factor. Courtesy of Byrd (private communication) and ALS.

We mention here an elegant piece of accelerator physics, using the beam energy calibration (via resonant depolarization), to accurately measure the momentum compaction factor of the ring (Steier *et al* 2000). For ultrarelativistic particles, we can approximate

$$\frac{\Delta E}{E} = -\frac{1}{\alpha}\frac{\Delta f_{\rm rf}}{f_{\rm rf}}. \tag{30.21}$$

The beam energy was changed slightly by varying the frequency of the rf cavities, but *without* altering the magnetic field in the bending dipole magnets. This shifted the energy (and spin tune) and the orbital revolution frequency. A graph of $\Delta E/E$ against $\Delta f_{\rm rf}/f_{\rm rf}$ is plotted in figure 60. The value of α is the negative inverse slope of the line. The value so obtained is $\alpha = (1.628 \pm 0.004) \times 10^{-3}$. This agrees well with calculations, based on a calibrated model of the machine, which yield $\alpha = (1.616 \pm 0.008) \times 10^{-3}$. The momentum compaction factor has also been measured in this way at BESSY I (Klein *et al* 1997) and at the SLS (Leemann *et al* 2002a).

An extremely pretty graph showing depolarization from the parent resonance and its first synchrotron sideband is shown in figure 61 (Leemann *et al* 2002a). The measurements were made at the SLS (see figure 17). Two frequency sweeps are displayed. The synchrotron tune varies with the rf voltage like $Q_s^2 \propto V_{\rm rf}$. Hence, the rf voltage was increased by 11% in the second sweep, thereby raising the value of the synchrotron tune Q_s from 0.006 17 to 0.006 48, a roughly 5% increase. The synchrotron sideband can be clearly distinguished because its location shifts, whereas that of the parent resonance does not. Using the data in figure 61, a more detailed fit of the depolarization across the parent resonance was performed by fitting to the Froissart–Stora formula. This led to an energy calibration of (2.4361 ± 0.000 24) GeV, where the uncertainty is half of the FWHM of the fit. Later work improved the calibration to (2.4361±0.000 18) GeV. This is 1.5% higher than the design energy. The difference has not yet been explained (Leemann 2002b). The momentum compaction factor was also measured at the SLS, including the second order term. The results are $\alpha_1 = 5.6 \times 10^{-4}$ and $\alpha_2 = 4.4 \times 10^{-3}$. (See Leemann *et al* (2002a) or (21.33) for the definition of α_1 and α_2.) No error bars are quoted because only three energy points were measured. Independent measurements (not using polarized beams) yield $\alpha_1 = 6.0 \times 10^{-4}$ and $\alpha_2 = 4.2 \times 10^{-3}$.

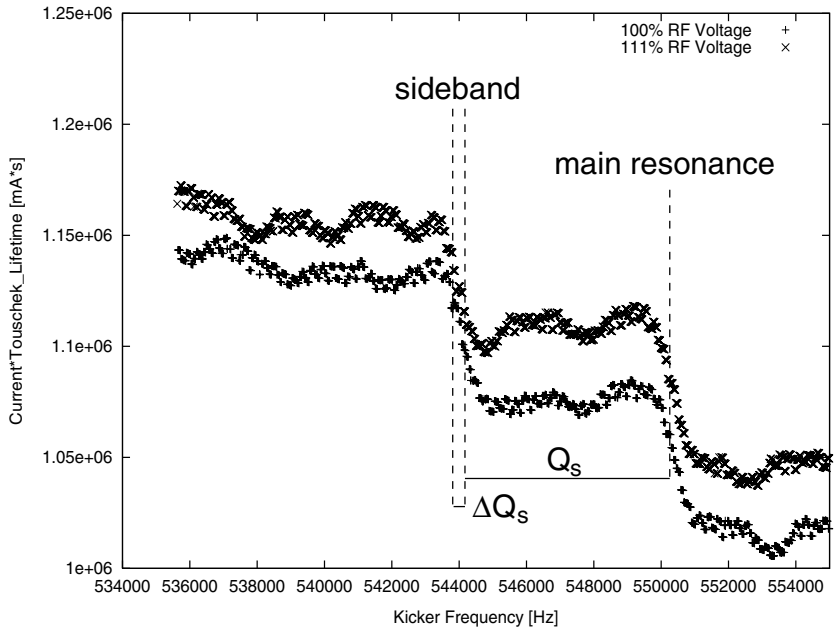

Figure 61. Dip patterns of two sweeps at the SLS differing by an 11% increase of the rf voltage (shift in the value of the synchrotron tune). Courtesy of Leemann (private communication) and SLS.

We are grateful to Byrd (2004) and Steier (2004) who kindly supplied copies of data and information about the experimental techniques employed at the ALS and to Leemann (2004) who kindly supplied details about the SLS and his work.

31. Precision measurements II

31.1. General remarks

In the previous section, we reviewed work on precision measurements with radiatively polarized beams at a number of accelerators. Here we shall review work at one accelerator only, the biggest ever built to date, where the concept of 'energy calibration' became not just an occasional measurement but part of the very soul of the machine. That accelerator is LEP. The figures below were kindly supplied by Wenninger (2004), also including a list of relevant references to the literature.

31.2. Background

CERN (Centre Européen pour la Recherche Nucléaire) is the European Laboratory for Particle Physics in Geneva, Switzerland. In the late 1980s and through the 1990s, the high-energy frontier was the mass scale of the Z^0 and $W^{\pm}$ bosons of the electroweak theory. The Z^0 and $W^{\pm}$ were discovered at CERN, using the S$p\bar{p}$S, the Super Proton Synchrotron converted into a $p\bar{p}$ collider. The next step after the discovery of the Z^0 and $W^{\pm}$ was to study their properties in detail. CERN met this challenge by building the e^+e^- collider LEP. Because of its high beam energy (approximately 46 GeV in LEP1, increased to about 100 GeV in the second phase LEP2), the dissipated synchrotron radiation power output was enormous (several tens of MW).

To mitigate this, LEP was designed with a circumference of 27 km, sitting astride the Swiss–French border. LEP operated from 1989 to 2000, initially as a dedicated Z^0 factory with a centre-of-mass energy of approximately 91 GeV (LEP1, 1989–95) and later (LEP2, 1995–2000) with higher beam energies up to a centre-of-mass energy of 209 GeV, for open W^+W^- production.

Since the Z^0 boson can be (copiously) produced on resonance via e^+e^- annihilation, LEP not surprisingly operated in its initial phase as a dedicated Z^0 factory (the so-called LEP1) to measure the parameters of the electroweak theory with precision. Two of the most important parameters are the mass M_Z and the decay width Γ_Z of the Z^0. LEP was uniquely positioned to measure both parameters to an accuracy unrivalled by other machines and it did so. Over 20 million Z^0 decays were recorded by the various detectors, by operating LEP at the peak of the Z^0 resonance, and at two energy points just above and below the peak.

Accumulating many decay events was not sufficient, however; the machine beam energy should also be accurately calibrated. We have seen that the technique of resonant depolarization furnishes the most accurate method of measuring the beam energy, and thereby for determining the masses of vector mesons produced in e^+e^- annihilation. The Z^0 boson can also be produced as a resonance in e^+e^- annihilation and its mass can, therefore, be accurately determined by setting the e^+e^- beam energy on the peak of the Z^0 resonance. The decay width Γ_Z can be determined by operating the machine at energy points slightly above and below the resonance peak. This section is devoted to a description of the development of the 'LEP Energy Model'. It was fortunate that the mass of the Z^0 is approximately 91.2 GeV, because this meant that the required spin tune was

$$a\gamma = \frac{(1/2)M_Z}{m_e/a} \simeq \frac{45.6}{0.440\,6486} \simeq 103.5. \tag{31.1}$$

Hence, the peak of the Z^0 resonance cross-section was also a point where the fractional spin tune was nearly one-half, i.e. an optimal value for polarization measurements. In practice, LEP1 was mainly run at a spin tune of $a\gamma = 103.5$.

The world average value for the mass of the Z^0 is, from the Particle Data Book (Eidelman *et al* 2004),

$$M_{Z^0} = 91.1876 \pm 0.0021\ \text{GeV}. \tag{31.2}$$

The above figure is based on data from all four LEP experiments, but one must be aware that an accurate calibration of the LEP beam energy is also essential to obtain the small error of 2.1 MeV, a relative accuracy of $\pm 2.3 \times 10^{-5}$.

LEP operated exclusively with transversely polarized beams, which were used for energy calibration (the polarization was zero during high-energy physics data taking). The polarization was generated naturally by the synchrotron radiation. Although plans were mooted for spin rotators to provide longitudinal polarization at the interaction points and a design of a spin rotator matched to the LEP optics was proposed (Grote 1995), no spin rotators were ever installed.

31.3. Early work and initial measurements: 1990–1

Interest in utilizing the radiative polarization at LEP was present from the inception of the project. We are not competent to offer a historical review of all such early work; the CERN archives, no doubt, have detailed information. We begin with the publication of plans for a Compton backscattering polarimeter at LEP (Placidi and Rossmanith 1989) (see figure 28 for a schematic of the LEP polarimeter). The commissioning of the Compton polarimeter was reported by Badier *et al* (1991b). Transverse polarization was first observed at LEP in 1990

(Badier *et al* 1991a, Knudsen *et al* 1991). The asymptotic degree of the polarization was $(9.1 \pm 0.3\,(\text{stat}) \pm 1.8\,(\text{syst}))\%$. The spin tune was approximately $\nu_0 = 103.53$, close but (by choice) not exactly equal to the centre of the Z^0 peak. The essential point being that transverse polarization had been observed at the desired energy scale.

By 1991, the combined 1989–90 experimental data from the four LEP experiments had established a statistical precision of ± 5 MeV on M_Z and ± 9 MeV on Γ_Z, whereas the systematic error due to the beam energy uncertainties was ± 20 MeV on M_Z and ± 6 MeV on Γ_Z. The need for an improved calibration of the LEP beam energy was clear. The first measurement of the LEP beam energy, by means of resonant spin depolarization, took place in four scans from 16 September to 11 November 1991 and was reported by Arnaudon *et al* (1992). Even though the LEP beam energy was high, the machine circumference was also large so that the Sokolov–Ternov buildup time at LEP at 46 GeV was in fact quite large, $\tau_{\text{ST}} \simeq 5$–$6$ h. The depolarizing resonance driving terms reduced the polarization buildup time to only 35 min, but at the cost of a greatly reduced asymptotic polarization level. Nevertheless, the minimum required polarization level to perform reliable resonant depolarization measurements at LEP was 5%, and a polarization of 10% met this criterion.

The radio-frequency kicks to induce depolarization were applied using a vertical kicker, which was normally used for vertical betatron tune measurements. It was noted that the use of this kicker could also excite the vertical betatron oscillations leading to large fluctuations in the electron beam position and distorting the readings in the polarimeter. This could happen if the kicker frequency or one of its harmonics were in tune with a higher order vertical betatron resonance. These are some of the practical difficulties which a review devoted purely to theory could not point out. It was also observed that the beam energy of LEP (i.e. the location of the resonant frequency) would drift over a timescale of a few hours, not inconsistent with the short term stability of LEP, of order 10^{-5}.

The availability of stable transverse polarization and the use of resonant depolarization allowed the systematic uncertainties in the Z^0 mass and width to be reduced to ~ 6.3 MeV for M_Z and ~ 4.9 MeV for Γ_Z in 1991. Perhaps most significantly, however, the analysis of the 1991 data suggested that the reproducibility of the LEP beam energy might be affected by sources other than temperature changes in the LEP dipoles. Fischer and Hofmann (1992) pointed out that tidal effects might be the cause. Arnaudon *et al* (1992) reported fluctuations in the energy calibrations indicating a correlation to gravity variations in the Geneva area related to tidal forces. This set the stage for one of the most delightful pieces of accelerator physics that we shall encounter in this review: the LEP TidExperiment.

31.4. LEP and the moon: the TidExperiment

The gravitational attraction of the Moon and the Sun is not uniform over the globe because of the $1/r^2$ dependence of the gravitational force, where r is the spatial separation between the bodies. This results in a small elastic deformation of the Earth's crust. The lunar and the weaker solar tides interfere to daily produce two tide bulges. These tides are of the same origin as the water tides of the oceans. In addition to the diurnal variation, there are also a number of other periodicities, including eccentricity and small oscillations of the Earth's and Moon's orbits. A sketch of the deformation of the Earth (greatly exaggerated) due to the lunar tides is shown in figure 62.

What this means to us is that the circumference of LEP got stretched and this affected the beam energy. Recall the momentum compaction factor, which we shall write in the

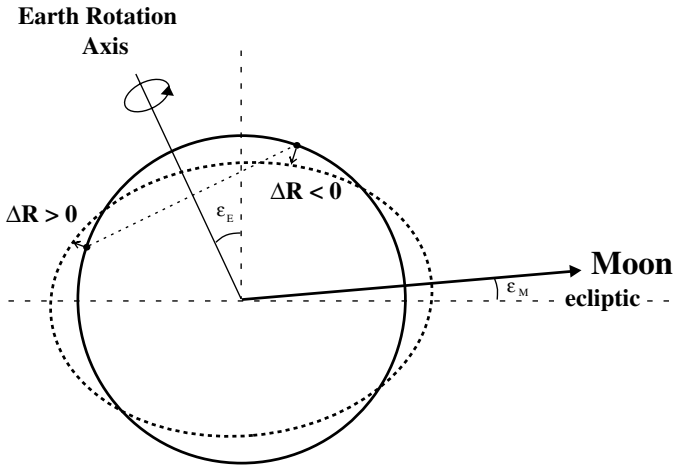

Figure 62. Schematic of tide bulges (greatly exaggerated) in the Earth due to the Moon. Courtesy of Wenninger (private communication) and CERN.

following way:

$$\frac{\Delta E}{E} = -\frac{1}{\alpha}\frac{\Delta C}{C} \tag{31.3}$$

and $\alpha \simeq 1.86 \times 10^{-4}$ for LEP. This meant that a fractional change in the circumference was magnified by around 6000, in its effect on the fractional change in the energy. Based on this information, let us consider a few simple numerical estimates. First, we wish to calibrate the Z^0 mass to better than 10 MeV, say, given $M_Z \simeq 91$ GeV. Hence, we seek an accuracy level of $\Delta E/E \simeq 10 \times 10^{-3}/90 \simeq 1.1 \times 10^{-4}$. Hence, we need a knowledge of $\Delta C/C$ to an accuracy of $\alpha(\Delta E/E) \simeq 1.86 \times 1.11 \times 10^{-8} \simeq 2 \times 10^{-8}$. Given the LEP circumference $C = 26.7$ km, the energy calibration is therefore sensitive to a variation in the ring circumference at the level of $\Delta C \simeq 26.7 \times 10^6 \times 2 \times 10^{-8} \simeq 0.5$ mm or half a millimeter. Really!

The local strain on the Earth's crust is a tensor and is difficult to monitor. Much simpler to measure and predict is the time-dependent local gravity variation $\Delta g(t)$. To a good accuracy, the horizontal strain is proportional to the gravity variation and one can write

$$\alpha_{\rm str} = \frac{\Delta C(t)/C_0}{\Delta g(t)/g_0}, \tag{31.4}$$

where $g_0 = 980$ gal (1 gal $= 1\,{\rm cm\,s^{-2}}$), and we stated earlier that $C_0 = 26.7$ km. The value of $\Delta g(t)$ reaches a maximum of about 140 μgal at high tide in the Geneva area. Hence, overall one has

$$\frac{\Delta E(t)}{E_{\rm tide=0}} = -\frac{\alpha_{\rm str}}{\alpha}\frac{\Delta g(t)}{g_0} \equiv \kappa_{\rm tide}\,\Delta g(t). \tag{31.5}$$

Figure 63 shows a graph of the correlation of the LEP energy variation (measured using resonant depolarization) against the local gravity at Geneva in 1991.

Based on the above reasonings, a dedicated beam energy calibration experiment was scheduled, on the night of a full moon, to record the LEP beam energy as a function of the time of day: this was the LEP TidExperiment, which took place over a 24 h interval on 11 November, 1992. All the LEP experimental detector solenoids were switched off and the machine given over entirely to beam energy calibration (Arnaudon *et al* 1993). The variation of the energy

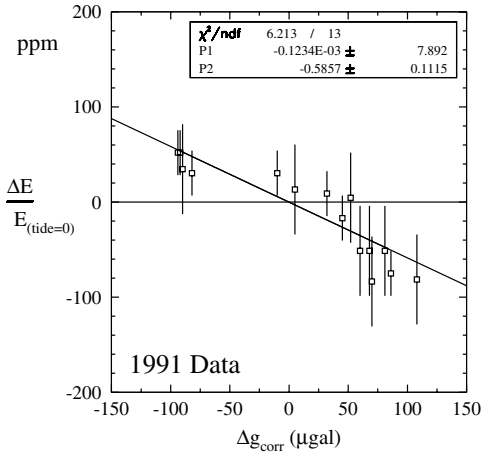

Figure 63. Correlation between relative energy measurements and the local gravity at LEP in 1991. Courtesy of Wenninger (private communication) and CERN.

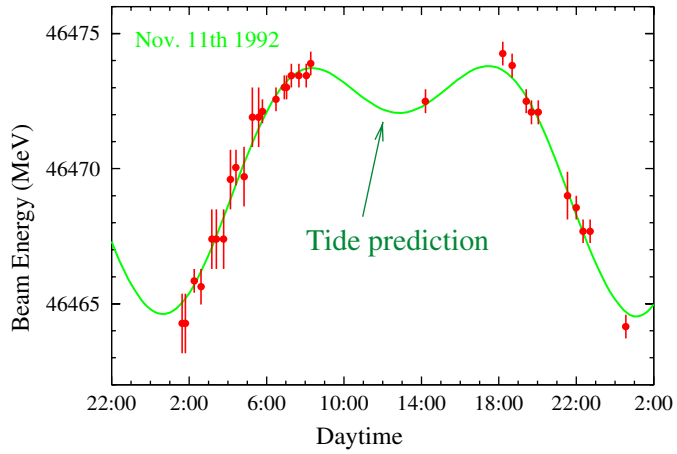

Figure 64. The LEP TidExperiment: predicted and measured variation of the LEP energy calibration with the time of day over a 24 h interval on the night of a full Moon. Courtesy of Wenninger (private communication) and CERN.

calibration with the time of day is shown in figure 64, the famous LEP TidExperiment graph. The fitted value of $\kappa_{\rm tide}$ is $\kappa_{\rm tide} = -0.86 \pm 0.08\,{\rm ppm}\,\mu{\rm gal}^{-1}$ (Arnaudon *et al* 1995a). The change in the LEP circumference was about ± 1 mm. When the effect of the Moon on LEP was announced, it made the headlines. Starting in 1993, all energy calibrations of the LEP beam energy also recorded the phase of the Moon.

A detailed exposition on the radial deformations of the LEP ring is given by Wenninger (1995b), for example, the changes in beam energy calibration as a function of the water level in lake Leman: the lake is emptied between January and April and refilled in May. This is done to produce electricity and also to make room for the influx of melting water from the Alps. Over a two-year period the LEP circumference displayed periodic fluctuations of about 2 mm. Wenninger (1999) reports the variation of the LEP circumference for a period of six years, 1993–8 (see figure 65).

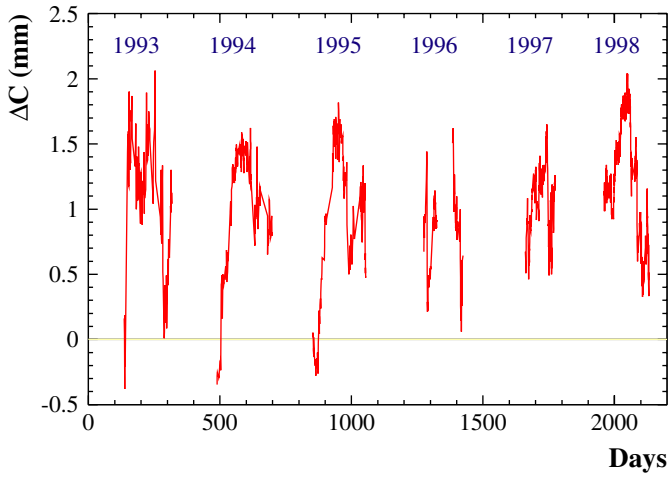

Figure 65. Variation of the LEP circumference in the period 1993–8. Courtesy of Wenninger (private communication) and CERN.

A detailed description of the accurate measurement of the LEP beam energy, using the 1993 data, was published by Arnaudon *et al* (1995b). Tidal effects were taken into account, including longer term variations not treated in the abbreviated description above, and also details of the increased sophistication of the resonant depolarization measurements were provided. The paper also discussed other effects such as spin tune shifts due to radial magnetic fields (imperfections in the vertical closed orbit resulting in radial perturbing fields in the LEP quadrupoles). Significantly, Arnaudon *et al* (1995b) also stated that NMR probes were installed in reference magnets and read out every few minutes. It was stated that 'this instrument is not completely understood'. This will take us to the next episode on the LEP Energy Model.

31.5. TGV

Most of the information below is taken from Assmann *et al* (1999b). This paper is the definitive CERN publication on the beam energy calibrations for LEP1. Up to 1993, the only measurement of the dipole field in LEP was provided by a special reference magnet connected in series with the LEP dipoles. The reference dipole was not the same as the regular machine dipoles; it was a high-precision iron-core magnet, unlike the cheaper concrete-reinforced ring dipoles, and it was installed in a thermally controlled environment in a surface building, not underground in the LEP tunnel. The reference magnet housed a flip-coil device and an NMR probe, both of which were read every eight minutes. In 1995 direct measurements of the ring dipole fields were provided by two additional NMR probes which were mounted on top of the vacuum chamber in two dipoles in the LEP tunnel near IP4 and IP8. (An additional 14 probes were installed in 1996, covering all eight LEP octants.)

Glossing over many details, the tunnel NMR data indicated that instead of remaining constant, the field in the LEP dipoles increased throughout a fill. This rise was significantly larger than that previously recorded in the reference magnet. Part, but not all, of the rise could be attributed to temperature effects. Of principal interest to us is that the NMR probes also displayed significant short-term fluctuations which were correlated with the time of day: things were much quieter between midnight and 05:00, after which the noise resumed.

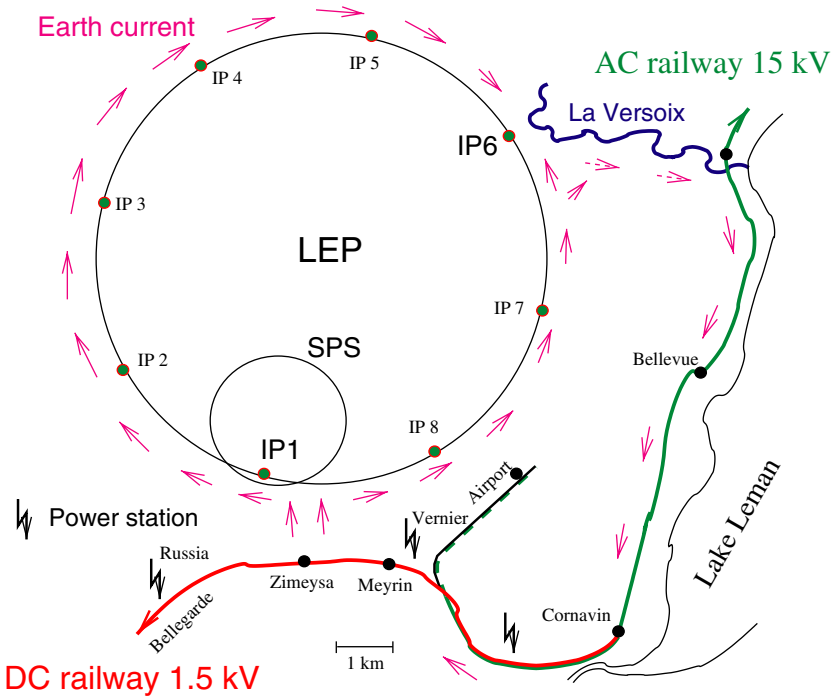

Figure 66. Sketch map of train leakage currents at LEP. Courtesy of Wenninger (private communication) and CERN.

This correlation suggested human activity. Measurements revealed an extra current flowing on the LEP beam pipe. This brings us to the LEP Train Effect.

The TGV is an electric train, and the current nominally returns to the power station through the train rails. However, it is known that as much as 25% of the current does not do this, but finds other pathways through the ground. These leakage currents are known as *vagabond currents* and are a well-documented source of electrical nuisance and electrochemical corrosion. The leakage currents from the local railway system were finding their way underground and found the LEP beam pipe to be a very good electrical pathway. To be precise, the leakage currents came from the French lines, which operated on dc, for historical reasons. Vagabond currents are mainly due to dc lines. The Swiss rail network operated on ac, and caused no observable effects on the LEP beam energy. A schematic sketch of the path of the currents is shown in figure 66. Figure 67 shows the synchronous measurement of the voltage difference between the ground and the train rails (*a*), the voltage difference between the LEP beam pipe and ground (*b*) and the NMR readings (*c*). Armed with this knowledge of the vagabond currents, the LEP Energy Model had to be revised.

31.6. LEP1 energy model

Ultimately, for LEP1 operations, the beam energy was computed as a function of the time t every 15 min (Assmann *et al* 1999b) according to the formula

$$E_b(t) = E_{\text{norm}}(\text{fill}) \cdot (1 + C_{\text{rise}}(t_{\text{day}}, t_{\text{fill}})) \cdot (1 + C_{\text{T-dipole}}(t) \cdot (1 + C_{\text{tide}}(t)) \cdot (1 + C_{\text{orbit}}(\text{fill})) \cdot (1 + C_{\text{h.corr}}(t)) \cdot (1 + C_{\text{QFQD}}(t)). \quad (31.6)$$

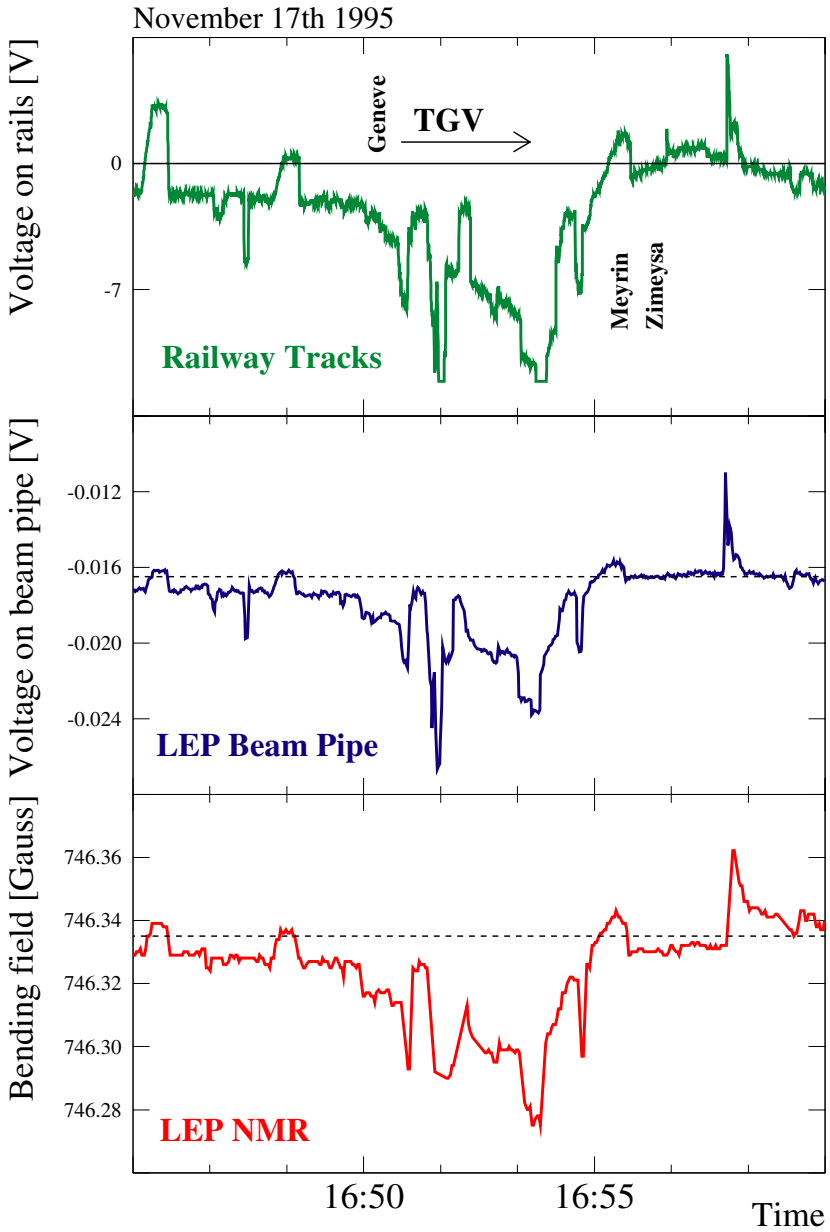

Figure 67. The LEP train effect: (*a*) voltage difference between ground and rails, (*b*) voltage difference between LEP beam pipe and ground and (*c*) NMR readings as a function of time of day. Courtesy of Wenninger (private communication) and CERN.

Here E_{norm} was used for absolute normalization. All the other terms follow relative energy variations. The meanings of the terms in the above formula are:

- E_{norm} was the energy from the resonant depolarization calibration for that fill. Some fills were not calibrated by resonant depolarization, if, for example, the beam was

lost prematurely. In 'uncalibrated fills', the value of $E_{\rm norm}$ was set equal to the mean normalization for all of the calibrated fills at that energy point.

- $C_{\rm rise}(t_{\rm day}, t_{\rm fill})$ was the term accounting for the rise in the bending field due to the leakage currents (vagabond currents) from the TGV trains. This term was not present in earlier versions of the LEP energy model.
- $C_{\rm T\text{-}dipole}$ was the temperature correction for the ensemble of ring dipole magnets.
- $C_{\rm tide}$ was the correction due to the tides.
- $C_{\rm orbit}$ was the correction for the deviation of the horizontal position of the orbit from the design orbit (which has no quadrupole bending). This effect was calculated after the expected variations for the tide had been removed.
- $C_{\rm h.corr}$ was the correction due to the setting of the horizontal correctors, and was not present in earlier versions of the LEP Energy Model.
- $C_{\rm QFQD}$ was a correction for the current in a QFQD compensation loop.

Consult Assmann *et al* (1999b) for a detailed description of these effects, and a quantification of their magnitudes. Based on the information gleaned in 1995, the energy calibrations for 1993 and 1994 were revised; the energy had been overestimated by about 4 MeV.

31.7. Harmonic spin matching

We mentioned earlier that the asymptotic polarization level in the early resonant depolarization measurements was only about 10%. What we did not say was that in 1992, as much as 12 h of optimization were required to achieve that 10% polarization. It was, therefore, decided in 1993 to improve the theoretical and experimental handling of the polarization. Most of the information below is taken from Arnaudon *et al* (1994) and Assmann *et al* (1994b).

Prior to 1993, the energy calibration measurements were performed in separate shifts with the experimental detector solenoids switched off. If polarization measurements were attempted with the detector solenoids on, an insignificant degree of polarization was observed. However, the spin rotations induced by the detector solenoids could be compensated by a configuration of vertical closed orbit bumps (Blondel 1990). This was an instance of harmonic spin matching (see section 28).

The harmonic correction procedure involved two steps, as explained by Wenninger (1995a). The solenoids were compensated using a set of vertical closed orbit bumps; this procedure was called SOLSPIN. The maximum orbital excursion was about 7 mm. Next, the Fourier spectrum of the harmonics in LEP was measured. The most significant harmonics were corrected using a different set of vertical closed orbit bumps. This procedure was called Harmonic Spin Matching (HSM). The maximum orbit amplitude was a few mm. The results are shown in figure 68. First SOLSPIN was applied, and then HSM. A polarization level of over 40% was attained. According to Assmann *et al* (1994b), the whole HSM procedure took less than 5 min. Using HSM, an asymptotic polarization level of over 35% could always be achieved in dedicated machine shifts, with the average around 50%. A value of between 10–25% was more typical in the end-of-fill energy scans in regular operations. The best level attained in 1993 was $(57 \pm 3)\%$ (see figure 5). The success of HSM vindicates, *a posteriori*, the validity of the approximation of first-order perturbation theory for LEP, even at a beam energy of 45.6 GeV. With these improvements it became unnecessary to devote dedicated machine shifts to measure the beam energy; instead it became possible to perform resonant depolarization at the end of LEP fills.

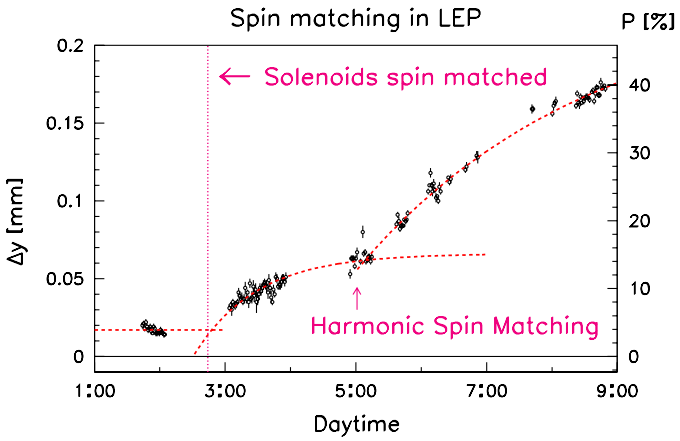

Figure 68. Polarization level at LEP after compensation of the spin rotations in the detector solenoids (procedure SOLSPIN) and harmonic spin matching (HSM). Courtesy of Wenninger (private communication) and CERN.

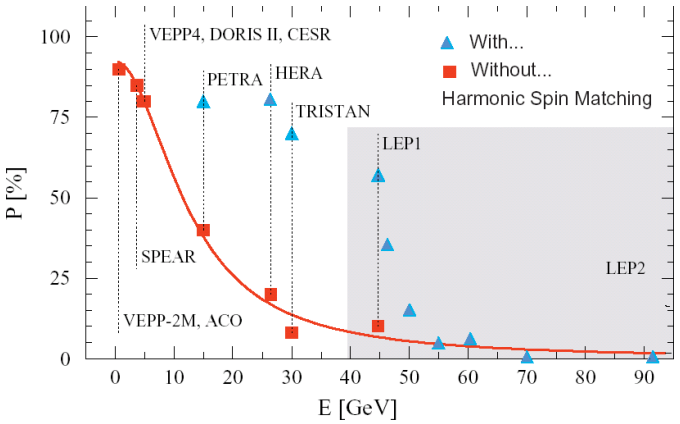

Figure 69. The maximum attained asymptotic polarization levels at different high-energy e^+e^- storage rings, with and without harmonic spin matching. Courtesy of Wenninger (private communication) and CERN.

31.8. Maximum attained polarization

We remarked earlier, in section 28, that the maximum achievable radiative polarization in a storage ring roughly follows the rule

$$P \simeq \frac{P_{\mathrm{ST}}}{1 + (\alpha E)^2}. \tag{31.7}$$

This formula assumes first-order perturbation theory in the orbital amplitudes, and that the major perturbation is due to motion in the quadrupoles, but we have seen that these are reasonable approximations, even for LEP at 45.6 GeV. A comparison of the maximum measured transverse polarizations in various storage rings is shown in figure 69. As can also

be seen, the polarization level dropped precipitously at high energies (beyond the Z^0 peak) at LEP.

31.9. PIC: polarization in collision

Usually only the polarizaton of the electron beam was measured. The positron polarization was measured once or twice per year (Assmann *et al* 1999b). Once harmonic spin matching became a standard part of LEP operations, the resonant depolarization measurements could be performed routinely, but with separated beams. When carrying out resonant depolarization measurements at the end of a physics fill, the positron beam was first dumped, or else the beams were separated at the interaction points. Transverse polarization with colliding beams was obtained only in special conditions, far from the parameter values of normal operation. The effect of the beam–beam interaction on the polarization is poorly understood. Three studies with colliding beams in LEP were reported by Assmann *et al* (1995). It was found that the beam–beam interaction does not necessarily depolarize the spins.

31.10. LEP2

By 1995, the luminosity of LEP had increased to the level where one good weekend produced as many data as the whole of the 1989 run. Dedicated running on the Z^0 peak ceased in October 1995. The next phase LEP2 then began, to push to higher beam energies to attain open W^+W^- production. LEP ultimately reached a centre-of-mass energy of 209 GeV (Arduini *et al* 2001). A detailed paper describing the energy calibration of LEP2 is in preparation (Assmann *et al* 2004).

Transverse radiative polarization was observed at LEP at energies beyond the Z^0 peak. However, the strengths of the depolarizing resonances increased with energy. Resonant depolarization was practicable at LEP up to a beam energy of 60.6 GeV. This was the highest energy at which a polarization level useful for resonant depolarization (minimum 5% required) was observed (Assmann *et al* 1999a). The polarization level was $(7.7 \pm 0.4)\%$. Note the error bar of $\pm 0.4\%$, compare this to the early error bars of $\pm(2\text{–}3)\%$. Resonant depolarization was not possible in LEP2 beyond 60.6 GeV.

31.11. Concluding remarks

The success of the energy calibration was one of the highlights of LEP1. It was originally expected that the mass of the Z^0 would be measured to an accuracy of ± 20 MeV; instead the accuracy achieved was ± 2.1 MeV, a full order of magnitude better. As an example of particle physics work on the Z^0, we present just one example, by Abbiendi *et al* (2001), on 'Zedometry' (simply because of its title). At LEP, the energy calibration via resonant depolarization was an essential part of the daily machine operations, not just an occasional exotic exercise. There was no other technique of comparable accuracy to measure the Z^0 mass. The CERN scientists quantified the systematic errors in the resonant depolarization technique to an unprecedented level of detail. LEP demonstrated, perhaps more clearly than any other machine, the enormous variety and subtlety of the systematic errors which must be accounted for in the actual usage of the spin dynamics. The CERN scientists met the challenge required to extract precision information via the spin dynamics, and succeeded well beyond their initial expectations. It is worthwhile to recall that all of the spin dynamics was derived from the humble equation $\nu = a\gamma$. Who would think that the Moon and TGV trains would contribute to the systematic errors in the use of this formula?

32. Linear accelerators

32.1. General remarks

We consider only one linear accelerator below, namely, the two-mile long linac of SLAC, the Stanford Linear Accelerator Center. Within that framework, we briefly review two items. The first is the SLC, the Stanford Linear Collider. As e^+e^- colliders increase in energy, the financial cost of the synchrotron radiation output becomes prohibitive. To reduce the power output, rings of large radius are required. The 'new physics' frontier for e^+e^- colliders in the late 1980s was 50 GeV beams, to study electroweak physics at the scale of the Z^0 mass (approximately 91 GeV). Two laboratories met this challenge, CERN and SLAC. We have seen that CERN built LEP, a conventional circular storage ring. To minimize the power loss, LEP was constructed with a circumference of 27 km. Even so the synchrotron radiation power output was tens of MW, especially with 100 GeV beams in LEP2. SLAC pioneered a novel solution to the problem by converting its two-mile long linac into a linear collider, the SLC. The linac energy was upgraded to 50 GeV. Electron and positron beams were sent down the linac in alternating bunches, and diverted to two oppositely bending arcs, to bring the beams into head-on collision at an interaction point, where a detector recorded the events. The SLC was, therefore, not only a high-energy physics accelerator but also a pioneer of a new technology. It is anticipated that high-energy e^+e^- accelerators of the future will be linear colliders. However, partly because of the newness of the technology, the luminosity of the SLC was far lower than that of LEP. Each of the four LEP experiments acquired a data sample about ten times larger than the total events accumulated at the SLD (the detector at SLC: by its nature the SLC could only have one detector), roughly 5 million Z^0 decays at each LEP experiment and 500 k decays at the SLD. Nevertheless, the SLC did achieve results competitive with LEP. The key to this success was the use of polarized beams. Starting in 1992, the SLC accelerated exclusively *longitudinally polarized* electron beams. (The positrons were unpolarized.) Because of the parity-violating coupling of the Z^0 boson to fermions, the availability of even single-spin longitudinal polarization enabled the SLC to obtain results competitive with LEP. LEP operated exclusively with transversely polarized beams, for energy calibration only (typically $P \simeq 10$–25%, after optimization). Longitudinally polarized beams were, therefore, truly the saving grace of the SLC. A good overview of the combined LEP and SLC electroweak results is given by the LEP Collaborations *et al* (2003). This report presents results from all four LEP experiments and the SLD, from data presented at various conferences in 2003.

The SLC concluded operations in 1997/98. SLAC also has a long history of fixed-target experiments with polarized beams and polarized targets, starting with the historic experiment by Prescott *et al* (1978), observing parity violation in inelastic electron scattering. There was a series of fixed target experiments lasting almost a decade, with polarized beams and polarized targets, to measure the neutron and proton spin structure functions. The experiments were E-142, E-143, E-154 and E-155. E-142 and E-154 used an optically pumped ^{3}He target, and E-143 and E-155 used polarized NH_3 for the neutron and proton, respectively. For E-142, an AlGaAs photocathode source was used with a polarization of about 40%. E-143 and the later experiments used strained GaAs, with a higher polarization level of 78–80%. These were the most high-tech fixed target experiments ever carried out at SLAC, resulting in the most precise measurements of the spin structure functions in the SLAC kinematic range. They addressed what was known at the time as the 'spin crisis', namely, the quark spin polarization only accounted for about a third of the proton and neutron spins. Today, we know that the gluons contribute an important part of the nucleon spin, and that a full QCD treatment is needed to

explain things. In this sense, there never was a 'spin crisis'. Following the above series of experiments, the recently concluded E-158 experiment addressed electroweak physics with a parity violation measurement in Møller scattering. Improvements to the polarized source resulted in a source polarization level of $>80\%$ for this experiment. For the final E-158 run in 2003, further improvements resulted in a polarization of 85–90%, better than almost anything that has ever been achieved with radiatively polarized beams. We include a *very* brief description of the E-158 experiment below.

Much of the information below was kindly supplied by Prepost (2004) and Woods (2004b). We are indebted to them both.

32.2. SLC

A schematic view of the 'polarized SLC' was shown in figure 19. Let us follow the history of the electron beam as it travels from the source to the interaction point. A lucid account of the SLC machine operations is given by Woods (1997), and is the principal source of the information below (plus ancillary sources as cited along the way). The electrons were produced by a polarized electron source (Alley *et al* 1995). For a more recent description, see Clendenin *et al* (2003). The electron polarization at the source was 78–80% (see above), and was longitudinal. Almost the full polarization was preserved to the interaction point (about 77%, see Woods *et al* (1997) for a description of the SLC longitudinal Compton polarimeter, also Shapiro *et al* (1993) for a description of earlier work). The helicity of the electrons could be of either sign, and was varied quasi-randomly to avoid systematic errors arising from correlation with the accelerator periodicities. The pulse rate of the SLC was 120 Hz. Two electron bunches at a time were produced from the source and were accelerated down the linac to an energy of 1.19 GeV, and kicked by a pulsed magnet to the LTR (Linac-to-Ring) transfer line to be transported to the electron damping ring (DR). The DR was a small storage ring, whose purpose was to generate synchrotron radiation to induce radiation damping of the beam emittances. The beam was stored in the DR for 8 ms. There is no significant Sokolov–Ternov radiative polarization buildup in such a short time. The electron polarization was vertical in the damping ring. The longitudinal polarization in the injector before the DR was rotated by an angle of 450° by dipole bending magnets in the LTR transfer line, and then to the vertical direction by a solenoid. Upon exit from the DR, the polarization was vertical, and remained so upon injection into the linac, and subsequent acceleration to 46.6 GeV (but see below). The two electron bunches were preceded by a positron bunch. The three bunches were accelerated down the linac. The positron bunch and first electron bunch were accelerated to the final energy of approximately 46.6 GeV, while the trailing bunch was accelerated to 30 GeV, and was extracted and sent to a positron production target. Positrons in the energy range of 2–20 MeV were collected, accelerated to 200 MeV, and transported to near the start of the linac for transport to the positron damping ring, where they were stored for 16 ms. The 2 : 1 ratio relative to the electron damping ring was because two electron bunches were extracted for every positron bunch. At the end of the linac, the positron and electron energies were 46.6 GeV. Note that a linac does not suffer from any resonance crossing issues during acceleration. At the end of the linac, a magnet deflected the electron (positron) bunch into the north (south) collider arc, for transport to the interaction point (IP). The beams lost about 1 GeV due to synchrotron radiation in just a single pass through the arcs, so the centre-of-mass collision energy matched the Z^0 rest energy of 91.2 GeV. The beam energies were measured to an accuracy of 20 MeV by energy spectrometers. Significantly, the SLC arcs were *not* flat. They were 'terrain following'. Each arc comprised 23 achromats, each of which consisted of 20 combined function (dipole + quadrupole) magnets.

At 46.6 GeV, the spin precession in each arc achromat was 1085°, while the vertical betatron phase advance was 1080°. Hence, although an arc was a single-pass system, it operated near a spin tune resonance. The term 'resonance' is used here to denote a large response to a small input, which adds coherently in the successive achromats. Because of this resonance, and the fact that vertical rotations do not commute with horizontal rotations from the horizontal bend magnets, the vertical betatron oscillations in the arcs could tilt the spins away from the vertical, and the effect added cumulatively in successive achromats. The resulting spin component in the plane of the arc would then precess significantly. The spin tune resonance, combined with the misalignments and complicated rolls in the arcs, meant that it was actually not possible to calculate the spin transport through an SLC arc. However, two methods were available to control the spin direction of the electron bunches. In the first method, used up to 1993, two solenoids were employed, one in the RTL (ring-to-linac) transfer line, and one in the linac itself, to rotate the spin direction to any direction along the x, y and z axes. The longitudinal component of the arc spin transport matrix was measured using the SLC Compton polarimeter (Woods *et al* 1997). The longitudinal polarization was measured for each of the x, y or z spin orientations at the end of the linac. From the relation

$$P_z^{\mathrm{C}} = R_{zx} P_x^{\mathrm{L}} + R_{zy} P_y^{\mathrm{L}} + R_{zz} P_z^{\mathrm{L}}, \tag{32.1}$$

where 'C' and 'L' stand for Compton and linac, respectively, one could determine the matrix elements R_{zx}, R_{zy} and R_{zz}, which is sufficient to determine the full rotation matrix. The matrix R was inverted to determine the desired spin orientation at the end of the linac to achieve longitudinal polarization at the IP. The solenoids in the RTL and linac were then set appropriately. As pointed out earlier, a polarization of about 77% was attained at the IP. This demonstrates that the spin tune resonance in the arcs induced precession, but *not* depolarization.

However, the above solenoids also introduced significant x–y coupling of the horizontal and vertical betatron oscillations. Since 1993, the SLC operated in 'flat-beam' mode, where the emittance in the vertical plane was much smaller than in the horizontal. This was of course to increase the luminosity. Hence, another method was employed to orient the spins, which was to take advantage of the spin tune resonance itself. A pair of vertical betatron oscillations ('spin bumps'), each spanning 7 achromats in the last third of the arc, was introduced to rotate the spin. The amplitudes of the spin bumps were empirically adjusted to achieve longitudinal polarization at the IP. Viewed in this way, the use of spin bumps was not dissimilar to the technique of vertical closed orbit bumps in circular accelerators to induce a spin rotation of controlled magnitude. Indeed, we saw that LEP used spin bumps for the harmonic spin matching (HSM) procedure. Since $a\gamma \gtrsim 100$, at an energy of 45.5–46.5 GeV, the spin rotations were greatly amplified relative to the orbit; hence the orbital deflections did not have to be large. The use of spin bumps was the preferred method since 1993, because they did not couple the horizontal and vertical betatron oscillations.

As already pointed out, the SLC was equipped with a longitudinal Compton polarimeter. Circularly polarized laser photons hit the electron beam after the e^+e^- collision region, but before the electrons passed through any dipole magnets. Unique to this Compton polarimeter, the scattered *electrons* were detected, rather than the backscattered photons. During the period 1992–5, several dedicated accelerator physics studies were carried out to establish the integrity of the polarimetry. The electron bunch helicity transmission was verified by setting up a current/helicity correlation in the SLC, and additional Møller and Mott polarimeters confirmed the precision of the Compton polarimeter to about 3%. In 1997, two additional devices were added to detect the Compton backscattered photons (Berridge *et al* 1999)—recall the Compton scattered electrons were detected in the primary device. More details about these secondary

devices are given by Onoprienko (2000). In addition, experiments at EndStation A with a fixed target polarimeter confirmed that the positron polarization was consistent with zero. This was an important point, because the expression for the asymmetry $A^0_{\rm LR}$ (see below) changes if the positrons are polarized.

We have previously pointed out that a Compton polarimeter only measures a small sample of the electron spins, i.e. the electron polarization $P_{\rm e}$ averaged over the beam. This can differ by a small amount from the luminosity weighted beam polarization $P_{\rm e}(1+\xi)$. The polarization is uniform across the beam for radiative Sokolov–Ternov polarization, but it need not be so for nonradiatively polarized beams. The dominant effect at SLC was a chromatic one due to the beam energy spread: because of the energy spread of the particles, the spin orientation after passage through the arc, has an energy dependence, and chromatic aberrations in the final focus just before collision result in a luminosity dependence on the beam energy. The use of the spin bumps allowed a reduction of the polarization chromaticity ($E(\mathrm{d}P/\mathrm{d}E)$), reducing the polarization correction from $\xi > 1\%$ in 1993, to $\xi < 0.2\%$ by 1995.

Rowson *et al* (2001) gives a good summary of the SLC physics. A high-precision measurement of the left–right Z^0 boson cross-section asymmetry was published by Abe *et al* (2000). The result, combined with earlier SLD data, yielded a value for the weak mixing angle of

$$\sin^2\theta^{\rm eff}_{\rm W} = 0.230\,97 \pm 0.000\,27. \tag{32.2}$$

This determination of $\sin^2\theta^{\rm eff}_{\rm W}$ is comparable in accuracy to the average of the measurements performed by all four LEP experiments, despite the fact that each LEP detector had a data sample about ten times bigger than the SLD. The LEP experiments had several other ways to measure the weak mixing angle (not requiring longitudinally polarized beams), from forward–backward leptonic and b-quark asymmetries, and from τ polarization.

The left–right asymmetry is defined as

$$A^0_{\rm LR} = \frac{\sigma_{\rm L} - \sigma_{\rm R}}{\sigma_{\rm L} + \sigma_{\rm R}}, \tag{32.3}$$

where $\sigma_{\rm L}$ and $\sigma_{\rm R}$ are the $\mathrm{e^+e^-}$ production cross-sections for Z^0 bosons at the Z^0 pole energy, with left-handed and right-handed electrons, respectively, and the positrons are unpolarized. Recall from above that it was verified that the positrons at the SLC were unpolarized. The Z^0 polarization depends on the polarization of both the $\mathrm{e^-}$ and $\mathrm{e^+}$ beams, and the expression given below is only valid if the positrons are unpolarized. The Standard Model predicts that $A^0_{\rm LR}$ depends on the effective vector ($v_{\rm e}$) and axial-vector ($a_{\rm e}$) couplings of the Z^0 boson to the electron current

$$A^0_{\rm LR} = \frac{2v_{\rm e}a_{\rm e}}{v_{\rm e}^2 + a_{\rm e}^2} = \frac{2[1 - 4\sin^2\theta^{\rm eff}_{\rm W}]}{1 + [1 - 4\sin^2\theta^{\rm eff}_{\rm W}]^2}, \tag{32.4}$$

where the effective electroweak mixing parameter is defined as $\sin^2\theta^{\rm eff}_{\rm W} = (1 - v_{\rm e}/a_{\rm e})/4$. The quantity $A^0_{\rm LR}$ is a sensitive function of $\sin^2\theta^{\rm eff}_{\rm W}$ and depends upon virtual electroweak radiative corrections, including those involving the Higgs boson and phenomena beyond the Standard Model. Presently, the most stringent bounds on the Higgs mass are from measurements of $\sin^2\theta^{\rm eff}_{\rm W}$.

32.3. Fixed target experiments at SLAC: E-158

The SLC ceased operations in 1997/98. Work with polarized electron beams continues at SLAC, with fixed-target experiments. We include a very brief description of the recently concluded E-158 experiment. Most of the information below is from Woods (2004a).

This experiment collided polarized electrons from the linac against a fixed target of unpolarized electrons. The source electron polarization was longitudinal and remained longitudinal through the linac. There is no need for damping rings and spin rotations by solenoids, etc. See Clendenin *et al* (2003) for a description of improvements to the polarized electron source. The spins precess in the 'A-line' bending magnets to EndStation A. The overall bend is 24.5°, so the spin precession angle increases by 180° for every 3.2 GeV increase in beam energy, leading to a set of so-called 'magic energies'. (These magic energies should not be confused with the magic energy of the muon $g-2$ storage rings at BNL and CERN.) The E-158 experiment recorded the first observation of parity violation in Møller scattering, caused by the interference between the exchange of a virtual photon and a virtual Z^0 boson (Anthony 2004). The parity violation measurements yield a value for $\sin^2\theta_{\rm W}$, but at a much lower energy scale than the Z^0 resonance. The experiment measured the parity-violation asymmetry

$$A_{\rm PV} = \frac{\sigma_{\rm L} - \sigma_{\rm R}}{\sigma_{\rm L} + \sigma_{\rm R}}, \tag{32.5}$$

for small-angle Møller scattering, where $\sigma_{\rm L}$ and $\sigma_{\rm R}$ are the cross-sections for left-handed and right-handed incident electrons, respectively, on an unpolarized electron target (cf (32.4) above). The asymmetry arises from the interference between the weak and electromagnetic amplitudes, and is sensitive to the weak mixing angle. The lowest-order (tree-level) expression for $A_{\rm PV}$ is

$$A_{\rm PV} = \frac{G_{\rm F}Q^2}{\sqrt{2}\,\pi\alpha}\,\frac{1-y}{1+y^4+(1-y)^4}\,(1-4\sin^2\theta_{\rm W}). \tag{32.6}$$

Here, $G_{\rm F}$ is the Fermi constant, Q^2 is the invariant four-momentum transfer, and is approximately $0.03\,{\rm GeV}^2$ for the E-158 kinematics and $y = Q^2/s$. For E-158, $\langle y\rangle \simeq 0.6$. The expected asymmetry at the tree level is approximately 3.2×10^{-7}. Radiative corrections reduce this asymmetry by about 50%. The E-158 value for the asymmetry is[5]

$$A_{\rm PV}^{\rm exp} = (-131 \pm 14\,({\rm stat.}) \pm 10\,({\rm syst.}))\times 10^{-9}, \tag{32.7}$$

with a significance of about 6.3σ for observing parity violation. In the context of the Standard Model, the weak mixing angle is, at $Q^2 = 0.026\,{\rm GeV}^2$,

$$\sin^2\theta_{\rm W}^{\overline{\rm MS}} = 0.2397 \pm 0.0010\,({\rm stat.}) \pm 0.0008\,({\rm syst.}). \tag{32.8}$$

33. Recirculating linacs

We treat only one recirculating linac below, which is CEBAF, the Continuous Electron Beam Accelerator Facility at the Jefferson Laboratory (JLab) in Newport News, Virginia. A recent overview of the CEBAF facility was published by Leemann (2001). A schematic view of CEBAF was shown in figure 20. Most of the information below was supplied by Sinclair (2004) and Grames (2004). We thank them both. CEBAF delivers a continuous electron beam, of energy up to approximately 5.7 GeV, to fixed-target experiments for nuclear physics. The electron source delivers a continuous series of electron bunches at the characteristic frequency (1497 MHz) of the linacs. Since 1999, CEBAF has operated *exclusively* with polarized electron beams. It is the only accelerator facility which currently operates exclusively with polarized beams. (The SLC operated exclusively with polarized electrons starting in 1992, until it ceased operations in 1997/8.) Due to improvements in polarized electron source technology, the CEBAF polarized gun delivers far greater intensity than did that at the SLC.

[5] *Note added in Proof* The E-158 collaboration announced their final results while this article was going to press (Anthony *et al* 2005). We quote their final measurements below.

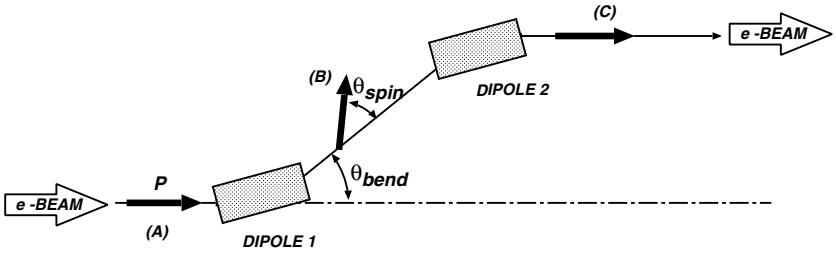

Figure 70. Schematic of chicane in a CEBAF spreader. Courtesy of Grames (private communication) and JLab.

The CEBAF polarized gun is the world's most intense source of polarized electrons. The integrated charge amounts to hundreds of Coulombs per year, and as much as $8\,\mathrm{C\,day^{-1}}$. A recent review of polarized electron sources is given by Sinclair (1999), which includes a description of the CEBAF polarized electron gun. See also Sinclair (1989), for an earlier review of polarized electron sources. The CEBAF source delivers longitudinally polarized electrons with a polarization level of approximately 75%. By virtue of the very high intensity of the polarized electrons, and the high degree of polarization, the experiments at CEBAF are able to probe nuclear sructure to a level of detail that is difficult to attain elsewhere. For example, parity violation experiments by the HAPPEX collaboration (Hall A Proton Parity EXperiment) to probe the proton structure have revealed that the proton is 'not strange' (Aniol *et al* 2001). See the statements about the 'spin crisis' in connection with fixed-target polarized beam experiments at SLAC. A practical way to measure the strange vector elements is to measure the electroweak asymmetry in polarized electron scattering. The HAPPEX experiments have demonstrated that the strange nucleon form factors are negligible. This experiment was also the first fixed-target parity-violation experiment to use a strained GaAs photocathode to produce highly polarized electrons, and also (for fixed target parity-violation work), the first to use a laser Compton polarimeter to continuously monitor the electron beam polarization. Longitudinally polarized electrons with 67–76% polarization and 3.3 GeV energy were scattered from a 15 cm liquid hydrogen target. The latest findings have been published by Aniol *et al* (2004).

As shown in figure 20, the CEBAF layout is a racetrack with a pair of linacs joined by 180° arcs. The beams make a total of five passes through each linac, increasing their energy significantly on each pass. Hence, the beam energy in the arcs is very different on each pass. Therefore, each 'arc' (East and West) consists of a set of 180° arcs, stacked vertically. A 'spreader' directs a beam, upon exit from a linac, into the arc appropriate to its energy, and a 'recombiner' redirects the beam, upon exit from an arc, into the other linac. Beams with the least (most) energy bend the most (least), and are directed to the top (bottom) arc. The transfer of the beam from a linac to the arcs, and vice-versa, is achieved using a 'chicane', which is, essentially, a set of two vertical bends of equal and opposite integrated field strength as shown in figure 70. Since there are no interleaved horizontal and vertical bends, and also no quadrupoles between the bends, the orbit undergoes a simple vertical translation, and the spin rotations cancel out.

The essential point is that, as far as the spin is concerned, CEBAF is equivalent to a planar machine. The vertical bends simply cancel out. Despite the term 'recirculating', as far as the spin is concerned, CEBAF is effectively a single-pass system, since the beams pass through each arc only once. Spin resonance issues are basically negligible in CEBAF. Admittedly, the chicane generates some vertical dispersion in the arcs, so particles with different energy offsets travel in slightly different vertical orbits, and see slightly different

radial perturbing fields. However, (i) the energy spread of the CEBAF beam is very small, and (ii) because CEBAF is a single-pass system, there is no opportunity for the perturbations to accumulate coherently.

Grames (2000) investigated the sensitivity of the spin rotations and polarization to vertical orbit perturbations in arc 7 of CEBAF. His results basically confirm that the perturbations to the electron beam polarization, under normal CEBAF operating conditions, are negligible. Hence, in CEBAF, the spins precess in the arcs, but they do not decohere. The beams are delivered from source to target essentially without depolarization. What is more important in CEBAF is spin control to deliver a beam of the desired spin orientation to an external beamline.

CEBAF has three experimental halls. Since the electron polarization is longitudinal at the source, and precesses in the arcs, the polarization will not, in general, be longitudinal in any of the external beamlines. There are two solutions to this issue. One is to determine those energies at which the final polarization *is* longitudinal. This, of course, constrains the operating energy of the facility to a certain set of values. The other solution is to rotate the spins upon exit from the source, so that the final delivered polarization will be longitudinal. A combination of both methods is used. Note that the three halls imply three external beamlines. At certain energies, the spin precession angle between successive beamlines is a π rotation, hence longitudinal polarization can be delivered to all three beamlines simultaneously. However, the choice of electron helicity in the beamlines is not independent. In practice, the situation is not so simple because of the differing needs of the various experiments. Hence, a compromise must sometimes be made as to the polarization direction in each beamline.

Since for spin rotations, CEBAF is effectively planar and the injected polarization is longitudinal, it is sufficient, in principle, to have a spin rotator whose axis points vertically. In practice, there are inevitably imperfections in the system, and so it is prudent to install a second spin rotator with a different spin rotation axis. CEBAF employs a Wien filter to rotate the spins about the vertical axis, followed by a solenoid to rotate them about the longitudinal axis. (see figure 20). In the studies carried out by Grames (2000), two solenoids in series were employed to achieve adequate integrated field strength. The overall spin rotator system is located after the polarized electron source, but before the preaccelerator and the rest of the CEBAF transport system. One can set the spin rotation angles in the Wien filter and the solenoids, to orient the spins (polarization) as desired.

CEBAF is equipped with Mott, Møller and Compton laser polarimeters. As pointed out in section 12 on polarimetry, a recent comparison was made of the analysing powers of five different electron polarimeters, of four different types (Grames *et al* 2004). The comparison was possible because CEBAF delivers a beam of the same polarization to all the polarimeters simultaneously, since, as we just noted, there is no depolarization through the system. A graph of the relative analysing powers of the CEBAF polarimeters is shown in figure 71.

As we have noted, the principal accelerator physics use of the polarization is to calibrate the beam energy, and CEBAF is no different in this respect. In June 1999, a two-day event called the *energy festival* took place (Mitchell 1999) to determine the final beam energy in the three CEBAF experimental halls. The beam energy was measured using three different techniques. The information below is taken from Grames (2000). Briefly, the first method was to measure the precession of the beam polarization between two polarimeters, at the injector and an end station, respectively. The second method involved the calibration of the magnetic field (bend angle) in the beam extraction switchyard to the experimental Halls A and C, plus a calibration of the beam trajectory. From this information, the beam momentum (hence energy) could be determined. The third method involved the measurement of the kinematics of elastic electron–proton scattering in Hall A to determine the opening angle between the scattered electron and recoil proton. Such equipment is part of the standard Hall A hardware.

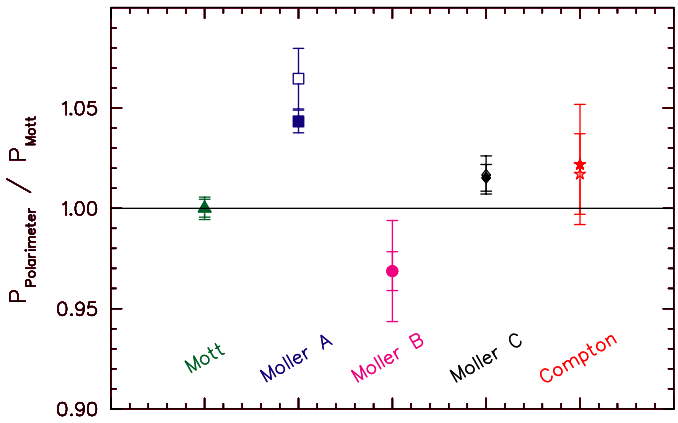

Figure 71. Relative analysing powers of the Jefferson Laboratory electron beam polarimeters, normalized to the Mott polarimeter for comparison. Solid symbols: dataset limited to be within 25% of the maximum measured polarization. Open symbols: all data. Reprinted with permission from Grames *et al* (2004). Copyright (2004) by the American Physical Society.

Table 5. Summary of the average CEBAF linac energy ($\overline{E_{\rm linac}}$) determined during the experiment in Grames (2000) as compared to the *energy festival* result. From Grames (2000). Courtesy of Grames (private communication) and JLab.

Description	$\overline{E_{\rm linac}}$ (MeV)
Hall C arc method	420.51 ± 0.11
Spin precession	420.00 ± 0.50
Energy fest (for comparison)	420.19 ± 0.39

Grames (2000) presents the results of energy measurements of the average linac energy $\overline{E_{\rm linac}}$ from two techniques carried out in his thesis, and the results of the energy festival. The results are displayed in table 5. All three sets of results match closely.

Acknowledgments

We are grateful to Vladimir Anferov, Ralph Assmann, William and Beverly Barletta, Mari Berglund, Richard Borcherds, Volker Burkert, John Byrd, Lali Chatterjee, Yaroslav Derbenev, Wilbur Franklin, Dennis Friesel, Frank Frommberger, Joseph Grames, Michael Harrison, Haixin Huang, Peter Karpius, S Y Lee, Simon C Leemann, Alfredo Luccio, Waldo MacKay, Yousef Makdisi, Richard Milner, Igor Passchier, Richard Prepost, Charles Prescott, Vadim Ptitsyn, Rajendran Raja, Thomas Roser, Hikaru Sato, Charles Sinclair, Christoph Steier, Edward Stephenson, Steven Tepikian, David Underwood, Jo van den Brand, Jan van der Laan, Johannes van Zeijts, Wolther von Drachenfels, Fuhua Wang, Jorg Wenninger, Michael Woods and Townsend Zwart.

Appendix A. Formal canonical transformation theory

Appendix A.1. General remarks

The formal canonical transformation theory to diagonalize the spin–orbit Hamiltonian is very abstract. The principal papers on the subject are by Derbenev and Kondratenko (1973), which introduced the concept of a phase-space dependent spin quantization axis, (although, preliminary steps in this direction were published earlier by Derbenev and Kondratenko (1972))

and by Yokoya (1986). The latter paper presents a more detailed exposition of the subject and corrects some loopholes in Derbenev and Kondratenko's logic. A few additional details were added by Mane (2003b). We do not review Mane's work below. Other formalisms, such as map-based algorithms and computer programs, are ultimately based on the foundation laid down by the formal canonical transformation theory. We mainly employ Yokoya's formalism below.

Appendix A.2. Canonical transformation

The orbital motion is treated semiclassically and the spin is modelled by a classical spin vector. The standard canonical transformation theory then makes two crucial assumptions:

- First, it is assumed that in the absence of the spin term, the orbital motion is integrable. More precisely, starting from $\mathscr{H} = \mathscr{H}_{\rm orb}(\boldsymbol{q}, \boldsymbol{p})$ we assume that the orbital motion is expressible using action-angle variables $(\boldsymbol{I}, \boldsymbol{\phi})$, so $\mathscr{H}_{\rm orb} = \mathscr{H}_{\rm orb}(\boldsymbol{I})$.
- The second important assumption is that, when the spin term is included, the perturbation to the orbital motion caused by the spin is so weak that the orbital motion *remains integrable* and the change to the orbital action-angles can validly be calculated using (first order in $\hbar$) canonical perturbation theory.

It is necessary to distinguish between the dynamical variables before and after the canonical transformation. Hence, the original Hamiltonian has the form

$$\mathscr{H}^0 = \mathscr{H}_{\rm orb}(\boldsymbol{I}^0) + \boldsymbol{W}(\boldsymbol{I}^0, \boldsymbol{\phi}^0) \cdot \boldsymbol{s}. \tag{A.1}$$

The next step is to find action-angle variables for the spin motion so as to express the entire spin–orbit motion in action-angle form. This requires a canonical transformation of the variables in (A.1). It was a key insight by both Derbenev and Kondratenko (1973) and later by Yokoya (1986) that the generating function of such a canonical transformation must involve *both* the orbital and spin variables—we cannot transform only the spin variables. Basically, this is a consequence of the Stern–Gerlach force; if the spin precession vector $\boldsymbol{W}$ contains gradient terms, as it must in the quadrupoles, etc, then the spin motion must react back on the orbit. The canonical transformation is carried out only to first order in $\hbar$, because throughout our work we have retained the spin terms only to the first order in $\hbar$. This is again a recognized approximation. We denote the spin action-angles by (J, ψ) and the spin tune by ν and the perturbed orbital action-angles by $(\boldsymbol{I}, \boldsymbol{\phi})$, without superscripts. Then we seek to express the transformed Hamiltonian in the form

$$\mathscr{H} = \mathscr{H}_{\rm orb}(\boldsymbol{I}) + \nu J, \tag{A.2}$$

where $\mathscr{H}_{\rm orb}$ is actually the same as before with the substitution $\boldsymbol{I}^0 \leftarrow \boldsymbol{I}$. Up to $O(\hbar)$, $\boldsymbol{I}$ and J are true actions because

$$\frac{{\rm d}I_j}{{\rm d}\theta} = -\frac{\partial \mathscr{H}}{\partial \phi_j} = {\rm O}(\hbar^2), \qquad \frac{{\rm d}J}{{\rm d}\theta} = -\frac{\partial \mathscr{H}}{\partial \psi} = {\rm O}(\hbar^2). \tag{A.3}$$

We now describe the formal canonical transformation to diagonalize the spin–orbit motion. The unperturbed orbital variables are $(\boldsymbol{q}^0, \boldsymbol{p}^0)$ and we recognize that the unperturbed Hamiltonian may depend explicitly on θ. To handle this situation, one employs an 'extended phase-space'. We promote θ to a dynamical variable and introduce a new independent variable τ, such that ${\rm d}\theta/{\rm d}\tau = 1$ so that $\theta = \tau +$ constant along a trajectory. We also introduce a dynamical variable $-E$, conjugate to θ. The extended Hamiltonian is

$$\mathscr{H}^0 = \mathscr{H}_{\rm orb}(\boldsymbol{q}^0, \boldsymbol{p}^0, \theta^0) + (-E^0) + \boldsymbol{W}(\boldsymbol{q}^0, \boldsymbol{p}^0, \theta^0) \cdot \boldsymbol{s}, \tag{A.4}$$

where we have written θ^0 and $-E^0$, in keeping with the fact that these are unperturbed variables. It is more elegant to treat all of the orbital variables in a unified notation by defining $q_4 = \theta$

and $p_4 = -E$ (and a tune $Q_4 = 1$). We shall employ Greek subscripts to denote a range $\lambda = 1, 2, 3, 4$, while Roman subscripts will denote a range $j = 1, 2, 3$ below. We *do* assume that the unperturbed orbital motion (without spin) is expressible in action-angle form, so the Hamiltonian is expressible as

$$\mathscr{H}^0 = \mathscr{H}_{\rm orb}(\boldsymbol{p}^0_\lambda) + \boldsymbol{W}(\boldsymbol{q}^0_\lambda, \boldsymbol{p}^0_\lambda) \cdot \boldsymbol{s}, \tag{A.5}$$

i.e. $\boldsymbol{q}^0_\lambda$ does not appear in $\mathscr{H}_{\rm orb}$. We also assume that $\mathscr{H}^0$ is unaltered under a shift $q^0_\lambda \to q^0_\lambda + 2\pi$, for any $\lambda = 1, 2, 3, 4$. In other words, $\mathscr{H}^0$ can be Fourier-expanded in the q^0_λ. The Fourier coefficients would be functions of the p^0_λ. The unperturbed orbital tunes are

$$\frac{{\rm d}q^0_\lambda}{{\rm d}\tau} = \frac{\partial \mathscr{H}^0_{\rm orb}}{\partial p^0_\lambda} \equiv Q_\lambda(\boldsymbol{p}^0_\mu), \tag{A.6}$$

with $Q_4 = 1$. The spin equation of motion is

$$\frac{{\rm d}\boldsymbol{s}}{{\rm d}\tau} = \{\boldsymbol{s}, \mathscr{H}^0\} = \boldsymbol{W} \times \boldsymbol{s}. \tag{A.7}$$

However, to formulate the canonical transformation properly, we must express the spin in terms of components in a clearly defined basis. We denote the original basis by $\{\boldsymbol{e}_1, \boldsymbol{e}_2, \boldsymbol{e}_3\}$, and we express $\boldsymbol{s}$ in terms of components in this basis as

$$\boldsymbol{s} = \sum_j s^0_j \boldsymbol{e}_j. \tag{A.8}$$

Then the Hamiltonian is

$$\mathscr{H}^0 = \mathscr{H}_{\rm orb}(\boldsymbol{p}^0_\lambda) + \sum_{j=1}^{3} \boldsymbol{W}(\boldsymbol{q}^0_\lambda, \boldsymbol{p}^0_\lambda) \cdot \boldsymbol{e}_j \, s^0_j. \tag{A.9}$$

The transformation is to a new basis $\{\boldsymbol{u}_1, \boldsymbol{u}_2, \boldsymbol{u}_3\}$ with spin components

$$\boldsymbol{s} = \sum_j s_j \boldsymbol{u}_j, \tag{A.10}$$

with suitably defined properties. This new basis must be found.

We only present the final results here; consult Derbenev and Kondratenko (1973) and Yokoya (1986) for the derivations. Since the Hamiltonian must be a function of dynamical variables only, the vectors $\boldsymbol{u}_j$ must be functions of phase-space variables only, i.e. $\boldsymbol{p}^0_\lambda$ and $\boldsymbol{q}^0_\lambda$. They must be explicitly independent of τ. Furthermore, they must be periodic in the q^0_λ, i.e. expressible as Fourier series in $\boldsymbol{q}^0_\lambda$, because $(p^0_\lambda, q^0_\lambda)$ and $(p^0_\lambda, q^0_\lambda + 2\pi)$ represent the same phase-space point. We choose $\boldsymbol{n} = \boldsymbol{u}_3$ as the spin quantization axis, so we want $(s_1, s_2, s_3) = (0, 0, J)$ where J is *invariant* to be a solution of the spin equation of motion. Hence, $\boldsymbol{s} = J\boldsymbol{u}_3$ satisfies (A.7), i.e. $\boldsymbol{u}_3$ must be a solution of (A.7). Thus, the transformed Hamiltonian $\mathscr{H}$ must be a function of s_3 only. So the prescription for $\boldsymbol{u}_3$ is that it is an explicitly τ-independent solution of (A.7):

$$\frac{{\rm d}\boldsymbol{u}_3}{{\rm d}\tau} = \boldsymbol{W} \times \boldsymbol{u}_3, \qquad \frac{\partial \boldsymbol{u}_3}{\partial \tau} = 0. \tag{A.11}$$

We also find two other orthonormal solutions of (A.7), say $\boldsymbol{\eta}_1$ and $\boldsymbol{\eta}_2$. These vectors depend explicitly on τ in general. By partial differentiation, we see that

$$\frac{\rm d}{{\rm d}\tau}\frac{\partial \boldsymbol{\eta}_j}{\partial \tau} = \boldsymbol{W} \times \frac{\partial \boldsymbol{\eta}_j}{\partial \tau} \qquad (j = 1, 2), \tag{A.12}$$

so $\partial\boldsymbol{\eta}_{1,2}/\partial\tau$ also satisfies the spin precession equation (A.7). Using $\boldsymbol{\eta}_j \cdot \boldsymbol{n} = 0$, it follows that $(\partial\boldsymbol{\eta}_j/\partial\tau) \cdot \boldsymbol{n} = 0$. Hence, $\partial\boldsymbol{\eta}_1/\partial\tau \parallel \boldsymbol{\eta}_2$ and $\partial\boldsymbol{\eta}_2/\partial\tau \parallel \boldsymbol{\eta}_1$. We construct the vector

$$\boldsymbol{a} \equiv \frac{1}{2}\left(\boldsymbol{\eta}_1 \times \frac{\partial \boldsymbol{\eta}_1}{\partial \tau} + \boldsymbol{\eta}_2 \times \frac{\partial \boldsymbol{\eta}_2}{\partial \tau}\right). \tag{A.13}$$

From the discussion about the directions of $\partial\boldsymbol{\eta}_{1,2}/\partial\tau$, it follows that $\boldsymbol{a} \parallel \boldsymbol{n}$, say $\boldsymbol{a} = F\boldsymbol{n}$. One also sees that $\mathrm{d}\boldsymbol{a}/\mathrm{d}\tau = \boldsymbol{W} \times \boldsymbol{a}$, so $|\boldsymbol{a}|$ is constant, i.e. $\mathrm{d}F/\mathrm{d}\tau = 0$ so $F = F(\boldsymbol{q}_\lambda^0 - \boldsymbol{Q}_\lambda\tau)$. Yokoya (1986) (and earlier, Derbenev and Kondratenko (1973)) concluded that F can be expanded in a Fourier series in $\boldsymbol{q}_\lambda^0$. Mane (2003b) showed that this is not always possible. However, the circumstances where a Fourier expansion is not possible are very rare and not important here. We assume the Fourier expansion is valid below. To this level of approximation, we can drop the superscript '0':

$$F = F_0 + \sum_{\boldsymbol{m}_\lambda \neq 0} F_{\boldsymbol{m}_\lambda}\, \mathrm{e}^{\mathrm{i}\boldsymbol{m}_\lambda\cdot(\boldsymbol{q}_\lambda - \boldsymbol{Q}_\lambda\tau)}. \tag{A.14}$$

We then choose $\boldsymbol{\eta}_1$ and $\boldsymbol{\eta}_2$ such that all the $F_{\boldsymbol{m}_\lambda}$ vanish for the nonconstant Fourier harmonics, leaving $F = F_0$ only. Consult Yokoya (1986) for a proof that this is possible. Then

$$\frac{\partial\boldsymbol{\eta}_j}{\partial\tau} = F_0\boldsymbol{n} \times \boldsymbol{\eta}_j \qquad (j = 1, 2). \tag{A.15}$$

We then set

$$\boldsymbol{u}_1 + \mathrm{i}\boldsymbol{u}_2 = (\boldsymbol{\eta}_1 + \mathrm{i}\boldsymbol{\eta}_2)\,\mathrm{e}^{\mathrm{i}F_0\tau}. \tag{A.16}$$

It is easily verified that $\partial\boldsymbol{u}_{1,2}/\partial\tau = 0$ and

$$\frac{\mathrm{d}\boldsymbol{u}_j}{\mathrm{d}\tau} = (\boldsymbol{W} - F_0\boldsymbol{u}_3) \times \boldsymbol{u}_j \qquad (j = 1, 2). \tag{A.17}$$

We can extend the above equation to $j = 3$ because $F_0\boldsymbol{u}_3 \times \boldsymbol{u}_3 = 0$. The basis vectors satisfy the equation of motion

$$\frac{\mathrm{d}\boldsymbol{u}_j}{\mathrm{d}\tau} = \boldsymbol{U} \times \boldsymbol{u}_j \qquad (j = 1, 2, 3), \tag{A.18}$$

where we see that $\boldsymbol{U} = \boldsymbol{W} - F_0\boldsymbol{u}_3$. The equation of motion for the spin in the new reference frame is

$$\frac{\mathrm{d}s_i}{\mathrm{d}\tau} = \sum_{jk} \epsilon_{ijk}\,(\boldsymbol{W} - \boldsymbol{U})\cdot\boldsymbol{u}_j\, s_k. \tag{A.19}$$

We must clearly identify the spin basis we are referring to (the $\boldsymbol{u}_j$). The transformed Hamiltonian, starting from (A.9), is

$$\mathscr{H} = \mathscr{H}_{\mathrm{orb}}(\boldsymbol{p}_\lambda) + \sum_{j=1}^{3}(\boldsymbol{W}(\boldsymbol{q}_\lambda, \boldsymbol{p}_\lambda) - \boldsymbol{U}(\boldsymbol{q}_\lambda, \boldsymbol{p}_\lambda))\cdot\boldsymbol{u}_j\, s_j. \tag{A.20}$$

The superscript '0' has been dropped from $\boldsymbol{q}_\lambda$ and $\boldsymbol{p}_\lambda$ because they have been transformed as well. In $\boldsymbol{W}$ and $\boldsymbol{U}$, we can simply ignore the distinction between $(\boldsymbol{q}_\lambda^0, \boldsymbol{p}_\lambda^0)$ and $(\boldsymbol{q}_\lambda, \boldsymbol{p}_\lambda)$ because the term is already of $\mathrm{O}(\hbar)$ because of the s_j. Note that $\mathscr{H}_{\mathrm{orb}}$ is a function of $\boldsymbol{p}_\lambda$ only, just as it was a function of only $\boldsymbol{p}_\lambda^0$ in (A.9). The transformed orbital Hamiltonian $\mathscr{H}_{\mathrm{orb}}$ is the same as the untransformed one with the simple substitution $\boldsymbol{p}_\lambda^0 \leftarrow \boldsymbol{p}_\lambda$. We also see that $\boldsymbol{\Omega} = \boldsymbol{W} - \boldsymbol{U} = F_0\boldsymbol{u}_3$, so the transformed Hamiltonian is of the desired form

$$\mathscr{H} = \mathscr{H}_{\mathrm{orb}}(\boldsymbol{p}_\lambda) + \Omega(\boldsymbol{p}_\lambda)\, s_3. \tag{A.21}$$

The value of $\Omega = F_0$ is the spin tune and is an invariant. The canonical transformation of the orbital variables is

$$\begin{aligned} q_\lambda &= q_\lambda^0 + \frac{1}{2}\sum_{jk} s_j\,\boldsymbol{u}_j\cdot(\boldsymbol{u}_k \times \{\boldsymbol{u}_k, q_\lambda^0\}), \\ p_\lambda &= p_\lambda^0 + \frac{1}{2}\sum_{jk} s_j\,\boldsymbol{u}_j\cdot(\boldsymbol{u}_k \times \{\boldsymbol{u}_k, p_\lambda^0\}). \end{aligned} \tag{A.22}$$

If the vector $\boldsymbol{n} = \boldsymbol{u}_3$ exists, it is unique, as long as the motion is not on a spin resonance. Suppose there is a vector $\boldsymbol{n}' \neq \pm\boldsymbol{n}$, which is also explicitly τ-independent and satisfies (A.7). Since it is easily seen that $\mathrm{d}(\boldsymbol{n}\cdot\boldsymbol{n}')/\mathrm{d}\tau = 0$, the vectors maintain a fixed angle with respect to each other, so they are never parallel for any τ. Then construct a third vector $\boldsymbol{n}'' \equiv \boldsymbol{n}\times\boldsymbol{n}'$. Clearly, $\boldsymbol{n}''$ is also explicitly independent of τ, and is linearly independent of $\boldsymbol{n}$ and $\boldsymbol{n}'$. Its equation of motion is

$$\frac{\mathrm{d}\boldsymbol{n}''}{\mathrm{d}\tau} = (\boldsymbol{W}\times\boldsymbol{n})\times\boldsymbol{n}' + \boldsymbol{n}\times(\boldsymbol{W}\times\boldsymbol{n}') = \boldsymbol{W}\times(\boldsymbol{n}\times\boldsymbol{n}') = \boldsymbol{W}\times\boldsymbol{n}''. \tag{A.23}$$

Hence, we have three linearly independent solutions of (A.7), all explicitly independent of τ, which we shall see in a moment means that the spin motion is resonant. Unlike $\boldsymbol{n}$, however, the vectors $\boldsymbol{u}_1$ and $\boldsymbol{u}_2$ are not unique. We can define another pair via

$$\boldsymbol{u}_1' + \mathrm{i}\boldsymbol{u}_2' = (\boldsymbol{u}_1 + \mathrm{i}\boldsymbol{u}_2)\,\mathrm{e}^{-\mathrm{i}\boldsymbol{m}_\lambda\cdot\boldsymbol{q}_\lambda}, \tag{A.24}$$

where $\boldsymbol{m}_\lambda$ is a set of integers. Then

$$\frac{\mathrm{d}}{\mathrm{d}\tau}(\boldsymbol{u}_1' + \mathrm{i}\boldsymbol{u}_2') = (\boldsymbol{U} + \boldsymbol{m}_\lambda\cdot\boldsymbol{Q}_\lambda\,\boldsymbol{u}_3)\times(\boldsymbol{u}_1' + \mathrm{i}\boldsymbol{u}_2'). \tag{A.25}$$

Clearly

$$\frac{\mathrm{d}\boldsymbol{u}_3}{\mathrm{d}\tau} = (\boldsymbol{U} + \boldsymbol{m}_\lambda\cdot\boldsymbol{Q}_\lambda\,\boldsymbol{u}_3)\times\boldsymbol{u}_3, \tag{A.26}$$

so $\boldsymbol{U}' = \boldsymbol{U} + (\boldsymbol{m}_\lambda\cdot\boldsymbol{Q}_\lambda)\,\boldsymbol{u}_3$, $\boldsymbol{W} - \boldsymbol{U}' \parallel \boldsymbol{u}_3$ and $\Omega' = \Omega - \boldsymbol{m}_\lambda\cdot\boldsymbol{Q}_\lambda$. Evidently $\mathrm{d}\Omega'/\mathrm{d}\tau = \partial\Omega'/\partial\tau = 0$, hence Ω' is an equally valid candidate spin tune. This is the proof that the spin tune is arbitrary up to a linear combination of the orbital tunes (plus an integer). If the value of Ω is such that we can find a set of integers $\boldsymbol{m}_\lambda$, such that $\Omega' = 0$, then all three vectors $\boldsymbol{u}_{1,2,3}$ satisfy (A.7) and all are explicitly independent of τ. Then we choose $\boldsymbol{U} = \boldsymbol{W}$, it follows that $\Omega = 0$ and $\boldsymbol{n}$ is not uniquely defined.

Let us comment briefly on the non-uniqueness of the spin tune. For planar rings, we have stated in several places that 'the' spin tune is $a\gamma$ (or $G\gamma$ in hadron rings), but according to the formal canonical transformation theory this is not a unique choice for the value of the spin tune. However, when performing a canonical transformation to a new spin basis, one must note that the spectrum of all the Fourier harmonics which drive the spin resonances also gets shifted. For example, the AGS has a superperiodicity of 12 and a weaker superperiodicity of 60. The intrinsic resonance $G\gamma = 60 - Q_y \simeq 51.25$ is so strong that it sets an effective upper limit on the energy up to which polarized protons can be accelerated at the AGS. A canonical transformation to change the value of the spin tune (say by an integer) would shift the locations of all the resonances by the *same* integer. The upper limit on the energy up to which polarized protons can be accelerated at the AGS, cannot be changed by a canonical transformation. Hence, in practice, there may be certain choices of spin bases which are more 'natural' or 'useful' than others. The formal canonical transformation theory treats all the choices for $\boldsymbol{u}_1$ and $\boldsymbol{u}_2$ as equally good.

Appendix A.3. Single resonance model

We apply the above formal procedure to the single resonance model. In section 16, we simply 'transformed to a frame rotating at a tune Q around the vertical axis'. We now solve the model following the formal procedure. The choice for $\boldsymbol{U}$, to rotate at a tune Q around the vertical axis, is $\boldsymbol{U} = Q\,\boldsymbol{e}_3$. Then

$$\tilde{\boldsymbol{W}} = (\nu_0 - Q)\,\boldsymbol{e}_3 + \epsilon(\boldsymbol{e}_1\cos\phi + \boldsymbol{e}_2\,\sin\phi) = \boldsymbol{\Omega}. \tag{A.27}$$

Define the auxiliary orthonormal vectors

$$\boldsymbol{v}_1 = \boldsymbol{e}_1 \cos\phi + \boldsymbol{e}_2 \sin\phi, \qquad \boldsymbol{v}_2 = -\boldsymbol{e}_1 \sin\phi + \boldsymbol{e}_2 \cos\phi, \qquad \boldsymbol{v}_3 = \boldsymbol{e}_3. \tag{A.28}$$

Then we set

$$\boldsymbol{u}_1 = \frac{1}{\Omega}[(\nu_0 - Q)\,\boldsymbol{v}_1 - \epsilon\,\boldsymbol{v}_3], \qquad \boldsymbol{u}_2 = \boldsymbol{v}_2, \qquad \boldsymbol{u}_3 = \frac{1}{\Omega}[(\nu_0 - Q)\boldsymbol{v}_3 + \epsilon\,\boldsymbol{v}_1]. \tag{A.29}$$

It is easily verified that $\mathrm{d}\boldsymbol{u}_j/\mathrm{d}\theta = \boldsymbol{U} \times \boldsymbol{u}_j$ for $j = 1, 2, 3$, and furthermore that $\mathrm{d}\boldsymbol{u}_3/\mathrm{d}\theta = \boldsymbol{W} \times \boldsymbol{u}_3$. Then $\boldsymbol{u}_3 = \boldsymbol{\Omega}/\Omega$, which we have seen earlier is the correct answer for $\boldsymbol{n}$. Also $\tilde{\boldsymbol{W}} = \Omega\,\boldsymbol{u}_3$ and so the spin tune is

$$\nu = \Omega = \sqrt{(\nu_0 - Q)^2 + \epsilon^2}. \tag{A.30}$$

As we have noted, the spin tune is arbitrary up to the addition of an integer linear combination of orbital tunes, so we can define new suitable new vectors $\boldsymbol{u}_1'$ and $\boldsymbol{u}_2'$ to change the value of the spin tune to $\nu \to Q \pm \sqrt{(\nu_0 - Q)^2 + \epsilon^2}$, if desired. Hence, we have confirmed the previously derived solution for the single resonance.

What the solution (without a canonical transformation) did *not* indicate was that the orbital variables would also be transformed. For brevity, we display only the change to the orbital action, which is a more interesting case. We do not distinguish between $(\boldsymbol{I}^0, \phi^0)$ and $(\boldsymbol{I}^1, \phi^1)$ below because the spin term is already of $\mathrm{O}(\hbar)$. There is only one orbital mode (I, ϕ) in the SRM. Then

$$\begin{aligned}
\{\boldsymbol{u}_1, I\} &= \frac{\partial \boldsymbol{u}_1}{\partial \phi} = \frac{\nu_0 - Q}{\Omega}\frac{\partial \boldsymbol{v}_1}{\partial \phi} = \frac{\nu_0 - Q}{\Omega}\,\boldsymbol{v}_2, \\
\{\boldsymbol{u}_2, I\} &= \frac{\partial \boldsymbol{u}_2}{\partial \phi} = -\boldsymbol{v}_1, \\
\{\boldsymbol{u}_3, I\} &= \frac{\partial \boldsymbol{u}_3}{\partial \phi} = \frac{\epsilon}{\Omega}\frac{\partial \boldsymbol{v}_1}{\partial \phi} = \frac{\epsilon}{\Omega}\,\boldsymbol{v}_2.
\end{aligned} \tag{A.31}$$

Omitting the tedious algebra, the answer is

$$I^0 = I^1 - \frac{\nu_0 - Q}{\Omega}\,J + \frac{\epsilon}{\Omega}\sqrt{s^2 - J^2}\cos\psi. \tag{A.32}$$

Recall that the value of I^1 is constant along a trajectory. Hence, the value of I^0 is shifted away from I^1 by a constant which is of $\mathrm{O}(\hbar)$, plus an oscillatory term (which averages to zero) which is also of $\mathrm{O}(\hbar)$. This implies a nonzero time-average shift in the value of the orbital action:

$$\overline{\Delta I} = \overline{I^1 - I^0} = \frac{\nu_0 - Q}{\Omega}\,J. \tag{A.33}$$

Setting $J = \pm\hbar/2$, we obtain two values of opposite sign for $\overline{\Delta I}$, i.e. a spatial separation of the spin states for *charged particle beams*. As explained above, we must recognize that the orbital trajectory itself has an uncertainty of $\mathrm{O}(\hbar)$, which is neglected in the semiclassical model.

Nevertheless, we *cannot* simply claim (as some authors do) that the change to the orbital motion in the canonical transformation does not exist. We have set up a formal (semiclassical) accelerator model and to diagonalize it, we must operate within the proper rules of Hamiltonian theory. It is then our responsibility to realize that the model orbital variables are approximations to the true coordinates and momenta of the actual particles in an accelerator, and no violation of the basic principles of quantum mechanics is implied.

References

Abbiendi G *et al* 2001 *Eur. J. Phys.* C **19** 587–651
(Abbiendi G *et al* 1999 *Preprint* hep-ex/9902068)
Abe K *et al* 2000 *Phys. Rev. Lett.* **84** 5945–9
Airapetian A *et al* 2001 *Phys. Rev. Lett.* **87** 182001
Akchurin N *et al* 1992 *Phys. Rev. Lett.* **69** 1753–6
Akhmetshin R R *et al* 2002 *AIP Conf. Proc.* **619** 15–29
Akhmetshin R R *et al* 2004 *Phys. Lett.* B **578** 285–9
Alekseev I *et al* 2003 *Nucl. Instrum. Methods* A **499** 392–414
Alley R *et al* 1995 *Nucl. Instrum. Methods* A **365** 1–27
Alsharo'a M M *et al* 2003 *Phys. Rev. ST Accel. Beams* **6** 081001
Anferov V A *et al* 1992 *Phys. Rev.* A **46** R7383–6
Anferov V A 1999 *Phys. Rev. Lett.* **83** 2738–40
Aniel T, Laclare J L, Leleux G, Nakach A and Ropert A 1985 *J. Physique Coll.* **46** C2-499–507
Aniol K A *et al* 2001 *Phys. Lett.* B **509** 211–16
Aniol K *et al* 2004 *Phys. Rev.* C **69** 065501
(Aniol K *et al* 2004 *Preprint* nucl-ex/0405006)
Anthony P L 2004 *Phys. Rev. Lett.* **92** 181602
Anthony P L *et al* 2005 *Preprint* hep-ex/0504049
Arduini G *et al* 2001 *Proc. 2001 Particle Accelerator Conf. (Chicago, IL)* (Piscataway, NJ: IEEE) pp 356–8
Arnaudon L, Knudsen L, Koutchouk J P, Olsen R, Placidi M, Schmidt R, Crozon M, Blondel A, Assmann R and Dehning B 1992 *Phys. Lett.* B **284** 431–9
Arnaudon L *et al* 1993 *Proc. 1993 Particle Accelerator Conf. (Washington, DC)* (Piscataway, NJ: IEEE) pp 44–6
Arnaudon L *et al* 1994 *Proc. 4th European Particle Accelerator Conf. (London)* (Geneva: EPAC) pp 187–9
Arnaudon L *et al* 1995a *Nucl. Instrum. Methods* A **357** 249–52
Arnaudon L *et al* 1995b *Z. Phys.* C **66** 45–62
Artamonov A S *et al* 1982 *Phys. Lett.* B **118** 225–9
Artamonov A S *et al* 1984 *Phys. Lett.* B **137** 272–6
Artamonov A S *et al* 2000 *Phys. Lett.* B **474** 427–9
Assmann R and Koutchouk J P 1994 *CERN Report* SL/94-13
Assmann R *et al* 1994a *CERN Report* SL/94-08 (AP)
Assmann R, Blondel A, Dehning B, Grosse-Wiesmann P, Jacobsen R, Koutchouck J P, Miles J, Placidi M, Schmidt R and Wenninger J 1994b *Proc. 4th European Particle Accelerator Conf. (London)* (Geneva: EPAC) pp 932–4
Assmann R, Blondel A, Dehning B, Grosse-Wiesmann P, Grote H, Placidi M, Schmidt R, Wenninger J, Drees A and Tecker F 1995 *Proc. 1995 Particle Accelerator Conf. (Dallas, TX)* (Piscataway, NJ: IEEE) pp 567–9
Assmann R *et al* 1999a *Proc. 1999 Particle Accelerator Conf. (New York)* (Piscataway, NJ: IEEE) pp 2999–3001
Assmann R *et al* 1999b *Eur. J. Phys.* C **6** 187–223
Assmann R *et al* 2001 *AIP Conf. Proc.* **570** 169–78
Assmann R *et al* 2004 CERN AB/2004-030
Aul'chenko V M *et al* 1975 Institute of Nuclear Physics, Novosibirsk (in Russian) http://www-spires.slac.stanford.edu/spires/find/hep/www?key=87157
Aul'chenko V M *et al* 2003 *Phys. Lett.* B **573** 63–79
Badier J, Blondel A, Crozon M, Dehning B, Knudsen L, Koutchouk J P, Placidi M and Schmidt R 1991a *Proc. 1991 Particle Accelerator Conf. (San Francisco, CA)* (Piscataway, NJ: IEEE) pp 147–9
Badier J *et al* 1991b *Proc. 1991 Particle Accelerator Conf. (San Francisco, CA)* (Piscataway, NJ: IEEE) pp 1213–15
Bai M, Lee S Y, Glenn J W, Huang H, Ratner L, Roser T, Syphers M J and van Asselt W 1997 *Phys. Rev.* E **56** 6002–7
Bai M *et al* 1998 *Phys. Rev. Lett.* **80** 4673–6
Bai M *et al* 2000 *Phys. Rev. Lett.* **84** 1184–7
Bai M, MacKay W W, Roser T and Ranjbar V 2002 *Proc. 8th European Particle Accelerator Conf. (Paris)* (Geneva: EPAC) pp 299–301
Baier V N 1969 *XLVI Corso Scuola Int. di Fizika 'Enrico Fermi'* (Orlando, FL: Academic) p 4
Baier V N 1972 *Sov. Phys.—Usp.* **14** 695–714
Baier V N and Katkov V M 1967 *Sov. Phys.—JETP* **25** 944–7
Baier V N, Katkov V M and Strakhovenko V M 1970 *Sov. Phys.—JETP* **31** 908–11
Baier V N, Katkov V M and Strakhovenko V M 1978 *Sov. Phys.—Dokl.* **23** 573–5
Baier V N and Orlov Yu F 1966 *Sov. Phys.—Dokl.* **10** 1145
Bailey J, Bartl W, von Bochmann G, Brown R C A, Farley F J M, Giesch M, Jostlein H, van der Meer S, Picasso E and Williams R W 1972 *Nuovo Cimento* A **9** 369

Bailey J *et al* 1978 *J. Phys. G: Nucl. Phys.* **4** 345–52
Bailey J *et al* 1979 *Nucl. Phys.* B **150** 1–75
Balandin V and Golubeva N 1992 *Int. J. Mod. Phys.* A **2B** 998
Balandin V and Golubeva N 1993 *Proc. 1993 Particle Accelerator Conf. (Washington, DC)* (Piscataway, NJ: IEEE) pp 444–6
Balandin V V and Golubeva N I 1997 *AIP Conf. Proc.* **391** 282–90
(Balandin V V and Golubeva N I 1999 *Preprint* physics/9903032)
Barber D P, Bialowons W, Klanner R, Lewin H C, Camerini U, Lomperski M, Goetschel H, Lohrmann E, Patel P and Romanowski T 1990 *Part. Accelerators* **32** 173–8
Barber D P, Bremer H D, Kewisch J, Lewin H C, Limberg T, Mais H, Ripken G, Rossmanith R, Schmidt R and Pelfer P 1983a DESY M-83-15
Barber D P, Bremer H D, Kewisch J, Lewin H C, Limberg T, Mais H, Ripken G, Rossmanith R and Schmidt R 1983b *Proc. 1983 Particle Accelerator Conf. (Santa Fe, NM)* (Piscataway, NJ: IEEE) pp 2710–12
Barber D P *et al* 1984 *Phys. Lett.* B **135** 498–504
Barber D P and Mane S R 1988 *Phys. Rev.* A **37** 456–63
Barber D P *et al* 1993 *Nucl. Instrum. Methods* A **329** 79–111
Barber D P *et al* 1994 *Nucl. Instrum. Methods* A **338** 166–84
Barber D P 1995a *Proc. 1995 Particle Accelerator Conf. (Dallas, TX)* (Piscataway, NJ: IEEE) pp 511–13
Barber D P *et al* 1995b *Phys. Lett.* B **343** 436–43
Barber D P and Gianfelice E 2002 *Acta Phys. Pol.* B **33** 3943–8
Barber D P (for the HERA team) 2004 *Proc. 9th European Particle Accelerator Conf. (Lucerne)* (Geneva: EPAC) pp 644–6
Bargmann V, Michel L and Telegdi V L 1959 *Phys. Rev. Lett.* **2** 435–6
Barkov L M *et al* 1979 *Nucl. Phys.* B **148** 53–60
Barkov L M *et al* 1987 *Sov. J. Nucl. Phys.* **45** 630–4
Barr G, Gaisser T K and Stanev T 1989 *Phys. Rev.* D **39** 3532–4
Baru S E *et al* 1992 *Z. Phys.* C **56** 547–52
Beckmann M *et al* 2002 *Nucl. Instrum. Methods* A **479** 334–48
Bell J S, Hughes R J and Leinaas J M 1985 *Z. Phys.* C **28** 75–80
Bell J S and Leinaas J M 1983 *Nucl. Phys.* B **212** 131–50
Bell J S and Leinaas J M 1987 *Nucl. Phys.* B **284** 488–508
Belomesthnykh S A, Bondar A E, Yegorychev M N, Zhilitch V N, Kornyukhin G A, Nikitin S A, Saldin E L, Skrinsky A N and Tumaikin G M 1984 *Nucl. Instrum. Methods* A **227** 173–81
Bennett G W *et al* 2002 *Phys. Rev. Lett.* **89** 101804
Bennett G W *et al* 2004 *Phys. Rev. Lett.* **92** 161802
Berglund M, Barber D P and Gianfelice E 1998 *Proc. 5th European Particle Accelerator Conf. (Stockholm)* (Geneva: EPAC) pp 1253–5
Berglund M 2001 *PhD Thesis* Royal Institute of Technology, Stockholm
Berglund M 2004 private communication
Berridge S C, Bugg W M, Cohn H O, Efremenko Yu V, Kamyshkov Yu A, Onoprienko D V, Shmakov K D, Weidemann A W and Woods M B 1999 *Proc. 13th Int. Symp. on High Energy Spin Physics (Protvino)* ed N E Tyurin *et al* (Singapore: World Scientific) pp 534–7
Biscari C, Buon J and Montague B W 1984 *Nuovo Cimento* B **81** 128–42
Bleistein N and Handelsman R A 1986 *Asymptotic Expansions of Integrals* 2nd edn (Mineola: Dover)
Blinov B B *et al* 1994 *Phys. Rev. Lett.* **73** 1621–3
Blinov B B *et al* 1998 *Phys. Rev. Lett.* **81** 2906–9
Blinov B B *et al* 1999 *Phys. Rev. ST Accel. Beams* **2** 064001
Blinov B B *et al* 2000 *Phys. Rev. ST Accel. Beams* **3** 104001
Blinov B B *et al* 2002 *Phys. Rev. Lett.* **88** 014801
Blinov V E *et al* 2002 *Proc. 8th European Particle Accelerator Conf. (Paris)* (Geneva: EPAC) pp 422–4
Bloch F 1946 *Phys. Rev.* **70** 460–74
Blondel A 1990 *LEP Note* 629
Bondar A E and Saldin E L 1982 *Nucl. Instrum. Methods* A **195** 577–80
Bordovitsyn V A, Ternov I M and Bagrov V G 1995 *Sov. Phys.—Usp.* **39** 1037–47
Bravar A 2003 *AIP Conf. Proc.* **675** 830–5
Budker G I 1967 *Sov. At. Energy* **22** 438–40
(Budker G I 1967 *At. Energ.* **22** 346–8 (in Russian))
Budker G I 1970 *Proc. 7th Int. Conf. on High-Energy Accelerators (Yerevan, 1969)* ed A I Alikhanian (Yerevan: Publishing House of the Academy of Sciences of Armenia SSR) p 33

Bukin A D, Kurdadze L M, Serednyakov S I, Sidorov V A, Skrinsky A N, Shatunov Yu M, Shvarts B A and Eidelman S I 1978 *Sov. J. Nucl. Phys.* **27** 516–21
Buon J 1981 NI/07-81
Buon J 1982 *DESY Report* M-82/08
Buon J and Steffen K 1986 *Nucl. Instrum. Methods* A **245** 248–61
Buon J 1989 *AIP Conf. Proc.* **187** 963–74
Buon J 1990 *Part. Accelerators* **32** 153–9
Buttimore N H, Kopeliovich B Z, Leader E, Soffer J and Trueman T L 1999 *Phys. Rev.* D **59** 114010
Byrd J M 2004 private communication
Camerini U, Cline D, Learned J, Mann A K and Resvanis L K 1975 *Phys. Rev.* D **12** 1855–78
Carrassi L M 1958 *Nuovo Cimento* **7** 524
Chao A W 1979 *J. Appl. Phys.* **50** 595–8
Chao A W 1981a *Nucl. Instrum. Methods* **180** 29
Chao A W 1981b *AIP Conf. Proc.* **87** 395–449
Chao A W and Yokoya K 1981 KEK Report 81-7
Charpak G, Farley F J M, Garwin R L, Muller T, Sens J C, Telegdi V L and Zichichi A 1961 *Phys. Rev. Lett.* **6** 128–32
Cho Y, Martin R L, Parker E F, Potts C W, Ratner L G, Gareyte J, Johnson C, Lefevre P, Mohl D and Krisch A D 1976 *AIP Conf. Proc.* **35** 396
Chu C M *et al* 1998 *Phys. Rev.* E **58** 4973–6
Clendenin J E, Brachmann A, Galetto T, Luh D A, Maruyama T, Sodja J and Turner J L 2003 *AIP Conf. Proc.* **675** 1042–6
Combley F H 1981 *Phys. Rep.* **68** 2
Courant E D 1990 *Part. Accelerators* **32** 127–37
Courant E D and Ruth R D 1980 *Brookhaven National Laboratory Technical Report* BNL 51270
Courant E D and Snyder H S 1958 *Ann. Phys.* **3** 1–48
Crabb D G *et al* 1979 *Phys. Rev. Lett.* **43** 983–6
Crandell D A *et al* 1996 *Phys. Rev. Lett.* **77** 1763–5
Danby G T *et al* 2001 *Nucl. Instrum. Methods* A **457** 151–74
de Jager C W, Ptitsyn V and Shatunov Yu M 1997 *Proc. 12th Int. Symp. on High Energy Spin Physics (Amsterdam)* ed C W de Jager *et al* (Singapore: World Scientific) pp 555–7
Dehmelt H 1986 *Proc. Natl Acad. Sci. USA* **83** 2291
Derbenev Ya S and Kondratenko A M 1971 *Sov. Phys.—JETP* **33** 658–64
Derbenev Ya S and Kondratenko A M 1972 *Sov. Phys.—JETP* **35** 230–6
Derbenev Ya S and Kondratenko A M 1973 *Sov. Phys.—JETP* **37** 968–73
Derbenev Ya S and Kondratenko A M 1976 *Sov. Phys.—Dokl.* **20** 562
Derbenev Ya S and Kondratenko A M 1978 *Sov. Phys.—Dokl.* **24** 366–8
Derbenev Ya S, Kondratenko A M and Saldin E N 1979a *Nucl. Instrum. Methods* A **165** 15–19
Derbenev Ya S, Kondratenko A M and Saldin E N 1979b *Nucl. Instrum. Methods* A **165** 201–8
Derbenev Ya S, Kondratenko A M and Saldin E N 1982 *Nucl. Instrum. Methods* A **193** 415–21
Derbenev Ya S, Kondratenko A M and Skrinsky A N 1979c *Part. Accelerators* **9** 247–66
Derbenev Ya S, Kondratenko A M, Skrinsky A N and Shatunov Yu M 1977 *Proc. 1977 Particle Accelerator Conf. (New York)* vol 2 (Piscataway, NJ: IEEE) p 75 (in Russian)
Doll D, Fischer P, Hillert W, Kruger H, Stammschroer K and Wermes N 2002 *Nucl. Instrum. Methods* A **492** 356–64
Dragt A J and Finn J M 1976 *J. Math. Phys.* **17** 2215–27
Dutz H *et al* 2003 *Phys. Rev. Lett.* **91** 192001
Edwards D A and Syphers M J 1993 *An Introduction to the Physics of Particle Accelerators* (New York: Wiley)
Edwards D A and Teng L C 1973 *IEEE Trans. Nucl. Sci.* **20** 885
Efstathiadis E *et al* 2003 *Nucl. Instrum. Methods* A **496** 8–25
Ehrenfest P 1927 *Z. Phys.* **45** 455
Eidelman S *et al* 2004 *Phys. Lett.* B **592** 1–1109
Eidelman Yu and Yakimenko V 1993 *Proc. 1993 Particle Accelerator Conf. (Washington, DC)* (Piscataway, NJ: IEEE) pp 450–2
Eidelman Yu and Yakimenko V 1994 *Part. Accelerators* **45** 17–35
Eidelman Yu and Yakimenko V 1995 *Part. Accelerators* **50** 261–78
Farley F J M and Picasso E 1990 *Quantum Electrodynamics* ed T Kinoshita (Singapore: World Scientific) pp 479–559
Farley F J M *et al* 2004 *Phys. Rev. Lett.* **93** 052001
(Farley F J M 2003 *et al Preprint* hep-ex/0307006)
Farley F J M and Semertzidis Y 2004 *Prog. Part. Nucl. Phys.* **52** 1–83

Fischer G E, Gustavson D B, Johnson J R, Murray J J, Phillips T J, Prepost R, Schwitters R F, Sinclair C K and Wiser D E 1979 *PEP Note* 316 (also *SPEAR Note* 218)
Fischer G and Hofmann A 1992 CERN SL/92-35 337
Ford G W and Hirt C W 1961 *University of Michigan Report* unpublished
Ford G W and Mullin C J 1957 *Phys. Rev.* **108** 477–81
Ford G W and Mullin C J 1958 *Phys. Rev.* **110** 1485
Ford W T, Mann A K and Ling T Y 1972 *SLAC Report* 158
Forest E 1992 *J. Comput. Phys.* **99** 209
Franklin W A 2000 *Prog. Part. Nucl. Phys.* **44** 61
Franklin W A, Akdogan T, Dutta D, Farkhondeh M, Hurwitz M, Matthews J L, Tsentalovich E, Turchinetz W, Zwart T and Booth E C 2003 *AIP Conf. Proc.* **675** 1058–62
Frenkel J 1926 *Z. Phys.* **37** 243
Friesel D 2005 private communication
Froissart M and Stora R 1960 *Nucl. Instrum. Methods* A **7** 297–305 (in French)
Frommberger F 2004 private communication
Garwin R L, Lederman L M and Weinrich M 1957 *Phys. Rev.* **105** 1415–17
Gerlach W and Stern O 1922 *Z. Phys.* **9** 349–52
Gianfelice E 2003 DESY-PROC-1999-03, pp 77–91
Goldstein H, Poole C P and Safko J L 2002 *Classical Mechanics* 3rd edn (Englewood Cliffs, NJ: Prentice-Hall)
Golubeva N I, Kondratenko A M and Filatov Yu N 1994 *Proc. International Symp. on 'Dubna Deuteron-93'* (Dubna: JINR) pp 374–7
Good R H 1961 *Phys. Rev.* **125** 2112–15
Goodwin J E *et al* 1990 *Phys. Rev. Lett.* **64** 2779–82
Grames J 2000 *PhD Thesis* University of Illinois at Urbana-Champaign
Grames J 2004 private communication
Grames J M *et al* 2004 *Phys. Rev. ST Accel. Beams* **7** 042802
Grorud E, Laclare J L, Leleux G, Nakach A and Ropert A 1982 *AIP Conf. Proc.* **95** 407–11
Grote H 1995 *AIP Conf. Proc.* **343** 307–11
Gustavson D, Murray J J, Phillips T J, Schwitters R, Sinclair C K, Johnson J R, Prepost R and Wiser D E 1979 *Nucl. Instrum. Methods* **165** 177
Hacyan S and Sarmiento A 1989 *Phys. Rev.* D **40** 2641–6
Hand L N and Skuja A 1987 *Phys. Rev. Lett.* **59** 1910–13
Hand L N and Skuja A 1989 *Phys. Lett.* A **139** 291–8
Harrison M, Peggs S and Roser T 2002 *Ann. Rev. Nucl. Part. Sci.* **52** 425–69
Hasty R *et al* 2000 *Science* **290** 2117–19
Hatanaka K *et al* 1997 *Proc. 16th RCNP Osaka International Symp. on 'Multi-GeV High-Performance Accelerators and Related Technology'* (Osaka: RCNP) pp 269–71
Hawking S 1974 *Nature* **248** 30–1
Heinemann K 1997 *Preprint* DESY 97-166
(Heinemann K 1997 *Preprint* physics/9709025)
Heinemann K and Barber D P 2001a *Nucl. Instrum. Methods* A **463** 62–7
Heinemann K and Barber D P 2001b *Nucl. Instrum. Methods* A **469** 294–4
Heinemann K and Hoffstätter G H 1996 *Phys. Rev.* E **54** 4240–55
Henry G R, Schrank G and Swanson R A 1969 *Nuovo Cimento* A **63** 995
Hiramatsu S, Sato H and Toyama T 1989 *AIP Conf. Proc.* **187** 1436–41
Hirayama T and Hara T 1999 *Prog. Theor. Phys.* **103** 907–28
Hoffmann M 2001 *PhD Thesis* Bonn University
(Hoffmann M 2001 *Internal Report* BONN-IR-2001-17)
Hoffmann M *et al* 2001 *AIP Conf. Proc.* **570** 756–760
Hoffstaetter G, Vogt M and Barber D P 1999 *Phys. Rev. ST Accel. Beams.* **2** 114001
Hoffstätter G and Willeke F 1999 *Proc. 1999 Particle Accelerator Conf. (New York)* (Piscataway, NJ: IEEE) pp 407–9
Holt C R 1984 *Part. Accelerators* **16** 19
Huang H, Lee S Y and Ratner L G 1993 *Proc. 1993 Particle Accelerator Conf. (Washington, DC)* (Piscataway, NJ: IEEE) pp 432–4
Huang H *et al* 1994 *Phys. Rev. Lett.* **73** 2982–5
Huang H *et al* 2001 *Proc. 2001 Particle Accelerator Conf. (Chicago, IL)* (Piscataway, NJ: IEEE) pp 2443–5
Huang H *et al* 2003a *AIP Conf. Proc.* **675** 794–8
Huang H *et al* 2003b *AIP Conf. Proc.* **667** 40–9

Huang H *et al* 2003c *Proc. 2003 Particle Accelerator Conf. (Portland, OH)* (Piscataway, NJ: IEEE) pp 51–3
Huang H 2005 private communication
Igo G and Tanihata I 2003 *AIP Conf. Proc.* **675** 836–40
Jackson J D 1976 *Rev. Mod. Phys.* **48** 417–33
Jackson J D 1998 *Classical Electrodynamics* 3rd edn (New York: Wiley)
Johnson J R, Prepost R, Wiser D E, Murray J J, Schwitters R and Sinclair C K 1983 *Nucl. Instrum. Methods* A **204** 261–8
José J V and Saletan E J 1998 *Classical Dynamics: A Contemporary Approach* (Cambridge: Cambridge University Press)
Jowett J M 1987 *AIP Conf. Proc.* **153** 864
Karpius P 2003 *Hampton University Graduate Studies at Jefferson Lab* at press
Kessler J 1985 *Polarized Electrons* 2nd edn (Berlin: Springer)
Kewisch J, Rossmanith R and Limberg T 1989 *Phys. Rev. Lett.* **62** 419–21
Kezerashvili G Ya, Lysenko A P, Shatunov Yu M and Vorobyov P V 1992 *Nucl. Instrum. Methods* A **314** 15–20
Khiari F Z *et al* 1989 *Phys. Rev.* D **39** 45–85
Khoe T, Kustom R L, Martin R L, Parker E F, Potts C W, Ratner L G, Timm R E, Krisch A D, Roberts J B and O'Fallon J R 1975 *Part. Accelerators* **6** 213–36
Khoze V A 1971 *Proc. 6th Winter School on the Theory of Nuclear and High Energy Physics* (Leningrad: Akademiya Nauka SSR) pp 393–415
Klein R, Mayer T, Kuske P, Thornagel R and Ulm G 1997 *Nucl. Instrum. Methods* A **384** 293–8
Klein R, Thornagel R, Ulm G, Mayer T and Kuske P 1998 *J. Synchrotron Radiat.* **5** 392–4
Knudsen L, Koutchouk J P, Placidi M, Schmidt R, Crozon M, Badier J, Blondel A and Dehning B 1991 *Phys. Lett.* B **270** 97–104
Kondratenko A M 1982 *Novosibirsk Preprint* 82-28
Koop I A, Lysenko A P, Nesterenko I N, Polunin A A and Shatunov Yu M 1989 *AIP Conf. Proc.* **187** 1023–7
Koop I and Shatunov Yu M 1995 *AIP Conf. Proc.* **343** 317–20
Korostelev M and Shatunov Yu M 2001 *Proc. 2001 Particle Accelerator Conf. (Chicago, IL)* (Piscataway, NJ: IEEE) pp 3496–8
Kramers H 1958 *Quantum Mechanics* (Amsterdam: North-Holland)
Krisch A D *et al* 1989 *Phys. Rev. Lett.* **63** 1137–40
Kuske P and Goergen R 2000 *Proc. 7th European Particle Accelerator Conf. (Vienna)* (Geneva: EPAC) pp 1771–3
LeDuff J, Marin P C, Masnou J L and Sommer M 1973 *Proc. 3rd All-Union Conf. Charged Particle Accelerators (Moscow, 1972)* (Moscow: Akademiya Nauka SSR) p 371
Leader E 2001 *Spin in Particle Physics* (*Cambridge Monographs on Particle Physics, Nuclear Physics and Cosmology*) (Cambridge: Cambridge University Press)
Learned J G, Resvanis L K and Spenser C M 1975 *Phys. Rev. Lett.* **35** 1688–90
Lee S Y 1997 *Spin Dynamics and Snakes in Synchrotrons* (Singapore: World Scientific)
Lee S Y 2005 private communication
Lee S Y and Berglund M 1996 *Phys. Rev.* E **54** 806–14
Leemann C 2001 *Ann. Rev. Nucl. Part. Sci.* **51** 413–50
Leemann S C 2002b *Master's Thesis* ETHZ/PSI *ETHZ-IPP Internal Report* 2002-02
Leemann S C 2004 private communication
Leemann S C, Böge M, Dehler M, Schlott V and Streun A 2002a *Proc. 8th European Particle Accelerator Conf. (Paris)* (Geneva: EPAC) pp 662–4
Leinaas J M 2002 *Quantum Aspects of Beam Dynamics* ed P Chen (Singapore: World Scientific) pp 336–52
Leonova M A *et al* 2004 *Phys. Rev. Lett.* **93** 224801
LEP Collaborations, LEP Electroweak Working Group and SLD Electroweak and Heavy Flavour Groups 2003 *Preprint* hep-ex/0312023
Lorentz B *et al* 2004 *Proc. 9th European Particle Accelerator Conf. (Lucerne)* (Geneva: EPAC) pp 1746–8
Luccio A, Lehrach A, Niederer J, Roser T, Syphers M and Tsoupas N 1999 *Proc. 1999 Particle Accelerator Conf. (New York)* (Piscataway, NJ: IEEE) pp 1578–80
Lyboshitz V L 1967 *Sov. J. Nucl. Phys.* **4** 195
Lysenko A P, Polunin A A and Shatunov Yu M 1986 *Part. Accelerators* **18** 215–22
MacKay W W *et al* 1984 *Phys. Rev.* D **29** 2483–90
MacKay W W *et al* 2003a *Proc. 2003 Particle Accelerator Conf. (Portland, OH)* (Piscataway, NJ: IEEE) pp 405–9
MacKay W W *et al* 2003b *Proc. 2003 Particle Accelerator Conf. (Portland, OH)* (Piscataway, NJ: IEEE) pp 1697–9
MacKay W W 2005 private communication
Maggiora A 1995 *Nucl. Phys. News* **5** 23–30

Makdisi Y 1998 *AIP Conf. Proc.* **451** 40–52
Mane S R 1986 *Phys. Rev. Lett.* **57** 78–81
Mane S R 1987a *Phys. Rev.* A **36** 105–19
Mane S R 1987b *Phys. Rev.* A **36** 120–30
Mane S R 1987c *FNAL Report* FN-465
Mane S R 1988a *FNAL Report* FN-503
Mane S R 1988b *FNAL Report* TM-1515
Mane S R 1989a *AIP Conf. Proc.* **187** 959–62
Mane S R 1989b *Proc. 1989 Particle Accelerator Conf. (Chicago, IL)* (Piscataway, NJ: IEEE) pp 1798–800
Mane S R 1990 *Nucl. Instrum. Methods* A **292** 52–74
Mane S R 1992a *BNL AGS/AD/Technical Note* No 364
Mane S R 1992b *Nucl. Instrum. Methods* A **321** 21–41
Mane S R 1993 *Phys. Lett.* A **177** 411–14
Mane S R 2003a *Nucl. Instrum. Methods* A **498** 1–15
Mane S R 2003b *Nucl. Instrum. Methods* **498** 52–89
Mane S R, Shatunov Yu M and Yokoya K 2005 *J. Phys. G: Nucl. Part. Phys.* **31** R151–R209
Margaritondo G 2002 *Elements of Synchrotron Light* (Oxford: Oxford University Press)
Mendlowitz H and Case K M 1955a *Phys. Rev.* **97** 33–8
Mendlowitz H and Case K M 1955b *Phys. Rev.* **97** 1551–7
Michel L and Wightman A S 1955 *Phys. Rev.* **98** 1190
Mitchell J M 1999 *JLab Internal Report* JLAC-ACC-99-25
Mizumachi Y, Kawamoto T, Mori Y, Nakajima K, Ogata A and Yokoya K 1990 *Part. Accelerators* **32** 179–84
Morozov V S *et al* 2001 *Phys. Rev. ST Accel. Beams* **4** 104002
Morozov V S *et al* 2003a *AIP Conf. Proc.* **675** 776–80
Morozov V S *et al* 2003b *Phys. Rev. Lett.* **91** 214801
Nagaitsev S S 1997 *Part. Accelerators* **56** 181–93
Nakajima K 1993 *Proc. 10th International Symp. on High Energy Spin Physics (Nagoya)* ed T Hasegawa *et al* (Japan: Universal Academic Press) pp 919–22
Nakajima K, Arinaga M, Kawamoto T, Mizumachi Y, Mori Y, Ogata A, and Yokoya K 1991 *Phys. Rev. Lett.* **66** 1697–700
Nakamura S *et al* 1998 *Nucl. Instrum. Methods* A **411** 93–106
Ohmori C *et al* 1995 *Phys. Rev. Lett.* **75** 1931–3
Onoprienko D V 2000 *SLAC Report* 556
Orlov Yu, Ozben C S and Semertzidis Y K 2002 *Nucl. Instrum. Methods* A **482** 767–75
Orsay Storage Ring Group 1971 *Proc. 8th Int. Conf. on High-Energy Accelerators (CERN)* (Geneva: CERN) p 127
Parker E F, Brandeberry F E, Crosbie E A, Knott M J, Potts C W, Ratner L G, Schultz P F and Suddeth D E 1979 *IEEE Trans. Nucl. Sci.* **26** 3200
Passchier I 2000 The charge form factor of the neutron from double-polarized electron-deuteron scattering *PhD Thesis* Free University Amsterdam
Passchier I, Higinbotham D W, de Jager C W, Norum B E, Papadakis N H and Vodinas N P 1998 *Nucl. Instrum. Methods* A **414** 446–58
Perevedentsev E A, Shatunov Yu M and Ptitsin V 2003 *AIP Conf. Proc.* **675** 761–5
Phelps R A and Anferov V A 1998 *Part. Accelerators* **59** 169–74
Placidi M and Rossmanith R 1989 *Nucl. Instrum. Methods* A **274** 79–94
Pollock R E 1991 *Nucl. Instrum. Methods* A **300** 210–12
Polunin A A and Shatunov Yu M 1982 *Novosibirsk Preprint* IYF 82-16
Prepost R 2004 private communication
Prescott C W *et al* 1978 *Phys. Lett.* B **77** 347–52
Ptitsyn V, Luccio A U and Ranjbar M 2003 *AIP Conf. Proc.* **675** 746–9
Ptitsyn V and Shatunov Yu M 1995 *Proc. 1995 Particle Accelerator Conf. (Dallas, TX)* (Piscataway, NJ: IEEE) pp 3331–3
Ptitsyn V and Shatunov Yu M 1997 *Nucl. Instrum. Methods* A **398** 126–30
Ptitsyn V *et al* 2004 *Proc. SPIN 2004 (Trieste)* (Singapore: World Scientific) at press
Purcell E M and Ramsey N F 1950 *Phys. Rev.* **78** 807
Raja R 2005 private communication
Raja R and Tollestrup A 1998 *Phys. Rev.* D **58** 013005
Ramsey N F 1982 *Rep. Prog. Phys.* **45** 95

Ranjbar V, Lee S Y, Bai M, Courant E and MacKay W W 2001 *Proc. 2001 Particle Accelerator Conf. (Chicago, IL)* (Piscataway, NJ: IEEE) pp 3177–9
Ranjbar V *et al* et al 2002a *Proc. 8th European Particle Accelerator Conf. (Paris)* (Geneva: EPAC) pp 356–8
Ranjbar V, Bai M, Luccio A U, MacKay W W, Roser T and Lee S Y 2002b *Proc. 8th European Particle Accelerator Conf. (Paris)* (Geneva: EPAC) pp 359–61
Ranjbar V H, Lee S Y, Huang H, Luccio A U, MacKay W W, Ptitsyn V, Roser T and Tepikian S 2003 *Phys. Rev. Lett.* **91** 034801
Regan B C, Commins E D, Schmidt C J and DeMille D 2002 *Phys. Rev. Lett.* **88** 071805
Rich A and Wesley J C 1972 *Rev. Mod. Phys.* **44** 250–83
Roberts B L (for the E821 Collaboration) 2002 *Proc. 8th European Particle Accelerator Conf. (Paris)* (Geneva: EPAC) pp 154–8
Roberts B L (for the E821 Collaboration) 2004 *AIP Conf. Proc.* **698** 13–22
Roser T 1989 *AIP Conf. Proc.* **187** 1442–6
Roser T 2002 *Handbook of Accelerator Physics and Engineering* ed A Chao and M Tigner (Singapore: World Scientific) pp 594–5
Roser T 2003 *Proc. 2003 Particle Accelerator Conf. (Portland, OH)* (Piscataway, NJ: IEEE) pp 24–8
Roser T 2005 private communication
Roser T *et al* 2003 *AIP Conf. Proc.* **667** 1–8
Rossmanith R and Schmidt R 1985 *Nucl. Instrum. Methods* A **236** 231–48
Rowson P C, Su D and Willocq S 2001 *Ann. Rev. Nucl. Part. Sci.* **51** 345–412
Ruth R 1983 *IEEE Trans. Nucl. Sci.* **30** 2669
Sands M 1970 *SLAC Report* 121
Sato H 1988 *Japan. J. Appl. Phys.* **27** 1022
Sato H, Arakawa D, Hiramatsu S, Mori Y, Ikegami K, Takagi A, Toyama T, Ueno A and Imai K 1988 *Nucl. Instrum. Methods* A **272** 617–25
Sato H *et al* 1997 *Nucl. Instrum. Methods* A **385** 391–17
Sato H 2004 private communication
Sato K 1997 *Proc. 16th RCNP Osaka International Symp. on 'Multi-GeV High-Performance Accelerators and Related Technology'* (Osaka: RCNP) pp 1–7
Schwinger J 1948 *Phys. Rev.* **73** 416–17
Schwinger J 1949 *Phys. Rev.* **75** 1912–25
Schwinger J and Tsai W 1974 *Phys. Rev.* D **9** 1843–5
Semertzidis Y K *et al* 2003 *Nucl. Instrum. Methods* A **503** 458–84
Serednyakov S I, Sidorov V A, Skrinsky A N, Tumaikin G M and Shatunov Yu M 1977 *Phys. Lett.* B **66** 102–4
Serednyakov S I, Skrinsky A N, Tumaikin G M and Shatunov Yu M 1976 *Sov. Phys.—JETP* **44** 1063
Shapiro G *et al* 1993 *Proc. 1993 Particle Accelerator Conf. (Washington, DC)* (Piscataway, NJ: IEEE) pp 2172–4
Shatunov Yu M 1969 unpublished
Shatunov Yu M 1990 *Part. Accelerators* **32** 139–52
Shatunov Yu M 2001 *AIP Conf. Proc.* **592** 279–316
Sinclair C K 1989 *AIP Conf. Proc.* **187** 1412–27
Sinclair C K 1998 *AIP Conf. Proc.* **451** 23–39
Sinclair C K 1999 *Proc. 1999 Particle Accelerator Conf. (New York)* (Piscataway, NJ: IEEE) pp 65–9
Sinclair C K 2004 private communication
Skrinsky A N and Shatunov Yu M 1989 *Sov. Phys.—Usp.* **32** 548–54
Sokolov A A and Ternov I M 1964 *Sov. Phys.—Dokl.* **8** 1203–5
Speckner T, Anton G, von Drachenfels W, Frommberger F, Helbing K, Hoffmann M, Kiel B, Michel T, Naumann J and Zeitler G 2004 *Nucl. Instrum. Methods* A **519** 518–31
Spinka H 2003 *AIP Conf. Proc.* **675** 807–11
Spinka H *et al* 1983 *Nucl. Instrum. Methods* A **211** 239–61
Steier C 2004 private communication
Steier C 1999 *PhD Thesis* Bonn University (in German)
(Steier C 1999 *Internal Report* BONN-IR-1999-07)
Steier C, Byrd J and Kuske P 2000 *Proc. 7th European Particle Accelerator Conf. (Vienna)* (Geneva: EPAC) pp 1566–8
Steier C and Husmann D 1998 *Proc. 1997 Particle Accelerator Conf. (Vancouver)* (Piscataway, NJ: IEEE) pp 1033–5
Steier C, von Drachenfels W, Frommberger F, Hoffmann M, Husmann D, Keil J and Nakamura S 1998 *Proc. 6th European Particle Accelerator Conf. (Stockholm)* (Geneva: EPAC) pp 433–5
Steier C, von Drachenfels W, Frommberger F, Hoffmann M, Husmann D, Keil J, Nakamura S and Nakanishi T 1999 *Proc. 1999 Particle Accelerator Conf. (New York)* (Piscataway, NJ: IEEE) pp 3098–100

Streun A 2001 *Swiss Light Source Report* SLS-TME-TA-2001-0191
Ternov I M, Loskutov Yu M and Korovina L I 1962 *Sov. Phys.—JETP* **14** 921
Thomas L H 1927 *Phil. Mag.* **3** 1–22
Tojo J *et al* 2002 *Phys. Rev. Lett.* **89** 052302
Tolhoek H A and de Groot S R 1951 *Physica* **17** 1–16
Tolhoek H A 1956 *Rev. Mod. Phys.* **28** 277–98
Toyama T, Hiramatsu S, Sato H and Holt J A 1989 *KEK Preprint* 89-112
Toyama T, Hiramatsu S, Sato H and Holt J A 1990 *Part. Accelerators* **32** 167–72
Unruh W G 1976 *Phys. Rev.* D **14** 870–92
Unruh W G 1998 *Quantum Aspects of Beam Physics* ed P Chen (Singapore: World Scientific) pp 594–619
Van Dyck Jr R, Dehmelt H and Schwinberg P 1987 *Phys. Rev. Lett.* **59** 26–9
van Guilder B S 1993 *PhD Thesis* University of Michigan
Vasserman I B *et al* 1987a *Phys. Lett.* B **187** 172–4
Vasserman I B *et al* 1987b *Phys. Lett.* B **198** 302–6
Vogt M 2000 *PhD Thesis* University of Hamburg
Vorobyov P V, Kezerashvili G Ya, Lysenko A P, Polunin A A and Shatunov Yu M 1986 *Proc. 7th Int. Symp. on High Energy Spin Physics (Protvino)* (Serpukhov: Institute of High Energy Physics) pp 175–9
Wang D 2001 *Proc. 2001 Particle Accelerator Conf. (Chicago, IL)* (Piscataway, NJ: IEEE) pp 3523–4
Wenninger J 1995a *Proc. 5th Workshop on LEP Performance (Chamonix, France)* ed J Poole, CERN SL/95-08 (DI) pp 40–3
Wenninger J 1995b CERN SL/95-21 (OP)
Wenninger J 1999 *Proc. 1999 Particle Accelerator Conf. (New York)* (Piscataway, NJ: IEEE) pp 3014–16
Wenninger J 2004 private communication
Woods M 1997 *Proc. 12th Int. Symp. on High Energy Spin Physics (Amsterdam)* ed C W de Jager *et al* (Singapore: World Scientific) pp 623–7
Woods M 2004a *SLAC PUB 10338*
(Woods M 2004 *Preprint* hep-ex/0403010)
Woods M 2004b private communication
Woods M *et al* 1997 *Proc. 12th Int. Symp. on High Energy Spin Physics (Amsterdam)* ed C W de Jager *et al* (Singapore: World Scientific) pp 843–5
Yokoya K 1982 *Proc. Workshop on Polarized Electron Acceleration and Storage* (Hamburg: DESY) pp R19–29
Yokoya K 1983a *Part. Accelerators* **13** 85–93
Yokoya K 1983b *Part. Accelerators* **13** 95–100
Yokoya K 1983c *Part. Accelerators* **14** 39–61
Yokoya K 1986 *DESY Report* 86-057
Yokoya K 1987 *Nucl. Instrum. Methods* A **258** 149–60
Yokoya K 1992 *KEK Report* 92-6
Yokoya K 1993 *Proc. 10th International Symp. on High Energy Spin Physics (Nagoya)* (Japan: Universal Academic Press) pp 415–18
Yokoya K 1999 *DESY Report* 99-006
(Yokoya K 1999 *Preprint* physics/9902068)
Yoshida H 1990 *Phys. Lett.* A **150** 262–8
Zelensky A N 1999 *Proc. 1999 Particle Accelerator Conf. (New York)* (Piscataway, NJ: IEEE) pp 106–8
Zetsche F 1997 *Proc. 12th Int. Symp. on High Energy Spin Physics (Amsterdam)* ed C W de Jager *et al* (Singapore: World Scientific) pp 846–8
Zholents A A *et al* 1981 *Sov. J. Nucl. Phys.* **34** 814–20